FATIGUE CRACK GROWTH UNDER SPECTRUM LOADS

ASTM STP 595

AMERICAN SOCIETY FOR TESTING AND MATERIALS

FATIGUE CRACK GROWTH UNDER SPECTRUM LOADS

A symposium
presented at the
Seventy-eighth Annual Meeting
AMERICAN SOCIETY FOR
TESTING AND MATERIALS
Montreal, Canada, 23-24 June 1975

ASTM SPECIAL TECHNICAL PUBLICATION 595
R. P. Wei and R. I. Stephens
symposium cochairmen

List price $34.50
04-595000-30

AMERICAN SOCIETY FOR TESTING AND MATERIALS
1916 Race Street, Philadelphia, Pa. 19103

Library of Congress Catalog Card Number: 75-32902

NOTE

The Society is not responsible, as a body, for the statements and opinions advanced in this publication.

Printed in Tallahassee, Fla.
May 1976

Foreword

The Symposium on Fatigue Crack Growth Under Spectrum Loads was held on 23-24 June 1975 at the Seventy-eighth Annual Meeting of the American Society for Testing and Materials in Montreal, Quebec, Canada. Committee E-24 on Fracture Testing of Metals and Committee E-9 on Fatigue sponsored the symposium. R. P. Wei, Lehigh University, and R. I. Stephens, The University of Iowa, served as the symposium cochairmen. Serving as members of the Symposium Organizing/Program Committee and as session chairmen were J. M. Barsom, U. S. Steel Corp.; W. G. Clark, Jr., Westinghouse R & D Center; N. E. Dowling, Westinghouse R & D Center; C. M. Hudson, NASA Langley Research Center; E. K. Walker, Lockheed California Co.; and Howard Wood, AFFDL/FBR, Wright-Patterson AFB.

Related ASTM Publications

Handbook of Fatigue Testing, STP 566 (1974), $17.25, 04-566000-30

Fatigue at Elevated Temperatures, STP 520 (1973), $45.50, 04-520000-30

Probabilistic Aspects of Fatigue, STP 511 (1972), $19.75, 04-511000-30

A Note of Appreciation to Reviewers

This publication is made possible by the authors and, also, the unheralded efforts of the reviewers. This body of technical experts whose dedication, sacrifice of time and effort, and collective wisdom in reviewing the papers must be acknowledged. The quality level of ASTM publications is a direct function of their respected opinions. On behalf of ASTM we acknowledge with appreciation their contribution.

ASTM Committee on Publications

Editorial Staff

Contents

Introduction

The importance of load interactions in variable-amplitude loading on the accurate prediction of fatigue lives or inspection intervals or both of engineering structures has been recognized for some time. A number of symposia have been held over the past 20 years (many of them under the auspices of the American Society for Testing and Materials (ASTM)). Most of these symposia were directed to the problems of fatigue behavior of smooth and mildly notched specimens, and of structural components. In more recent years, fatigue crack growth has begun to receive increasing attention both in research and in structural design. Fracture mechanics has emerged and matured as an important tool for design analyses and for studying fatigue crack growth during the past decade.

As a result of these developments and of well-publicized problems with several aerospace and highway structures, a considerable amount of effort has been and is now being devoted to the understanding of load interaction effects in fatigue, and to the development of rational procedures for predicting fatigue behavior under spectrum (service) loads. It was clear that a major symposium was needed to review and assess current technology and understanding in this important area, to provide a forum for the exchange of ideas, and to help define problem areas and directions for new research. In recognition of this need, independent planning for such a symposium was initiated in early 1973 within ASTM Committee E-24 on Fracture Testing of Metals and Committee E-9 on Fatigue. The symposium became a joint venture between ASTM Committees E-24 and E-9 in late 1973.

Because of the complexity of the problem, it was decided to restrict the symposium only to those topics that are related to fatigue crack growth so that each topic could be treated in some depth. The primary objective of this symposium was to bring the current state of the art and information into focus such that reliable predictive procedures can be identified or developed or both for use in the design of engineering structures. In support of this primary objective, the following topics were considered:

1. Review and assessment of current technology.
2. Description of service loading and environmental conditions.
3. Characterization of load spectrum for use in testing and in design.
4. Crack growth under simple load spectra, including the influence of service/test environment.
5. Crack growth under complex/random load spectra, including the influence of service/test environment.
6. Mechanism(s) and modeling.

7. Predictive methods and correlations with service performance.
8. Identification of test procedures and of need for standardization.

This volume details the proceedings of the Symposium on Fatigue Crack Growth Under Spectrum Loads and provides a reasonable representation of the current state of the art and thinking. It is organized into four separate sections, with an introductory overview paper by J. Schijve:

I. Simple Spectra—Effect of Loading Variables
II. Simple Spectra—Environmental Effects and Modeling
III. Complex Spectra—Load Definition, Modeling, and Service Simulation
IV. Life Prediction and Applications

The various topics listed are covered in each of these sections and in the overview paper by Dr. Schijve. The volume serves to reemphasize the highly complex nature of fatigue crack growth under spectrum loads, and the diversity of views on the subject. Load interaction effects result from complex processes that occur at or near the crack tip and are difficult to assess analytically or experimentally. The difficulty is compounded by a range of combined load and environment (chemical and thermal) interactions. Nevertheless, by recognizing the difference between *pragmatism* and *fundamental understanding*, significant progress can be made. By realizing the importance of various loading and environmental variables, rational life prediction procedures can be developed for specific applications. By avoiding broad generalizations, development of understanding can proceed in an orderly fashion. The contributions of this symposium are to be viewed in light of these comments, and represent a good beginning.

The information contained in this volume will be of use to designers, materials scientists and test engineers, and structural and reliability engineers who are concerned with this important problem. It is hoped that interactions between the various disciplines involved will be promoted and that this volume will serve as a starting point and provide impetus for rapid advance in the field of fatigue crack growth under spectrum loads.

The success of a symposium and the publication of its proceedings depend on the tireless efforts of many people. The contributions of the authors, the reviewers, the members of the Symposium Organizing/Program Committee, and Jane B. Wheeler and her staff are gratefully acknowledged. Donald Wisdom, who encouraged and assisted in the initial planning of this symposium, and who through untimely death could not see it come to fruition, is warmly remembered by us all.

R. P. Wei,

Lehigh University, Bethlehem, Pa.; ASTM Committee E-24, symposium cochairman.

R. I. Stephens,

The University of Iowa, Iowa City, Iowa; ASTM Committee E-9, symposium cochairman.

J. Schijve[1]

Observations on the Prediction of Fatigue Crack Growth Propagation Under Variable-Amplitude Loading

REFERENCE: Schijve, J., **"Observations on the Prediction of Fatigue Crack Growth Propagation Under Variable-Amplitude Loading,"** *Fatigue Crack Growth Under Spectrum Loads, ASTM STP 595,* American Society for Testing and Materials, 1976, pp. 3–23.

ABSTRACT: The paper starts with a discussion on loads in service, after which a survey is given of various types of variable-amplitude loading as applied in test programs. The various phenomenological aspects of fatigue damage associated with fatigue cracks are indicated. Interaction effects between cycles of different magnitudes are defined. Methods for measuring interaction effects, examples of interaction effects, and possible explanations are reviewed. This includes both tests with simple types of variable-amplitude loading (overloads and step loading) and more complex load-time histories (program loading, random load, and flight-simulation loading). New evidence on crack closure is presented. Various types of prediction methods are discussed. The paper is primarily a survey of the present knowledge, with an analysis of the consequences for prediction techniques.

KEY WORDS: crack propagation, fatigue (materials), loads (forces), predictions

For an operator of a machine or a structure, cracks are of little interest as long as they cannot be detected by available inspection techniques. However, as soon as detection is possible, the situation is different. If crack growth is sufficiently slow, routine inspections can be adopted to prevent failures in service. In aircraft structures this has led to the well-known fail-safe philosophy. The crack propagation curve in Fig. 1 illustrates this point. Obviously, the time available

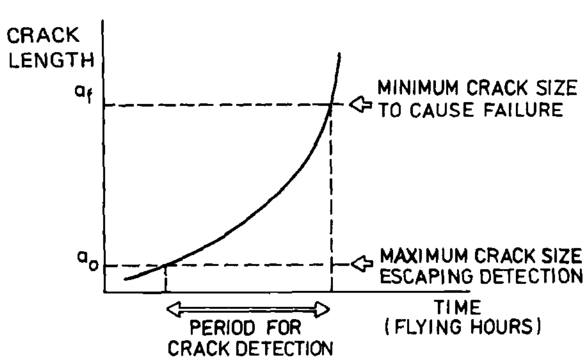

FIG. 1–*Limitations of fail-safety.*

[1] Professor, Department of Aeronautical Engineering, Delft University of Technology, Delft, The Netherlands.

for crack detection depends on both a_0 and a_f. Since the growth of a crack is usually an accelerating process, the time is less dependent on a_f and more dependent on a_0. This emphasizes the significance of inspection techniques. For a long time, the arbitrary choice was a_0 = ½ in. (12.6 mm), but more optimistic values, say a few millimetres, appear to be justified, provided the crack location is accurately known. The time available for crack detection is clearly related to the crack propagation curve (Fig. 1), and the problem of predicting this curve is the leading question of this paper.

Crack growth is dependent on numerous variables (see Table 1 which lists the main groups). This paper attempts to survey the various aspects of predicting

TABLE 1 – *Variables affecting crack growth.*

Variables outside the structure	load-time history chemical environment
Variables inside the structure	type of structure material

crack growth curves, which should include a discussion of many variables. However, the main topic will be the effect of the load-time history including a few comments on environmental effects. It is well known, especially for aircraft structures, that crack growth can be retarded and temporarily stopped by adopting specific design features. Fail-safe design procedures, however, will not be discussed, nor will material selection for slow crack growth. The discussion in this paper includes: loads in service, present knowledge about crack growth under variable-amplitude loading, and present prediction methods. These problems are discussed as they occur in aeronautics, but the situation is similar to other diciplines.

Loads in Service

The major aspects of service load-time histories include:

1. load occurrences,
2. load sequences,
3. speed of load variations, and
4. environment.

The definition of the varying load is a problem in itself. Two samples are shown in Fig. 2 to illustrate this point. The first sample is characteristic of an amplitude-modulated signal [*1*][2] with a constant mean and frequency, and the random feature is in the modulation. The second sample shows a random nature, which is less easily defined than the first sample. Such samples can be statistically analyzed with respect to peak loads, load ranges, etc. (counting

[2] The italic numbers in brackets refer to the list of references appended to this paper.

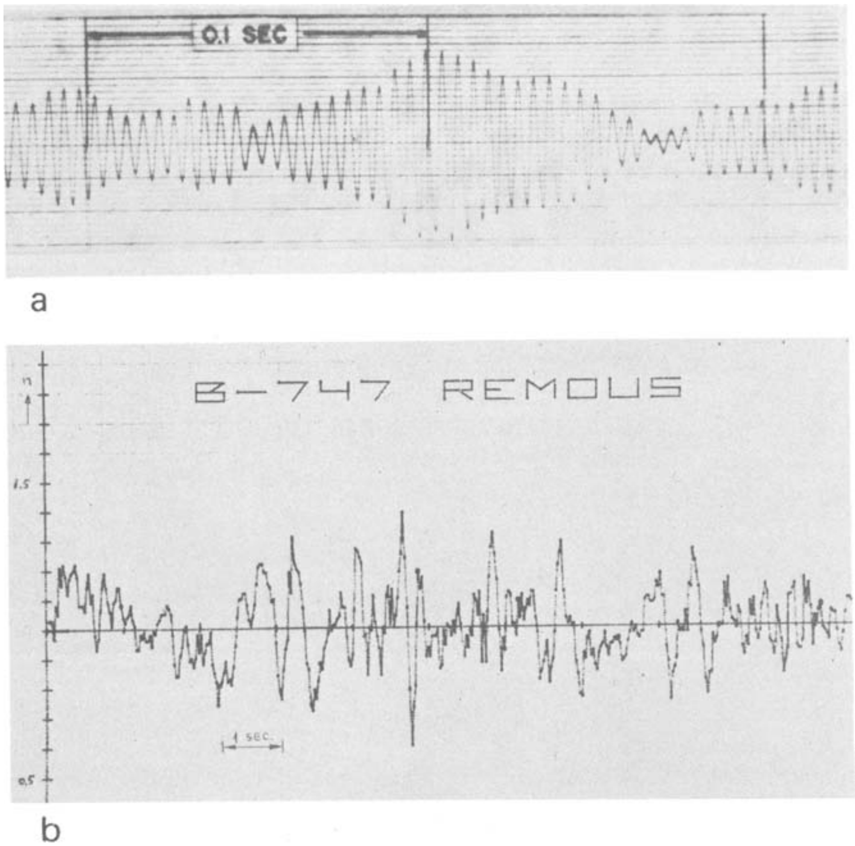

FIG. 2–*Two samples of service load-time histories: (a) narrow-band random vibrations [1], and (b) gust loading on a wing.*

methods) [*2,3*]. However, information on the sequence of load occurrences is lost in such a statistical description.

Investigations on sequence effects have clearly shown their significance. Results of a comparative study on crack growth with random and programmed sequences are summarized in Fig. 3 [*4*]. Although all sequences were statistically

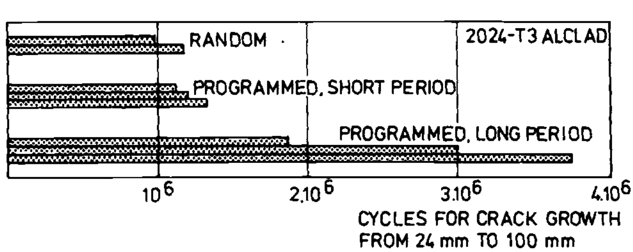

FIG. 3–*Comparison between crack propagation lives under random loading and "statistically equivalent" programmed loading [4].*

equivalent with respect to load occurrences, the crack growth rates were significantly different. Moreover, the fracture surfaces were also different, even macroscopically, and this will be discussed later.

The conclusion to be drawn here is that complete knowledge about loads in service should include information on load sequences. If the loading is a stationary random process, the sequence appears to be well defined in statistical terms. However, in many practical situations the loading conditions are non-stationary. Moreover, mixtures of random loads and deterministic loads frequently occur. A well-known example is the (non-stationary) random gust loading on a wing, combined with the deterministic ground-to-air cycles.

An inherent problem of predicting loads in service is the scanty information on the rarely-occurring very high loads. This feature is disturbing, because these high loads can have a great effect on crack growth. High tensile loads can drastically reduce crack growth. Unfortunately, accurate predictions on the occurrence of such loads in service are difficult to make. This implies a severe limitation to the practical significance of predicted crack rates.

Service conditions also include the operating environment. If the environment is affecting crack growth, the phenomenon has to be associated with corrosion fatigue. The speed of load variations can be significant (effects depending on time and loading rates). Three groups of environments are:

1. nonaggressive dry environments,
2. water vapor as the most detrimental element, and
3. more aggressive electrolytic conditions.

Nonaggressive environments do not frequently occur in aerospace conditions, although they are relevant to space structures and to aircraft at very high altitudes. However, the second group is applicable in many cases. The third group encompasses wet environments.

The detrimental effect of water vapor on crack growth in aluminum alloys is well known. Present knowledge appears to indicate the constant effect of water vapor on many service conditions as well as on testing in the laboratory. Sufficient water vapor is available for the same maximum detrimental effect. Comparative flight-simulation tests at 10 Hz, 1 Hz, and 0.1 Hz have shown the same crack rates in 2024-T3 Alclad and 7075-T6 clad material [5]. This simplified picture is a most desirable result in view of the relevance of laboratory results for service conditions. It should be clearly recognized, however, that the picture is only wishful thinking unless it can be backed up by physical understanding. Moreover, for more agressive wet environments, the time scale will certainly be significant. An outstanding example of this is the growth of cracks in marine environments, which would apply to off-shore structures. It then becomes extremely difficult to obtain relevant information from high-speed laboratory tests.

Differences Between Crack Growth Studies

The first impression from the literature is the overwhelming variety of different types of variable-amplitude loading. For an analysis of present knowledge, the various types of loading have been classified in a number of groups in Table 2. The variety of fatigue loads is partly, but not fully, illustrated by the second column of the table. The variety of investigations on crack growth

TABLE 2 – *Types of variable-amplitude loading with main variables.*

Overloads	single overload repeated overloads blocks of overloads magnitude of overloads (including R) sequence in overload cycles
Step loading	sequence of steps (hi-lo or lo-hi) magnitude of steps (including R)
Programmed block loading	sequence of amplitudes size of blocks distribution function of amplitudes
Random loading	spectral density function (narrow band, broad band) crest factor (clipping ratio) irregularity factor
Flight-simulation loading	distribution function of load cycles sequence of flights sequence of loads in flight maximum load in the test

is significantly larger because, in addition to the loading history, there are several additional variables. It is sufficient to mention:

1. type of specimen;
2. material;
3. loading system (tension, bending, etc.);
4. loading rate (frequency); and
5. environmental conditions.

The effect of the type of specimen is generally covered by relevant K-values. However, differences between thick and thin specimens are significant (plane strain/plane stress). The other variables further contribute to a large variety of investigations reported in the literature. It then becomes possible that the relative amount of duplication is rather limited, despite an impressive number of publications.

The goals of investigations can also be grouped into different categories. Three general goals frequently recognized from the literature are:

1. to increase the fundamental understanding of the crack growth mechanism under variable-amplitude loading,
2. to check crack growth prediction models, and
3. to generate data from which useful empirical trends might be derived.

Investigations on overload effects and step loading are usually aimed at the first goal. Conclusions of papers suggest some degree of understanding of a mechanism. Investigations on program loading, random loading, or flight-simulation are more directed to the second and the third goals. Relevant papers suggest that a technical problem is treated in a practical way.

Definition and Measurement of Interaction Effects

It would be very convenient for the prediction of crack growth if the growth was a simple addition process of crack length increments (Δa) in each load cycle

$$a = a_0 + \Sigma\, \Delta a_i \tag{1}$$

This process should be understood to be simple if Δa was dependent on the momentary size of the crack, a, only and independent of the history of the preceding crack growth. Unfortunately, this is not true as a consequence of so-called interaction effects. The crack growth increment, Δa, in a certain load cycle will be a function of [*6*]:

1. the crack geometry being present before the cycle started,
2. the condition of the crack tip material, and
3. the magnitude of the load cycle.

These arguments are further illustrated in Table 3.

The arguments compiled in Table 3 imply that Δa will be a function of the preceding cyclic load history. Similarly, a stress cycle will affect crack growth

TABLE 3 – Δa *in a certain load cycle will depend on.*

Amount of cracking	crack length shape of crack front	crack geometry	fatigue damage caused by the preceding load-history
Crack front orientation	tensile mode shear mode mixed modes		
Crack tip blunting	shape of crack tip blunted/sharpened		
Crack closure	plastic deformation in wake of crack		
(Cyclic) strain hardening Residual stress and strain	distribution in crack tip zone	condition of material at tip of crack	
Magnitude of load cycle Environment and frequency	ΔS, R	external conditions of present load cycle	

increments in subsequent cycles. These effects are referred to as "interaction effects." Several examples will be shown later on.

Initially, interaction effects were measured from crack propagation curves as obtained by visual observations of the tip of a crack at the surface of the specimen. Examples for a thin and a thick specimen are given in Fig. 4 [7]. It

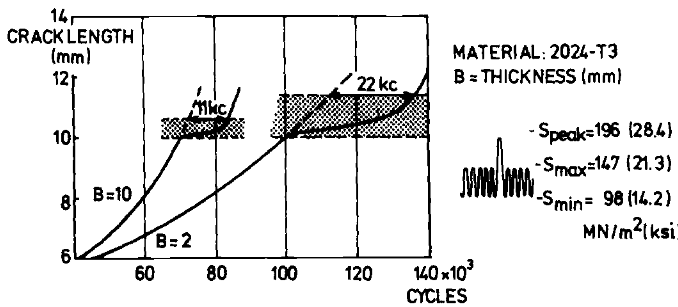

FIG. 4—*The effect of sheet thickness on crack growth delays [7].*

should be pointed out that the tip of a crack cannot always be located accurately. Especially after an overload, the more extensive plastic deformation at the tip of a crack will give some extra blurring of the surface image. Moreover, it is generally recognized now that the two-dimensional picture of the surface does not give sufficient information about the three-dimensional phenomenon occurring in the material. This was borne out by fractographic observations which showed that the curvature of the crack front could change by varying the fatigue load (for example, forming of "tongues" by peak loads). The topography could also vary (amount of shear lips).

Another fractographic refinement was due to measurements of striation spacings. It essentially added to a more detailed picture of interaction effects. Local accelerations or retardations of crack growth can hardly be observed from crack growth curves, but striations can reveal such effects [8].

A different approach is associated with crack closure measurements [9,10]. Such measurements give indirect indications about plastic deformations left in the wake of the crack (see Fig. 5). Unfortunately, more information on the changes of the fatigue damage in the material can hardly be obtained. It is difficult, if not impossible, to measure crack tip blunting and resharpening. The same applies to the cyclic strain-hardening or softening in the crack tip zone and the related residual stress field.

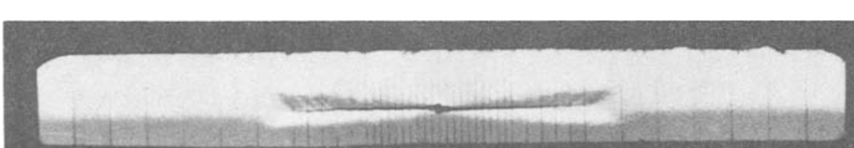

FIG. 5—*Plastic deformation in the wake of a crack (real size). Crack viewed through a window. The upper light part is the reflection of a fluorescent tube lamp.*

Interaction Effects in Tests with Overloads or Step Loading

Originally, most information was obtained on aluminium alloys. Later on, similar tests were conducted on titanium alloys [*11–20*] and high-strength steels [*11,12,15,21–29*]. More or less similar trends were observed. Several test series were also performed on mild steel and other non-aircraft steels [*30–39*]. The behavior of these materials is not fully similar, but crack growth delays were found as well. Apparently, similar results may be expected for materials with a similar (cyclic) strain behavior. For most aeronautical materials this implies a fairly high $\sigma_{0.2}/\sigma_u$ ratio, a limited ductility, and a rapid cyclic strain hardening. Mild steel does not conform to this picture, which should be related to its characteristic yielding and strain aging behavior.

The more prominent observations on interaction effects in tests with overloads or step loading are summarized in the following:

1. *Positive overloads* introduce significant crack growth delays [*6,12,14–20,22,27,29,34,40–50*]. In general, longer delays are obtained by:
   (a) increasing the magnitude of the overload,
   (b) repeating the overload during the crack propagation life, and
   (c) application of blocks of overloads instead of single overloads.
   The retarded growth need not immediately follow the overloads. Some further growth may be required before the crack rate decreases [*29,34,43,45–47,50*]. Sometimes a small initial acceleration was even observed. This *delayed retardation* was clearly verified by observations of striation spacings.
2. The crack extension caused by the overloads themselves is larger than expected from constant-amplitude tests [*49,51*]. This *acceleration* usually requires fractography also.
3. *Negative overloads* have a relatively small detrimental effect on crack growth [*20,40,52*]. However, a negative overload added immediately after positive overloads can significantly reduce the crack growth delay of the latter ones. If the negative overload precedes the positive overload, the reduction of the delay is much smaller. There is an apparent *sequence effect* of the overload cycles [*12,20,40,41,43,49*].
4. In step loading, a hi-lo sequence produces qualitatively similar results as overload cycles [*9,10,40,41,45,46,49,50,53–55*]. Once again, delayed retardation was observed. Interaction effects after a *lo-hi sequence* are hardly detected from macroscopic crack growth observations. However, more accurate measurements and striations do reveal locally accelerated crack growth [*21,25,45,46,50*].
5. Delays clearly depend on the ductility of the material. If the ductility of an alloy is controlled by heat treatment, a lower yield strength will produce longer delays [*27,29,54*].

Originally, the explanation of crack growth delay was based on residual stresses in the crack tip zone [*40,54*]. Later it turned out that this view was too simple. Crack closure, discovered by Elber [9,10], explained both retardations and accelerations by the mechanism. Elber pointed out that crack growth retardation did not occur immediately after an overload. The crack had to penetrate into the plastic zone created by the overload before crack closure could become effective (delayed retardation). This was amply confirmed by the work of others.

Some exploratory tests were recently carried out [7] to study crack closure and delays in relation to specimen thickness. The crack-opening stress, S_{op} (that is, the stress at which crack closure is removed) was measured in constant-amplitude tests for three different thicknesses. A small crack opening displacement (COD) meter was used for this purpose. Results in Fig. 6 show that S_{op} is lower for a larger thickness. In the thicker specimen the plastic zone size will be smaller (approximately plane strain) than in the thinner specimen (approximately plane stress). Similarly, the elongation in the plastic zone is smaller and the residual deformation in the wake of the crack will be smaller. This explains the lower crack opening stress. Adding one overload cycle gives a significant reduction of S_{op} immediately after the overload cycle (see Fig. 6). This has to

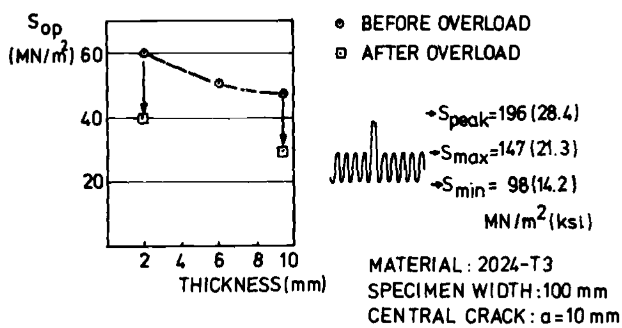

FIG. 6—*Effect of sheet thickness and overload on crack closure [7].*

be expected, because the plasticity ahead of the crack opens the wake of the crack. The results of these overloads on subsequent crack growth are shown in Fig. 4. The crack growth delay is twice as long in the thinner specimen. In view of more crack closure occurring in the thinner specimen, this result had to be expected. The investigation is still in progress, but some data on measurements of S_{op} during the delay period for a thin specimen can already be given here. As shown by Fig. 7, $S_{op} < S_{min}$ before the overload is applied. Immediately after the overload, S_{op} is reduced still further. This would allow an accelerated growth for a small number of cycles, which was reported to occur in the literature [43]. However, shortly afterwards, S_{op} is significantly raised beyond S_{min}. Later, S_{op} again decreases and S_{eff} increases. After $S_{op} = S_{min}$, the retardation of the growth has vanished. In Fig. 4 the crack length increment affected by the overload is approximately equal to its estimated plastic zone size. In Fig. 7 this increment is larger than the plastic zone. As pointed out by Van Lipzig and Nowack [50], the retardation due to crack closure can very well be effective beyond the overload plastic zone.

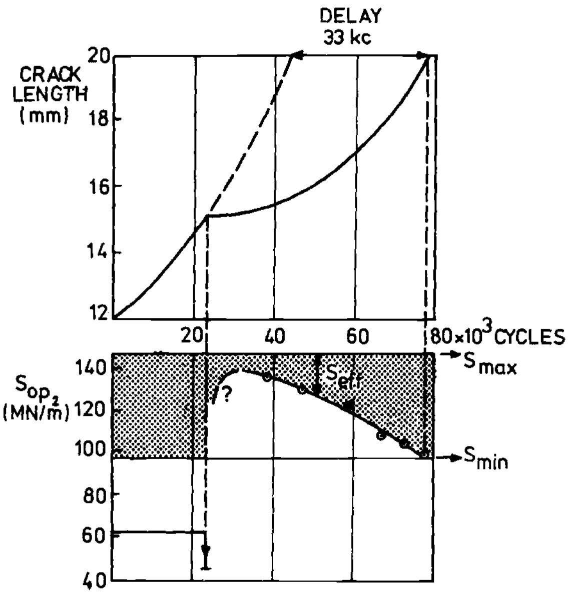

FIG. 7—*Crack-opening stress before and during delay period (material and stress levels, see Fig. 6) [7].*

Results on crack closure in flight-simulation tests, discussed later on, also confirm that crack closure is a real phenomenon. Surprisingly enough, its existence was overlooked for a long time, but recently, the first attempts to incorporate crack closure into calculations were published [*17,56–58*]. The more rigorous calculations made by Newman and Armen [*58*] produced promising results, but such calculations are still rather expensive. More progress, however, may be expected. The question to be raised here is whether interaction effects might be due to crack closure alone. Keeping in mind the fatigue damage picture outlined in the previous section (Table 3), this assumption appears to be somewhat too optimistic. It would be surprising if the cyclic straining of the material in the crack tip zone, the crack tip geometry, and the crack front orientation would be fully irrelevant. Interaction effects as described in Ref *49* cannot be explained completely by crack closure. The crack extension during an overload (for instance, tongues [*29,42,49,59*]) is too large to be due to a low S_{op}. The conditioning of the material in the crack tip zone during the preceding low-amplitude cycles may be another contributing factor. Incompatible crack front orientation [*49*] may further add to the observed behavior. More research is needed to unravel the complex phenomena occurring during variable-amplitude loading. For further studies on this issue a mandatory requirement is to include measurements on crack closure. Tests with load sequences avoiding the occurrence of crack closure should also be enlightening, as shown by Shih and Wei [*17*]. It should be recognized, however, that highly localized crack tip closure might not be detected by "macro crack closure measurements."

Interaction Effects in Tests with Program Loading, Random Loading, or Flight-Simulation Loading

During a complex load sequence, it is more difficult to observe the local interaction effects separately. The overall effect, however, can easily be deduced from macroscopic measurements of the crack growth. The predicted crack rate without interaction effects is obtained from the predicted crack growth curve

$$a = a_0 + \Sigma\, \Delta a_i \tag{1}$$

$$\text{with } \Delta a_i = \text{crack extension in one cycle} = da/dN = f_R\,(\Delta K) \tag{2}$$

It is generally observed that the actual crack rates are considerably different from the predicted values. More detailed observations were obtained by fractographic techniques and crack closure measurements. A summary of the main results is given in the following.

(*a*) Crack rates derived from crack growth curves were usually found to be significantly lower than the values predicted by Eqs 1 and 2 [*5,15,24,26,28,41,59–63*]. Values two to eight times lower were frequently found. Apparently, retardation effects are predominating the possibilities for acceleration effects.

(*b*) In program tests, similar sequence effects were found as observed in step loading [*4,8,16,19,25,26*]. Specifically, a retarded crack growth after a drop of the stress amplitude was clearly observed. In tests with a lo-hi-lo sequence, the crack rate in the descending part was lower than in the ascending part of the program.

(*c*) Nowack [*64*] studied crack growth under random loading with a constant S_{rms}, but a step wise change of S_m. A decrease of S_m caused retarded crack growth.

(*d*) The effect of high loads is similar to the effect of overloads in constant-amplitude loading. In flight-simulation tests, it is well established that the application of rarely occuring very high loads can decrease the crack rate significantly. Truncation of these high loads to lower levels gives faster growth [*6,13,23,26,61,65,66*]. Overloads applied to a structure (for instance fail-safe loads) can drastically reduce subsequent crack growth [*66*].

(*e*) Comparison of program loading and random loading has revealed significant sequence effects [*4*]. These effects were not restricted to crack rates (see Fig. 3) but also applied to the topography of the fracture surface. Macroscopically, the roughness of the fracture surface and the transition from the tensile mode to the shear mode were completely different for the two types of loading, in spite of the same load spectrum applying to both.

(*f*) Crack closure was recently shown to occur during flight-simulation tests [*67,68*]. A sample of the loads in a flight with severe gusts is shown in Fig. 8. Crack closure measurements made by a COD meter during a

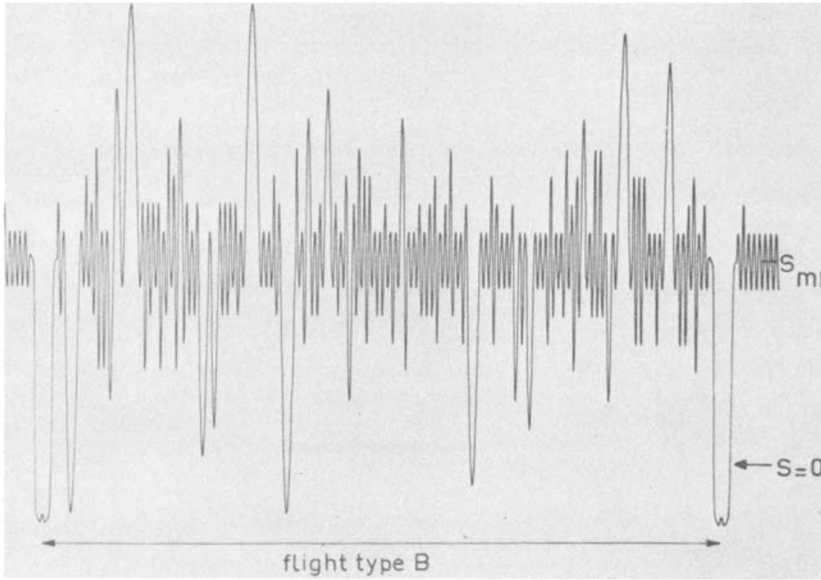

FIG. 8–*Load history during a flight-simulation test [66,67]. Flight with severe gust loads.*

severe flight are shown in Fig. 9. The measurements were made only for larger stress amplitudes of the flight. When the load passed the mean stress in flight, small horizontal shifts were given to the recorder to separate the loops of the various loads. Two interesting observations can be made. First, five maximum peak loads occurring in the same flight do not have the same effect. The nonlinearity at the top of the first one is mainly due to crack extension and crack tip plasticity. Apparently, the other four

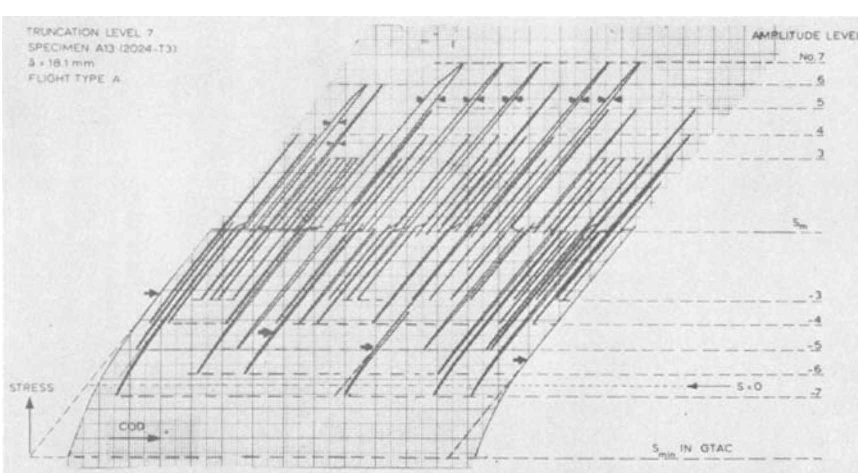

FIG. 9–*COD measurements during a severe flight of a flight-simulation test [66,67].*

peak loads produce smaller contributions. This is in agreement with results from a more elementary study [*47,49*]. The second observation is related to crack closure which is easily observed from the nonlinearities in the bottom part of the recording. Arrows indicate the stress levels below which the crack is partly closed (S_{op}). The first high load widens the crack and thus causes a similar decrease of S_{op} as reported in the previous section. After further crack growth during subsequent flights with milder gust spectra, the crack opening stress was again restored to a higher level.

It appears that the observations of the tests with more complex load histories are qualitatively in good agreement with the results of the more simple types of loading, discussed in the previous section. The agreement concerns the effect of high loads, delays, sequence effects, and crack closure. In view of all this evidence, it is opportune to reconsider the occurrence of both crack growth delaying and acceleration effects during complex load-time histories. A useful comment was recently made by Katcher [*15*]. He started from the observation that crack growth retardation after a high load requires a number of cycles before it becomes effective (delayed retardation). He then pointed out that a reapplication of a high load, before the retardation could become effective, may considerably reduce the delay effect. A similar suggestion can be made for acceleration effects. Accelerations were observed after lo-hi sequences, occurring immediately after the lo-hi transition. This is in agreement with the crack closure concept, although it need not be the only explanation. Anyhow, the acceleration requires some prehistory of lower-amplitude cycles. Consequently, high-load cycles which have not seen a prehistory of lower-amplitude cycles, will not be associated with the same acceleration effect. This was illustrated before (see subsection (*e*) and Fig. 9).

The conclusion now is that accelerations and delays in a complex load history are very sensitive to the sequence of the various loads. The assumption that random sequences and equivalent programmed sequences could give the same overall crack rate has to be considered wishful thinking.

There is another conclusion to be drawn from the present knowledge. During variable-amplitude loading, accelerations occur during the high loads. Retardations occur during the low-amplitude cycles. The result may well be that the major part of the crack extension will occur during the high-amplitude cycles. Crack growth observations during flight-simulation tests and fractography appear to confirm this view [*59,65*]. This appears to be important for the mutually related effects of environment and frequency. Environmental effects during crack growth (corrosion fatigue) were amply shown in the literature to be large for low ΔK values and relatively small during high ΔK values. If it is true that the major contribution in $\Sigma\ \Delta a$ is coming from the higher load-amplitude cycles a relatively small environmental effect should be expected. This is now being investigated at the National Aerospace Laboratory, Amsterdam (NLR). Flight-simulation tests are carried out on 2 and 10-mm sheet specimens (width 160 mm) of 2024-T3 and 7075-T6 material at 15 Hz. Some preliminary results for 2-mm specimens of 2024-T3 are shown in Table 4.

TABLE 4 – *Preliminary results of 2-mm 2024-T3 specimens.*

Environment	Crack growth life ($a = 10$ mm to failure)	Ratio
Dry air ($H_2O < 20$ ppm)	23 120 flights	1.3
Lab air (RH 50%, 20 to 25°C)	18 210 flights	1
Salt water	7 845 flights	0.43

Life in dry air is only 30 percent longer than in wet air, whereas constant-amplitude data [*69*] would suggest it to be about three times longer. The effect of salt water is probably not much different from the expected ratio derived from constant-amplitude data. The problem of environmental effects under service loading requires further clarification [*19*]. The present considerations, however, already emphasize the need for realistic testing if realistic answers are to be found.

Prediction Methods for Variable-Amplitude Loading

After the conclusive proof of the usefulness of ΔK for correlating constant-amplitude crack rate data, it was all but natural that extensions to variable-amplitude loading were proposed. Available propositions can be classified in five groups:

1. non-interaction,
2. interaction based on K_{eff},
3. equivalent K-concept,
4. characteristic K-concept, and
5. empirical trends.

The non-interaction method simply assumes that Δa in any load cycle is dependent on the applicable K-value pertaining to that cycle. As discussed before, this is physically incorrect and leads to overconservative crack rate estimates.

Interaction methods based on K_{eff} also start from the idea that the crack rate is uniquely related to ΔK and R values. In addition, attempts are made to account for the effect of crack tip plasticity in preceding load cycles on the real values of K (K_{eff}) and R. A notable example is the Willenburg model [*70*]. More comments on this model and the Wheeler model [*11*] are given later on.

The equivalent K method was proposed for random loading [*60,62,71*]. The basic assumption is that an equivalent ΔK can be indicated, which under constant-amplitude (CA) loading will give the same crack rate as the random loading.

$$\left[da/dN = f(\Delta K_{eq})_{\text{random loading}}\right] = \left[da/dN = f(\Delta K)_{\text{CA loading}}\right] \qquad (3)$$

The root mean square (rms) value of the random loading was proposed for this purpose: $\Delta K_{eq} = \Delta K_{rms}$. There are no theoretical reasons to see that the basic assumption is plausible. Checks in the literature have shown systematic deviations [*60,62,71*].

The characteristic K-concept was proposed by Paris [*72*] for stationary random loading. Contrary to the equivalent K-method, a relationship to constant-amplitude data was abandoned. The basic idea is that the random variations of the stress in the crack tip zone are fully described by ΔK_{rms}

$$da/dN = f_R\ (\Delta K_{\mathrm{rms}}) \tag{4}$$

$$\text{with } \Delta K_{\mathrm{rms}} = C\,S_{\mathrm{rms}}\sqrt{\pi a} \tag{5}$$

Available evidence in the literature [*60,71,73*] appears to confirm the validity of this approach. It should not be overlooked that the relationship in Eq 4 will be a function of a stress ratio, which was defined by S. H. Smith [*60*] as $\gamma = S_{\mathrm{m}}/S_{\mathrm{rms}}$. Two more important variables of random loading are the spectral density function and the crest factor (clipping ratio). The first one appears to have a small effect on the crack rate [*60,71*], although the evidence is still limited. It is difficult to indicate theoretical expectations on this topic. The effect of the crest factor is practically unknown, but a significant effect should be expected in view of results obtained in flight-simulation tests [*6,61*].

The promising results obtained for random loading have promoted a similar approach to flight-simulation loading [*5,74*]. A characteristic K-value can also be defined easily for this type of loading. Unfortunately, the test results indicated that a relation similar to Eq 4 did not hold. In a theoretical analysis of this observation, it was shown that Eq 4 should be replaced by

$$da/dN = f_R\ (\Delta K, dK/da) \tag{6}$$

In constant-amplitude tests and random load tests, the effect of dK/da turned out to be negligible, but for flight-simulation loading this did no longer apply. A more extensive discussion is given in Refs *5* and *74*.

*The Willenborg Model [*26,69*] and the Wheeler Model [*11*]*

Both the Willenborg and Wheeler models were proposed to explain crack growth delays induced by high loads. Both employ plastic zone sizes as indicated in Fig. 10, however, the concepts are different. Wheeler related the retardation

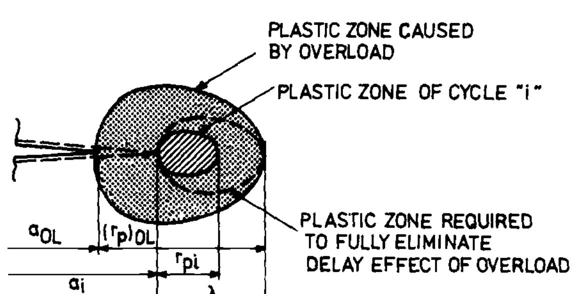

FIG. 10—*Plastic zone size concepts in the models of Wheeler and Willenborg.*

to r_{pi}/λ. Willenborg made a different assumption about the effective stress as affected by the plastic deformation of the overload. As a result, ΔK_{eff} and R_{eff} are calculated and used to obtain the applicable da/dN values.

Both models were checked by various authors [*14,15,26,62,63,75*], but a systematic agreement with test results was rarely found. The advantage of the Willenborg model was said to be that no empirical material constants were required. However, in order to improve the reliability of the Willenborg model a material constant was again introduced [*29,62*]. Actually, the number of variables of complex load-time histories is rather large, and it would be surprising if a single empirical constant would be sufficient to account for all variables. This can be expected only if the model itself is physically correct. Unfortunately, this does not appear to be true. The Willenborg model and the Wheeler model consider plasticity in the crack tip zone only with a simple assumption about the plastic zone size. A reversed plastic zone as discussed by Rice [*76*] is not included. Both models predict maximum retardation immediately after an overload, while the retardation is assumed to pass off as soon as $r_{pi} = \lambda$ (Fig. 10). These features were shown to be incorrect, which can easily be explained by crack closure. The models exclude the possibility of accelerated growth, which is also a real phenomenon.

In Ref *68* requirements for a more realistic model were indicated. The complexity of the problem became clearly evident. The first approach would be to incorporate crack closure, but, it cannot be ruled out that this will not be enough to make a model sufficiently reliable for prediction problems. Extensive research is still required to reach this goal.

Empirical approach

If fundamentally correct laws are not available, it is a practical solution to look for a systematic empirical rule. Attempts were made to start from delays as observed in tests with overloads. Delay factors were derived from such tests, which were then translated to more complex loading programs [*12,14,18,19,48*]. The more complex programs were still rather simple as compared to service load-time histories. Since these propositions start from delays only, ignoring accelerations, it is doubtful whether it will ever lead to a useful rule. Checking empirical rules by unpractical types of loading is not a logical approach. Similarly, it is also illogical to disprove an empirical rule by tests with unpractical types of loading.

The prediction method proposed by Habibie [*77–79*] for application to service load-time histories is starting from crack growth retardations as observed in flight-simulation tests. Apparently, this is a more practical approach. Habibie employs the K factor to arrive at crack growth retardation formulas. Originally he adopted eight material constants, but this number was later reduced. His predictions for flight-simulation test results are quite good, but the method was less successful in predicting the trends for program tests. For an empirical method, the latter result need not be a disadvantage if the prediction for realistic load sequences is considered.

Multi-Variable Regression Analysis

Habibie was still employing the K-factor to support his method by physical arguments. A more rigorous empirical approach is to start directly from empirical data and to look for mathematical relations which best represent the trends. This leads to multi-variable regression analysis of test data. An example of this approach was recently suggested for flight-simulation loading by Simpkins, Neulieb, and Golden [80]. The regression function proposed is

$$N = D \cdot (\sigma^2)^a \cdot (\overline{S}_{1g})^b \cdot (\overline{n})^c \cdot (1\text{-}\overline{Z})^d \tag{7}$$

where D is a constant, σ^2 is the variance of the load spectrum in flight, $\overline{S}_{1g}$ is the average mean stress in flight, $\overline{n}$ is the average number of cycles per flight, and $\overline{Z}$ is the average of S_{min} of the ground-to-air cycle divided by S_{1g}. The equation accounts for four independent variables which are supposed to characterize the severity of the load history. The five constants D, a, b, c, and d are determined by a regression analysis applied to empirical data. Equation 7 applies to the fatigue life, N, under flight loading. A similar approach was proposed for random loading [81]. Applications to crack propagation although not yet made so far, could occur in the same way. The problem is to indicate the independent variables, which sufficiently characterize the load-time history.

Incidentally, a rigorous analysis is still hampered by insufficient available test data. For this purpose a systematic test program was proposed earlier [61]. The purpose should be to obtain systematic data on the effect of the more important variables of realistic load-time histories.

Conclusions

1. The problem of predicting crack growth rates in service cannot be solved without a thorough knowledge of the load-time histories occurring in service. A statistical distribution function of peak loads is insufficient, and knowledge about load sequences is essential.

2. During crack growth under variable-amplitude loading, significant interaction effects will occur. Both crack growth retardations and accelerations have been amply demonstrated. Relevant evidence is available from tests with simple types of loading (overloads, step loading), but similar trends were observed in tests with more complex load sequences (random loading, program loading, and flight-simulation loading).

3. Several mechanisms can contribute to interaction effects, and it is difficult to separate the contributions of each. Actually, the picture of damage accumulation during crack growth under variable-amplitude loading is very complex. However, it has been shown that crack closure gives a significant contribution, and new evidence is reported in this paper. It is strongly recommended that empirical studies on crack growth under variable-amplitude loading should include crack closure measurements.

4. During complex load-time histories, high-amplitude cycles contribute more crack extension than the non-interaction concept will predict, whereas low-

amplitude cycles contribute less. This observation could be significant for environmental effects.

5. Since interaction effects are very sensitive to the sequence of the loads the "equivalence" of complex load-time histories and simplified histories (for example, program loading) is illusory. Actually, realistic answers from tests can only be expected if realistic load-time histories are simulated.

6. There is an increasing activity reported in the literature to develop prediction techniques. Unfortunately, available crack growth models are too simple, and reliable predictions cannot be expected with any certainty. Observations on crack closure as affected by overloads in relation to material thickness and yield strength strongly emphasize the controlling influence of plastic deformation on fatigue crack growth. Therefore, it should be attempted to include crack closure in a fatigue model, although this alone may not be sufficient.

7. For random loading the applicability of ΔK_{rms} is promising. Information on the effect of the crest factor (clipping ratio) is insufficient.

8. For the time being, a prediction method based on multi-variable regression analysis could provide useful information for practical problems. However, sufficient empirical data is not yet available. Empirical investigations to fill this gap should be recommended.

References

[1] Hillbery, B. M. in *Effects of Environment and Complex Load History on Fatigue Life, ASTM STP 462*, American Society for Testing and Materials, 1970, pp. 167–183.

[2] V. Dijk, G. M. in *Advanced Approaches to Fatigue Evaluation*, NASA SP-309, 1972, pp. 565–598.

[3] Schijve, J. in *Fatigue of Aircraft Structures*, Pergamon, 1963, pp. 115–149.

[4] Schijve, J., *Engineering Fracture Mechanics*, Vol. 5, 1973, pp. 269–280.

[5] Schijve, J., Jacobs, F. A., and Tromp, P. J., "Fatigue Crack Growth in Aluminium Alloy Sheet Material under Flight-Simulation Loading. Effects of Design Stress Level and Loading Frequency," NLR TR 72018, Amsterdam, 1972; also in AGARD-CP-118, 1972.

[6] Schijve, J., "The Accumulation of Fatigue Damage in Aircraft Materials and Structures," AGARDograph No. 157, 1972.

[7] Recent test results of W. J. Arkema, Aerospace Department, Delft University of Technology, The Netherlands.

[8] McMillan, J. C. and Pelloux, R. M. N., in *Fatigue Crack Propagation, ASTM STP 415*, American Society for Testing and Materials, 1967, pp. 505–532.

[9] Elber, W., *Engineering Fracture Mechanics*, Vol. 2, 1970, pp. 37–45.

[10] Elber, W. in *Damage Tolerance in Aircraft Structures, ASTM STP 486*, American Society for Testing and Materials, 1971, pp. 230–242.

[11] Wheeler, O. E., *Journal of Basic Engineering, Transactions*, ASME, March 1972, pp. 181–186.

[12] Porter, Th. R., *Engineering Fracture Mechanics*, Vol. 4, 1972. pp. 717–736.

[13] Schütz, W. and Zenner, H., "Crack Growth in Titanium Alloy Sheets under Flight-Simulation Loading" (in German), IABG Report TF-224, Ottobrunn, Jan. 1972.

[14] Jones, R. E., *Engineering Fracture Mechanics*, Vol. 5, 1973, pp. 585–604.

[15] Katcher, M., *Engineering Fracture Mechanics*, Vol. 5, 1973, pp. 793–818.

[16] Wei, R. P., Shih, T. T., and Fitz Gerald, J. H., "Load Interaction Effects on Fatigue Crack Growth in Ti-6Al-4V Alloy," NASA Report CR 2239, 1973.
[17] Shih, T. T. and Wei, R. P., "A Study of Crack Closure in Fatigue," NASA Report CR-2319, Oct. 1973.
[18] Wei, R. P. and Shih, T. T., *International Journal of Fracture*, Vol. 10, 1974, pp. 77–85.
[19] Shih, T. T. and Wei, R. P. in *Prospects of Fracture Mechanics*, Noordhoff, Leyden, 1974, pp. 231–248.
[20] Hsu, T. M. and Lassiter, L. W., "Effects of Compressive Overloads on Fatigue Crack Growth," AIAA Paper No. 74-365, April 1974.
[21] Matthews, W. T., Baratta, F. I., and Driscoll, G. W., *International Journal of Fracture Mechanics*, Vol. 7, 1971, pp. 224–228.
[22] Feddersen, Ch. E., "Fatigue Crack Propagation in D 6 AC Steel Plate for Several Flight Loading Profiles in Dry Air and JP-4 Fuel Environments," AFML-TP-72-20, Air Force Materials Laboratory, Jan. 1972.
[23] Davidson, J. R., *Engineering Fracture Mechanics*, Vol. 4, 1972, pp. 777–788.
[24] Keays, R. H., "Numerical Evaluation of Wheeler's Model of Fatigue Crack Propagation for Programmed Load Spectra," ARL/SM 736, Melbourne, April 1972.
[25] Ryan, N. E., "The Influence of Stress Intensity History on Fatigue Crack Growth," ARL/Met. 92, Melbourne, June 1973.
[26] Wood, H. A. in *Fatigue Life Prediction for Aircraft Structures and Materials*, AGARD Lecture Series No. 62, May 1973.
[27] Gallagher, J. P., Stalnaker, H. D., and Rudd, J. L., "A Spectrum Truncation and Damage Tolerance Study Associated with the C-5A Outboard Pylon Aft Tress Lugs," AFFDL-TR-74-5, Air Force Flight Dynamics Laboratory, May 1974.
[28] Petrak, G. J., *Engineering Fracture Mechanics*, Vol. 6, 1974, pp. 725–733.
[29] Gallagher, J. P. and Hughes, T. F., "Influence of Yield Strength on Overload Affected Crack Growth Behavior in 4340 Steel," AFFDL-TR-74-27, Air Force Flight Dynamics Laboratory, July 1974.
[30] Griffiths, J. R., Mogford, I. L., and Richards, C. E., *Metal Science Journal*, Vol. 5, 1971, pp. 150–154.
[31] Von Stubendorff, A., "Fatigue Crack Growth in Notched Steel Plates Loaded in Tension," Ph.D. thesis, Delft University of Technology, Dec. 1971.
[32] Klesnil, M. and Lukas, P., *Engineering Fracture Mechanics*, Vol. 4, 1972, pp. 77–92.
[33] Lukas, P. and Klesnil, M., "Transient Effects in Fatigue Crack Propagation," Institute of Physical Metallurgy, Czechoslovak Academy of Sciences, Brno, Jan. 1975.
[34] Rice, R. L. and Stephens, R. I. in *Progress in Flaw Growth and Fracture Toughness Testing, ASTM STP 536*, American Society for Testing and Materials, 1973, pp. 95–114.
[35] Gardner, F. H. and Stephens, R. I. in *Fracture Toughness and Slow Stable Cracking, ASTM STP 559*, American Society for Testing and Materials, 1974, pp. 225–244.
[36] Barsom, J. M. in *Progress in Flaw Growth and Fracture Toughness Testing, ASTM STP 536*, American Society for Testing and Materials, 1973, pp. 147–167.
[37] Priddle, E. K., "Fatigue Crack Propagation due to Random Amplitude Vibrations: Prediction Using Constant Amplitude Data," Central Electricity Generating Board, Report RD/B/N2784, Nov. 1973.
[38] Priddle, E. K., "Fatigue Crack Propagation Due to Random Amplitude Vibrations: the Influence of Stress Intensity Mean on Propagation Rate," Central Electricity Generating Board, RD/B/N 3097, Sept. 1974.
[39] Lindley, T. C. and Richards, C. E., *Materials Science and Engineering*, Vol. 14, 1974, pp. 281–293.
[40] Schijve, J. in *Advances in Aeronautical Sciences*, Vol. 3, Pergamon, 1962, pp. 387–408.
[41] Schijve, J. and Broek, D., *Aircraft Engineering*, Vol. 34, 1962, pp. 314–316.
[42] Hudson, C. M. and Hardrath, H. F., "Investigation of the Effects of Variable-Amplitude Loadings on Fatigue Crack Propagation Patterns," NASA, TN D-1803, Aug. 1963.

[43] McMillan, J. C. and Hertzberg, R. W. in *Electron Fractography, ASTM STP 436*, American Society for Testing and Materials, 1968, pp. 89–123.
[44] Hudson, C. M. and Raju, K. N., "Investigation of Fatigue Crack Growth Under Simple Variable-Amplitude Loading," NASA, TN-D-5702, 1970.
[45] Von Euw, E. F. J., Hertzberg, R. W., and Roberts, R. in *Stress Analysis and Growth of Cracks, ASTM STP 513*, American Society for Testing and Materials, 1972, pp. 230–259.
[46] Trebules, V. W., Roberts, R., and Hertzberg, R. W. in *Progress in Flaw Growth and Fracture Toughness Testing, ASTM STP 536*, American Society for Testing and Materials, 1973, pp. 115–146.
[47] Corbly, D. M. and Packman, P. F., *Engineering Fracture Mechanics*, Vol. 5, 1973, pp. 479–497.
[48] Probst, E. P. and Hillberry, B. M., "Fatigue Crack Delay and Arrest Due to Single Peak Tensile Overloads," AIAA Paper No. 73-325, 1973.
[49] Schijve, J., *Engineering Fracture Mechanics*, Vol. 6, 1974, pp. 245–252.
[50] Van Lipzig, H. T. M. and Nowack, H., "Fatigue Crack Growth and Residual Strength of Light Metals under Multi-Level Loading" (in German), paper of the Institut für Werkstoff-Forschung (DFVLR), Porz-Wahn, Oct. 1974.
[51] Swift, T., "The Application of Fracture Mechanics to the Design of Damage-Tolerant Stiffened Aircraft Structure," Douglas Paper 5981, 1972.
[52] Schijve, J. and De Rijk, P., "The Effect of Ground-to-Air Cycles on the Fatigue Crack Propagation in 2024-T3 Alclad Sheet Material," NLR-TR M 2148, Amsterdam 1965.
[53] Christensen, R. H. in *Metal Fatigue*, McGraw-Hill, 1959, p. 376.
[54] Hudson, C. M. and Hardrath, H. F., "Effects of Changing Stress Amplitude on the Rate of Fatigue-Crack Propagation in Two Aluminium Alloys," NASA, TN D-960, 1961.
[55] Plunkett, R. and Viswanathan, N., *Journal of Basic Engineering, Transactions*, ASME, March 1967, pp. 55–68.
[56] Crews, J. H. and White, N. H., "Fatigue Crack Growth from a Circular Hole With and Without High Prior Loading," NASA, TN-D-6899, Sept. 1972.
[57] Hanel, J. J., "Crack Growth Prediction for Programmed Loading, Including Crack Closure as Based on the Dugdale Barenblatt Model" (in German), paper of the Technische Hochschule Darmstadt, Oct. 1973.
[58] Newman, J. C. and Armen, H., "Elastic-Plastic Analysis of a Propagating Crack under Cyclic Loading." AIAA Paper No. 74-366, April 1974.
[59] Brussat, T. R. in *Damage Tolerance in Aircraft Structures, ASTM STP 486*, American Society for Testing and Materials, 1971, pp. 122–143.
[60] Smith, S. H. in *Acoustical Fatigue in Aerospace Structures*, Syracuse University Press, 1965, pp. 331–360.
[61] Schijve, J., *The Aeronautical Journal*, Vol. 74, 1970, pp. 517–532.
[62] Gallagher, J. P. and Stalnaker, H. D., "Methods for Analyzing Fatigue Crack Growth Rate Behavior Associated with Flight-by-Flight Loading," AIAA Paper No. 74-367. April 1974.
[63] Sayer, R. B., "Non-linear Effects of Spectrum Loading on Fatigue Crack Growth in Transport Wings," AIAA Paper No. 74-984, Aug. 1974.
[64] Nowack, H. and Mukherjee, B. in *Fail-Safe Aircraft Structures*, RAE TR 73183, Vol. 1, Farnborough, 1974.
[65] Impellizzeri, L. F. in *Effects of Environment and Complex Load History on Fatigue Life, ASTM STP 462*, American Society for Testing and Materials, 1970, pp. 40–68.
[66] Schijve, J. in *Advanced Approaches to Fatigue Evaluation*, NASA, SP-309, 1972, pp. 253–273.
[67] Schijve, J., Jacobs, F. A., and Tromp, P. J., "Flight-Simulation Tests on Notched Elements," NLR TR 74033, Amsterdam, Feb. 1974.
[68] Schijve, J., "Fatigue Crack Growth under Variable-Amplitude Loading," Delft University of Technology, Report VTH-181, April 1974.
[69] Hartman, A. and Schijve, J., *Engineering Fracture Mechanics*, Vol. 1, 1970, pp. 615–631.

[70] Willenborg, J. D., Engle, R. M., and Wood, H. A., "A Crack Growth Retardation Model Using an Effective Stress Concept," AFFDL-TM-FBR-71-1, Air Force Flight Dynamics Laboratory, 1971.
[71] Paris, P. C. in *Fatigue, an Interdisciplinary Approach*, Syracuse University Press, 1964, pp. 107–132.
[72] Paris, P. C., "The Growth of Cracks due to Variations in Load," Ph.D. thesis, Lehigh University, 1962.
[73] Swanson, S. R., Cicci, F., and Hoppe, W. in *Fatigue Crack Propagation, ASTM STP 415*, American Society for Testing and Materials, 1967, pp. 312–362.
[74] Schijve, J. in *Fail-Safe Aircraft Structures, Proceedings*, ICAF Symposium London, July 1973, RAE TR 73183, Vol. 1, March 1974.
[75] Engle, R. M. and Rudd, J. L., "Analysis of Crack Propagation under Variable Amplitude Loading Using the Willenborg Retardation Model," AIAA Paper No. 74-369, April 1974.
[76] Rice, J. R. in *Fatigue Crack Propagation, ASTM STP 415*, American Society for Testing and Materials, 1967, pp. 247–309.
[77] Habibie, B. J., "A Prediction Method for Crack Growth under Random Loading. Comparison with Test Results" (in German), Paper No. 71-111, DGLR Conference, Baden-Baden, Oct. 1971.
[78] Habibie, B. J., "On the Integration Method of Crack Propagation in Elastic Plastic Material under Operational Loads and Plane Stresses," paper of 3rd Conference on Fracture, Munich, April 1973.
[79] Habibie, B. J., *Zeitschrift für Flugwissenschaften*, Vol. 4, 1974, pp. 120–127.
[80] Simpkins, D., Neulieb, R. L., and Golden, D. J., *Journal of Aircraft*, Vol. 11, 1974, pp. 563–570.
[81] Bussa, S. L., Sheth, N. J., and Swanson, S. R., *Materials Research and Standards*, Vol. 12, 1972, pp. 31–43.

Simple Spectra: Effect of Loading Variables

R. I. Stephens,[1] *D. K. Chen,*[1] *and B. W. Hom*[1]

Fatigue Crack Growth with Negative Stress Ratio Following Single Overloads in 2024-T3 and 7075-T6 Aluminum Alloys

REFERENCE: Stephens, R. I., Chen, D. K., and Hom, B. W., "**Fatigue Crack Growth with Negative Stress Ratio Following Single Overloads in 2024-T3 and 7075-T6 Aluminum Alloys,**" *Fatigue Crack Growth Under Spectrum Loads, ASTM STP 595,* American Society for Testing and Materials, 1976, pp. 27–40.

ABSTRACT: Modified pre-cracked compact specimens of 2024-T3 and 7075-T6 aluminum alloys were subjected to four different overload patterns followed by subsequent constant-amplitude steady-state loading with $R = P_{\ell min}/P_{\ell max}$ equal to 0, −1/2, −1, and −2. The overload patterns were tension, compression-tension, tension-compression, and compression. Cyclic loading with negative stress ratio, R, drastically reduced crack-growth retardation. The higher the negative R ratio the greater the reduction in retardation. Overload ratios, OLR $= P_{h max}/P_{\ell max}$, ranging from 2.0 to 3.0 were used. For compression overloads, the OLR ranged from −2.0 to −4.0. High compression overloading was detrimental and dependent upon subsequent R ratio loading. Substantial fracture surface abrasion near the mid-thickness occurred for higher negative R ratios. Striations were not readily found in this region, however, they were quite evident near the edges, which indicated crack closure was greater near the mid-thickness. The 2024-T3 gave better crack growth life than 7075-T6 in some loading conditions, while the opposite was true for other loadings. The results indicate negative R ratio must be considered in retardation models and that retardation life cannot be modeled based solely on overload plastic zone sizes.

KEY WORDS: fatigue (materials), crack propagation, fracturing, residual stress, loads (forces), plastic zone, stress ratio, aluminum alloys

Fatigue crack-growth retardation following high tensile excursions has recently received widespread interest. In most instances cyclic loading following a high tensile excursion was also in the tensile region and resulted in appreciable crack-growth retardation and even crack arrest. Representative crack-growth retardation with zero or positive $R = P_{\ell min}/P_{\ell max}$ following high tensile excursions have been reported in 2024-T3 aluminum [*1*],[2] 7075-T6 aluminum [*2*], Ti-6Al-4V [*3*], austenitic manganese steel [*4*], cold-rolled low carbon steel [*5*], hot-rolled low carbon steel [*6*], and 4340 steel [*7*]. These materials represent both cyclic strain hardening and cyclic strain softening behavior.

[1] Professor and research assistants, respectively, Materials Engineering Division, The University of Iowa, Iowa City, Iowa 52242.

[2] The italic numbers in brackets refer to the list of references appended to this paper.

Crack-growth retardation has been attributed to both compressive residual stresses ahead of the crack tip and to crack closure. Stephens et al, however, in a brief current research report [*8*] showed fatigue crack-growth retardation following a high single tensile excursion could be substantially reduced and even eliminated if the subsequent load ratio, $R = P_{\ell_{min}}/P_{\ell_{max}}$, was negative. The present paper provides an in-depth extension of the original brief report and indicates the importance of load ratio R when considering fatigue crack-growth retardation.

Material and Experimental Procedures

The 2024-T3 and 7075-T6 aluminum plate alloys with yield strengths of 355 and 558 MN/m^2, respectively, in the rolled direction were used in this research. Modified compact specimens shown in Fig. 1*a* were cut from the 10.1-mm-thick

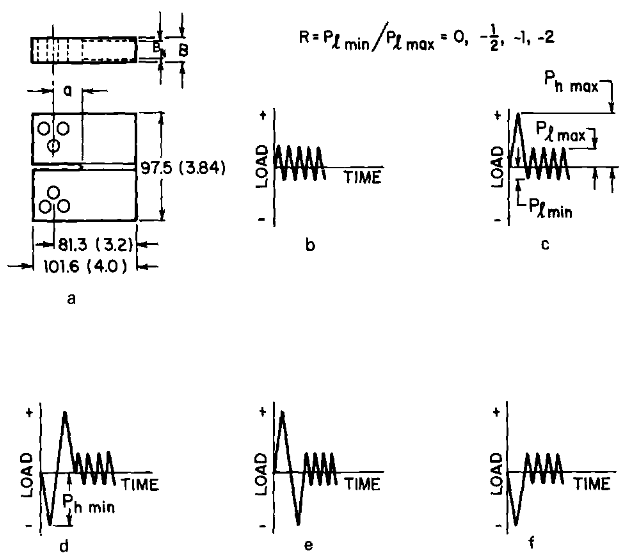

FIG. 1—*Modified compact specimen and loading spectrum: (*a*) modified compact specimen, mm (in.); (*b*) no overload (reference); (*c*) tension overload (T); (*d*) compression-tension overload (C-T); (*e*) tension-compression overload (T-C); and (*f*) compression overload (C).*

2024-T3 and 9.5-mm-thick 7075-T6 aluminum plates. The six holes provided facility to fasten specimens to a spherical monoball gripping system which allowed both tensile and compressive loadings. The tests were performed in an 88 960 N closed-loop electrohydraulic test system with ram loading transferred through the spherical monoball bearings which prevented external bending moments. The loading direction was parallel to the rolled direction. The crack length, *a*, was measured from the centerline of the axial ram loading. Specimen side grooves were used to ensure crack growth path direction and resulted in net thicknesses of 9.15 mm for 2024-T3 and 8.9 mm for 7075-T6. The side grooves were polished in order to better monitor crack growth which was measured optically using x36 magnification and stroboscopic lighting. A least-reading 0.25-mm scale was taped directly adjacent to the side groove. Fatigue crack-growth tests were run at room temperature with relative humidity between 68 and 74 percent.

The loading spectrum incorporated is shown in Fig. 1*b* thru *f* and consisted of four different overload patterns followed by constant load cycling with $R = P_{\ell min}/P_{\ell max} = 0, -1/2, -1$, and -2 for each overload pattern. The four overload patterns were tension (T) (Fig. 1*c*), compression-tension (C-T) (Fig. 1*d*), tension-compression (T-C) (Fig. 1*e*), and compression only (C) (Fig. 1*f*). When both tension and compression occurred in the overload cycle, P_{hmax} was always equal to $-P_{hmin}$. No-overload tests (Fig. 1*b*), used as reference, were also obtained for each R ratio. The machined V-notch was pre-fatigue sharpened in all specimens with $R = 0$ to a crack length of 25.4 mm with the maximum load equal to $P_{\ell max} = 8580$ N for 2024-T3 and 8310 N for 7075-T6. This resulted in a final stress intensity of 19.7 $MNm^{-3/2}$. Overload patterns were then applied at 0.5 Hz with overload ratio (OLR) $= P_{hmax}/P_{\ell max}$ equal to 2.0, 2.3, 2.5, or 3.0. Compression overloads only were applied with OLR $= -2, -2.3, -2.5, -3.0$, and -4.0. Subsequent steady-state constant-load cycling always had $P_{\ell max}$ equal to the pre-overload value. $P_{\ell min}$ was established from the particular R value for each specimen. Thus, if no crack extension occurred during overload, then each test for both materials would begin with identical initial $K_{\ell max} = 19.7$ $MNm^{-3/2}$. Crack tension during overloading, however, did occur in many tests and is described later.

The maximum overload stress intensity for OLR = 2.0, 2.3, 2.5, and 3.0 was 39.4 $MNm^{-3/2}$, 45.3 $MNm^{-3/2}$, 49.2 $MNm^{-3/2}$, and 59.1 $MNm^{-3/2}$, respectively. Monotonic fracture toughness tests using the same specimen geometry, maximum load, and initial crack length of 25.4 mm resulted in non-valid average fracture toughness, K_e, of 70.6 $MNm^{-3/2}$ for 2024-T3 and 51.9 $MNm^{-3/2}$ for 7075-T6. Two tests were performed for each material. OLR equal to 3.0 was therefore not possible for 7075-T6 since fracture would occur during the overload. The ratio of the maximum overload stress intensity, K_{hmax} to K_e, ranged from 0.56 to 0.835 for 2024-T3 and 0.76 to 0.95 for 7075-T6.

Steady-state constant-load amplitude following overloading was at 10 to 20 Hz depending upon the R ratio. The larger negative R ratios required lower frequencies in order to maintain proper frequency response. As the crack grew to about 40 mm, the frequency had to be lowered to about 5 Hz for the larger negative R ratios. Total fatigue crack growth life following overloads was taken from a_0 equal to 25.4 mm to fracture. If crack growth following an overload did not occur in 300 000 cycles then complete crack arrest was assumed and the test terminated. A total of 60 tests were performed with 2024-T3 and 52 tests with 7075-T6.

Test Results

A summary of all crack growth life following single overloads is shown in Table 1 for both 2024-T3 and 7075-T6. Some duplicate tests were run and both

TABLE 1 – *Summary of crack growth lives*

Loading Patterns	2024-T3 OLR \ R	0	−1/2	−1	−2	7075-T6 OLR \ R	0	−1/2	−1	−2
No overload (Fig. 1*b*)	no overload	38 800 36 100	33 700 30 700	29 700	29 500 27 700	no overload	21 600 22 800	22 400	22 300	22 300
Tension overload (Fig. 1*c*)	2.0	85 200	39 400 38 000	36 100	31 300	2.0	25 900[a]	. . .	27 000 22 200	26 500
	2.3	. . .	. . .	. . .	. . .	2.3	222 700	119 900	64 500	26 700
	2.5	>300 000	135 700	46 600	30 900 26 600	2.5	>300 000	253 400	174 000	51 400 40 000
	3.0	√	>300 000	187 600	45 800	3.0	. . .	. . .	. . .	. . .
Compression-tension overload (Fig. 1*d*)	2.0	50 600	29 900	26 800 30 200	28 800	2.0	. . .	. . .	. . .	. . .
	2.3	. . .	. . .	. . .	. . .	2.3	119 400	106 000	59 400	27 100
	2.5	271 100	58 900	40 600	29 300	2.5	278 000	230 000	172 000	52 600
	3.0	√	>300 000	133 200	43 400	3.0	. . .	. . .	. . .	. . .
Tension-compression overload (Fig. 1*e*)	2.0	36 900	30 500	28 400	28 500	2.0	. . .	. . .	. . .	. . .
	2.3	. . .	. . .	. . .	. . .	2.3	33 900	30 500	28 300	26 400
	2.5	34 200	30 600	25 400	28 500	2.5	57 600	37 000	36 800	36 300
	3.0	30 900	29 400	23 900	25 800	3.0	. . .	. . .	. . .	. . .

Compression overload (Fig. 1*f*)	−2.0	34 000	27 700	26 900	27 400	−2.0	. . .	. . .	. . .	. . .
	−2.3	. . .	. . .	. . .	. . .	−2.3	21 000	21 700	24 100	24 600
	−2.5	31 000	24 800	25 800	23 000	−2.5	17 400	18 800	19 800	21 400
	−3.0	25 700	21 000	21 400	20 600	−3.0	. . .	. . .	. . .	. . .
	−4.0	25 500	18 400	18 400	14 200	−4.0	15 800	18 600	19 500	21 500

[a] Average of seven tests.

values are included in the table. Normal scatter existed within these duplicate tests. No-overload constant-amplitude reference tests are included for both materials. For 2024-T3, a decrease in constant-amplitude life of approximately 25 percent occurred as R increased from 0 to −2. A general conclusion should not be made that under constant-amplitude loading increased negative R ratio decreases 2024-T3 life, because these data only include the upper portion of the sigmoidal log da/dN versus log ΔK curve due to their high crack growth rates. The constant amplitude 7075-T6 crack growth life was essentially constant as R varied from 0 to −2. This data was also in the upper portion of the sigmoidal crack-growth rate curve. For these identical constant-amplitude no-overloading tests, 2024-T3 had greater life than 7075-T6 and, thus, lower crack growth rates for all R ratios.

The OLR = 2.0 for 7075-T6 was applied to just tension overloading since a negligible amount of crack-growth retardation or crack life increase occurred. The effect of negative R ratio for a given overload pattern and material can be determined by traversing across a row in Table 1. The effect of overload ratio for a given R ratio can be obtained by scanning a column within a given overload pattern section. A check mark in Table 1 implies crack arrest would occur for the specific loading conditions. Tests labeled >300 000 indicate crack arrest occurred.

Representative crack length versus applied cycles following a specific overload pattern and overload ratio with R ratio as the parameter are shown in Figs. 2 thru 4. Figure 2 indicates that crack-growth life in 2024-T3, for a tensile overload

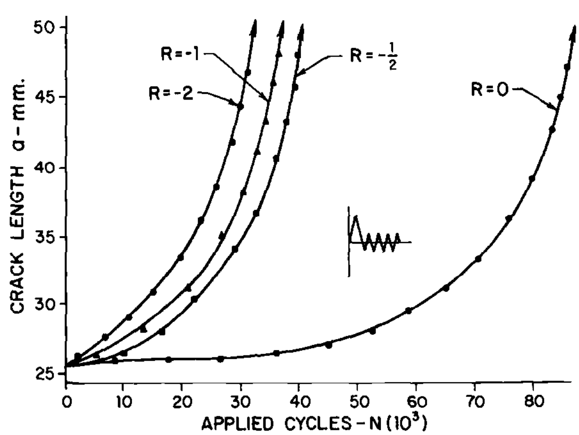

FIG. 2—*Crack growth following single tensile overload in 2024-T3 aluminum, OLR = 2.0.*

ratio of 2.0, is drastically reduced for $R = -1/2$, −1, and −2 compared with life at $R = 0$. Figure 3 indicates the same result for 7075-T6 with a tension overload ratio of 2.5. Compression-tension overloading for 2024-T3 with an overload ratio equal to 2.5 illustrates similar reduction in crack-growth life in Fig. 4. A general conclusion from these representative curves along with scanning the rows in Table 1 is that increasing the value of R from 0 to −2 following a given

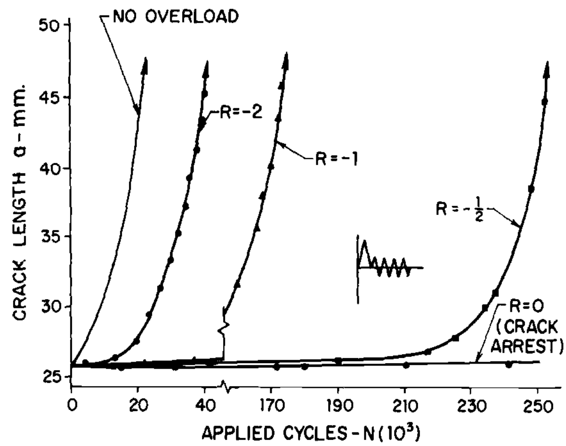

FIG. 3—*Crack growth following single tensile overload in 7075-T6 aluminum, OLR = 2.5.*

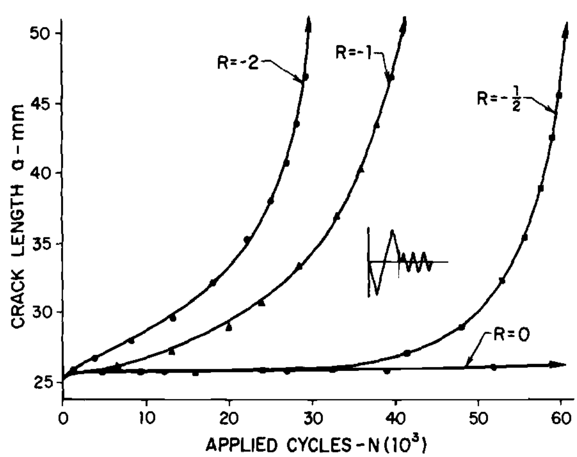

FIG. 4—*Crack growth following single compression-tension overload in 2024-T3 aluminum, OLR = 2.5.*

tension or compression-tension overload causes drastic reduction in crack-growth retardation and hence total crack-growth life. Under constant-load amplitude cycling following overloads, retardation is best characterized by the constant crack-growth region (straight line) of the a versus N curve. It is apparent that with higher overload ratios, complete crack arrest occurred for $R = 0$ whereas only small increases in crack-growth life resulted with negative R ratios.

In order to better visualize the drastic effects of negative R ratio following tension or compression-tension overloads, the data from Table 1 for these two loading patterns has been normalized and plotted against R in Fig. 5. The normalized life was obtained by dividing the total life to fracture for a given overload and R ratio by the no-overload constant-amplitude life at the same R ratio. This figure indicates that with $R = -2$, very little benefit results from the overloads even with the highest overloads. Figure 5 also indicates that

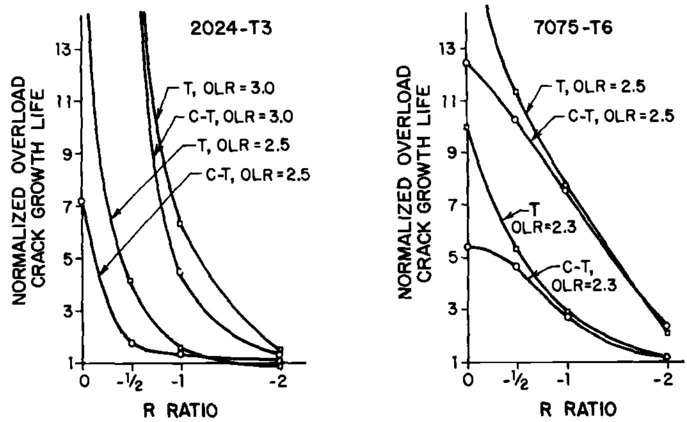

FIG. 5—*Normalized overload crack growth life versus* R *ratio, tension (T) and compression-tension (C-T) overloads.*

compression-tension overload life was slightly less than tension-only overload life for most conditions. This implies a high compression overload preceding a high tension overload should not be completely neglected, but its effect is not large.

The tension-compression overload pattern, Fig. 1*e*, for 2024-T3 caused either little change in crack-growth life or decreased life. For all R ratios, the higher the overload ratio the smaller the life. However, for 7075-T6 the tension-compression overload was beneficial in all cases with the higher the overload ratio the greater the life. The increase in life was substantially less than tension or compression-tension overloads, however, and as R went from 0 to −2 this increase became very small.

Compression overloads, Fig. 1*f*, ranging from −2.0 to −4.0 resulted in either no affect on crack-growth life or decrease in life for both materials. In general, the higher compression overload ratios caused greater decrease in life. The decrease in life was due to higher crack-growth rates (accelerated crack growth) immediately following the compressive overload. Life decreases ranged from 0 to 50 percent. For 2024-T3 increasing the negative R ratio caused greater decreases in life, whereas with 7075-T6 increasing the negative R ratio tended to eliminate the detrimental effects of the compression overload. Thus, 2024-T3 and 7075-T6 behaved in somewhat opposite manners for the compression and tension-compression overload patterns.

The general effect of overload pattern on crack-growth behavior for a given OLR and R is illustrated in Fig. 6. It is seen that tension or compression-tension overloads can cause appreciable retardation while compression or tension-compression overloads showed somewhat the same behavior as the no-overload constant-amplitude loading.

Partial macroscopic fracture surfaces of specimens subjected to tensile overloads are shown in Fig. 7. Crack extension during overload is easily seen as the very dark area. For both materials, the higher the overload ratio the greater the macroscopic crack extension during overload. The 7075-T6 shows crack

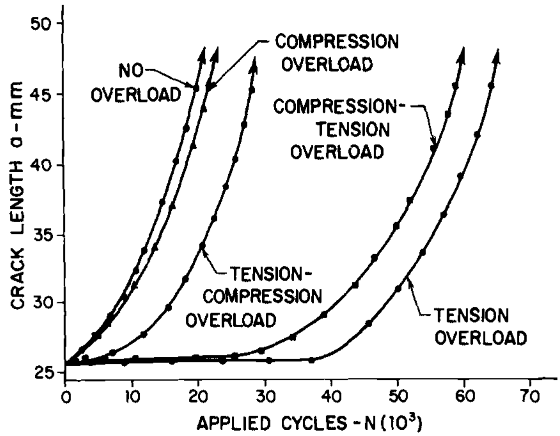

FIG. 6—*Crack growth following different overload patterns in 7075-T6 aluminum; OLR = 2.3,* R = *−1.*

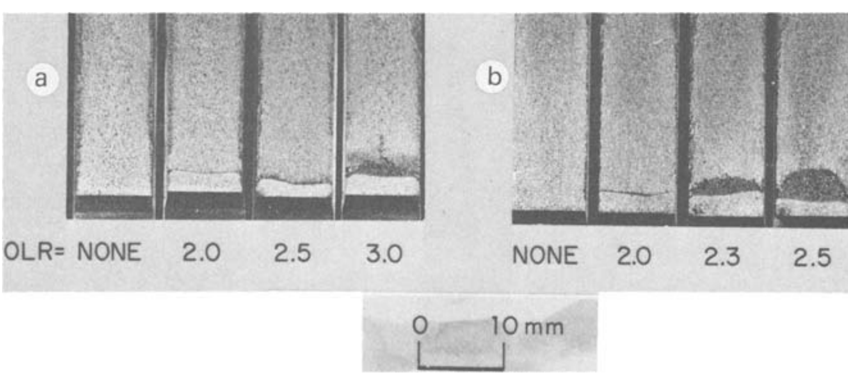

FIG. 7—*Macroscopic fracture surfaces of tensile overload specimens as dependent upon overload ratio: (a) 2024-T3 and (b) 7075-T6.*

tunneling at the OLR = 2.3 and 2.5, and some crack tunneling also occurred with the 2024-T3 for OLR = 3.0. Crack extension during overload ranged from approximately 0.1 to 1.5 mm for 2024-T3 and 0.2 to 4.0 mm for 7075-T6. The ratio of K_{hmax}/K_e was between 0.56 and 0.835 for 2024-T3 and 0.76 and 0.95 for 7075-T6. However, K_{hmax} was the same for each material for a given OLR. The large crack extension that occurred with the higher overload ratios are undesirable, however, crack tip plasticity and crack closure more than offset the increase in crack length.

In general, overload crack extension for a given OLR was similar for tension, compression-tension, and tension-compression overloading. Fatigue crack-growth surfaces remained flat following overloads due to specimen side grooves.

The effect of negative R ratio on macroscopic fracture appearance for both materials is indicated in Fig. 8 for 2024-T3. As R was increased from 0 to −2,

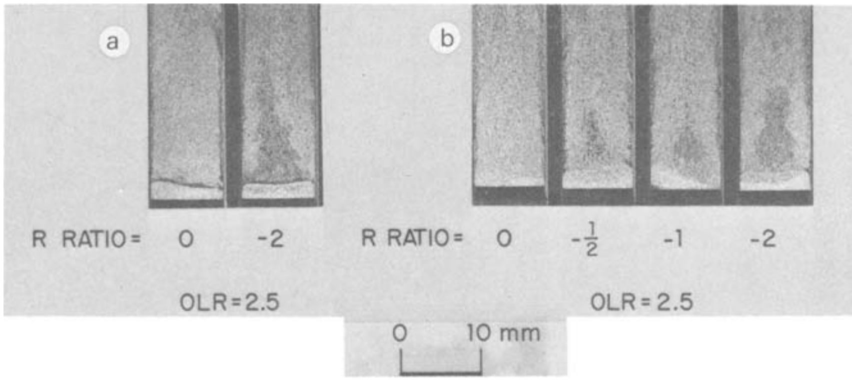

FIG. 8—*Macroscopic fracture surfaces as dependent upon negative* R *ratio, 2024-T3 aluminum: (*a*) compression-tension overload and (*b*) compression overload.*

substantial abrasion resulted in the mid-thickness region following the overload. This abrasion region is darker and increased in magnitude as the negative R value increased. This indicates that crack closure was most predominant on the inner surfaces. The abrasion was evident for all four loading patterns, however, the greatest abrasion, for a given R ratio, occurred with compression and tension-compression overloads. It is also shown in Fig. 8*b* that no crack extension occurred under the compressive overloads which was consistent for both materials for all OLR.

Discussion of Results

Crack-growth retardation or acceleration occurred within a small crack-growth region immediately following the overload pattern. That is, the overall effect on total life was controlled primarily in the overload plastic zone region immediately following the overload. Reversed plane stress plastic zones formed from the tensile portion of an overload can be approximated as one-fourth the monotonic plane stress plastic zone, $2r_y$, [*9*] where

$$2r_y = 2\left(\frac{1}{2\pi}\right)\left(\frac{K_{\text{hmax}}}{\sigma_{ys}}\right)^2$$

and

$$K_{\text{hmax}} = \frac{P_{\text{hmax}}}{B_N\sqrt{W}} f(a/W)$$

according to ASTM Test for Plane-Strain Fracture Toughness of Metallic Materials (E 399-74). Values of the reversed plane stress plastic zone varied from 1.1 to 2.4 mm for 2024-T3 and 0.4 to 0.62 mm for 7075-T6. This plastic zone size, however, can be drastically altered by subsequent cycling, particularly with negative R ratio. Thus, the significance of the reversed stress plastic zone is substantially reduced under subsequent negative R cycling. It is also substantially reduced under tension-compression overload patterns.

Delayed retardation following overloads could not be depicted from macroscopic observations of a versus N curves. This can be attributed to the small effective crack-growth region where retardation occurred, crack tunneling effects, least scale reading of 0.25 mm, and difficulties of observing crack tips during negative R cycling. Scanning electron fractographs shown in Fig. 9, however, do show delayed retardation for 2024-T3 following a tensile OLR = 2.5 with $R = -1/2$. This is indicated in Fig. 9*a* by fine striation spacings before overloading, coarser spacing immediately after the overload region, and eventual return to finer spacing in Fig. 9*b*. The overload band is indicated in Fig. 9*a*.

In general, fatigue crack striations could easily be depicted with the scanning electron microscope in the pre-overload region for all R values. They were also easily found after overloading for $R = 0$ and $-1/2$. However, with the higher negative R ratios, it became more difficult to find striations. This was particularly true in the abrasion regions indicated previously in Fig. 8. A representative scanning electron fractograph of this region for $R = -2$ is shown in Fig. 10*a*, and the lack of clear distinct striations is evident. Figure 10*b* shows distinct striations near the edge of this same specimen.

Under constant-amplitude loading the use of the log-log linear relationship, $da/dN = A(\Delta K)^n$ has been predominant. ΔK has been taken as the positive stress intensity range which implies the negative or compression portion of constant-amplitude loading and has either no effect or negligible effect on crack-growth life. The experimental results described, however, indicate that under spectrum loading conditions the negative portion of a loading spectrum cannot be neglected if possible retardation is to be considered in the crack-growth-life analysis.

The Wheeler [*10*] and Willenborg [*11*] retardation models, and extensions of these models, have received the widest application to crack-growth life under spectrum loading. As pointed out by Wood [*12*] however, these models still have appreciable need for improvement and incorporation of new behavior as it becomes known, such as these negative R effects.

Summary and Conclusions

1. Negative R-ratio cycling following tension or compression-tension overloading drastically reduced crack-growth retardation in both 2024-T3 and 7075-T6 aluminum. As the negative R ratio was increased, retardation decreased. An R ratio of just $-1/2$ was sufficient to eliminate from 10 to 80 percent of the total life found with $R = 0$. However, even with $R = -2$ the tension or compression-tension overloads were either slightly beneficial or had no effect on crack-growth life.

2. Tension-compression or compression overloading in 2024-T3 was detrimental or caused no change in life. For 7075-T6, tension-compression overloading was somewhat beneficial, however, compression overloads were either detrimental or had no effect. Compression overloading with overload ratios of -2.0 to -4.0 reduced life from 0 to 50 percent.

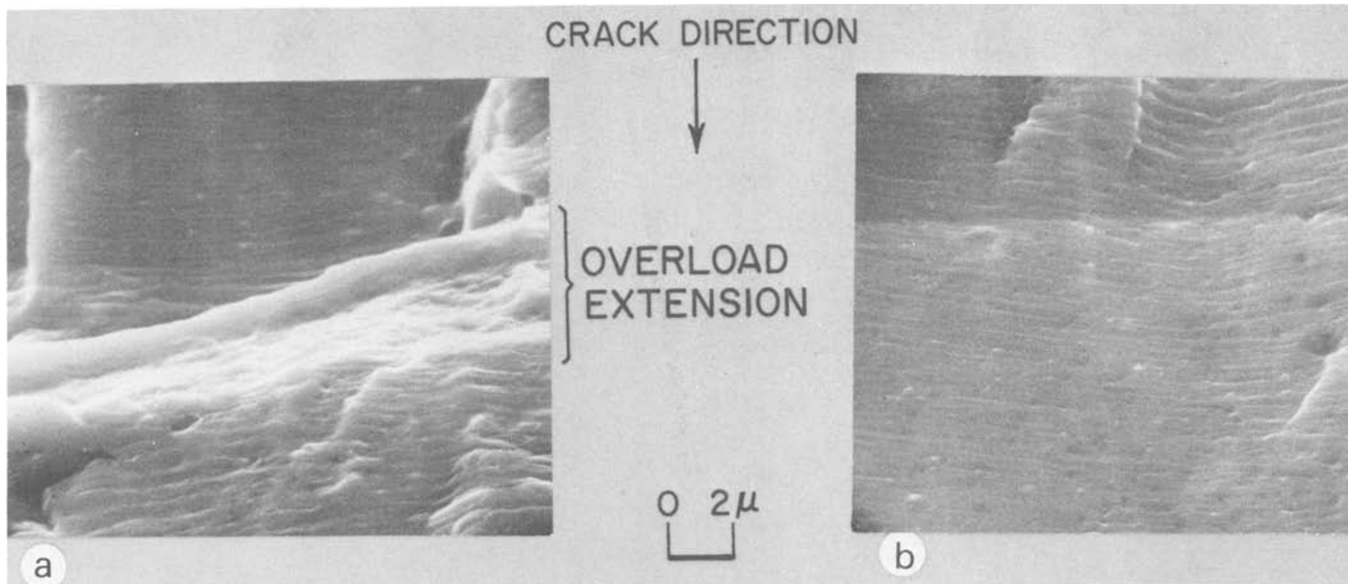

FIG. 9—*SEM fractographs indicating delayed retardation following tensile overload in 2024-T3 aluminum; OLR* $= 2.5$, $R = -1/2$: *(a) overload region and (b) 0.13 mm after overload.*

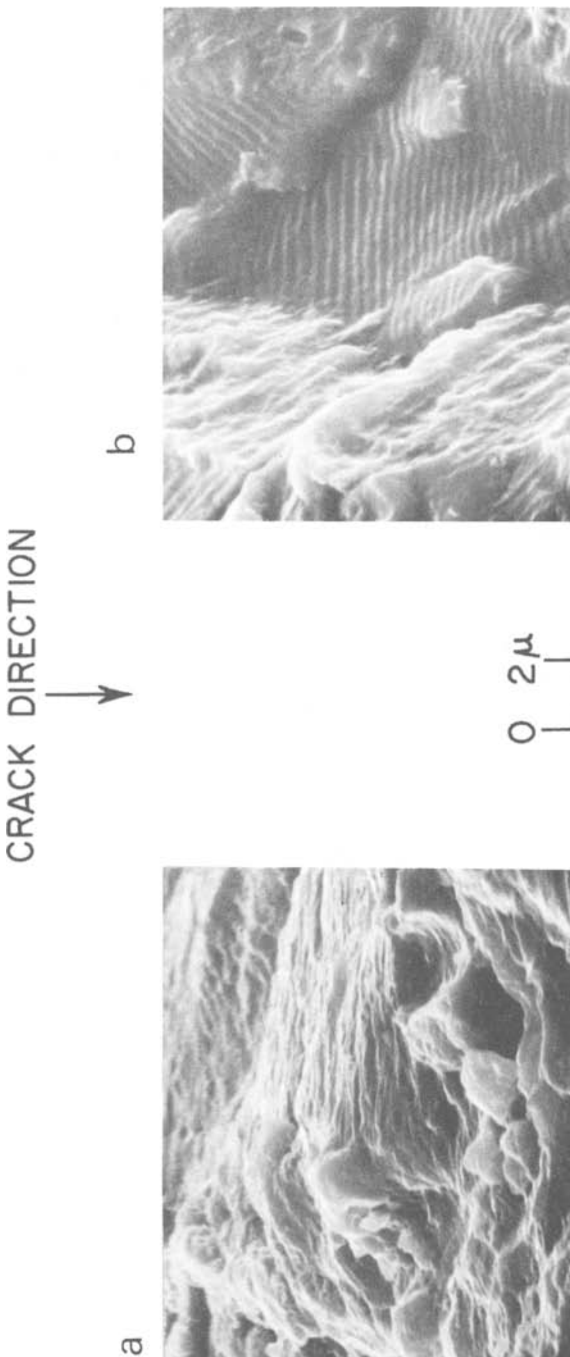

FIG. 10—*SEM fractographs in 7075-T6 aluminum following compression-tension overload,* R = −2: *(a) mid-thickness and (b) near edge.*

3. For a given R ratio, the higher tension or compression-tension overload ratios caused the greatest crack-growth retardation.

4. Compression-tension overloading caused slightly less retardation than tension overloading and, thus, a high compression loading preceding a high tension loading should not be completely neglected. Compression overloads following tension overloads were extremely detrimental.

5. Crack extension during overloads (except for compression-only overloads) ranged from 0.1 to 1.5 mm in 2024-T3 and 0.2 to 4.0 mm in 7075-T6. Overload crack-tip tunneling was most evident in 7075-T6.

6. Appreciable fracture surface abrasion occurred in the mid-thickness region following overloads as the negative R ratio increased. Striations were not readily found in these regions, however, they were quite evident near the edges for all R ratios. This implies greater mid-thickness crack closure following overloads.

7. Under identical loading conditions 2024-T3 had better life than 7075-T6 in some loading patterns and poorer life in others. Thus, overload plastic zone sizes do not completely control fatigue crack-growth behavior.

8. Negative R ratio loading following overloads must be considered in any mathematical model involving crack-growth retardation life predictions.

Acknowledgment

The authors would like to thank Ronald Kelsey, Richard Feild, and Mick Christensen of Alcoa Corporation for providing the material.

References

[*1*] vonEuw, E. F. J., Hertzberg, R. W., and Roberts, R. in *Stress Analysis and Growth of Cracks, ASTM STP 513*, American Society for Testing and Materials, 1972, pp. 230–259.

[*2*] Corbly, D. M. and Packman, P. F., *Engineering Fracture Mechanics*, Vol. 5, 1973, pp. 479–497.

[*3*] Wei, R. P. and Shih, T. T., *International Journal of Fracture Mechanics*, Vol. 10, No. 1, 1974, pp. 77–85.

[*4*] Rice, R. C. and Stephens, R. I. in *Progress in Flaw Growth and Fracture Toughness Testing, ASTM STP 536*, American Society for Testing and Materials, 1973, pp. 95–114.

[*5*] Vargas, L. G. and Stephens, R. I. in *Proceedings*, Third International Conference on Fracture, Munich, Germany, Vol. 6, April, 1973, p. V–325.

[*6*] Sheets, E. C., "Predicting Fatigue Crack Propagation in Steel Plates Under the Effects of Periodic Overloads", MS thesis, The University of Iowa, Dec. 1973.

[*7*] Gallagher, J. P. and Hughes, T. F., "The Influence of Yield Strength on Overload Affected Fatigue Crack Growth Behavior in 4340 Steel," AFFDL-TR-74-27, Air Force Flight Dynamics Laboratory, Wright-Patterson AFB, Ohio, 1974.

[*8*] Stephens, R. I., McBurney, G. W., and Oliphant, L. J., *International Journal of Fracture*, Vol. 10, No. 4, 1974, pp. 587–589.

[*9*] Rice, J. R., *Fatigue Crack Propagation, ASTM STP 415*, American Society for Testing and Materials, 1967, pp. 247–309.

[*10*] Wheeler, O. E., "Spectrum Loading and Crack Growth," ASME, Paper No. 71-Met-X, American Society of Mechanical Engineers, 1971.

[*11*] Willenborg, J., Engle, R. M., and Wood, H. A., "A Crack Growth Retardation Model Using an Effective Stress Concept," Air Force Flight Dynamics Laboratory, Technical Memorandum 71-1-FBR, Wright-Patterson AFB, Ohio, Jan. 1971.

[*12*] Wood, H. A. in *Fatigue Life Prediction for Aircraft Structures and Materials*, AGARD Lecture Series No. 62, NATO, May, 1973, pp. 8-1 to 8-31.

W. X. Alzos,[1] *A. C. Skat, Jr.,*[2] *and B. M. Hillberry*[2]

Effect of Single Overload/Underload Cycles on Fatigue Crack Propagation

REFERENCE: Alzos, W. X., Skat, A. C., Jr., and Hillberry, B. M., "**Effect of Single Overload/Underload Cycles on Fatigue Crack Propagation,**" *Fatigue Crack Growth Under Spectrum Loads, ASTM STP 595*, American Society for Testing and Materials, 1976, pp. 41–60.

ABSTRACT: Tests, represented in a three-dimensional matrix, were performed to investigate the effects of a single overload/underload sequence on the fatigue crack-growth rate in 2024-T3 aluminum alloy. Three different stress intensity ratios were studied to investigate the delay phenomenon: (1) overload level to maximum cyclic level, K_{ol}/K_{max}; (2) underload level to overload level, K_{ul}/K_{ol}; and (3) minimum cyclic level to overload level, K_{min}/K_{ol}. These ratios ranged from 1.6 to 3.0, −1.0 to +0.3, and 0.11 to 0.3, respectively. All tests had the same overload stress intensity level. Sufficient data were recorded to accurately determine the crack-growth rate through the overload affected zone. The crack length versus number of cycles data for each test were represented by a spline function which was then analytically differentiated to obtain the growth rate. The number of delay cycles was found to be directly related to the minimum growth rate following the overload/underload sequence. The ratios K_{ol}/K_{max} and K_{ul}/K_{ol} were shown to be of particular significance to the delay while the ratio K_{min}/K_{ol} was shown to be of less significance. The results were correlated with an extended crack closure concept. From this the maximum value of the opening stress intensity level following the overload/underload sequence can be determined and used to predict the number of delay cycles.

KEY WORDS: crack propagation, fatigue (materials), loads (forces), stress ratio, stress cycle, overload, underload

The load interaction effects on fatigue crack propagation due to variable-amplitude loading has been a subject of investigation for many years and will undoubtedly continue to be so for some time. The inability to adequately predict these interaction effects has prompted recent interest in studying the interaction due to simple load patterns and its influence on fatigue crack propagation. Of particular interest is the decrease in growth rate (delay effect or crack retardation) which normally follows a high overload or a reduction in the load level. As pointed out by Schijve [*1*][3] and Gallagher and Stalnaker [*2*] as

[1] Mechanical engineer, Engineering Service Division, E. I. DuPont de Nemours and Company, Wilmington, Del. 19898; formerly, graduate research assistant, Purdue University, West Lafayette, Ind. 47907.

[2] Graduate research assistant and professor, respectively, School of Mechanical Engineering, Purdue University, West Lafayette, Ind. 47907.

[3] The italic numbers in brackets refer to the list of references appended to this paper.

well as many others, this delay can have a significant influence on the fatigue life of a structure.

The crack-growth reduction resulting from a single overload preceded and followed by the same level of cyclic loading has been studied by several investigators including Von Euw [3], Jonas and Wei [4], Wei and Shih [5,6], Probst and Hillberry [7], Gardner and Stephens [8], Trebules et al [9], Corbly and Packman [10], and Himmelein and Hillberry [11]. Trebules et al [9], Corbly and Packman [10], Gardner and Stephens [8], Wei and Shih [5], and Hsu and Lassiter [12] also examined the effect of single periodic and multiple overloads. Petrak and Gallagher [13] examined the effect of yield strength level on the retardation behavior. Probst and Hillberry [7] observed complete crack arrest for an overload sufficiently higher than the steady-state loading and established an arrest/delay boundary. The boundary was found to be a function of the stress ratio by Himmelein and Hillberry [11]. Jonas and Wei [4], Corbly and Packman [10], and Stephens et al [14] report that the delay following an overload is reduced if the overload is followed by an underload before the constant-amplitude cycling is resumed. Several techniques have been proposed to describe the delay phenomenon [2,15–19]. Crack closure [20] has also been used to explain the delay phenomenon [9,21,22].

Crack-growth retardation is known to be related to many factors. Following the overload there is generally a rapid decrease in the growth rate to a minimum level followed by a gradual increase back to the steady-state growth rate. Since this minimum growth rate is very slow, it significantly affects the total number of delay cycles. Small variations can result in considerable variation in the resulting number of delay cycles. This study [23] was undertaken to investigate the crack-growth rate behavior through the interaction zone following the overload/underload sequence on otherwise steady-state load cycling and to determine the correlation of the minimum growth rate with the applied load conditions and number of delay cycles.

Test Program

The test program was designed so that the effects of each of the loading parameters in the overload/underload sequence would be isolated. The test matrix was defined in terms of the three stress ratios (the corresponding ranges are given in parentheses)

$$R_{uo} = K_{ul}/K_{ol} \quad (-1.00 \text{ to } 0.30)$$

$$Q_{ol} = K_{ol}/K_{max} \quad (1.6 \text{ to } 2.2)$$

$$R_{m} = K_{min}/K_{ol} \quad (0.11 \text{ to } 0.30)$$

The overload/underload test sequence is shown in Fig. 1. The level of K_{ol} was the same for all tests, and therefore varying each of the preceding ratios one at a time corresponded to varying K_{ul}, K_{max}, or K_{min}, respectively, with the remaining stress intensity levels constant.

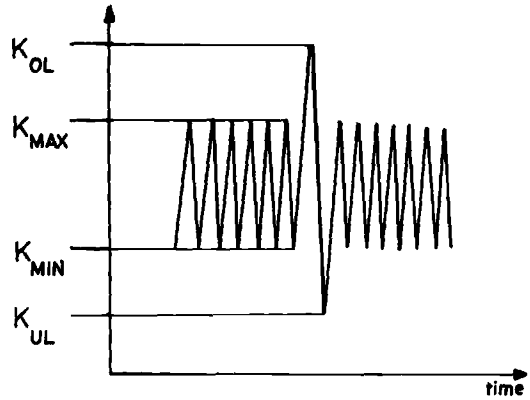

$$Q_{OL} = \frac{K_{OL}}{K_{MAX}} \qquad R_M = \frac{K_{MIN}}{K_{OL}}$$

$$R_{UO} = \frac{K_{UL}}{K_{OL}} \qquad R_F = \frac{K_{MIN}}{K_{MAX}}$$

FIG. 1—*Overload/underload sequence and definition of variables.*

Previous results [*3,11*] have indicated that the delay behavior is different for overloads which create plane stress as opposed to plane strain conditions. For this investigation, the overload level (which was the same for all tests) was chosen to create plane stress conditions. K_{ol} was selected such that the plastic zone diameter, $2r_y$, was greater than the specimen thickness, that is

$$2r_y = \frac{1}{\pi}\left[\frac{K_{ol}}{\sigma_{ys}}\right]^2 \geq 2.54 \text{ mm} \tag{1}$$

For each test, the specimen was cycled to establish steady-state growth, overloaded into a state of plane stress and then cycled again at the pre-overload level.

The principal tests in the test matrix are illustrated in Figs. 2 and 3 which show the stress intensity levels for each test. Tests in addition to these were also run and are included in Table 1. It can be seen in Figs. 2 and 3 that each row on either plane isolates the R_{uo} variable. Each column isolates the effect of either Q_{ol} or R_m (also K_{max} or K_{min}) depending on the plane. It should be pointed out that the middle row in each of the two figures represents the same set of tests.

Experimental Procedure

The material used for this investigation was 2024-T3 aluminum alloy from the same stock as that used by Himmelein and Hillberry [*11*]. The specimen geometry was a center crack panel (558.8 by 152.4 by 2.54 mm thick) of the same dimensions as used by Probst and Hillberry [7] and Himmelein and Hillberry [*11*].

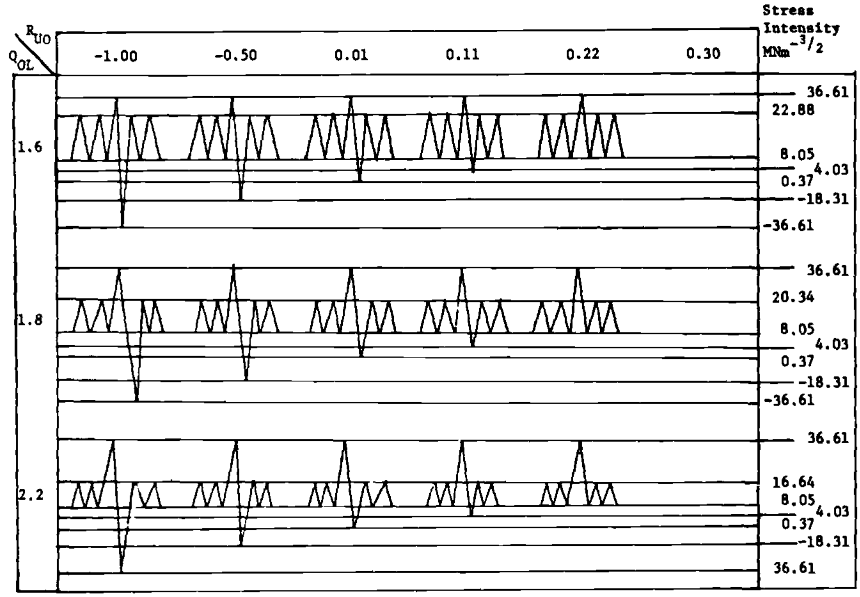

R_M = 0.22

FIG. 2—Q_{ol} *versus* R_{uo} *plane of test matrix;* R_m *constant.*

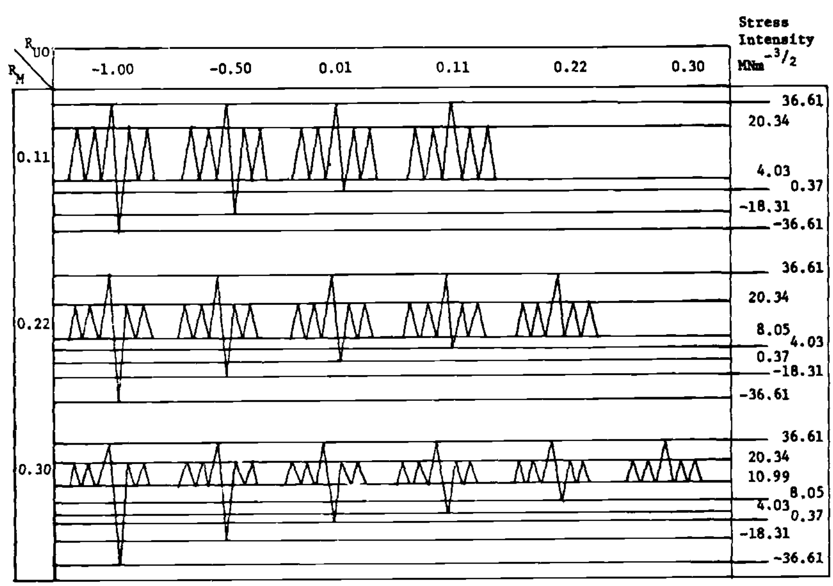

FIG. 3—R_m *versus* R_{uo} *plane of test matrix;* Q_{ol} *constant.*

The material had the following tensile properties; yield strength = 392 MN/m², ultimate strength = 476 MN/m², and percent elongation = 14.2 percent. The test specimens were polished to a mirror finish in the vicinity of the crack path to facilitate optical observation of the crack tip during crack-growth measurement. The specimens were loaded parallel to the direction of rolling of the material with a closed-loop, electrohydraulic test system. Lightweight aluminum compression guides lined with 1.5 mm felt were used to support the specimen when the compressive underloads were applied.

Since the scope of this study strictly involved the effects of loading on fatigue crack propagation, care was taken to control as many other variables as possible. All tests were subjected to nearly identical environmental conditions of dessicated air and room temperature. All fatigue cycling was done at 20 Hz except for Tests 1, 2, and 3, which were cycled at 10 Hz due to the rapid crack propagation. All overload and underload cycles were applied at 0.02 Hz. In order to have a basis for comparison between tests in the test matrix, the stress intensity factors were held at quasi-constant values throughout each test. This was accomplished by changing the load required to produce a specified K for every 5 percent increase in crack length. This ensured that the actual value of K was within 3 percent of the desired value. Care was taken in each test to establish equilibrium before the application of the overload/underload sequence. The steady-state condition was achieved by propagating the fatigue crack at least 6 mm (over twice the diameter of the theoretical overload plastic zone of each test) at the quasi-constant stress intensity values specified for the test. The overload/underload sequence was then applied when the crack had propagated 5 percent past the point of the previous load shed. Cycling was continuous for both pre-overload and post-overload fatigue cycling to negate the possibility of time or unloading to zero load affecting subsequent crack growth.

The crack length was measured optically with a x100 microscope mounted on a two-directional traverse. The traverse had a resolution of 0.001 mm in the horizontal direction and a direct digital display. The number of cycles was recorded with a printer connected to a counter. Data were actually recorded by advancing the optical system the specified increment (0.01, 0.02, or 0.05 mm depending on growth rate). When the crack had grown this incremented distance, the trigger button to the printer was pressed, recording the number of cycles.

Data Reduction–Numerical Differentiation

One of the objectives of this study was to characterize the growth-rate behavior through the overload affected zone following the overload/underload sequence. To obtain this growth rate, da/dN, it was necessary to record sufficient a versus N data and then differentiate these data. Several different techniques have been used for the numerical differentiation of experimental data. Incremental differentiation methods tend to amplify any small-scale variation in the acutal data. As an alternative, the spline method was selected in which a series of cubic polynomials were fit to the experimental data and then analytically differentiated to obtain the crack-growth rate. This method,

TABLE 1 – *Test results.*

Test No.	K_{max} (MN/m$^{-3/2}$)	ΔK (MN/m$^{-3/2}$)	R_f	Q_{ol}	R_{uo}	R_m	$\frac{da}{dN}\Big\vert_{ss}^{pre.\ ol}$ (mm/cycle)	$\frac{da}{dN}\Big\vert_{ss}^{post.\ ol}$ (mm/cycle)	$\frac{da}{dN}\Big\vert_{min}$ (mm/cycle)	Δa^* (mm)	K_{op}^{max} (MN/m$^{-3/2}$)	$N_D^{exper.}$ (cycles)	$N_D^{predict}$ (cycles)
1	36.61	12.45	0.65	1.00	0.11	0.65	6.55×10^{-4}	6.60×10^{-4}	6.60×10^{-4}	0	27.34	0	650
2	28.17	12.63	0.55	1.30	0.11	0.42	5.18×10^{-4}	5.38×10^{-4}	9.27×10^{-5}	1.55	22.60	6 800	3 470
3	22.88	12.63	0.45	1.60	0.11	0.28	3.53×10^{-4}	3.58×10^{-4}	9.63×10^{-6}	2.01	19.16	22 000	21 740
4	19.27	12.63	0.34	1.90	0.11	0.18	3.02×10^{-4}	2.54×10^{-4}	4.72×10^{-6}	3.51	16.70	121 000	247 800
5	16.64	12.63	0.24	2.20	0.11	0.11	1.66×10^{-4}	...	0	...	$\geq$16.64	∞	∞
6	22.88	14.83	0.35	1.60	−1.00	0.22	1.03×10^{-3}	9.02×10^{-4}	2.45×10^{-4}	2.03	15.72	5 850	8 330
7	22.88	14.83	0.35	1.60	−0.50	0.22	6.30×10^{-4}	6.76×10^{-4}	1.28×10^{-4}	2.62	16.83	10 600	7 960
8	22.88	14.83	0.35	1.60	0.01	0.22	5.82×10^{-4}	4.52×10^{-4}	7.44×10^{-5}	1.88	17.62	11 400	14 100
9	22.88	14.83	0.35	1.60	0.11	0.22	4.55×10^{-4}	5.08×10^{-4}	5.38×10^{-5}	2.36	18.04	18 400	20 700
10	22.88	14.83	0.35	1.60	0.22	0.22	4.78×10^{-4}	4.52×10^{-4}	1.34×10^{-5}	2.36	19.51	44 000	40 200
11	20.34	12.29	0.40	1.80	−1.00	0.22	3.53×10^{-4}	4.01×10^{-4}	1.09×10^{-4}	1.88	14.52	11 800	16 600
12	20.34	12.29	0.40	1.80	−0.50	0.22	4.93×10^{-4}	3.58×10^{-4}	1.02×10^{-4}	2.36	14.63	14 400	18 200
13	20.34	12.29	0.40	1.80	0.01	0.22	3.15×10^{-4}	2.54×10^{-4}	2.37×10^{-5}	3.23	16.43	42 600	50 200
14	20.34	12.29	0.40	1.80	0.11	0.22	2.95×10^{-4}	2.54×10^{-4}	6.48×10^{-6}	2.59	17.55	53 000	98 900
15	20.34	12.29	0.40	1.80	0.22	0.22	2.84×10^{-4}	3.05×10^{-4}	2.72×10^{-6}	3.05	18.11	142 000	395 300
16	16.64	8.59	0.48	2.20	−1.00	0.22	1.21×10^{-4}	1.27×10^{-4}	2.67×10^{-5}	2.79	12.61	52 000	43 400
17	16.64	8.59	0.48	2.20	−0.50	0.22	1.66×10^{-4}	2.02×10^{-4}	4.88×10^{-6}	4.32	14.05	127 000	79 400
18	16.64	8.59	0.48	2.20	0.01	0.22	1.24×10^{-4}	...	0	...	$\geq$16.64	∞	∞
19	16.64	8.59	0.48	2.20	0.11	0.22	1.51×10^{-4}	...	0	...	$\geq$16.64	∞	∞
20	16.64	8.59	0.48	2.20	0.22	0.22	1.22×10^{-4}	...	0	...	$\geq$16.64	∞	∞
21	20.34	16.31	0.20	1.80	−1.00	0.11	5.54×10^{-4}	4.52×10^{-4}	1.36×10^{-4}	1.98	14.19	10 300	13 800
22	20.34	16.31	0.20	1.80	−0.05	0.11	7.87×10^{-4}	3.58×10^{-4}	1.12×10^{-4}	3.18	14.50	17 600	15 800
23	20.34	16.31	0.20	1.80	0.01	0.11	5.89×10^{-4}	4.52×10^{-4}	8.36×10^{-6}	1.73	17.36	44 500	43 700
24	20.34	16.31	0.20	1.80	0.11	0.11	5.13×10^{-4}	5.08×10^{-4}	8.99×10^{-6}	3.48	17.30	63 700	84 600

[a]													
30	20.34	9.36	0.54	1.80	−1.00	0.30	1.93×10^{-4}	1.84×10^{-4}	2.69×10^{-5}	2.36	16.30	25 000	19 200
31	20.34	9.36	0.54	1.80	−0.50	0.30	2.44×10^{-4}	2.02×10^{-4}	6.07×10^{-5}	1.65	15.36	17 600	20 300
32	20.34	9.36	0.54	1.80	0.01	0.30	1.69×10^{-4}	1.60×10^{-4}	1.50×10^{-5}	1.50	16.87	52 800	55 700
33	20.34	9.36	0.54	1.80	0.11	0.30	1.60×10^{-4}	1.61×10^{-4}	7.14×10^{-6}	3.00	17.47	83 200	111 500
34	20.34	9.36	0.54	1.80	0.22	0.30	1.61×10^{-4}	1.80×10^{-4}	2.62×10^{-6}	3.12	18.14	197 000	469 800
35	20.34	9.36	0.54	1.80	0.30	0.30	1.80×10^{-4}	. . .	0	. . .	$\geq$20.34	∞	∞
16-2.4	15.26	7.21	0.53	2.40	−1.00	0.22	9.35×10^{-5}	7.16×10^{-5}	7.98×10^{-6}	2.87	12.31	124 000	54 500
16-2.6	14.08	6.03	0.57	2.60	−1.00	0.22	3.86×10^{-5}	6.68×10^{-5}	3.23×10^{-6}	2.92	11.74	260 000	58 000
17-2.4	15.26	7.21	0.53	2.40	−0.50	0.22	9.07×10^{-5}	5.44×10^{-5}	1.41×10^{-5}	3.48	11.83	126 000	143 000
3A/D-.4a	12.20	8.55	0.30	3.00	−0.40	0.10	1.31×10^{-4}	. . .	0	0	$\geq$12.20	∞	387 000
3A/D-.4b	12.20	8.55	0.30	3.00	−0.40	0.10	1.02×10^{-4}	. . .	0	0	$\geq$12.20	∞	387 000
3A/D-.5	12.20	8.55	0.30	3.00	−0.50	0.10	1.25×10^{-4}	7.16×10^{-5}	2.67×10^{-6}	3.81	9.99	593 000	204 700
R-12	20.34	12.29	0.40	1.80	−0.50	0.22	1.02×10^{-3}	2.54×10^{-4}	1.96×10^{-6}	2.26	. . .	160 500	. . .
R-13	20.34	12.29	0.40	1.80	0.01	0.22	2.67×10^{-4}	2.37×10^{-4}	3.86×10^{-6}	2.54	. . .	169 000	. . .

NOTE—$K_{ol} = 36.61$ MN/m$^{-3/2}$ for all tests. Overload preceeded underload except in Tests R-12 and R-13.

[a] Tests 25 to 29 are for the same set of tests as Tests 11 to 15.

frequently used to differentiate experimental data [24,25], provides a smoothed crack-growth rate curve.

To apply the spline method, third order polynominals were fit to three intervals of the entire post-overload a versus N data of a given test. The values of the polynomials and their first two derivatives were matched at the knots (points where the polynomials join). The computer technique of de Boor and Rice [26,27] was modified to allow the first interior knot to be fixed at a specified position. This first knot was located after the initial deceleration of the crack where the a versus N curve started to level out. It was found for all tests that this knot could be located at a point equal to 5 percent of the calculated plastic zone size. The computer routine then optimally located the second knot and determined the coefficients of the three polynomials which minimized the least-square error over the entire range of the data.

Figure 4 shows a typical fit of the spline function to a versus N data, and Fig. 5 shows the corresponding analytically differentiated curve, that is, da/dN versus a. The spline method of differentiation was compared to a linear, seven-point least-squares movable-strip method [2,28]. The resulting growth rate from this method is also shown in Fig. 5 for the same data. To compare the two methods, the da/dN from the movable-strip method was numerically integrated and compared with the original data. This is shown in Fig. 4. With the spline method, integration of da/dN will simply reproduce the original spline function since the derivation is obtained analytically. As can be seen from Figs. 4 and 5, the spline

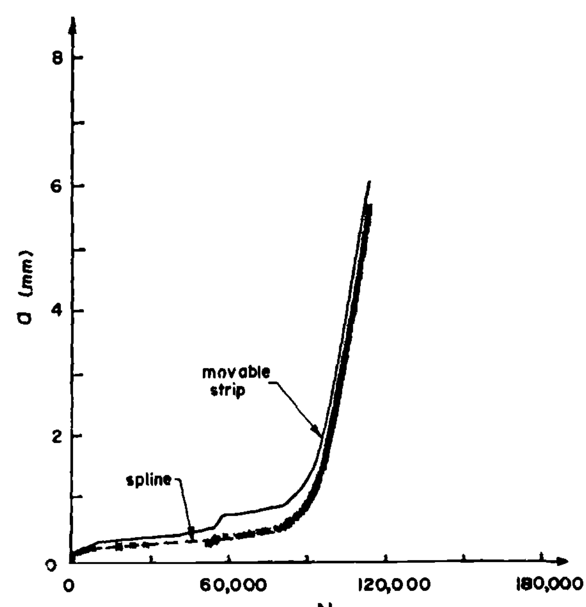

FIG. 4—*Spline function and integrated* da/dN *from the movable strip fit of* a *versus* N *data for Test 15.*

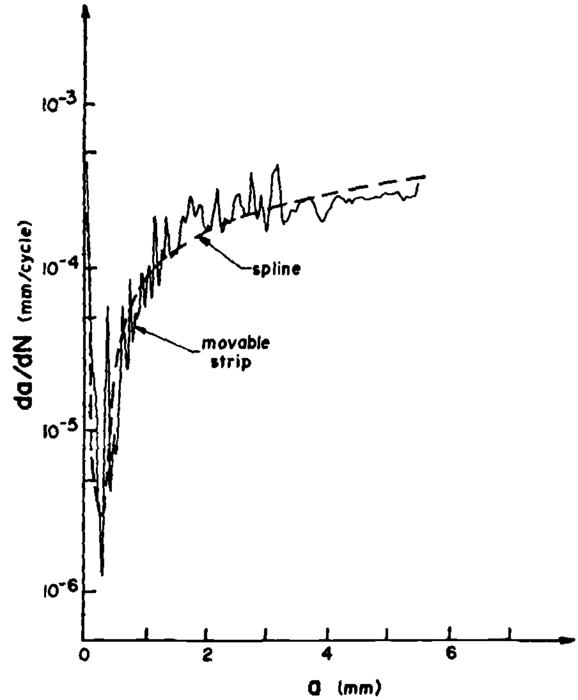

FIG. 5—*Comparison of* da/dN *obtained from spline function and from the movable strip method from* a *versus* N *data for Test 15.*

method provides a good representation of the *a* versus *N* data and a smoothed *da/dN* curve. An analytical expression is also obtained for an entire data set.

One of the important characteristics of the delay behavior is the minimum growth rate following the overload. Therefore, the minimum growth rate for each test as determined from the spline method was compared with the data graphically. In some of the tests the spline method produced a slightly lower value for the minimum growth rate. For these tests (10, 17, 23, 32, 33, and 34) the graphical values were used.

Test Results

Constant-Amplitude Test Results

A total of ten constant stress amplitude tests were run with five stress ratios, R_f, ranging from 0.01 to 0.55. By keeping the load amplitude constant in these tests, R_f remained constant, but the stress intensity level and also the ΔK level increased with increasing crack length. Data was collected every 0.01 mm of growth. Spline functions were fit to the data from which *da/dN* values were determined for each of the tests. Because of the density of the data, the ten tests provided over 1700 data points for *da/dN*. The resulting growth rate data were fit to Elber's form of the growth rate equation using a least-squares method which gave

$$\frac{da}{dN} = C(\Delta K_{eff})^n \text{ mm/cycle}$$

$$C^4 = 1.22 \times 10^{-7}$$

$$n = 3.86$$

$$\Delta K_{eff} = \Delta K(0.5 + 0.4R_f)$$

Overload/Underload Test Results

For each of the tests, the following experimental variables were determined: (1) the number of delay cycles, N_D; (2) the overload affected crack length increment, Δa^*; (3) the minimum growth rate following the overload/underload sequence, $(da/dN)|_{min}$; (4) pre and post-overload crack-growth rates; and (5) the coefficients for the spline function describing the a versus N data. N_D is the number of cycles following the overload before the crack growth returns to a steady-state rate, and Δa^* is the interval over which N_D is observed. Both quantities were determined graphically from plots of the data. The results are presented in Table 1. Tables 2 and 3 give the values of $(da/dN)|_{min}$ and N_D in the matrix form as functions of the test variables Q_{ol}, R_{uo}, and R_m. These results are for the corresponding test conditions shown in Figs. 2 and 3. Examination of the results of Table 2 show an increase in N_D and a corresponding decrease in $(da/dN)|_{min}$ as either R_{uo} or Q_{ol} is increased with R_m held constant. A trend is less pronounced for R_m as columns of Table 3 reveal. These results indicate that R_m has less influence on the delay phenomenon than the two parameters R_{uo} and Q_{ol}.

The calculated value of the load interaction zone, $Z_{ol} = 2r_y$, from Eq 1 was 2.77 mm and was the same for all of the tests since K_{ol} was the same. This can be compared to the experimental results, Δa^*, given in Table 1. The average value for Δa^* was 2.61 mm.

Tests 1 to 5 are in a plane of constant R_{uo} and illustrate the effects of changing only the mean level of the fatigue cycling, that is, R_f. Tests R-12 and R-13 were performed to determine the effect of reversing the load sequence by applying the underload before the overload. These results, when compared with the same test conditions having no underload (Test 15) indicate that any effect of the underload is essentially eliminated by the subsequent overload. Tests 16-2.4 to 3A/D-.5 in Table 1 were run with larger values of Q_{ol} and negative values of R_{uo} to more accurately establish trends in that region of the Q_{ol} versus R_{uo} plane.

Observation during data collection and examination of the shape of the growth rate curve following the overload indicated that the minimum growth rates were directly related to the total number of delay cycles. The correlation

[4] Here, C is defined as a constant and differs from that defined in the Glossary.

TABLE 2 – *Minimum growth rate and number of delay cycles for Q_{ol}/R_{uo} plane of text matrix.*

Q_{ol}		R_{uo}					
		−1.00	−0.50	0.01	0.11	0.30	0.30
1.6	$\left.\frac{da}{dN}\right\rvert_{min}$	2.45×10^{-4}	1.28×10^{-4}	7.44×10^{-5}	5.38×10^{-5}	1.34×10^{-5}	
	N_D	5 850	10 600	11 400	18 400	44 000	
1.8	$\left.\frac{da}{dN}\right\rvert_{min}$	1.09×10^{-4}	1.02×10^{-4}	2.37×10^{-5}	6.48×10^{-6}	2.72×10^{-6}	
	N_D	11 800	14 400	42 600	53 000	142 000	
2.2	$\left.\frac{da}{dN}\right\rvert_{min}$	2.67×10^{-5}	4.88×10^{-6}	0	0	0	
	N_D	52 000	127 000	∞	∞	∞	

TABLE 3 – *Minimum growth rate and number of delay cycles for* R_m/R_{uo} *plane of test matrix.*

R_m		R_{uo}					
		−1.0	−0.5	0.01	0.11	0.22	0.30
0.11	$\left.\frac{da}{dN}\right\|_{min}$	1.36×10^{-4}	1.12×10^{-4}	8.36×10^{-6}	8.99×10^{-6}		
	N_D	10 300	17 600	44 500	63 700		
0.22	$\left.\frac{da}{dN}\right\|_{min}$	1.09×10^{-4}	1.02×10^{-4}	2.37×10^{-5}	6.48×10^{-6}	2.72×10^{-6}	
	N_D	11 800	14 400	42 600	53 000	142 000	
0.30	$\left.\frac{da}{dN}\right\|_{min}$	2.69×10^{-5}	6.07×10^{-5}	1.50×10^{-5}	7.14×10^{-6}	2.62×10^{-6}	0
	N_D	25 000	17 600	52 800	83 200	197 000	∞

of the minimum growth rate with the delay cycles is illustrated in Figure 6. Therefore, if $(da/dN)|_{min}$ is known, N_D can be determined. It should be recalled, however, that K_{ol} was the same for all of the tests in this investigation. This correlation should be investigated for other levels of K_{ol} and also other metals.

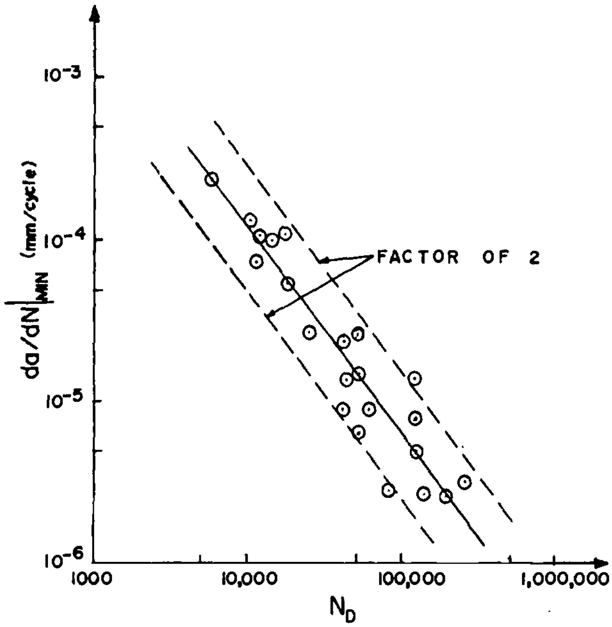

FIG. 6—*Minimum growth rate following overload/underload cycle versus the number of delay cycles.*

Comparison with Crack Closure

Elber's crack closure concept has been used to qualitatively explain the delay behavior following an overload condition. However, by knowing the crack-growth rate through the overload affected zone it is possible to provide a more quantitative comparison of crack closure with the delay behavior. For crack closure [*20*], the effective stress intensity range is

$$\Delta K_{eff} = K_{max} - K_{op} \tag{3}$$

where K_{op} is the stress intensity at which the crack opens. At the minimum growth rate following the overload, K_{op} is a maximum and Eq 2 becomes

$$\left.\frac{da}{dN}\right|_{min} = C(K_{max} - K_{op}^{max})^n \tag{4}$$

In Eq 4, C and n were determined from the constant-amplitude test results, K_{max} from the test conditions and $(da/dN)|_{min}$ from the test results. Therefore, this equation could be solved for K_{op}^{max} following the overload [*29*].

These results are given in Table 1. (This is not restricted to the point where da/dN is a minimum since K_{op} can be determined throughout the overload affected zone [23].) For constant-amplitude loading, Elber defined

$$U = \frac{K_{max} - K_{op}}{K_{max} - K_{min}} \tag{5}$$

For 2024-T3 aluminum alloy, he found

$$U = 0.5 + 0.4R_f \tag{6}$$

At the minimum growth rate following an overload/underload cycle, U_{ol} can be defined, analogous to Eq 5,

$$U_{ol} = \frac{K_{ol} - K_{op}^{max}}{K_{ol} - K_{ul}} \tag{7}$$

Since K_{op}^{max} can be determined from the experimental results as just described, U_{ol} can be determined. It is expected that U_{ol} would be related to the loading conditions as well as environmental and material factors, that is

$$U_{ol} = f(Q_{ol}, R_{uo}, R_m, R_f, K_{ol}, \ldots) \tag{8}$$

If crack closure, as presented for constant-amplitude loading, describes the results, then this function would be, analogous to Eq 6,

$$U_{ol} = 0.5 + 0.4\,R_{uo} \tag{9}$$

Examination of the data, however, suggested that this equation should be of the form

$$U_{ol} = C_1 + C_2R_{uo} + C_3R_{uo}{}^2 + C_4Q_{ol} \tag{10}$$

Using the results from the tests that did not arrest, a multiple linear regression analysis was performed to determine the C_i constants. From the regression analysis,

$$\begin{aligned} C_1 &= 0.408 \\ C_2 &= 0.367 \\ C_3 &= 0.117 \\ C_4 &= 0.075 \end{aligned} \tag{11}$$

By combining Eqs 7 and 10 and solving for K_{op}^{max} gives

$$K_{op}^{max} = K_{ol}\,[1 - (1 - R_{uo})\,(C_1 + C_2R_{uo} + C_3R_{uo}{}^2 + C_4Q_{ol})] \tag{12}$$

The values for K_{op}^{max} calculated from Eq 12 are compared with the experimentally determined values (obtained using $(da/dN)\big|_{min}$ and Eq 4) in Fig. 7. The calculated maximum opening stress intensity value correlates almost exclusively within 5 percent of the measured value.

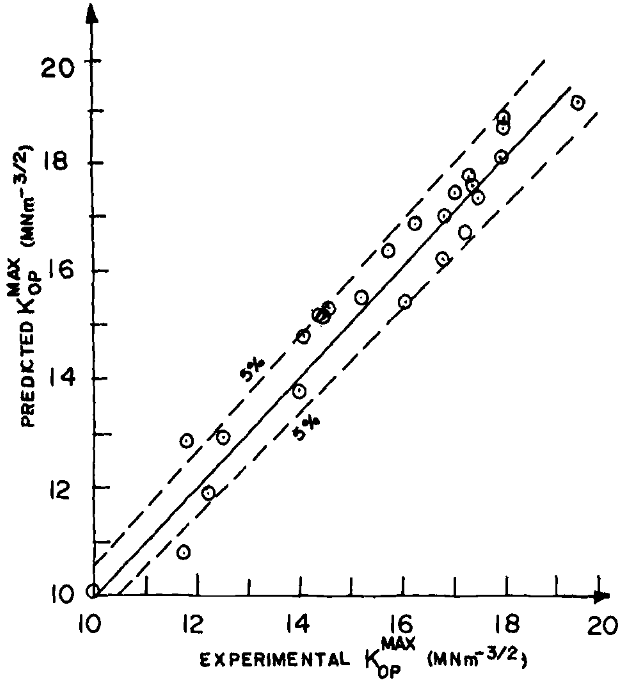

FIG. 7—*Comparison of the predicted and experimentally determined values of the maximum opening stress intensity.*

With C_5R_m added to Eq 10, the regression analysis showed that R_m was statistically insignificant.

The effects of the test parameters on the minimum growth rate can be more readily illustrated by substituting K_{op}^{max} from Eq 12 into Eq 4 and plotting the results for constant values of $(da/dN)|_{min}$. Figure 8 shows several level curves of constant $(da/dN)|_{min}$ as functions of Q_{ol} and R_{uo}. In this study, if the growth was less than 0.01 mm in 10^6 cycles, the test was stopped and the crack was assumed to have arrested. Therefore, a minimum growth rate of 10^{-8} mm/cycle which is the experimental resolution for the data, can be considered arrest. The curve in Fig. 8 with this growth rate is then an arrest/delay boundary. It should be pointed out that this arrest/delay boundary is based entirely on finite growth test results, however, it compares favorably with the experimentally determined arrest/delay boundary found by Himmelein and Hillberry [*11*] which was for an overload with no underload, that is, $R_{uo} = R_m$ [*23*]. The arrest/delay boundary defined by Elber's crack closure equation (Eqs 5 and 6) is also shown in Figure 8. In evaluating the validity of the correlation of the results of this study with crack closure, it is important to keep in mind the number of tests and the distribution of the loading conditions of these tests. Of the 24 tests used in determining the coefficients of Eq 10, only three tests had $Q_{ol} > 2.2$. Furthermore, eleven of the tests were performed in the small region of $0 \leq R_{uo}$

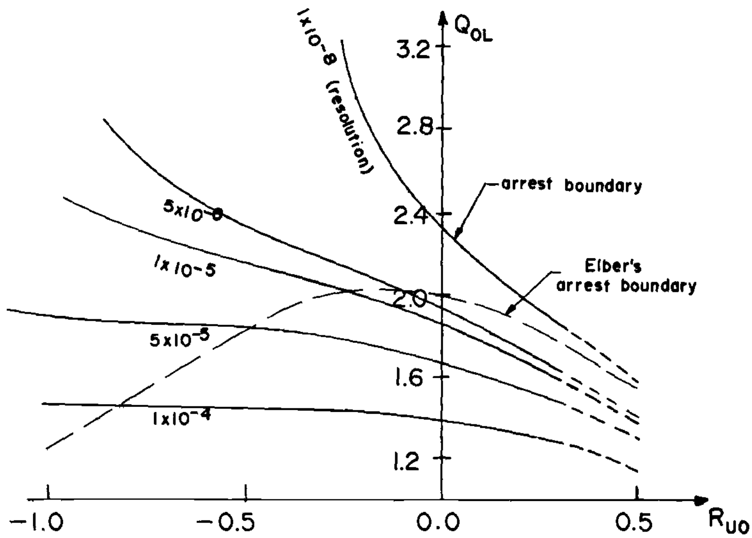

FIG. 8—*Curves of constant* da/dN$|_{min}$ *for* $R_m = 0.22$ *and* $K_{ol} = 36.61$ $MN/m^{3/2}$.

≤ 0.3 and $1.6 \leq Q_{ol} \leq 1.8$. Even with this very unequal distribution of the data, the correlation is exceptionally good.

In Figure 6, the correlation of the minimum growth rate and the number of delay cycles was shown. This, along with Eq 4, suggests that an average growth rate $2r_y/N_D$ would correlate with $K_{max} - K_{op}^{max}$, that is,

$$\frac{2r_y}{N_D} = A(K_{max} - K_{op}^{max})^b \tag{13}$$

The results showed a straight line on a log-log plot and Constants A and b were then determined from a least-squares fit. Using the resulting equation, the number of delay cycles were calculated. These predicted number of delay cycles are compared with the experimental results in Table 1. Comparison with the experimental results show the prediction to be nearly within a factor of two for all tests. It should be mentioned, however, that for these tests $2r_y$ was the same.

Conclusions

1. Utilizing a three-dimensional test matrix approach, the effects of each of the selected loading parameters could be isolated and studied.
2. The number of delay cycles correlates directly with the minimum growth rate following the overload/underload sequence.
3. The extension of the crack closure theory to include the effects of the underload accurately predicts values of K_{op}^{max} which may be used to calculate the minimum growth rate following the overload/underload cycle and the corresponding numbers of delay cycles.

4. The method of cubic splines may be used to represent the a versus N data and for determining da/dN.

Acknowledgments

The authors wish to express their appreciation to the Air Force Flight Dynamics Laboratory, Wright-Patterson Air Force Base, for their support, under Contract F33615-73-C-3056, of this investigation and to the Aluminum Company of America for providing the test samples.

References

[1] Schijve, J., "The Prediction of Fatigue Crack Propagation Under Service Load-Time Histories," National Aerospace Laboratory, NLR, The Netherlands, NLR MP 73016U, 1973.

[2] Gallagher, J. P. and Stalnacker, H. D., "Methods for Analyzing Fatigue Crack Growth Rate Behavior Associated with Flight by Flight Loading," AIAA Paper No. 74-367, April 1974.

[3] Von Euw, E. F. J., "Effect of Overload Cycle(s) on Subsequent Fatigue Crack Propagation in 2024-T3 Aluminum Alloy," Ph.D. thesis, Lehigh University, 1971.

[4] Jonas, O. and Wei, R. P., *International Journal of Fracture Mechanics*, Vol. 7, 1971, pp. 116–118.

[5] Wei, R. P. and Shih, T. T., *International Journal of Fracture Mechanics*, Vol. 10, 1974, pp. 77–85.

[6] Wei, R. P., Shih, T. T., and Fitzgerald, J. H., "Load Interaction Effects on Fatigue Crack Growth in Ti-6Al-4V Titanium Alloy," NASA CR2239, 1973.

[7] Probst, E. P. and Hillberry, B. M., *AIAA Journal*, Vol. 12, 1974, pp. 330–335.

[8] Gardner, F. H. and Stephens, R. I. in *Fracture Toughness and Slow-Stable Cracking, ASTM STP 559*, American Society for Testing and Materials, 1973, pp. 225–244.

[9] Trebules, V. W., Roberts, R., and Hertzberg, R. W. in *Progress in Flaw Growth and Fracture Toughness Testing, ASTM STP 536*, 1973, pp. 115–146.

[10] Corbly, D. M. and Packman, P. F., *Engineering Fracture Mechanics*, Vol. 5, 1973, pp. 479–497.

[11] Himmelein, M. K. and Hillberry, B. M., "The Effect of Stress Ratio and Overload Ratio on Fatigue Crack Delay and Arrest Behavior Due to Single Peak Overloads," Proceedings of the Eighth National Symposium on Fracture Mechanics (1974), *Mechanics of Crack Growth, ASTM STP 590*, to be published.

[12] Hsu, T. M. and Lassiter, L. W., "Effects of Compressive Overloads on Fatigue Crack Growth," AIAA Paper No. 74-365, April 1974.

[13] Petrak, G. J. and Gallagher, J. P., "Predictions of the Effect of Yield Strength on Fatigue Crack Growth Retardation in HP-9Ni-4Co-3OC Steel," accepted for publication in *Journal of Engineering Materials and Technology*, ASME.

[14] Stephens, R. I., McBurney, G. W., and Oliphant, L. J., "Fatigue Crack Growth with Negative R Ratio Following Tensile Overloads," *International Journal of Fracture*, Vol. 10, 1974.

[15] Porter, T. R., *Engineering Fracture Mechanics*, Vol. 4, 1972, pp. 717–736.

[16] Wheeler, O. E., *Journal of Basic Engineering*, Vol. 94, 1972, pp. 181–186.

[17] Willenborg, J., Engle, R. M., and Wood, H. A., "A Crack Growth Retardation Model Using an Effective Stress Concept," AFFOL-TM 71-1-FBR, 1971.

[18] Gray, T. D. and Gallagher, J. P., "Predicting Fatigue Crack Retardation Following a Single Overload Using a Modified Wheeler Model," Proceedings of the Eighth National Symposium on Fracture Mechanics (1974), *Mechanics of Crack Growth, ASTM STP 590*, to be published.

[19] Gallagher, J. P., "A Generalized Development of Yield Zone Models," AFFDL-TM-FBR-74-28, Air Force Flight Dynamics Laboratory, Wright-Patterson Air Force Base, Ohio, Jan. 1974.

[20] Elber, W. in *Damage Tolerance in Aircraft Structures, ASTM, STP 486* American Society for Testing and Materials, 1971, pp. 230–242.

[21] Newman, J. C., "Finite Element Analysis of Fatigue Crack Propagation–Including the Effects of Crack Closure," Ph.D. thesis, Virginia Polytechnic Institute and State University, 1974.

[22] Sharpe, W. M. and Grandt, A. F., "A Preliminary Study of Fatigue Crack Retardation Using Laser Interferometry to Measure Crack Surface Displacements," proceedings of the Eighth National Symposium on Fracture Mechanics (1974), *Mechanics of Crack Growth, ASTM STP 590*, to be published.

[23] Alzos, W. X., "The Effects of Single Overload/Underload Cycles on Fatigue Crack Propagation," M.S. thesis, Purdue University, May 1975.

[24] Wold, S., "Spline Functions in Data Analysis," Research Group for Chemometrics, Institute of Chemistry, Umea University, S 901 87, Umea, Sweden.

[25] Ahlberg, J. H., Nilson, N. H., and Walsh, J. L., *The Theory of Splines and Their Applications*, Academic Press, New York, 1967.

[26] de Boor, C. and Rice, J. R., "Least Squares Cubic Spline Approximation: I–Fixed Knots," Purdue University Computing Center Publications, 1968.

[27] de Boor, C. and Rice, J. R., "Least Squares Cubic Spline Approximation: II–Variable Knots," Purdue University Computing Center Publication, 1968.

[28] Clark, W. G., Jr., and Hudak, S. J., "Variability in Fatigue Crack Growth Rate Testing," ASTM E-24.04.01 Task Group Report, 18 Sept. 1974.

[29] James, L. A and Anderson W. E., *Engineering Fracture Mechanics*, Vol. 1, 1963, pp. 565–568.

DISCUSSION

R. P. Wei[1] *and T. T. Shih*[2] *(written discussion)*—The authors are to be complimented for introducing factorial design into their experiments on load interaction effects in fatigue crack growth. Unfortunately, they did not follow this approach to its logical conclusion. The authors' statement regarding *prediction* and its implications in the context of Fig. 7 and Eqs 4 to 12 appears to us to be inappropriate and misleading. One gets the mistaken impression that Fig. 7 represents a comparison between the predictions of an analytically derived model and experimental results. In actuality, the authors had simply *assumed* the validity and applicability of a "crack closure" model to account for load interaction effects (see Eq 4), and had made an ad hoc assumption regarding the functional form of the load interaction parameter (defined to be U_{0l}; Eqs 7 and 10). Incidentally, the authors could have dealt with K_{op}^{max} directly without having to invoke U_{0l}). The authors then used a multiple linear regression analysis to determine the unknown coefficients C_i in the *assumed* equation (Eq 10 or 12) so as to obtain a least-error fit to the values of K_{op}^{max} computed from their experimental data, using Eq 4. As such, Fig. 7 depicts only the closeness of this fit, and *does not* represent a comparison between prediction and experimentation, and a test of the model. Although there is merit in the authors' approach, one needs to remain objective in its implementation.

B. M. Hillberry (author's closure)—I agree that the word *prediction* in Figure 7

[1] Department of Mechanical Engineering and Mechanics, Lehigh University, Bethlehem, Pa. 18015.

[2] Ebasco Services, Inc., New York, N. Y.

is possibly misleading and I wish to thank Drs. Wei and Shih for pointing this out.

In response to the remaining comments I find it particularly interesting that they were able to so clearly describe what we *actually* did in analyzing our data. Unfortunately their conclusions did not arrive at the logical approach. In *actuality* the authors *did not* assume the validity or applicability of any model in this study. The results were however compared with several models to see if the model described the observed behavior. There was no apparent correlation with either the Wheeler model [*16*] or the Willenborg model [*17*]. In comparing the crack closure model with the results, the only assumption made was that the overload/underload cycle establishes the residual stress field in the vicinity of the crack tip and is not affected by subsequent cycling. This in turn establishes the crack opening stress intensity level throughout the overload affected region. The functional form for U given in Eq 5 was defined by Elber and for the overload/underload cycle is, by definition, U_{ol} as given in Eq 7. As stated in the text the functional form for U_{ol} given in Eq 10 was predicted by the data, and no ad hoc assumption as to the form of Eq 10 was made as Drs. Wei and Shih suggest. Plotting U_{ol} versus Q_{ol} showed a linear relationship between U_{ol} and Q_{ol} for R_{uo} constant. This accounts for the Q_{ol} term of Eq 10. Plotting U_{ol} versus R_{uo} showed a definite second order relationship between U_{ol} and R_{uo} for Q_{ol} constant. This accounts for the quadratic form in R_{uo} contained in Eq 10. By finding the slope, m, of the U_{ol} versus Q_{ol} curve, the data collapsed to nearly a single line on a plot of ($U_{ol} - mQ_{ol}$ versus R_{uo}). From this, it was clearly evident that U_{ol} was related to R_{uo} and Q_{ol} as given in Eq 10 and the crack closure did in fact describe the behavior due to the overload/underload cycle. Possibly, we should have quit at this point to avoid the possibility of confusing our readers. However, since the functional relation between U_{ol} and Q_{ol} and R_{uo} was known (*not assumed*), the constants were determined using a regression analysis. This in turn provides an equation for calculating U_{ol} which can be used to calculate K_{op}^{max}. This along with Eq 13 can then be used to *predict* delay behavior as is done in Fig. 8. It is interesting to note that in comparing U_{ol} from Eqs 9 and 10, there is very close agreement for $0 \leq R_{uo} \leq 0.5$ which is the region over which Eq 9 would be expected to be applicable.

In the recent studies of delay behavior due to overloads, there has been very little success in correlation of the results. Several investigators have qualitatively described their results using the crack closure concept. The results presented here, however, provide a quantitative correlation (within 5 percent, Fig. 7). It is also interesting to note that in subsequent studies Eqs 10 and 13 have provided excellent *prediction* of delay behavior.[3,4]

[3] Skat, A. C., Jr., "Evaluation of Extended Crack Closure in Fatigue Crack Delay Prediction for Single Overload/Underload Sequences, M. S. thesis, Purdue University, May 1975.

[4] Crandall, G. M., "Residual Stress Intensity Parameters for Predicting Delay in Fatigue Crack Propagation," M. S. thesis, Purdue University, Dec. 1975.

As I have just described, our objectives and procedures for analyzing the data were not the same as that suggested by Drs. Wei and Shih. The procedure they suggest is an elementary approach which can be very misleading. In this study, the regression analysis was used only to find the magnitude of the constants for an equation whose functional form was predicted by the data. As they point out one should remain objective in their approach.

W. N. Sharpe, Jr.,[1] *D. M. Corbly,*[2] *and A. F. Grandt, Jr.*[2]

Effects of Rest Time on Fatigue Crack Retardation and Observations of Crack Closure

REFERENCE: Sharpe, W. N., Jr., Corbly, D. M., and Grandt, A. F., Jr., "**Effects of Rest Time on Fatigue Crack Retardation and Observations of Crack Closure,**" *Fatigue Crack Growth Under Spectrum Loads, ASTM STP 595*, American Society for Testing and Materials, 1976, pp. 61–77.

ABSTRACT: Fatigue cracks grown in compact tension specimens of 2024-T851 aluminum at $\Delta K = 6.93$ MN/m$^{3/2}$ ($R = 0.1$) were subjected to single-peak overloads of 17.31 MN/m$^{3/2}$. After the overload, the specimens were held at zero load for periods of 3 min, 1 h, and 20 or more hours before recycling at $\Delta K = 6.93$ MN/m$^{3/2}$. Increasing the rest time had the effect of slightly reducing the crack retardation as measured on the specimen surface.

The load at which the fatigue crack faces fully separate was measured on the specimen surface by laser interferometric techniques and in the specimen interior by through-transmission ultrasonic methods. Crack opening loads measured on the specimen surface were found to increase with application of an overload and then decrease to the original value when the specimen was allowed to rest at zero load, while opening loads measured through the sample by the ultrasonic method did not vary significantly with peak loads or rest times. Varying specimen thickness between 0.64 and 2.54 cm had little effect on surface measured retardation or opening loads. The relationship between applied load and crack surface displacement as measured by ultrasonics varied significantly with specimen thickness.

KEY WORDS: crack propagation, fatigue (materials), loads (forces), stress cycle, retarding, ultrasonics

It is well known that tensile peak overloads may significantly delay subsequent constant-amplitude fatigue crack propagation in many materials. Since real structures are usually subjected to complex load histories, the ability to predict accurate crack-growth lives under realistic service conditions is of major engineering interest. Thus, several mechanisms have been proposed to account for load history effects on crack growth, including crack closure [*1*],[3] effective stress concepts [*2–4*], and crack tip blunting [*5*].

Although these models differ in their explanation for fatigue crack retardation, all share the view that crack tip plasticity is the controlling parameter. The

[1] Professor, College of Engineering, Michigan State University, East Lansing, Mich. 48842.

[2] Research metallurgist and materials research engineer, respectively, Metals Behavior Branch, Metals & Ceramics Division, Air Force Materials Laboratory, Wright-Patterson AFB, Ohio 45433.

[3] The italic numbers in brackets refer to the list of references appended to this paper.

differences between mechanisms arise in how the plasticity affects crack growth. They agree that any variable which would alter the amount of crack tip yielding would be expected to have an influence on subsequent crack extension. Factors which have been considered by previous investigators include the size and sign of the overload, the number and sequence of overloads, the mean stress level, the influence of material properties, and the effects of temperature.

This paper examines two other variables which could influence fatigue crack retardation: rest periods and specimen thickness. Although residual stresses could be expected to relax out with time, the authors are aware of only limited data on the effect of hold times [*6*]. Thus, a series of experiments are described in which a tensile overload was applied and the specimen allowed to rest at zero load prior to resuming the original cyclic loading. Since the size of the plastic zone is larger for conditions of plane stress than for plane strain, these tests were repeated for several specimen thicknesses.

An optical interference method was employed to measure the opening load required to separate the crack faces in order to interpret the results in terms of the closure model. As discussed in previous work [*7,8*], this technique provides an accurate and sensitive magnification of the crack opening displacements at the specimen surface. In an attempt to "look" into the interior of the aluminum specimens to determine if internal crack behavior is similar to that on the specimen surface, corresponding measurements were made by ultrasonic transmission. These observations tend to support other evidence [*9,10*] that surface measurements are not necessarily indicative of the internal crack behavior.

Retardation Measurements

Procedure

Compact tension specimens (with specimen width W = 5.08 cm and height-to-width ratio of 0.6) were machined from 2024-T851 aluminum in thicknesses of 2.54, 1.27, and 0.64 cm. Fatigue cracks approximately 3-mm long were grown from machined starter notches (a/W = 0.25) in these specimens by cyclic loading at large values of $\Delta K = K_{max} - K_{min}$, with a gradual reduction to K_{max} = 7.7MN/m$^{3/2}$ and $R = K_{min}/K_{max}$ = 0.1. These values of K_{max} and R were chosen for baseline conditions because the crack growth rate was fast enough for reasonable test times and ΔK was small enough to allow overloads that did not cause fracture. All subsequent testing was done with crack lengths in the range $0.3 \leq a/W \leq 0.7$ where a is the total crack length. By shedding load in predetermined increments as the crack extended, it was possible to keep the baseline ΔK constant to within ±5 percent.

All tests were performed in a closed-loop electrohydraulic testing machine with the baseline fatigue cycling run at 40 Hz. The overload was a load pulse that rose linearly to a maximum value of 17.31 MN/m$^{3/2}$ in 0.1 s, stayed at that value for 60 s, and unloaded linearly in 0.1 s. This overload magnitude was chosen because it gave appreciable, but not excessive, retardation (on the order of 30 000 cycles). The particular pulse shape was chosen because it was controllable and reproducible on the test machine. Following the overload, the specimen was allowed to rest at zero load in the test machine for the specified period of time.

Crack lengths were measured during the fatigue testing with the aid of a small plastic scale taped to the specimen surface parallel to the crack. By examining the crack tip and scale through a microscope, it was possible to resolve 0.051 mm of crack extension. For each rest-time data point, the crack was grown approximately 3 mm under baseline conditions, overloaded, allowed to rest at zero load, and then subjected to baseline loading conditions until it started to grow again. The number of cycles of baseline loading required to restart the crack growth is the number of retardation cycles, N_D.

Wei et al [6] noted that interaction effects due to sequential applications of single peak overloads were negligible when the crack had grown approximately ten plastic zone sizes between overloads. The maximum plastic zone size for experiments conducted here (using the relationship, $r_y = \frac{1}{2\pi}(K_{hmax}/\sigma_{ys})^2$, with K_{hmax} = 17.31 MN/m$^{3/2}$ and σ_{ys} = 448 MN/m^2) is 0.238 mm. Therefore, interaction effects should be negligible for these experiments. Moreover, care was taken to ensure that steady-state growth rates were reestablished well before the application of a subsequent overload. In addition, in order to avoid any bias in the results due to possible load/rest-time interaction effects, the test sequence was randomly mixed. The results in Tables 1 and 2 are listed in order of increasing rest times solely for the purpose of clarifying data presentation.

Results and Discussion

Figure 1 is a plot of a representative crack-growth curve. The crack was grown from Points A to B under the baseline loading conditions (K_{max} = 7.7 MN/m$^{3/2}$ and $R = 0.1$). At Point B, the 17.31 MN/m$^{3/2}$ overload was applied

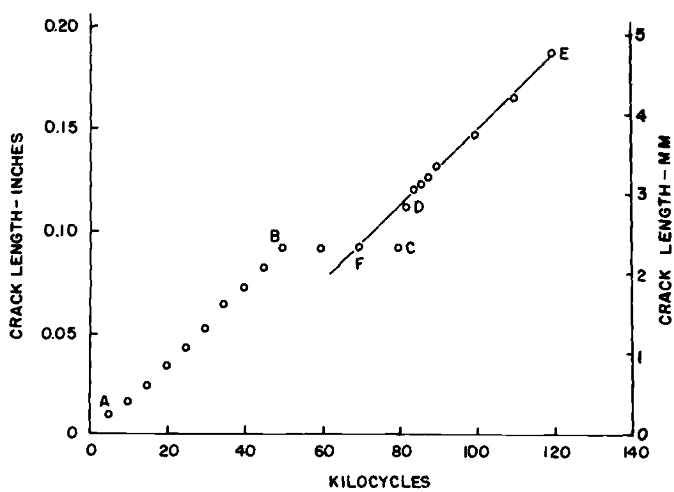

FIG. 1—*Typical crack-growth curve. Overload of 2.25* K_{max} *was applied at Point* B; *rest time was 3 min.*

TABLE 1 – *Summary of retardation data and effective stress intensity ratio (U) measurements by optical techniques.*

Specimen	Test Condition[a]	N_D[b] (direct)	N_D[b] (slope)	U (IDG)	U (P–δ)
1					
(2.54 cm thick)	baseline	...	...	0.83	0.78
	3 min	...	...	0.72	0.78
	growth	36 K	32K	0.78	0.81
2					
(2.54 cm thick)	baseline	...	...	0.81	0.75
	3 min	...	...	0.61	0.67
	growth	48 K	40 K	0.78	0.72
	1 h	...	...	0.67	0.72
	growth	32 K	26 K	0.72	0.75
	70 h	...	...	0.78	0.75
	growth	32 K	30 K	0.83	0.78
3					
(2.54 cm thick)	baseline	...	...	0.83	0.78
	3 min	...	...	0.69	0.81
	growth	32 K	20 K	0.83	0.83
	1 h	...	...	0.78	0.86
	growth	44 K	35 K	0.72	0.83
4					
(2.54 cm thick)	baseline	...	...	0.86	0.78
	3 min	...	...	0.72	0.81
	growth	38 K	33 K	0.81	0.81
	1 h	...	...	0.75	0.81
	growth	28 K	21 K	0.83	0.86
	66 h	...	...	0.83	0.81
	growth	14 K	12 K	0.83	0.89
5					
(1.27 cm thick)	baseline	...	...	0.86	0.86
	3 min	...	...	0.75	0.83
	growth	28 K	22 K	0.86	0.86
	1 h	...	...	0.78	0.83
	growth	36 K	29 K	0.83	0.86
	24 h	...	...	0.83	0.83
	growth	28 K	26 K	0.89	0.83
6					
(0.64 cm thick)	baseline	...	...	0.83	0.86
	3 min	...	...	0.75	0.78
	growth	38 K	30 K	0.81	0.86
	1 h	...	...	0.78	0.78
	growth	34 K	27 K	0.83	0.86
	20 h	...	...	0.83	0.86
	growth	24 K	22 K	0.83	0.86

[a] The time given in this column is the time between application of overload and commencement of cycling at the original baseline conditions.

[b] In cycles.

TABLE 2 – *Summary of retardation data and effective stress intensity ratio (U) measurements by ultrasonic techniques.*

Specimen	Test Condition[a]	N_D[b] (direct)	N_D[b] (slope)	U (ultrasonic) Before Overload	After Overload
7 (2.54 cm thick)	3 min + growth	33 K	26 K	0.76	0.78
	1 h + growth	32 K	23 K	0.79	0.79
	1 h + growth	34 K	29 K	0.80	0.80
	1 h + growth	40 K	32 K	0.76	0.76
	1 h + growth	40 K	19 K	0.73	0.76
	24 h + growth	30 K	25 K	0.84	0.84
8 (1.27 cm thick)	3 min + growth	34 K	29 K	...	...
	3 min + growth	30 K	22 K	...	...
	3 min + growth	34 K	26 K	...	...
	1 h + growth	27 K	24 K	...	...
	24 h + growth	22 K	20 K	...	...
	24 h + growth	24 K	22 K	...	...
	24 h + growth	28 K	25 K	...	...
9 (0.64 cm thick)	3 min + growth	34 K	25 K	0.70	0.73
	3 min + growth	25 K	10 K	0.72	0.73
	1 h + growth	25 K	17 K	0.66	0.72
	1 h + growth	34 K	25 K	0.71	0.74
	1 h + growth	30 K	25 K	0.72	0.79
	24 h + growth	30 K	26 K	0.64	0.64
	24 h + growth	25 K	20 K	0.66	0.74

[a] The time given in this column is the time between application of overload and commencement of cycling at the original baseline conditions.

[b] In cycles.

and the baseline loading was restarted after the appropriate delay (in this case 3 min). Crack growth was not visible on the specimen surface until Point C. The crack then grew very rapidly until Point D, at which time the previous baseline growth rate was reestablished. Since the crack length was not uniform through the specimen thickness, leading somewhat in the interior, it may be possible that the crack really started growing earlier inside the specimen than observed on the surface. If this is the case, it is more appropriate to extrapolate the line DE back to Point F and take the distance BF as N_D instead of the distance BC.

Tables 1 and 2 present the experimental results in detail. The two values of N_D were obtained by taking the point at which the crack growth was visible on the surface (direct) or by extrapolating the growth curve (slope). The number of delay cycles is plotted against the rest time between overload and restart of baseline cycling in Fig. 2. The values plotted there are average values with the

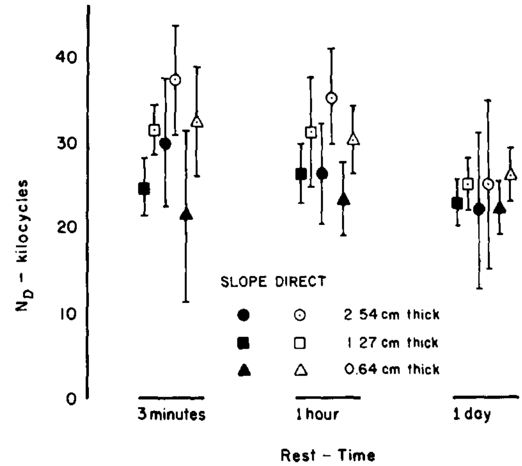

FIG. 2–*Number of cycles delay versus rest time.*

vertical bars representing a best estimate of one standard deviation. There is a tendency for the amount of retardation to decrease with increasing rest time, although examination of Tables 1 and 2 shows a few tests where the opposite effect was observed. There is no great difference in the behavior because of thickness, although the 2.54-cm specimens usually exhibited delays that were slightly longer than the thinner ones. The decrease in delay cycles after long rest times at zero load is not very large in this material under these test conditions. Although, as expected, the slope method gives smaller N_D values than the direct procedure, results obtained by the two methods do not differ greatly.

Surface Measurement of Opening Loads

Procedure

The load at which the crack became completely open on the specimen surface was measured by laser interferometry in a manner described earlier [*8*]. Briefly, two shallow reflective grooves were impressed on either side of the crack extending ahead of the crack tip. A laser beam incident on the grooves generates two interference fringe patterns, one on either side of the beam. The fringes are basically straight when the crack is closed, and the fringes emanating from the grooves astride the crack become displaced as the crack opens. The load required to produce measurable fringe displacement over the entire crack length is defined here as the opening load.

The opening load was measured by photographing both fringe patterns at each load increment. These photographs were referenced to the zero load photograph, and the fringes compared to determine the opening load. The opening load was thus determined to lie within a certain range of load. The data are presented in terms of U ($U = \Delta K_{eff}/\Delta K$), the effective stress intensity ratio. Because of the incremental nature of the measurements, U may be underestimated by approximately 0.06.

The interferometric displacement measurement technique permits measurements of the crack displacement at any point along the crack. As an additional measure of U, crack surface displacements were plotted as a function of load for a position 1 mm from the crack tip, and U was determined by the departure from linearity of the load-displacement curve in a manner described by Elber [1]. The fringe motion technique for finding U is referred to as the IDG method, and the load-displacement technique referred to as the $P - \delta$ method. Values of U found by both methods are presented in Table 1.

Results and Discussion

Figure 3 shows the variation of the effective stress intensity ratio U with rest time. The vertical bars on the 2.54-cm-thick specimens denote extreme values. The original data for Fig. 3 are given in Table 1. U for the baseline fatigue

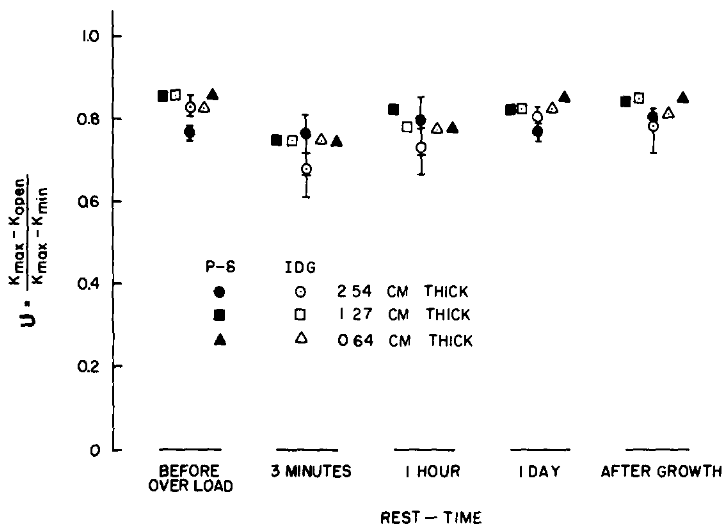

FIG. 3–*Effective stress intensity ratio versus rest time. Vertical bars represent extreme values.*

growth is approximately 0.84, meaning that 84 percent of the applied load is effective in growing the crack. After an overload plus a 3-min rest, the value of U drops slightly; for longer rest periods it tends to return to its original value. There is little difference in the behavior for specimens of different thicknesses or between the two techniques for measuring U.

The closure model can be used, with the data of Fig. 3, to predict the amount of delay due to retardation. The Elber model states that the growth rate is given by

$$da/dN = A\ (\Delta K_{\text{eff}})^n \tag{1}$$

or

$$da/dN = A\ (\Delta K)^n\ U^n \tag{2}$$

Now, basically the Elber model says if one decreases U, da/dN will decrease to such a very low value that "retardation" will be observed. The average value of this slow crack growth rate following the overload is specified by dividing the minimum resolvable increment of crack extension by the number of delay cycles.

Denote the conditions before overload, that is, the baseline growth rate, by the subscript 1, and the average conditions after the overload by subscript 2. Then

$$\frac{da/dN_2}{da/dN_1} = \left(\frac{U_2}{U_1}\right)^n \tag{3}$$

Baseline growth rate data on these specimens give a value of $n = 3.76$, $U_1 = 0.84$ and $da/dN\big|_1 = 3.8 \times 10^{-5}$ mm/cycle. The microscope and scale setup for measuring crack length had a sensitivity of 0.051 mm. Using these values plus the measured U values, one can predict the amount of delay for a given rest time. The results of such calculations are given in Table 3. The $\bar{U}$ and $\bar{N}_D$ values in that table are an average of the U (IDG method) and N_D (direct method) measurements made on Specimens 1 through 6.

In examining the data of Table 3, it is evident that values of N_D predicted in this manner are significantly less than actually observed. In this case the closure

TABLE 3 – *Comparison of number of cycles of delay measured experimentally and predicted by closure model.*

Rest Condition	$\bar{U}$	$\bar{N}_D$ [a]	N_D [a] (closure model)
Baseline	0.84	. . .	. . .
3-min rest	0.71	37 K	2.5 K
1-h rest	0.75	35 K	2.1 K
1-day rest	0.82	24 K	1.5 K

[a] In cycles.

predictions are in error by over an order of magnitude. Since it was assumed here that U remained at its minimum value following the overload instead of gradually increasing to U_1, the predictions of Table 3 represent upper limits for N_D. Although the value of n used for these calculations was determined from conventional da/dN-ΔK data rather than the more appropriate da/dN-ΔK_{eff} representation, the computations of Eq 3 are not very sensitive to n. Using the prior approach, it would be necessary for the overload to cause U to drop from 0.84 to approximately 0.35 in order to achieve the number of delay cycles actually observed. In addition, since there is still significant delay after a 24-h rest period when U_2 has nearly relaxed back to U_1, it is evident that the closure model does not completely account for retardation in this case.

Ultrasonic Measurements

Procedure

A through-transmission ultrasonic testing procedure was used to make measurements of the fatigue crack response to loading variables. Two longitudinal-wave piezoelectric ceramic transducers, 0.64 cm in diameter, were used for the majority of the tests. The transducers were placed on opposite edges of the specimen with the wave propagation direction normal to the crack plane (see Fig. 4*a* for test conditions). Care was taken to place the transducers directly

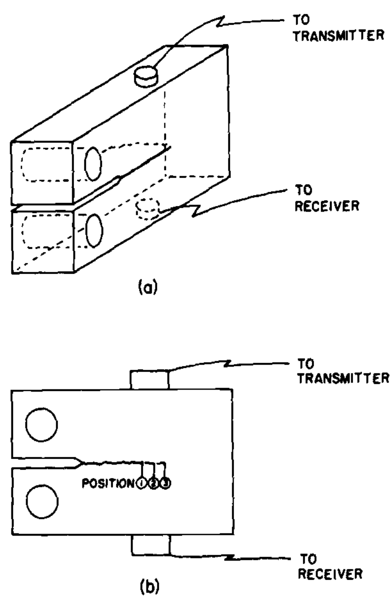

FIG. 4–*(a) Schematic illustration of ultrasonic transducer placement on the compact specimen. (b) Approximate crack tip positions relative to ultrasonic transducer.*

opposite each other along the centerline of the test specimen. Several schemes were investigated to define a holding and coupling method which would give reproducible results in the fatigue loading environment. The method finally selected involved using a viscous liquid couplant (6-phenyl ether) and a rubber band-metal clip arrangement around the transducers and specimen. The transducer case was then visually aligned with a scribe mark on the specimen surface, and the transducers were wrung against the specimen surface. An uncracked specimen was repeatedly subjected to the fatigue overload test spectrum, and it was shown that the vibrations involved had virtually no effect on the ultrasonic signal.

To avoid introducing unwanted electronic artifacts in the ultrasonic results, a very simple system was employed. The transmit transducer was excited at its nominal 5 MHz center frequency by a 1-μs high-voltage sinusoidal pulse burst from a Matec Model 9000 Attenuation Comparator. The receive transducer was connected directly to the high impedance input vertical amplifier of a wide bandwidth Hewlett-Packard Model 180A oscilloscope. Initially, Polaroid photographs were taken of both the reflected signal as presented on the Matec cathode ray tube and the transmitted signal on the H-P oscilloscope at each applied load increment. The pulse-echo signal received by the transmit transducer is rectified by the Matec circuitry and the video envelope is displayed. It was found that due to stability problems the reflected signal was not sufficiently reliable and sensitive enough for these experiments. It was therefore decided to photograph and measure only the through transmitted r-f peak-to-peak signal amplitudes.

Figures 5 and 6 are representative plots of ultrasonic through-transmission results versus applied load for 0.64 and 2.54-cm-thick specimens, respectively. Each figure contains three sets of data which represent the three relative

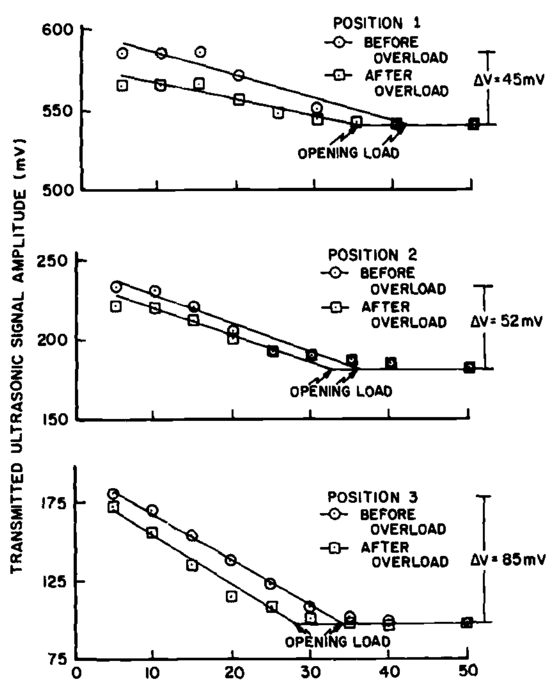

FIG. 5—*Transmitted ultrasonic signal amplitude versus applied load, before application of overload and following a 1-h rest period. Specimen thickness is 0.64 cm.*

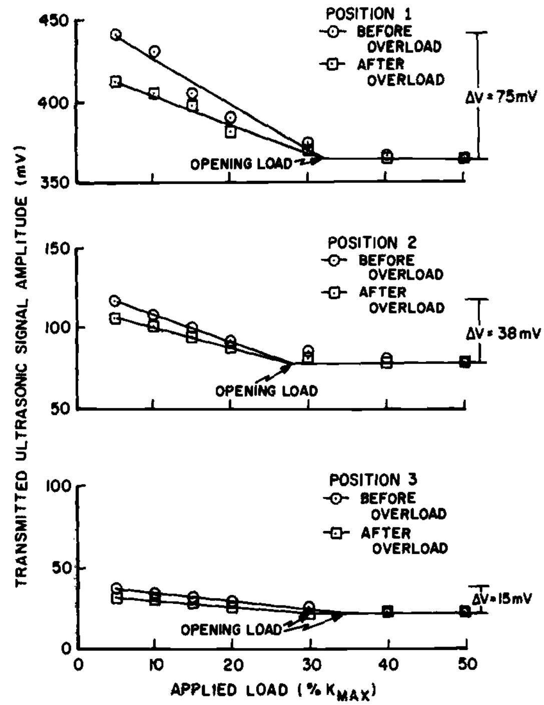

FIG. 6—*Transmitted ultrasonic signal amplitude versus applied load, before application of overload and following a 1-h rest period. Specimen thickness is 2.54 cm.*

positions of the crack tip with respect to the ultrasonic field (refer to Fig. 4*b*). Due to curvature of the crack tip through the specimen thickness there is a certain degree of imprecision as to the exact position of the ultrasonic field with respect to the crack tip. Roughly speaking, however, Position 1 corresponds to the crack plane interrupting approximately 40 to 50 percent of the ultrasonic beam, Position 2 corresponds to 60 to 80 percent, and Position 3 corresponds to 85 to 95 percent.

At each position the peak-to-peak r-f amplitude of the received signal is plotted versus load before and after the application of the overload as shown in Figs. 5 and 6. It should be noted that although these plots do not show the ultrasonic signal amplitude at zero applied load, this value was periodically checked and found to be proportionately greater than the 5 percent value. This value was not always measured, however, because of the difficulty in maintaining load control stability very near zero load. Also, at the other end of the applied load range, that is, at the 225 percent overload value, the ultrasonic signal was shown not to vary significantly from the 50 percent load condition indicating the crack was fully open at this load. The crack growth due to the overload was not sufficient to cause a detectable change in the ultrasonic signal amplitude.

Results and Discussion

The following remarks are based on some general observations which were commonly observed on several sets of similar experiments. In all cases the ultrasonic signal amplitude at low values of applied load was less after the overload than that observed prior to the overload, indicating that less energy is being transmitted through the crack following the peak load. Since the signals again match at higher loads when the crack faces are completely separated (see Figs. 5 and 6), this result suggests that the effect of crack closure, as measured by the ultrasonic technique, decreases with application of an overload. The surface observations made by the laser interferometry method described previously, however, indicated an increase in closure on the specimen surface following the overload.

This discrepancy between the effects of closure observed on the surface and in the specimen interior agrees with prior measurements of fatigue crack surface displacements in a transparent polymer [*10*] and with electropotential measurements in titanium [*9*]. In the latter reference, Shih and Wei suggested that due to the differences in plane stress and plane strain plastic zone behavior, the closure distribution through the thickness would be of the form shown in Fig. 7.

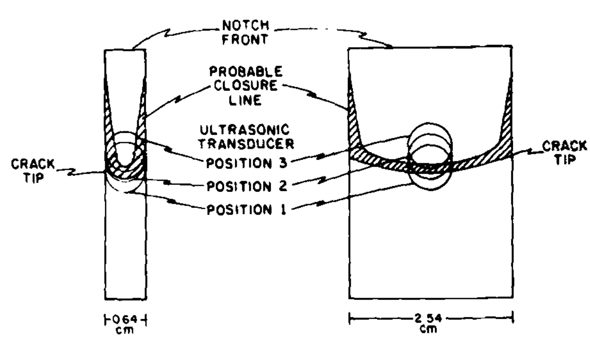

FIG. 7–*Schematic illustration of probable closure distribution through specimen thickness [9].*

This is also in agreement with the interferometric measurements of crack opening [*10*] which showed that the crack surfaces were closed around the crack perimeter, but separated in the specimen interior.

The ultrasonic experiments reported here tend to support the distribution of closure affected area shown in Fig. 7. Note in Figs. 5 and 6, for example, that there are some basic differences indicated between the ultrasonic results as the thickness of the sample increases. In the thinner specimen the magnitude of the signal change between minimum and maximum applied load (ΔV) tended to increase as the crack extended (going from Position 1 to Position 3). This is in general agreement with 2-dimensional closure model predictions. However, it can be seen in Fig. 6, that this is not the case in the thicker material. A possible explanation of this discrepancy can be seen schematically in Fig. 7. The relative position of the transducers is indicated on the figure. If the closure affected area is as assumed then the area sampled by the transducers would increase in the thinner sample and stay constant or decrease in thicker specimen. Although definite conclusions as to the exact shape of the closure affected zone cannot be made on the basis of these experiments, it is clear that closure does not extend uniformly back from the tip in the specimen interior.

Crack closure stresses were defined from the ultrasonic results before and after the overload using the extrapolation approach as defined by Buck et al [*11*] and are recorded in Table 2. It can be seen in Figs. 5 and 6 that the knee of the curve (that point beyond which the ultrasonic signal does not change with increasing load) either stays in the same place or decreases following the overload. This is again in opposition to the surface measurements (and the closure model) which indicated an increase in crack closure stress (that is, reduction in U) following the overload.

The time dependency of the ultrasonic results following the overload were somewhat ambiguous. In some cases there was a tendency for the after-overload curve to shift toward the before condition with increasing time at zero load. This relaxation behavior was not clear cut and will require more detailed study. The surface measurements on these samples indicated that this was not a very pronounced effect in this alloy and it could be just outside the resolution threshold of this ultrasonic technique.

Conclusions

1. Rest periods at zero load following a tensile peak overload had a slight influence on subsequent fatigue crack retardation in 2024-T851 aluminum alloy. For the conditions examined, the number of delay cycles (N_D) decreased slightly as the rest time was varied between 3 min and 24 h.

2. The zero load rest periods also had a slight influence on surface measurements of the effective stress intensity range ratio U. Tensile peak overloads initially decrease U below the steady-state value. As the rest time at zero load was increased from 3 min to 24 h, U gradually returned to the original value prior to the overload.

3. Varying specimen thickness from 0.64 to 2.54 cm had no appreciable effect on N_D or surface measured values of U.

4. Although the surface measured values of U decreased following an overload as suggested by the closure model, the change was not of sufficient magnitude to cause the actual amount of crack retardation. As U increased with rest time, there was a corresponding decrease in N_D. The fact that measurable fatigue crack retardation remained after a 24-h rest period when U had returned to its initial steady-state value further indicates that the closure model does not completely account for surface measured crack delay.

5. Ultrasonic measurements of the internal crack behavior raise basic questions regarding application of the closure model to predict crack delay in the specimen interior. Although these measurements are preliminary in nature, they tend to support other published observations. Thus, the authors suggest that future research be directed toward understanding the complex relation between surface and internal measurements of fatigue crack retardation.

Acknowledgments

The authors appreciate the assistance of M. B. Strope and G. E. Mescher with the experiments. W. N. Sharpe, Jr., very gratefully acknowledges the support of the National Research Council and the Air Force Materials Laboratory while on sabbatical from Michigan State University.

References

[*1*] Elber, W. in *Damage Tolerance in Aircraft Structures, ASTM STP 486*, American Society for Testing and Materials, 1971, pp. 230–242.

[*2*] Wheeler, O. E., *Journal of Basic Engineering, Transactions*, ASME, Vol. 94, Series D, No. 1, March 1972, pp. 181–186.

[*3*] Willenborg, J., Engle, R. M., and Wood, H. A., "A Crack Growth Retardation Model Using an Effective Stress Concept," AFFDL-TM-71-1-FBR, Air Force Flight Dynamics Laboratory, Wright-Patterson AFB, Ohio, Jan. 1971.

[*4*] Gray, T. D. and Gallagher, J. P., "Predicting Fatigue Crack Retardation Following a Single Overload Using a Modified Wheeler Model," presented at the Eighth National Symposium on Fracture Mechanics, Brown University, Providence, R.I., 26–28 Aug. 1974.

[*5*] Christensen, R. H., *Metal Fatigue*, McGraw-Hill, New York, 1959, pp. 376–412.

[*6*] Wei, R. P., Shih, T. T., and Fitzgerald, J. H., "Load Interaction Effects on Fatigue Crack Growth in Ti-6Al-4V Alloy," NASA CR-2239, National Aeronautics and Space Administration, Washington, D.C., April 1973; also Wei, R. P. and Shih, T. T., *International Journal of Fracture Mechanics*, Vol. 10, 1974, p. 77.

[*7*] Sharpe, W. N., Jr., and Grandt, A. F., Jr., "A Laser Interferometric Technique for Crack Surface Displacement Measurements," *Proceedings*, 20th International Instrumentation Symposium of the Instrument Society of America, Albuquerque, N.M., May 1974; also published as Technical Report AFML-TR-74-75, Air Force Materials Laboratory, Wright-Patterson AFB, Ohio.

[*8*] Sharpe, W. N., Jr., and Grandt, A. F., Jr., "A Preliminary Study of Fatigue Crack Retardation Using Laser Interferometry to Measure Crack Surface Displacements," *Mechanics of Crack Growth, ASTM STP 590*, American Society for Testing and Materials, to be published.

[*9*] Shih, T. T. and Wei, R. P., "A Study of Crack Closure in Fatigue," NASA CR-2319, National Aeronautics and Space Administration, Washington, D.C., Oct. 1973; also Shih, T. and Wei, R. P., *Engineering Fracture Mechanics*, Vol. 6, 1974, p. 19.

[*10*] Pitoniak, F. J., Grandt, A. F., Montulli, L. T., and Packman, P. F., *Engineering Fracture Mechanics*, Vol. 6, No. 4, Dec. 1974, pp. 663–670.

[*11*] Buck, O., Ho, C. L., and Marcus, H. L., *Engineering Fracture Mechanics*, Vol. 5, No. 1, Feb. 1973, pp. 23–34.

DISCUSSION

R. I. Stephens[1] *(written discussion)*—Your results indicate that hold or rest time at zero load following a single tensile overload have little influence on crack delay. You also indicate thicknesses from 6.4 to 25.4 mm have little influence on delay and surface crack opening stress intensity. Are these results due to plane strain conditions existing for all your thicknesses? What results would you expect for thicknesses of say 1 to 2 mm? Can you perform these additional tests for verification?

W. N. Sharpe, Jr., D. M. Corbly, and A. F. Grandt, Jr. (authors' closure)—As Professor Stephens indicates, all the specimen thicknesses considered here were sufficient for plane strain conditions based on the requirement $B \geq 2.5 (K_{Ic}/\sigma_{ys})^2$. Using fracture toughness and yield strength values determined for this plate of material in an earlier effort (Ref *8*) where $K_{Ic} = 23.2$ MN/m$^{3/2}$ and $\sigma_{ys} = 448$ MN/m^2, the minimum thickness for plane strain fracture toughness is 6.7 mm. Since all testing was done at loads less than K_{Ic} it would be reasonable to assume that plane strain conditions also prevailed for the 6.4-mm-thick specimens tested here. We have not tested thinner specimens. The 1 to 2-mm-thick specimens suggested by Professor Stephens would be difficult to test with the specimen geometry and ultrasonic techniques employed here. Although we would not care to speculate on the results with thinner specimens, perhaps the following discussion by Dr. Chanani will assist in understanding the closure behavior for thinner specimens.

G. R. Chanani[2] *(written discussion)*—The crack closure results presented by the authors, even though contrary to most of the reported results indicating importance of crack closure in retardation, are in agreement with our results.[3] We used electrical potential and strain gage techniques for crack closure measurements before and after an overload cycle during the delay period. The strain gage technique met the "hysteresis loop" criteria for sensitivity as described by Elber. For the specimen geometry (0.063-in. SEN), alloy (7075-T6), and instrumentation used, we did not measure significant changes in crack closure as the cycling progressed after the overload cycle (Fig. 8). The small change was not enough to explain the delay. However, after relaxation for 16 h, as well as after a high overload ratio, significant crack closure was observed by the potential method (Fig. 9). This crack closure disappeared within 200 cycles. Nevertheless, the overall conclusion from these preliminary observations was that no substantial changes in crack closure were taking place to account for

[1] Materials Engineering Division, The University of Iowa, Iowa City, Iowa 52242.

[2] Northrop Corporation, Hawthorne, Calif. 90250.

[3] Chanani, G. R. and Mays, B. J., "Observation of Crack-Closure Behavior After Single Overload Cycles in 7075-T6 SEN Specimens," submitted for publication in *Engineering Fracture Mechanics.*

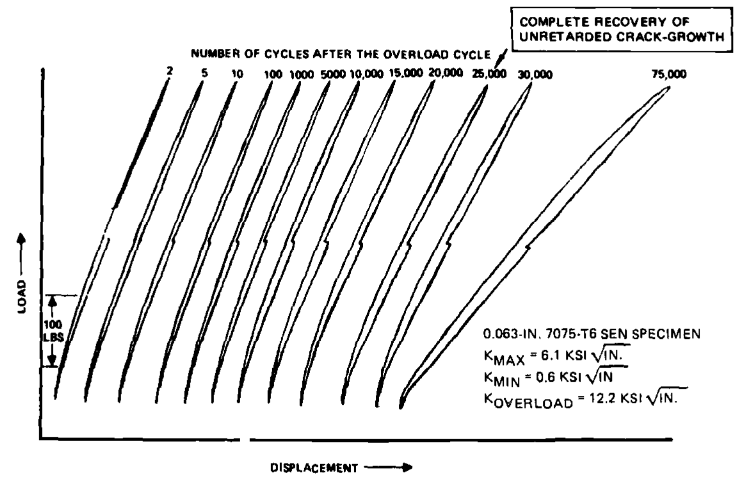

FIG. 8—*Load versus displacement at intervals during fatigue testing; overload ratio of 2.*

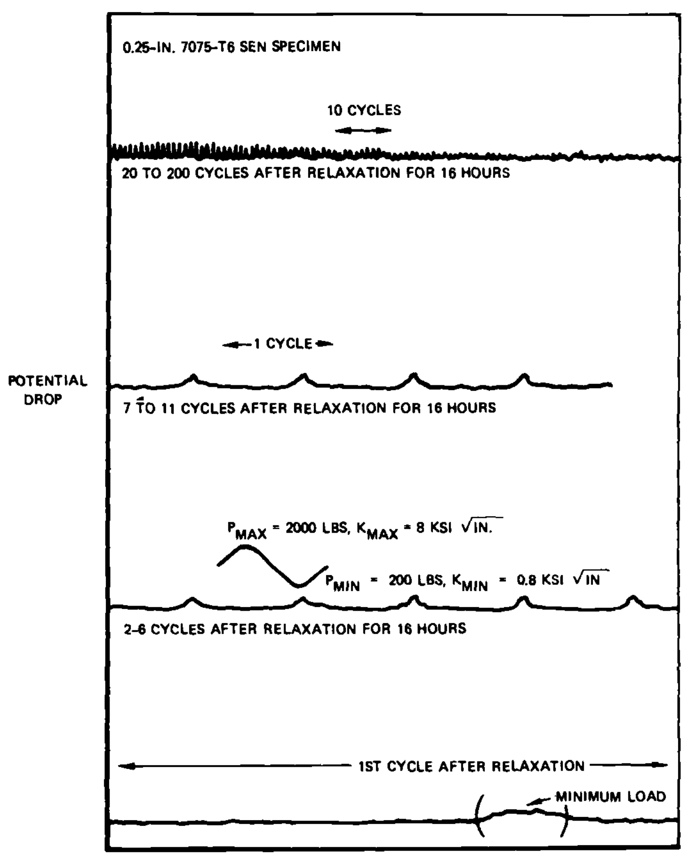

FIG. 9—*Effect of relaxation of crack closure.*

the observed number of delay cycles. These preliminary observations which appear contrary to the results described in the past and at this symposium are in agreement with your basic conclusion. However, we feel that these results are applicable to the alloy, specimen geometry, thickness, and sensitivity of the instrumentation used in this investigation. Further work is needed before definite conclusions can be reached.

W. N. Sharpe, Jr., D. M. Corbly, and A. F. Grandt, Jr. (authors' closure)—The authors find Dr. Chanani's results interesting and thank him for supplying a preprint of the paper from which his comment is excerpted. Based on these results, it is interesting to note that four different experimental approaches for measuring closure lead to similar conclusions regarding the apparent inability of the crack closure mechanism for completely explaining observed retardation. The authors would agree with Dr. Chanani that much more work needs to be done in this complex area.

P. J. Bernard,[1] *T. C. Lindley,*[2] *and C. E. Richards*[2]

Mechanisms of Overload Retardation During Fatigue Crack Propagation

REFERENCE: Bernard, P. J., Lindley, T. C., and Richards, C. E., "**Mechanisms of Overload Retardation During Fatigue Crack Propagation,**" *Fatigue Crack Growth Under Spectrum Loads, ASTM STP 595,* American Society for Testing and Materials, 1976, pp. 78–97.

ABSTRACT: The effect of single overloads on room-temperature fatigue crack growth has been studied in two steels of markedly different yield stresses. The observed retardation effects have been presented and the evidence suggests that overload retardation is primarily due to residual compressive stresses generated in the crack tip region, and associated with crack closure effects. The results have been rationalized in terms of a fatigue crack growing through overload plastic zones of different shapes and sizes associated with plane stress and plane strain deformation.

KEY WORDS: crack propagation, fatigue (materials), loads (forces), retarding, plastic deformation

There are many reports in the literature that "overloading" a cracked specimen reduces the crack growth rate or arrests the crack, for example, Jones [*1*],[3] Jonas and Wei,[*2*] etc. Many structures are overloaded for other reasons, for example, during proof tests on pressure vessels which may contain weld and other defects, or overspeed testing of rotating machinery [*3,4*]. Overloading a component or structure is therefore a possible method of providing protection from fatigue failure. The retardation, or arrest of fatigue cracks, is not cited as a major reason for proof testing, perhaps because of the quantitative, and even qualitative uncertainties in overload effects reported in the literature and the absence of fundamental understanding of the mechanisms. The following models have been proposed in an attempt to explain retardation following single overloads or high-low amplitude block loading sequences:

1. residual compressive stresses at or near the crack tip [*5–7*] and associated yield zone interaction effects [*8*],
2. crack closure [*9–11*],
3. crack tip blunting [*12*], and
4. crack tip strain hardening [*1*].

The purpose of this investigation was to study the effect of a single overload in

[1] Now research metallurgist, Electricity Supply Board, Dublin.

[2] Research officers, Central Electricity Research Laboratories, Leatherhead, United Kingdom.

[3] The italic numbers in brackets refer to the list of references appended to this paper.

a detailed and systematic manner to increase our understanding of the mechanisms of overload retardation and thereby to relate laboratory data to service conditions with greater confidence.

Fatigue crack propagation testing is usually carried out under either constant load or constant stress intensity. In constant load tests, the maximum and minimum loads in the fatigue cycle, P_{max} and P_{min}, are kept constant. In the majority of fracture mechanics specimens, the maximum and minimum stress intensities, K_{max} and K_{min}, increase with increasing crack length giving a steadily increasing propagation rate and, hence, a curve, when crack length is plotted against number of cycles (Fig. 1*a*(ii)).

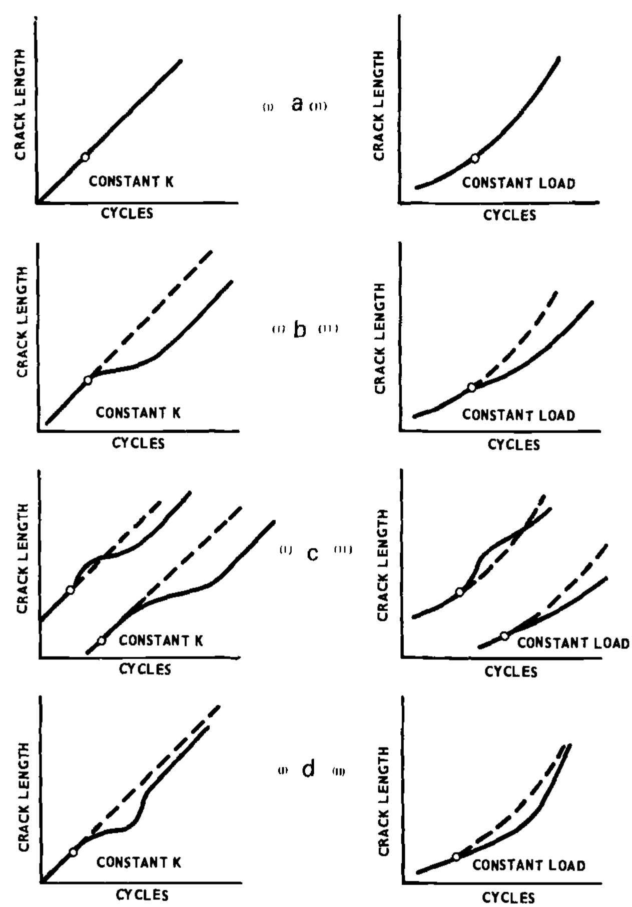

FIG. 1—The different types of fatigue crack growth retardation behavior: (a) no effect, (b) retardation, (c) delayed retardation, and (d) lost retardation.

During a constant K test the maximum and minimum loads are reduced in steps that are sufficiently small ($\sim$2.5 percent of K_{max}) to avoid transient effects. When crack length is plotted against number of cycles in this type of test a straight line is obtained (Fig. 1*a*(i)). For given ΔK and K_{max} conditions, the fatigue crack growth rates obtained by the two methods will be the same.

In overload work, constant stress intensity testing has obvious advantages, in that deviation from the straight line plot of crack length versus cycles (Fig. 1) is more easily detected than deviation from a curve obtained under constant load conditions. The present work involved constant stress intensity testing.

Types of Single Overload Effect

The types of single overload effects that have been observed are discussed in this section.

No Effect

Small overloads generally have no detectable influence on fatigue crack growth (see, for example, Jones [*1*], Jonas and Wei [*2*]). Curves of the type shown in Fig. 1*a* are obtained. The threshold level, the lowest overload level at which significant retardation occurs, is generally around 40 to 60 percent overload [*1*] relative to the baseline $K_{\ell max}$,

$$\left[\% \text{ overload} = \frac{K_{hmax} - K_{\ell max}}{K_{\ell max}} \times 100\right]$$

but lower values have been reported [*13*]. There is apparently no explanation for this variation in threshold level.

Retardation

Almost all investigations have revealed that retardation occurs above a threshold overload value in all materials and specimen geometries so far tested. Several empirical expressions have been proposed which quantify the retardations observed for particular specimen geometries, materials, and loading conditions [*1,8,9,14,15*], but few attempts have been made to obtain a generalized expression. Simple retardation is shown in Fig. 1*b*.

Delayed Retardation

The phrase "delayed retardation" has apparently been used to describe two different phenomena, Fig. 1*c*. It has been used to describe an increase in propagation rate immediately following an overload application, followed by retardation [*13,16*]. Delayed retardation has also been described simply as a delay (Fig. 1*c*) after an overload, prior to retardation [*17*]. It has been proposed that a crack extends by brittle fracture in the center region of a specimen on overloading [*5*] and this could account for an apparent increase in rate, thus masking an immediate retardation.

Delayed retardation does not always occur, and some authors have provided evidence of an immediate decrease in propagation rate [*6,18*].

Lost Retardation

Lost retardation is retardation followed by acceleration to a rate higher than the baseline rate before returning to the original rate (Fig. 1*d*). This effect has only been observed by the present authors and will be described more fully later in the text.

Most investigators have studied constant load specimens [*1,5,17,18*] and under these circumstances, lost retardation would be difficult to detect, since the crack accelerated continuously with increasing crack length.

Arrest

Complete arrest has been reported in the literature [*1,13*], but there is evidence that the crack may propagate very slowly at a rate undetected by the crack-following technique [*18*].

In general, the previous responses to overloads with increasing overload levels are likely to occur in the following order: (*a*) no effect, (*b*) retardation, (*c*) delayed retardation, (*d*) lost retardation, and (*e*) "arrest," but one or more may be absent. All of these effects, with the possible exception of complete arrest, have been observed during this investigation.

Experimental

Two steels with contrasting yielding and strain hardening characteristics were examined, a low alloy pressure vessel steel, Ducol W30B, and a "corrosion resistant" high strength steel, FV520B. The composition and mechanical properties are summarized in Table 1.

TABLE 1 – *Material composition and mechanical properties at 20°C.*

	C	Mn	Ni	Cr	Mo	V	Cu	Nb	σ_{ys} (MNm^{-2})	σ_u (MNm^{-2})	% Elongation
Ducol W30B	0.12	1.17	0.8	0.6	0.26	0.08	0.13	...	366	534	38
FV520B	0.04	0.92	5.6	15.1	1.35	...	1.8	0.2	940	1110	20

The Ducol was normalized at 920°C and tempered at 640°C for 3 h. The FV520B was normalized for 30 min at 1050°C, air-cooled to 800°C, and held at 800°C for 2 h before air-cooling to 20°C. Finally, it was tempered at 450°C for 4 h.

Compact tension (CKS) test pieces were machined with all the dimensions as for a 25-mm thick specimen, except for the thickness which was varied from 1 to 25 mm. The ratio $H/W = 0.6$ where $2H$ was the specimen height and W the width measured from the pin-hole centers.

The crack length in side-grooved specimens [*19*] was measured by a d-c potential drop method [*20*]. In specimens without side-grooves, crack lengths were measured optically using 1-mm grid lines scribed on the .pre-polished surfaces, several specimens being monitored by both methods. One 75-mm thick CKS specimen of Ducol W30B with no side-grooving was also tested and was monitored optically on both faces and at the center of the crack front by an ultrasonic technique. When two methods of crack length measurements were used on a single specimen, the surface readings were used for calculating loads and stress intensities. Optical crack length measurements were estimated to within 0.1 mm, and potential drop readings to ±0.1 mm. The ultrasonic technique could locate the crack tip position to within ±0.5 mm. Changes in crack length of 0.2 mm could however be detected.

All fatigue cycling was performed on servohydraulic machines at a frequency of 1 Hz for the 75-mm-thick CKS specimen, and at 3 Hz for all the other specimens. Baseline cycling was carried out under "constant" ΔK and K_{max} conditions, the maximum stress intensity, K_{max}, and minimum stress intensity, K_{min}, being maintained to within ±2.5 percent by reducing the loads every 0.5 mm of growth (discussed earlier). Cracks were initiated from spark machined notches, and baseline

$$\Delta K = 30\ \mathrm{MNm}^{-3/2}; R = \frac{K_{\ell min}}{K_{\ell max}} = 0.05$$

propagation rates were established, usually over a distance of 4 mm, before the first overload. In many cases, several single overloads were applied to one specimen provided that the baseline crack growth rate could be reestablished following previous overloads. Overload levels were held for 30 s, and the load returned to $K_{\ell min}$ before fatigue cycling was continued. Overloads were usually applied in an increasing series, starting with an overload at 40 $\mathrm{MNm}^{-3/2}$, and subsequently raising this by increments of 10 $\mathrm{MNm}^{-3/2}$.

In some cases a single specimen was overloaded to the same K_{hmax} at different crack lengths in order to establish whether the ratio, a/W, of crack length, a, to specimen width, W, influenced the degree of overload retardation.

Stress intensities were calculated from the tables of Walker and May, [*21*] and load modifications for side-grooving as described by Freed and Krafft [*19*].

Results

Shapes of Curves

Figure 2 (Curve A) is representative of the results obtained on FV520B and shows a sharp decrease in rate immediately following an overload. During the retarded period, the crack grew at a very low, but measurable rate, for periods which increased with increasing overload level. At the end of the retarded growth rate region the rate abruptly reverted to the baseline rate, except at an overload of 80 $\mathrm{MNm}^{-3/2}$ where the behavior was similar to that observed for Ducol.

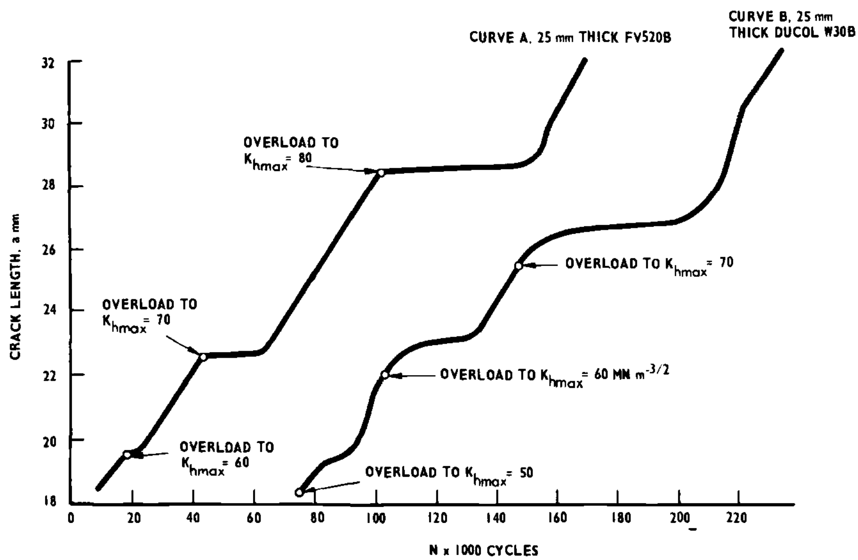

FIG. 2—*Typical crack growth retardation curves for 25-mm-thick Ducol and FV520B steels.*

Figure 2 (Curve B) shows a curve representative of the softer Ducol W30B steel. There are several differences in response compared to the high strength FV520B.

1. The transitions from baseline to retarded rate, and retarded to baseline rate were gradual in contrast to the FV520B.
2. The rates in the retarded position were higher than for the FV520B, even though the baseline rates for the two steels were very similar.
3. There was a region following the application of the overload where the crack continued to grow at approximately the baseline rate before slowing down.
4. The rate of growth following the delay period was initially higher than the baseline rate (as measured on the surface of the specimen) before returning to the original rate (see earlier discussion).

The overload response due to changing specimen thickness and other variables are treated in the appropriate sections.

Threshold Effects

In both materials there existed a threshold overload level below which retardation was not detected. For a given specimen thickness, this threshold was higher in the higher yield stress FV520B (Table 2). The threshold level in the case of Ducol W30B decreased with decreasing thickness but was essentially independent of thickness in FV520B over the range of thicknesses tested (Table 2).

TABLE 2 – *Summary of overload retardation results.*

Specimen No.	Thickness (mm)	K_{hmax} Overload ($MNm^{-3/2}$)	Retardation Cycles (thousands)	Affected Crack Length (mm) (Δa^*)	Calculated-Overload Plane Stress Plastic Zone Size (mm) (Δa_c*)	Calculated-Overload Plane Strain Plastic Zone Size (mm) (Δa_c*)
DUCOL 14	75	40	3	1.8	3.8	1.27
	75	50	15	2.0	5.94	1.98
	75	60	38	2.4	8.55	2.85
	75	70	130	4.5	11.64	3.85
DUCOL 10	25	40	0	0	3.8	1.27
	25	50	10	1.5	5.94	1:98
	25	60	25	1.9	8.55	2.85
	25	70	50	2.6	11.54	3.85
DUCOL 11	19	40	0	0	3.8	1.27
	19	50	6	0.8	5.94	1.98
	19	60	40	1.8	8.55	2.85
	19	70	170	3.2	11.64	3.85
DUCOL 7	19	60	33	1.8	8.55	2.85
	19	60	29	2.2	8.55	2.85
	19	60	38	2.0	8.55	2.85
	19	60	29	1.7	8.55	2.85
DUCOL 2	19[a]	40	0	0	3.8	1.27
	19[a]	50	0	0	5.94	1.98
	19[a]	60	20	1.8	8.55	2.85
DUCOL 4	19	40	0	0	3.8	1.27
	19	50	6	1.0	5.94	1.98
	19	60	12	1.8	8.55	2.85

DUCOL 5	5	40	0	0	3.8	1.27
	5	50	40	2.9	5.94	1.98
	5	60	100	7.4	8.55	2.85
DUCOL 9	5	50	28	2.9	5.94	1.98
	5	50	27	2.4	5.94	1.98
	5	50	44	2.9	5.94	1.98
	5	50	15 GY	1.6	5.94	1.98
DUCOL 15	1	35	3	0.2	2.91	0.97
	1	40	7	0.3	3.8	1.27
	1	50	10 GY	0.4	5.94	1.98
FV520B-1	25[a]	40	0	0	0.58	0.19
	25[a]	50	0	0	0.9	0.30
	25[a]	60	4	0.3	1.30	0.43
	25[a]	70	12	0.8	1.82	0.61
	25[a]	80	50	1.3	2.30	0.77
FV520B-2	25	40	0	0	0.58	0.19
	25	50	1	0.1	0.9	0.30
	25	60	6	0.3	1.3	0.43
	25	70	17	0.3	1.82	0.61
FV520B-3	25	60	7	0.2	1.30	0.43
	25	80	50	0.3	2.30	0.77
FV520B-4	5	40	0	0	0.58	0.19
	5	50	0	0	0.90	0.30
	5	60	9	0.1	1.30	0.43
	5	70	22	0.1	1.82	0.61
	5	80	43	0.2	2.30	0.77

GY = general nett section yielding.

[a] Side grooving, crack length measured by d-c potential drop.

Effect of Overload Level

In both steels beyond the threshold, an increase in overload level was accompanied by an increase in retardation. The relationship between the percentage overload and retardation is not linear, as shown in Figs. 3 and 4, a given increment being progressively more effective as the overload level increases. However, limited results (Table 2) indicate that if the overload is sufficiently large to cause general (nett section) yielding, smaller retardations are obtained than for overloads within linear elastic conditions.

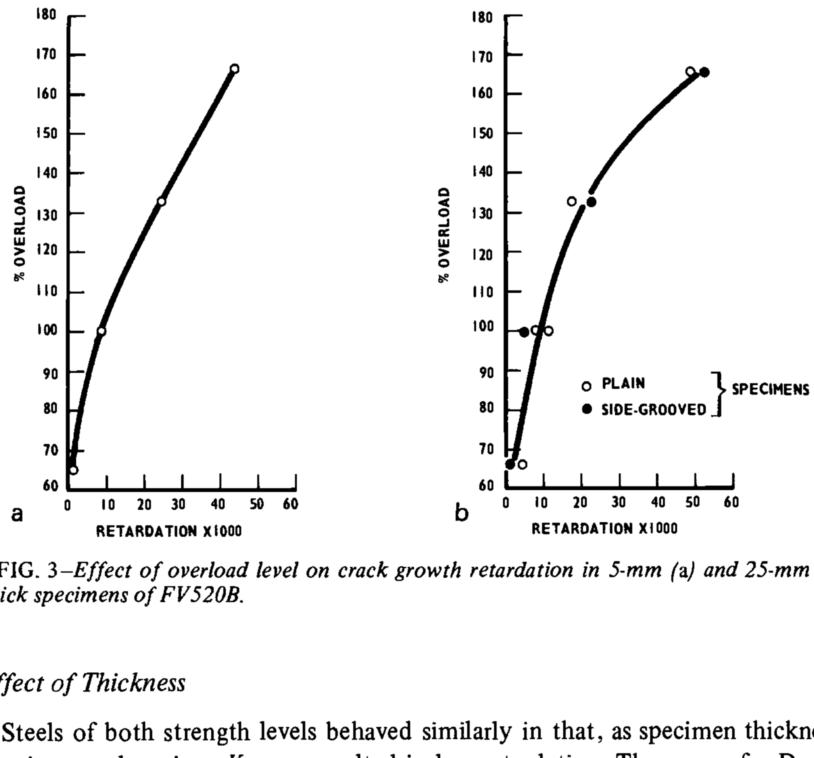

FIG. 3—*Effect of overload level on crack growth retardation in 5-mm (*a*) and 25-mm (*b*) thick specimens of FV520B.*

Effect of Thickness

Steels of both strength levels behaved similarly in that, as specimen thickness was increased, a given K_{hmax} resulted in less retardation. The curves for Ducol W30B are shown in Fig. 4.

Effect of Yield Stress

The higher yield stress material, FV520B, gave a smaller retardation than the low yield stress material for the same overload level and specimen thickness (Fig. 2).

Effect of Side Grooving

Table 3 gives details of the effect of side grooving on retardation. The lower overload levels gave less retardation in the side-grooved specimens than in the

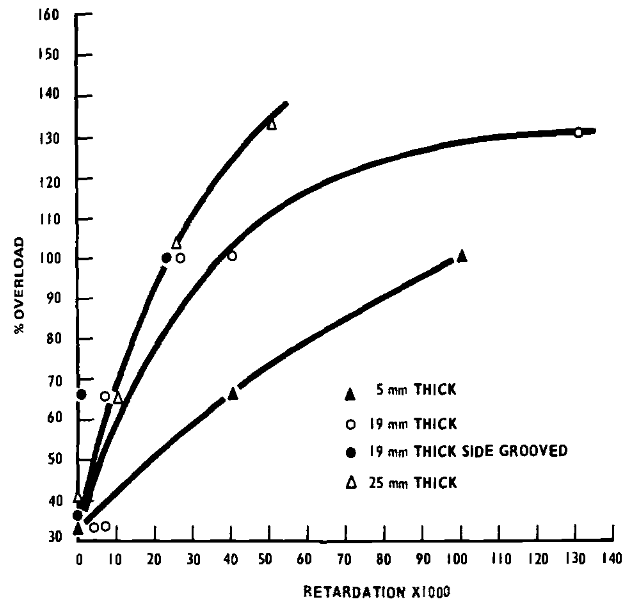

FIG. 4—*Effect of overload level on crack growth retardation in Ducol W30B specimens of various thicknesses.*

plane-sided specimens, although the effect is relatively small. At higher overload levels there was little difference.

TABLE 3 – *Effect of side-grooving on crack growth retardation (number of cycles lost) in Ducol W30B and FV520B.*

% Overload	Ducol W30B 19-mm Thick		FV520B 25-mm Thick	
	Plain Specimen	Side-Grooved	Plain Specimen	Side-Grooved
33	0[a]	0	0	0
66	6 000[a]	0	1 000	0
100	34 000[a]	20 000	6 500[a]	4 000
133	170 000	...	17 000	12 000
166	...	...	50 000	50 000

[a] Average of two or more results.

Effect of Crack Depth (a/W)

The retardations, in terms of cycles lost, obtained in the two specimens loaded to the same level at different crack lengths are shown in Table 4.

There was no systematic variation in retardation with crack length or a/W. The scatter in results shows a variation of 18 percent from the mean in the 19-mm

TABLE 4 – *The effect of* a/W *on overload retardation.*

Specimen	B (mm)	a/W	Overload (%)	Retardation
Ducol 7	19	0.360	100	33 000
	19	0.476	100	29 000
	19	0.653	100	38 000
	19	0.641	100	29 000
Ducol 9	5	0.380	66	28 000
	5	0.476	66	27 000
	5	0.548	66	44 000
	5	0.624	66	15 000 (GY)

GY = general yield.

specimen, and 33 percent from the mean in the 5-mm specimen, excluding the general yield overload.

For the largest overloads in Ducol specimens, plastic zone size corrections became significant. For example, in specimen Ducol 7 (see Table 4 and Fig. 5) overloaded to a nominal K_{hmax} value of 60 $\mathrm{MNm}^{-3/2}$ at four different values of a/W, K_{hmax} overload levels were estimated using surface measurements of plastic zone sizes. Assuming plane stress conditions, the corrected values of K_{hmax} were approximately 66, 70, and 75 $\mathrm{MNm}^{-3/2}$. Assuming the plastic zone in the center is about one third of that on the surface, the corresponding values were approximately 62, 63, and 64 $\mathrm{MNm}^{-3/2}$. The results for the overload at the largest a/W were just outside the ASTM calibration range and were therefore probably invalid.

For overloads in the high yield strength FV520B and for lower overloads in the softer Ducol material, the overload plastic zone size corrections were insignificant.

There was an indication (Table 4) that general (nett section) yielding of the specimen reduced the retardation, but further testing will be necessary.

75-mm Ducol W30B Specimen

The two crack growth curves shown in Fig. 6 are similar to the retardation Curves A and B in Fig. 2, characteristic of FV520B and Ducol W30B behavior, respectively. The center of the 75-mm Ducol W30B specimen behaved similarly to the FV520B material and the edge regions reflected thin Ducol W30B specimen behavior.

Under baseline ΔK conditions, the crack front in the 75-mm-thick Ducol W30B achieved an equilibrium curvature whereby the crack surface lagged behind the central regions by 6.8 mm (see Fig. 6). Following the application of a

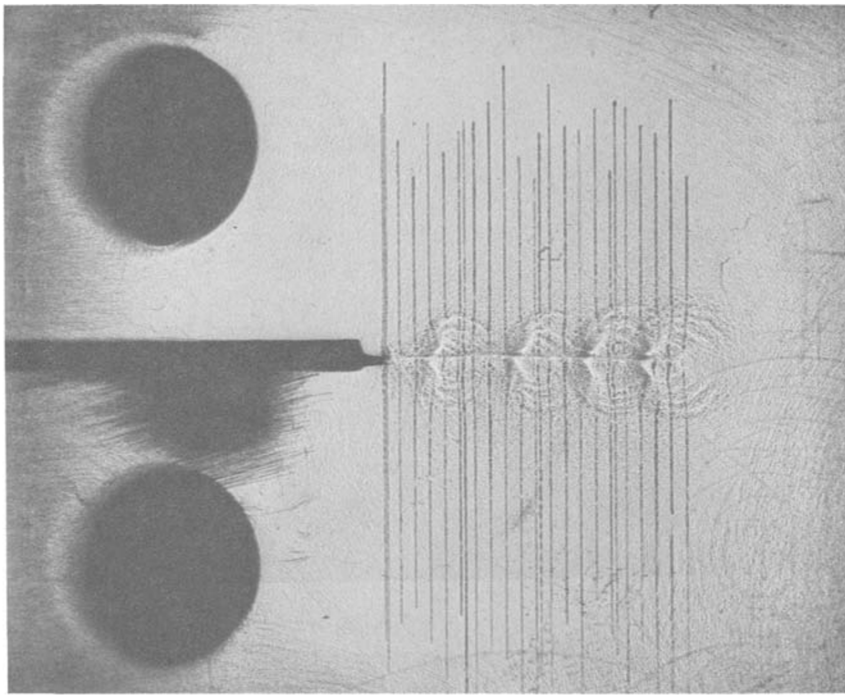

FIG. 5–*Surface of specimen Ducol 7 overloaded at different values of* a/W *to same overload* K_{hmax} *of 60* $MNm^{-3/2}$.

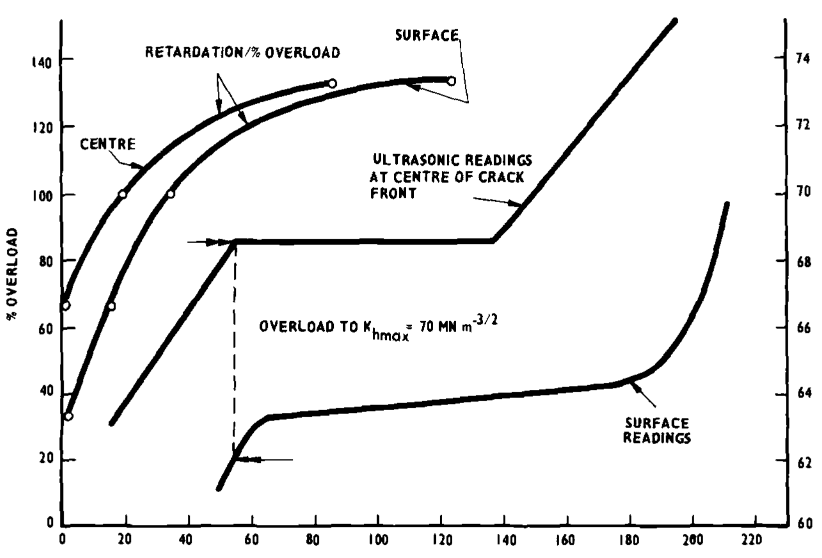

FIG. 6–*Surface and midthickness crack growth retardation in 75-mm-thick Ducol W30B.*

large overload, the curvature of the crack front initially decreased since retardation was immediate at the center but delayed at the surface. The curvature was further reduced by the more significant growth through the surface plane stress regions during retardation than through the central plane strain regions. However, since retardation is completed after a smaller number of cycles at the specimen center, the curvature then increased until retardation was completed at the surfaces. Thereafter, the curvature decreased toward the equilibrium curvature characteristic of the baseline fatigue conditions (lost retardation). It is noted that the constant K conditions were calculated from surface crack length measurements and that the shapes of the growth rate curves in Fig. 6 would have been different if the crack length at the center of the specimen had been used instead.

Macroscopic Fracture Appearance

The polished surface of a Ducol specimen overloaded at four different values of a/W to the same overload K_{hmax} of 60 $MNm^{-3/2}$ is shown in Fig. 5.

Examination of the fatigue fracture surfaces revealed a dark band associated with the application of each overload. These bands were well defined at high overload stress intensities but hardly discernible at low peak stress intensities. The shear lip was small in the retardation region and then increased gradually to approximately the original value found prior to the overload. This was reflected in a change in direction of crack propagation at the specimen surface (Fig. 7).

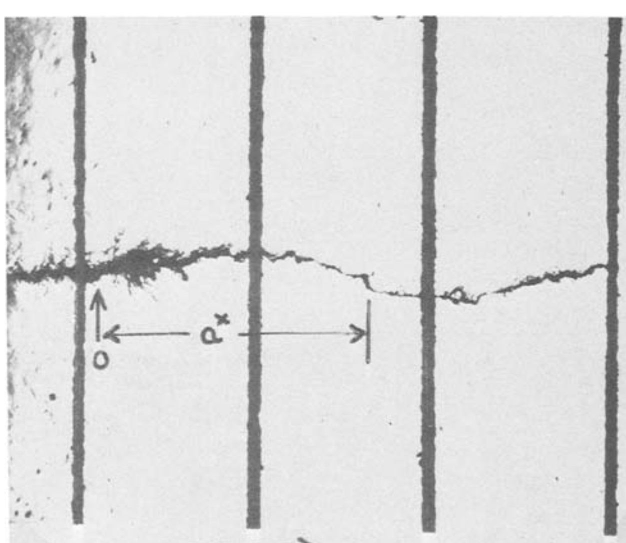

FIG. 7–*Effect of overload on crack growth at surface of Ducol W30B (x23).*

Discussion

Models for Crack Growth Retardation Following Overloads

Crack tip strain hardening has been discounted as a mechanism by Jones [1] following a study of overload effects on fatigue crack growth in pre-strained material.

It is argued that the importance of crack tip blunting is different in plane stress and plane strain situations, and it is convenient to consider separately the evidence for either case.

A crack tip blunting mechanism would suggest that the crack length affected by the overload, Δa^*, should be restricted to the crack tip region which is clearly not the case for plane stress surface measurements (Fig. 8*a*) where the affected crack length spans several millimetres.

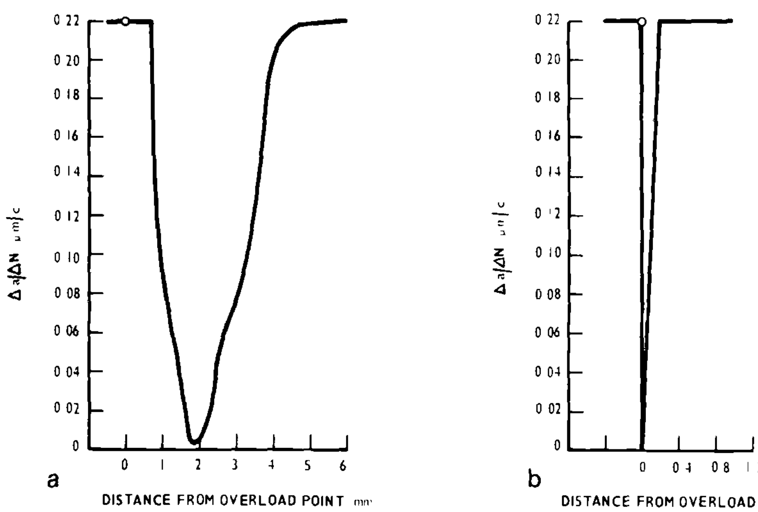

FIG. 8—*Growth rate through the overload retardation region for specimen Ducol 14 measurements at specimen surface (*a*) and center (*b*).*

In the present investigation, the only case where complete crack arrest could have occurred (and where crack tip blunting might be applicable) was at the center of the 75-mm-thick Ducol 14 (see previous section) which is under predominantly plane-strain conditions. The ultrasonic crack following technique was incapable of discriminating between arrest and very slow growth over a very short distance. The crack length affected by overloading (Fig. 8*b*) was much more localized than for the plane stress case. However, clip (displacement) gage measurements made immediately before and after a single overload on a Ducol 14 specimen indicate that an overload has no significant effect on edge opening displacement for this predominantly *plane-strain* situation. Furthermore, the shape of the retardation curve was similar to that for the high-strength FV520B with side notching. In this case, which was also predominantly plane strain, the crack-following technique (potential drop) was sufficiently sensitive to detect very slow, but perceptible, crack growth over the small affected distance. These observations are again inconsistent with a crack blunting model.

Preliminary results on overloads approaching general yield suggest a smaller retardation effect than for those applied at small values of a/W. Further work on retardation approaching and beyond general yield might increase our understanding of the relevance of crack tip blunting which would be more severe under these circumstances.

The results presented in Table 2, particularly those on the 75-mm-thick Ducol specimen, may be rationalized by proposing that retardation effects differ markedly between plane stress and plane strain conditions. It is proposed that compressive residual stresses generated in the overload plastic zone, accompanied by crack closure effects, are responsible for retardation and that the magnitude and distribution of these stresses are different in plane stress and plane strain. The variety of retardation effects described earlier are considered in terms of these differences and to the variation in constraint that can occur from the surface to the center of a test piece.

Following the arguments of Elber [*9*], it is probable that during growth through the overload plastic zone, the surface (plane stress) regions of the crack close above the minimum stress intensity K_{min} of the fatigue cycle. This is consistent with abrasion of the fracture surfaces previously observed where specimens were tested at larger values of ΔK [*11*]. At present, it is unclear if significant closure occurs in a predominantly plane-strain situation [*22*].

Residual Compressive Stress Mechanism for Overload Retardation

The residual stress levels were estimated by measuring the crack propagation rate at intervals during retarded growth after an overload (Fig. 8). The effective ΔK responsible for crack growth, ΔK_{eff}, is less than the applied ΔK, (ΔK_{app}), due to residual compressive stresses and consequent crack closure effects in the affected crack length region. Values of ΔK_{eff} were obtained from the standard $(da/dN)/\Delta K$ plots previously obtained for the two steels [*22*]. The magnitude of the residual stresses are reflected in the quantity ($\Delta K_{app} - \Delta K_{eff}$) which is plotted in Fig. 9 as a function of distance from the point of overload. Two types of curve were obtained, one characterizing plane stress deformation (Curve A in Fig. 9) and the other plane strain deformation (Curve B in Fig. 9). The plane strain plastic zone consists of two shear bands, inclined at 45° or more to the plane of the crack, with only a small region of plasticity ahead of the crack tip. By contrast, the maximum dimension of the plane stress zone is in the plane of the crack. The shapes of the plastic zones under monotonic loading have been illustrated schematically by Hahn et al [*23*] and directly by etch-pitting a high nitrogen steel (Griffiths and Richards [*24*], see Fig. 10). The residual stress patterns reflected by ($\Delta K_{app} - \Delta K_{eff}$) in Fig. 9 are qualitatively consistent with these plastic zones. Thus in predominantly plane-strain conditions, the retardation is immediate on application of the overload, and retarded growth occurs at a very slow rate over a small distance (Curve A in Fig. 2 and Fig. 8*b*). For plane

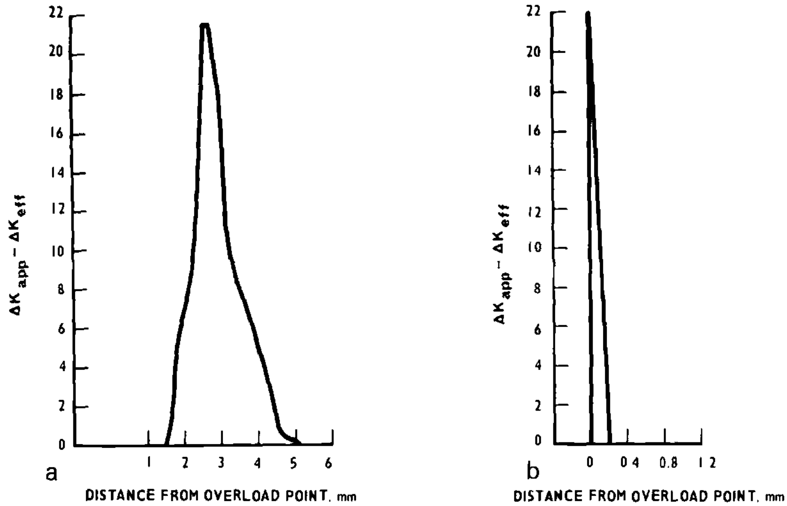

FIG. 9—$\Delta K_{baseline} - \Delta K_{effective}$ *as a function of distance from point of overload for specimen Ducol 14, (a) surface and (b) center.*

stress, the affected crack length after overload is more extensive and the rate of growth through the overload zone (Curve B in Fig. 2 and Fig. 8*b*) diminishes progressively to a minimum level, which is typically one quarter to one third of the affected crack length, before eventually returning to the "baseline" rate. This suggests that the maximum tensile strains and residual stresses after overloading are not at the crack tip. The crack growth rate over much of the affected crack length is significantly greater in plane stress (Fig. 8). This implies that residual stresses will generally be higher under predominantly plane strain conditions, and the present results are consistent with the view that residual stresses will increase with increasing yield stress, specimen thickness, and overload level (below general yield).

The monotonic plastic zone sizes, $2r_y$, due to overloading were calculated using the relation

$$\Delta a_c^* = 2r_y = \frac{2}{d\pi}\left(\frac{K_{hmax}}{\sigma_{ys}}\right)^2$$

where $d = 2$ for plane stress and 6 for plane strain given in Table 2. Not surprisingly, in view of the proposed importance of plastic zone shape, poor correlation was generally obtained between Δa_c^* (either plane stress or plane strain) and the measured affected crack length, Δa^*, which was usually appreciably less than Δa_c^* (Table 2). In terms of this simple comparison, better correlation would be expected for a plane stress situation than for plane strain. In fact, best correlation was found for 5-mm-thick Ducol (appreciable plane stress) and surprisingly for the 25-mm side-notched FV520B (predominantly plane strain). In calculating plastic zone sizes, the use of σ_{ys} allows no work-hardening and σ_u might be a more appropriate parameter, thereby

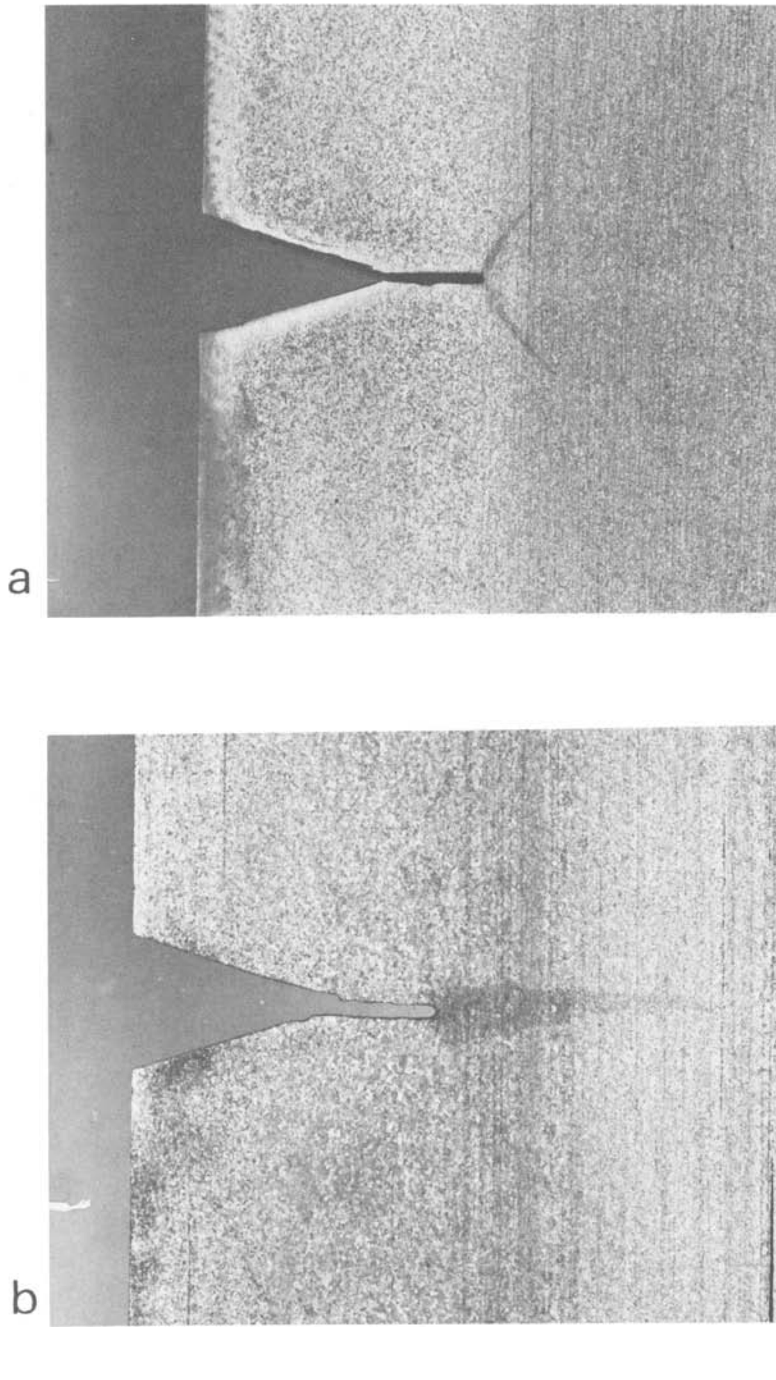

FIG. 10–*The plastic zones at the midthicknesses of (a) 24-mm and (b) 2-mm thick, double edge notched specimens of high nitrogen steel loaded to give the same nett-section stress (∿0.8 of the general yield stress) (x4).*

reducing Δa_c^* by 47 percent for Ducol and 72 percent for FV520B. In reality, a flow stress intermediate between σ_{ys} (giving an upper bound) and σ_u (lower bound) is probably relevant.

Further support for the residual stress mechanism was obtained by performing stress relieving experiments. An initial stabilizing treatment of 40 h at 640°C was performed to eliminate possible microstructural changes during stress relief of 25 and 5-mm Ducol specimens. In the 25-mm-thick specimen, a delay of 15 000 cycles was obtained following an overload of 50 $MNm^{-3/2}$. The same overload followed by stress relief anneal (2 h at 640°C), however, caused a delay of only 1000 cycles. Similarly, when a 5-mm-thick Ducol specimen undergoing what would normally have been an extensive retarded growth region was subjected to a stress relief anneal, continued cycling caused the growth rate to return abruptly to the baseline rate.

There is a minimum cyclic stress intensity, ΔK_0, below which fatigue cracks do not grow significantly. If the effective stress intensity ΔK_{eff} does not exceed ΔK_0 then the crack should arrest. These conditions were not achieved in this investigation where the baseline ΔK_ℓ of 30 $MNm^{-3/2}$ was relatively large and further tests are planned at smaller values of baseline ΔK_ℓ.

It was noted during this investigation that, with plane strain deformation, there was a definite threshold level which must be exceeded during the overload before significant retardation occurred. In both materials, this level was about 100 percent higher than $K_{\ell max}$ for the baseline fatigue cycling. In contrast, for conditions approaching plane stress, there appeared to be no clearly-defined threshold and small overloads ($\sim$20 percent) resulted in detectable retardation (Table 2). The prediction of fatigue life of a cracked component under variable-amplitude loading using the Paris [25] or other crack growth laws available in the literature will be more successful where the material is deforming under predominantly plain-strain conditions, since transient effects due to overloading will be absent (below the threshold) or minimal compared to plane-stress situations.

Conclusions

The various retardation effects resulting from the application of a single overload have been examined and discussed. The evidence suggests that overload retardation is primarily due to residual compressive stresses, generated in the crack tip region, and associated with crack closure effects. The results have been rationalized in terms of a fatigue crack growing through overload plastic zones of different shapes and sizes found for predominantly plane stress and plane strain deformation.

A threshold level existed below which retardation did not occur, and this level was higher for plane strain than plane stress. Above the threshold, the fatigue crack growth rate through the overload region was higher in plane stress than plane strain. The results are consistent with the view that residual stresses will increase with increasing yield stress, specimen thickness, and overload level (below general yield).

Acknowledgments

The work was carried out at the Central Electricity Research Laboratories and the paper is published by permission of the Central Electricity Generating Board.

References

[1] Jones, R. E., *Engineering Fracture Mechanics*, Vol. 5, 1973, pp. 585–604.
[2] Jonaš, O. and Wei, R. P., *International Journal of Fracture Mechanics*, Vol. 7, 1971, pp. 116–118.
[3] Nichols, R. W., *Pressure Vessel Engineering Technology*, Elsevier, 1971, p. 225.
[4] Nichols, R. W., *British Welding Journal*, 1968, Vol. 15, p. 21.
[5] Hudson, C. M. and Hardrath, M. F., NASA, TN D-1803, Aug. 1963.
[6] Hudson, C. M. and Raju, K.N., NASA, TN D-5702, March 1970.
[7] Schijve, J. and Broek, D., *Aircraft Engineering*, Vol. 34, 1962, p. 314.
[8] Wheeler, O. E., *Journal of Basic Engineering*, Vol. 4, 1972, pp. 181–186.
[9] Elber, W., *Engineering Fracture Mechanics*, Vol. 2, 1970, pp. 37–45.
[10] Elber, W., *Damage Tolerance in Aircraft Structures, ASTM STP 486*, American Society for Testing and Materials, 1971, p. 230.
[11] von Euw, E. F. J., Hertzberg, R. W., and Roberts, R., *Stress Analysis and Growth of Cracks, ASTM STP 513*, American Society for Testing and Materials, 1972, p. 230.
[12] Christensen, R. H., *Metal Fatigue*, McGraw Hill, New York, 1959.
[13] Corbly, D. M. and Packman, P. F., *Engineering Fracture Mechanics*, Vol. 5, 1973, pp. 479–497.
[14] Probst, E. P. and Hilberry, B. M., AIAA Paper No. 73-325, 1973.
[15] Schijve, J., *Advances in Aeronautical Sciences*, Pergamon Press, 1962, pp. 387–408.
[16] Vargas, L. G. and Stephens, R. I., *Proceedings*, Third International Conference on Fracture, Munich, Germany, Vol. VI, April, 1973.
[17] McMillan, J. C. and Hertzberg, R. W. in *Electron Fractography, ASTM STP 436*, American Society for Testing and Materials, 1968, pp. 89–123.
[18] McMillan, J. C. and Pelloux, R. M. N. in *Fatigue Crack Propagation, ASTM STP 415*, American Society for Testing and Materials, 1967, pp. 505–532.
[19] Freed, C. N. and Krafft, J. M., *Journal of Materials*, Vol. 1, 1966, p. 770.
[20] Ritchie, R. O., Garrett, G. G., and Knott, J. F., *International Journal of Fracture Mechanics*, Vol. 7, 1971, pp. 462–467.
[21] Walker, E. F. and May, M. J., BISRA Report, MG/E/307/67, 1967.
[22] Lindley, T. C. and Richards, C. E., *Materials Science and Engineering*, Vol. 10, 1972, p. 235.
[23] Hahn, G. T., Hoagland, R. G., and Rosenfield, A. R., Battelle Final Technical Report, AR-016067, 1971.
[24] Griffiths, J. R. and Richards, C. E., CERL Report, RD/L/N 132/72, 1972.
[25] Paris, P. C. and Erdogan, F., *Transactions*, American Society of Mechanical Engineering, Vol. 85, 1963, p. 528.

DISCUSSION

R. I. Stephens[1] *(written discussion)*—Your results indicated the lower yield strength steel had greater crack retardation than the higher strength steel for a given overload and thickness with $R_\ell = P_{\ell\min}/P_{\ell\max} > 0$. Based upon greater cyclic plasticity in the lower yield strength steel, I might think the opposite effect could occur with $R_\ell = -1$. That is, residual stresses and crack closure can

[1] Materials Engineering Division, The University of Iowa, Iowa City, Iowa 52242.

be more readily removed in the lower yield strength steel—we are currently investigating this behavior. Could the authors comment on this?

P. J. Bernard, T. C. Lindley, and C. E. Richards (authors' closure)—We have no results concerning the effect of overloads on retardation for baseline tension-compression cycling ($R_\ell = -1$). However, we suspect that residual stresses and crack closure can indeed be more readily removed in a lower yield strength steel, for a given overload and thickness. We look forward to the results of your investigation.

Simple Spectra: Environmental Effects and Modeling

Otto Buck,[1] *J. D. Frandsen,*[1] *and H. L. Marcus*[2]

Spike Overload and Humidity Effects on Fatigue Crack Delay in Al 7075-T651

REFERENCE: Buck, Otto, Frandsen, J. D., and Marcus, H. L., **"Spike Overload and Humidity Effects on Fatigue Crack Delay in Al 7075-T651,"** *Fatigue Crack Growth Under Spectrum Loads, ASTM STP 595*, American Society for Testing and Materials, 1976, pp. 101–112.

ABSTRACT: This paper describes experiments on fatigue crack growth, $\Delta a/\Delta N$, in part-through crack specimens of 7075-T651 aluminum alloy. The effects of dry and humid environment in combination with single-spike overloads on $\Delta a/\Delta N$, the crack growth delay, N_D, and the "effective" stress intensity range, ΔK_{eff}, are discussed. Using an acoustic monitoring technique, it was observed that the crack closure not only reflects the influence of the environment, but also of the spike overload on the plastic deformation at the crack tip and therefore on $\Delta a/\Delta N$. The relationship $\Delta a/\Delta N = A\ (\Delta K_{eff})^n$ describes both environmental and spike overload effects, uniquely. Delay is more pronounced in a dry environment and increases strongly with increasing overload ratio.

KEY WORDS: crack propagation, fatigue (materials), aluminum alloys, humidity, plastic deformation

Delay, or retardation, of the fatigue crack growth rate due to tensile overloads is an important phenomenon in that the fatigue life of a structure can be increased by the overloads. Only recently, however, have systematic studies been aimed at the phenomenology of the process [*1–8*].[3] Corbly and Packman [*4*] have summarized many of the observations that are generally agreed upon in various investigations and, therefore, a review will not be repeated here.

It has recently been indicated [*3,5,7*] that crack closure [*9*] is a likely model to quantitatively explain delay effects. Trebules et al [*5*] indeed have shown the great potential of crack closure by using the Elber equation [*9*] to explain their data. This paper describes results from closure measurements made directly before, during, and after application of single overload spikes using an acoustic technique [*10*] which was previously used to study the effects of overload

[1] Group leader and senior staff associate, respectively, Science Center, Rockwell International, Thousand Oaks, Calif. 91360.

[2] Formerly, group leader, Science Center, Rockwell International, Thousand Oaks, Calif. 91360; now, professor, Mechanical Engineering Department, University of Texas, Austin, Tex. 78712.

[3] The italic numbers in brackets refer to the list of references appended to this paper.

blocks on fatigue crack delay. Also, if crack closure is important in explaining delay, one might expect large effects of mildly aggressive environments on the delay since an environment can change the crack closure stress and the crack propagation rate severely [*11*]. Thus, it was decided to check these hypotheses on the aluminum alloy 7075-T651 and apply single-spike overloads in dry and humid gaseous environments. The results of this investigation are reported in this paper.

Experimental Procedures

To study both load spike and environmental effects on fatigue crack growth, the aluminum alloy 7075-T651 with a nominal yield stress $\sigma_{ys} \approx 480$ MN/m^2 was selected since its fatigue crack propagation rate is known to be very sensitive to humidity [*11*]. Specimen geometry was of the part-through crack (PTC) type (1.25 cm thick, 10 cm wide) with a semi-elliptical starter notch (1.3 mm deep and 6 mm long). The starter notch was covered with a glass bell filled with flowing dry nitrogen or moist air.

All experiments were performed in tension-tension loading with the load axis perpendicular to the starter notch (Mode I). A sinusoidal gross section stress with a maximum amplitude $\sigma_{\ell max} = 0.225\sigma_{ys}$ and a load ratio $R = (\sigma_{\ell min}/\sigma_{\ell max}) = 0.1$ was applied until a crack depth of about 0.2 to 0.4 cm was obtained. At this time a single sinusoidal load spike with an overload ratio $\sigma_{hmax}/\sigma_{\ell max}$ of either 2.0 or 2.5 was applied using a paper-tape controlled arbitrary function generator. Thereafter, the program reverted to the previous stress conditions. During all measurements of crack depth and closure, the stress was cycled at a rate of 0.1 s^{-1} and in between measurements at 5 s^{-1}.

The acoustic device for monitoring crack depth and crack closure has been described in several previous publications [*10–13*]. The device was positioned across the starter notch and mounted within a glass bell [*11*]. Crack growth and crack closure produce changes in the acoustic wave attenuation which result in a direct measurement of true and "apparent" crack depth.

After fracture of each specimen, the fatigue crack growth region of the fracture surfaces was examined by scanning electron microscopy (SEM) and by replicas in the transmission electron microscope (TEM) to characterize the fatigue fracture morphology.

Results

Crack depth measurements obtained from acoustic wave attenuation on five specimens are shown in Fig. 1 as a function of the number of fatigue cycles applied. In four of the cases the humidity was well controlled (0 to 80 percent relative humidity (RH)); in the fifth case, the humidity was about 10 percent RH at the beginning and dropped to 0 percent towards the end of the experiment. Some of the effects observed on the fifth specimen were more pronounced than they were in the other four samples, but this is more likely the

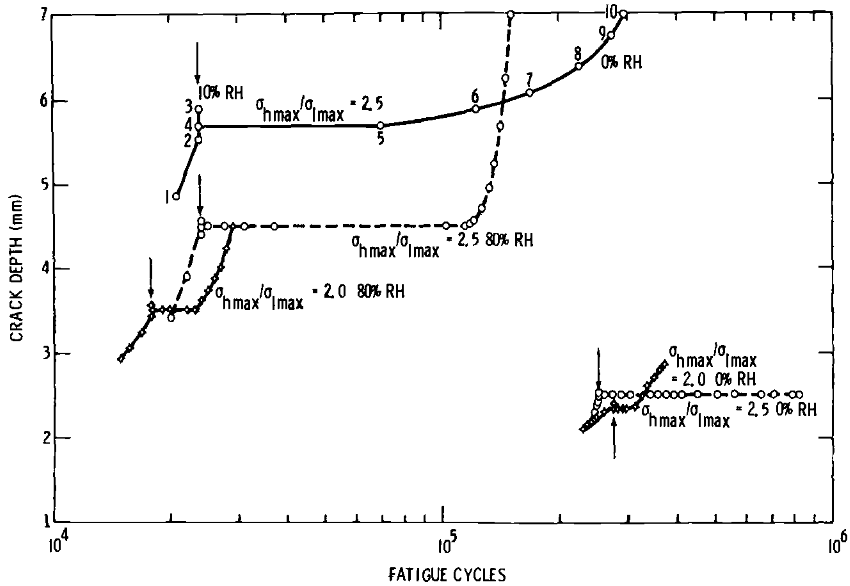

FIG. 1—*Crack depth versus number of fatigue cycles. Arrows indicate application of the overload spike.*

result of the slightly higher K levels involved rather than the variation within the environment.

The four experiments with controlled relative humidity were performed as outlined in the previous section. Fatigue cycling at $\sigma_{\ell max} = 0.225\sigma_{ys}$ and $R = 0.1$ established an initial crack propagation rate, $\Delta a/\Delta N$, which was appreciably higher at 80 percent RH than at 0 percent RH (dry N_2). After a number of fatigue cycles in this initial condition, a single-spike overload of amplitude σ_{hmax} with ($\sigma_{hmax}/\sigma_{\ell max}$) equal to either 2.0 or 2.5 was applied (indicated by arrows in Fig. 1) in both humidity conditions. The crack growth was delayed for a certain number of fatigue cycles, N_D, before further growth occurred. The end of the delay can easily be detected using the acoustic technique since the signal strength starts to drop again. In one case, after application of the overload ratio $\sigma_{hmax}/\sigma_{\ell max} = 2.5$ at 0 percent RH, the specimen broke in the grip section after fatigue cycling for 560 000 cycles without resumption of crack growth. All external parameters as well as the results on these four experiments are listed in Table 1. Also included are the stress intensity range, ΔK, just before the overload and the corresponding effective stress intensity range, ΔK_{eff}, as deduced from crack closure data [10] on these specimens. ΔK_{eff} has been derived using the following extrapolation method [10]. Before and during application of the overload ΔK_{eff} is defined to be proportional to ($\sigma_{\ell max} - \sigma_{op}$), with σ_{op} being the closure load (and equal to the opening load, since no hysteresis was observed) given by the intersection of the tangents to the two extreme segments of the closure curves. Although the ΔK levels prior to

TABLE 1 – *Fatigue crack growth before application of various overloads, ΔK, ΔK_{eff}, and delay data for four experiments with well controlled humidity (see Fig. 1).*

$\sigma_{hmax}/\sigma_{\ell max}$	Relative Humidity (%)	a_0(mm), Initial Crack Length	$\Delta a_0/\Delta N$ (μm/cycle), Prior to Overload	ΔK(MNm$^{-3/2}$), Prior to Overload	ΔK_{eff}(MNm$^{-3/2}$), Prior to Overload	N_D
2.0	0	2.35	0.012	7.60	3.88	24 000
2.0	80	3.50	0.20	8.59	6.18	5 000
2.5	0	2.50	0.019	7.71	3.31	>560 000
2.5	80	4.50	0.25	9.14	6.03	93 000

overload were not quite the same for the four specimens, Table 1 demonstrates:

1. $\Delta a_0/\Delta N$ and ΔK_{eff} increase as relative humidity increases in agreement with Ref *11*,
2. N_D increases as $\sigma_{hmax}/\sigma_{\ell max}$ increases in agreement with Ref *6* (correction to a constant ΔK prior to overload is such that N_D slightly decreases with increasing ΔK), and
3. N_D decreases as relative humidity increases.

These points will be discussed more fully in a later section.

The initial crack growth rate observed on the fifth specimen (at RH $\approx$ 10 percent) was intermediate to the ones observed in the 0 and 80 percent RH experiments, in agreement with earlier observations [*11*]. During the spike overload ($\sigma_{hmax}/\sigma_{\ell max} = 2.5$) the acoustic signal indicated relatively large crack growth ($\approx$300 μm) as shown by Points 2 and 3 in Fig. 1. Point 4 shows the crack depth as observed in the first load cycle after the overload: the crack does not open up to the full depth it did during the overload cycle. At Point 6 the crack depth again has reached the actual crack depth established during the overload. The crack propagation rate thereafter is typical of the crack growth rate observed in the dry environment (0 percent RH) experiments after delay.

Actual closure curves (crack depth versus applied stress) for the fifth specimen tested in a mixed environment are shown in Fig. 2. The identification of each of the closure curves corresponds to similar identifications in Fig. 1 for this specimen. As has been pointed out before [*10,11*], the interpretation of these

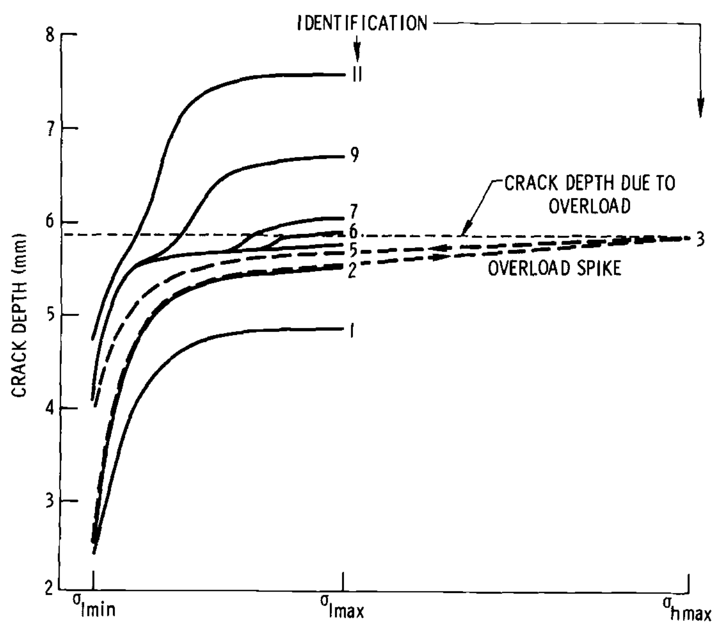

FIG. 2—*Crack closure curves before, during, and after application of overload spike. Identification as in Fig. 1.*

closure curves is that the crack is fully open only at high load levels. The crack stays open over a load range (defining ΔK_{eff} and the true crack depth) as the stress level is lowered and then the crack closes down on itself (a typical example is shown in Curve 1). As may be seen, the acoustic measurements indicate that the crack grew about 300 μm during the overload spike. After the overload the crack does not fully open over the full crack depth established during the overload for a large number of cycles, therefore $\Delta K_{eff} = 0$. As an example, the maximum crack depth indicated by Curve 5 is less than that indicated during the overload cycle. Finally (Curve 6), the crack opens again over the full extent of the crack depth established during the overload cycle. The load corresponding to the crack opening decreases slowly with increasing number of fatigue cycles. After the crack has started to move again, it is proposed that σ_{op} is given by the intersection of the tangent at the upper inflection point of the closure curve with the tangent at $\sigma_{\ell max}$. The consequence of these definitions will be discussed more fully in a later section. Curve 11 still shows an effect of the overload on the low stress region of the closure curve as indicated by the two inflection points on the curve. The crack has grown about 2 mm since application of the overload as indicated by Curve 11. This distance is roughly three times the plastic zone site generated during overload, in qualitative agreement with Wei and Shih [6].

A typical example of the fracture surface features of the area, where the spike overload has been applied, is shown in Fig. 3. A ledge, about 1 to 3 μm high (depending on the overload ratio) corresponds with the position of the crack at the time the overload was applied. Striation spacing in front of the ledge is in good agreement with the crack propagation rate observed acoustically. However, the SEM pictures do not clearly reveal a crack extension of the magnitude indicated by the acoustic measurements (Fig. 1). No striations have been found for a zone greater than the measured crack growth; however, the lack of features may be associated with the damage done by repeated loading during the delay. Replicas taken in the vicinity of the ledges and examined by TEM have not yielded conclusive results so far.

Discussion

The present results on constant-amplitude cycling are, in general, in very good agreement with earlier observations [11,13] in that a gaseous, mildly aggressive environment affects the crack propagation rate, $\Delta a/\Delta N$, the crack closure stress, σ_{op}, and, consequently, the effective stress intensity range, ΔK_{eff}. Furthermore, it was observed that both the size of spike overloads (as in Ref 6) and the environment affect the subsequent delay in fatigue crack growth.

In particular, the present results seem to indicate that the acoustic technique to observe crack propagation is also a valuable tool to study delay effects. As was pointed out before, the closure results from the fifth sample at the higher stress intensity level are amplified somewhat with respect to the other tests. Although somewhat atypical in this respect, these results (Fig. 2) show the effects of the

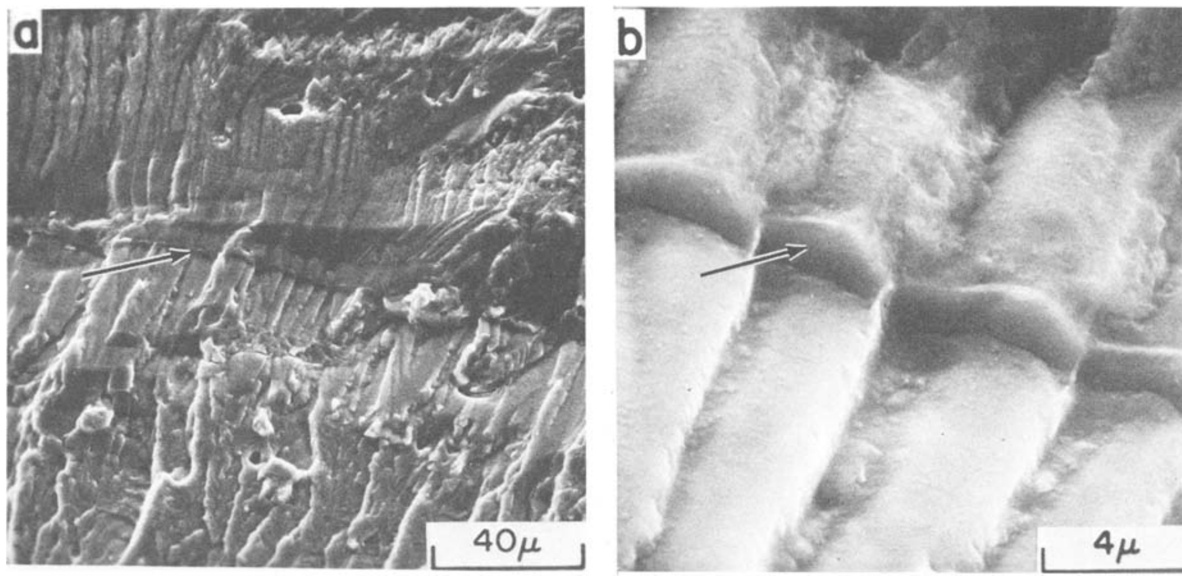

FIG. 3—*Scanning electron microscopy of the fracture surface in the vicinity of application of an overload. The crack propagation direction is from bottom to top with the application of the load spike in the center of the fractographs. The ledge is indicated by an arrow.*

spike overload quite clearly: the crack tip stays closed over the period of delay. Once the crack starts to propagate again, ΔK_{eff} increases slowly, which is reflected in a much smaller $\Delta a/\Delta N$, even at the larger crack depth than before application of the overload.

An attempt was made to quantize this observation by plotting $\Delta a/\Delta N$ versus ΔK and ΔK_{eff}. Both curves are shown in Fig. 4. The identifications given in this

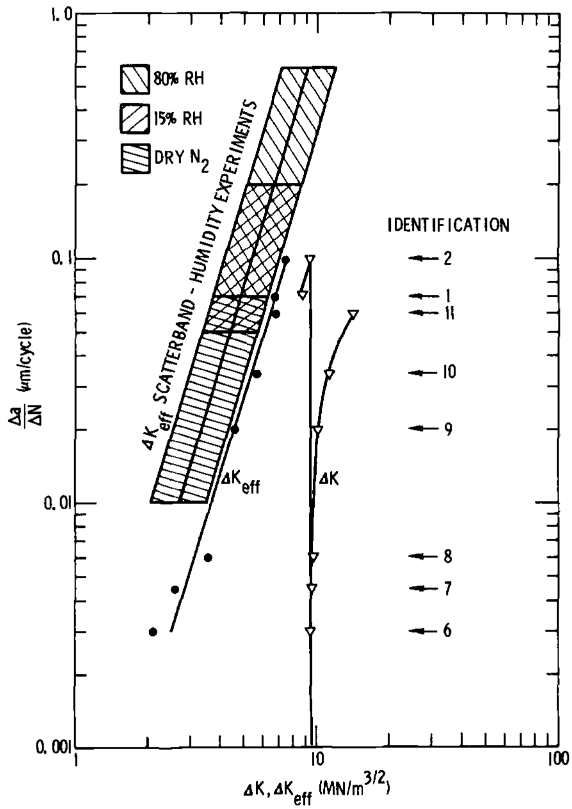

FIG. 4—$\Delta a/\Delta N$ *versus* ΔK *and* ΔK_{eff}, *respectively. Identification as in Figs. 1 and 2. The* ΔK_{eff} *scatterband shows humidity experiments, obtained earlier [11].*

figure again refer to the same identifications in Fig. 2. Before the overload is applied both ΔK and the corresponding ΔK_{eff} increase, with ΔK_{eff} being somewhat smaller than ΔK due to partial closure. After the overload $\Delta a/\Delta N$ approaches zero, resulting in a vertical drop in the $\Delta a/\Delta N$ versus ΔK curve. At the same time ΔK_{eff} goes to zero. As the crack starts to propagate again, ΔK increases slowly above the value it had before the overload with a much reduced $\Delta a/\Delta N$. This results in a second branch of the $\Delta a/\Delta N$ versus ΔK curve (6 through 11). At the same time $\Delta a/\Delta N$ versus ΔK_{eff} shows the same relationship it had before the overload, resulting in a unique functional relation [*9,11,13*] $\Delta a/\Delta N = A\ (\Delta K_{eff})^n$ for the crack propagation rate before and after the overload.

In other words, the effect of the overload is just to operate at a lower value of ΔK_{eff} after the overload but otherwise to follow the prior $\Delta a/\Delta N$ versus ΔK_{eff} relation. Figure 4 also contains the $\Delta a/\Delta N$ versus ΔK_{eff} scatterband on earlier 7075-T651 results [*11*] which were obtained by fatiguing the different gaseous environments. As was shown, $\Delta a/\Delta N$ versus ΔK_{eff} yields a unique functional relation for three environments: dry N_2, 15 percent RH, and 80 percent RH. Although the present overload experiment is just at the lower boundary of the humidity scatter band, both experiments are in good agreement on the exponent $n = 3.27$ [*11*]. The values of ΔK and ΔK_{eff} obtained during the overload have not been plotted. The maximum K value during the overload approached the expected fracture toughness of the material.

The $\Delta a_0/\Delta N$ versus ΔK_{eff} data (Table 1) obtained from the four controlled humidity experiments before application of the overload fell into the appropriate parts of the scatterband in Fig. 4, thus verifying the earlier results [*11*]. In view of the limited data obtained so far, it is difficult to quantize the effects of overload ratio and environment on the delay N_D for this alloy. Indications from the $(\sigma_{hmax}/\sigma_{\ell max}) = 2.0$ experiments are, however, that the delay N_D is a function of the form

$$N_D \propto f\left[\frac{1}{\Delta a/\Delta N}\right] = f\left[(\Delta K_{eff})^{-n}\right] \tag{1}$$

Assuming that this functional relation is merely

$$N_D \propto (\Delta K_{eff})^{-n} \tag{2}$$

the relative change of the delay N_D is in good agreement with the relative change of ΔK_{eff} (using $n = 3.27$ for $(\sigma_{hmax}/\sigma_{\ell max}) = 2.0$. Applying Eq 2 to the $(\sigma_{hmax}/\sigma_{\ell max}) = 2.5$ data one would estimate that the delay in the RH = 0 percent experiment should be about 660 000 cycles. Unfortunately, this specimen broke at the grips after 560 000 cycles delay. Equations 1 or 2, furthermore, would suggest that the delay decreases as the stress intensity increases. Qualitatively, this is in agreement with observations on titanium alloys [*6*], which show N_D decreases as ΔK increases for a constant overload ratio.

Further indications are that for experiments at a constant $\Delta a/\Delta N$ (before application of an overload), the delay N_D is a strong function of the overload ratio $(\sigma_{hmax}/\sigma_{\ell max})$, again in qualitative agreement with observations on titanium alloys [*6*]. Quantification of this effect has not as yet been accomplished due to the limited data available.

The point most likely to be subject to criticism in the present paper is the way the ΔK_{eff} values have been derived. The authors do not deny the weaknesses in their extrapolation technique used in the definition of the closure stress, σ_{op}. One has to keep in mind, however, that the present definitions yield information on the relative changes in the closure stress, and this is the main objective of the present investigations as well as of earlier ones [*10,11,13*]. Definition of σ_{op} by the first deviation from the tangent to the closure curve at $\sigma_{\ell max}$ [*9*] would lead to much smaller ΔK_{eff} values than quoted in the present case. At present there is no means to judge on the preference of one method over the other, however. Future experiments have to decide on this question of the absolute value of ΔK_{eff}, as has been pointed out before [*14*].

One may speculate on the physical picture of the effects of single overload spikes. A rough model based upon the residual strain produced by the deformation in the plastic zone [*9*] (which does not intend to show actual fracture features) is shown in Fig. 5. The identification numbers in Fig. 5 refer

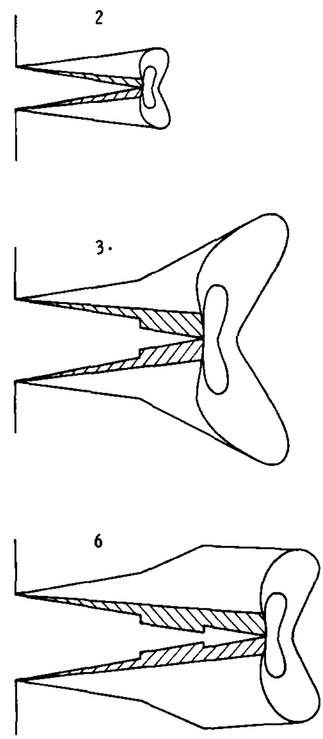

FIG. 5—*Model of overload effects on the residual strain in the wake of the crack tip. (Not intended to represent fracture features.) Identification as in Figs. 1, 2, and 4.*

back to Fig. 2. At the top of Fig. 5 the crack is shown just before the overload spike is applied. The shaded area symbolizes the residual strain causing closure. The center part shows the large crack growth during the overload with the increased residual strain due to an increase in the plastic zone size and the amount of strain at the crack tip. This increased residual strain prevents the crack from opening fully to the crack tip after the overload, thus causing the crack growth delay. Furthermore, it seems likely that the ledges observed by SEM (Fig. 3) are a result of increased crack tip opening displacement and increased residual strain during the overload. Another effect predicted here during unloading would be a large reduction of the area over which crack closure occurs on the fracture surface, which indeed has been observed (compare Curve

2 and the unloading part of Curve 3 in Fig. 2). At the bottom of Fig. 5 a situation is shown after the crack started to grow again. The residual strain is reduced due to the smaller plastic zone size and reduced strain at the crack tip. During unloading, the fracture surface will close down over the fracture surface produced during the overload. As the crack continues to grow and move away from the fracture surface produced during the overload, the effect of the overload becomes less pronounced so that ΔK_{eff} will increase with the corresponding increase in crack growth rate.

It has to be mentioned that the closure phenomenon certainly is not only due to the residual strain in the wake of the crack, but is also caused, to a certain degree, by the residual stresses in the plastic zone. However, as has been discussed before, in the present study the growth rate after an overload is affected over distances many times the plastic zone diameter due to the overload. Thus, it seems that the residual strain, as shown in Fig. 5, dominates the delay effects after an overload.

Many more experiments are necessary to more fully quantize the delay due to spike overloads in terms of ΔK_{eff}. Furthermore, it will be necessary to include block overloads into research of this kind, although some trends under such conditions have been observed earlier [*5,10*]. In the aluminum alloy 2024-T851, it was noted [*10*] that crack growth is stabilized during the overload block. Decreasing the maximum load by only 20 percent yielded a growth delay with a large decrease in ΔK_{eff}. Here, too, the ΔK_{eff} increases slowly due to a decrease in σ_{op}. The exact details of this delay had not been studied at that time, due to experimental problems.

Conclusions

The following conclusions can be drawn from the present studies on the aluminum alloy 7075-T651:

1. The change in the crack growth rate due to a single overload can be explained on the basis of crack closure and the corresponding ΔK_{eff}.
2. Humidity strongly decreases the delay due to an overload which is also explainable in terms of crack closure and ΔK_{eff}.

Acknowledgment

The authors would like to acknowledge the experimental assistance of R. V. Inman and discussions with M. W. Mahoney.

References

[*1*] Wheeler, O. E., "Crack Growth Under Spectrum Loading," General Dynamics Report FZM 5602, 1970.

[*2*] Jonas, O. and Wei, R. P., *International Journal of Fracture Mechanics*, Vol. 7, 1971, p. 116.

[*3*] Van Euw, E. F. J., Hertzberg, R. W., and Roberts, R. in *Stress Analysis and Growth*

of Cracks, ASTM STP 513, American Society for Testing and Materials, 1972, p. 230.

[*4*] Corbly, D. M. and Packman, P. F., *Engineering Fracture Mechanics*, Vol. 5, 1973, p. 479.

[*5*] Trebules, V. W., Roberts, R., and Hertzberg, R. W. in *Progress in Flaw Growth and Fracture Toughness Testing, ASTM STP 536*, American Society for Testing and Materials, 1973, p. 115.

[*6*] Wei, R. P. and Shih, T. T., *International Journal of Fracture*, Vol. 10, 1974, p. 77.

[*7*] Gardner, F. H. and Stephens, R. I., *Fracture Toughness in Slow-Stable Cracking, ASTM STP 559*, American Society for Testing and Materials, 1974, p. 225.

[*8*] Adetifa, O. A. and Gowda, C. B., *International Journal of Fracture*, Vol. 10, 1974, p. 614.

[*9*] Elber, W. in *Damage Tolerance in Aircraft Structures, ASTM STP 486*, American Society for Testing and Materials, 1971, p. 230.

[*10*] Buck, O., Ho, C. L., and Marcus, H. L., *Engineering Fracture Mechanics*, Vol. 5, 1973, p. 23.

[*11*] Buck, O., Frandsen, J. D., and Marcus, H. L., *Engineering Fracture Mechanics*, Vol. 7, 1975, p. 167.

[*12*] Buck, O., Ho, C. L., Marcus, H. L., and Thompson, R. B. in *Stress Analysis and Growth of Cracks, ASTM STP 513*, American Society for Testing and Materials, 1972, p. 280.

[*13*] Buck, O., Frandsen, J. D., Ho, C. L., and Marcus, H. L. in *Microstructure and Design of Alloys, Proceedings*, 3rd International Conference on Strength of Metals and Alloys, Vol. 1, The Institute of Metals and The Iron and Steel Institute, 1973, p. 462.

[*14*] Frandsen, J. D., Inman, R. V., and Buck, O., *International Journal of Fracture*, Vol. 11, 1975, p. 345.

T. T. Shih[1] *and R. P. Wei*[2]

Influences of Chemical and Thermal Environments on Delay in a Ti-6Al-4V Alloy

REFERENCE: Shih, T. T. and Wei, R. P., "**Influences of Chemical and Thermal Environments on Delay in a Ti-6Al-4V Alloy,**" *Fatigue Crack Growth Under Spectrum Loads, ASTM STP 595*, American Society for Testing and Materials, 1976, pp. 113–124.

ABSTRACT: The influences of chemical and thermal environments on delay in fatigue crack growth under elemental load spectra were examined for a mill-annealed Ti-6Al-4V alloy. The results indicate that delay is significantly affected by the hold time at high load in 3.5 percent NaCl solution at room temperature, and by both temperature and thermal history. In 3.5 percent NaCl solution, delay may be increased by 40 times through increasing the hold time from zero to 900 s, the specific amount depends on the overload ratio ($K_{hmax}/K_{\ell max}$) and the maximum value of the low-amplitude fatigue load (or $K_{\ell max}$). Delay is generally higher at the higher test temperature (560°F or 293°C), although the trend in behavior associated with changes in loading variables is similar to that observed at room temperature. Delay is significantly increased when the high load is applied at a high temperature, with subsequent fatigue at room temperature. It is reduced by intermediate heating at a high temperature following a high-load excursion at room temperature, and is lowest when fatigue loads are applied at high temperature following a high-load excursion at room temperature. The significance of these results in terms of modeling and life prediction procedures is discussed.

KEY WORDS: crack propagation, fatigue (materials), delay, titanium alloys, environmental tests, temperature, thermal environments

The importance of delay (retardation in the rate of fatigue crack growth), produced by load interaction in variable-amplitude loading, on the accurate prediction of fatigue lives of engineering structures has been well recognized for some time [*1–11*].[3] Delay properly refers to the period of abnormally low rate, or approximately zero rate, of fatigue crack growth between a decrease in load level and the establishment of a rate of growth commensurate with that for constant-amplitude loading at the prevailing (lower) load; that is, between Points a and c in a simplified schematic diagram shown in Fig. 1. It is usually measured

[1] Formerly, research assistant, Department of Mechanical Engineering and Mechanics, Lehigh University, Bethlehem, Pa. 18015; now with Ebasco Services, Inc., New York, N. Y.

[2] Professor of Mechanics, Department of Mechanical Engineering and Mechanics, Lehigh University, Bethlehem, Pa. 18015.

[3] The italic numbers in brackets refer to the list of references appended to this paper.

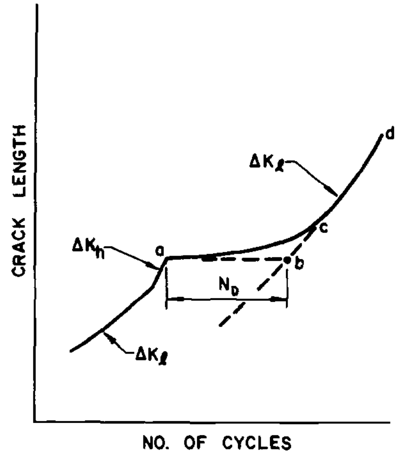

FIG. 1–*Schematic illustration of delay in fatigue crack growth and definition of* N_D.

in terms of the number of elapsed load cycles. For experimental accuracy and potential engineering utility, however, it is more convenient to define delay (N_D) artificially as a period of zero crack growth, represented by the dashed line segment (a-b) in Fig. 1, which is obtained by extrapolating the constant-amplitude growth curve, Curve cd, to b. Following Jonáš and Wei [5], this definition of delay will be used here. The actual crack-growth response of materials following a high load excursion is more complex, and is incorporated indirectly in this definition for delay.

Systematic studies of delay on a mill-annealed Ti-6Al-4V alloy [5–8] showed that the phenomenon is very complex and is affected by a broad range of loading variables. The possible influence of chemical and thermal environments on delay, however, has received little attention thus far. Although the influence of environment on fatigue crack growth under constant-amplitude loading is relatively well established [12–14], it is not clear that this information can be applied directly to the case of fatigue crack growth under variable-amplitude loads. Since engineering structures can be expected to encounter a wide range of operating conditions, a systematic study of load and environment (chemical and thermal) interactions on delay is needed. A brief examination of the effects of chemical and thermal environments on delay was therefore carried out and is reported here. The studies on the effect of chemical environment represent an extension of the results reported previously [7], and are directed specifically at the influence of hold time at high load on delay in a 3.5 percent NaCl (sodium chloride) solution at room temperature. Studies of the effects of thermal environment involve investigations of the influences of temperature and of thermal history. Experiments were carried out within the framework of linear fracture mechanics. The crack tip stress intensity factor K or ΔK was used to characterize the mechanical crack driving force.

Material and Experimental Work

A 0.2-in.-thick (5.08-mm), mill-annealed, Ti-6Al-4V alloy plate was used in this investigation. The chemical composition, heat treatment, and longitudinal and transverse tensile properties of this material are given in Refs *6* and *9*. Constant-load-amplitude fatigue crack growth data in several test environments at room temperature, and in dehumidified argon at room temperature and at about 580°F (305°C) are also given in Refs *6* and *9*.

Two-in.-wide (50.8-mm), wedge opening load (WOL) specimens and 3-in.-wide (76.2-mm) center-cracked specimens, oriented in the long transverse (TL) direction [*15*], were used [*9*]. The specimens were precracked in air at a stress ratio, R, of 0.05 through a sequence of loads that reduced K_{max} to a level that is equal to or less than the selected starting K_{max} level for the actual experiments [*16*]. This precracking procedure provided fatigue cracks of at least 0.08 in. (2 mm) in length from the end(s) of the electro-discharge-machined (EDM) starter notch, such that subsequent fatigue crack growth will be through material that has not been altered by the notch preparation procedure and will be unaffected by the starter notch geometry. The stress intensity factor, K, for the WOL specimens was computed from Eq 1 [*17,18*]

$$K = \frac{P\sqrt{a}}{BW}\left[30.96 - 195.8\left(\frac{a}{W}\right) + 730.6\left(\frac{a}{W}\right)^2 - 1186.3\left(\frac{a}{W}\right)^3 + 754.6\left(\frac{a}{W}\right)^4\right] \quad (1)$$

and from Eq 2, for the center-cracked specimens [*19,20*]

$$K = \frac{P}{BW}\sqrt{\pi a \sec\frac{\pi a}{W}} \quad (2)$$

where P = applied load; a = crack length (or, half-crack length for the center-cracked specimens); B = specimen thickness; and W = specimen width. A continuous recording electrical potential system was used for monitoring crack growth [*9,21,22*]. Resolution in the measurement of crack length, a, was estimated to be about 0.001 in. (0.025 mm) for this material and these specimen configurations [*9*]. The accuracy in crack length measurement was better than 1 percent.

The chemical environment used in these studies was 3.5 percent NaCl solution. The solution was made from reagent grade NaCl and triple-distilled water, and was deaerated continuously in a reservoir and circulated through Plexiglas environment chambers clamped onto the faces of the specimens. For convenience, studies of the effects of temperature and thermal history were carried out in air. Specimen heating was accomplished by the use of electrical resistance heating tapes. The temperature was monitored continuously during the tests by means of thermocouples spot welded to the test specimen. Temperature stability was better than ±5°F (±2.8°C) during a delay test.

Delay experiments were carried out under tension-tension (sinusoidal) loading in a closed-loop electrohydraulic testing machine operated in load control at 5

Hz. Deviations from this loading frequency or the sinusoidal waveform or both were made only when a single or a small number of high load cycles were to be applied (either manually or with the aid of the function generator). Load control was estimated to be better than ±1 percent. Because previous experiments indicated the existence of a significant effect on delay when a high-load excursion occurs during delay produced by a previous high-load excursion [*5,6*], and that this influence can be minimized or eliminated by allowing at least 0.08 in. (2 mm) of crack extension between the successive high-load excursions, such a procedure was used in this investigation and permitted an average of six individual delay experiments to be performed on each test specimen. (The actual crack-growth increments between successive high-load excursions were selected on the basis of crack growth response for the individual cases.) To minimize error, delay (N_D) data were determined directly from the electrical potential (crack length) versus time (cycles) records.

Results and Discussions

Experimental results on the effects of chemical and thermal environments on delay in fatigue crack growth will be reported and discussed separately.

Effect of Chemical Environment (3.5 percent NaCl Solution) on Delay at Room Temperature

In a previous series of experiments [7], the effects of 3.5 percent NaCl solution on delay in fatigue crack growth following single and multiple high-load excursions were examined. The results for single high-load excursion tests (high loads applied by manual control) did not conform to companion test results in air and in dehumidified argon, and exhibited considerable scatter. The multiple high-load cycle data indicated that delay may be dependent on the cycling frequency, f_h, for the high-amplitude loads. These results, along with preliminary test data, suggested that there may be a significant effect of hold time, t_h, at high load on delay for this alloy in 3.5 percent NaCl solution. In this investigation, a more detailed examination of the hold time effect was made. Experimental work was limited to single high-load excursions at various $K_{\ell max}$, for prescribed values of $K_{hmax}/K_{\ell max}$, R_h, and R_ℓ. The test results are shown in Figs. 2 through 4, and are summarized in the following.

1. For reference, single high-load excursion experiments with zero hold time, using a triangular waveform at 0.5 Hz, were carried out. The results show that delay, N_D, decreases monotonically with increasing $K_{\ell max}$ at a constant ratio $K_{hmax}/K_{\ell max}$, and increases with $K_{hmax}/K_{\ell max}$ for fixed values of $K_{\ell max}$ (Fig. 2). They suggest that the previously observed anomalous behavior may indeed reflect a hold time effect engendered by "manual" application of the high loads [7].

2. Data on the effect of hold time (t_h), at $K_{hmax}/K_{\ell max} = 2.0$ and $K_{hmin} = K_{\ell min} = 0.05\ K_{\ell max}$, indicate that delay, N_D, increases with hold time and

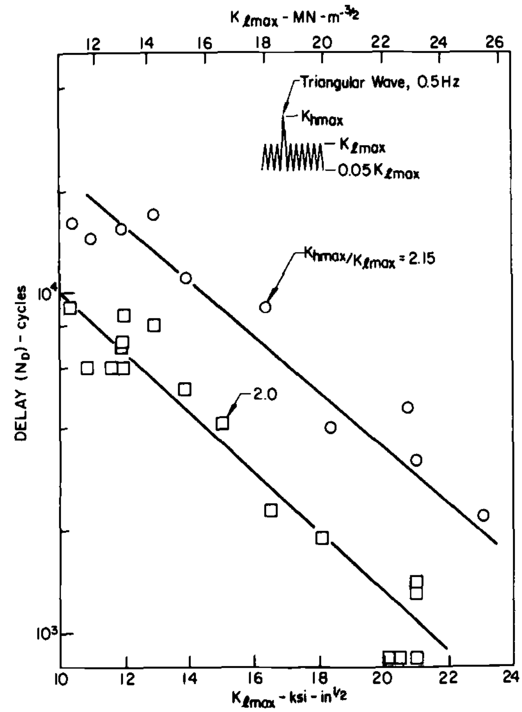

FIG. 2–*Effect of* $K_{\ell max}$ *and* $K_{hmax}/K_{\ell max}$ *on delay in 3.5 percent NaCl solution.*

reaches a limit (Fig. 3). The effect of hold time on delay is dependent on $K_{\ell\,max}$. For t_h from zero[4] to 900 s, N_D can vary from about 10^3 to 4 x 10^4 cycles (a 40-fold increase) at $K_{\ell max}$ = 21 ksi$\sqrt{\text{in.}}$ (23.1 MN/m$^{3/2}$), and from about 7 x 10^3 to 4 x 10^4 cycles (a six-fold increase) at $K_{\ell max}$ = 12 ksi$\sqrt{\text{in.}}$ (13.2 MN/m $^{3/2}$). These results suggest that delay becomes much less sensitive to $K_{\ell max}$ at the longer hold times.

3. The same trend in the hold time effect was observed at $K_{hmax}/K_{\ell max}$ = 1.85, with $K_{\ell\,max}$ = 21 ksi$\sqrt{\text{in.}}$ (23.2 MN/m $^{3/2}$) and $K_{hmin} = K_{\ell min}$ = 0.05 $K_{\ell max}$ (Fig. 4). Here, delay varied from about 4 x 10^2 to 10^4 cycles with increases in t_h from zero to 900 s. Delay was shorter for the lower ratios of $K_{hmax}/K_{\ell max}$.

The experimental results suggest that delay in fatigue crack growth (N_D) for this titanium alloy in 3.5 percent NaCl solution, at a constant $K_{hmax}/K_{\ell\,max}$, may be represented by a surface in the $N_D - K_{\ell max} - t_h$ space as illustrated schematically in Fig. 5. This surface (that is, N_D) would be expected to increase with increasing $K_{hmax}/K_{\ell max}$ (Figs. 2 and 4). Delay produced by a single high-load excursion with zero hold time (triangular waveform, Figs. 2 to 5) decreased with increasing $K_{\ell max}$ in a well-behaved manner, and is consistent

[4] High Loads were applied using a triangular waveform at 0.5 Hz (see Fig. 2).

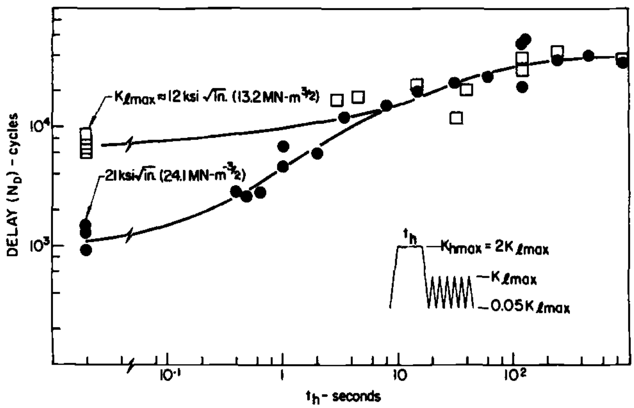

FIG. 3—*Effect of hold time on delay with* $K_{hmax}/K_{\ell max} = 2.0$ *and two different values of* $K_{\ell max}$ *in 3.5 percent NaCl solution.*

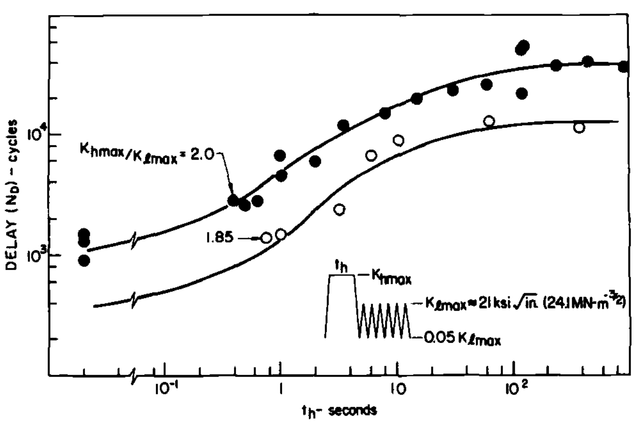

FIG. 4—*Effect of hold time on delay with* $K_{\ell max} = 21$ *ksi*$\sqrt{in.}$ *and two different values of* $K_{hmax}/K_{\ell max}$ *in 3.5 percent NaCl solution.*

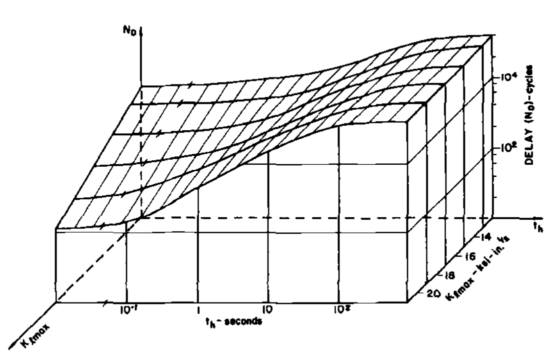

FIG. 5—*Three-dimensional representation of effects of* $K_{\ell max}$ *and* t_h *on delay in 3.5 percent NaCl solution.*

with results obtained in the other environments [*5–7*]. The small reduction in delay in comparison with the other environments is consistent with the higher rates of fatigue crack growth in 3.5 percent NaCl solution for this alloy [*7*]. The extensive increase in delay with increasing hold time is unique to the salt-water environment. Although hold time effects have been observed previously on this alloy in air [*5*], the increase in delay amounted to less than a factor of two for hold times up to 15 h as compared to over one order of magnitude increase observed here. The strong dependence of delay on hold time provides a reasonable basis for explaining the anomalous behavior of the single high-load excursion delay data reported previously [*7*]. A more extensive investigation of hold time effects in 3.5 percent NaCl solution is required to develop a clearer understanding of this load/environment interaction effect in this titanium alloy. Meanwhile, the significant influences of environment-induced frequency and hold time effects on delay must be recognized and be taken into account in the development of life prediction procedures. It is likely that each material-environment system will need to be treated separately. Thus, generalization of existing data should be avoided.

A plausible explanation for the increased delay at long hold times may be advanced. As suggested by the ligament model [*23*], the material immediately ahead of the crack tip has accumulated a substantial amount of fatigue damage caused by the loading cycles prior to the high-load excursion. In the presence of 3.5 percent NaCl solution, stress corrosion cracking may occur during the high-load excursion and cause the crack tip to penetrate through this zone of damaged material. The extent of stress corrosion crack extension depends on K_{hmax} and t_{h}. Thus, after the high-load excursion, the crack tip may now reside in material that has experienced no prior fatigue damage. The residual (compressive) stress introduced by the high-load excursion, however, is not expected to be affected by stress corrosion cracking, since the zone of plastic strain moves forward with the crack tip. It is suggested, therefore, that the increase in delay is the consequence of a reduced (residual stress modified) mechanical driving force encountering a more damage-resistant material. This suggestion is consistent with the experimental observations that there was significant stress corrosion crack growth during the high-load cycle [*9*], and that the increase in N_{D} with hold time, t_{h}, was substantially higher at the higher $K_{\ell\mathrm{max}}$ (Fig. 3) commensurate with greater amount of stress corrosion crack extension. A more extensive study, however, will be needed to better quantify this coupled load/environment interaction effect.

Effect of Thermal Environment on Delay (in Air)

In this part of the investigation, the influences of temperature and some simple thermal history on delay under selected elemental load spectra were examined. For simplicity, the experiments were carried out in air (with relative humidity of 40 to 60 percent at room temperature). Experimental results are shown in Figs. 6 to 9, and are summarized in this section. Wherever possible, comparison data for the same load spectra at room temperature are also given.

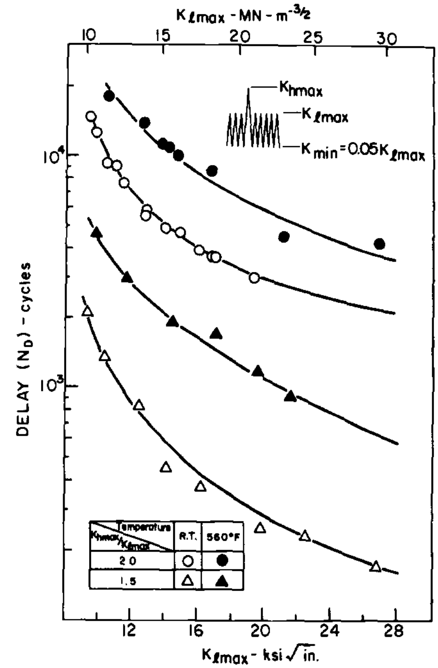

FIG. 6–*The influence of temperature on delay.*

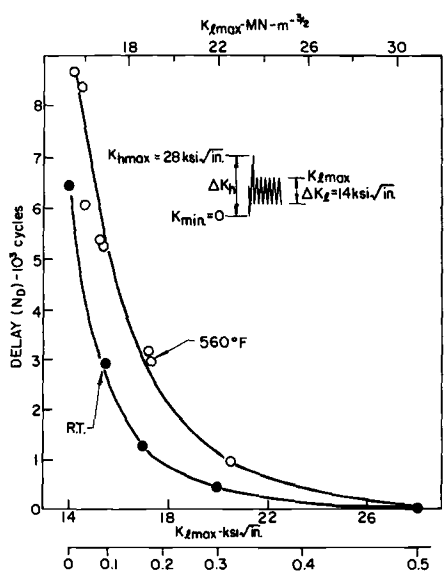

FIG. 7–*Effect of* R_ℓ *on delay for fixed values of* K_{hmax} *and* ΔK_ℓ *at two temperatures.*

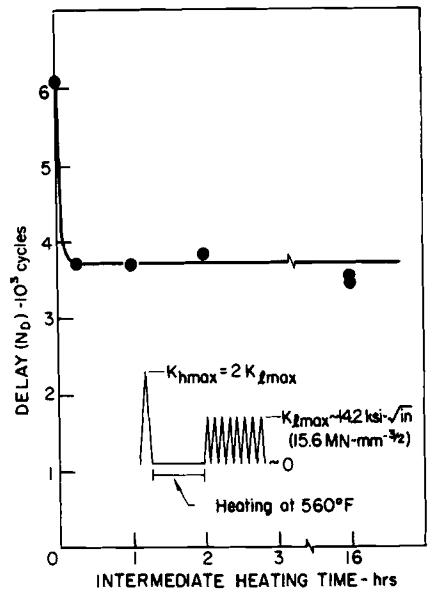

FIG. 8—*The effect of intermediate heating at 560°F on delay at room temperature.*

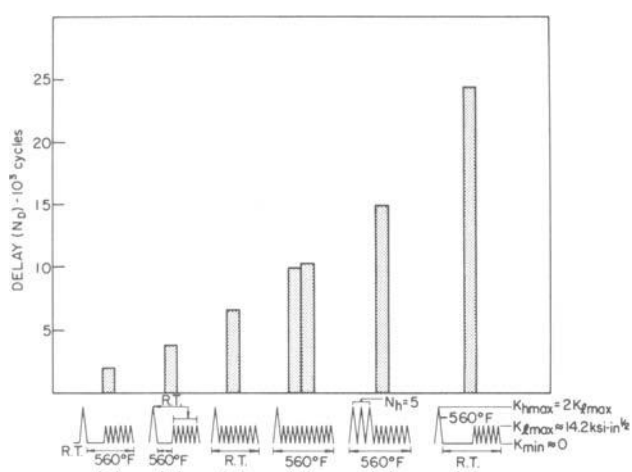

FIG. 9—*Delay under changing temperature and loading conditions at* $K_{\ell max}$ = *14.2 ksi*$\sqrt{in.}$ *and* $K_{hmax}/K_{\ell max}$ = *2.0.*

1. For a single high-load excursion, delay at high temperature decreases with increasing $K_{\ell max}$ at a given value of $K_{hmax}/K_{\ell max}$, and increases with $K_{hmax}/K_{\ell max}$ for fixed values of $K_{\ell max}$ (Fig. 6). These trends are identical to those observed at room temperature [*5,6*]. Delay at 560°F (293°C), however, are some 2 to 4 times longer than at room temperature (Fig. 6), although

temperature had only a minor effect on the rate of fatigue crack growth [*9,24*].

2. For fixed values of $\Delta K_h/\Delta K_\ell$ and K_{hmin}, delay at high temperature is strongly affected by R_ℓ or by the ratio between K_{hmax} and $K_{\ell max}$ (Fig. 7). If $K_{\ell max}$ is equal to K_{hmax}, no delay is experienced. These results are again consistent with those obtained at room temperature [*5,6*].

3. The effect of intermediate heating at 560°F (293°C), following a high-load excursion, on delay was examined. Intermediate heating decreases delay at room temperature by about 40 percent (Fig. 8). The reduction in delay appears to be relatively unaffected by the intermediate heating time (Fig. 8).

4. Various simple combinations of changes in load and temperature were also examined, and the results are summarized in Fig. 9 in order of increasing delay. In Fig. 9, loadings *c* and *d* may be regarded as references for comparisons among the different combinations. It is seen that multiple high-load excursions increase delay at high temperature (Fig. 9*e*). This is consistent with previous results obtained at room temperature. Comparisons between the various combinations show that delay is longest when the high load is applied at a high temperature followed by low-load cycling at room temperature (Fig. 9*f*) and is the shortest when the high load is applied at room temperature and the low-load cycling at high temperature.

These results show that the general behavior of delay with changing loading conditions at an elevated temperature (560°F or 293°C) is the same as that at room temperature. Delay, however, is generally longer at the higher temperature, Figs. 6 and 7. Since, for this alloy, relative humidity was found to have little effect on delay [*7*] and the rate of fatigue crack growth is relatively insensitive to temperature [*9,24*], the observed differences in delay are most likely related to those differences pertaining to the high-load excursions. It is known that the plastically deformed zone ahead of the crack tip is inversely proportional to the yield strength, and that the yield strength of a material decreases with increasing temperature. As such, the interaction zone (residual stress affected zone) would tend to be larger at the higher temperature, and may account for the increased delay. The increased plastic zone size also reduces constraint at the crack tip, and would thereby increase delay [*8*]. The influence of yield strength on delay was studied by using the same material heat treated to different strength levels [*25*]. The results showed that delay was longer for the lower yield strength material, and tend to support the foregoing rationale. The possible causes just discussed are to be rationalized in terms of the influences of residual stresses ahead of the crack tip. This residual stress concept, although difficult to quantify, draws support from the observations that (*a*) intermediate heating (some stress relieving) reduces delay (Fig. 8); (*b*) fatigue at elevated temperature, following a high load excursion at room temperature, reduces delay (Fig. 9*a*); and (*c*) high-load excursion at high temperature followed by fatigue at room temperature tends to prolong delay (Fig. 9*f*). Even though residual stress may not provide a complete explanation for delay, it certainly must be an important part of any complete explanation.

Summary

The influences of chemical and thermal environments on delay in fatigue crack growth under elemental load spectra were examined for a mill-annealed Ti-6Al-4V alloy. Experiments carried out in 3.5 percent NaCl solution showed a significant effect of load/environment interactions. Specifically, delay was strongly affected by the hold time at high load. With zero hold time, delay decreased with $K_{\ell max}$ in a well-behaved manner and was slightly lower than that observed in less aggressive environments (air, for example). By increasing hold time from zero to 900 s, delay was increased by up to 40-fold depending on $K_{\ell max}$ and $K_{hmax}/K_{\ell max}$. Tests at a high temperature (560°F or 293°C) showed that delay was generally longer than that observed at room temperature under identical loading conditions. Room temperature delay was reduced by intermediate heating at 560°F (293°C). Delay was found to be longest if the high-load excursion occurred at high temperature and the subsequent fatigue was at room temperature, and shortest if the temperature profile is reversed. These results suggest that residual stresses ahead of the advancing crack play an important role in delay, although this aspect of the problem is difficult to quantify at this time. The significant effects of combined load and environment (chemical and thermal) interactions must be recognized and be taken into account in the development of life prediction procedures. It is likely that each material-environment system will need to be treated separately, and that broad generalization of existing data should be avoided.

Acknowledgment

Partial support of this work by the National Aeronautics and Space Administration under Grant NGL 39-007-040, and by the Office of Naval Research under Contract N00014-67-A-0370-0008, NR 036 097, is gratefully acknowledged.

This paper is based on a part of the research performed in partial fulfillment of requirements for a Ph.D. in Applied Mechanics, Lehigh University.

References

[1] Christensen, R. H. in *Proceedings*, Crack Propagation Symposium, Cranfield, The College of Aeronautics, Vol. 2, 1961, p. 326.

[2] Schijve, J., *Advances in Aeronautical Sciences*, Vol. 3-4, 1962, p. 387.

[3] Hudson, C. M. and Hardrath, H. F., "Effects of Changing Stress Amplitude on the Rate of Fatigue-Crack Propagation in Two Aluminum Alloys," NASA TN D-960, 1961.

[4] Hudson, C. M. and Raju, K. N., "Investigation of Fatigue-Crack Growth under Simple Variable-Amplitude Loading," NASA TN D-5702, 1970.

[5] Jonáš O. and Wei, R. P., *International Journal of Fracture Mechanics*, Vol. 7, 1971, p. 116.

[6] Wei, R. P. and Shih, T. T., *International Journal of Fracture*, Vol. 10, 1974, p. 77.

[7] Shih, T. T. and Wei, R. P. in *Proceedings–The Prospects of Advanced Fracture Mechanics*, Noordhoff, 1975, p. 231.

[8] Shih, T. T. and Wei, R. P., *Journal of Testing and Evaluation*, Vol. 3, No. 1, 1975, p. 46–47.
[9] Shih, T. T., "Fatigue Crack Growth under Variable Amplitude Loading," Ph.D. thesis, Lehigh University, Bethlehem, Pa., 1974.
[10] von Euw, E. F. J., Hertzberg, R. H., and Roberts, R. in *Stress Analysis and Growth of Cracks, ASTM STP 513*, American Society for Testing and Materials, 1972, p. 230.
[11] Trebules, V. W., Roberts, R., and Hertzberg, R. W. in *Progress in Flaw Growth and Fracture Toughness Testing, ASTM STP 536*, American Society for Testing and Materials, 1973, p. 115.
[12] Wei, R. P., *International Journal of Fracture Mechanics*, Vol. 4, 1968, p. 159.
[13] Wei, R. P., *Engineering Fracture Mechanics*, Vol. 1, 1970, p. 633.
[14] Hartman, A., *International Journal of Fracture Mechanics*, Vol. 1, 1965, p. 167.
[15] Goode, J., *Materials Research and Standards*, Vol. 1, 1961, p. 389.
[16] FitzGerald, J. and Wei, R. P., *Journal of Testing and Evaluation*, Vol. 2, No. 2, 1974, p. 67.
[17] Wilson, W. K., Analytical Determination of Stress Intensity Factors for the Manjonie Brittle Fracture Test Specimen, Report No. WERL-0029-3, Westinghouse Research Laboratories, 1965.
[18] Wilson, W. K., Optimization of WOL Brittle Fracture Test Specimen, Report No. 66-1B4BTLFR-R1, Westinghouse Research Laboratories, 1966.
[19] Brown, W. F., Jr., and Srawley, J. E., *Plane Strain Crack Toughness Testing of High-Strength Metallic Materials, ASTM STP 410*, American Society for Testing and Materials, 1966.
[20] Isida, M., "Crack Tip Stress Intensity Factors for the Tension of an Eccentrically Cracked Strip," Lehigh University, Dept. of Mechanics Report, 1965.
[21] Johnson, H. H. *Materials Research and Standards*, Vol. 5, 1965, p. 442.
[22] Li, C. Y. and Wei, R. P., *Materials Research and Standards*, Vol. 6, 1966, p. 392.
[23] Majumdar, S. and Morrow, J. D., "Correlation Between Fatigue Crack Propagation and Low Cycle Fatigue Properties," T & AM Report No. 364, University of Illinois, Urbana, Ill., 1973.
[24] Wei, R. P. and Ritter, D. L., *Journal of Materials*, Vol. 7, No. 2, 1972, p. 240.
[25] Gallagher, J. P. and Hughes, T. F., "The Influence of Yield Strength on Overload Affected Crack Growth Rate Behavior in 4340 Steel," AFFDL-TR-74-27, 1974.

DISCUSSION

R. I. Stephens[1] *(written discussion)*—In Fig. 9, loadings *c* and *d*, your results indicate delay was greater at 560°F than at room temperature with $R_\ell = K_{\ell \min}/K_{\ell \max} \approx 0$. I would like to suggest the opposite might occur had you tested with R_ℓ equal to say −1.0. This idea is based upon greater cyclic plasticity at elevated temperature and $R_\ell = -1$ such that residual compressive stresses and crack closure due to the overload are reduced. This in turn would decrease the elevated temperature delay. Could the authors comment on this?

T. T. Shih and R. P. Wei (authors' closure)—It is the authors' experience that the application of a compressive load following a high-load excursion reduces delay. One would expect, therefore, fatigue at $R_\ell < 0$ would also reduce delay. The authors can agree that the reversal in behavior suggested by Dr. Stephens is within the realm of possibility (although very unlikely), but do not believe that there is a valid basis or data to permit the type of extrapolation suggested by Dr. Stephens at the present time.

[1] Materials Engineering Division, The University of Iowa, Iowa City, Iowa 52242.

S. W. Hopkins,[1] *C. A. Rau,*[1] *G. R. Leverant,*[1] *and A. Yuen*[1]

Effect of Various Programmed Overloads on the Threshold for High-Frequency Fatigue Crack Growth

REFERENCE: Hopkins, S. W., Rau, C. A., Leverant, G. R., and Yuen, A., "Effect of Various Programmed Overloads on the Threshold for High-Frequency Fatigue Crack Growth," *Fatigue Crack Growth Under Spectrum Loads, ASTM STP 595*, American Society for Testing and Materials, 1976, pp. 125–141.

ABSTRACT: A threshold value of crack tip stress intensity range (ΔK_{th}) exists below which Mode I cracks do not propagate in high-frequency fatigue. The response of ΔK_{th}, in a commercial nickel-base and titanium-base alloy, to single and multiple cycle overloads (that is, the behavior of an overload modified threshold, ΔK_{th}*) has been defined for a variety of fatigue conditions. Both alloys responded similarly and showed an exponential increase of ΔK_{th}* with increased magnitude of the overload. The effects of overload rate, temperature, cycle shape and number, and the fatigue conditions of mean stress and cyclic frequency have lesser, but significant, effects on ΔK_{th}*. Metallography and scanning electron fractography have been used to define the changes in crack size and tip shape which contribute to the overload effects.

KEY WORDS: crack propagation, fatigue (materials), loads (forces), crack propagation, cyclic loads

The strong effects of spectrum loads on the rate of fatigue crack propagation have been appreciated for some time [*1*].[2] The loading spectrums are often so complex and involve such large numbers of small load excursions that there is a need to define the limits below which load excursions do not contribute to the crack growth rate ($\Delta a/\Delta N$). Many loading spectrums, like those for rotating equipment, consist of two major cyclic loads: low cycle fatigue (LCF) produced by a relatively few number of large load (rotating speed or rpm) excursions, and high cycle (vibratory) fatigue which may superimpose large numbers of low-amplitude cycles on specific portions of the LCF cycle. For cases where vibratory excitation occurs below the maximum LCF load, each LCF cycle acts as an overload which may affect crack growth during the vibratory fatigue. The present approach utilizes the observation that Mode I cracks do not extend in fatigue for ranges of crack tip stress intensity factor below a threshold (ΔK_{th}). ΔK_{th} can therefore be used directly to establish design allowables for some load spectrums or as part of the lifetime prediction analysis of more complex load

[1] Pratt Whitney Aircraft, Materials Engineering and Research Laboratory, E. Hartford, Conn. 06108; Mr. Rau is now with Failure Analysis Associates, Palo Alto, Calif. 94304.

[2] The italic numbers in brackets refer to the list of references appended to this paper.

spectrums. Because of experimental difficulties in valid precracking, much of the early threshold data is suspect. Furthermore, the response of ΔK_{th} to various operating conditions, including overload, has not previously been defined. The present work determines ΔK_{th} and ΔK_{th}^* (an overload modified threshold) for two engineering alloy systems under several important special cases. Specifically, ΔK_{th}^* is evaluated after single and multiple cycle overloads of various magnitude under a range of fatigue (mean stress, frequency, temperature) and overload (shape, temperature) conditions.

Experimental Procedure

Center-cracked sheet specimens, Fig. 1, were used to evaluate the threshold and subsequent fatigue crack growth for two commercial alloys. The titanium-base alloy (Ti-6Al-4V) specimens were machined from a pancake forging that

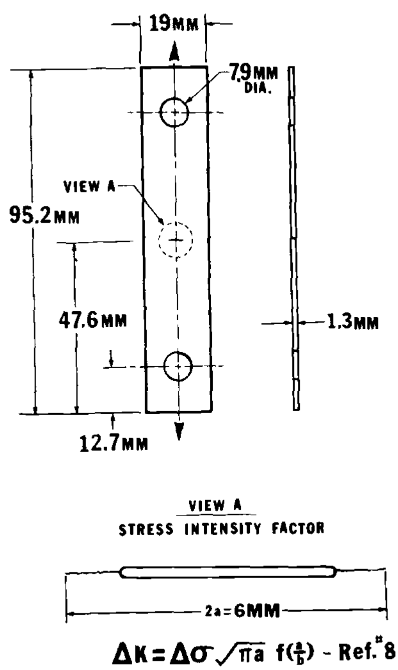

FIG. 1—*Center notched crack growth and threshold specimen design.*

had been forged at 1241 K (1775°F) in the $\alpha + \beta$ phase field and then annealed at 1227 K (1750°F) for 1 h, water quenched, and aged at 977 K (1300°F) for 2 h. The chemical composition in weight percent was the following 0.02 to 0.033 carbon, 0.10 to 0.18 iron, 6.3 to 6.43 aluminum, 4.28 to 4.30 vanadium, 0.172 to 0.183 oxygen, 0.0050 to 0.0062 hydrogen, and 0.013 to 0.015 nitrogen. The microstructure, Fig. 2*a*, consisted of 20 to 40 percent primary α and the

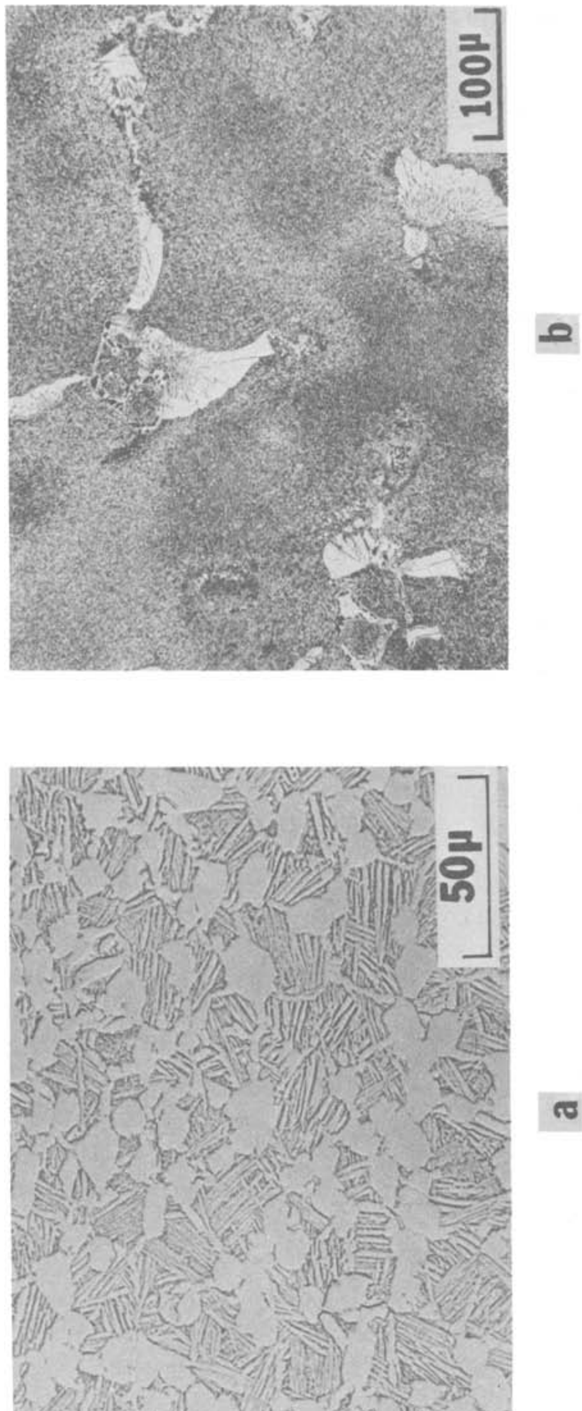

FIG. 2—*Photomicrographs showing the microstructure of (a) Ti-6Al-4V after being forged at 1241 K, annealed at 1227 K/1 h, water quenched, and aged at 977 K/2 h, and (b) DS nickel-base alloy (MarM-200 plus hafnium) after being solutioned at 1477 K/2 h, air cooled, aged at 1144 K/32 h, and air cooled.*

remainder Widmanstatten α. The average α grain size, as determined by lineal analysis, was 14 μm.

The nickel-base alloy (MarM-200 plus hafnium) specimens were machined from two directionally-solidified (DS) castings so that loading was parallel to the longitudinal growth direction. The DS alloy is composed of a γ solid solution matrix, precipitation hardened by ordered γ' particles and containing both bulk and grain boundary carbides, Fig. 2*b*. The large grains are elongated in the growth direction, have a <100> texture, and random transverse orientation. The chemical composition was the following in weight percent: 4.8 to 5.0 aluminum, 0.009 to 0.018 boron, 0.11 to 0.16 carbon, 9.5 to 10.2 cobalt, 8.11 to 9.3 chromium, 0.03 to 0.08 iron, 1.9 to 2.25 hafnium, <0.001 manganese, 1.8 to 2.1 titanium, 0.04 to 0.06 silicon, 11.8 to 12.8 tungsten, and 1.0 (nominal) columbium.

In past experience with the nickel-base alloy, it was found that ΔK_{th} could vary significantly if the final precracking was done at a temperature other than the test temperature. For example, with a room temperature precrack, ΔK_{th} = 7.6 MNm$^{-3/2}$, but with a 950 K (1250° F) precrack, ΔK_{th} = 4.4 MNm$^{-3/2}$ when both specimens were tested at 950 K (1250°F) and R ($\equiv \sigma_{min}/\sigma_{max}$) = 0.695. Therefore, all specimens were precracked at 30 Hz and at the test temperature. The fatigue precrack was extended a minimum of one sheet thickness from the slot. The final step in precracking was done at a maximum load less than or equal to the maximum load for the first step in the test condition. Once the specimen was precracked, the ΔK_{th} or $\Delta K_{th}{}^*$ value was determined by cycling for 10^7 cycles and then examining either a cellulose acetate replica or the specimen surface directly in an optical microscope at x1000 magnification. If the crack had not propagated, then ΔK was incremented up by 0.22 MNm$^{-3/2}$, keeping the ratio (R) constant, and cycled for an additional 10^7 cycles. This procedure was continued until crack growth was observed. The ΔK_{th} or $\Delta K_{th}{}^*$ reported in this paper is the highest ΔK which did not cause the crack to propagate in 10^7 cycles, that is, the load step just below the growth step. Since crack extensions of 25 μm could be resolved, ΔK_{th} or $\Delta K_{th}{}^*$ is equivalent to $\Delta a/\Delta N < 2.5\text{x}10^{-9}$ mm/cycle (10^{-10} in./cycle). Once the $\Delta K_{th}{}^*$ was determined and crack growth occurred, the specimen was overloaded again in various ways, and the resulting $\Delta K_{th}{}^*$ was evaluated in the same manner. With this procedure, a number of $\Delta K_{th}{}^*$ values were obtained from the same specimen. Care was taken to ensure that each successive evaluation was not influenced by previous ones on the same specimen.

$\Delta K_{th}{}^*$ was determined after different magnitudes of the overload (K_{hmax}) ranging from no overload to K_{hmax} approaching K_c of the material. The standard overload test sequence is shown in Fig. 3. This was done for five different stress ratios R = (0.1, 0.3, 0.5, 0.7, and 0.9) in the titanium-base alloy and three different R ratios (0.694, 0.785, and 0.887) in the nickel-base alloy. Two different testing frequencies (1000 and 30 Hz) were examined and two different overload rates were used (1 Hz and 1 min hold at maximum load) for the titanium-base alloy. For the nickel-base alloy, three different overload

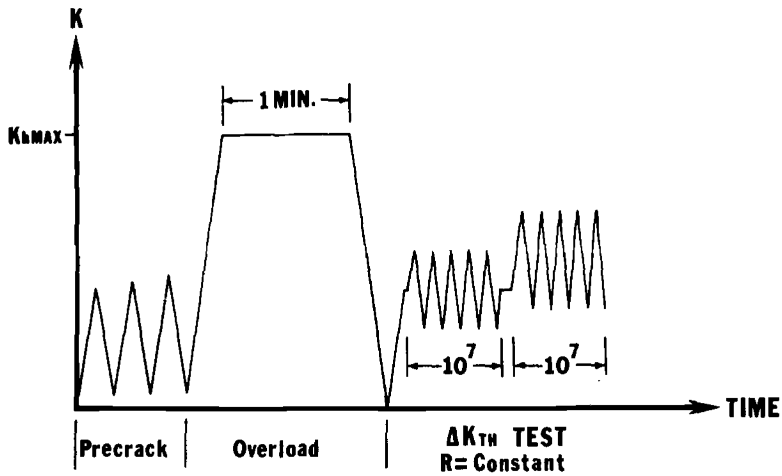

FIG. 3–*Standard overload test sequence for determining* ΔK_{th} *by uploading a non-propagating crack.*

temperatures (299, 866, and 1200 K) were also investigated, with $\Delta K_{th}{}^*$ always being determined at 866 K (1100°F).

Experimental Results and Discussion

Basic Threshold and Slow Crack Growth

The basic ΔK_{th} without overload is shown as a function of R in Fig. 4 for the Ti-6Al-4V alloy at room temperature and for 30 and 1000-Hz testing frequencies. The 1000-Hz frequency produces a slightly higher ΔK_{th} than did the 30 Hz testing frequency. The ΔK_{th} at $R = 0.1$ is an extrapolated value rather than a measured value because of the experimental problems involved in obtaining a valid precrack without overloading. Irving and Beevers [*2*] have stated that they observed a difference of 2.0 $MNm^{-3/2}$ in the ΔK_{th} at $R = 0.35$ for Ti-6Al-4V material cycled in high vacuum, depending on whether they down-loaded with a growing crack or up-loaded a non-propagating crack to obtain the ΔK_{th}, with down-loading producing the lower results.[3] All the basic ΔK_{th} results presented here will necessarily be for up-loading to compare directly with the overload results which can only be evaluated by up-loading non-propagating cracks to keep the crack tip under the influence of the overload's plastic zone. The basic ΔK_{th} for the DS nickel alloy is shown in Fig. 4 as a function of R at 866 K and 1000 Hz frequency.

The basic ΔK_{th} values for the Ti-6Al-4V at 294 K are about 50 percent of the ΔK_{th} for the nickel-base alloy at 866 K for the same R ratio, although both have the same modulus of elasticity at their respective test conditions. The modulus

[3] Down-load here means decreasing the load amplitude until a growing crack is brought to "rest" (or stop), and up-load means increasing the load amplitude until a stationary crack begins to grow.

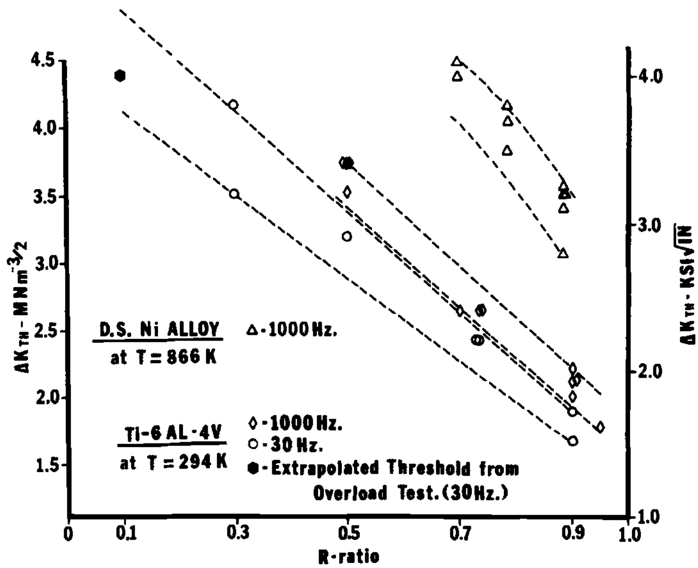

FIG. 4—*Basic threshold stress intensity factor as a function of stress ratio for Ti-6Al-4V at 294 K and 30 and 1000 Hz and for directionally solidified DS nickel alloy at 866 K and 1000 Hz.*

of elasticity for Ti-6Al-4V at 294 K is 1.10×10^5 MNm^{-2} (16×10^6 psi) and for the nickel-base alloy at 866 K is 1.08×10^5 MNm^{-2} (15.7×10^6 psi). Weiss and Lal [*3*] have suggested that ΔK_{th} is only a function of the material's modulus of elasticity. The present results show that such models are at best crude approximations of the basic threshold (ΔK_{th}) that do not account for the important effects of overloads.

The low crack growth rates ($\Delta a/\Delta N$) as a function of stress intensity ranges (ΔK) just larger than the basic ΔK_{th} were obtained and are shown in Fig. 5*a* for the titanium-base alloy at 294 K for $R = 0.5$, 0.7, and 0.9 and in Fig. 5*b* for the DS nickel alloy at 866 K for $R = 0.785$ and 0.887. It was noted that crack growth rate just above ΔK_{th} differed considerably between the two materials. Specifically, in the titanium alloy, Fig. 5*a*, the crack growth rate jumps one order of magnitude from below 2.5×10^{-9} mm/cycle or no growth to 2.54×10^{-8} mm/cycle for $R = 0.7$, and only a factor of 5 to 1.3×10^{-8} mm/cycle for $R = 0.9$ when ΔK is increased 0.22 $MNm^{-3/2}$ above ΔK_{th}. With the DS nickel alloy, Fig. 5*b*, the crack growth rate jumps three orders of magnitude to 2.0×10^{-6} and 2.5×10^{-6} mm/cycle for $R = 0.785$ and 0.887, respectively, when ΔK is similarly incremented. Once this jump occurs, the crack growth rates are the same for all three R-ratios in the titanium alloy and nearly the same in the nickel-base alloy. In 2024-T3 aluminum, Schmidt and Paris [*4*] found the same ΔK at a growth rate of 5×10^{-7} mm/cycle from $R = 0.5$ to 0.8 at 300 Hz and from $R = 0.75$ to 0.9 at 580 Hz. The observation from Fig. 5*a* is that ΔK to produce $\Delta a/\Delta N = 2.5 \times 10^{-7}$ mm/cycle is R-ratio independent; however, the threshold ΔK_{th} at a growth rate of 2.5×10^{-9} mm/cycle is strongly R-ratio

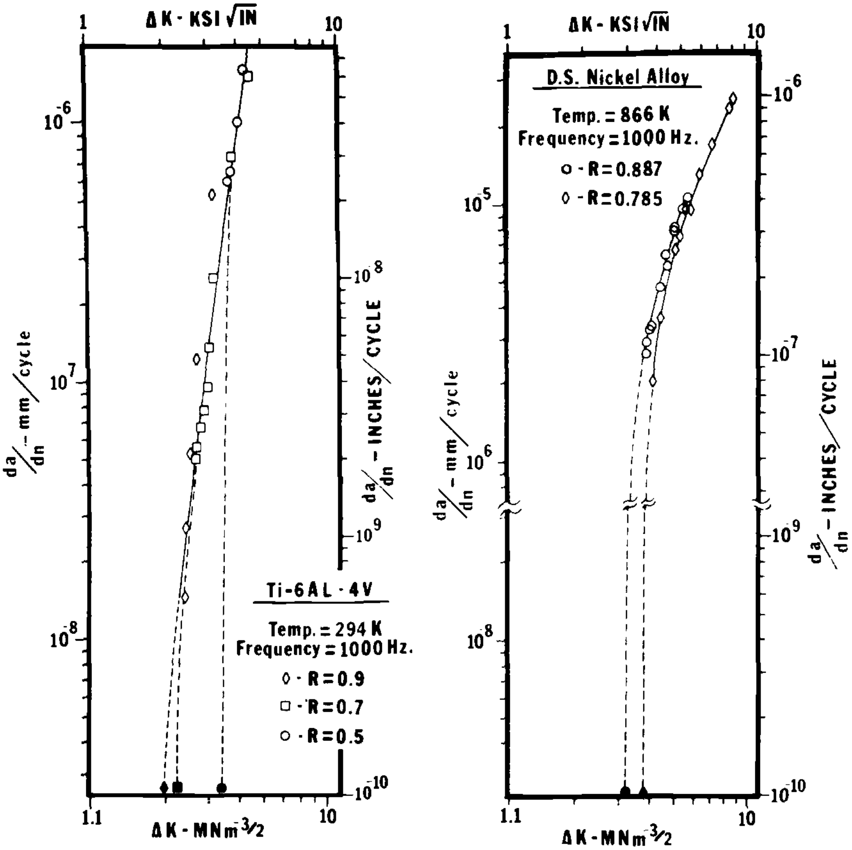

FIG. 5—*Fatigue crack growth rate immediately after the basic threshold as a function of stress intensity factor for (a) Ti-6Al-4V at 1000 Hz and 294 K, and (b) DS nickel alloy at 1000 Hz and 866 K.*

dependent. Great patience is obviously required to examine sufficiently slow $\Delta a/\Delta N$ where the large effects on ΔK_{th} are present. Schmidt and Paris [*4*] also observed a lowering of the threshold with increasing cyclic frequency from 342 to 1000 Hz and suggested localized heating of the crack tip as a possible reason. With the Ti-6Al-4V alloy, we do not observe a strong frequency effect. Furthermore, the crack growth rate is insensitive to temperature up to 616 K [*5*]. The slight increase in ΔK_{th} with increased frequency is more likely the result of less plasticity at the crack tip and less time for environmental interaction.

Threshold After a Single Cycle Overload

The ΔK_{th}^* is a strong function of the single cycle overload magnitude K_{hmax}, as shown in Fig. 6 for the titanium alloy at 294 K and Fig. 7 for the DS nickel alloy at 866 K. The open symbols represent the basic ΔK_{th} with its corresponding K_{max} and the filled-in symbols represent the ΔK_{th}^* after an

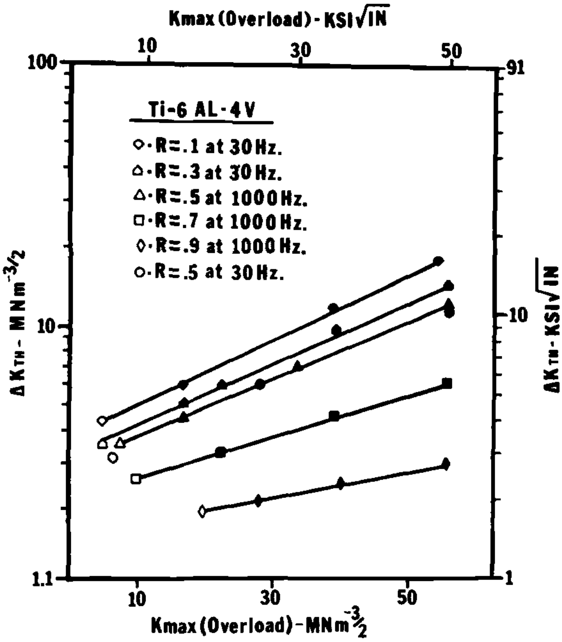

FIG. 6—*Overload modified threshold stress intensity factor as a function of the maximum single cycle overload stress intensity factor for Ti-6Al-4V at 294 K and at both 1000 and 30 Hz. (Open symbols represent ΔK_{th} without overload.)*

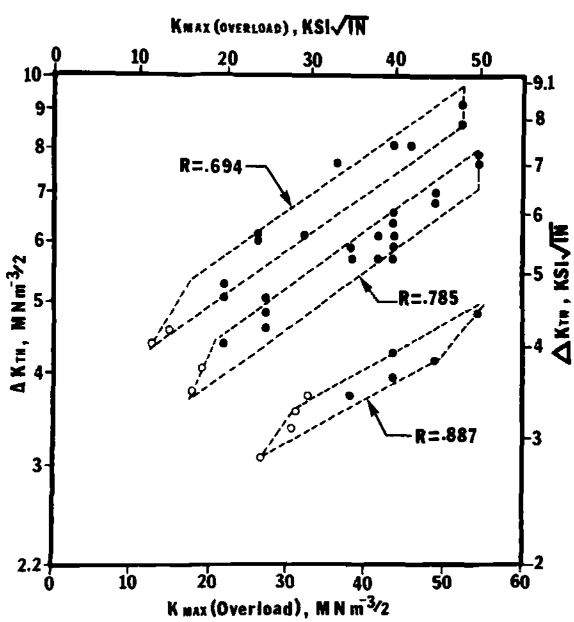

FIG. 7—*Overload modified threshold stress intensity factor for the DS nickel alloy at 1000 Hz and 866 K after single cycle overloads to various K_{max}. (Open symbols represent ΔK_{th} without overload.)*

overload to the K_{hmax} plotted. Figures 6 and 7 show that by overloading to near the fracture toughness of the material, $\Delta K_{th}{}^*$ at $R = 0.1$ can be increased by 400 percent and $\Delta K_{th}{}^*$ at $R = 0.9$ can be increased by 50 percent. For smaller overloads, the $\Delta K_{th}{}^*$ is increased by smaller amounts. For both alloys, log $\Delta K_{th}{}^*$ increases nearly linearly with overload K_{hmax}. Using the linear relationship of log $\Delta K_{th}{}^*$ versus K_{hmax} along with the relationship $\Delta K = (1 - R)\,K_{max}$, the basic ΔK_{th} at $R = 0.1$ in Fig. 4 was obtained by extrapolation.

In Fig. 4 it was shown that the basic threshold, ΔK_{th}, was slightly dependent on fatigue frequency for the Ti-6Al-4V. However, Fig. 6 shows that the $\Delta K_{th}{}^*$ after overload at $R = 0.5$ is not dependent on testing frequency between 30 and 1000 Hz. The specific shape and loading rate of the overload cycle affected the resultant $\Delta K_{th}{}^*$ in the Ti-6Al-4V as shown in Fig. 8. The standard overload

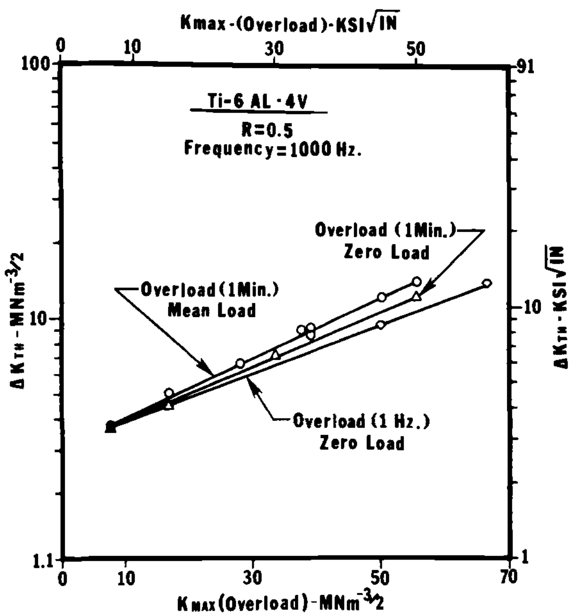

FIG. 8—*Overload modified threshold stress intensity factor for Ti-6Al-4V after single cycle overloads to* K_{max} *at different overload rates at 294 K and 1000 Hz.*

cycle was to load up to the maximum load (K_{hmax}) and hold for 1 min, return to zero load, and then load to mean load for the first attempt at determining $\Delta K_{th}{}^*$ as shown in Fig. 3. The effect of the overload of magnitude K_{hmax} was increased (that is, $\Delta K_{th}{}^*$ increased) by not unloading to zero load and instead returning directly to the mean load for test after the overload as designated by "Overload (1 min) Mean Load" in Fig. 8. Some of the apparent scatter in $\Delta K_{th}{}^*$ of the nickel alloy (Fig. 7) results from not unloading to zero after overload. By not returning to zero load, the crack tip is apparently left more blunted and thus produces a higher $\Delta K_{th}{}^*$. Conversely, the effect of the overload on $\Delta K_{th}{}^*$ is less when applied at 1 Hz and eliminating the 1 min hold at maximum load as designated by "Overload (1 Hz) Zero Load" in Fig. 8. This higher loading rate apparently reduces the amount of crack tip deformation during overload and, therefore, the effect of the overload.

Single cycle overloads were also applied to the nickel alloy at a lower (294 K) and higher (1200 K) temperature, and the corresponding ΔK_{th}^* was obtained at 866 K after each overload, Fig. 9. The four different magnitude single cycle

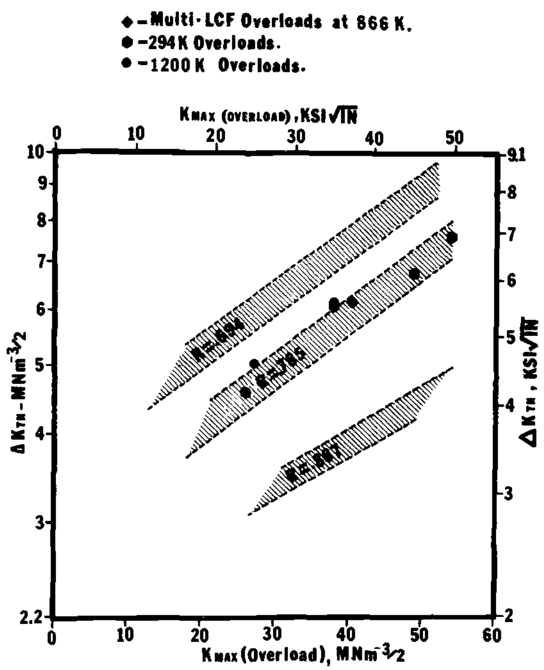

FIG. 9—*Overload modified threshold stress intensity factor of DS nickel alloy at* R = *0.785, 866 K, and 1000 Hz as a function of the overload magnitude for multiple overload cycles put on at 866 K and single cycle overloads put on at 294 and 1200 K compared with the scatterband for single cycle overloads at 866 K.*

overloads which were introduced at 294 K produced resultant ΔK_{th}^* at R = 0.78 and 866 K which were the same as the ΔK_{th}^* measured when the overload was applied at 866 K. The two different magnitude single cycle overloads introduced at 1200 K produced ΔK_{th}^* at R = 0.78 and 866 K which were on the high boundary of the scatterband for the 866 K overloads. Because the yield stresses for this alloy at 294, 866, and 1200 K are 897, 890, and 573 MNm^{-2}, respectively, the size of the plastic zone in front of the crack tip due to K_{hmax} was different for each temperature. Even though the plastic zone size of the overloads varied, the resultant ΔK_{th}^* was unchanged, which indicates that the plastic zone size during overload cannot be the controlling parameter.

Multiple consecutive cycle overloads have also been investigated in a limited number of tests. For the titanium-base alloy, 50 overload cycles were applied at

$R = 0.1$, and ΔK_{th}^* was then evaluated at both $R = 0.5$ and 0.9. With 50 consecutive overload cycles applied, the ΔK_{th}^* at $R = 0.5$ was only slightly (20 percent) above that after a single identical overload, while at $R = 0.9$, ΔK_{th}^* after multiple overloads was indistinguishable from that after the single cycle overload (Fig. 6). Similarly, for the DS nickel alloy, Fig. 9, ΔK_{th}^* at $R = 0.785$, was the same after 50 overload cycles as after a single overload of the same magnitude. This limited multiple overload testing shows that multiple cycle overloads do not produce markedly larger effects than a single overload.

Metallography and Fractography

In order to better understand the mechanisms responsible for the large effects of overloads on ΔK_{th}^*, extensive metallographic and scanning electron fractography was performed. The crack length, path, and shape during and after each overload was examined on the sheet surface. Since fractography revealed some unusual crack front behavior near the sheet surface, for the DS nickel-base alloy, some specimens were sectioned and examined along the mid-plane of the sheet. Figure 10*a* shows the crack tip on the plate surface before an overload to

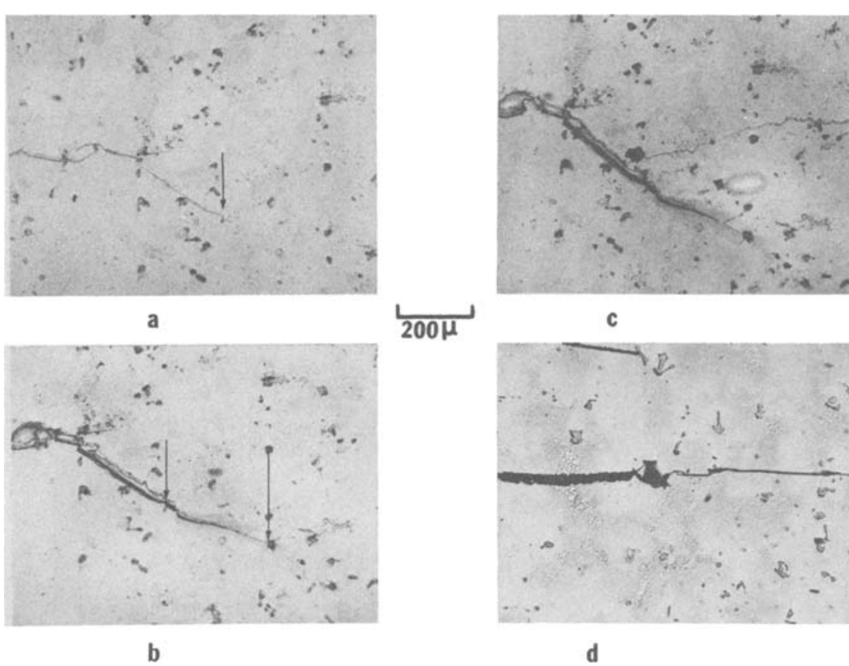

FIG. 10—*Crack path for DS nickel alloy with a single cycle overload at* R = *0.785 and 866 K: (a) Precrack before overload is applied (plate surface); (b) Crack growth due to a single cycle overload of 55 MNm*$^{-3/2}$ *(plate surface); (c) Crack growth after single cycle overload and threshold has been exceeded (plate surface); (d) Crack path at mid-thickness after single cycle overload and threshold has been exceeded.*

55 $MNm^{-3/2}$ (almost K_c), and Fig. 10*b* is the crack tip after the overload. The surface observations indicate that during the overload the crack grew approximately 0.25 mm along a plane other than the primary plane. Figure 10*c* shows the same surface area after $\Delta K_{th}{}^*$ had been exceeded, and the crack extended. Note that on the sheet surface, the subsequent high cycle fatigue crack did not propagate out of the overloaded crack tip. Figure 10*d* shows the same crack location after polishing down to view the center thickness of the specimen. In contrast to the surface behavior, the majority of the fatigue crack remained planar through the overload zone. In this material, cracks on the surface often deviated from planar and extended somewhat at $\Delta K < \Delta K_{th}{}^*$ before arresting permanently until ΔK was increased. Most of the crack away from the surface did not extend until $\Delta K_{th}{}^*$ was exceeded. Figure 11*a* illustrates crack extension

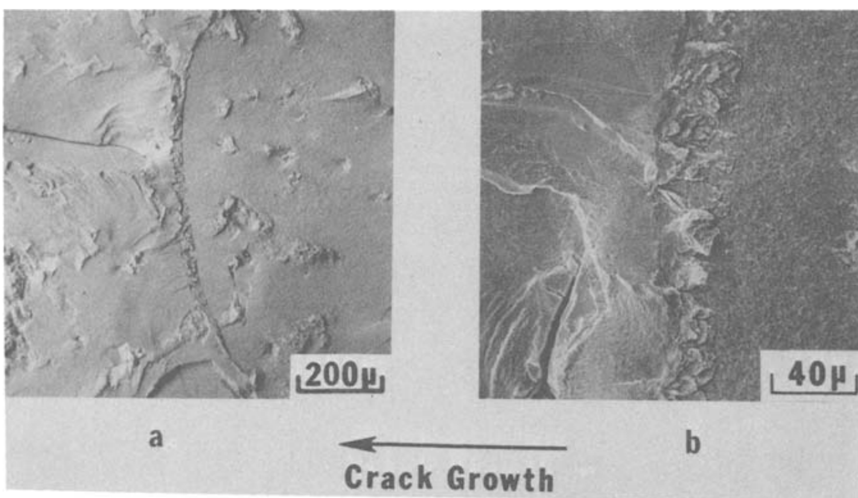

FIG. 11—*Scanning electron fractographs of the DS nickel alloy after a single cycle overload to 53 $MNm^{-3/2}$ and threshold evaluation at 866 K and R = 0.694: (a) Low magnification showing crack curvature and incremental surface growth; (b) High magnification showing the change in elevation at the center thickness due to the overload.*

and arrest near the sheet surface at a typical fracture surface after a 53 $MNm^{-3/2}$ overload. To ensure that these surface crack extensions were truly arrested, further cycling at the same ΔK conditions was performed every time surface extension occurred. No additional crack growth occurred in up to 5 x 10^7 additional cycles. The specimen shown in Fig. 11*a* experienced five up-loads before $\Delta K_{th}{}^*$, and it can be seen that the surface crack length increased incrementally and arrested while the center portion of the crack was stationary. Figure 11*b* is a higher magnification of the center portion of the overload region showing ductile crack advance during the overload and an elevation change of the crack plane from before the overload to after the overload. The change in elevation was measured from the fracture surface and found to be between 8 to

12 μm. The value of the crack tip opening displacement (CTOD) was calculated to be 7 μm using the approximate Eq 1 from Ref *6*,

$$\mathrm{CTOD} = \frac{0.25\ \Delta K^2}{E\ \sigma_{ys}} \tag{1}$$

where

E = Young's modulus,
ΔK = stress field intensity range, and
σ_{ys} = yield stress.

Scanning electron microscopy work on the DS nickel-base alloy specimens in this investigation indicated, that during the larger overloads, the crack tip was blunted in such a way that sharp corners were produced at the top and bottom of the tip. After the overload, the high cycle fatigue crack propagated from either the top or bottom corner of the overloaded crack tip, and in some cases both. This crack tip bifurcation would certainly reduce the crack tip stress intensity and thus contribute to the increased ΔK_{th} that results from the overload.

The fractographic observations of the Ti-6Al-4V are more difficult to interpret due to the material's fine grain size which caused microscopic crack plane irregularities. Replica fractography provided additional resolution and assisted in identification of the following two regimes:

(*a*) Overload $K_{hmax} \leq 33$ $\mathrm{MNm}^{-3/2}$ –Macroscopically, the position of the crack front at the overload (beach marks) is not well defined, Fig. 12*a*. Microscopic observations in the overload areas reveal slight changes in the fracture plane elevation and subtle differences in the crystallographic, cleavage-like appearance [*5*].

(*b*) Overload $K_{max} > 33$ $\mathrm{MNm}^{-3/2}$ –Macroscopically, distinct beach marks on the fracture surface clearly delineate the crack front location at overload application, Fig. 12*b*. Microscopically, each overload cycle is accompanied by crack advance by ductile rupture. The amount of crack advance (width of the dimpled-rupture area) increases with increasing K_{hmax} of the overload.

In all cases, the fatigue growth just after ΔK_{th}^* occurs in the crystallographic mode and proceeds from the overloaded crack tip.

General Discussion

The threshold (ΔK_{th}^*), below which cracks do not grow in Mode I fatigue, has been shown to increase markedly with magnitude of a prior overload. Figures 6 and 7 show that with overloads much larger absolute increases in ΔK_{th}^* can be obtained at low stress ratios than at higher stress ratios. The main reason for this is that a much larger percentage overload can be applied at the lower stress ratios without exceeding the fracture toughness of the material. Figure 13 shows the same results normalized and plotted as relative threshold

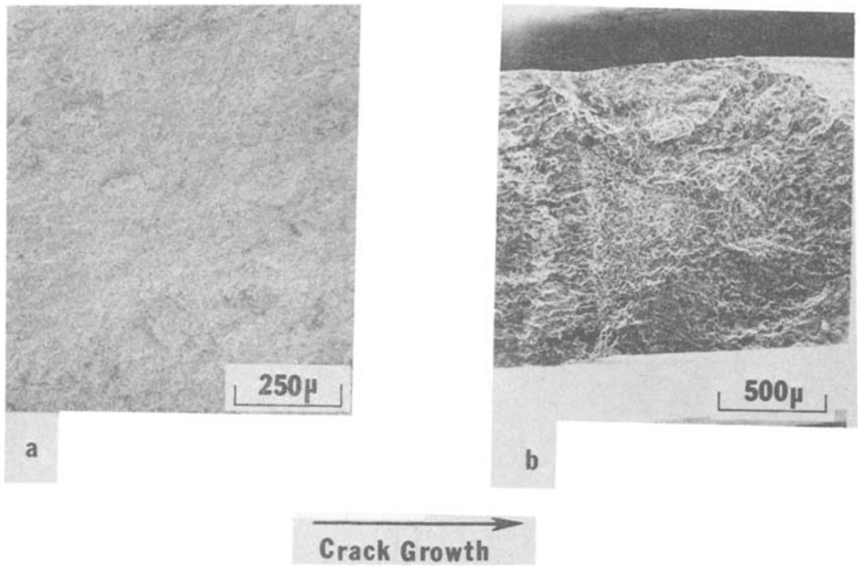

FIG. 12–*Scanning electron fractographs of Ti-6Al-4V after single cycle overloads and the threshold evaluations at 1000 Hz and 294 K: (a) Overload* $K_{max} = 27.5$ *MNm*$^{-3/2}$ *showing no apparent difference in fracture appearance due to the overload; (b) Overload* $K_{max} = 66$ *MNm*$^{-3/2}$ *showing crack advancement by ductile rupture during the single cycle overload.*

$\Delta K_{th}{}^{*}/\Delta K_{th}$, where $\Delta K_{th}{}^{*}$ is the threshold after a given overload to K_{hmax} and ΔK_{th} is the basic threshold at a given stress ratio and temperature, against relative overload K_{hmax}/K_{max}, where K_{max} is that reached in the basic ΔK_{th} evaluation. Normalized in this way, data for all stress ratios investigated fall on the same line indicating that the effect of relative overload on relative threshold is independent of R. Both materials behave similarly, although the threshold of the DS nickel superalloy is slightly more sensitive to overloads. Therefore, it may be possible to write a relationship for $\Delta K_{th}{}^{*}$ after overload which is independent of R and only slightly dependent on microstructure. However, since under the conditions investigated both materials had almost the same modulus of elasticity and fracture toughness, more work with different materials and overload conditions needs to be done to examine this and other possible relationships.

The observation of crack closure at loads greater than zero has led to the definition of an effective ΔK, less than the applied ΔK, which better predicts many fatigue crack growth effects. The contribution of closure effects to the overload effect on ΔK_{th} has been considered. For Ti-6Al-4V Shih and Wei [7] did not observe crack closure above $R = 0.3$. In the present work, we made some limited closure measurements which agree with their results. In fact, for single cycle overloads, we measured crack opening at $K_o = 0.25\ K_{hmax}$. Effective ΔK_{th} can be calculated by subtracting K_o or K_{min}, whichever is larger, from K_{max} of the fatigue cycle. Analysis of the effective ΔK_{th} data indicated that

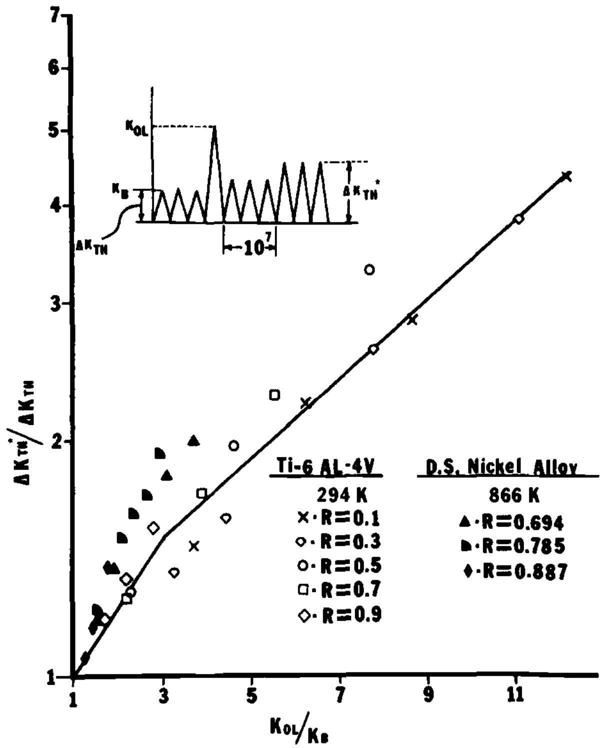

FIG. 13—*The relative change in fatigue threshold after single cycle overloads as a function of the relative overload for both alloys and all stress ratios.*

crack closure, in addition to residual compressive stresses at the crack tip, could contribute to the increase in ΔK_{th}^{*} due to the overloads. However, closure is not a factor at high values of R.

The effect of overloads on subsequent ΔK_{th} have been shown to be quite large and reproducible. The effect appears to be nearly independent of microstructure. However, the observations are such that no single mechanism appears responsible. For instance, for overloads at higher temperature where the yield stress is much lower, much more crack tip blunting and residual strains should occur; but ΔK_{th} was only marginally higher. Perhaps the lower flow stress at high temperature reduces the magnitude of beneficial residual compressive stresses. Crack tip blunting, bifurcation, closure, and residual stress fields may all contribute to the overload effect, and additional work is necessary to quantitatively define their individual and cumulative effects.

Conclusions

1. The basic fatigue threshold decreases nearly linearly with increasing stress ratio (R) for both alloys and is frequency dependent for Ti-6Al-4V.

2. The overload modified fatigue threshold increases exponentially with magnitude of the prior overload.

3. At low R, overloads produce much larger absolute magnitude increases in the threshold than at high R; but the effect of relative overload on relative threshold is independent of R, as shown in Fig. 13.

4. The number of overloads and their detailed shape and rate can affect threshold but are much less important than overload magnitude.

5. Fatigue thresholds after overloads of various magnitudes can be extrapolated to obtain the basic threshold at low R ratios where valid precracking is impractical.

Acknowledgments

The authors wish to acknowledge the assistance of K. V. Mattson and R. Perkins for the care they took in the testing of these specimens.

References

[1] *Fracture Mechanics of Aircraft Structures*, Liebowitz, H., Ed., AGARD-AG-176, Technical Editing and Reproduction Ltd., London, 1974.
[2] Irving, P. E. and Beevers, C. J., *Metallurgical Transactions*, Vol. 5, 1974, p. 391.
[3] Weiss, V. and Lal, D. N., *Metallurgical Transactions*, Vol. 5, 1974, p. 1946.
[4] Schmidt, R. A. and Paris, P. C. in *Progress in Flaw Growth and Fracture Toughness Testing, ASTM STP 536*, American Society for Testing and Materials, 1973, p. 79.
[5] Yuen, A., Hopkins, S. W., Leverant, G. R., and Rau, C. A., *Metallurgical Transactions*, Vol. 5, 1974, p. 1833.
[6] Hahn, G. T., Hoagland, R. G., and Rosenfield, A. R., *Metallurgical Transactions*, Vol. 3, 1972, p. 1189.
[7] Shih, T. T. and Wei, R. P., *Engineering Fracture Mechanics*, Vol. 6, 1974, p. 19.
[8] Koiter, W. T., "Note on the Stress Intensity Factors for Sheet Strips with Cracks under Tensile Loads," Technological University, Department of Mechanical Engineering, Report No. 314, 1965.

DISCUSSION

Otto Buck[1] *(written discussion)*—You showed a figure that indicates a dependence of K_{th} on R for Ti-6-4. How much of the effect is due to precracking at low R? I also wanted to point out that one ought to be very careful with threshold data since the crack closure load changes rapidly at low $\Delta a/\Delta N$. The effect is that threshold is much lower than you showed in your figure.[2]

S. W. Hopkins, C. A. Rau, G. R. Leverant, and A. Yuen (authors' closure)—It is agreed that one ought to be very careful with threshold data. Specifically at low stress ratios, the ability to obtain a valid precrack without exceeding K_{max}

[1] Science Center, Rockwell International, Thousand Oaks, Calif. 91360.

[2] Frandsen, J., Inman, R. V., and Buck, O., *International Journal of Fracture Mechanics*, Vol. 11, 1975, p. 345.

of the threshold test is difficult. For all ΔK_{th} data presented in this paper, low stress ratio ($R \approx 0$) precracks were used at various final K_{max} conditions which never exceeded K_{max} of the threshold test.

Additional work has since been done on this titanium alloy which shows an effect of precracking condition on the low stress ratio threshold value and no effect of precracking condition on the high stress ratio threshold value. Tubular specimens were precracked at various negative stress ratios down to $R = -9.0$ prior to obtaining ΔK_{th} at positive stress ratios. The largest reduction in ΔK_{th} was 1 $MNm^{-3/2}$ for all the various negative stress ratio precracking conditions investigated and this occurred at $R = 0.1$; the reduction in ΔK_{th} value was reduced with increasing stress ratio. At $R = 0.7$ and above no reduction in ΔK_{th} was obtained regardless of the precracking condition. For applications where low-amplitude high cycle (vibratory) fatigue is superimposed on high-amplitude low cycle fatigue, the high stress ratio results are of most technological importance. Under these conditions the precracking effects do not exist. These new results of negative mean stress precracking will be reported in the future.

O. A. Adetifa,[1] C. V. B. Gowda,[2] and T. H. Topper[1]

A Model for Fatigue Crack Growth Delay Under Two-Level Block Loads

REFERENCE: Adetifa, O. A., Gowda, C. V. B., and Topper, T. H., "A Model for Fatigue Crack Growth Delay Under Two-Level Block Loads," *Fatigue Crack Growth Under Spectrum Loads, ASTM STP 595*, American Society for Testing and Materials, 1976, pp. 142–156.

ABSTRACT: After reviewing previous attempts to quantify delay, a composite stress intensity parameter, $(K_{\ell max}/K_{hmax}) \cdot \Delta K_{\ell}$, is proposed to correlate the number of delay cycles in simple two-level variable-load amplitude tests for various combinations of stress levels. Its application is restricted in the present investigation to room temperature tests in an air environment. Delay (cycles) is defined herein as the period of apparent zero crack growth after the overload, and the stress intensity factors, $K_{\ell max}$ and K_{hmax} refer to the stress intensities accompanying the lower and higher load levels, respectively. It is hypothesized on the basis of experimental observations that material under different two-level block loading sequences, but having equal values of the parameter, will experience the same delay.

Good correlations for data on aluminum alloys, titanium alloys, and carbon steel taken from the work of several investigators are obtained using the parameter. An empirical model relating the delay to a power function of the parameter is suggested. Limitations of the model are pointed out and discussed. The engineering significances of the parameter with respect to the determination of crack propagation life and crack arrest conditions are discussed.

KEY WORDS: fatigue (materials), crack propagation, stress ratio, aluminum alloys, titanium alloys, carbon steels, delay cycles, loads (forces), cyclic loads

Qualitatively, the effects of tensile peak overloads on fatigue crack growth at a lower level of cyclic load are now well known. A general conclusion reached by most investigators [*1–6*][3] is that high tensile overloads will cause crack growth rate retardation (or delay), and sometimes even crack arrest, during subsequent cycling at a constant lower load level. From the point of view of safely predicting crack life endurance, this is beneficial because crack propagation life predictions based on the usual crack propagation rate expression will be smaller than the actual life. However, for better and less conservative predictions of crack propagation lives for engineering structures subjected to variable amplitude loading, delay effects should be considered.

Several explanations of the fatigue crack delay phenomenon have been

[1] Research student and professor, respectively, Department of Civil Engineering, University of Waterloo, Waterloo, Ontario N2L 3G1, Canada.

[2] Senior engineer, Advanced Reactors Division, Westinghouse Corp., Madison, Pa. 15663.

[3] The italic numbers in brackets refer to the list of references appended to this paper.

proposed [1,2,7–9] but the most often discussed theories in this regard are: (a) the residual compressive stresses theory [1,2], (b) the crack closure theory [7], and (c) the crack tip blunting theory [8]. At present, no single mechanism appears to be capable of satisfactorily explaining all the features of mixing high and low load cycles on fatigue crack propagation. In reality, delay and other load interaction effects are probably caused by a combination of these mechanisms.

Few attempts [1,3,5,10–13] have been made to quantify the delaying effect. An accurate quantitative description of this effect, which would allow the prediction of the crack growth retardation behavior of several materials without recourse to testing each individual material, would be invaluable to analysts and designers. The objective of this paper is to present a simple method of predicting delay cycle trends due to a two-level loading. Before the development of this method, previous attempts to quantify delay will be briefly reviewed in order to put the method in perspective.

Previous Quantitative Models

Hudson, Hardrath, and McEvily [1,3,5] made what are probably the first serious attempts to correlate the number of delay cycles with the applied stress levels. Graphs of the delay cycles versus the low stress for different peak stress levels were presented for 2024-T3 and 7075-T6 aluminum alloys. Stulen et al [10] and Wei et al [14] also presented data in graphical forms for titanium alloys. Essentially, these graphical approaches are attempts to produce "delay stress-life (S–N) curves" for the materials investigated.

Other methods used to quantify delay were based on data obtained from constant stress intensity tests [11–13,15]. These methods assume that the average growth rate during the retardation period can be determined using an effective stress intensity in the basic growth rate equation [7]. For 2024-T3 aluminum subjected to a single peak overload, Von Euw [11] proposed the parameter r_0/bN_D^* as a measure of delay (r_0 is the overload plastic zone, b is the steady growth rate after the overload, and N_D^* is the number of delay cycles corresponding to r_0), while Probst and Hillberry [12] proposed the following expression for the same material ($R = 0.3$)

$$N_D = \frac{r_0}{C[K_{\ell\,\max} - EK_{\text{hmax}}]^n} \tag{1}$$

where $K_{\ell\max}$ is the maximum lower load stress intensity factor, K_{hmax} is the maximum high load or overload stress intensity factor, E is a constant relating the critical stress intensity to cause crack arrest and the overload stress intensity (to be experimentally determined), C and n are constants from the constant-amplitude growth rate expression ($da/dN = C\Delta K^n$). Equation 1 is applicable for cases when $K_{\text{hmax}} > K_{\ell\max}$ and $(K_{\ell\max} - EK_{\text{hmax}}) > 0$.

Using an effective stress intensity concept, Himmelein and Hillberry [13] and

Gray and Gallagher [15] obtained N_D by an integration of the constant amplitude crack propagation equation within the overload plastic zone. The overload residual stress intensity factor was experimentally determined by Himmelein and Hillberry while Gray and Gallagher used a modified form of the Wheeler retardation model [16] to account for load interaction effects. In all of these methods, it was found that for a single peak overload, the correlation between predictions and experimental data was within a factor of two.

In this paper, a simple phenomenological method of determining the number of delay cycles for simple two-level loading is presented. A composite stress intensity parameter is introduced to correlate the delay for single peak overloads and for high-low block loadings for a variety of materials. When a consistent definition of delay period is adopted, the proposed parameter provides a good correlation of delay trends for two-level loadings.

Composite Stress Intensity Parameter

One of the difficulties encountered in using work from different investigations is the lack of a consistent definition of delay. Consequently, delay will be defined herein as the period of apparent zero macrocrack growth following a peak overload or a block of overloads and is determined as illustrated in Fig. 1.

Experimental results [1,14,17–19] have shown delay to depend on a large number of variables including ΔK_ℓ, ΔK_h, R_ℓ, R_h, N_h, t_h, and metallurgical, environmental, and geometrical factors (temperature, thickness, yield stress (σ_{ys}), strain hardening (n'), and stress intensity gradient (dK/da)). In functional notation

$$N_D = f[\Delta K_\ell, \Delta K_h, R_\ell, R_h, N_h, t_h, \sigma_{ys}, n', \ldots\ldots\ldots] \tag{2}$$

where ΔK is the stress intensity factor range, R is the stress ratio ($R = K_{min}/K_{max}$), the subscript ℓ is for the low load level, h is for the high load level, N_h is the number of applications of the high load, and t_h is the hold time at the high load level. The present work deals only with the influence of a subset of these variables while others are held constant or treated separately. Specifically, variations in delay with N_h are bounded by dealing with the extreme cases in which N_h is one or very large. Environmental and hold time effects are minimized by considering only results from room temperature tests in air without deliberate hold periods. Metallurgical and thickness effects are dealt with by considering materials and stress states (plane strain or plane stress) separately. Since only step changes in load were introduced in the two-level tests of this study, the effects of (dK/da) on delay is expected to be constant for all cases considered. Within these restrictions, the following hypothesis relating the delay cycles to various values of the variables in Eq 2 is now advanced.

Hypothesis—The composite stress intensity parameter $(K_{\ell max}/K_{hmax}) \cdot \Delta K_\ell$ governs the number of delay cycles in variable-amplitude load fatigue crack propagation, and, as a consequence, delay will be the same for a given N_h and material in all two-level load sequences having the same value of the parameter.

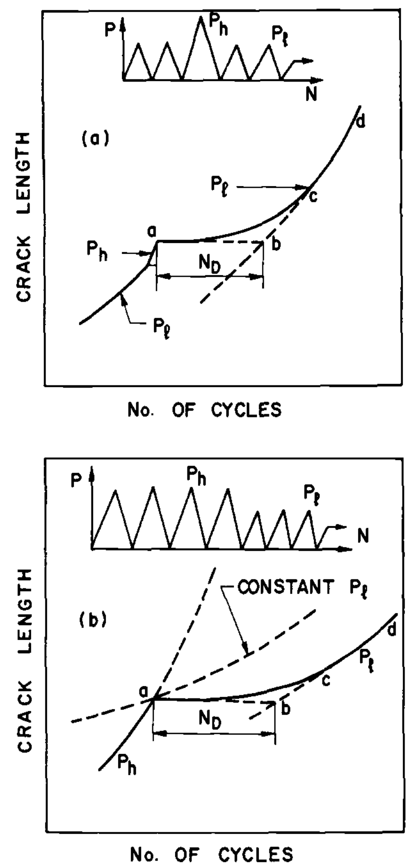

FIG. 1—*Schematic illustration of delay in fatigue crack growth and definition of delay cycles,* N_D [20].

The validity and usefulness of the composite stress intensity parameter will now be examined for various metals.

Delay Data Correlation

The preceding hypothesis is tested for the materials listed in Table 1. The results for API X-65 steel are from tests conducted at the University of Waterloo while results for other materials are taken from the work of other investigators (referenced in Table 1), and delay is determined as shown in Fig. 1. All of the tests were load controlled, except those reported in Refs *11* thru *13* which were constant-K tests. The tests were conducted under zero-tension or tension-tension sinusoidal loading. Specimen types used by various investigators included a compact tension specimen, a center-notched specimen, and single edge notch specimen.

Figures 2 thru 8 show correlations between the proposed composite stress intensity parameter and delay for the various materials. Different correlations

TABLE 1 – *Mechanical properties of metals investigated.*

Material	Yield Stress (0.2% Offset), MN/m^2 (ksi)	Ultimate Strength, MN/m^2 (ksi)	Elongation in 2-in. Gage Length, %	% Reduction in Area	Ref	Specimen Details
Ti-6Al-4V (titanium)	923.2 (133.9)	984.6 (142.8)	13.3	. . .	[20]	center-notched specimen t = 1.6 mm (0.06 in.)
	975.6 (141.5)	1042.5 (151.2)	12.0	. . .	[14]	center-notched specimen t = 5.08 mm (0.20 in.)
2024-T3 (aluminum)	358.9 (52.05)	497.4 (72.14)	21.0	. . .	[1]	center-notched specimen t = 2.29 mm (0.09 in.)
7075-T6 (aluminum)	520.6 (75.50)	571.9 (82.94)	12.0	. . .	[1]	center-notched specimen t = 2.29 mm (0.09 in.)
SAE 1020 cold rolled steel	627.4 (91.0)	668.8 (97.0)	. . .	. . .	[21]	[a]compact tension specimen t = 6.35 mm (0.25 in.)
Austenitic manganese steel[b]	420.6 (61.0)	1048.0 (152.0)	49.0(1″)	34	[22]	[a]compact tension specimen t = 6.35 mm (0.25 in.)
API X-65 steel[b]	449.0 (65.1)	688.3 (99.82)	. . .	51	University of Waterloo	center-notched specimen t = 2.54 mm (0.10 in.) modified compact specimen t = 6.35 mm (0.25 in.)
Ti-8Al-1Mo-1V (titanium)	937.69 (136.0)	1051.45 (152.5)	12.5	. . .	[9]	center-notched specimen t = 1.14 mm (0.045 in.)

[a] Flat fracture surface reported.

[b] Cyclic strain hardening material.

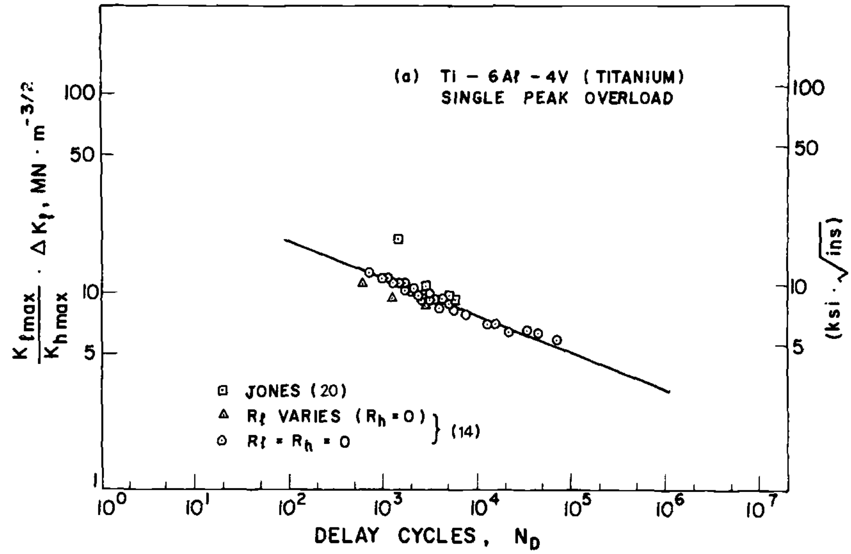

FIG. 2—*Relationship between* $(K_{\ell max}/K_{hmax}) \cdot \Delta K_{\ell}$ *and delay cycles for Ti-6Al-4V (titanium).*

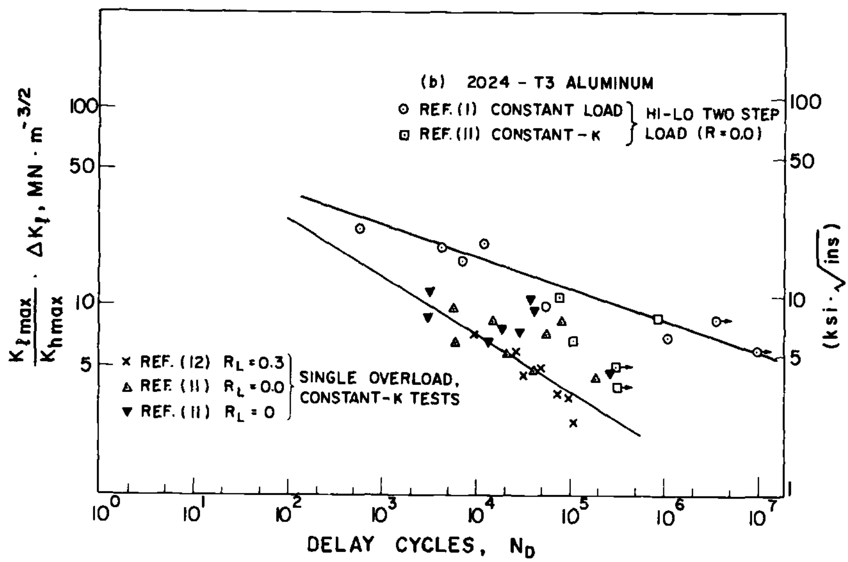

FIG. 3—*Relationship between* $(K_{\ell max}/K_{hmax}) \cdot \Delta K_{\ell}$ *and delay cycles for 2024-T3 (aluminum).*

are shown for the single-cycle peak load and for high-low two-step tests. The plots imply an empirical relationship for N_D of the form

$$N_D = A\left[\frac{K_{\ell\,max}}{K_{hmax}} \cdot \Delta K_{\ell}\right]^m \tag{3}$$

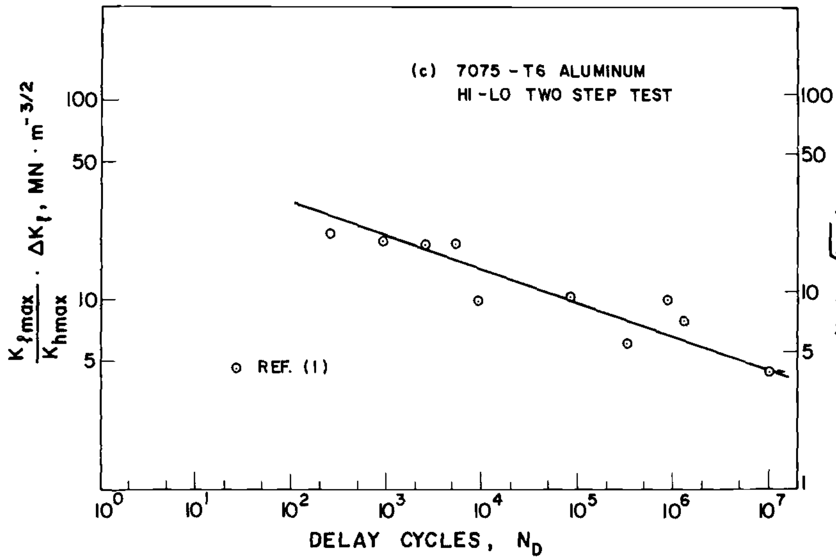

FIG. 4—*Relationship between* $(K_{\ell max}/K_{hmax}) \cdot \Delta K_\ell$ *and delay cycles for 7075-T6 (aluminum).*

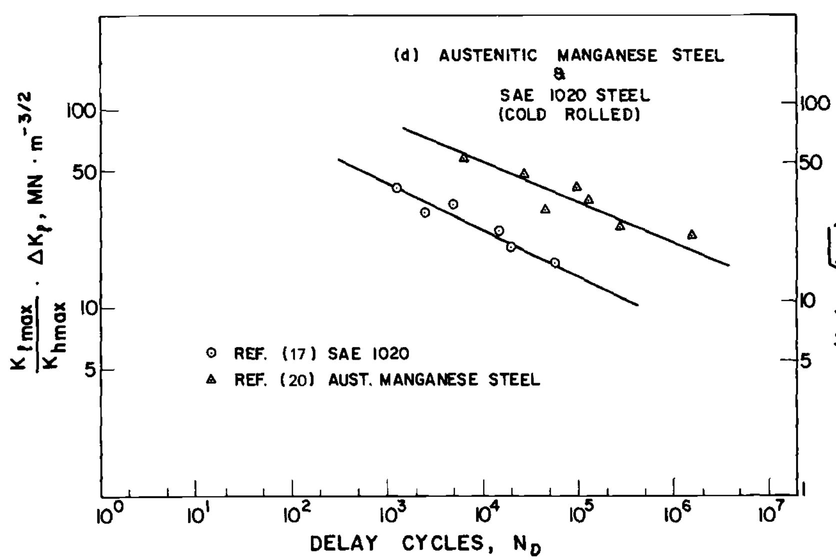

FIG. 5—*Relationship between* $(K_{\ell max}/K_{hmax}) \cdot \Delta K_\ell$ *and delay cycles for SAE 1020 steel and austenitic manganese steel.*

where A and m are constants for the data used in this work. Values of A and m obtained from a least-square fit of the plots are given in Table 2. It should be noted that Eq 3 is valid for only K_{hmax} greater than $K_{\ell max}$ (for constant amplitude loading $K_{hmax} = K_{\ell max}$, and Eq 3 would predict delay, which is not correct).

Data plotted in Figs. 6 and 8 are obtained for different values of R_ℓ and R_h ($R \geq 0$). In Fig. 6, the data for $R > 0$ lie below the data for $R = 0$, indicating that the delay for the former case is less than for the latter. There is no data available for $R = 0$ for the titanium alloy in Fig. 8, however, it is evident from the graph

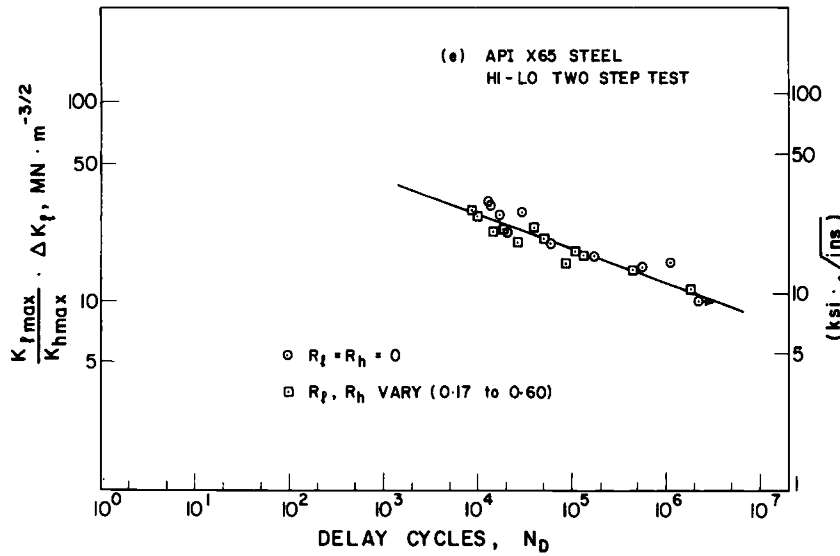

FIG. 6—*Relationship between* $(K_{\ell max}/K_{hmax}) \cdot \Delta K_\ell$ *and delay cycles for API-X65 steel (high-low).*

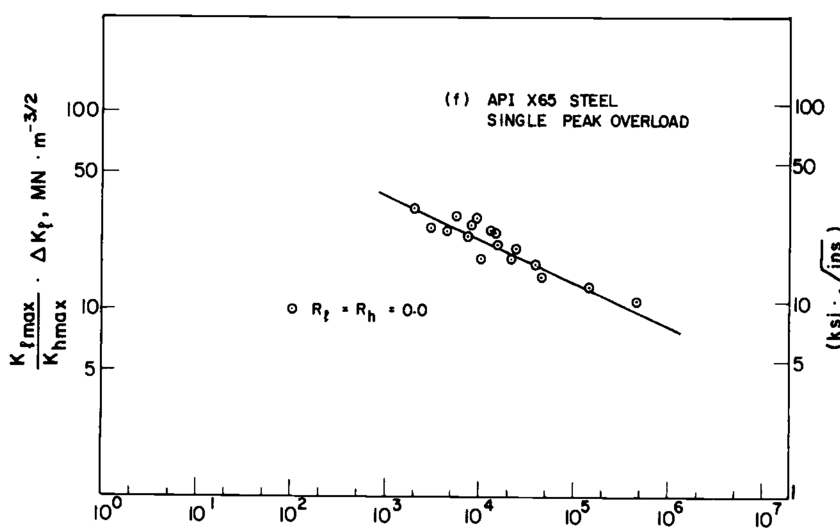

FIG. 7—*Relationship between* $(K_{\ell max}/K_{hmax}) \cdot \Delta K_\ell$ *and delay cycles for API-X65 steel (SO).*

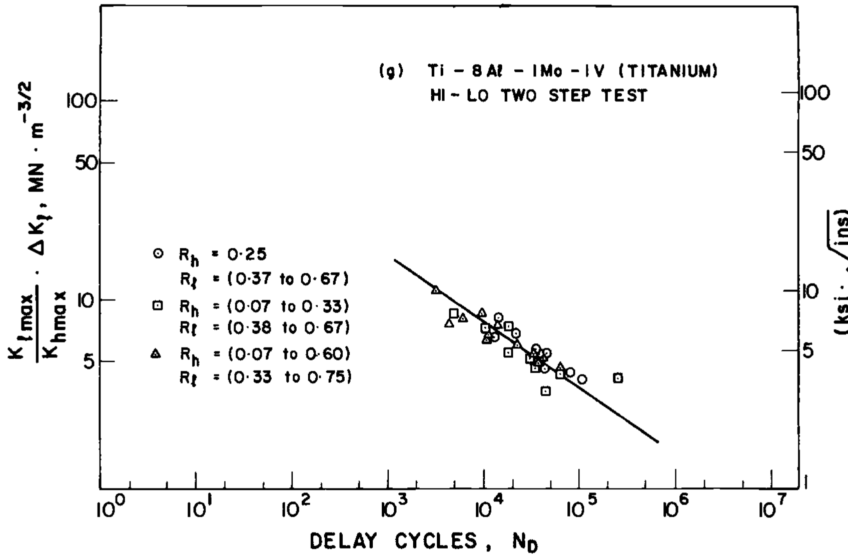

FIG. 8—*Relationship between* $(K_{\ell max}/K_{hmax}) \cdot \Delta K_{\ell}$ *and delay cycles for Ti-8Al-1Mo-1V (titanium).*

TABLE 2 – *Values of* A *and* m *in Eq 3.*

MATERIAL	A^a	m
Ti-6Al-4V (titanium)	4.35×10^{8}	−5.5
2024-T3[b] (aluminum)	1.21×10^{11}	−5.69
7075-T6 (aluminum)	3.28×10^{10}	−5.86
SAE 1020 steel	5.25×10^{9}	−4.22
Austenitic manganese steel	2.43×10^{12}	−4.95
API-X65 steel (high-low)	9.1×10^{11}	−5.72
(Single overload)	7.57×10^{9}	−4.49
Ti-8Al-1Mo-1V (titanium)	3.67×10^{6}	−3.01

[a] Units in $\dfrac{1}{(\mathrm{ksi}\sqrt{\mathrm{in.}})^m}$.

[b] High-low only.

that for a range of values of R_ℓ and R_h, the data fall essentially within a narrow band. If it is assumed that data for $R = 0$ for the material will lie above those for $R > 0$, as is the case in Fig. 6, conservative predictions for the former case will be obtained from Fig. 8.

Figure 3 gives a plot of the data for single overload constant-K tests [*11,12*]. The parameter correlates relatively well with the data by Probst and Hillberry [*12*], but the correlation is poor and there is considerable scatter in the data taken from Von Euw [*11*].

It is interesting to note that specimen type and thickness do not appear to greatly affect delay. In Figs. 6 and 7, data obtained from a 2.54-mm-thick center-notched specimen cannot be distinguished from those obtained from a 6.35-mm-thick modified compact tension specimen. This finding is contrary to that recently reported by Shih and Wei [*19*] who found delay to be a function of specimen thickness for a 7075-T6 aluminum alloy. It may be significant that the specimens for which data are given in Figs. 6 and 7 all showed the slant fracture typical of plane stress. Thus, if a change in delay with specimen thickness is due to differences between a plane strain mode and a plane stress mode of cracking, the thickness effect is not expected in test results shown in Figs. 6 and 7.

Crack Arrest Condition

The condition for crack arrest can be determined using the proposed parameter if arrest is equated to some suitably long delay. If, for instance, crack arrest is defined as a number of delay cycles in excess of 2×10^6 for the API X-65 steel of Fig. 7, a value of the parameter of 7.91 is required for arrest. Then if ΔK_ℓ were 21.98 MN/m$^{3/2}$ for a crack, the overload ratio for crack arrest would be 0.34 for $R = 0$. A different value of overload ratio would be obtained for a different ΔK_ℓ. From the foregoing, it is apparent that the overload ratio to cause crack arrest depends on the stress intensity level range, ΔK_ℓ, and the deduction is consistent with the experimental results of Corbly and Packman [*23*]. In another example, Wei et al [*14*] found that for a low stress intensity level of 10.99 MN/m$^{3/2}$ the crack did not propagate in 450 000 cycles. For this condition, the value of the parameter is 3.92 which gives a predicted delay (Fig. 2) of 400 000 cycles—a conservative prediction.

Compared with the "zero-in" technique used by Probst and Hillberry [*12*] to determine the arrest condition in Eq 1, this parameter offers a simpler procedure and eliminates the trial-and-error approach inherent in the zero-in method.

Discussion

The results from the analysis of data on delay for a variety of materials indicate that the parameter, $(K_{\ell max}/K_{h max}) \cdot \Delta K_\ell$ adequately correlates delay for the data examined and Eq 3 can be used to determine delay cycles (defined in Fig. 1). Effects of metallurgical and environmental variables (for example,

σ_{ys}, strain hardening (n'), temperature, etc.) can only be accounted for at present through variations in the parameters A and m in Eq 3. Applicability of the composite parameter so far has been shown only for first-order delay effects where the influences of peak loads do not interact. Second-order effects due to periodic overloads may cause an increase or a decrease in delay [*17,18*] depending on the interval of repetition. Other load interaction effects [*9*] (for example, delayed retardation) are not considered in this phenomenological model. Furthermore, the effects of stress intensity gradient, dK/da, on delay period pointed out by Schijve [*9*] and discussed by Bucci [*24*] is not considered. In the context of the loading pattern considered here, the effect of stress intensity gradient, dK_{ℓ}/da, should be constant since a step change in load amplitude is applied in all cases. If this were not the case, the stress intensity gradient effect would probably be important [*24*]. The proposed parameter suggests that primary variables in Eq 2 governing the delay period are $K_{\ell\,\max}$, ΔK_{ℓ}, and K_{hmax}.

It should be noted that only the two extreme cases of overloads, namely, the single overload and two-step high-low block loading cases, were considered in the preceding delay model. Therefore Eq 3 does not account for an increase in delay cycles with an increase in the number of applied overloads. However, it is expected that the delaying effect of multiple overloads will be bounded by the two cases considered here. In a situation where the overload is repeated often enough that there is appreciable crack growth during its repeated application, a reasonable estimate of the expected delay cycles should result from the high-low loading case.

No similar parameter describing delay has been found in the literature, but it is interesting to compare it with parameters used by other investigators to predict crack initiation and crack propagation. Jack and Price [*25*] proposed a function $\Delta K\ (\rho_0/\rho')^{1/2}$ to predict crack initiation cycles in a mild steel under constant amplitude loading. In the function, ρ_0 is the critical value of the crack tip radius and ρ' is the effective crack tip radius. If we extend this to the case of variable amplitude loading, (for example, a high-low two-step test), and assume that ρ_0 is the crack root radius at the low load level and ρ' is the crack root radius at the high load, we can show that the function reduces to the same form as the parameter used herein. Let the crack root radius be represented by the crack opening displacement (COD) at the respective load level. COD $\propto \epsilon_y\ (K^2/\sigma_{ys}{}^2)$. By substitution, $\Delta K(\rho_0/\rho')^{1/2}$ becomes $\gamma \cdot (K_{\ell\max}/K_{\mathrm{hmax}}) \cdot \Delta K_{\ell}$ where γ is a constant, which is, except for the constant, identical to the parameter proposed in this paper.

During the delay period, crack growth can be visualized as continuing on a relatively small scale ($\sim 10^{-7}$ cm/cycle for a very long delay). In the high strain region in the plastic zone ahead of the crack tip, many microcracks are propagating and coalescing until a dominant crack is formed [*26*]. Under these circumstances, initiation and propagation intermix and the growth process can be described by a damage accumulation theory [*25–28*]. The equation for crack propagation rate, based on a damage accumulation mechanism is given by [28]

$$\frac{da}{dN} = \lambda \frac{\Delta\bar{\epsilon}_{\rho}{}^{2} \cdot \Delta K^{2}}{4B^{2}\sigma_{ys}} \tag{4}$$

where $\Delta\bar{\epsilon}_{\rho}$ is the weighted average strain range close to the crack tip, B is a measure of ductility, and λ is a constant. It is evident from the expression that the function, $\Delta\epsilon_{\rho}\cdot\Delta K$ is the controlling variable for crack growth. For variable-amplitude loading, Rice [29] has shown by analysis that the strain range at a blunted crack tip depends on the ratio of the stress intensities, K_{ℓ} and K_{h}. That is, $\Delta\epsilon_{\rho} \propto (K_{\ell}/K_{h})$. With this expression, the function can be written as $\Delta\bar{\epsilon}_{\rho}$ ΔK α $(K_{\ell}/K_{h}) \cdot \Delta K_{\ell}$. Assuming a proportionality factor of β, it becomes $\Delta\bar{\epsilon}_{\rho}\cdot\Delta K = \beta(K_{\ell}/K_{h}) \cdot \Delta K_{\ell}$ which again is identical to the parameter proposed except for the constant.

Finally, the engineering significance of the proposed parameter lies in its provision of a simple method of estimating delay, thereby, making possible an adjustment of crack propagation life obtained from a direct integration of a constant-amplitude crack propagation "law," for example

$$\Sigma N = \int_{a_i}^{a_f} \frac{da}{f(\Delta K)} + N_D$$

Also, the delay model can be used to estimate crack growth behavior under block programmed loading by accounting for the delay after a step down in load. When using Eq 3 for multi-step increasing or decreasing block loading, it must be borne in mind that it was developed for the simple cases of two-level (high-low) block loading. It does not account for the initial acceleration of growth rate after an increase in load level and the interaction of delay effects in a multi-step decreasing load sequence. Many other variables will also have to be included in the model to make it suitable for spectrum loading.

Summary and Conclusions

This study has demonstrated that there is a relationship between the proposed composite stress intensity parameter, $(K_{\ell max}/K_{hmax}) \cdot \Delta K_{\ell}$, and the number of delay cycles due to simple two-step load blocks with different R_h and R_{ℓ} ($R \geq 0$) values for a variety of materials: aluminum alloys, titanium alloys, and carbon steels. The functional form of N_D is

$$N_D = A\left[\frac{K_{\ell max}}{K_{hmax}} \cdot \Delta K_{\ell}\right]^{m}$$

where A and m are experimentally determined. In this form, the model is limited to the estimation of delay for cases when K_{hmax} is greater than $K_{\ell max}$, and ΔK_{ℓ} is due to constant-amplitude sinusoidal loading.

The engineering usefulness of this parameter at present lies in its provision of a simple method of estimating delay and, perhaps, in its utilization in determining the combination of stress intensities that would produce crack arrest.

Acknowledgment

This work was supported by grants from the National Research Council under Grant No. (A.1694), the Defense Research Board of Canada under Grant No. (9535-49), and the Office of Scientific Research of the United States Air Force (AFOSR-71-2120). Mr. Adetifa would also like to acknowledge financial support from the Canadian Commonwealth Scholarship Programme.

References

[1] Hudson, C. M. and Hardrath, H. F., "Effects of Changing Stress Amplitude on the Rate of Fatigue-Crack Propagation in Two Aluminum Alloys," NASA, TN D-960, Sept. 1961.
[2] Schijve, J. and Broek, D., *Aircraft Engineering*, Vol. 34, 1962, p. 314.
[3] Hudson, C. M. and Raju, K. N., "Investigation of Fatigue-Crack Growth Under Simple Variable-Amplitude Loading," NASA, TN D-5702, March 1970.
[4] Trebules, V. W., Roberts, R., and Hertzberg, R. W. in *Progress in Flaw Growth and Fracture Toughness Testing, ASTM, STP 536*, American Society for Testing and Materials, 1973, p. 115.
[5] Hardrath, H. F. and McEvily, A. J. in *Proceedings*, Crack Propagation Symposium, Vol. 1, Cranfield, England, Oct. 1961.
[6] Hudson, C. M. and Hardrath, H. F., "Investigation of the Effects of Variable-Amplitude Loadings on Fatigue Crack Propagation Patterns," NASA, TN D-1803, May 1963.
[7] Elber, W. in *Damage Tolerance in Aircraft Structures, ASTM STP 486*, American Society for Testing and Materials, 1971, pp. 230–251.
[8] Christensen, R. H. in *Metal Fatigue*, McGraw Hill, New York, 1959.
[9] Schijve, J., "The Accumulation of Fatigue Damage in Aircraft Materials and Structures," AGARDograph No. 157, NATO, Jan. 1972.
[10] Stulen, F. B., Redfern, J. H., and Schulte, W. C., "An Approach to Metal Fatigue," NASA, CR-246, June 1965.
[11] Von Euw, E. F. J., "Effect of Overload Cycles on Subsequent Fatigue Crack Propagation in 2024-T3 Aluminum Alloy." Ph.D. thesis, Lehigh University, March 1971.
[12] Probst, E. and Hillberry, B., *AIAA Journal*, Vol. 12, No. 3, March 1974, p. 330.
[13] Himmelein, M. K. and Hillberry, B., "The Effect of Stress Ratio and Overload Ratio on Fatigue Crack Delay and Arrest Behavior Due to Single Peak Overloads," presented at the Eighth National Symposium on Fracture Mechanics, Brown University, Aug. 1974.
[14] Wei, R., Shih, T., and Fitzgerald, J., "Load Interaction Effects on Fatigue Crack Growth in Ti-6Al-4V Alloy," NASA CR-2239, April 1973.
[15] Gray, T. D. and Gallagher, J. P., "Predicting Crack Retardation Following a Single Overload Using a Modified Wheeler Model," presented at the Eighth National Symposium on Fracture Mechanics, Brown University, Aug. 1974.
[16] Wheeler, O. E., *Journal of Basic Engineering, Transactions*, ASME, Series D, Vol. 94, March 1972, p. 181.
[17] Petrak, J., *Engineering Fracture Mechanics*, Vol. 6, 1974, pp. 725–733.
[18] Jonas, O. and Wei, R. P., *International Journal of Fracture Mechanics*, Vol. 7, No. 1, 1971, pp. 116–118.
[19] Shih, T. T. and Wei, R. P., *Journal of Testing and Evaluation*, Vol. 3, No. 1, Jan. 1975, pp. 46–47.
[20] Jones, R. E., *Engineering Fracture Mechanics*, Vol. 5, 1972, pp. 585–604.

[21] Vargas, L. G. and Stephens, R. I., "Subcritical Crack Growth Under Intermittent Overloading in Cold-Rolled Steel," *Proceedings*, Third International Conference on Fracture, Munich, Germany, Vol. 6, April 1973.
[22] Rice, R. C. and Stephens, R. I. in *Progress in Flaw Growth and Fracture Toughness Testing, ASTM STP 536*, American Society for Testing and Materials, 1973, pp. 95–114.
[23] Corbly, D. M. and Packman, P. F., *Engineering Fracture Mechanics*, Vol. 5, 1973, pp. 479–497.
[24] Bucci, R. J., Discussion on paper by J. Schijve, *Engineering Fracture Mechanics*, Vol. 7, March 1975, pp. 181–185.
[25] Jack, A. R. and Price, A. T., *International Journal of Fracture Mechanics*, Vol. 6, 1970, pp. 401–409.
[26] Lehr, K. R. and Liu, H. W., *International Journal of Fracture Mechanics*, Vol. 5, 1969, p. 45.
[27] McClintock, F. A. in *Fracture of Solids*, Drucker and Gilman, Eds., Gordon and Breach, New York, 1963, p. 65.
[28] Hahn, C. T., Rosenfield, A. R., and Sarrate, M., "Elastic-Plastic Fracture Mechanics," AFML-TR-67-143, Part III, Air Force Materials Laboratory, Wright-Patterson AFB, Ohio, Jan. 1970.
[29] Rice, J. R. in *Fatigue Crack Propagation, ASTM STP 415*, American Society for Testing and Materials, 1967, pp. 247–311.

DISCUSSION

R. I. Stephens[1] *(written discussion)*—Could the authors indicate how this composite stress intensity model might be extended to more complex interaction spectra? How might this model be applied to design situations?

C. V. B. Gowda (author's closure)—The proposed model estimates delay caused by either a single overload or a block of overloads in a high-low load case. However, delay cycles caused by most forms of variable-amplitude loads can be estimated from the model in the following manner. It is known that delay increases as the number of overloads increases. Therefore, the effects of multiple overloads on delay should be bounded by the single overload and high-low step load cases; with the extent of delay increasing toward the higher limit as the number of overloads increases. If the overload is repeated until a quasi-constant growth rate ensues before cycling at the low load level, delay can be reasonably estimated from the high-low case data. Therefore, a combination of careful analysis of load history, good engineering judgement during interpolation or extrapolation, and enough test data to back the proposed model will enable one to estimate delay due to most practical variable-amplitude load cases.

Once an estimate of delay is obtained, integration of crack growth equations (for example, equation in text) or a cumulative damage evaluation procedure will provide data necessary for design or integrity (serviceability) decisions.

For very unusual load histories like random load histories, it is not a simple matter to adopt the proposed model. However, a thorough statistical analysis of load histories may provide information suitable to estimate delay (or inter-

[1] Materials Engineering Division, The University of Iowa, Iowa City, Iowa 52242.

action) effects by procedures similar to the ones discussed in this paper. As a conjecture (first attempt) one could start with

$$\frac{(K_{\ell\max})_{\rm rms}}{(K_{\rm hmax})_{\rm rms}}(\Delta K_{\ell})_{\rm rms}$$

as the parameter which controls the extent of delay. In practical applications of great importance and value, incorporation of simple models, like the one proposed here, in computer programs for crack growth integration would yield quicker and physically interpretable results.

P. D. Bell[1] *and A. Wolfman*[1]

Mathematical Modeling of Crack Growth Interaction Effects

REFERENCE: Bell, P. D. and Wolfman, A., "Mathematical Modeling of Crack Growth Interaction Effects," *Fatigue Crack Growth Under Spectrum Loads, ASTM STP 595*, American Society for Testing and Materials, 1976, pp. 157–171.

ABSTRACT: A combined analytical and experimental program was performed to obtain additional insight into the growth of cracks subjected to simple variable-amplitude loading. The experimental results were used to examine methods of mathematically modeling crack propagation behavior to enhance predictive capability for arbitrary spectrum loading.

The mathematical modeling consisted, primarily, of using the crack closure concept to correlate predicted crack propagation behavior with observed behavior for various simple loading spectra. Two analytical schemes were developed, one of which calculated the crack opening load based on residual forces acting on the crack surface, and another where empirical relationships between loading sequences and crack opening behavior were utilized. Difficulties with the Residual Force Model in correctly representing some of the experimentally observed crack opening and closing effects led to emphasizing the development of the more empirical Crack Closure Model.

The test program encompassed constant-amplitude tension loads, single and multiple tensile overloads, compression spikes, and simplified variable-amplitude load sequences applied to 2219-T851 aluminum and Ti-6Al-4V annealed titanium alloy specimens. Detailed crack-growth and crack closure measurements were obtained. These measurements were used to quantify crack closure behavior as a function of stress ratio, including negative values, and various loading sequences.

KEY WORDS: crack propagation, fatigue (materials), retarding, stress ratio, tension, aluminum alloys, titanium alloys, compressing

The introduction of fracture control criteria for new aerospace structures has necessitated a mathematical model which accurately predicts crack growth during spectrum loading. At the initiation of this development effort, existing mathematical models attempted to predict crack-growth retardation resulting from previous tensile overloads [*1,2*].[2] However, they did not account for a number of factors which could critically affect crack growth. These included the effect of the number of overloads on subsequent retarded crack-growth rates, the effect of compression spikes, and the effect of stress ratio (ratio of minimum stress to maximum stress in a load cycle).

This paper presents two new mathematical models for predicting crack growth

[1] Senior structural mechanics engineer and member, Systems Engineering Staff, respectively, Grumman Aerospace Corporation, Bethpage, N. Y. 11714.

[2] The italic numbers in brackets refer to the list of references appended to this paper.

under arbitrary spectrum loading. These models, which account for some of the previously-mentioned deficiences, were empirically developed during the course of an analytical and experimental investigation of crack growth carried out at Grumman and its subcontractors for the Air Force Flight Dynamics Laboratory [*3*].

Results and Discussion

Crack Closure Model

The Crack Closure Model is an empirically based model which uses an effective stress range concept. The closure variations were defined as functions of previous load history. Since it is a strictly empirical model, certain specific test data, in addition to constant-amplitude data, are required for each new material where predictions are desired. Based on the results of the test programs used to verify the model, it provides fairly good predictions for a variety of load histories.

Concepts—Elber [*4*] showed that cracks subjected to tension-tension loading close when the remotely applied stress, S, is some value greater than zero. Assuming that crack extension occurs only when the applied stress is greater than the crack opening stress, the pertinent stresses involved in the crack-growth process should be the crack opening and maximum stresses. It has been shown [*4–6*] that the crack opening stress differs from the crack closure stress, but for the purposes of this discussion, they will be considered to be equal and will be referred to as the closure stress.

The effective stress range, ΔS_{eff}, is then equal to the difference between the maximum stress, $S_{\max}$, and the closure stress, S_c:

$$\Delta S_{\text{eff}} = S_{\max} - S_c \tag{1}$$

Defining the closure factor, C_f, as

$$C_f = \frac{S_c}{S_{\max}} \tag{1a}$$

Equation 1 becomes

$$\Delta S_{\text{eff}} = S_{\max}(1 - C_f) \tag{1b}$$

For the purpose of this model, a Paris type growth equation was modified and written in terms of ΔK_{eff} as

$$\frac{\Delta a}{\Delta N} = A(\Delta K_{\text{eff}})^n \tag{2}$$

Equation 2 can be written in terms of the effective stress range for a crack of length $2a$, in an infinite sheet as

$$\frac{\Delta a}{\Delta N} = A\left[(S_{\max} - S_c)\sqrt{\pi a}\right]^n \tag{3}$$

The coefficient A and exponent n can be determined by fitting the crack growth rate data plotted against the effective stress intensity range, say for $R = 0$.

Equation 3 is the basis for all crack-growth calculations performed by the model. Elber [4] showed that S_c was a function of S_{max} and R during steady-state (constant-amplitude) crack growth. If S_c in Eq 3 is defined as a function of R, then Eq 3 will predict the effect of stress ratio on crack-growth rates. Further, if S_c is defined as a function of the previous load history, then Eq 3 would predict crack-growth interaction effects. It remains then, to define S_c as a function of stress ratio and previous load history (and any other pertinent parameters) so that Eq 3 will properly predict crack-growth rates for any condition.

Application of Crack Closure to Mathematical Model—In the past, it has been suggested that many parameters influence crack-growth interactions. The most significant parameters were determined from the test data as far as possible. In some areas, quantitative values were not divulged by the data and a certain amount of intuition was employed. In all cases, the model was verified by comparing predicted crack growth with the test data. The most significant parameters found during this program were: effect of R, including compression, on constant-amplitude growth; and the effects on subsequent crack growth of overload stress, previous minimum stress relative to current minimum stress, number of overload cycles, and compression.

Effect of Stress Ratio on Closure—Crack closure measurements were made for both materials under constant-amplitude loading conditions. Some of the results obtained for aluminum are shown in Fig. 1. The closure factor is plotted against stress ratio, and the data show a definite trend towards increasing closure factor with increasing stress ratio. The data scatter shown is typical of that obtained throughout the program. Scatter was more extensive when measurements were taken during and subsequent to transient loading sequences. It was determined

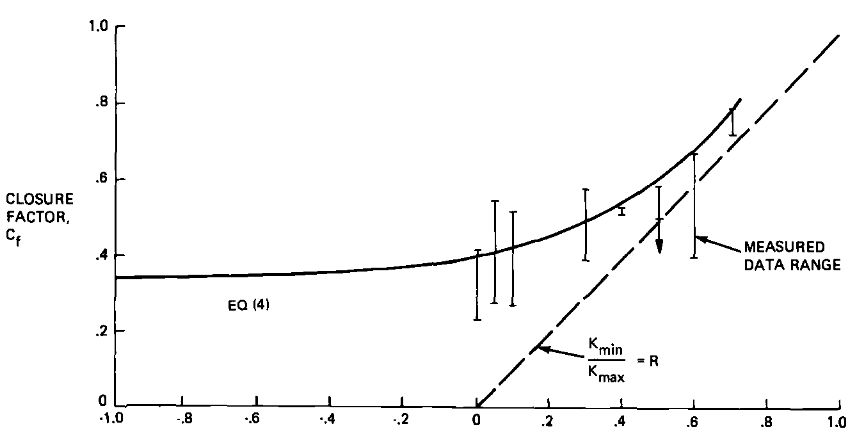

FIG. 1—*Comparison of closure factor versus stress ratio for 2219-T851 aluminum.*

that the measured closure values possessed too much scatter to be used directly for modeling purposes. The absolute value of C_{f_0} (at a stress ratio of zero) was determined from multiple-overload (high-low) crack-growth data by utilizing the crack-growth rates immediately after the load change. Elber [*4*] and the qualitative trend of the measured closure factors indicated that C_f was stress ratio dependent. As a result, C_f was determined indirectly from crack-growth rate data as follows.

Equation 3 may be rewritten as

$$\frac{\Delta a}{\Delta N} = A \left[\frac{\Delta S}{(1-R)} \cdot (1-C_f) \sqrt{\pi a} \right]^n \tag{3a}$$

or more generally as

$$\frac{\Delta a}{\Delta N} = A \left[\frac{\Delta K}{(1-R)} \cdot (1-C_f) \right]^n \tag{3b}$$

The parameter C_f is the closure factor at any stress ratio, R. It can be seen that for a given value of ΔK, C_f can be related to C_{f_0}, the closure factor at $R = 0$, by the measured crack-growth rates. An analysis of the data revealed that C_f can be expressed by the equation

$$C_f = C_{f_{-1}} + (C_{f_0} - C_{f_{-1}})(1 + R)^p \tag{4}$$

where $C_{f_{-1}}$ is the closure factor at $R = -1$. The final values for the parameters in Eq 4 are shown in Table 1.

TABLE 1 – *Crack closure parameters.*

	2219-T851 Aluminum	Ti-6Al-4V Titanium
C_{f_0}	0.4	0.4
$C_{f_{-1}}$	0.347	0.332
p	3.93	3.33

These results were compared with the limited data available in the literature (that is, with 2024-T3 from Ref *3*). The behavior is similar for positive stress ratios and agree within 20 percent with Elber's value at $R = 0$. No data were available for negative stress ratios.

Equation 4 is presented in Fig. 1 for 2219-T851 aluminum. The most significant aspect of these results is that the closure factor was determined experimentally for stress ratios as low as −1, thus providing a convenient technique for including negative stresses in crack-growth calculations.

Effect of Overload Stress—It is well known that when many cyclic overloads have been applied to a cracked specimen, the crack-growth rates during a subsequent, lower cyclic loading are retarded. Investigators [*3,7,8*] have shown that after the crack propagates some distance, the degree of retardation decreases and the rates return to constant-amplitude values. The Crack Closure Model considered herein assumes that subsequent to such a load change the rate is immediately retarded, and that the crack extension required for the rates to return to constant amplitude is related to the plastic zone radius caused by the overload.

Although delayed retardation could also have been included in the model, the experimental data generated in this investigation did not provide sufficient indications of this phenomenon. Further, it was concluded that delayed retardation was a second-order effect during most variable-amplitude loading applications.

Consider the loading shown in Fig. 2 for the case of many cycles of high stress, S_1, followed by a lower stress, S_2. For convenience, the stress ratio for both

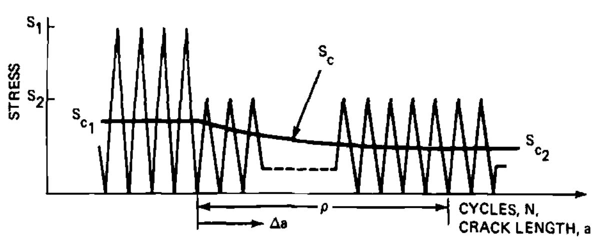

FIG. 2–*Schematic of closure variation through affected length caused by overload.*

stresses is taken as zero. The Crack Closure Model assumes that the closure stress, S_c, varies as shown. Immediately prior to the change in stress, the closure level is the stabilized level, S_{c1}, associated with S_1, and varies, as shown, through some affected length, ρ, to the stabilized value, S_{c2}, associated with level S_2. The expression assumed to define the closure stress variation is given by

$$S_c = S_{c1} - \left(S_{c1} - S_{c2}\right) \left(\frac{\Delta a}{\rho}\right)^b \text{ for } 0 \leq \Delta a \leq \rho \tag{5}$$

An analysis of the aluminum and titanium data revealed that when ρ is taken to be equal to the plane stress plastic zone radius and b is 1.0, they produced a good fit to the data. Some typical results, obtained by numerically integrating Eq 5 are shown in Fig. 3 for aluminum and in Fig. 4 for titanium.

Effect of Number of Overloads–It has been shown [*7,9,10*] that a single overload produces a lesser degree of subsequent retardation than several overload cycles. This effect was modeled by assuming that the increase in closure level is a function of the number of overload cycles applied. An equation of the form

$$\gamma = \gamma_1 + (1 - \gamma_1) \cdot \left(\frac{N_{ol} - 1}{N_{sat} - 1}\right) \tag{6}$$

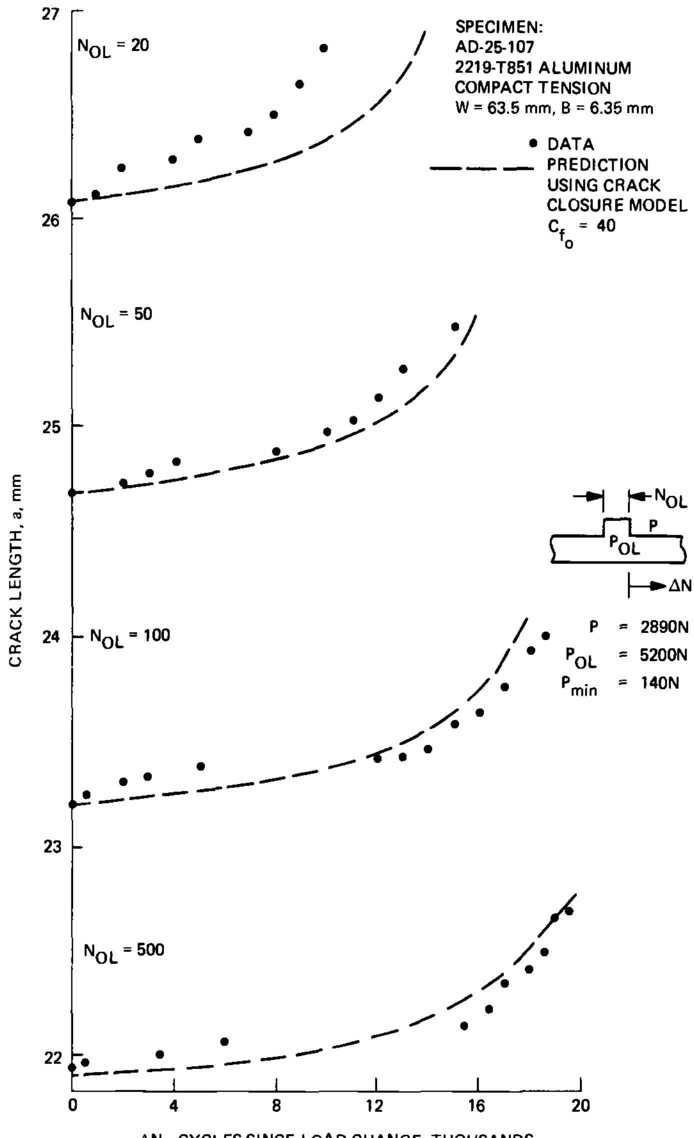

FIG. 3—*Comparison of predictions with data for high-low sequence, 2219-T851 aluminum.*

was fitted to data where the number of overloads, N_{ol}, was varied. Here, γ is the ratio of the closure stress after N_{ol} overloads to the stabilized overload closure stress; γ_1 is the value of γ for $N_{ol} = 1$; and N_{sat} is the number of overload cycles required to achieve saturation (that is, beyond N_{sat}, the addition of overload cycles produces no additional retardation). Values of γ_1 and N_{sat} are shown in Table 2 for both materials. These results indicate that only 13 overload cycles

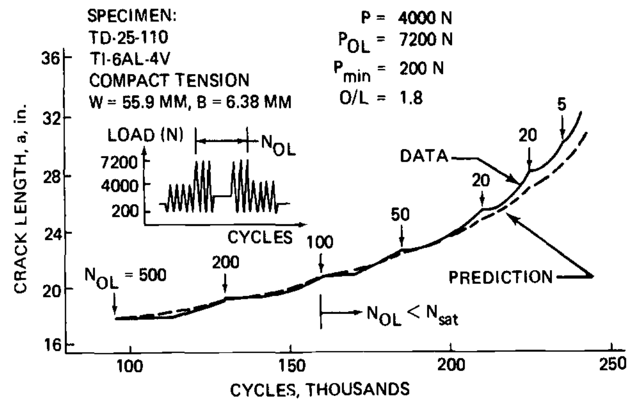

FIG. 4—*Predicted* a *versus* N *for Ti-6Al-4V titanium.*

are required to produce maximum retardation for aluminum, whereas 100 overload cycles are required for titanium, values which are indirectly supported by Refs *10* and *9*, respectively. Figure 4 also shows that the model provides a good prediction for titanium where $N_{ol} < N_{sat}$. Similar results were obtained for aluminum.

TABLE 2 – *Increasing closure parameters.*

	2219-T851 Aluminum	Ti-6Al-4V Titanium
γ_1	0.67	0.80
N_{sat}	13	100

Effect of Compression and Minimum Stress—The test program revealed that whenever the minimum stress was reduced, the closure stress decreased to a new value almost immediately. For example, given a constant maximum cyclic stress with a positive stress ratio, when the minimum cyclic stress was reduced to zero, usually one to three load cycles were required to produce a new stabilized closure level. This effect was modeled by assuming that only one cycle of the new lower minimum stress was required to produce a new stabilized closure stress. The concept was then extended to more complex loading sequences (see Fig. 5).

It was found that when the new minimum stress was compression, the same approach held. The justification for extending the model to handle compression is that, based on the data, the closure stress is always positive. Therefore, from a closure standpoint, a compression load is the same as a reduction of the minimum load. Figure 6 presents a prediction and data for an aluminum

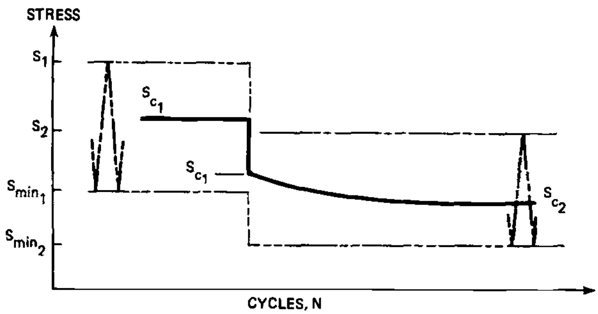

FIG. 5—*Schematic of minimum stress adjustment.*

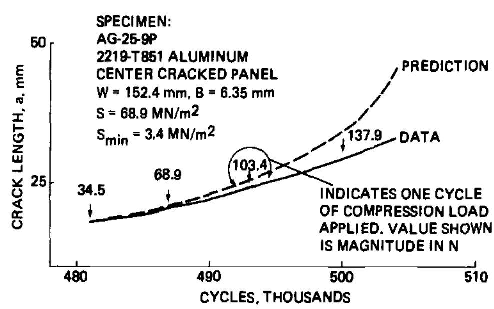

FIG. 6—*Predicted* a *versus* N *for occasional compression loads, 2219-T851 aluminum.*

specimen subjected to several discrete compression spikes, and indicates that the model properly accounts for compression spikes.

The model was verified by predicting the lives of specimens subjected to two, three, and four-level block loading sequences. The stresses within the blocks were ordered high-to-low, low-to-high, and randomized within each block. Numerous comparisons, presented in Ref *3*, show good correlation with the data.

Residual Force Model

The Residual Force Model is essentially the same as the Crack Closure Model except that it attempts to account for the actual closure forces acting on the crack faces instead of basing closure on the externally applied loads. The effective stress range is taken as the difference between the maximum remotely applied stress, S_{max}, and the crack closure stress, S_c. Elber [*4*] suggested that crack closure resulted from plastic deformations left in the wake of a propagating crack. The Residual Force Model assumes that when the crack is closed, a compressive stress distribution develops along the crack surfaces. Figure 7 shows the development of the residual stresses. A crack of half-length a_0, in an infinite sheet, is subjected to the remote tensile stress, S_{max}, which produces a plastic zone of extent ρ_y (Fig. 7*a*). When the remote stress is removed, a reverse

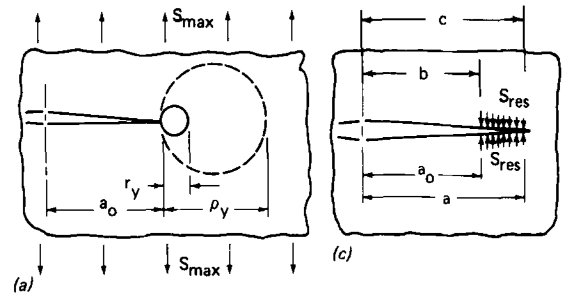

FIG. 7–*Residual stress distributions.*

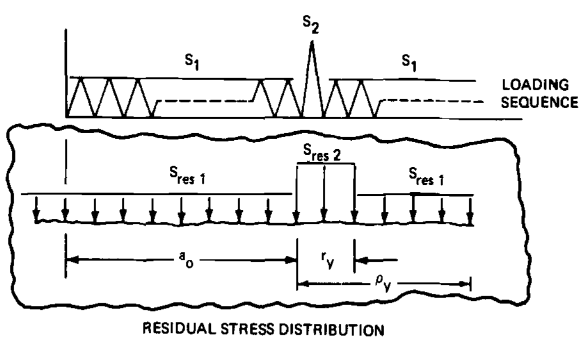

FIG. 8–*Effect of a single overload on residual stresses.*

plastic zone of extent r_y[3] remains defining an area of compressive residual stresses. Figure 8*b* shows the crack after it has propagated to a new half-length, a. The crack tip is part way through the envelope of compressive residual stresses which were developed as the crack propagated to its new length. Figure 8*c* shows an average residual stress distribution, S_{res}, which represents the integrated value of the residual stresses from a_0 to a.

The following assumptions were made:

(*a*) $$\Delta K_{eff} = K_{max} - K_{res} \tag{7}$$

[3] Here, r_y is defined as the reversed plastic zone and differs from that defined in the Glossary.

where ΔK_{eff} is the effective stress intensity range, K is the stress intensity caused by S_{max}, and K_{res} is the stress intensity produced by the residual stresses acting along the crack face only.

(*b*) S_{res} is proportional to S_{max}.

(*c*) The extent of S_{res} due to the application of one cycle of tensile loading is one quarter of the maximum plastic zone size and is given by

$$r_y = \beta \left[\frac{K_{max}}{2\,\sigma_{ys}}\right]^2 \tag{8}$$

where $\beta = \frac{1}{2\pi}$ for plane stress and $\beta = \frac{1}{6\pi}$ for plane strain.

Initially, it seemed that S_{res} should be equal to the material compression yield stress. However, a review of Eq 7 revealed that the crack could only be opened by the application of $S \geq \sigma_{ys}$, the material compression yield stress. Experience indicates that this is not the case and that S_{res} must therefore be something less than σ_{ys}. It was therefore assumed that $S_{res} = \alpha S_{max}$.

An interesting effect produced by this model is that delayed retardation is predicted. It was found that the delay period depends on the number of overloads applied and that as the number of overloads increases to the saturation value, the delay period decreases to zero, and the minimum crack growth rate occurs immediately after the load change. In addition, the model predicts acceleration when changing from a low load to a high load. These results are included in the following discussion of the development of the working model.

Development of Working Model—Figure 8 shows a crack which has propagated to a half-length, a_0, under the influence of remote stress S_1, which has caused the residual stress, S_{res1}, to be developed. At half-length, a_0, a remote stress, S_2 (where $S_2 > S_1$), has been applied and then removed. The plastic zone, ρ_y, caused by S_2 is shown along with the reverse plastic zone, r_y, which exists when S_2 returns to zero. The crack then continues to propagate under the influence of S_1.

Immediately after the application of S_2, the residual forces (stresses) acting behind the crack are those caused only by the application of S_1 and the residual stress intensity is the same as for the constant-amplitude case for S_1. However, as the crack begins to propagate into the reverse plastic zone caused by S_2, the residual stresses, S_{res2}, begin to act behind the crack tip and an increase in K_{res} occurs. When the crack half-length is $a + r_y$ the influence of S_{res2} is most prominent and K_{res} is a maximum. As the crack continues to propagate, S_{res2} becomes remote from the crack tip so that its effect on K_{res} is reduced, and when the crack half-length is large relative to $a + r_y$, the effect of S_{res2} on K_{res2} approaches zero.

If a crack propagation law of the Paris type is used such that

$$\frac{da}{dN} = A \left(\Delta K_{eff}\right)^n \tag{9}$$

then ΔK_{eff} is smallest when the crack half-length is $a + r_y$ and $\Delta a/\Delta N$ is the smallest at the same point. Therefore, the minimum crack growth rate occurs at a point r_y from where the overload was applied and delayed retardation has been represented by the model.

To test this approach, an equation of the form

$$K_{\text{res}} = S_{\text{res}}\sqrt{\frac{a}{\pi}}\left[\sin^{-1}\left(\frac{c}{a}\right) - \sin^{-1}\left(\frac{b}{a}\right) - \sqrt{1-\left(\frac{c}{a}\right)^2} + \sqrt{1-\left(\frac{b}{a}\right)^2}\right]$$

was taken from Ref *11*, and the equation was doubled to account for forces acting on both surfaces of the crack. Dimensions b and c are shown in Fig. 7*c*. At any crack length, a, it is a simple matter to sum the effects of the various residual stress distributions over the crack half-length from zero to a, to obtain the total K_{res}.

Recent experimental investigations [*6–8*] indicate that the effect of the overload should have dissipated by the time the crack has propagated through a distance approximately equal to the plastic zone caused by the overload. It was found, however, that when Eqs 7 and 9 were used, the effect of an overload on subsequent crack growth persisted for crack extensions of several plastic zones. It was therefore assumed that only those residual stresses which exist from one plastic zone radius, ρ_y, behind the crack tip, to the crack tip, should be included in the calculations. In this way, the effect of an overload on subsequent crack growth is only included in the calculation while the crack tip is within the area from a_0 to $a_0 + \rho_y$ in Fig. 8. Then, ΔK_{eff} was normalized so that steady-state crack-growth conditions would exist when appropriate.

The final crack-growth rate equation is given by

$$\frac{\Delta a}{\Delta N} = A\left\{\frac{\left\{S\sqrt{\pi a} - \sum_{a-\rho_y}^{a}\left\{S_{\text{res}_i}\sqrt{\frac{a}{\pi}}\left[\sin^{-1}\left(\frac{c_i}{a}\right) - \sin^{-1}\left(\frac{b_i}{a}\right) - \sqrt{1-\left(\frac{c_i}{a}\right)^2} + \sqrt{1-\left(\frac{b_i}{a}\right)^2}\right]\right\}\right\}^n}{1 - \frac{\alpha}{\pi}\left[\frac{\pi}{2} - \sin^{-1}\left(\frac{a-\rho_y}{a}\right) + \sqrt{1-\left(\frac{a-\rho_y}{a}\right)^2}\right]}\right\} \tag{10}$$

Results—The model was tested using data from the literature [*7*] which strongly exhibited delayed retardation. Figure 9 shows crack-growth rate data versus crack-growth increment after a load change for the cases where the number of overloads, N_{ol}, were 0, 1, 450, and 9000. The dashed lines represent predictions for $N_{\text{ol}} = 1$ and ≥ 300. The values of α and β were selected to provide a reasonable fit to the $N_{\text{ol}} = 1$ data and were then used for the other predictions. The basic trend is evident and shows that for the case of $N_{\text{ol}} = 1$, a minimum crack-growth rate occurs when Δa is about 0.2 mm. A comparison of the predicted and test curves indicates that the curve shapes and magnitudes agree fairly well. However, when the limiting case of 300 or more overloads is applied, the residual force model predicts a crack-growth rate which is much lower than the data suggests.

Figure 10 shows a case of acceleration where the crack-growth rate versus

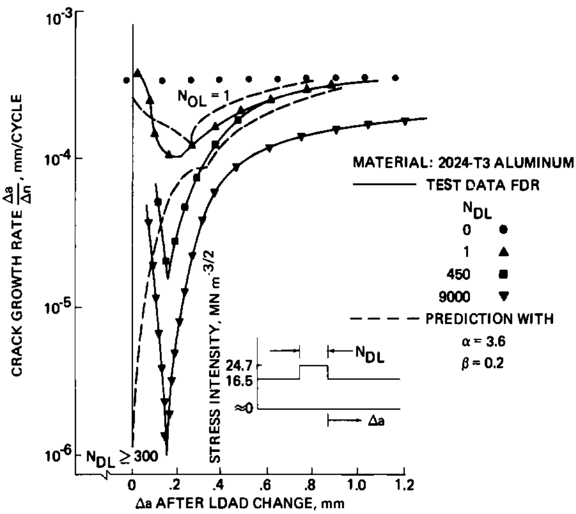

FIG. 9—*Residual force predictions versus data.*

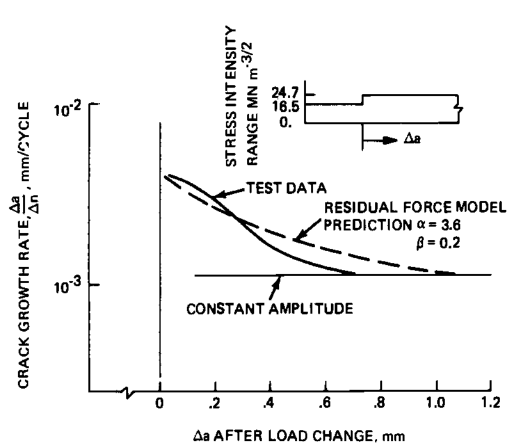

FIG. 10—*Residual force predictions versus data for low-high loading.*

distance after load change is plotted for the case of a low-high loading. Here, the predictions are based on the same values of α and β used for the delayed retardation cases. Prediction and test agree fairly well.

Some predictions are compared in Fig. 11 to test data from more complex loading cases [*12*]. Cases 1 and 2 were used to determine the Paris crack-growth parameters while α and β were determined to be 2.6 and 0.1, respectively, from Case 3. These values were then used to predict the lives for the remaining cases. In general, the correlation between test and predicted lives is good. The difference between the shapes of the predicted and test curves is attributed to the block-wise integration scheme [*13*] used to calculate lives.

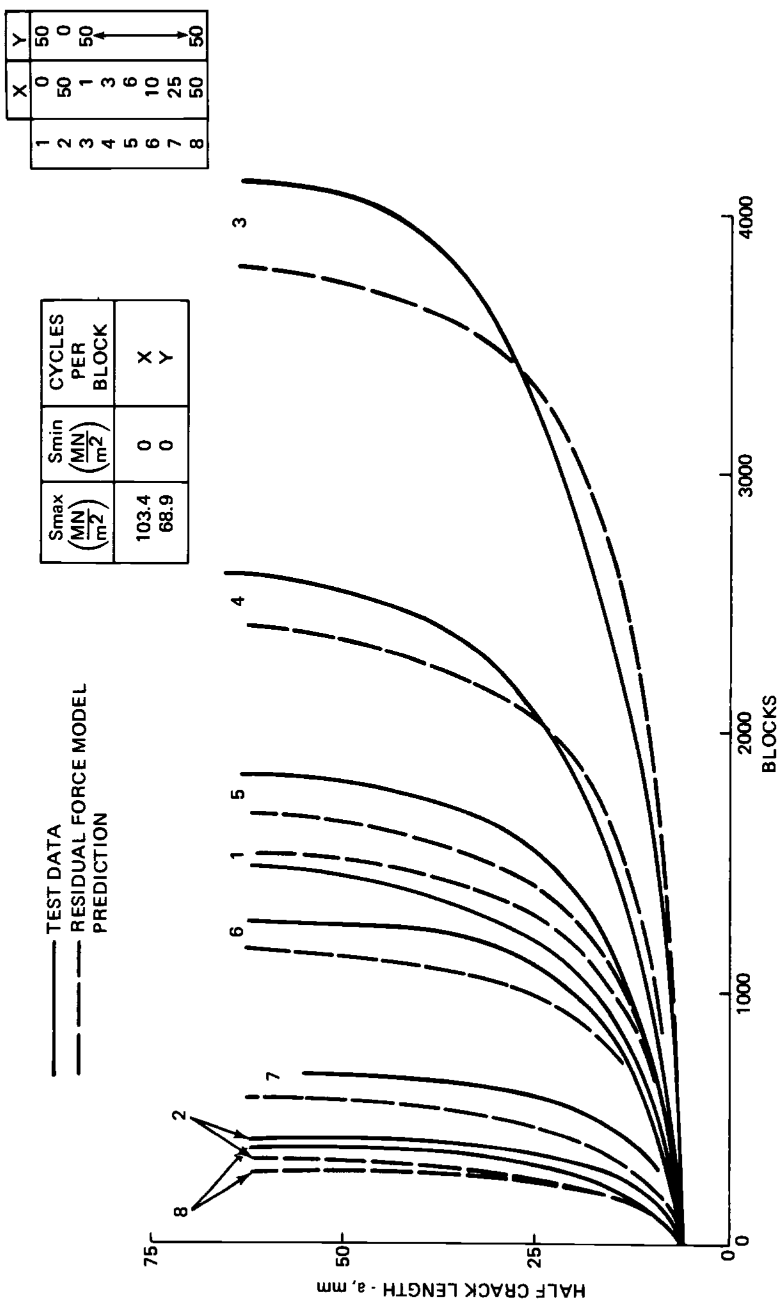

FIG. 11—*Comparison of predicted and test lives for 7075-T6 aluminum panel specimens.*

Concluding Remarks

Both the Residual Force and Crack Closure Models offer new methods of predicting crack growth under variable-amplitude loading. The Residual Force Model is elementary and requires only basic input data for its use. However, its predictive ability is currently limited to simple loading sequences. Conversely, the Crack Closure Model is considerably more versatile but requires more complex input data. The development of both models and many comparisons of predictions and data are presented in Ref *3*.[4]

Acknowledgments

The authors wish to acknowledge J. C. Newman, Jr., NASA Langley Research Center, and R. Bucci, formerly of Del Research Corporation, for their contributions in formulating the initial versions of the Crack Closure Model; and P. C. Paris and M. Creagar of Del Research and Del West, respectively, for their extensive efforts and advice in generating the experimental data and analytical approaches reported in this paper. A grateful acknowledgment is also extended to R. M. Engle, Air Force Flight Dynamics Laboratory, for his assistance in the overall program.

References

[*1*] Wheeler, O. E., "Crack Growth under Spectrum Loading," Report No. FZM-5602, General Dynamics Corporation, Fort Worth Division, June 1970.

[*2*] Willenborg, J., Engle, R., and Wood, H. A., "A Crack Growth Retardation Model Using an Effective Stress Concept," Technical Memorandum 71-1FBR, Air Force Flight Dynamics Laboratory, Wright-Patterson AFB, Jan. 1971.

[*3*] Bell, P. D. and Creager, M., "Crack Growth Analysis for Arbitrary Spectrum Loading," AFFDL-TR-74-129, 1974.

[*4*] Elber, W. in *Damage Tolerance in Aircraft Structures, ASTM STP 486*, American Society for Testing and Materials, 1971, pp. 230–242.

[*5*] Newman, J. C., Jr., and Armen, H., Jr., "Elastic-Plastic Analysis of a Propagating Crack," Paper 74-366, AIAA/ASME/SAE 15th Structures, Structural Dynamics and Materials Conference, Las Vegas, Nev., April 1974.

[*6*] Newman, J. C., Jr., "Finite-Element Analysis of Fatigue Crack Propagation Including the Effects of Crack Closure," Ph.D. thesis, Virginia Polytechnic Institute, 1974.

[*7*] Trebules, V. W., Roberts, R., Jr., and Hertzberg, R. W. in *Progress in Flaw Growth and Fracture Toughness Testing, ASTM STP 536*, American Society for Testing and Materials, July 1973, pp. 115–146.

[*8*] von Euw, E. F. J., Hertzberg, R. W., and Roberts, R. in *Stress Analysis and Growth of Cracks, ASTM STP 513*, American Society for Testing and Materials, 1972, pp. 230–259.

[*9*] Wei, R. P. and Shih, T. T., "Delay in Fatigue Crack Growth," Lehigh University Publications.

[*10*] Hudson, C. M. and Raju, K. N., "Investigation of Fatigue Crack Growth under Simple Variable-Amplitude Loading," NASA TN D-5702, March 1970.

[*11*] Paris, P. C., and Sih, G. C. in *Fracture Toughness Testing and Its Applications, ASTM STP 381*, American Society for Testing and Materials, 1965, pp. 30–83.

[4] The Crack Closure Model has been programmed and incorporated into the Air Force crack growth computer program, CRACKS II.

[12] Porter, T. R., "Method of Analysis and Prediction for Variable-Amplitude Fatigue Crack Growth," *Engineering Fracture Mechanics*, Vol. 4, No. 4, 1972.
[13] Brussat, T. R. in *Fracture Toughness and Slow-Stable Cracking, ASTM STP 559*, American Society for Testing and Materials, 1974, pp. 298–311.

DISCUSSION

Otto Buck[1] *(written discussion)*—Do you think it would be possible to include stress relaxation and creep into your models?

P. D. Bell and A. Wolfman (authors' closure)—Yes, if creep is defined as either stable crack growth at sustained load or as stable tear. Both models could be modified to include relaxation of residual stresses and stable growth as functions of both time and temperature if empirical data, similar to crack growth rate data, are available. Stable tear has been incorporated in the Crack Closure Model with some success.

[1] Science Center, Rockwell International, Thousand Oaks, Calif. 91360.

G. H. Jacoby,[1] *H. Nowack,*[2] *and H. T. M. van Lipzig*[2]

Experimental Results and a Hypothesis for Fatigue Crack Propagation Under Variable-Amplitude Loading

REFERENCE: Jacoby, G. H., Nowack, H., and van Lipzig, H. T. M., "Experimental Results and a Hypothesis for Fatigue Crack Propagation Under Variable-Amplitude Loading," *Fatigue Crack Growth Under Spectrum Loads, ASTM STP 595,* American Society for Testing and Materials, 1976, pp. 172–183.

ABSTRACT: Many as yet inadequately-understood phenomena contribute to the sequence effects observed during fatigue crack propagation under variable-amplitude loading. In order to get an insight in the sequence effects, an extensive test program with 2024-T3 aluminum and Ti-6Al-4V sheet specimens with systematic variations in the loading conditions was performed, where special emphasis was placed on the accurate measurement of the crack propagation just after changes in the loading conditions. A hypothesis is proposed which explains the observed behavior. The hypothesis is based on deformation considerations within the plastic zones caused by the propagating crack.

KEY WORDS: fatigue (materials), crack propagation, aluminum alloys, titanium alloys, plastic deformation, fracture properties, damage, loads (forces)

Cumulative damage analysis of structures subjected to variable-amplitude loading is complex because of sequence effects. Many studies have been performed with respect to the accuracy of cumulative damage theories, program and random tests [*1,2*].[3] There is still, however, a lack of information about the crack propagation behavior resulting from changes in amplitude and mean stress. This is mainly because of experimental difficulties in determining the exact crack extension rates over a relatively short distance. With such crack propagation measurements from tests where the loading conditions are systematically varied it should be possible to get further insight into the mechanism of sequence effects [*3,4*]. Sequence effects are the consequence of the interaction of several phenomena which have been outlined in many investigations with

[1] Director, Carl Schenck AG, Darmstadt, West Germany.

[2] Department head and research fellow, respectively, Deutsche Forschungs- und Versuchsanstalt für Luft- und Raumfahrt (DFVLR), Institut für Werkstoff-Forschung, Porz, West Germany.

[3] The italic numbers in brackets refer to the list of references appended to this paper.

constant-amplitude loading (CAL). Some of these phenomena shall shortly be considered.

Figure 1*a* shows schematically the stresses and strains along the x-axis and also the plastic zones in front of the crack tip at the maximum and minimum load in

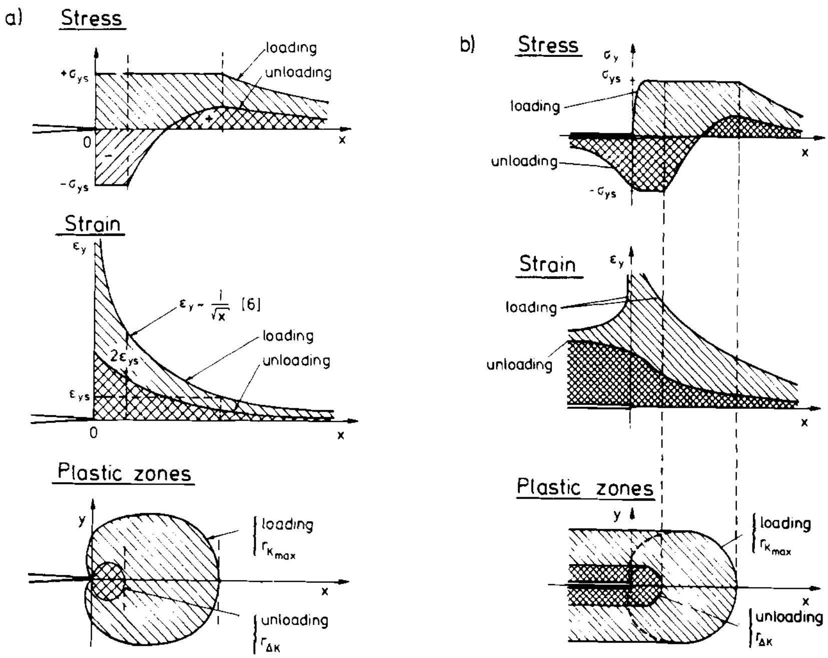

FIG. 1—*Stress and strain distributions along the crack line without and with considering residual deformations behind the propagating crack and plastic zones.*

a load cycle assuming an ideal elastic-plastic material behavior [*5*]. There exist two areas with different plastic deformation characteristics. Within the area denoted as $r_{K\max}$ the material is monotonically plasticly deformed. The size of this area is controlled by the maximum stress in a cycle. Within the area denoted as $r_{\Delta K}$, the material is subjected to reversed plastic deformations corresponding to the stress variation in the cycle.

Actual materials usually exhibit monotonic and cyclic strain hardening or softening properties. This leads to alterations in the plastic zone sizes and also to the buildup of a cyclic strain hardening (or softening) profile along $r_{\Delta K}$ [*7,8*].

During fatigue crack propagation residual deformations are built up in front of the crack tip and are left behind the propagating crack. The presence of these residual deformations is one of the main causes for the crack closure behavior as observed in several investigations [*9,10*]. The distributions of the stresses and strains along the x-axis, considering the residual deformations, are shown in Fig. 1*b*. The main consequence of the residual deformations is a reduction of the crack tip stress intensity variation during a load cycle. The crack propagation behavior is further influenced by the instantaneous stress state at the crack tip [*11*] and by microstructural mechanisms. The latter may, however, become a second order effect at higher loading levels [*12*].

In case of variations in the loading conditions, an interaction of the described phenomena and mechanisms occurs. In the following sections, an attempt is made to analyze these interactions on the basis of an extensive test program, where the crack propagation behavior due to a variation in mean stress during CAL, due to single and multiple high loads, and due to additional negative peak loads is studied. The interpretation of the experimental crack propagation behavior is further substantiated by the results from deformation measurements on the specimen surface and by microscopic observations.

The investigations were performed with both cyclic strain hardening 2024-T3 aluminum and cyclic softening Ti-6Al-4V. Center-cracked 80-mm-wide specimens were used. The thickness of the 2024-T3 aluminum specimens was 1 mm and that of the Ti-6Al-4V specimens was 1.6 mm. The crack propagation measurements were performed with two microscopes for both sides of the crack. The magnification was x125. Special scales in the optical systems enabled the observation of crack growth increments smaller than 0.01 mm.

Experimental Crack Propagation Behavior and Discussion

Constant-Amplitude Loading with an Increase in Mean Stress

Figure 2 shows the loading conditions; the observed crack length, a, as a function of the cycle number, N; and the crack rates, $\Delta a/\Delta N$, as a function of the crack length for 2024-T3 aluminum and Ti-6Al-4V. In both cases the crack rates increase above the CAL-rates immediately after the change in mean stress. The acceleration of the crack growth is, however, more pronounced for 2024-T3 aluminum resulting in a significant decrease in fatigue life in the crack stage. In Fig. 3*a* the crack propagation behavior of 2024-T3 aluminum is schematically replotted. Capital letters characterize the essential stages. In the figure the plastic deformed regions before and after the change in mean stress are also shown. The increase in the crack rates between (A) and (B) can be explained as follows: At the end of the low mean stress CAL-period, the plastic zones $r_{K_{\max 1}}$ and $r_{\Delta K_1}$ exist. Residual deformations are present on the crack surfaces and along the previous path of $r_{K_{\max 1}}$. Within $r_{\Delta K_1}$ a stable strain hardening profile corresponding to the low mean stress loading level exists. During the first load cycle after the increase in mean stress $r_{K_{\max 2}}$ develops, the size of this zone is mainly controlled by the monotonic strain hardening behavior of the material. At the very tip of the crack the material is subjected to high tensile strains. Since it is cyclic hardened from the preceding loading period, its deformation capability is limited. This brittle characteristic of the material increases the crack rates. Scanning microscopic observations revealed the formation of material regions separated by deep grooves parallel to the crack front. During unloading, the crack remains opened over a considerable range of the half cycle since the

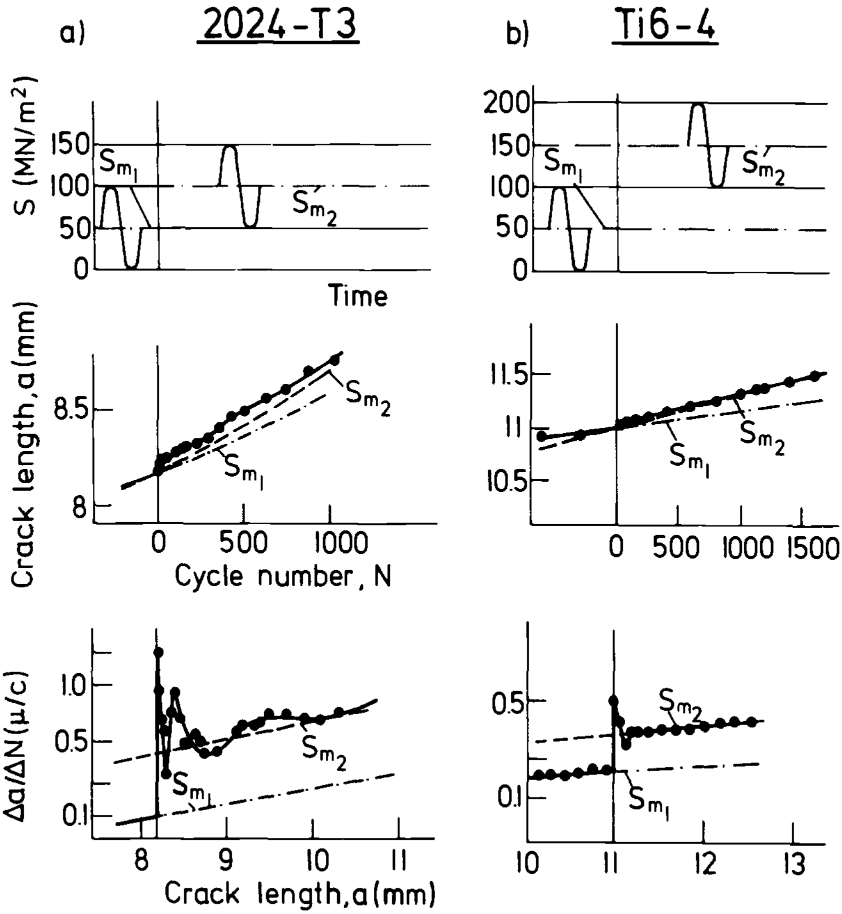

FIG. 2—*Crack propagation behavior due to an increase in mean stress.*

residual deformations along the fracture surfaces exhibit the low equilibrium extent of the preceding loading period. Therefore, both the brittle crack tip material and the high stress intensity variations, until crack closure occurs, are the reasons for the high crack rates at (B). Due to the fast crack extension, the crack tip and $r_{\Delta K_2}$ rapidly enter material regions which are less cyclic strain hardened than under CAL-conditions. From this and due to the fact that higher tensile deformations can develop in the high mean stress period, which reduce the stress intensity variation at the crack tip, $\Delta a/\Delta N$ decreases. The fact that the crack rates decrease below the CAL-rates and that they then increase above the CAL-rates indicates that the cyclic hardening of the crack tip regions plays an essential part. Variations in the $\Delta a/\Delta N$ behavior occur until new stable plastic zones at the crack tip are built up at (C). The given explanations for the $\Delta a/\Delta N$-variations could further be substantiated by ϵ_y-strain measurements

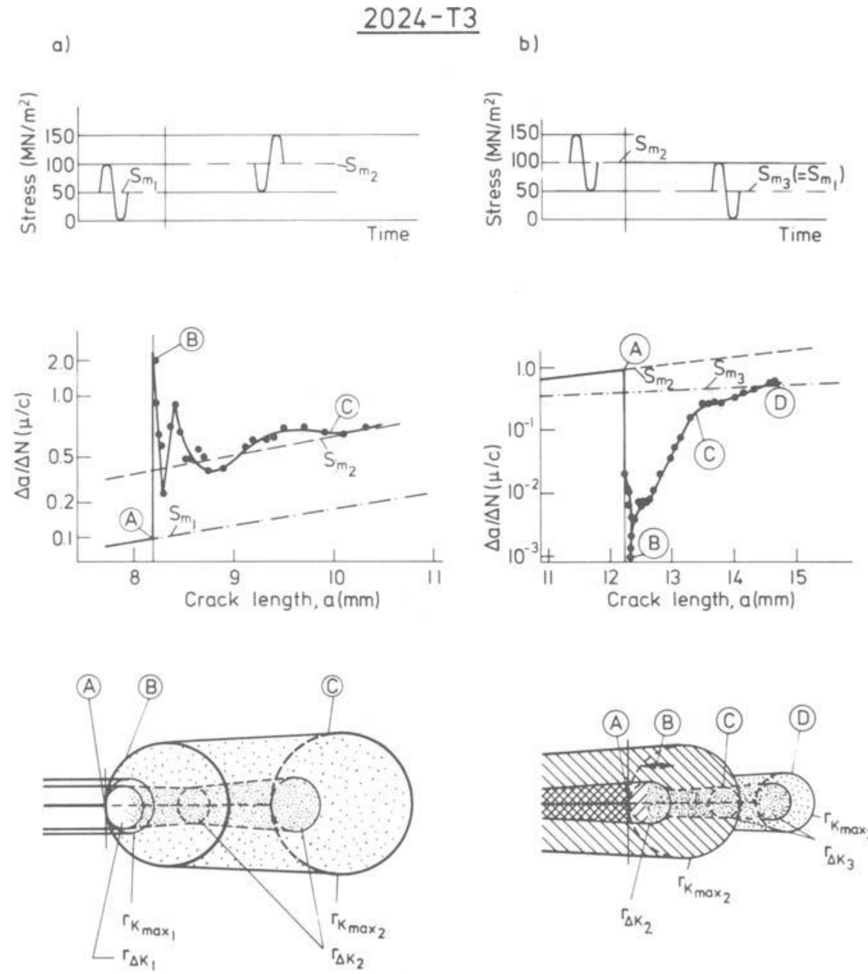

FIG. 3—$\Delta a/\Delta N$ *and plastic zone behavior due to a variation in mean stress.*

using a special grid technique.[4] The measurements showed that during the low mean stress CAL-period up to (A) no high deformations occured in the vicinity of the crack tip ($\Delta\epsilon_{y_{max}} \approx$ 3 to 5 percent). Immediately after the change in mean stress, however, extremely high strain variations ($\Delta\epsilon_{y_{max}} \approx$ 15 to 20 percent) were measured in the vicinity of the crack tip. These high strain variations reduced when the crack propagated. At (C), where the $\Delta a/\Delta N$-

[4] A fine 0.1-mm spaced grid was engraved ahead of the crack tip with a modified micro-hardness tester. Photographs were taken from the undeformed grids and from the deformed grids at several instances during the loading histories. The grid spacings were then measured with a special microscope and the ϵ_y-strains determined from the relative displacements of the grid.

behavior has reached a stable condition, maximum strain variations of 5 to 7 percent were measured.

The considerations so far have referred to a strain hardening material. In the case of Ti-6Al-4V, $r_{\Delta K_1}$ at the end of the low load period exhibits a high ductility. Consequently, the crack extension, due to the increase in mean stress, occurs in a ductile region accompanied by an extensive opening of the crack. The cyclic softened material and the high stress intensity variations, due to the comparatively small residual deformations left behind from the preceding loading period, lead to crack propagation rates which are higher than under high mean stress CAL. Along with the fast propagation of the crack, regions that have experienced less cyclic softening as compared to the stabilized condition are entered, and this increases the resistance against crack extension. In addition, the formation of higher residual deformations decreases the crack rates significantly. These low crack rates lead to a more extensive softening of the material within $r_{\Delta K_2}$ resulting in an increase in crack rates. In conclusion, the crack propagation behavior of cyclic softening materials and that of cyclic hardening materials is similar although the mechanisms differ.

Constant-Amplitude Loading with a Decrease in Mean Stress

Figure 3*b* shows schematically the $\Delta a/\Delta N$ versus a behavior of 2024-T3 aluminum and the plastic deformed areas. At the end of the high loading period, $r_{K_{\max 2}}$ and $r_{\Delta K_2}$ are present. The residual deformations along the previous path of $r_{K_{\max 2}}$ are in an equilibrium condition corresponding to the high loading level. After the decrease in mean stress, the crack rates fall below those under low mean stress CAL because the residual deformations generated in the previous loading period reduce the crack tip stress intensity variation. A satisfactory explanation for the further delayed decrease in $\Delta a/\Delta N$ could not be found. An incompatibility of the crack front orientation from the high loading period with the low loading conditions may have an influence. After passing through the minimum at B, the crack rates grow up rapidly along with an increase in $r_{\Delta K_3}$. At C, the influences of $r_{K_{\max 2}}$ and the residual deformations within this zone decay, and a new $r_{K_{\max 3}}$ develops. The described plastic zone and residual deformation behavior became clearly visible in the ϵ_y-distribution measurements using the previously mentioned grid technique.

Behind C, the crack rates are still lower than those under low mean stress CAL, since the influence of the residual deformations from the preceding loading period is still present. This influence gradually decays up to D. Simultaneously, $r_{K_{\max 3}}$ and $r_{\Delta K_3}$ which coincide with those under CAL are formed. The latter process can be recognized in the side view of the specimen surface shown in Fig. 4. Further on the fracture surface shown in the figure, dark areas in the range of the $r_{K_{\max 2}}$ path from the high mean stress loading period can be seen. Scanning microscopic observations revealed that these are material particles which have been abraded during the rubbing of the fracture surfaces due to the action of the residual deformations.

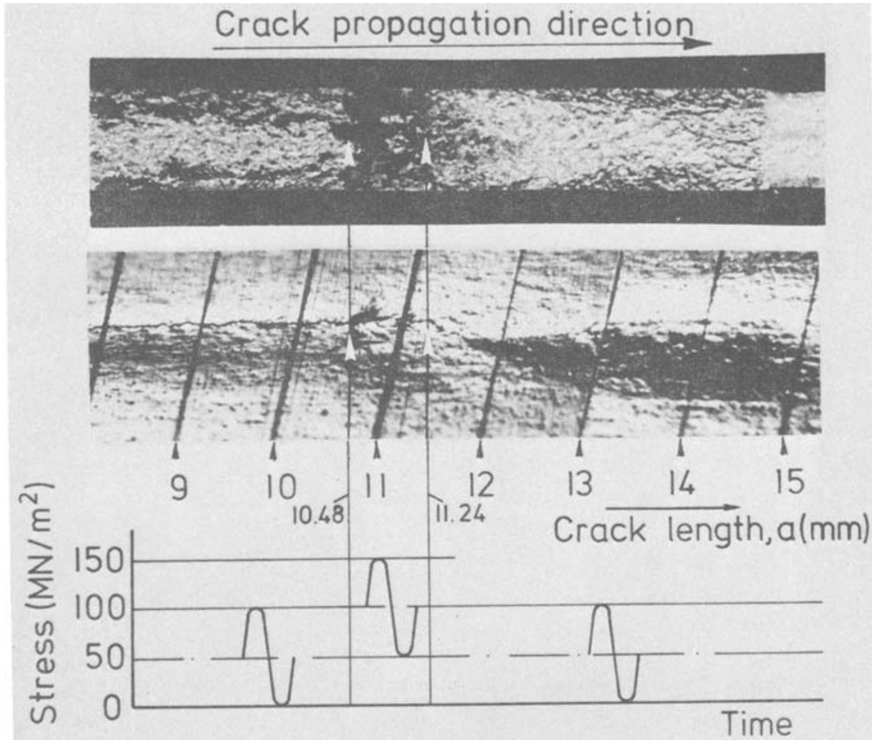

FIG. 4—*Influence of mean stress variations on the fracture surface and specimen surface appearance.*

Crack Propagation Under Single and Multiple High Loads

Under these loading conditions an interaction of the mechanisms described in the two previous sections occurs. The Figs. 5 and 6*a* show the $\Delta a/\Delta N$-behavior for $N_h = 1$, 40, and 100 high load cycles inserted in low load CAL for 2024-T3 aluminum, as well as for $N_h = 1$ for Ti-6Al-4V. Before the details of the $\Delta a/\Delta N$-behavior in the subsequent low load period are discussed, the differences in the plastic zone behavior and in the residual deformations as a function of N_h will first be considered. The plastic zone behavior for a single and a small number of high loads is shown in the lower part of Fig. 5. During the preceding low load period, $r_{K_{max1}}$ and $r_{\Delta K_1}$ have been formed. Due to the increase in load, $r_{K_{max2}}$ is generated. Within $r_{K_{max2}}$ high residual deformations are built up. In the case of a low number of high loads, $r_{K_{max2}}$ propagates by a small amount corresponding to the crack extension during the high loads. The area where residual deformations are built up increases just a little. There is, however, an essential difference compared to the behavior as described in the preceding section. In that case the $r_{K_{max2}}$ path and also the high residual deformations within $r_{K_{max2}}$ exist along the whole previous crack path. Under a single or a

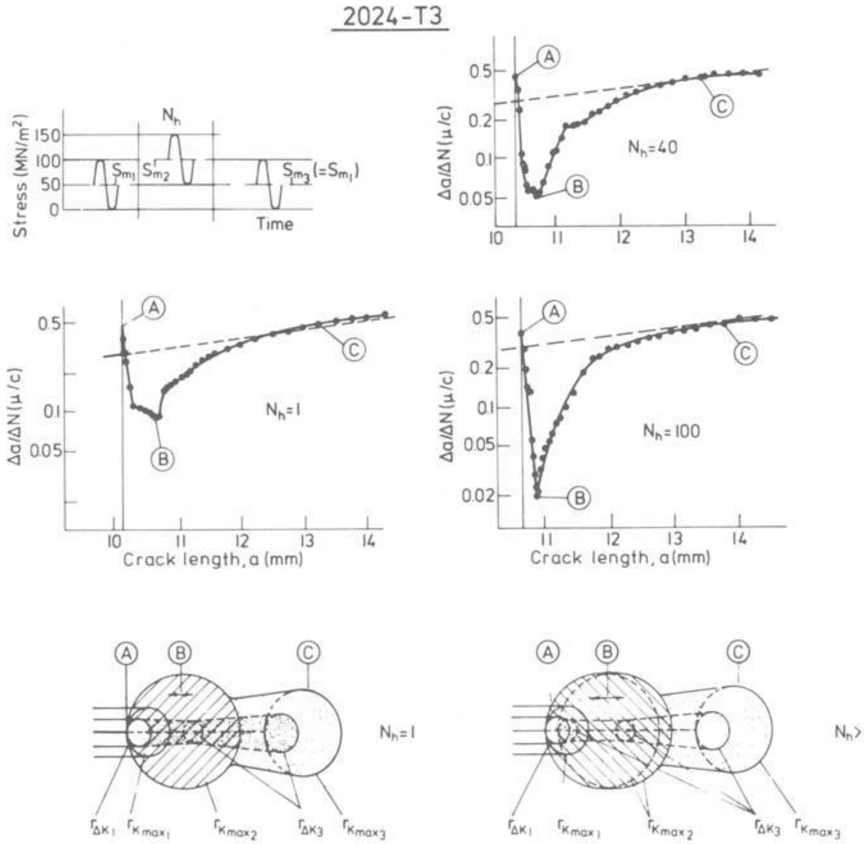

FIG. 5—*Crack propagation behavior due to single and multiple high loads and plastic zones.*

small number of high loads, significant high residual deformations are only formed ahead of the crack tip during the high loads.

The $\Delta a/\Delta N$-behavior caused by the application of the high loads is the same as described in the first section. Due to the aforementioned residual deformation behavior within the $r_{K_{max2}}$ path as a function of the number of high loads, the minimum in the $\Delta a/\Delta N$ at B is lower following multiple high loads and occurs at a smaller crack length. During the subsequent loading period, the crack rates increase again, whereby the crack extension mechanism is similar to that as described in the preceding section.

From the experimental $\Delta a/\Delta N$-behavior in Figs. 5 and 6*a*, it is seen that the cyclic strain hardening 2024-T3 aluminum and the softening Ti-6Al-4V behave in a similar manner. The experimental results further showed that the retardation in crack growth caused by different numbers of peak loads N_h is not directly proportional to N_h.

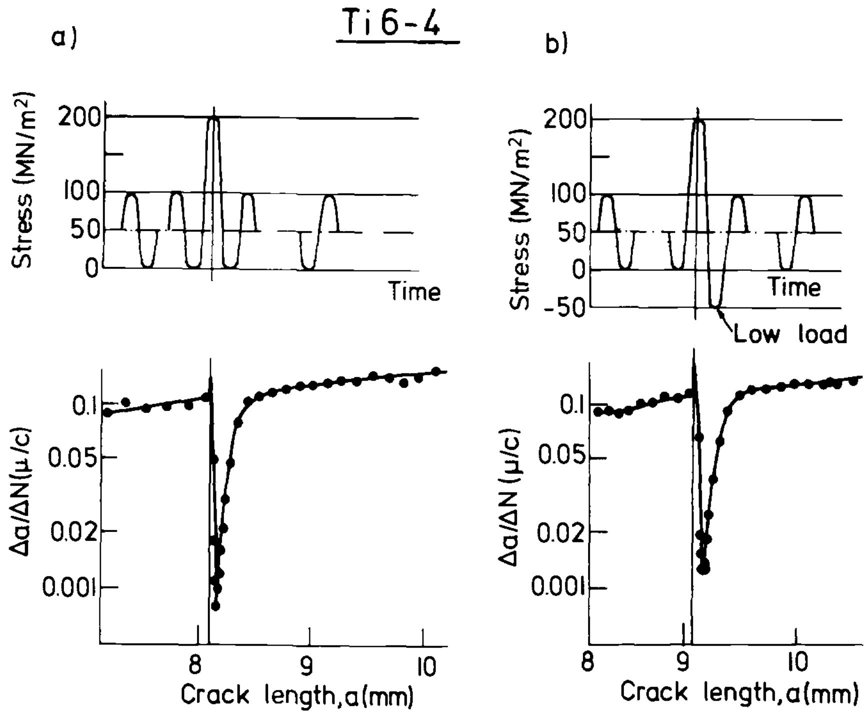

FIG. 6—*Crack propagation behavior due to a single high load (a) and due to a single high load followed by a compression load (b).*

Crack Propagation Due to a Low Peak Load Following Single and Multiple High Loads

These loading conditions represent a further approach to variable loading conditions. Figures 7 and 6*b* show the $\Delta a/\Delta N$-behavior for 2024-T3 aluminum and for Ti-6Al-4V. The changes in the crack propagation mechanism due to a negative peak load are schematically indicated in Fig. 7. Until the occurance of the negative peak load the plastic zone and residual deformation behavior is the same as already described in the preceding subsections. If the negative peak load would not occur, $r_{\Delta K_2^*}$ would be generated upon unloading. When the negative peak load is applied, however, a larger $r_{\Delta K_2^{**}}$ is generated. This leads to a reduction of the area of $r_{K_{\max 2}}$ where residual deformations exist after unloading and also to a larger redeformation of the residual deformations. Besides this, the crack tip is further resharpened. All these effects lead to the formation of a larger $r_{\Delta K_3^{**}}$ than under a loading situation where no negative peak loads occur, and the crack rates are higher. From these considerations it immediately follows that the crack propagation is more influenced by negative peak loads: the lower the peak loads are, the smaller the areas are where residual deformations are formed, and the smaller the residual deformations are.

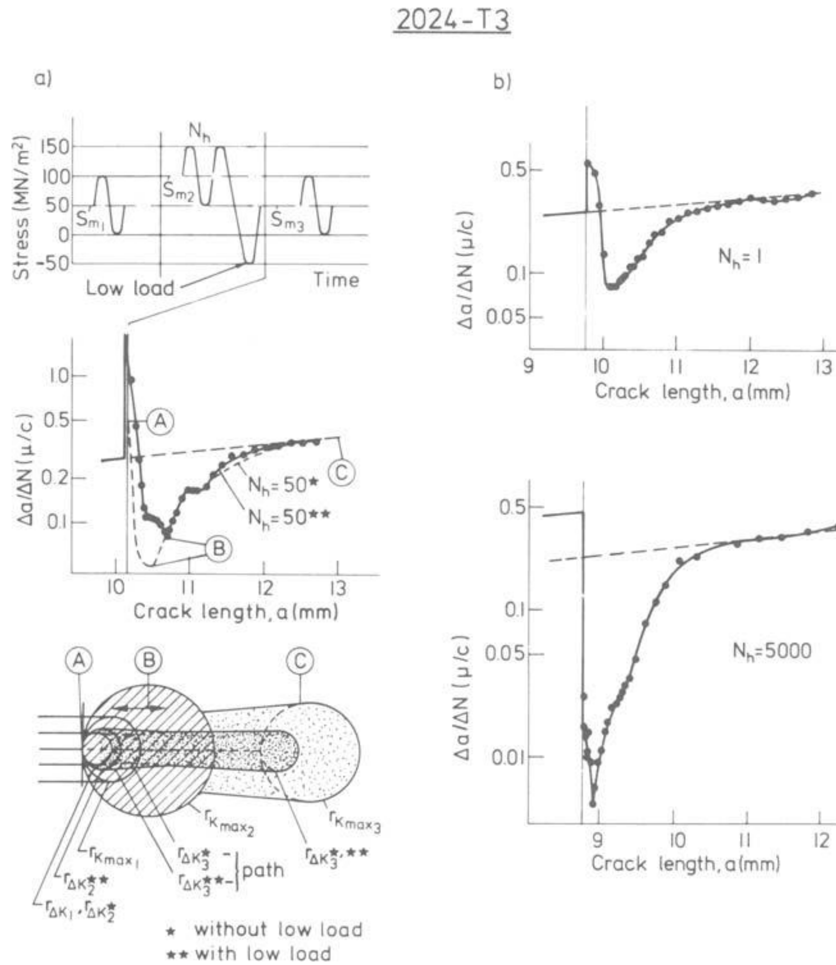

FIG. 7—*Crack propagation behavior due to single and multiple high loads followed by a compressive load and plastic zones.*

This coincides with the experimental results in Fig. 7 and, also, with the observations made by Schijve, where negative peak loads were applied during a loading history with a comparatively high mean stress [*11*]. Since the effect of the residual deformations along the crack surfaces is small, because of the high loading level, a comparatively larger $r_{\Delta K_2}$ due to the negative peak load can develop which also reduces the influence of the residual deformations ahead of the crack tip. This together with a pronounced resharpening of the crack tip leads to a nearly unretarded crack propagation.

The present test results further show that Ti-6Al-4V behaves in a similar manner as 2024-T3 aluminum.

Conclusions

1. Experiments with systematic variations in the loading conditions, where special emphasis was placed on an accurate measurement of the crack propagation behavior after changes in the loading conditions, have shown that significant variations in the crack rates occur until stabilization is reached.

2. A hypothesis is proposed which explains the observed behavior. This hypothesis is based on the deformations caused by the propagating crack. The deformations depend on:

   (*a*) the maximum stress intensity and the variation in stress intensity during a cycle and the stress intensity history, and

   (*b*) the monotonic and cyclic deformation characteristics of the material.

3. Under constant-amplitude loading a monotonic deformed plastic zone and a smaller cyclic deformed plastic zone exist directly in front of the crack tip. From these plastic zones, residual deformations are also left behind the propagating crack.

4. Sequence effects mainly occur due to the interaction of the plastic zones of the respective loads in the subsequent load cycles. Of predominant importance are the K_{max}-controlled plastic zones. The residual deformations built up within the area of the K_{max}-controlled plastic zones hinder the formation of a stable condition corresponding to constant-amplitude loading.

5. The ranges in crack length where sequence effects are observed are considerably larger than calculated on the basis of the linear elastic fracture mechanics equations for the plastic zone size.

Acknowledgment

The financial support for this work by the Deutsche Forschungsgemeinschaft (DFG) is gratefully acknowledged.

References

[*1*] Schijve, J., "The Accumulation of Fatigue Damage in Aircraft Materials and Structures," AGARDograph No. 157, NATO Advisory Group for Aerospace Research and Development, 1972.

[*2*] Jacoby, G. in *Effect of Environment and Complex Load History on Fatigue Life, ASTM STP 462*, American Society for Testing and Materials, 1970, pp. 184–202.

[*3*] Nowack, H. and van Lipzig, H. T. M., "Ermüdungsrissausbreitung bei Belastungen mit veränderlichen Mittelspannungen und Amplituden," DGM-Hauptversammlung, Bonn, June 1974.

[*4*] Van Lipzig, H. T. M. and Nowack, H., "Rissfortschrittsverhalten und Restfestigkeit von Leichtbauwerkstoffen bei nicht-einstufigen Belastungen," *Proceedings 6*, DVM-Arbeitskreissitzung "Bruchvorgänge," Deutscher Verband für Materialprüfung, 1974, pp. 129–141.

[*5*] Rice, J. R. in *Fatigue Crack Propagation, ASTM STP 415*, American Society for Testing and Materials, 1967, pp. 247–309.

[*6*] Lehr, K. R. and Liu, H. W., *International Journal of Fracture*, Vol. 5, No. 1, March 1969, pp. 45–55.

[*7*] Bathias, C. and Pelloux, R. M., *Metallurgical Transactions*, Vol. 4, May 1973, pp. 1265–1273.

[*8*] Schwalbe, K. H., *International Journal of Fracture*, Vol. 9, No. 4, Dec. 1973, pp. 381–395.

[9] Elber, W. in *Damage Tolerance in Aircraft Structures, ASTM STP 486*, American Society for Testing and Materials, 1971, pp. 230–242.
[10] Nowack, H., "Ein Beitrag zur Untersuchung der Schadensakkumulation auf der Grundlage biharmonischer Belastungsabläufe," DLR Forschungsbericht 71–23, Abteilung Wissenschaftliches Berichtswesen der DFVLR, Ed., Porz-Wahn (Germany), 1971.
[11] Schijve, J., *Engineering Fracture Mechanics*, Vol. 6, No. 2, Sept. 1974, pp. 245–252.
[12] Freudenthal, A. M., *Engineering Fracture Mechanics*, Vol. 6, No. 4, Dec. 1974, pp. 775–793.

Complex Spectra: Load Definition, Modeling, and Service Simulation

J. A. Reiman,[1] *M. A. Landy,*[1] *and M. P. Kaplan*[1]

Effect of Spectrum Type on Fatigue Crack Growth Life

REFERENCE: Reiman, J. A., Landy, M. A., and Kaplan, M. P., "Effect of Spectrum Type on Fatigue Crack Growth Life," *Fatigue Crack Growth Under Spectrum Loads, ASTM STP 595*, American Society for Testing and Materials, 1976, pp. 187–202.

ABSTRACT: An ever-present problem in airplane design has been the accurate prediction of fatigue crack growth rate in new (never flown) aircraft. This problem has become even more critical in light of the new U. S. Air Force Damage Tolerance Requirements (MIL-A-83444). Briefly, the purpose of this specification is to protect flight structures from potentially deleterious defects which can be introduced into the structure during processing, manufacturing, etc. One of the most important things to consider when performing a damage tolerance analysis is the type of fatigue loading spectrum to be used. The purpose of this paper is to present a method of deriving a randomized flight-by-flight loading spectrum which can be used in preliminary design, and to show the effect on crack growth life of varying certain important parameters.

The random spectrum is derived using mission profiles, MIL-A-008866A or flight recorder exceedance data, design loads, and stress data. The mission mix and actual load sequence is determined randomly. The spectrum is then analyzed using a conventional crack growth computer program which calculates crack growth (*a* versus *N*) curves, and critical crack length.

The sensitivity of fatigue crack growth life to the variation in a number of parameters was investigated. These parameters include different random sequences and cycle counting methods. Random sequence effects include randomizing the loads on a mission segment or on a flight-by-flight basis. The results of this study are compared to the results obtained when the basic exceedance data was combined into a conventional block loading sequence.

KEY WORDS: fatigue (materials), crack propagation, damage, randomization, flight tests, counting, sampling, defects

The increased awareness of the effects of load interaction has underscored the importance of defining a realistic loading spectrum for fatigue and crack growth analysis and test. This has led to much effort being expended to quantitatively determine exactly how the variation of key spectrum parameters affect crack growth life [*1–3*].[2] We would like to know how closely a design spectrum must simulate real life usage in order to accurately predict life.

The early fatigue spectra were all block-type. There were a number of reasons for this: the test equipment available could not handle complex load time histories, the contemporary analytical techniques such as Miner's Rule did not

[1] Aerospace engineers, Fatigue and Fracture Branch, Structures Division, ASD/ENF, Wright-Patterson AFB, Ohio, 45433.

[2] The italic numbers in brackets refer to the list of references appended to this paper.

recognize sequence, etc. Unfortunately, it was learned from fleet experience that these techniques of testing and analysis were not accurately predicting problems which were occurring in service. Therefore, it became necessary to go to a more complex test spectrum in order to improve the accuracy of test results by using a load-time history which was a closer simulation of the actual spectrum experienced by the fleet. Thus, the flight-by-flight spectrum was conceived, and it has generally become the accepted standard. In recent years, the widespread use of computers has allowed one to ever increase the complexity of the flight-by-flight spectra.

Although nearly everyone is in general agreement as to what kind of spectrum should be used, the exact methodology to derive the spectrum is ill-defined. It is the purpose of this paper to describe methods of deriving loading spectra which can be used in the preliminary phases of airframe design. Furthermore, the effect on crack growth life of varying certain important parameters will be demonstrated. These parameters include various sequences and cycle counting methods. Sequencing effects include block loading or randomizing the loads on a mission segment or flight-by-flight basis.

Mission Profile Definition

In determining a fatigue loading spectrum, it is important to know how the user plans to utilize the aircraft. To accomplish this, the user, together with the agency which is responsible for design development, determines a set of "mission profiles." These mission profiles characterize what type of missions will be flown; for example, close air support, armed reconnaissance, training, etc. Each mission profile outlines all the important parameters of the mission: the type of mission, its payload, fuel load, mission duration, and total amount of time spent flying this mission during the aircraft lifetime. Each mission profile is then subdivided into a number of mission segments such as takeoff, ascent, cruise, and combat. The important variables for each mission segment also are defined: initial and final velocity, altitude, and gross weight; and time spent in the segment. This is illustrated in Fig. 1.

With the mission profiles defined, a "load factor exceedance curve" is constructed [*4*]. The load factor exceedance curve, Fig. 2, shows the number of times a given load factor will be exceeded during the lifetime of the aircraft. As the mission profiles tell how much time will be spent flying a given mission segment, the total number of load factor exceedances for the aircraft in question can be determined. MIL-A-008866A [*4*] is one of many sources of exceedance data; there have been many flight load recorder programs which can provide useful information, depending on the type of aircraft being analyzed.

After construction of the load factor exceedance curve, a bending moment and then a stress-exceedance curve is developed. This is accomplished by associating each load factor occurrence with a given weight, velocity, and altitude. To determine how many occurrences one has of a certain load factor, the exceedance curve is discretized. The bending moment is calculated using a

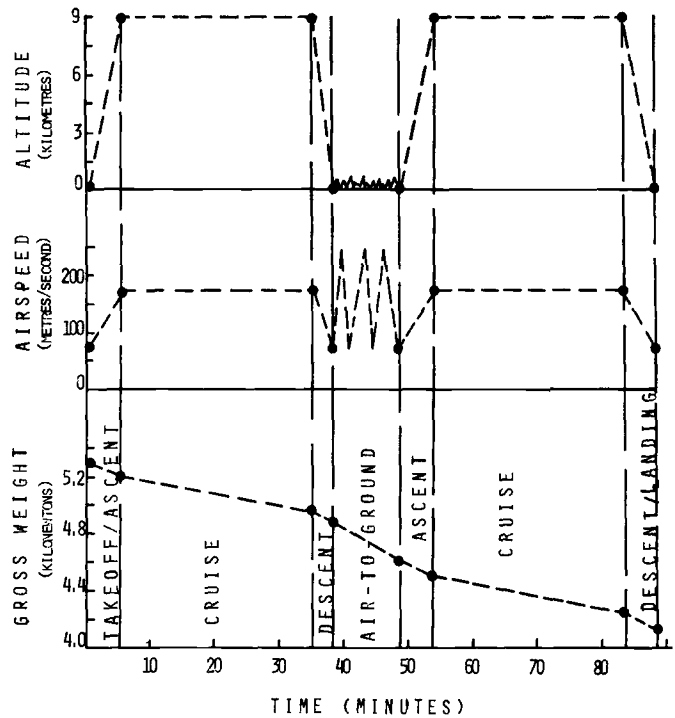

FIG. 1–*Mission profile: ground support.*

known functional relationship between load factor, weight, velocity, and altitude. Using another known relationship, the stress is calculated from the bending moment. Curves for positive and negative maneuvers and their corresponding 1 *g* stresses are developed.

Spectrum Development

For this study, two types of spectra for two different fighter aircraft were developed. These spectra represent the most widely used means of deriving the load-time (stress-time) history of an aircraft. The spectra developed were block (low-high-low) and flight-by-flight (quasi-random). The flight-by-flight spectra were developed by two different methods: one with the loads randomized on a mission segment basis and one with the loads randomized on a total mission basis. The load exceedance data used to generate these spectra were identical [*4,5*].

The two aircraft for which these spectra were developed consisted of an air-to-air fighter and an air-to-ground fighter. For the air-to-air fighter, both flight-by-flight spectra, and a block spectrum were developed. The air-to-ground aircraft did not have a flight-by-flight mission segmented spectrum.

A discussion of the methodology for developing each of these spectra follows.

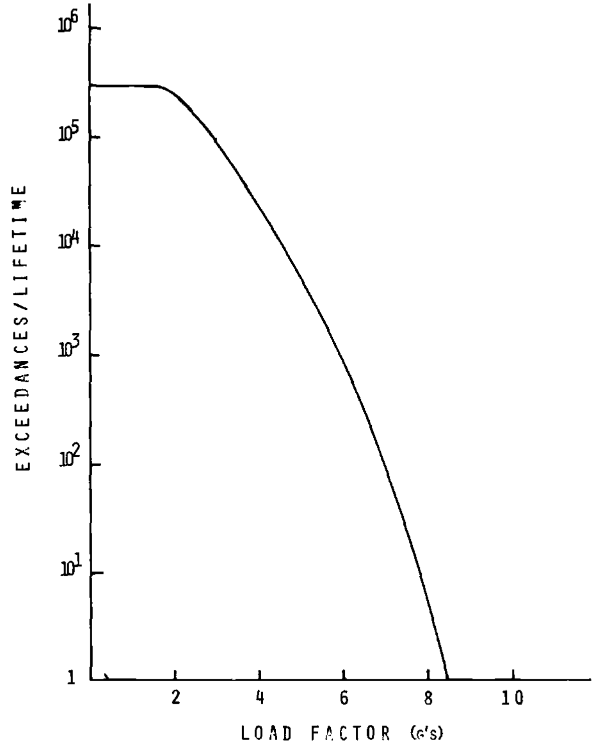

FIG. 2–*Typical stress/exceedance curve.*

Block

The block spectrum, the simplest to derive and test, consists of groups of stress cycles, with each group having the same maximum and minimum stress. The magnitude of the loads for each block are found by differentiating a load (stress) exceedance curve at a given number of load (stress) levels and using the resultant number of occurrences. The blocks so formed are ordered low-high-low.

Block spectra were developed for both the air-to-air fighter and the air-to-ground fighter. The air-to-air fighter's block spectrum consisted of ten unique stress levels for each block while the air-to-ground fighter's spectrum consisted of 14 unique stress levels for each block. To obtain one lifetime, each block was repeated 80 times for the air-to-air aircraft and 325 times for the air-to-ground aircraft. These spectra are illustrated in Fig. 3.

Flight-by-Flight

The importance of using a realistic flight-by-flight spectrum to predict life has been frequently discussed. Derivation of these spectra has only recently been accomplished. This is due to the increased use of high-speed computers, especially when used in conjunction with fatigue test apparatus.

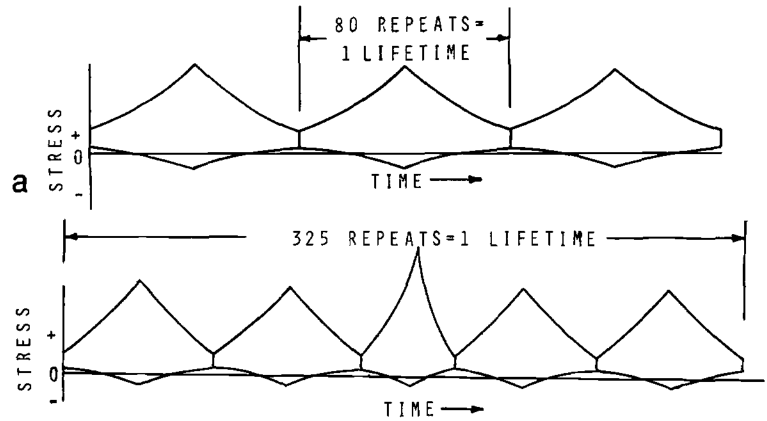

FIG. 3—*Block spectra shapes for (a) air-to-air and (b) air-to-ground fighter.*

A program for developing such a flight-by-flight spectrum has been written by the authors [*6*]. This program has the capability for pairing maximum and minimum stresses on a random basis. The program is written such that any number of missions and mission segments may be input. Ground loads also may be input into the program. The resulting spectrum contains as many different flights as desired. Each flight may be considered as a real-time history of the maneuver loads. For this study, two different flight-by-flight spectra were considered.

Mission Segment-by-Mission Segment—This type of spectrum is the most realistic representation of an aircraft load-time history. The spectrum is first broken into distinct flights, each flight being a certain mission-type such as a special weapons mission, air-to-air combat mission, etc. Each mission type is further divided into mission segments such as ascent, cruise, or descent. For the air-to-air fighter, there are 3195 total flights comprised of five different missions. Each mission contains up to seven segments. These 3195 flights represent 4000 h of flight time. Figure 1 shows a typical mission profile. Each segment (ascent, cruise, etc.) is comprised of a range of airspeeds, gross weights, and altitudes.

The mission ordering within the spectrum is random, but the segments retain their order in each flight. Within each segment the stress history is random. The stresses are divided among 20 unique stress levels, the levels being selected on a statistical basis using a program developed by Lincoln [*7*]. The 20 stress levels are unique for each segment of the mission, providing a total of 520 unique stress levels in the spectrum.

Flight-by-Flight—This spectrum was constructed in a manner similar to the mission segment-by-mission segment just described. The difference is that this spectrum is broken down no finer than on a mission basis. This type of spectrum was derived for both the air-to-air and the air-to-ground aircraft.

The air-to-air fighter's flight-by-flight spectrum was comprised of the same five mission types as in the mission segment-by-mission segment spectrum. The mission ordering was the same random ordering as in the mission segment-by-mission segment spectrum. The stress history within each flight was random. As in the mission segment-by-mission segment spectrum, there were 20 unique stress levels in each mission; thus, there are 100 unique stress levels in all.

The air-to-ground fighter flight-by-flight spectrum was comprised of 2921 unique flights consisting of eleven different missions. As in the air-to-air fighter's flight-by-flight spectrum, the mission ordering was random as was the ordering of the stresses within each flight. There are also 20 unique stress levels in each mission, thus giving 220 stress levels. The same method was used to generate this aircraft usage spectrum [7] as was used with the air-to-air fighter.

Analytical Model Verification

The motivation behind development of a spectrum is to determine the life characteristics, whether fatigue or fracture, of a component. Spectrum development cannot, in itself, determine these life characteristics. To obtain them, it is necessary to perform either a fatigue or fracture analysis or test of a particular component with each of the spectra and compare their results. For the tasks discussed within this report, a fracture mechanics analysis was performed.

It is believed by the authors that test results for each spectrum variation would be beneficial, yet the expense in time, material, and test equipment would be overwhelming. For this reason, the authors chose to utilize a crack growth program, EFFGRO [8] with the Vroman retardation model [9] as the means of comparing results. It is the purpose of this section to indicate that this analytical procedure is capable of predicting crack growth behavior of aluminum alloys for various aircraft spectra. The three spectra will be for a fighter, bomber, and cargo aircraft.

The first example is that of the fighter spectrum. The material used was 2024-T3511 aluminum. The test coupon, shown in Fig. 4 was 101.6 mm (4 in.)

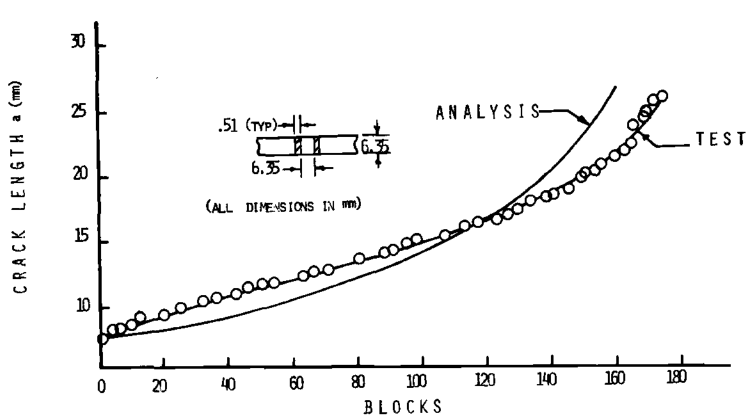

FIG. 4—*Experimental/analytical correlation: fighter spectrum.*

wide and 6.35 mm (0.25 in.) thick. A 6.35 mm (0.25 in.) hole was drilled into the center of the sheet. The specimen was precracked according to ASTM Test for Plane Strain Fracture Toughness of Metallic Materials (E 399-72). Actual spectrum testing was initiated when two diametrically opposed precracks were 0.51 mm (0.02 in.) long. The test spectrum (maximum spectrum stress of 23 MN/m^2 (34 ksi)), shown in Table 1, was a modified low-high-low block spectrum. Figure 4 shows the experimental test results and the analytical correlation.

The second example, that of a bomber spectrum, Table 2, used 2024-T851 aluminum. The specimen geometry, shown in Fig. 5, is a "dog-bone" type specimen, 25.4 mm (1.0 in.) thick. The initial flaw size was 1.78 mm (0.07 in.) with $a/2c = 0.5$, and the critical crack size was 9.14 mm (0.36 in.). The specimen was elox slotted, and the crack initiated using a bending fatigue apparatus. Again, the specimen was precracked consistent with ASTM Method E 399-72. The test spectrum was a flight-by-flight type representative of a wing lower surface. The maximum spectrum stress was 23 MN/m^2 (34 ksi). The test result and its correlation with the analytical study are shown in Fig. 5.

The third example is indicative of a cargo spectrum. Its loading parameters are shown in Table 3. The material is 7075-T6511 aluminum extrusion. The test coupon used, shown in Fig. 6, was 203.2 mm (8 in.) wide and 4.877 mm (0.192 in.) thick. A hole 6.35 mm (0.25 in.) in diameter with a through crack 1.27 mm (0.05 in.) in length was in the center of the specimen. Again, the crack was initiated according to ASTM Method E 399-72. The test spectrum was a low-high-low block spectrum with approximately 5600 cycles equivalent to 6000 flight hours. Figure 6 compares the experimental and analytical results. The maximum spectrum stress was approximately 21.7 MN/m^2 (31.5 ksi).

Thus, it can be seen that for these types of aircraft (bomber, fighter, and cargo) and for these types of spectra (flight-by-flight quasi-block, and block), EFFGRO is able to predict the crack growth characteristics. It also should be noted that the crack geometry for each of these specimens was different.

Results and Discussion

The analytical portion of this study was accomplished employing the same crack growth program (EFFGRO) with the same retardation model (Vroman) as used in the analytical model verification section. For this reason, justification exists for accepting qualitatively the analysis performed herein for spectrum studies. The studies performed for the air-to-air aircraft were as follows:

1. block spectrum versus flight-by-flight spectra,
2. segmented flight-by-flight spectrum versus unsegmented flight-by-flight spectrum,
3. cycle counting techniques: rain flow and range pair, and
4. randomization effects for the unsegmented flight-by-flight spectrum.

The results of the first study, shown in Fig. 7, indicated that a flight-by-flight spectrum was more damaging than a block spectrum: a result which agrees with

TABLE 1 – *Fighter spectrum.*

	Max Load (psi)	Min Load (psi)	Cycles
1	8370.00	3830.00	13.00
2	10870.00	5080.00	39.00
3	13620.00	4760.00	18.00
4	16010.00	5080.00	9.00
5	18320.00	5080.00	5.00
6	20530.00	990.00	1.00
7	22160.00	1320.00	1.00
8	24600.00	2010.00	1.00
9	20530.00	990.00	1.00
10	18320.00	5080.00	5.00
11	16010.00	5080.00	9.00
12	13620.00	4760.00	19.00
13	10870.00	5080.00	39.00
14	8370.00	3830.00	13.00
15	8370.00	3830.00	13.00
16	10870.00	5080.00	39.00
17	13620.00	4760.00	18.00
18	16010.00	5080.00	9.00
19	18320.00	5080.00	5.00
20	20530.00	990.00	1.00
21	22160.00	1320.00	1.00
22	20530.00	990.00	1.00
23	18320.00	5080.00	4.00
24	16010.00	5080.00	10.00
25	13620.00	4760.00	19.00
26	10870.00	5080.00	39.00
27	8370.00	3830.00	13.00
28	13620.00	4760.00	7.00
29	16010.00	5080.00	4.00
30	18320.00	5080.00	2.00
31	22160.00	1320.00	2.00
32	16010.00	5080.00	30.00
33	19250.00	6440.00	7.00
34	20530.00	990.00	5.00
35	27380.00	4260.00	5.00
36	29900.00	1670.00	1.00
37	22160.00	1320.00	1.00
38	20530.00	990.00	3.00
39	19250.00	6440.00	4.00
40	18320.00	5080.00	10.00
41	13620.00	4760.00	16.00
42	10870.00	5080.00	12.00
43	10870.00	5080.00	5.00
44	13490.00	5490.00	1.00
45	13620.00	4760.00	4.00
46	18320.00	5080.00	1.00
47	8370.00	3830.00	9.00
48	8370.00	3830.00	13.00
49	10870.00	5080.00	39.00
50	13620.00	4760.00	18.00
51	16010.00	5080.00	9.00
52	18320.00	5080.00	5.00

TABLE 1 Continued

	Max Load (psi)	Min Load (psi)	Cycles
53	20530.00	990.00	1.00
54	20530.00	990.00	1.00
55	18320.00	5080.00	5.00
56	16010.00	5080.00	9.00
57	13620.00	4760.00	19.00
58	10870.00	5080.00	39.00
59	8370.00	3830.00	13.00
60	8370.00	3830.00	13.00
61	10870.00	5080.00	39.00
62	13620.00	4760.00	18.00
63	16010.00	5080.00	9.00
64	18320.00	5080.00	5.00
65	20530.00	990.00	1.00
66	22160.00	1320.00	1.00
67	24600.00	2010.00	1.00
68	20530.00	990.00	1.00
69	18320.00	5080.00	5.00
70	16010.00	5080.00	9.00
71	13620.00	4760.00	18.00
72	10870.00	5080.00	39.00
73	8370.00	3830.00	13.00
74	10870.00	5080.00	.50
75	16010.00	5080.00	.03
76	20530.00	9900.00	.17
77	29900.00	1670.00	.17
78	31063.00	0.00	.02
79	34260.00	1190.00	.01
80	34260.00	1190.00	.06
81	31480.00	2370.00	.06
82	24600.00	2010.00	.06
83	19250.00	6440.00	.56
84	13490.00	−5490.00	.04
85	8370.00	3830.00	.08

NOTE—Steps with fractional cycles are only applied at interval shown, for example, step 74 is applied every 2nd block, step 78 every 50th, etc.

many investigators [*3,10,11*]. This is due at least in part, to flight duration. It has been shown [*3*] that the shorter the block the more closely the results agree with a flight-by-flight spectrum. It cannot be stated categorically that a block spectrum is nonrepresentative of actual flight conditions; however, it appears that a flight-by-flight spectrum is more realistic.

The results of the second study, also shown in Fig. 7, reveal that no discernable difference exists if a flight-by-flight spectrum is randomized on a flight basis, or randomized on a mission segment basis. This result indicates that it is not necessary to arrange a flight on a mission segment basis, which allows much time savings both in computer hours and test equipment.

TABLE 2 – *Bomber spectrum.*

	Load Range in Percent of Max Load			Randomized Load Step Schedule[a]	
				Flight A	Flight B
Step	Max Load (%)	Min Load (%)	Number of Cycles/Flight	Step No.	Step No.
1	100	60	1 every 100 Flights	4	4
2	90	60	1 every 10 Flights	7	1
3	70	60	2	6	2
4	60	49	2	5	6
5	85	58	1	39	7
6	71	42	3	...	5
7	66	43	1	3	39
8	79	47	1	...	3
9	46	21	1	15	9
10	57	47	1	11	11
11	47	40	1	8	15
12	63	33	1	9	12
13	33	13	1	14	14
14	44	33	1	13	13
15	33	28	1	10	8
16	38	14	1	12	10
17	26	15	1	16	17
18	36	27	1 every 10 Flights	17	16
19	30	15	1	26	21
20	25	19	7	...	19
21	26	5	1	24	23
22	22	8	9	23	20
23	17	10	32	20	22
24	16	0	1	22	25
25	13	1	9	21	26
26	11	5	32	19	18
27	99	55	1 every 100 Flights	25	24
28	89	55	1 every 10 Flights	...	28
29	76	55	1	36	38
30	55	37	1	...	33
31	64	55	19	...	30
32	55	50	19	29	37
33	83	51	1	34	29
34	72	59	1	31	27
35	72	36	1	30	34
36	65	43	9	37	32
37	62	46	48	32	31
38	0	0	1 every 10 Flights	33	36
39	0	0	1	35	35
40	0	0	1	40	40

[a] Apply alternately Flight A, Flight B, Flight A, etc.

NOTE–Steps 1, 2, 18, 27, 28, 38 are never applied on Flight A since "A" Flights are odd numbered flights only. These steps are applied on Flight B only on the 10th or 100th flights or both.

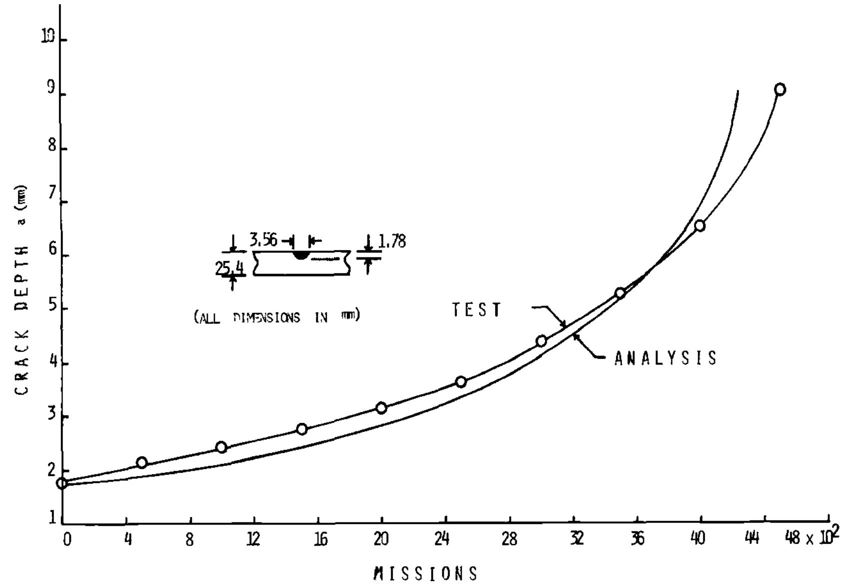

FIG. 5—*Experimental/analytical correlation: bomber spectrum.*

The third study showed that no meaningful difference existed between rain flow and range pair counting procedures. However, if the spectrum were not subjected to a cycle counting procedure, a substantial difference in life exists. Figure 8 shows this. The techniques of crack growth analysis demand that a spectrum be input as a series of whole cycles where a cycle consists of a maximum stress, a minimum stress, and a maximum stress. Thus, a whole cycle is defined as a load excursion with constant mean stress across it. Figure 9 illustrates a cycle with and without constant mean stress. The block type spectrum consists of, by definition, constant mean stress cycles and thus can be used in the crack growth analysis directly. The random spectra, either flight-by-flight or mission segment-by-mission segment, do not consist of whole

TABLE 3 – *Cargo spectrum.*

	Max Stress (psi)	Min Stress (psi)	Cycles
1	10103.00	505.00	1200.00
2	14064.00	5882.00	10823.00
3	17346.00	2540.00	94.00
4	17346.00	2540.00	94.00
5	14064.00	5882.00	10823.00
6	10103.00	505.00	1200.00

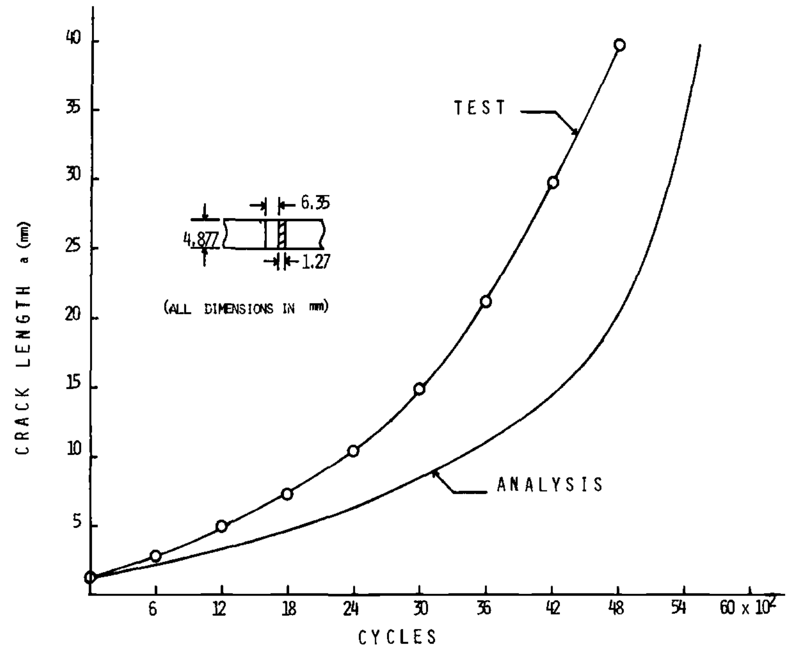

FIG. 6—*Experimental/analytical correlation: cargo spectrum.*

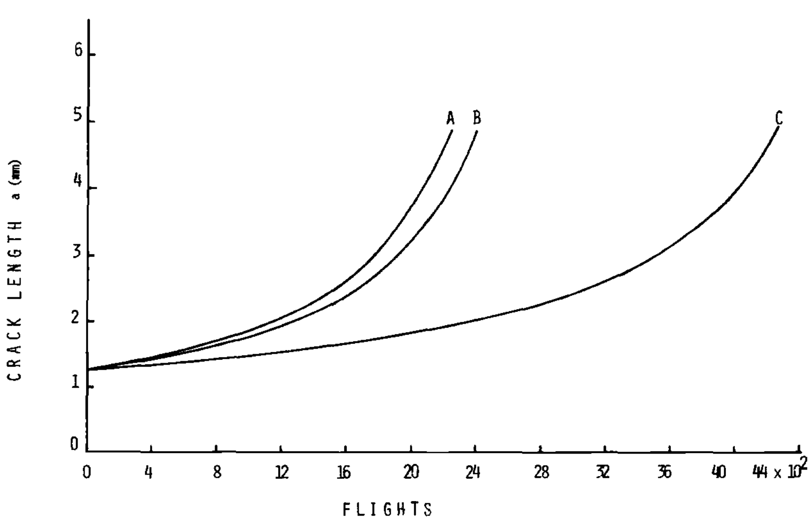

FIG. 7—*Air-to-air fighter: effect of spectrum type on crack growth life. (A) Random flight-by-flight spectrum (stresses randomized on mission basis) rain flow counted; (B) random flight-by-flight spectrum (stresses randomized on mission segment basis) rain flow counted; and (C) block spectrum.*

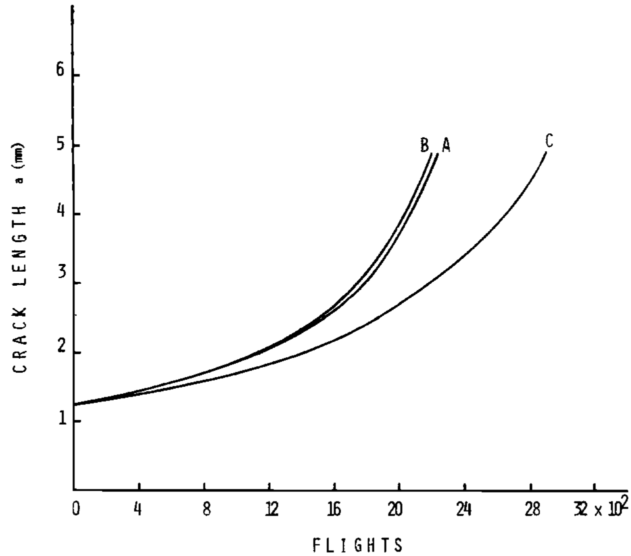

FIG. 8—*Air-to-air fighter: effect of cycle counting procedures on crack growth life. (*A*) Random flight-by-flight spectrum rain flow counted; (*B*) same spectrum as (*A*) range pair counted; and (*C*) same spectrum as (*A*) not counted.*

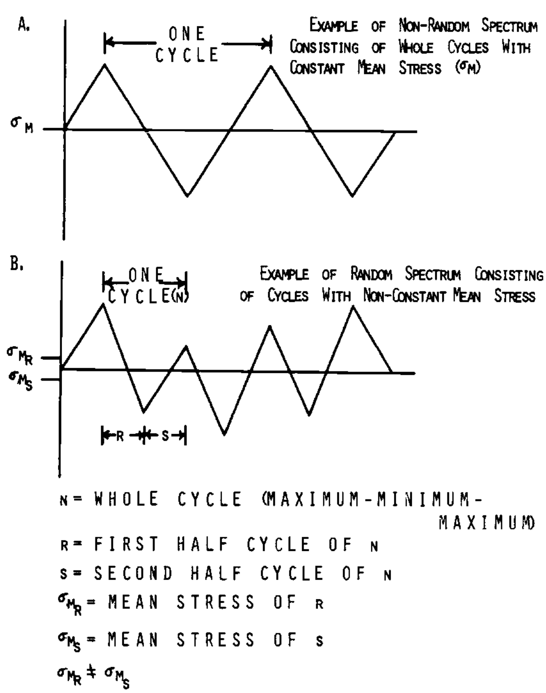

FIG. 9—*Definition of a cycle.*

cycles but, rather, of half-cycles (maximum to minimum or minimum to maximum). Thus, it is necessary to use a cycle counting technique that will redefine the random spectrum in terms of whole cycles with constant mean stress. The range pair method results in output consisting of whole cycles and this output is used directly as input to a crack growth analysis (*12*). The rain flow method results in output consisting of half-cycles (*13*), and different techniques developed by the authors [*6*] were used to form the half-cycles into whole cycles. These whole cycles are then used as input to a crack growth analysis. Both methods preserve the sequencing effects of the random spectrum.

The final study, randomization effects, suggests that one random sequence gives results similar to another, as shown in Fig. 10. This is not unexpected as

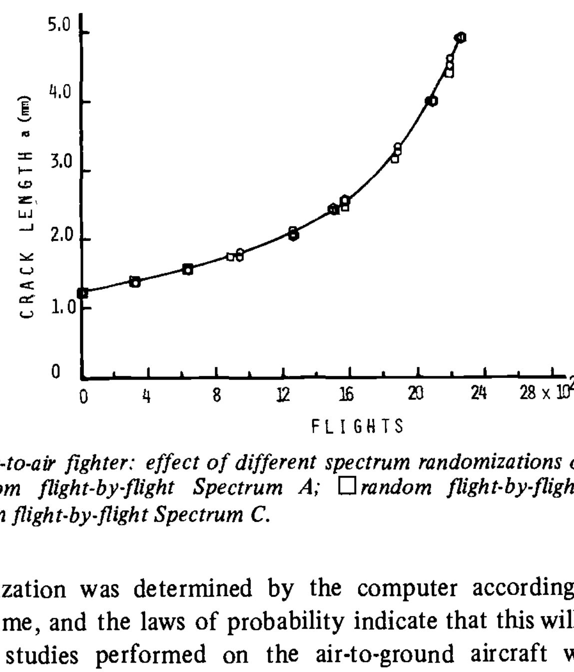

FIG. 10—*Air-to-air fighter: effect of different spectrum randomizations on crack growth life.* ○ *Random flight-by-flight Spectrum A;* □ *random flight-by-flight Spectrum B; and* ⬡ *random flight-by-flight Spectrum C.*

the randomization was determined by the computer according to a random number scheme, and the laws of probability indicate that this will be the result.

The two studies performed on the air-to-ground aircraft were: a block spectrum versus a flight-by-flight spectrum, and an evaluation of cycle counting procedures. It should be noted that each block of the block spectrum contained five low-high-low excursions as is shown in Fig. 3.

The first study indicated (Fig. 11) that a flight-by-flight spectrum results in shorter life than does a block spectrum. The second study, the evaluation of cycle counting procedure again showed, Fig. 12, that the difference between the range pair and rain flow techniques is negligible.

Conclusions

1. Flight-by-flight spectra appear to result in a more conservative life estimate than block spectra if proper cycle counting procedures are used.

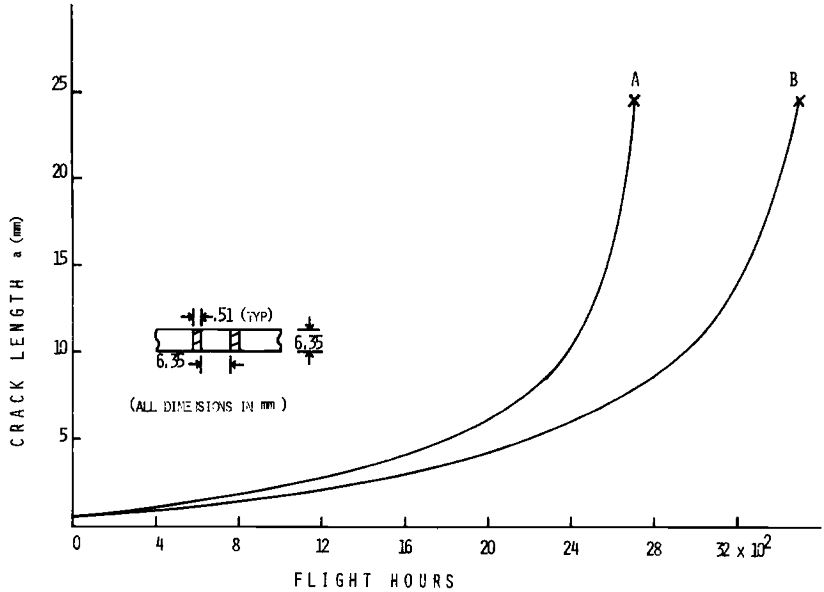

FIG. 11—*Air-to-ground fighter: effect of spectrum type on crack growth life. (A) Random flight-by-flight spectrum rain flow counted; and (B) block spectrum.*

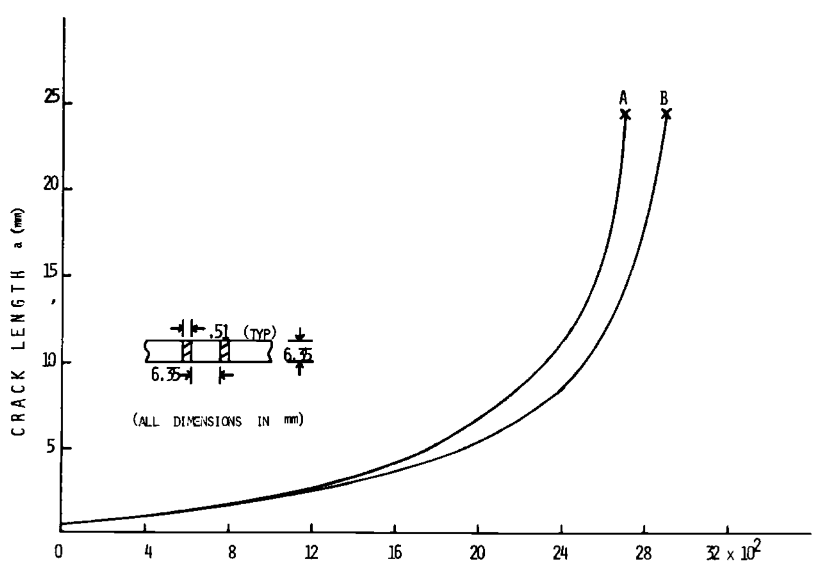

FIG. 12—*Air-to-ground fighter: effect of cycle counting procedures on crack growth life. (A) Rain flow counted; and (B) range pair counted.*

2. Negligible differences in analytical life exist between mission segmented and unsegmented flight-by-flight spectra.

3. In this study, a randomized flight-by-flight spectrum gives repeatable results independent of the exact random sequence.

Acknowledgments

The authors would like to thank the various System Program Offices from Wright-Patterson AFB which allowed us to use their test data for the Analytical Model Verification portion of this paper.

References

[*1*] Schijve, J., "Load Sequences for Fatigue Testing of Components and Fullscale Aircraft Structures," Paper No. 70-37, ICAF Congress, Rome, 1970.

[*2*] Barrois, W., "A Short Survey on Possibilities of Fatigue Life Assessment of Aircraft Structures Based on Random or Programmed Fatigue Tests," *Fracture Mechanics of Aircraft Structures*, AGARD-AG-176, NATO, Jan. 1974.

[*3*] Schijve, J., "The Effect of Load Sequence on Fatigue Crack Propagation Under Random Loading and Program Loading," NLR TR 71014, Amsterdam, 1971.

[*4*] Department of the Air Force, "Airplane Strength and Rigidity Reliability Requirements, Repeated Loads, and Fatigue," MIL-A-008866A(USAF), 31 March 1971.

[*5*] Clay, L., Nash, J., Rockafellow, R., and Shope, C., "Structural Flight Loads Data from F/RF-4 and Thunderbird F-4E Aircraft, January, 1972 through June, 1973," ASD-TR-74-2, Jan. 1974.

[*6*] Landy, M., Kaplan, M., and Reiman, J., "Derivation and Analysis of Loading Spectra for USAF Aircraft," ASD-TR-7X-XXXX, to be published.

[*7*] Lincoln, J. W., "Development of an Aircraft Maneuver Load Spectrum Based on VGH Data," ASD-TR-7X-XX, to be published.

[*8*] Szamossi, M., "Crack Propagation Analysis by G. Vroman's Model," NA-72-94, Rockwell International, 1 Feb. 1972.

[*9*] Vroman, G. A., "Analytical Prediction of Crack Growth Retardation Using a Residual Stress Concept," B-1 Division, Rockwell International, May 1971.

[*10*] Swanson, S. R., Cicci, F., and Hoppe, W. in *Fatigue Crack Propagation, ASTM STP 415*, American Society for Testing and Materials, 1966, pp. 312–362.

[*11*] Breyan, W. in *Effects of Environment and Complex Load History on Fatigue Life, ASTM STP 462*, American Society for Testing and Materials, 1970, pp. 127–166.

[*12*] Tischler, V. A., "A Computer Program for Counting Load Spectrum Cycles Based on the Range-Pair Cycle Counting Method," AFFDL-TM-72-4-FBR, Nov. 1972.

[*13*] Dowling, N. E., *Journal of Materials*, Vol. 7, No. 1, March 1972, pp. 71–87.

K. H. Klippstein[1] *and C. G. Schilling*[1]

Stress Spectrums for Short-Span Steel Bridges*

REFERENCE: Klippstein, K. H. and Schilling, C. G., "Stress Spectrums for Short-Span Steel Bridges," *Fatigue Crack Growth Under Spectrum Loads, ASTM STP 595*, American Society for Testing and Materials, 1976, pp. 203–216.

ABSTRACT: U. S. Steel's Research Laboratory is currently completing research on Project 12-12, sponsored by the National Cooperative Highway Research Program of the National Academy of Sciences, and entitled "Welded Steel Bridge Members Under Variable-Cycle Fatigue Loadings." The main objectives of the program are to develop fatigue data on welded bridge members under variable-amplitude random-sequence stress cycles representative of stress spectrums such as occur in actual bridges and to develop an analytical method of predicting the fatigue behavior under variable-amplitude stress spectrums from constant-amplitude fatigue data.

This paper summarizes available field measurements of stresses in short-span bridges under traffic, and describes the stress spectrums that were developed from these measurements for use in the testing program. The available field data show that the passage of a vehicle over a bridge produces a single major stress cycle and superimposed vibrational stress cycles. In most types of bridges, the vibrational stresses are small enough to be neglected; however, the described method of deriving a simple equation for the stress spectrum is applicable to field data with or without vibrational stresses. The frequency of occurrence of stress cycles can be defined by a family of skewed Rayleigh probability-density curves; a particular curve from the family is defined by the modal value, S_{rm}, and the dispersion, S_{rd}. The major stress cycles (or stress ranges) are added to the dead-load stress, S_{min}, which remains essentially constant during the life of the bridge. In general, the stress cycles are arranged in random sequence. The stress spectrums used in the main test program, therefore, are defined by three parameters: S_{rm}, S_{rd}, and S_{min}. The fatigue-test control tapes corresponding to these spectrums record 500 individual loads that satisfy one of the family of Rayleigh probability-density curves and are arranged in a random sequence. The tape is continuously cycled throughout a fatigue test.

KEY WORDS: crack propagation, fatigue (materials), steels, stresses, loads (forces), stress cycle

U. S. Steel's Research Laboratory is currently completing research on Project 12-12, sponsored by the National Cooperative Highway Research Program of the National Academy of Sciences, and entitled "Welded Steel Bridge Members

* The opinions and findings expressed or implied in this paper are those of the authors. They are not necessarily those of the Highway Research Board, the National Academy of Sciences, the Federal Highway Administration, the American Association of State Highway Officials, nor of the individual states participating in the National Cooperative Highway Research Program.

[1] Senior research engineer and section supervisor, respectively, Application Research Division, Research Laboratory, United States Steel Corporation, Monroeville, Pa. 15146.

Under Variable-Cycle Fatigue Loadings." The main objectives of the program are to develop fatigue data on welded bridge members under variable-amplitude random-sequence stress cycles representative of stress spectrums such as occur in actual bridges and to develop an analytical method of predicting the fatigue behavior under variable-amplitude stress spectrums from constant-amplitude fatigue data.

To accomplish these objectives, field measurements of stresses in bridges under traffic were analyzed, and various hypotheses of predicting the fatigue behavior of small specimens and beams tested during the program were used and compared. In the experimental part of this study, variable- and constant-amplitude fatigue tests of wedge-opening-loading specimens and plate specimens with a simulated cover-plate-end detail were conducted to obtain crack-growth data and to determine the effects of various stress-spectrum parameters on fatigue life. Also, more than 200 variable- and constant-amplitude fatigue tests of relatively large beams simulating bridge members were performed. Welded beams with and without cover plates and fabricated from either A36 or A514 steel were used to obtain the approximate upper and lower bounds of the variable-amplitude fatigue strength of fabricated bridge members. Various stress spectrums, defined in terms of the mode and dispersion of the frequency of occurrence of stress ranges, were used in the tests.

Currently, the last set of beams is being tested at stress levels representative of actual stresses observed in field measurements. The final report, which summarizes the results of this project, is being drafted and should soon be available through the sponsoring agencies. This paper describes the method employed to represent the available field measurements of stresses in short-span bridges under traffic by simple equations for stress spectrums that were subsequently used in the testing program of the research project.

Field Measurements

Individual Vehicle Passages

The stress or strain response of a bridge to the passage of a vehicle depends on the type of bridge, the weight, speed, and dynamic characteristics of the vehicle, the roughness of the pavement preceding the bridge, and many other factors [*1*].[2] Therefore, the exact shapes of stress-time curves from available field measurements [*2,3,4*] vary considerably, as shown (in Fig. 1) for five different bridges. However, most of the available curves can be characterized as illustrated by an idealized stress-time relationship (Fig. 2*a*).

Without a vehicle on the bridge, the weight of the bridge produces a static or dead-load stress that is not recorded during field measurements, because it existed when the strain gages were installed. The passage of a vehicle produces a single major cycle of additional stress that is controlled primarily by the weight of the vehicle. Smaller vibrational stress cycles, which depend on the dynamic

[2] The italic numbers in brackets refer to the list of references appended to this paper.

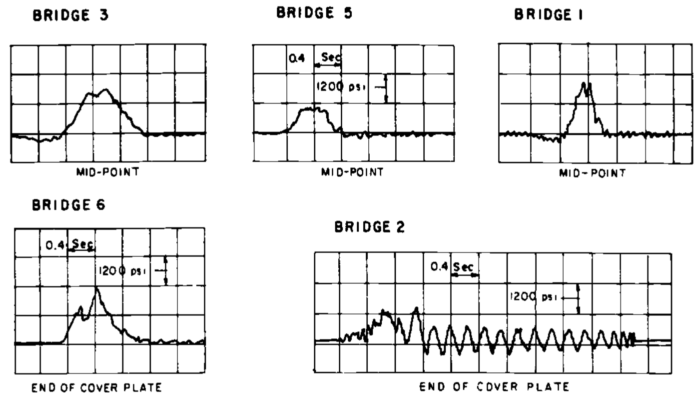

FIG. 1–*Experimental load traces for passage of a single vehicle (traces reproduced from Ref 2).*

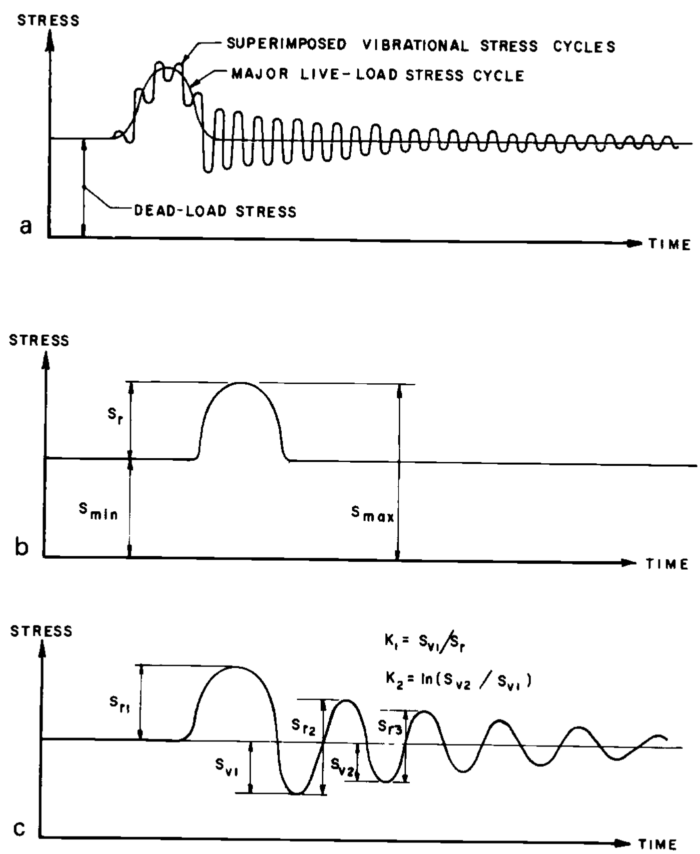

FIG. 2–*Idealized load traces for passage of a single vehicle.*

characteristics of the bridge and vehicle, are superimposed on this major stress cycle. Vibrational stress cycles also occur after the major stress cycle is complete and the vehicle has left the bridge. These vibrational stress cycles occur at the natural frequency of the bridge and usually decrease logarithmically due to viscous damping.[3]

In most of the available stress-time curves, the vibrational stress cycles are small compared with the major stress cycle. As confirmed by tests described in the final report, the small vibrational stress cycles superimposed on the major stress cycle can be neglected. Also, the vibrational stress cycles occurring after the major cycle can be included in the stress-cycle histogram. Thus, the stress caused by the passage of a vehicle can be approximated by a single stress-time cycle (Fig. 2*b*). The cycle is defined by any two of the three parameters: (1) the maximum stress, S_{max}, (2) the minimum stress, S_{min}, and (3) the stress range, S_r.

In a few stress-time curves, particularly curves for a girder bridge with a suspended span, large vibrational stress cycles occur after the major cycle. This type of curve can be approximated by logarithmically descending multiple stress-time cycles (Fig. 2*c*).

Frequency of Occurrence

The stress spectrum, or stress history, for a particular location in a bridge can be conveniently defined in terms of the frequency of occurrence of the maximum (peak) stress in each stress cycle. Usually, frequency-of-occurrence field data are presented as a histogram showing the percentage of recorded maximum live-load stresses that fall within a certain stress interval. Figure 3*a* illustrates a similar histogram for the total (dead plus live) stresses. For example, the figure shows that 20.2 percent of the recorded peak stresses were between 7.5 and 8.5 ksi (52 and 59 MPa). The frequency of occurrence of stress ranges can be represented by a plot with the vertical (stress) scale changed according to the relationship among S_{max}, S_{min}, and S_r. Since stress range is the most important stress parameter controlling the fatigue strength of bridge members [*5*], stress range is used to define the major stress cycle in the present program.

The frequency-of-occurrence data can be presented in a more general form by dividing the percentage of occurrence for each interval (Fig. 3*a*) by the interval width to obtain a probability-density curve[4] (Fig. 3*b*). The probability density is independent of the interval used in classifying the data and is a continuous curve. Thus, data from sources that use different stress-range intervals can be compared by using the probability-density curve. The area under the curve between any two stress-range values represents the proportion (or percentage) of stress ranges that fall within this interval. The probability-density curve can be defined mathematically by an appropriate equation; a nondimensional equation

[3] Viscous damping, in which a force proportional to the velocity opposes motion, causes a progressive decrease in the peak amplitudes, such that the logarithm of the ratio of any two consecutive peaks (the smaller divided by the larger) is a constant.

[4] The points representing each interval are connected by a smooth curve.

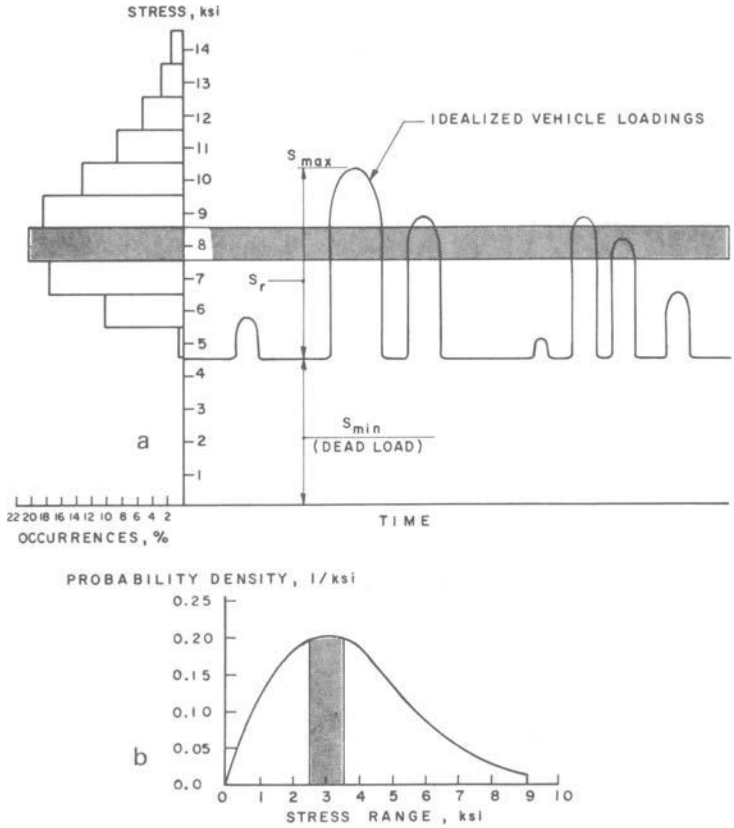

FIG. 3—*Frequency of occurrence data.*

that can be used to represent a family of different probability-density curves is most convenient.

Curve Fitting

Two mathematical expressions illustrated in Fig. 4 were considered for use in representing the frequency of occurrence of stress ranges[5]: (1) a two-parameter Rayleigh probability-density function and (2) a three-parameter Erlang probability-density function. The Rayleigh function is defined for $x' \geq 0$ by

$$p' = x' e^{-(1/2)\ (x')^2} \tag{1}$$

In this equation, p' is the nondimensional probability density, and

$$x' = \frac{S_r - S_{rmin}}{S_{rd}} \tag{2}$$

[5] Two additional expressions, normal and log-normal distributions, were considered during initial evaluations but were discarded.

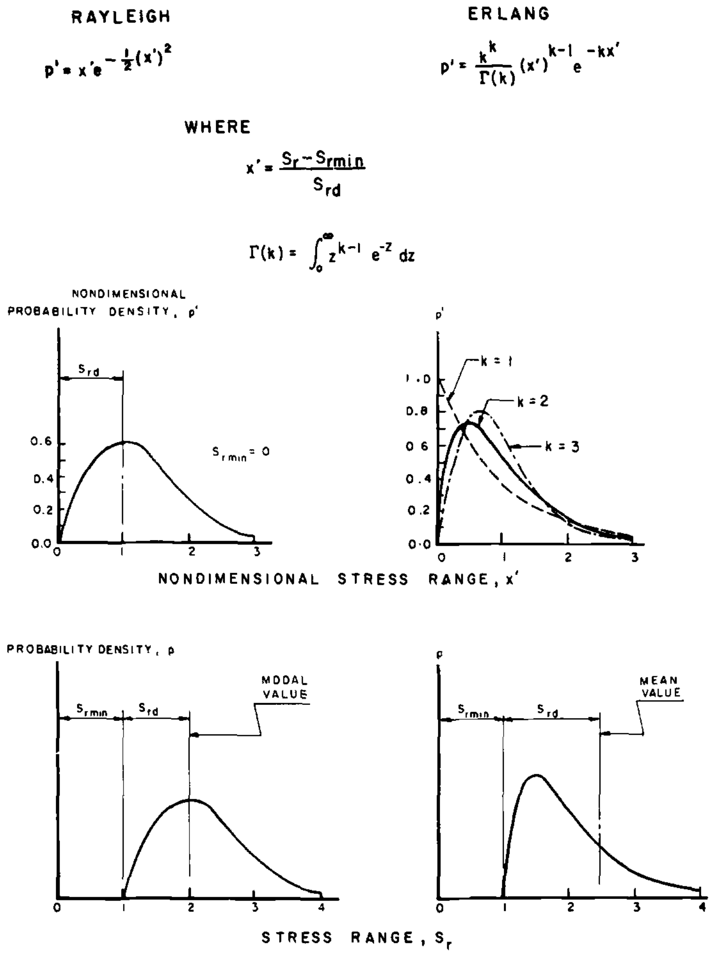

FIG. 4–*Rayleigh and Erlang probability density.*

in which S_r is the independent variable (stress range), and S_{rmin} and S_{rd} are the two parameters (constants) that define any particular probability-density curve[6] from the family represented by Eq 1. The Erlang function is defined for $x' \geq 0$ by

$$p' = \frac{k^k}{\Gamma(k)} (x')^{k-1} e^{-Kx'} \tag{3}$$

in which x' is defined by Eq 2, and k is the third parameter necessary to define a

[6] In both the Rayleigh and Erlang funtions, S_{rmin} represents the distance from the origin to the starting point of the function. S_{rd} represents the distance from the starting point to the modal value in the Rayleigh function and from the starting point to the mean value in the Erlang function. The Rayleigh function is a special case of the Erlang function.

particular probability-density curve. k is a nondimensional parameter greater than 0, and $\Gamma(k)$ is the gamma function defined by

$$\Gamma(k) = \int_0^\infty z^{k-1} e^{-z} dz \tag{4}$$

The Rayleigh curve always starts with zero probability density at the lowest x'. In contrast, the Erlang curve starts with the highest probability density at $x' = 0$ and steadily decreases if the paramenter, k, is equal to 1.0. If the parameter, k, is greater than 1, the Erlang curve has a shape similar to that of the Rayleigh curve; if $k < 1.0$, the curve is asymptotic to the vertical axis at $x' = 0$.

The two mathematical expressions, Eqs 1 and 3, were fitted to frequency-of-occurrence field data by using a curve-fitting computer program that is based on the least-square criterion. The NLWOOD program was selected from a group of available programs. Specifically, the program determines optimum values for the two or three parameters of the Rayleigh or Erlang functions, respectively, and defines an individual probability-density curve of each type. Using trial values of these parameters, the computer program calculates the theoretical frequency of occurrences (in percent) of stress ranges within each experimental interval. The theoretical frequency of occurrence is obtained by integrating the probability-density equations and by subsequently evaluating the integral over the limits defined by the stress-range interval of the experimental data. For the Rayleigh function, integrating Eq 1 for the interval defined at its left side by S_{rL} and at its right side by S_{rR} results in

$$P_R = e^{-1/2\left(\frac{S_{rL} - S_{rmin}}{S_{rd}}\right)^2} - e^{-1/2\left(\frac{S_{rR} - S_{rmin}}{S_{rd}}\right)^2} \tag{5}$$

The Erlang function, Eq 3, cannot be readily integrated. Consequently, the numerical integral utilizing Simpson's rule with 16 divisions for the stress-range interval was used to obtain the frequency of occurrence, P_E, for the Erlang function.

The algebraic difference between the experimental frequency of occurrence and the corresponding theoretical value is the residual (Fig. 5). The computer program automatically changes the parameters and recalculates the residuals until a minimum value of the sum of the squares of the residuals is obtained. When the difference in the sum of the squares between two successive iterations is less than 0.01 percent, it is assumed that the minimum value has been reached. Thus, the selected parameters give the best possible fit (according to the least-squares criterion) over the range of experimental S_r values.

The results of the curve fitting are summarized in Table 1. Fifty-one data sets collected from six sources [*2,4,6–9*][7] were used. For convenience in comparing

[7] This includes all data available during the early part (1971) of the project. Sources that did not contain suitable data because measurements were made under specific truck loadings rather than under normal traffic conditions were excluded.

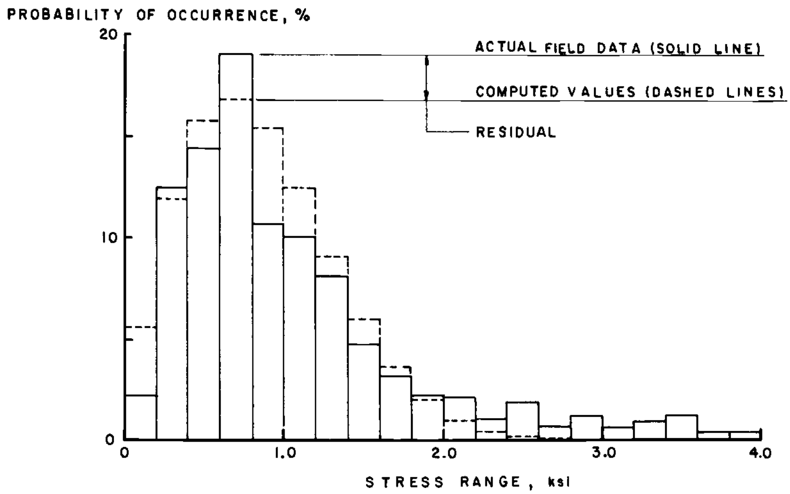

FIG. 5–*Actual versus computed frequency of occurrence.*

the Rayleigh and Erlang curves for a given set of data, the mean, S_{rmean}, and the minimum, S_{rmin}, instead of S_{rd} and S_{rmin}, are given to define a particular probability-density curve. The mean is equal to S_{rmin} + $1.23S_{rd}$ for the Rayleigh curve and S_{rmin} + S_{rd} for the Erlang curve. The parameter k is also given to complete the definition of the Erlang curve. The sum of the squares of the residuals, which is a measure of the closeness of fit, is listed.

As expected, the sum of the squares for the three-parameter Erlang curve was less than the corresponding sum for the two-parameter Rayleigh curve for most of the 51 sets of data. The Erlang curve provides a much closer fit than the Rayleigh curve for data (classified as "descending" in Table 1) that starts with the highest probability density at or near $S_r = 0$ and steadily decreases; such a probability-density curve usually results if the small vibrational stress cycles are included in the data. The closer fit provided by the Erlang curves, of course, results primarily from the use of the third parameter, k, which varied from 1.0 to 8.2 for the 51 sets of data.

The Rayleigh curve was chosen for use in the test program because two parameters were found to be sufficient to represent a wide variation of skewed data and because many more tests would be required to establish the fatigue strength in terms of three parameters than in terms of two parameters. Also, the asymptotic tail of the theoretical Rayleigh probability-density curve was truncated for the testing program. Specifically, a standard Rayleigh curve[8] that has a width of $3S_{rd}$ was used as shown in the upper part of Fig. 6. This width was chosen to permit a reasonable factorial experiment within the limitation that the peak loads must not exceed the yield load. The available field data were considered insufficient to provide an accurate representation of the probability

[8] "Standard Rayleigh curve" is used herein to refer to the family of truncated Rayleigh curves that are used as the standard probability-density curves for the testing program.

of extreme values of S_r ($3S_{rd}$ and above) in actual bridges. The probability of S_r values above $3S_{rd}$ is only 1.1 percent and suggests that the cutoff at $3S_{rd}$ is of little practical significance. Furthermore, the value of S_{rrms}, which is a very meaningful parameter to represent variable-amplitude fatigue data, is shifted only 2.6 percent by truncating a Rayleigh curve at $3S_{rd}$ and would cause an estimated shift in the fatigue life of less than 10 percent.

The constant 1.011 has been inserted into the mathematical expression defining the standard Rayleigh curve to make the area under the truncated curve equal to 1.000, so that the curve represents 100 percent of the occurrences. Thus

$$p' = 1.011x'e^{-(1/2)(x')^2} \tag{6}$$

The modal, median, mean, and root-mean-square values of x' for the standard truncated curve are shown in the figure. These values are slightly different from the corresponding x' values for a full curve, which are equal to 1.000, 1.177, 1.253, and 1.414, respectively. The root-mean-square (rms) value is equal to the square root of the mean of the squares of the individual values.

Based on the definition of x' (Eq 2), the standard Rayleigh curve represents a family of probability curves for stress ranges that may be shifted from the origin of the coordinate system by an amount equal to S_{rmin} and changed in width by varying S_{rd} as shown in the center of Fig. 6. Each particular probability-density curve from the family can be defined by any two of the following three parameters: S_{rm}, S_{rd}, and S_{rmin}. In the testing program, the curves are defined in terms of S_{rm} and S_{rd}/S_{rm}. Four values of S_{rd}/S_{rm} are used in the testing program: 0.00, 0.25, 0.50, and 1.00. Curves for these values are shown at the bottom of Fig. 6. While the root mean square of the x' value (x'_{rms}) is a constant for all curves from the Rayleigh family, the root mean square of the S_r values (S_{rrms}) varies slightly with the ratio S_{rmin}/S_{rd}. However, the maximum difference between the two root mean square values, which occurs when S_{rmin}/S_{rd} is between 1 and 2, is less than 3 percent.

Control Tapes for Fatigue Tests

Several methods were considered to generate and control the variable-amplitude random-sequence loads used in the experimental portion of this project such that these loads would follow a specific Rayleigh probability density function. A filtered one-sided signal of a random-noise generator was considered but rejected because this method would have caused extensive operating problems and the load sequence generated in a trial setup was not random. Also, a permanent computer hookup with an available random-sequence length of up to 2 million cycles or a three-track magnetic tape were considered. These possibilities were rejected because their reliability over a three-year period was considered questionable. Instead, it was decided to use a digital-tape control with looped tapes that contain 500 load cycles per tape in a random sequence. The chosen number of load cycles (500) approximately represents the observed average number of truck passages per day [*2,4,6–9*], and

TABLE 1 – *Comparison of Rayleigh and Erlang curves.*

Data Set	Type of Curve	Rayleigh Curve S_{rmin}, ksi	Rayleigh Curve S_{rmean}, ksi	Rayleigh Curve Fit Parameter	Erlang Curve S_{rmin}, ksi	Erlang Curve S_{rmean}, ksi	Erlang Curve k	Erlang Curve Fit Parameter
1	D	0.52	0.79	12.1	0.56	0.81	1.87	2.8
2	P	0.23	2.24	29.1	0.22	2.35	3.30	18.7
3	D	0.46	0.80	59.6	0.60	0.90	1.10	0.6
4	P	0.20	1.94	18.0	0.00	1.99	4.06	30.2
5	P	0.00	1.36	42.0	0.25	1.50	1.84	2.2
6	P	0.14	1.52	80.9	0.45	1.71	1.61	8.3
7	D	0.42	0.97	13.7	0.48	1.00	2.91	2.3
8	P	0.47	2.04	157.0	0.00	2.10	5.85	180.8
9	D	0.52	0.81	28.7	0.60	0.84	1.05	1.0
10	P	0.32	1.28	20.0	0.34	1.34	3.08	5.8
11	D	0.43	0.89	34.3	0.55	0.96	2.03	2.8
12	P	0.21	2.37	17.2	0.25	2.49	2.96	12.4
13	P	0.07	1.54	3.5	0.00	1.60	3.55	4.0
14	P	0.11	1.47	29.3	0.03	1.52	3.54	28.8
15	P	0.00	1.01	55.2	0.35	1.15	1.11	0.6
16	P	0.05	1.33	68.2	0.38	1.49	1.48	2.6
17	P	0.52	1.84	208.5	0.00	1.86	6.86	225.9
18	P	0.30	0.95	14.1	0.41	0.82	2.02	2.1
19	P	0.09	1.37	20.2	0.08	2.02	3.22	12.4
20	P	0.17	0.95	80.2	0.07	1.00	4.11	81.6
21	P	0.12	0.35	0.1	0.00	0.34	8.18	0.2
22	P	0.22	0.74	19.2	0.16	0.78	3.99	10.6
23	P	0.15	1.05	59.8	0.30	1.18	1.97	31.6
24	P	0.23	1.00	56.0	0.26	1.03	2.93	49.5
25	P	0.14	0.68	30.8	0.17	0.71	2.86	25.5
26	P	0.20	1.02	35.3	0.22	1.07	2.86	28.7
27	P	0.23	1.91	6.8	0.00	1.97	4.11	9.2
28	P	0.20	1.56	37.2	0.00	1.59	4.28	35.4
29	P	0.01	1.02	48.1	0.16	1.16	2.04	19.0
30	P	0.23	1.61	48.8	0.38	1.71	2.33	36.6
31	P	0.08	0.88	118.4	0.40	1.00	1.05	43.7
32	P	0.00	1.26	72.8	0.35	1.47	1.42	31.6
33	D	0.50	0.96	9.8	0.48	0.95	4.19	9.0
34	P	0.31	1.15	4.3	0.21	1.16	4.29	4.6
35	P	0.40	1.14	0.0	0.00	1.15	7.82	2.1
36	D	0.31	0.88	6.1	0.33	0.92	3.61	1.8
37	D	0.37	0.79	2.8	0.36	0.81	3.80	0.6
38	P	0.28	1.08	4.9	0.25	1.12	3.76	6.1
39	D	1.33	1.69	3.0	1.33	1.70	3.51	0.4
40	P	0.82	2.37	5.7	0.44	2.39	5.15	9.6
41	D	0.80	1.79	123.3	0.92	1.86	2.70	79.2
42	P	0.46	1.26	18.2	0.51	1.28	2.95	6.0
43	D	0.00	1.07	151.4	0.43	1.34	0.98	5.9
44	D	0.05	1.01	42.4	0.57	1.28	1.08	8.9

TABLE 1 Continued.

Data Set	Type of Curve	Rayleigh Curve S_{rmin}, ksi	Rayleigh Curve S_{rmean}, ksi	Rayleigh Curve Fit Parameter	Erlang Curve S_{rmin}, ksi	Erlang Curve S_{rmean}, ksi	Erlang Curve k	Erlang Curve Fit Parameter
45	D	0.26	0.78	22.9	0.33	0.80	2.19	9.6
46	P	0.21	1.20	4.6	0.40	1.29	2.46	0.0
47	D	0.16	0.81	110.6	0.35	0.88	1.08	36.7
48	D	0.00	1.19	70.3	0.40	1.38	1.63	31.6
49	P	0.27	1.17	3.9	0.15	1.21	4.52	7.1
50	P	0.32	1.20	3.6	0.30	1.23	3.78	0.6
51	D	0.31	0.75	15.8	0.43	0.76	1.11	13.8

NOTES—1 ksi = 6.895 MN/m^2.

Curves that start at a peak and steadily decrease are referred to as descending curves and are identified by a D; curves that increase to a peak and then decrease are called peak curves and are identified by a P.

S_{rmin} is the minimum stress range in the spectrum; S_{rmean} is the mean stress range for the spectrum; k is the nondimensional shape parameter; and the fit parameter is the sum of the squares of the residuals, lower values of the fit parameter indicate a closer fit.

the random sequence of the load cycles within each tape resembles the observed randomness of recorded stress-range histories [*8*].

The punched tapes that are used to control the fatigue tests were generated by a computer program [*10*]. Two methods were considered to determine the individual loads necessary to generate stress-range cycles that correspond to a given probability-density curve: (1) subdivide the width of the curve ($3S_{rd}$) into a certain number of stress-range intervals of equal widths to produce a frequency-of-occurrence graph similar to that shown in Fig. 5, and (2) subdivide the area below the probability-density curve into a certain number of intervals with equal areas but different widths. For the first method, each interval would contain a different percentage of the total area and thus would represent a different percentage of the total number of cycles on each test control tape. Each percentage would be multiplied by the total number of cycles on the tape to determine the number of cycles at the stress range corresponding to the midpoint of that interval. Since the number of cycles corresponding to each stress-range interval would not be an integer, rounding off of fractional cycles would be required. Therefore, the method was rejected and the computer program was written to make use of the second method.

The program calculates 500 individual loads that satisfy the standard Rayleigh probability-density curve, arranges them in a random sequence, and punches a control tape defining these loads in ASC II code. A separate tape is required for each different value of S_{rd}/S_{rm}, but different levels of S_{rm} and S_{min} are set

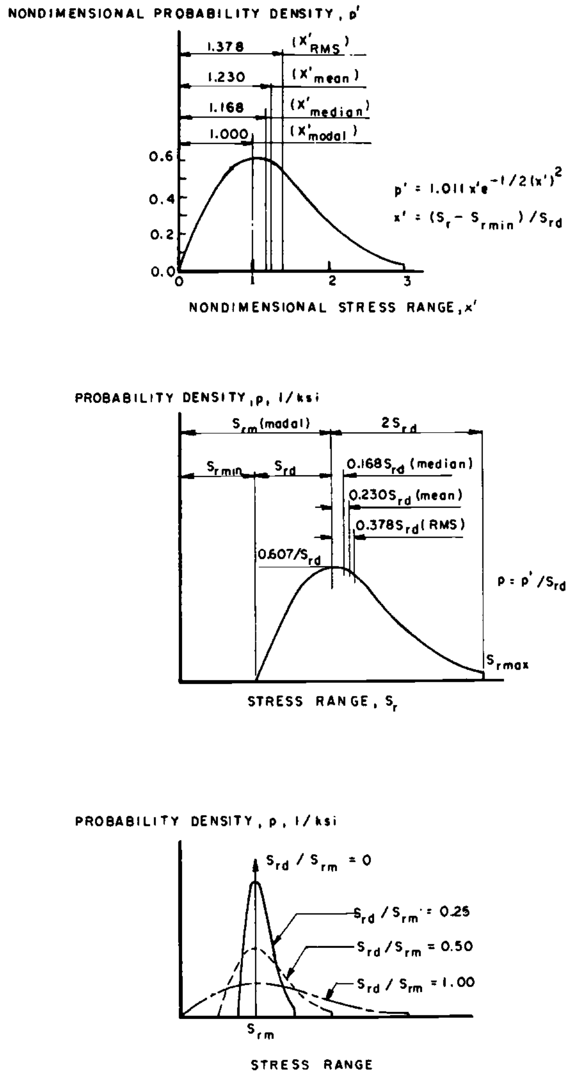

FIG. 6—*Characteristics of Rayleigh probability curves.*

manually on the testing-machine controls. The program is written in FORTRAN IV.

The 500 individual loads are calculated by dividing the area below the nondimensional probability-density curve, Eq 1, into 500 vertical segments (bars) of equal area. The width of the bars varies to provide equal areas. The midwidth (or more precisely, the value of x' that bisects the bar into segments of equal area) of each of these bars corresponds to a load with a frequency of occurrence of 1/500. The value x'_n corresponding to the midwidth of the nth bar is calculated by integrating the nondimensional probability-density curve from 0 to x'_n and equating the result to the desired area, $(n - 1/2)/500$. The result of the integration is 1.011 times $(1 - e^{-(1/2)(x'_n)^2})$. Thus

$$x'_n = \sqrt{-2 \ln[1 - 0.00198 (n - 0.5)]} \tag{7}$$

The values of x'_n vary from 0 to 3. In generating the tapes for the main testing program, the values of x'_n corresponding to the right side of the bars, rather than to midwidths, were used for convenience. This procedure is equivalent to omitting the 0.5 in Eq 7 and is permissible because the x' interval is very small. The resulting increase in S_{rrms} does not exceed 0.3 percent.

For convenience in operating the fatigue-testing equipment, the corresponding stress ranges, S_{rn}, on the control tape are expressed as a three-digit percentage of the maximum stress range, S_{rmax}; thus the control-tape values vary from a minimum of 000 to a maximum of 999 representing 0.0 and 99.9 percent, respectively. A different tape is required for each of the four different values of S_{rd}/S_{rm} in the program: 0.0 (constant amplitude), 0.25, 0.50, and 1.00.

The computer program arranges the calculated S_{rn}/S_{rmax} values in a random sequence by generating 500 random-sequence numbers, consecutively assigning these sequence numbers to the 500 S_{rn}/S_{rmax} values, and finally arranging the control-tape values according to the assigned sequence numbers. The random numbers are generated by an available CDC (Control Data Corporation) computer subroutine.

The control tape defines both the peak and valley of each load cycle; the valley is equal to 0, and the peak equals the calculated control-tape value. In the actual test, the level of maximum cyclic stress corresponding to a tape command of 999 is set by the testing-system controls, and a constant minimum stress may be superimposed on the cyclic stress. The ends of the tape are connected to form a loop which is continuously cycled through the test. Thus, within the loop of 500 cycles, the sequence of the load levels is fully random; however, since the loop is repeated many times before the specimens fail, the overall sequence is pseudo-random.

The control tape just described was used for the major test program. To assure that the chosen number of load levels within the spectrum and the number of load cycles and their relative positions within a sequence (or loop) would not affect the test results, 24 tests were conducted. In these tests, 100 and 500 load levels were used to subdivide the load spectrum, and sequence lengths of 100, 500, and 5000 cycles were used within a loop. The results of the additional tests were not significantly different from the tests conducted with the tape used for the major test program.

Conclusions

The investigated field data of steel bridges indicate that the passage of a vehicle over a bridge produces a single major stress cycle, S_r, with superimposed vibrational stress cycles that may continue after the vehicle has left the bridge. For most types of short-span bridges, the vibrational stress cycles are small enough to be neglected. The major stress cycle is added to the existing dead-load stress. Therefore, the stress spectrum for bridges can be defined in terms of the minimum (dead load) stress, S_{min}, which remains essentially constant during the life of the bridge, and the frequency of occurrence of major stress cycles, S_r. The chosen probability-density function, along with the available controls of the test equipment and the command signals generated by continuous control tapes, adequately permits variable-amplitude random-sequence fatigue testing representative of the actual stress spectrums for short-span steel bridges.

References

[*1*] Veletsos, A. S. and Huang, T., *Journal of the Structural Division*, American Society of Civil Engineers, Vol. 96, No. EM5, Oct. 1970, pp. 617–619.

[*2*] Cudney, G. R., "The Effects of Loadings on Bridge Life," Research Report No. R-638, Michigan Dept. of State Highways, Jan. 1968.

[*3*] Cudney, G. R., *Journal of the Structural Division*, American Society of Civil Engineers, Vol. 94, No. ST12, Dec. 1968, pp. 2725–2737.

[*4*] Heins, C. P. and Sartwell, A. D., "Tabulation of Dynamic Strain Data on Three-Span Continuous Bridge Structures," Civil Engineering Research Report No. 33, University of Maryland, Nov. 1969.

[*5*] Fisher, J. W., Frank, K. H., Hirt, M. A., and McNamee, B. M., "Effect of Weldments on Fatigue Strength of Steel Beams," NCHRP Report 102, 1970.

[*6*] Galambos, C. F. and Armstrong, W. L., "Loading History of Highway Bridges," Highway Research Record 295, Highway Research Board, 1969.

[*7*] Heins, C. P. and Sartwell, A. D., "Tabulation of 24-Hour Dynamic Strain Data on Four Simple-Span Girder-Slab Bridge Structures," Civil Engineering Research Report No. 29, University of Maryland, June 1969.

[*8*] Heins, C. P. and Sartwell, A. D., "Tabulation of Dynamic Strain Data on a Girder-Slab Bridge Structure During Seven Continuous Days," Civil Engineering Research Report No. 31, University of Maryland, Sept. 1969.

[*9*] Christiano, P., Goodman, L. E., and Sun, C. N., "Bridge Stress Range History and Diaphragm Stiffening Investigation," report by the Department of Civil Engineering and Hydraulics, University of Minnesota, June 1970.

[*10*] NCHRP Project 12-12, Interim Report, Research Laboratory, United States Steel Corporation, Project No. 76.019-001, 1 Oct. 1972.

J. M. Barsom[1]

Fatigue Crack Growth Under Variable-Amplitude Loading in Various Bridge Steels

REFERENCE: Barsom, J. M., "Fatigue Crack Growth Under Variable-Amplitude Loading in Various Bridge Steels," *Fatigue Crack Growth Under Spectrum Loads, ASTM STP 595*, American Society for Testing and Materials, 1976, pp. 217–235.

ABSTRACT: Well-conceived procedures used to study the safety and reliability of structures recognize that the performance of a structure or a structural component is governed not only by material properties but also by the design, fabrication, inspection, erection, and use of the structure. These parameters govern the initiation of subcritical cracks and their propagation to critical dimensions, and therefore, determine the useful fatigue life of structural components subjected to load fluctuations.

This paper presents the results of the first phase of an investigation sponsored by the National Cooperative Highway Research Program, Project 12-14, to study "Subcritical Crack Growth in Steel Bridge Members."

The paper describes the fatigue-crack-growth behavior of various bridge steels (A36, A588-A, A588-B, A514-B, A514-E, and A514-F) under variable-amplitude random-sequence stress spectra such as occur in actual bridges. The fatigue crack growth-rate data were obtained by using wedge-opening-loading specimens tested under variable-amplitude random-sequence load spectra that are represented by a Rayleigh distribution function.

The data obtained for these steels showed that the average fatigue crack growth rates, da/dN, under variable-amplitude random-sequence load fluctuation and under constant-amplitude load fluctuation agreed closely when da/dN was plotted as a function of the root-mean-square stress intensity factor range, ΔK_{rms}. Thus, within the limits of the present investigation, the average fatigue crack-growth rates, da/dN, of various bridge steels subjected to variable-amplitude random-sequence load fluctuations, such as occur in actual bridges and to constant-amplitude load fluctuations, can be represented by the equation

$$\frac{da}{dN} = A\,(\Delta K_{\mathrm{rms}})^n$$

where ΔK_{rms} is the root-mean-square stress intensity factor fluctuation, and A and n are material constants.

KEY WORDS: crack propagation, fatigue (materials), inspection, steels, loads (forces)

Steel bridges have an excellent service record extending over millions of operational years. However, the collapse of the Point Pleasant Bridge [*1*][2] has

[1] Section supervisor, Mechanical Behavior, Research Laboratory, United States Steel Corporation, Monroeville, Pa. 15146.

[2] The italic numbers in brackets refer to the list of references appended to this paper.

led to an increasing concern about the possibility of catastrophic fractures in steel bridges.

The safety and reliability of steel bridges are governed by many interrelated factors. Fracture of a bridge detail can occur as a result of improper material properties, design, fabrication, inspection, erection, or operating conditions. Consequently, a need exists for a systematic evaluation of the procedures used to select steels for bridges, of the philosophy and trends in bridge design and analysis, and of the procedures used to fabricate and to inspect bridge details. A thorough understanding of the several technologies used in bridges is the basis for the development of a systematic procedure to evaluate the safety and reliability of steel bridges. A description of these technologies and the development of fracture-control plans for steel bridges are beyond the scope of this paper.

The rate of fatigue crack growth has been investigated in many materials and has been found to depend on the magnitude of the stress range, $\Delta\sigma$, the crack length, a, and the material properties. The stress range and crack length can be incorporated in a single-term parameter, ΔK_I, which represents the fluctuation of the stress intensity in the vicinity of the crack tip. Consequently, the rate of fatigue crack growth, da/dN, has been related to ΔK_I by the empirical relationship

$$\frac{da}{dN} = A(\Delta K_I)^n \tag{1}$$

where

a = crack length,
N = number of cycles, and
ΔK_I = fluctuation of the stress-intensity factor.

A and n are constants that reflect effects of material properties and environments. Sufficient data obtained under constant-amplitude cyclic-load fluctuations are available in support of this observation [*2,3*].

Several investigators [*4–8*] have noted that changes in cyclic-load magnitude and the order (sequence) of the variation of cyclic-load magnitude can lead to accelerated or retarded rates of fatigue crack growth. Consequently, fatigue crack-growth rate models that account for these interaction effects must be developed to predict the crack growth of structural components under variable-amplitude random-sequence load fluctuations. Accordingly, the present investigation was undertaken to study fatigue crack growth in various bridge steels under constant-amplitude, and random variable-amplitude cyclic-load fluctuations such as occur in actual bridges. The data were analyzed by using linear-elastic fracture-mechanics methods.

Materials and Experimental Work

Materials

The steels studied in the present investigation are A36, A588-A, A588-B, A514-E, and A514-F. One-in.-thick (25.4-mm) plates of each steel were used in this study. The chemical composition and mechanical properties of the steels are given in Tables 1 and 2, respectively. This paper includes some data for A514-B that were published earlier [*9,10*].

Experimental Procedure

The details for the experimental procedure used in the present investigation have been published elsewhere [*9,10*]. A brief description of the procedure is presented in this section. The fatigue crack propagation data were obtained by using wedge-opening-loading (WOL) specimens. The data were obtained at a cyclic-load frequency equal to 300 cpm. The tests were conducted in a room-temperature air environment by using a 50-kip (222-kN) high-strain-rate Materials Testing System (MTS) machine. Alignment was obtained by carefully machining specimens and other auxiliary parts and by using universal joints to load the specimens.

The specimens were tested under constant-amplitude and under variable-amplitude cyclic-load fluctuations in the form of a sine wave. In each test the fatigue crack was initiated and propagated in tension-to-tension at a constant minimum load of 200 lb (890 N) and at a constant- or variable-amplitude maximum load, which were controlled within ±1.0 percent. The crack was initiated and propagated from the notch root so that at the time crack-length measurements were begun, the total crack length, a, was equal to 1.0 ± 0.001 in. (25.4 ± 0.0254 mm).

Fatigue-crack-growth rates were measured optically with a Type M-101 Gaertner microscope mounted in a micrometer slide. To improve the accuracy of measuring the rate of crack extension, a series of hardness indentations was made on the surface (with a Vickers pyramid hardness testing machine) along a line parallel to the plane of the initial crack and in the direction of expected crack extension.

The variable-amplitude random tests were conducted in a 50-kip high-strain-rate MTS machine, used in conjunction with a tape-controlled digital programmer [*11*]. The programmer accepts manually entered commands or programmed digital commands from punched tape, and produces an electronic control signal that varies with time as specified by the input instructions. Continuous cycling of tapes can be achieved by splicing the tape to form a closed loop.

Stress spectra, typical of bridge loadings, have been thoroughly investigated [*9,12*]. In the crack-growth tests, all loadings followed a Rayleigh distribution curve, with the ratio of the load-range deviation to the modal (peak) load (P_{rd}/P_{rm}) equal to either 0 or 1.0. A block of 500 individual (usually different) loads satisfying one of these distribution curves was repeated throughout each test. Within the block, the loads were arranged in random sequence.

Although the cyclic-loading spectrum was not changed during a test, the stress intensity factor range, ΔK, for successive blocks increases as the crack length increases. Thus, a single test gives crack-growth rates for a range of ΔK values. The value of ΔK corresponding to a given crack length and loading was calculated from an available theoretical analysis [*13*].

TABLE 1 – *Chemical composition of steels tested–percent (check analysis).*

Steel	Heat No.	Plate No.	C	Mn	P	S	Si	Cu	Ni	Cr	Mo	V	Ti	Sol Al	Insol Al	Total Al	N[a]	O[b]	B
A36	74C515	195264	0.26	1.14	0.009	0.023	0.038	0.031	0.042	0.05	0.016	<0.005	<0.005	0.001	0.001	0.002	0.004	90	ND[c]
A588-A	67C611	193804	0.13	1.14	0.011	0.026	0.22	0.31	0.022	0.57	0.020	0.033	0.005	0.040	0.001	0.040	0.006	15	ND
A588-B	662J487	551528	0.11	1.16	0.011	0.018	0.27	0.26	0.35	0.63	0.016	0.052	<0.005	0.021	0.001	0.022	0.009	27	ND
A514-E	50343	P70074	0.16	0.61	0.008	0.018	0.28	0.21	ND	1.84	0.53	ND	0.063	0.033	0.001	0.034	0.010	41	0.0020
A514-F	70C125	79873A1	0.17	0.60	0.014	0.013	0.22	0.28	0.78	0.56	0.45	0.050	0.005	0.024	0.001	0.025	0.005	26	0.0041

[a] Kjeldahl determination.
[b] Parts per million.
[c] ND = Not determined.

TABLE 2 – *Mechanical properties*[a] *of steels tested.*

Steel	Heat No.	Plate No.	Yield Strength (0.2% Offset), ksi	Tensile Strength, ksi	Elongation in 2 In., %	Reduction of Area, %	Charpy V-Notch Energy Absorption, at 72°F, ft · lb
				Longitudinal			
A36	74C515	195264	43.6	78.2	28.2	62.4	28
A588-A	67C611	193804	54.9	81.7	28.2	68.3	69
A588-B	662J487	551528	55.6	82.1	27.8	76.2	66
A514-E	50343	P70074	107.9	122.6	19.0	65.1	68
A514-F	70C125	79873A1	126.0	134.0	18.3	57.8	45
				Transverse			
A36	74C515	195264	43.9	78.6	25.3	57.4	26
A588-A	67C611	193804	54.6	81.3	24.2	54.0	31
A588-B	662J487	551528	55.8	82.7	24.2	60.5	29
A514-E	50343	P70074	106.1	123.1	17.3	55.5	43
A514-F	70C125	79873A1	126.0	134.0	18.3	58.0	32

[a] Tension and impact specimens were taken in the longitudinal orientation from the quarter-thickness point of the plates, which were all 1 in. thick. Tension-test results are the average of three 0.505-in.-diameter tension specimens, and impact results are the average of two Charpy V-notch specimens.

NOTE–Conversion factors:
1 inch = 25.4 mm
1 ksi = 6.895 MN/m^2
1 ft · lb = 1.36 J
C = 5/9 (F − 32)

Results and Discussion

Fatigue Crack-Growth Behavior

Most fatigue crack-growth tests are conducted by subjecting a fatigue cracked specimen to constant-amplitude cyclic-load fluctuations. Incremental increase of crack length is measured and the corresponding number of elapsed load cycles is recorded. Various a-versus-N curves can be generated by varying the magnitude of the cyclic-load fluctuation or the size of the initial crack or both. These curves reduce to a single curve when the data are represented in terms of crack-growth rate per cycle of loading, da/dN, and the fluctuation of the stress-intensity factor, ΔK_{I}, because ΔK_{I} is a single-term parameter that incorporates the effect of changing crack-length and cyclic-load magnitude.

Incremental increase of crack length and the corresponding number of elasped load cycles can be measured under variable-amplitude random-sequence load spectra. However, unlike constant-amplitude cyclic-load data, the magnitude of ΔK_{I} changes for each cycle. Reduction of data in terms of fracture-mechanics concepts requires the establishment of a correlation parameter that incorporates the effects of crack length, cyclic-load amplitude, and cyclic-load sequence.

It is desirable to determine the magnitude of constant-amplitude cyclic-load fluctuation that results in the same a-versus-N curve obtained under variable-amplitude cyclic-load fluctuation when both spectra are applied to identical specimens (including initial crack length). In other words, the objective is to find a single stress intensity parameter, such as mean, modal, or root mean square, that can be used to define the crack-growth rate under both constant and variable-amplitude loadings. The selected parameter *must* characterize the distribution curve.

Fatigue crack-propagation behavior under variable-amplitude random-sequence stress spectra such as occur in actual bridges has been investigated as part of NCHRP Project 12-12 [*9–13*]. The tests were conducted on A514-B steel under variable-amplitude random-sequence load spectra having $P_{\mathrm{rd}}/P_{\mathrm{rm}}$ values of 0.5 and 1.0; a typical portion of the 500-cycle loading block for each is shown in Fig. 1. The data showed that the average fatigue crack-propagation rates under variable-amplitude random-sequence and ordered-sequence load fluctuation, Fig. 2, are approximately equal to the rate of fatigue-crack propagation under constant-amplitude cyclic-load fluctuation equal to the root-mean-square (rms) value of the variable-amplitude function. The root mean square is the square root of the mean of the squares of the individual load cycles in a spectrum; it is related to the modal value of the spectrum, as indicated in Fig. 3. The average fatigue crack-propagation rates, da/dN, under variable-amplitude random-load fluctuation, ordered-load fluctuation, and constant-amplitude load fluctuation were found to agree closely when da/dN was plotted as a function of the root-mean-square stress intensity factor range, ΔK_{rms}, Fig. 4. Thus, within the limits of the available experimental data, the average fatigue crack-growth rates

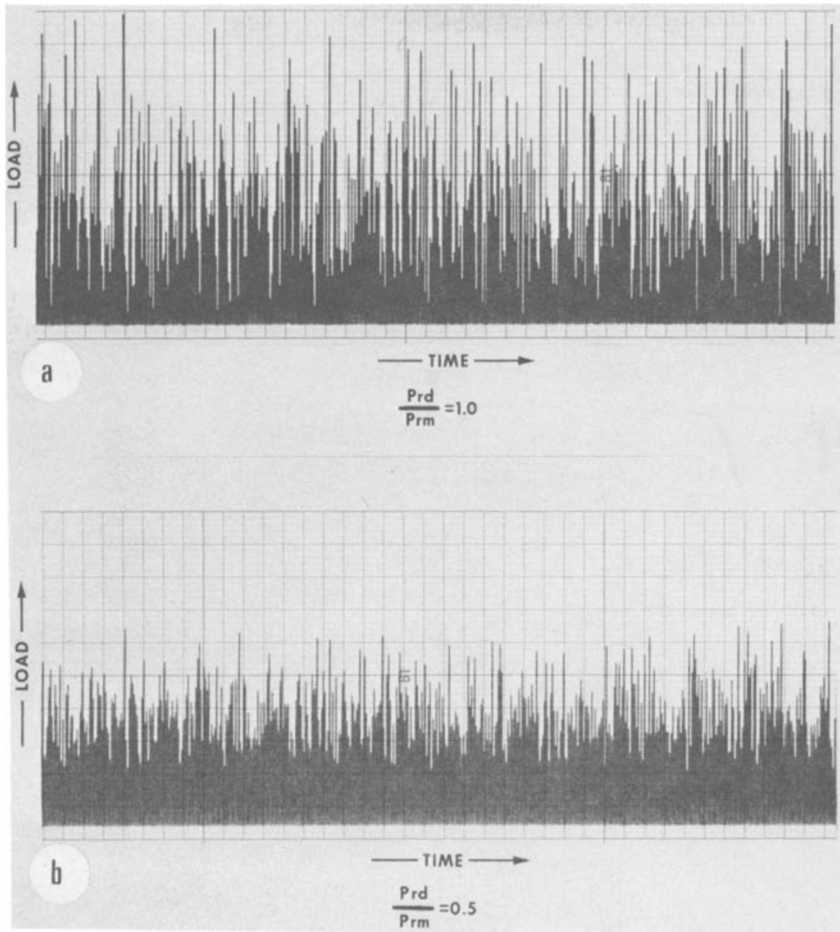

FIG. 1—*Two variable-amplitude random-sequence load fluctuations studied in this investigation: (a)* $P_{rd}/P_{rm} = 1.0$ *and (b)* $P_{rd}/P_{rm} = 0.5$.

per cycle, da/dN, under variable-amplitude stress spectra such as occur in actual bridges can be represented by the equation

$$\frac{da}{dN} = A(\Delta K_{\mathrm{rms}})^n \tag{2}$$

where A and n are material constants.

The root-mean-square value of the stress-intensity factor under constant-amplitude cyclic-load fluctuation is equal to the stress intensity factor fluctuation. Consequently, the average fatigue crack-growth rate can be predicted from constant-amplitude data by using Eq 2.

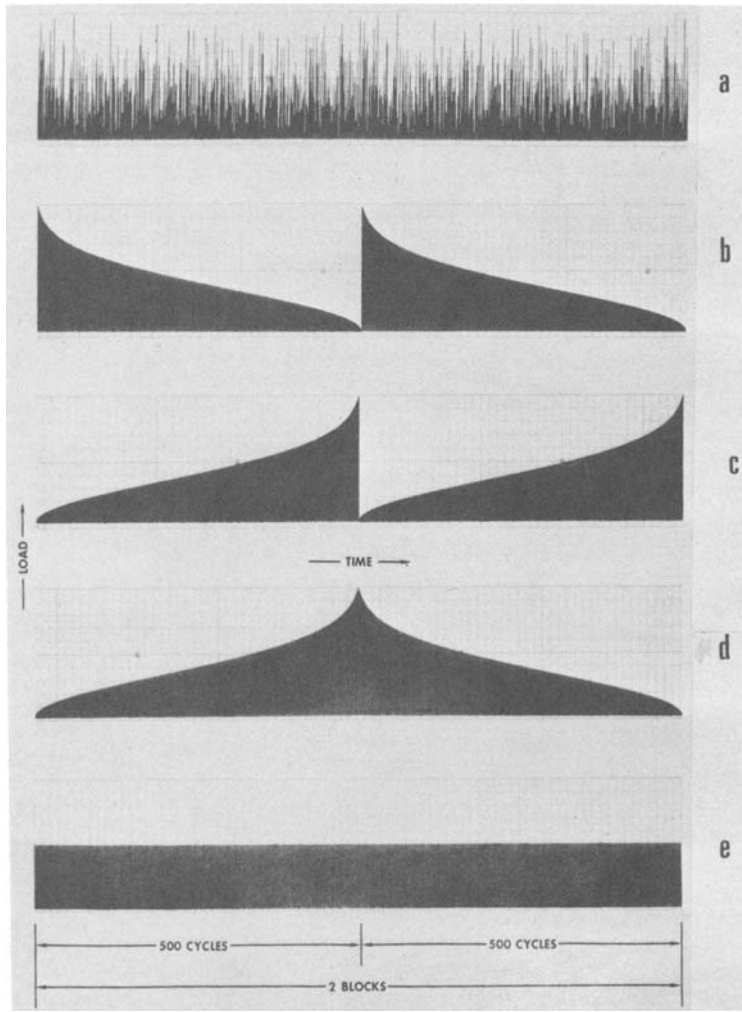

FIG. 2—*Various random-sequence and ordered-sequence load fluctuations studied in this investigation [18,19]: (a) random sequence, (b) ascending sequence, (c) descending sequence, (d) ascending-descending sequence, and (e) constant amplitude.*

Fatigue Crack Growth in Various Bridge Steels

The preceding results were obtained by testing A514-B steel. Because several investigators [4–8] have noted that changes in cyclic-load magnitude can lead to accelerated or retarded rates of fatigue crack growth, the applicability of the root-mean-square model for correlating crack-growth rates under random loading, such as occurs in actual bridges, must be established for bridge steels of various yield strengths. Consequently, the fatigue crack-growth rates under constant-amplitude and variable-amplitude random-sequence load fluctuations

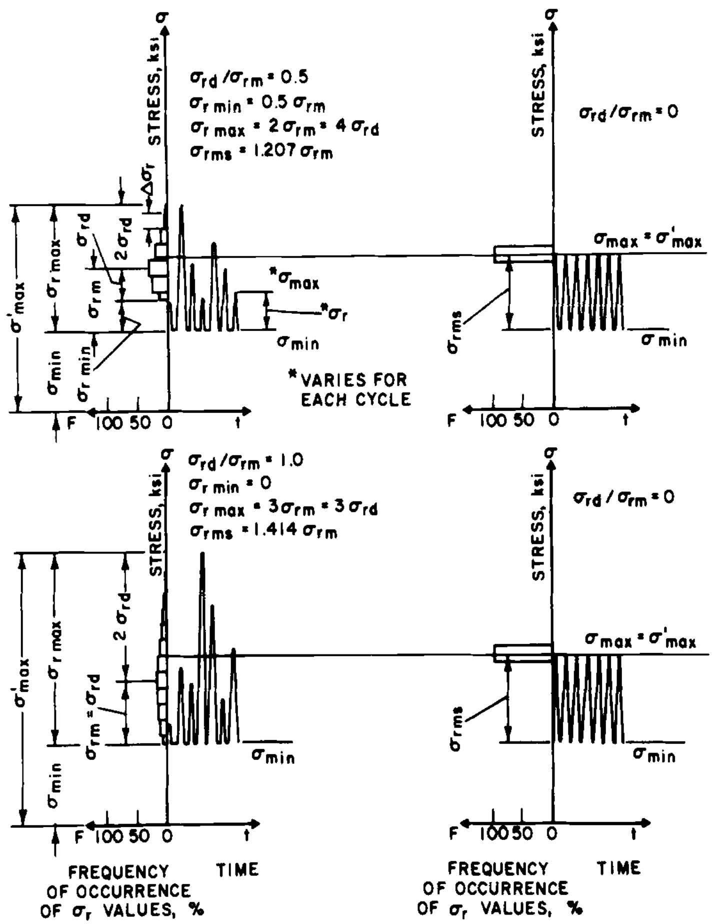

FIG. 3—*Stress spectra, constant* σ_{rms}.

were investigated in A36, A588-A, A588-B, A514-E, and A514-F steels. All loadings followed a Rayleigh distribution curve, with the ratio of the load-range deviation to the modal (peak) load (P_{rd}/P_{rm}) equal to either 0 or 1.0. Data of crack length and the corresponding number of elapsed load cycles obtained by subjecting identical specimens of A588-A steel to the variable-amplitude random-sequence load spectrum are presented in Fig. 5. Similar data were obtained for the other steels. The figure also includes data obtained under constant-amplitude cyclic-load fluctuation ($P_{rd}/P_{rm} = 0$). The load range, ΔP, for every cycle in the constant-amplitude tests was equal to ΔP_{rm}. The data show that the fatigue life under constant-amplitude cyclic-load fluctuations was longer than the life obtained under random-sequence load spectra having the same value of ΔP_{rm}. The data for each steel are represented in Figs. 6 through 10 in terms of crack-growth rate, da/dN, and the root-mean-square stress intensity factor range, ΔK_{rms}.

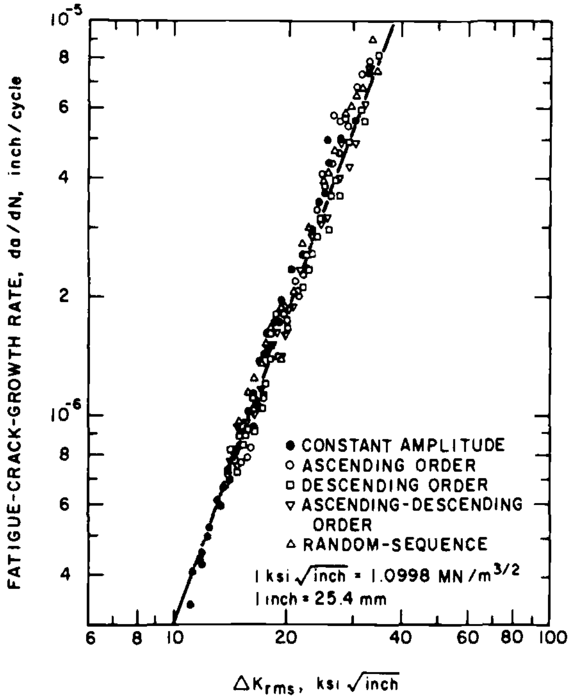

FIG. 4—*Summary of crack growth rate data under random-sequence and ordered-sequence load fluctuations for A514-B steel [18,19].*

The data presented in Figures 6 through 10 show that, within the limits of the present experimental work, the average fatigue crack-growth rates, *da/dN*, in various bridge steels subjected to variable-amplitude load spectra as occur in actual bridges can be represented by Eq 2. The root-mean-square value of the stress intensity factor range under constant-amplitude cyclic-load fluctuation is equal to the stress intensity factor range. Consequently, the average fatigue crack-growth rate under variable-amplitude load spectra as occur in actual bridges can be predicted from constant-amplitude data by using Eq 2.

Summary

The results of this phase of an investigation to study the fatigue crack-propagation behavior of various bridge steels under variable-amplitude stress spectra such as occur in actual bridges may be summarized as follows:

1. The average fatigue crack-growth rate, *da/dN*, under variable-amplitude random-sequence load spectra that can be represented by Rayleigh distribution functions can be related to various stress intensity factor ranges, ΔK, that are characteristics of the distribution function (for example, mean, root-mean, or root-mean-square ΔK).
2. The average fatigue crack-growth rates, *da/dN*, under variable-amplitude

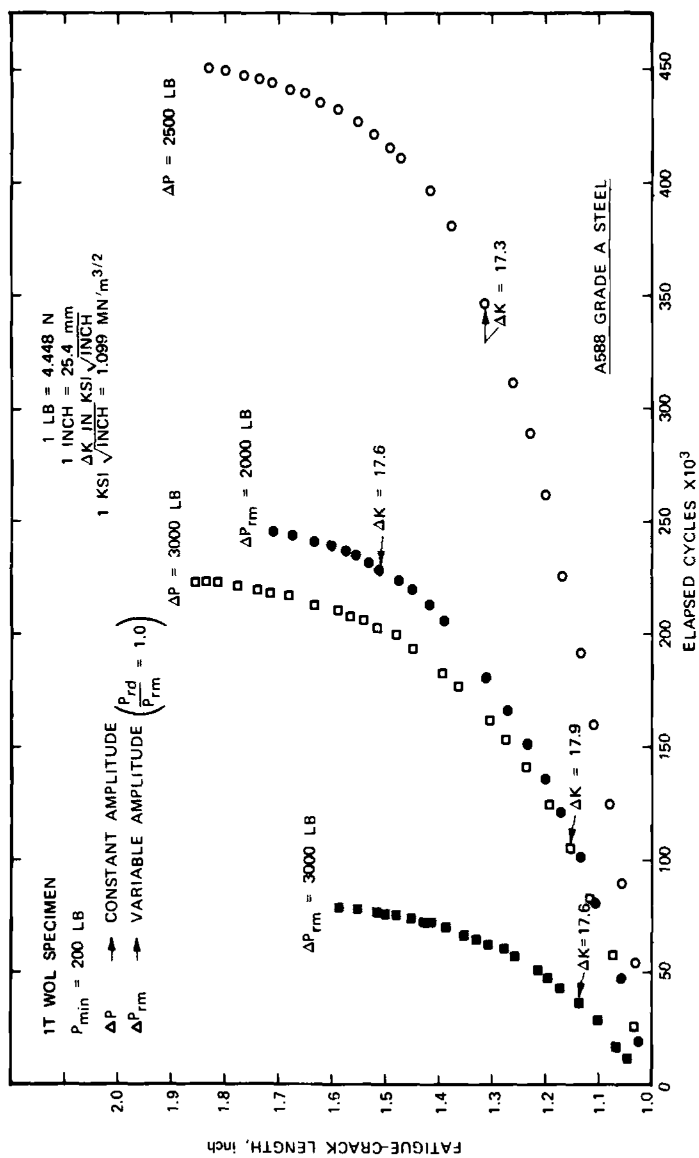

FIG. 5—*Fatigue crack growth under constant-amplitude and variable-amplitude load fluctuation for A588-A steel.*

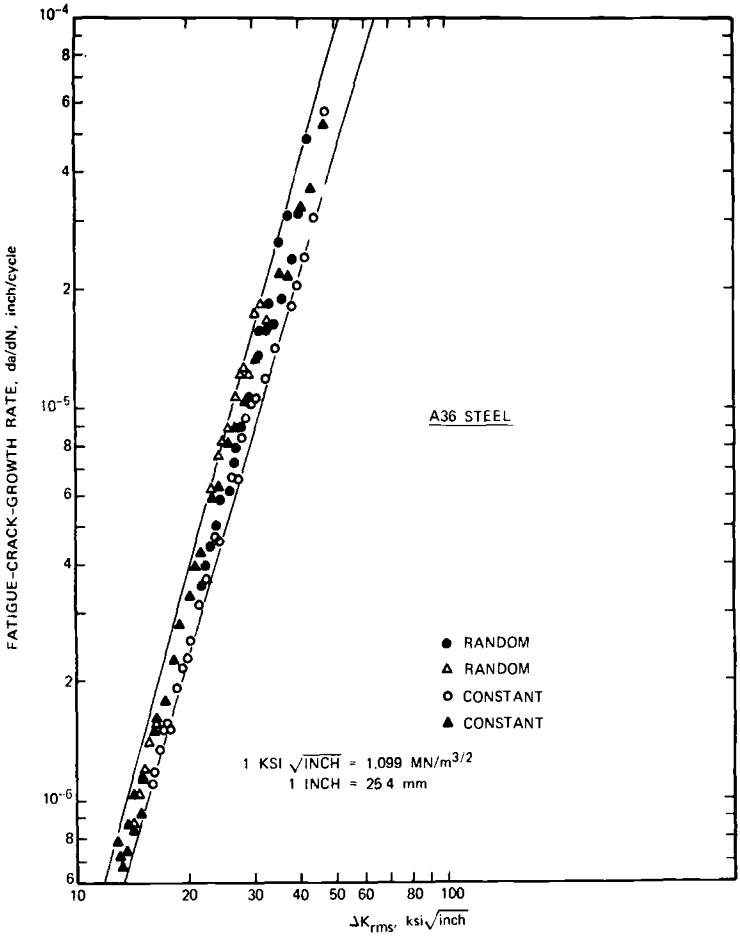

FIG. 6—*Crack growth rate as a function of the root-mean-square stress intensity factor for A36 steel.*

random-sequence load spectra such as occur in actual bridges and under constant-amplitude load fluctuations can be represented by the equation

$$\frac{da}{dN} = A(\Delta K_{\text{rms}})^n$$

where ΔK_{rms} is the root-mean-square stress intensity factor range, and A and n are constants for a given material.

3. The preceding relationship was found applicable to the following steels: A36, A588-A, A588-B, A514-B, A514-E, and A514-F.
4. The average fatigue crack-growth rates, da/dN, of the various steels studied under variable-amplitude random-sequence load fluctuations such as occur in actual bridges are equal to da/dN obtained under constant-amplitude load fluctuation when the stress intensity factor range, ΔK, under constant-

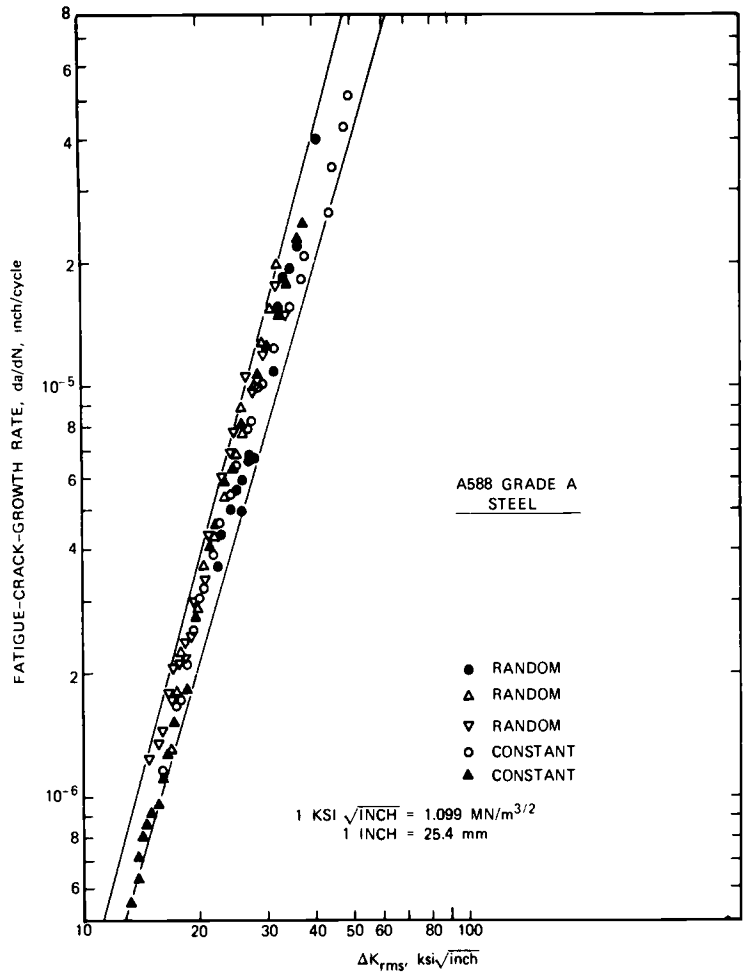

FIG. 7—*Crack growth rate as a function of the root-mean-square stress intensity factor for A588-A steel.*

amplitude load fluctuation is equal in magnitude to the ΔK_{rms} of the variable-amplitude spectra.

Acknowledgment

The author appreciates the assistance of E. J. Imhof, Jr., in developing the experimental procedure, conducting the experimental work, and analyzing and interpreting the data.

This study was conducted under National Cooperative Highway Research Program 12-14. The opinions and findings expressed or implied in this report are those of the author. They are not necessarily those of the Highway Research Board, the National Academy of Sciences, the Federal Highway Administration,

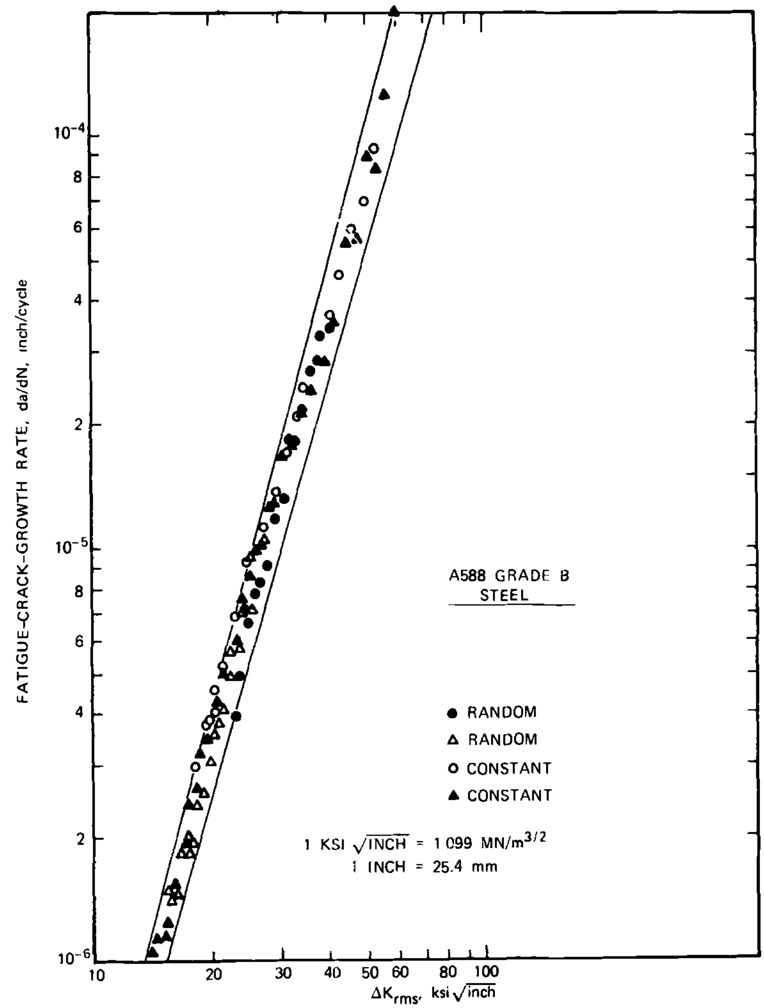

FIG. 8—*Crack growth rate as a function of the root-mean-square stress intensity factor for A588-B steel.*

the American Association of State Highway Officials, nor of the individual states participating in the National Cooperative Highway Research Program.

References

[*1*] "Collapse of U. S. 35 Highway Bridge, Point Pleasant, West Virginia, December 15, 1967," Point Pleasant Bridge, National Transportation Safety Board, Report No. NTSB-HAR-71-1, 1971.

[*2*] Barsom, J. M., *Journal of Engineering for Industry, Transactions*, ASME Series B, Vol. 93, No. 4, Nov. 1971, p. 1190.

[*3*] Paris, P. C. and Erdogan, F., *Journal of Basic Engineering, Transactions*, ASME, Series D, Vol. 85, No. 3, 1963, p. 528.

[*4*] Hardrath, H. F. and McEvily, A. T., "Engineering Aspects of Fatigue-Crack

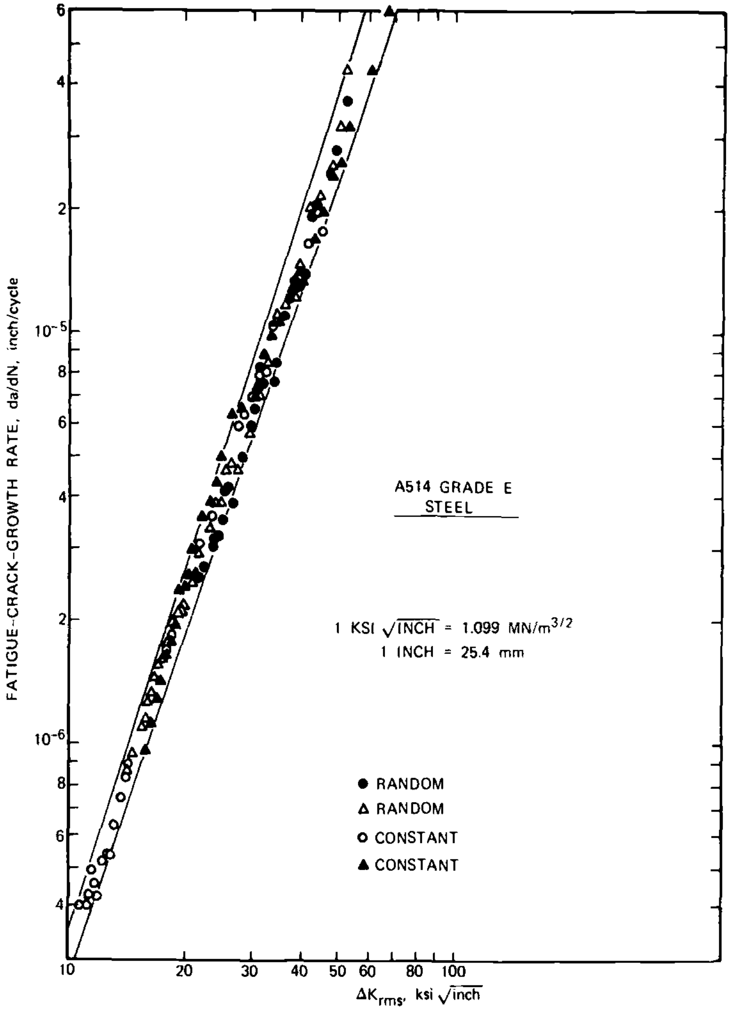

FIG. 9—*Crack growth rate as a function of the root-mean-square stress intensity factor for A514-E steel.*

Propagation," *Proceedings*, Crack Propagation Symposium, Vol. 1, Cranfield, England, Oct. 1961.

[5] Schijve, J., Jacobs, F. A., and Tromp, P. J., "Crack Propagation in Clad 2024-T3Al Under Flight Simulation Loading. Effect of Truncating High Gust Loads," National Aerospace Laboratory, NLR, The Netherlands, NLR TR-69050-U, June 1969.

[6] Hudson, C. M. and Hardrath, H. F., "Effects of Changing Stress Amplitude on the Rate of Fatigue-Crack Propagation of Two Aluminum Alloys," NASA Technical Note D-960, Sept. 1961.

[7] McMillan, J. C. and Pelloux, R. M. N. in *Fatigue Crack Propagation, ASTM STP 415*, American Society for Testing and Materials, 1967, p. 505.

[8] Wheeler, O. E., "Spectrum Loading and Crack Growth," General Dynamics Report FZM-5602, 30 June 1970.

[9] "NCHRP PROJECT 12-12: Interim Report," U. S. Steel Research Laboratory Report 76.019-001, 1 Oct. 1972.

[10] Barsom, J. M. in *Progress in Flaw Growth and Fracture Toughness Testing, ASTM STP 536*, American Society for Testing and Materials, 1973, pp. 147–167.
[11] Blake, G. T., Klippstein, K. H., and Schilling, C. G., "NCHRP PROJECT 12-12: Test Setup and Procedures for Beam and Plate-Specimen Tests," Research Laboratory Report 76.019-001(2), 30 June 1972.
[12] Klippstein, K. H. and Schilling, C. G., in this symposium.
[13] Wilson, W. K., "Review of Analysis and Development of WOL Specimen," 67-7D7-BTLPV-R1, Westinghouse Research Laboratory, 8 March 1967.

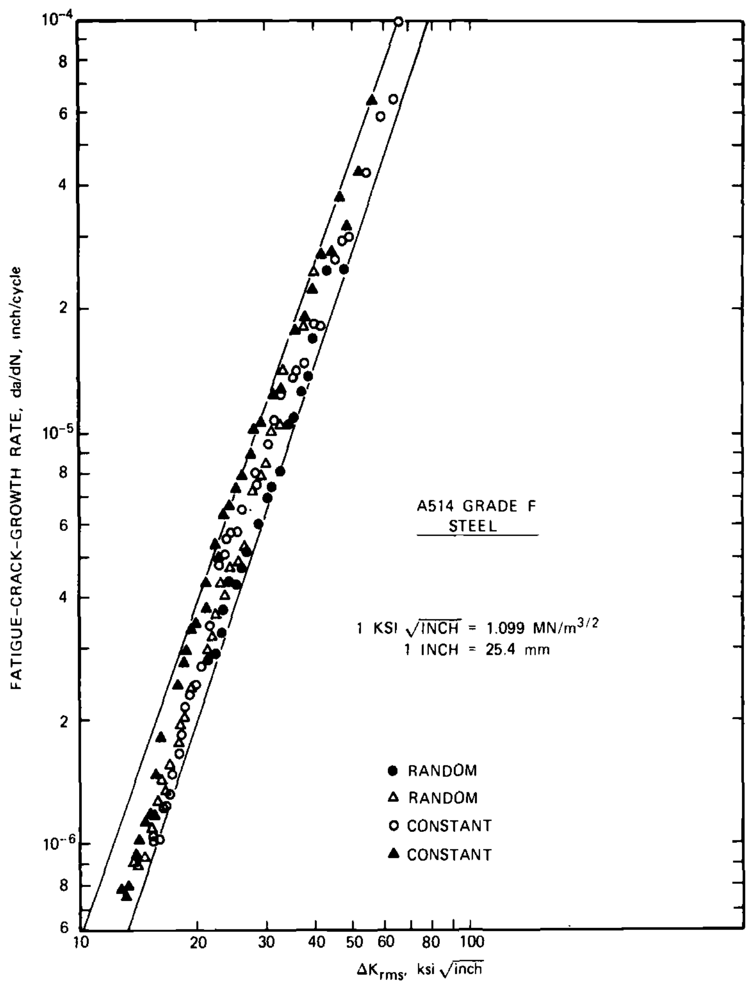

FIG. 10—*Crack growth rate as a function of the root-mean-square stress intensity factor for A514-F steel.*

DISCUSSION

R. P. Wei[1] *(written discussion)*—Dr. Barsom is to be complimented on his comprehensive and careful experimental work on fatigue crack growth under variable-amplitude loading in bridge steels. For the benefit of the unwary, I feel that one needs to emphasize the fact that the loading sequence used by Dr. Barsom is not truly *random* in the strictest sense. Although the selected load levels obtained from a Rayleigh distribution had been randomized within a given load block, this same load block was repeated *ad infinitum* in the actual experiments. As such, the actual load sequence may be viewed as being periodic in nature; the sequencing of loads within each period (block) being identical but complex. A plausible interpretation to be applied to the load sequence used by Dr. Barsom is that it represents, on average, the loading experienced by short span bridges, with each block representing the traffic load on a day-to-day or week-to-week basis.

A. J. McEvily[2] *(written discussion)*—The following expression based upon crack-opening displacement considerations has been developed to account for the contribution of fatigue and static modes to the amount of crack growth per cycle, $\Delta a/\Delta N$ [3]

$$\frac{\Delta a}{\Delta N} = \frac{A}{\sigma_{ys}E}(\Delta K^2 - \Delta K_{th}{}^2)\left(1 + \frac{\Delta K}{K_c - K_{max}}\right) \tag{3}$$

(Since $K_{max} = (\Delta K/1 - R)$, the effects of mean stress are incorporated in the expression.) Equation 3 can be modified to incorporate the effects of variable amplitude loading. Barsom [*10*] has reported on crack growth tests of an A514-B steel (yield strength 128 ksi) subjected to random loading. He found that the rate of crack growth could be expressed as

$$\frac{\Delta a}{\Delta N} = A'(\Delta K_{rms})^n \tag{4}$$

where A' and n are material constants, and ΔK_{rms} is the root-mean-square stress-intensity-factor fluctuation. It is of interest to compare predictions based upon Eq 3 with this result. Since Barsom observed that crack growth in this steel was independent of mean stress for crack growth less than 10^{-4} in. per cycle, the contribution due to static modes in Eq 3, that is, the $\Delta K/(K_c - K_{max})$ term, can be neglected. An average rate of crack growth under variable amplitude

[1] Department of Mechanical Engineering and Mechanics, Lehigh University, Bethlehem, Pa. 18015.

[2] Department of Metallurgy, School of Engineering, The University of Connecticut, Storrs, Conn. 06268.

[3] McEvily, A. J., "Phenomenological and Microstructural Aspects of Fatigue," presented at the Third International Conference on the Strength of Metals and Alloys, 1973, Cambridge, England; published by The Institute of Metals and The Iron and Steel Institutes, Publication No. 36, Vol. 2, 1974, p. 204.

loading, $(\Delta a/\Delta N)_{avg}$, can be taken to be equal to the average contribution from each of the cycles over the increment of crack growth considered, that is

$$\left(\frac{\Delta a}{\Delta N}\right)_{avg} = \frac{A}{\sigma_{ys}E} \sum_{i+N}^{i+N+\Delta N} \frac{\Delta K_i^2}{\Delta N} - \Delta K_{th}^2 \tag{5}$$

Note that the quantity $\Sigma \Delta K^2/\Delta N$ is the square of ΔK_{rms}, so that Eq 5 can be written

$$\left(\frac{\Delta a}{\Delta N}\right)_{avg} = \frac{A}{\sigma_{ys}E}(\Delta K_{rms}^2 - \Delta K_{th}^2) \tag{6}$$

Fig. 11 shows a comparison between Eq 4 and Eq 6 and the data obtained by

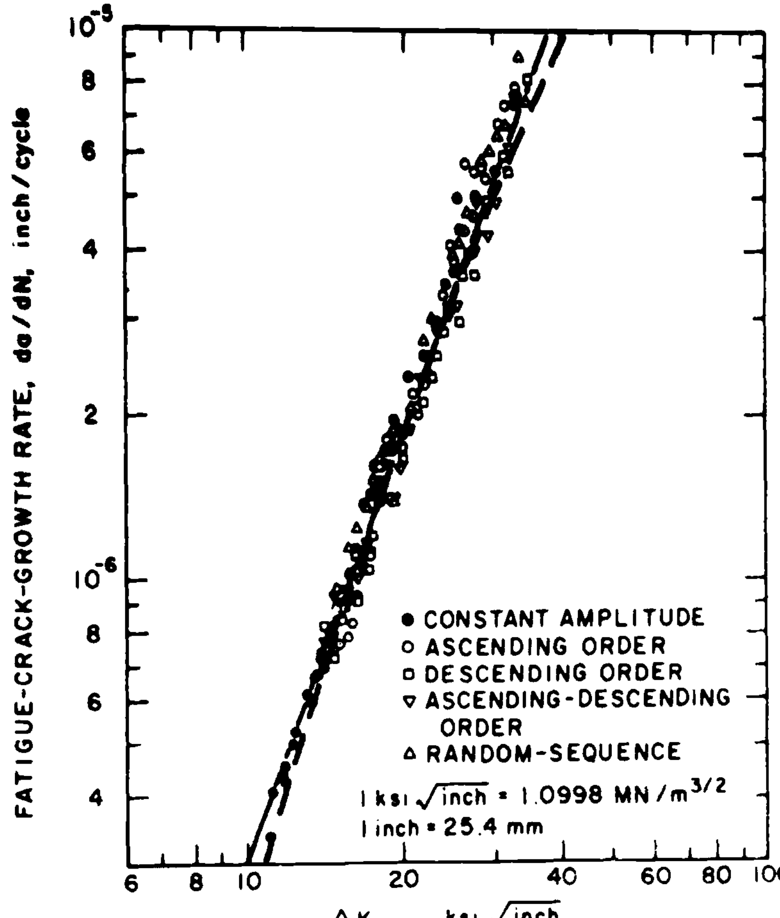

FIG. 11–*Dependence of the rate of crack growth for variable-amplitude loading on* ΔK_{rms}*: Eq 4 represented by the solid line, and Eq 6 represented by the dashed line (data from Barsom [10]).*

Barsom [10]. (In evaluating Eq 6, A was taken to be 0.023 and ΔK_{th} to be 8 ksi$\sqrt{in.}$) Agreement of both equations is quite good, however, for other more extreme types of loading the agreement may not be as good. For example, a single overload can greatly retard the rate of crack growth rate at a lower amplitude, and the preceeding equations would over-estimate the rate of crack growth. Nevertheless, for a large number of random cycles, the amplitudes of which do not fluctuate too widely, the agreement shown here indicates that reasonable predictions can be made.

J. M. Barsom (author's closure)—The author thanks Dr. McEvily for his comments concerning the applicability of the ΔK_{rms} parameter to analyze fatigue crack-growth rates under random loading and the fatigue crack growth expression that he developed using crack-opening displacement considerations. Similar expressions that are based on energy release rate or plastic zone size can also be developed. All these expressions result in a relationship between da/dN and ΔK^2. However, expressions based on energy release rate, crack opening displacement, and plastic zone size suggest that da/dN is not related to the yield strength, σ_{ys}, for the material, to σ_{ys}^{-1} and σ_{ys}^{-2}, respectively. The available fatigue crack-growth-rate data do not show any consistent dependence of growth rate on σ_{ys}. Consequently, further work is necessary to establish the correct fatigue crack-growth-rate model.

Wolf Elber[1]

Equivalent Constant-Amplitude Concept for Crack Growth Under Spectrum Loading

REFERENCE: Elber, Wolf, "Equivalent Constant-Amplitude Concept for Crack Growth Under Spectrum Loading," *Fatigue Crack Growth Under Spectrum Loads, ASTM STP 595*, American Society for Testing and Materials, 1976, pp. 236–250.

ABSTRACT: A concept based on the crack-closure phenomenon has been developed to replace random-load spectra with constant-amplitude loading in both analysis and tests. The maximum load and the crack-opening load in the constant-amplitude loading are chosen to be equal to those for the spectrum, so that both crack-growth mode and the crack length at failure are equivalent to those under the random-load spectra. The number of cycles of constant-amplitude loading is chosen so that the amount of crack growth is equal to that due to a given sequence or block of the random spectrum loading. The concept was tested experimentally after predicting the equivalent number of constant-amplitude cycles for six different random-load sequences. The agreement between predictions and test results was good.

KEY WORDS: crack propagation, fatigue (materials), analyzing, loads (forces)

To ensure the safety of aerospace structures, designers calculate the growth of possible cracks for the expected service loading conditions. The calculated crack growth is useful in determining inspection intervals, as well as in selecting materials and in establishing nominal operating stresses.

Currently available models of the crack-growth process require repetitive analyses, either cycle-by-cycle or block-by-block, of the service loading spectrum from the initial to the critical crack length. Analyses of the crack-growth process, such as those of Wheeler [*1*][2] and Willenborg et al [*2*], are usually based on plastic zone sizes which change with crack length. Even when combined with fast calculation methods such as that by Brussat [*3*], these crack-growth analyses are cumbersome.

The equivalent constant-amplitude concept developed here is based on the crack-closure phenomenon [*4*] and on results of pilot tests that showed that the crack-opening load remained essentially constant while cracks grew under repeating random-load sequences containing several thousand load peaks. When the crack-opening load is essentially constant and known, the equivalent

[1] Research engineer, NASA Langley Research Center, Hampton, Va. 23665.

[2] The italic numbers in brackets refer to the list of references appended to this paper.

constant-amplitude concept replaces the random loads with constant-amplitude loads in crack-growth calculations.

The concept hinges on the determination of the crack-opening load. To obtain a design method based on this concept will require empirical or analytical methods of predicting the crack-opening load for a particular load spectrum. Newman [5] has developed a numerical analysis to calculate the crack-opening load; however, at the moment such an analysis is more complex than desired for design use. Also, empirical rules for determining the crack-opening loads for an arbitrary spectrum do not exist.

The search for an equivalent constant-amplitude test to replace the random-load test is not new. Barsom [6] showed that for some random-load distributions the rate of crack growth was generally equivalent to the rate of crack growth under a constant-amplitude test with the same minimum load and an amplitude representing the root-mean-square amplitude of the random test. However, Barsom's approach did not attempt to obtain equivalent failure crack lengths or equivalent crack-growth modes.

In this report an equation of crack-growth equivalence was developed, and the validity of the concept was tested experimentally on six different random-load sequences. In the tests the crack-opening loads were measured in crack-growth tests run with both the random sequences and their predicted equivalent constant-amplitude sequences. To check the predicted number of equivalent constant-amplitude cycles, the number of random-loading sequences required to cause failure was compared to the number of equivalent constant-amplitude cycles required to cause failure.

Analysis

The Crack-Growth Law

The crack-growth law proposed by Elber [4], and experimentally verified under constant amplitude and some two-level variable amplitude loadings, states that the crack-growth rate is a power function of the effective stress intensity range only, that is,

$$\frac{da}{dN} = A\,(\Delta K_{\mathrm{eff}})^n \tag{1}$$

where the effective stress intensity range, ΔK_{eff}, is measured relative to the load at which the crack fully opens.

The Equivalent Constant-Amplitude Concept

The equivalent constant-amplitude concept was developed to replace a repeating random-load sequence containing several thousand load excursions by a shorter constant-amplitude sequence. Random-load sequence, in this context, represents a fixed number of load excursions whose distribution is known. The constant-amplitude sequence which replaces this random-load sequence is selected so that the total crack growth, the crack-growth mode, and the critical crack length are equivalent for the two loading sequences. To achieve this, the maximum gross section stress for the equivalent constant-amplitude sequence was chosen to be the same as the largest maximum stress in the random sequence. Therefore, the crack length at failure under the constant-amplitude loading represents the shortest possible failure crack length under the random-load sequence. Also, the minimum stress for the equivalent constant-amplitude sequence was chosen so that the crack-opening stress for that sequence is the same as the crack-opening stress in the random sequence. This produces equivalent maximum effective stress intensity ranges and, hence, the plastic zone envelopes are essentially equal for the two loading conditions. Also, this choice simplifies the equation of equivalence developed later. Last, the number of cycles in the equivalent constant-amplitude sequence was chosen so that the crack growth caused by those cycles is the same as the crack growth caused by the random-load sequence. This equivalent number of cycles, N_{eq}, was determined as follows.

If S_i is the maximum and $\widetilde{S}_i$ is the minimum stress in the ith excursion of the random sequence, S_{op} is the crack-opening stress, $\hat{S}_i$ is the effective minimum stress, and a is the crack length. Then from Eq 1, the growth increment due to the ith load excursion is

$$\delta_a = A(S_i - \hat{S}_i)^n (\sqrt{\pi a}\phi)^n \tag{2}$$

where

$$\hat{S}_i = \left\{ \begin{matrix} S_{op}, \widetilde{S}_i \leq S_{op} \\ \\ \widetilde{S}_i, \widetilde{S}_i > S_{op} \end{matrix} \right\} \tag{3}$$

If S_{max} is the highest maximum stress in the random sequence, then this growth increment, δ_a, can also be expressed as a fraction λ_i of the growth caused by one cycle of the equivalent constant-amplitude loading

$$\delta_a = \lambda_i A(S_{max} - S_{op})^n (\sqrt{\pi a}\,\phi)^n \tag{4}$$

Equating Eqs 2 and 4, yields the equation of equivalence

$$A(S_i - \hat{S}_i)^n (\sqrt{\pi a}\,\phi)^n = \lambda_i A(S_{max} - S_{op})^n (\sqrt{\pi a}\,\phi)^n \tag{5}$$

which, when solved for λ_i and then summed over all excursions in the random load sequence, simplifies to

$$N_{eq} = \sum \lambda_i = \sum \frac{(S_i - \hat{S}_i)^n}{(S_{max} - S_{op})^n} \tag{6}$$

With the crack-opening ratio, α, defined by

$$\alpha = \frac{S_{op} - S_B}{S_{max} - S_B} \tag{7}$$

S_{op} was expressed in terms of the highest maximum stress S_{max} and the lowest minimum stress S_B as

$$S_{op} = S_B + \alpha(S_{max} - S_B)$$

Then the final form of the equation of equivalence becomes

$$N_{eq} = \sum \frac{(S_i - \hat{S}_i)^n}{(1 - \alpha)^n (S_{max} - S_B)^n} \tag{8}$$

Equation 8 can be evaluated from the distribution of loads in the random sequence. The resulting relationship between N_{eq}, α, and n is a unique relationship for the particular spectrum. When the concept is applied, and a particular value of N_{eq} is obtained, that value depends on the crack-opening stress and the materials' crack-growth exponent, n. Differences in configuration and environment affect the crack-opening stress and, therefore, through α, will affect N_{eq}.

The relationship among N_{eq}, α, and n was obtained for the two spectrum shapes in this test series. The necessary steps are explained in the next section.

Spectrum Analysis

A pseudorandom noise generator was used to produce a continuous analog signal which is identically repeated after a given sequence length. Changes in the shape of this spectrum were made using a variable nonlinear amplifier in the output stage of the noise generator. Two spectra were selected. The main stress parameters are defined in Fig. 1. To calculate the equivalent number of cycles for these spectra from Eq 8, the distribution of stress excursions $(S_i - \tilde{S}_i)$ and the corresponding relative maxima $(S_i - S_B)$ was evaluated for the load spectrum. For simplicity of analysis and data presentation, the spectrum load

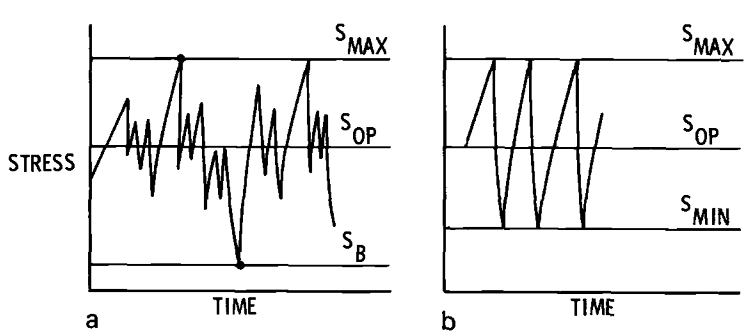

FIG. 1—*Definition of stress parameters: (a) spectrum load sequence, and (b) equivalent constant amplitude.*

excursions were sorted into a two-dimensional matrix of normalized stress excursions $(S_i - \tilde{S}_i)/(S_{max} - S_B)$ and normalized relative maxima $(S_i - S_B)/(S_{max} - S_B)$. The spectrum range $(S_{max} - S_B)$ was subdivded into approximately 20 intervals. The number of occurrences in each interval was then tabulated in the matrix.

The data from Spectra I and II are tabulated in Figs. 2 and 3, respectively. Using the values from these tables, Eq 8 was evaluated for each spectrum for a range of α, $(0 \leq \alpha \leq 1)$, and for a representative range of n, $(2.5 \leq n \leq 4)$. The resulting relationships between the equivalent number of cycles, N_{eq}, and the parameters n and α are plotted for Spectra I and II in Figs. 4 and 5, respectively.

Testing

Specimens and Material

Sheet specimens (100-mm wide, 3.29-mm thick) with 2.5-mm-long central notches were tested. The test section configuration is shown in Fig. 6. The specimens were made of 7075-T6 aluminum alloy, having a nominal tensile strength of 595 MPa, and a 0.2-percent offset yield strength of 540 MPa.

Testing Equipment

Both spectrum load tests and constant-amplitude tests were conducted in a 100-KN servo-hydraulic testing machine. The mean cyclic frequency for the

$\frac{S_i - S_{min}}{S_{max} - S_{min}}$ / $\frac{S_i - \tilde{S}_i}{S_{max} - S_{min}}$	0.00 - 0.05	0.05 - 0.09	0.09 - 0.14	0.14 - 0.18	0.18 - 0.23	0.23 - 0.27	0.27 - 0.32	0.32 - 0.36	0.36 - 0.41	0.41 - 0.45	0.45 - 0.50	0.50 - 0.55	0.55 - 0.59	0.59 - 0.64	0.64 - 0.68	0.68 - 0.73	0.73 - 0.77	0.77 - 0.82	0.82-- 0.86	0.86 - 0.91	0.91 - 0.95	0.95 - 1.00
0.00 - 0.05	2	0	0	0	0	0	0	0	0	0	0	0	0	0	0	0	0	0	0	0	0	0
0.05 - 0.09	0	4	0	0	0	0	0	0	0	0	0	0	0	0	0	0	0	0	0	0	0	0
0.09 - 0.14	15	5	8	0	0	0	0	0	0	0	0	0	0	0	0	0	0	0	0	0	0	0
0.14 - 0.18	58	50	22	10	0	0	0	0	0	0	0	0	0	0	0	0	0	0	0	0	0	0
0.18 - 0.23	158	168	126	68	15	0	0	0	0	0	0	0	0	0	0	0	0	0	0	0	0	0
0.23 - 0.27	150	228	242	201	99	8	0	0	0	0	0	0	0	0	0	0	0	0	0	0	0	0
0.27 - 0.32	44	105	158	197	167	74	2	0	0	0	0	0	0	0	0	0	0	0	0	0	0	0
0.32 - 0.36	2	11	25	36	37	40	15	1	0	0	0	0	0	0	0	0	0	0	0	0	0	0
0.36 - 0.41	0	4	2	18	19	28	30	7	2	0	0	0	0	0	0	0	0	0	0	0	0	0
0.41 - 0.45	0	0	1	4	12	18	32	19	5	1	0	0	0	0	0	0	0	0	0	0	0	0
0.45 - 0.50	0	0	0	0	4	4	13	13	12	4	0	0	0	0	0	0	0	0	0	0	0	0
0.50 - 0.55	0	0	0	0	0	1	1	3	1	7	3	1	0	0	0	0	0	0	0	0	0	0
0.55 - 0.59	0	0	0	0	0	0	2	0	4	4	4	1	0	0	0	0	0	0	0	0	0	0
0.59 -0.64	0	0	0	0	0	0	0	0	0	1	4	4	2	0	0	0	0	0	0	0	0	0
0.64 - 0.68	0	0	0	0	0	0	0	0	0	0	3	4	2	0	0	0	0	0	0	0	0	0
0.68 - 0.73	0	0	0	0	0	0	0	0	0	0	1	1	1	2	2	0	0	0	0	0	0	0
0.73 - 0.77	0	0	0	0	0	0	0	0	0	0	0	1	3	0	1	0	0	0	0	0	0	0
0.77 - 0.82	0	0	0	0	0	0	0	0	0	0	0	0	0	0	0	2	0	0	0	0	0	0
0.82 - 0.86	0	0	0	0	0	0	0	0	0	0	0	0	1	0	0	1	1	0	0	0	0	0
0.86 - 0.91	0	0	0	0	0	0	0	0	0	0	0	0	0	0	0	0	2	0	0	0	0	0
0.91 - 0.95	0	0	0	0	0	0	0	0	0	0	0	0	0	0	0	0	0	0	0	0	0	0
0.95 - 1.00	0	0	0	0	0	0	0	0	0	0	0	0	0	0	0	0	2	0	0	0	0	0
	0	0	0	0	0	0	0	0	0	0	0	0	0	0	0	0	0	0	0	0	0	0

FIG. 2–*Data from Spectrum I.*

$\frac{S_i - S_{min}}{S_{max} - S_{min}}$ \ $\frac{S_i - \bar{S}_i}{S_{max} - S_{min}}$	0.00 - 0.05	0.05 - 0.11	0.11 - 0.16	0.16 - 0.21	0.21 - 0.26	0.26 - 0.32	0.32 - 0.37	0.37 - 0.42	0.42 - 0.47	0.47 - 0.53	0.53 - 0.58	0.58 - 0.63	0.63 - 0.68	0.68 - 0.74	0.74 - 0.79	0.79 - 0.84	0.84 - 0.89	0.89 - 0.95	0.95 - 1.00
0.00 - 0.05	0	0	0	0	0	0	0	0	0	0	0	0	0	0	0	0	0	0	0
0.05 - 0.11	0	0	0	0	0	0	0	0	0	0	0	0	0	0	0	0	0	0	0
0.11 - 0.16	0	0	0	0	0	0	0	0	0	0	0	0	0	0	0	0	0	0	0
0.16 - 0.21	0	0	0	0	0	0	0	0	0	0	0	0	0	0	0	0	0	0	0
0.21 - 0.26	0	1	0	0	1	0	0	0	0	0	0	0	0	0	0	0	0	0	0
0.26 - 0.32	0	2	2	0	0	0	0	0	0	0	0	0	0	0	0	0	0	0	0
0.32 - 0.37	3	0	4	1	0	0	0	0	0	0	0	0	0	0	0	0	0	0	0
0.37 - 0.42	26	11	6	6	0	0	0	0	0	0	0	0	0	0	0	0	0	0	0
0.42 - 0.47	84	76	39	28	8	0	0	0	0	0	0	0	0	0	0	0	0	0	0
0.47 - 0.53	120	163	151	99	52	11	0	0	0	0	0	0	0	0	0	0	0	0	0
0.53 - 0.58	92	147	182	186	115	69	10	0	0	0	0	0	0	0	0	0	0	0	0
0.58 - 0.63	24	69	98	131	177	119	47	3	0	0	0	0	0	0	0	0	0	0	0
0.63 - 0.68	4	14	41	52	60	85	67	19	4	0	0	0	0	0	0	0	0	0	0
0.68 - 0.74	0	3	6	8	15	25	27	22	9	1	0	0	0	0	0	0	0	0	0
0.74 - 0.79	0	0	0	0	0	4	4	4	3	0	0	0	0	0	0	0	0	0	0
0.79 - 0.84	0	0	0	0	0	1	4	0	1	4	0	0	0	0	0	0	0	0	0
0.84 - 0.89	0	0	0	0	0	0	0	0	0	0	2	0	0	0	0	0	0	0	0
0.89 - 0.95	0	0	0	0	0	1	0	0	0	2	2	0	0	0	0	0	0	0	0
0.95 - 1.00	0	0	0	0	0	0	0	0	0	2	0	0	0	0	0	0	0	0	0

FIG. 3—*Data from Spectrum II.*

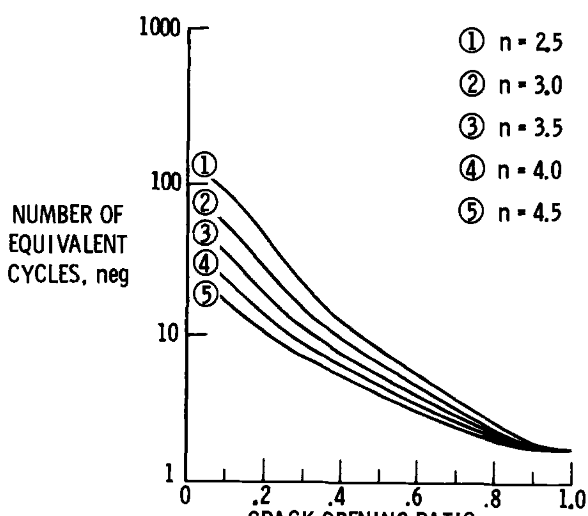

FIG. 4—*Equivalent cycles function for Spectrum I.*

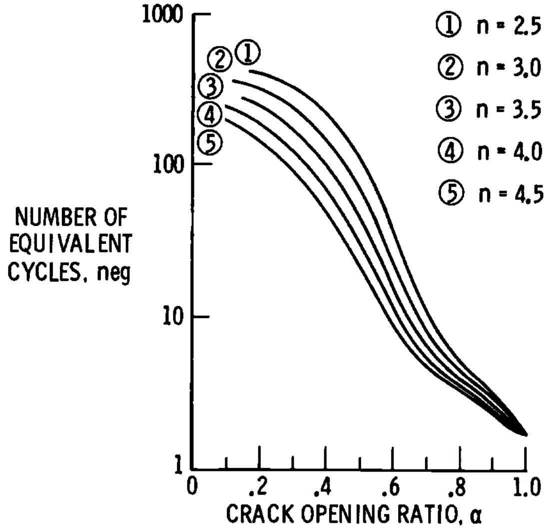

FIG. 5—*Equivalent cycles function for Spectrum II.*

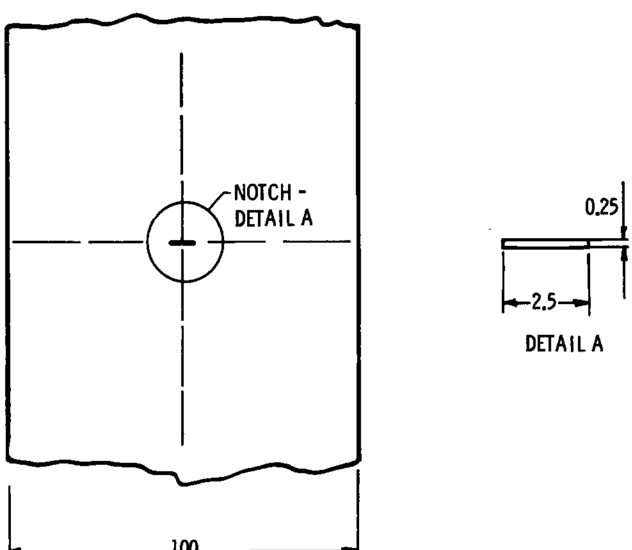

FIG. 6—*Specimen test section configuration.*

spectrum load tests was 5 Hz. The cyclic frequency for the constant-amplitude load tests was 1 Hz. Load tracking accuracy at those frequencies was within 1 percent.

Crack-Closure Measurements

The crack closure and opening behavior of all specimens was continuously measured with a crack-opening displacement (COD) gage [*4*]. The COD-gage output and the testing-machine load-cell output were analyzed to determine the stresses at which the cracks opened fully. The compliance method of Ref *4* was used for that analysis.

Spectrum Loading

Load Spectra I and II were applied as tensile loads to three specimens each at selected values of minimum stress level S_B, and spectrum range $S_{max} - S_B$. The matrix of test parameters is shown in Table 1.

TABLE 1 – *Test matrix for spectrum load tests.*

Specimen Number	Spectrum	S_{Bn}, MPa	$S_{max} - S_B$, MPa	S_{max}, MPa
1	I	20	180	200
2	I	10	90	100
3	I	50	100	150
4	II	20	180	200
5	II	10	90	100
6	II	50	100	150

Constant-Amplitude Loading

The equivalent constant-amplitude stresses were determined analytically from the measured values of the stabilized average crack-opening stresses in each of the six spectrum tests. Because of lack of data for 7075-T6, the crack-closure behavior was taken from the published results for 2024-T3 [*4*], where

$$U = \frac{S_{max} - S_{op}}{S_{max} - S_{min}} = 0.5 + 0.4R \text{ for } R > 0$$

from which S_{min}, the minimum constant-amplitude stress, was determined as

$$S_{min} = 1{\cdot}25 \left\{ \sqrt{1{\cdot}6\, S_{max}\, S_{op} - 0{\cdot}79\, S_{max}^2} - 0{\cdot}1\, S_{max} \right\} \tag{9}$$

The resulting test matrix for the constant-amplitude tests is tabulated in Table 2, where Specimen 7 is the constant-amplitude specimen corresponding to Specimen 1, as indicated in the first column.

Results and Discussion

Spectrum Load Tests

The equivalent constant-amplitude concept was based on the assumption that crack-opening stresses remain essentially constant during short (several thousand load peaks) random-load sequences. Figure 7 shows the relationship between

TABLE 2 – *Test matrix for constant-amplitude tests.*

Specimen Number	S_{max}, MPa	S_{op},[a] MPa	R
7, 1	200	104	0.13
8, 2	100	53	0.18
9, 3	150	87	0.34
10, 4	200	102	0.07
11, 5	100	56	0.28
12, 6	150	89	0.37

[a] Measured values from spectrum tests.

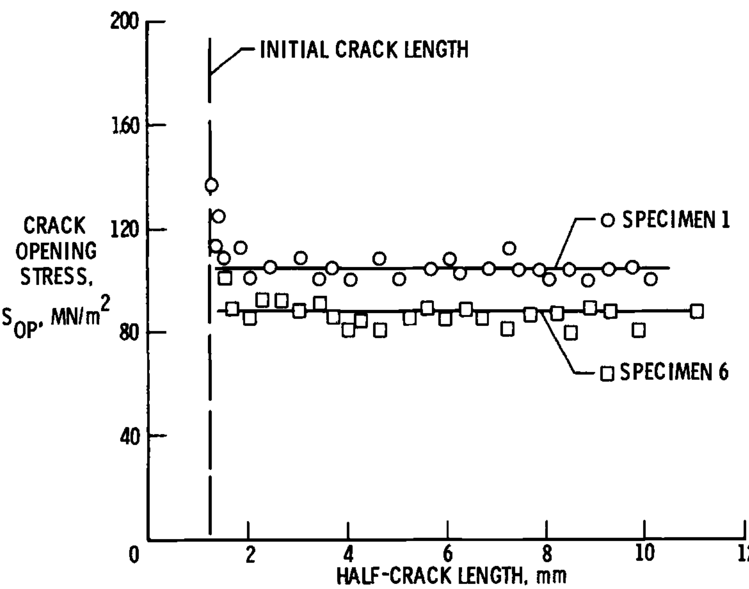

FIG. 7–*Crack-opening stress as a function of crack length for Specimens 1 and 6.*

crack length and crack-opening stress for two typical specimens from the test series. Specimen 1 was tested under Spectrum I with a minimum stress of approximately zero. Specimen 6 was tested under Spectrum II with a minimum stress of one third of the maximum. For both specimens, the crack-opening stresses were above the stabilized average just after initiation, and then stabilized to a constant value for the remainder of the test. This initiation effect has also been observed in surface crack growth in titanium alloy. The stabilized average crack-opening stresses and the number of sequences to failure are given in Table 3.

TABLE 3 – *Crack-opening stresses and number of sequences to failure* N_s *for spectrum tests.*

Specimen Number	S_{op}, MPa	N_s
1	104	372
2	53	3400
3	87	930
4	102	26
5	56	640
6	89	68

Constant-Amplitude Tests

The stresses for the equivalent constant-amplitude tests were calculated from the measured crack-opening stresses and Eq 9. The cyclic stress ratios and crack-opening loads are tabulated in Table 2. The values of crack-opening ratio α are obtained from Eq 7. Values for the equivalent number of cycles, N_{eq}, were obtained from Figs. 4 and 5 for these values of α, and the material's crack-growth exponent $n = 2 \cdot 7$ [7]. These values are tabulated in Table 4.

TABLE 4 – *Equivalent constant-amplitude parameters.*

Specimen Number	S_{max}, MPa	Desired S_{op}, MPa	R	α	N_{eq}
1, 7	200	104	0.13	0.465	8.1
2, 8	100	53	0.18	0.48	7.8
3, 9	150	87	0.34	0.37	12.9
4, 10	200	102	0.07	0.45	126
5, 11	100	56	0.28	0.51	83
6, 12	150	89	0.37	0.39	191

Results from the constant-amplitude tests consist of the stabilized average crack-opening stresses and the number of cycles to failure, N_{ca}. The values are given in Table 5. The measured crack-opening stresses were in good agreement with the opening stresses in Table 4, based on the 2024-T3 aluminum data. Failure crack lengths and failure modes of corresponding specimens were compared. Failure crack lengths were generally equivalent, except for the short-lived Specimens 10 and 4. The change of crack-growth mode from normal

TABLE 5 – *Measured results from constant-amplitude tests.*

Specimen Number	Measured S_{op}, MPa	N_{ca}
7	105	3 240
8	56	32 200
9	84	13 200
10	104	2 800
11	53	41 300
12	86	14 300

to slant mode generally occurred at equal crack lengths. In all cases, the fracture surfaces from the spectrum tests showed more discoloration due to corrosion or fretting than the corresponding constant-amplitude specimens.

Comparison of Results

The number of constant-amplitude cycles to failure, N_{ca}, was divided by the equivalent number of cycles, N_{eq}, for each test and compared with the number of spectrum sequences to failure, N_s. The results are shown in Table 6.

TABLE 6 – *Comparison of results.*

Specimen Numbers	N_{ca}, cycles	N_{eq}, cycles/ sequence	$\frac{N_{ca}}{N_{eq}}$	N_s, sequences	$\frac{N_{ca}}{N_{eq} \times N_s}$
1, 7	3 240	8.1	400	372	1.08
2, 8	32 200	7.8	4100	3400	1.21
3, 9	13 200	12.9	1020	930	1.10
4, 10	2 800	126	22	26	0.85
5, 11	41 300	83	500	640	0.78
6, 12	14 300	191	75	68	1.10

The ratio $N_{ca}/(N_{eq} \times N_s)$ ranges from 0 · 78 to 1 · 21, a range that is no greater than scatter that might be expected in fatigue crack-growth data. The results show no systematic differences between the test results and the predicted number of equivalent cycles, and that the crack-closure-based crack-growth law and the equation of crack-growth-equivalence gave valid predictions for these tests.

Concluding Remarks

To simplify crack-growth calculations, a concept has been developed for replacing relatively complex random-load tests and analyses with simpler constant-amplitude tests and analyses. An equation of crack-growth-equivalence resulting from derivations based on the crack-closure crack-growth law was obtained and was used to determine a relationship between an equivalent number of cycles of constant-amplitude loading (producing the same amount of crack growth as a fixed sequence of the random-load spectrum) and the distribution of the random loads, the exponent in the crack-growth law, and the ratio of the crack-opening load to the maximum load. That relationship, which is independent of crack length and stress level, is unique for a given spectrum.

The concept was tested experimentally for six different spectrum loadings and the six corresponding equivalent constant-amplitude loadings. Good agreement was obtained between the experimental results and the predictions.

References

[1] Wheeler, O. E., *Journal of Basic Engineering*, Vol. 94, March 1972, pp. 181–186.

[2] Willenborg, T., Engle, R. M., and Wood, H. A., "A Crack Growth Retardation Model Using an Effective Stress Concept," AFFDL Tech. Memo 71-1-FBR, Air Force Flight Dynamics Laboratory, Wright-Patterson AFB, Ohio, Jan. 1971.

[3] Brussat, T. R. in *Fracture Toughness and Slow-Stable Cracking, ASTM STP 559*, American Society for Testing and Materials, 1974, pp. 298–311.

[4] Elber, Wolf in *Damage Tolerance in Aircraft Structures, ASTM STP 486*, American Society for Testing and Materials, 1971, pp. 230–242.

[5] Newman, J. C., "A Finite-Element Analysis of Fatigue Crack Closure," presented at the Eighth National Symposium on Fracture Mechanics, Providence, R. I., 26–28 Aug. 1974; also NASA TM X-72005.

[6] Barsom, J. M. in *Progress in Flaw Growth and Fracture Toughness Testing, ASTM STP 536*, American Society for Testing and Materials, 1973, pp. 147–167.

[7] Hudson, C. M., and Newman, J. C., Jr., "Effect of Specimen Thickness on Fatigue-Crack-Growth Behavior and Fracture Toughness of 7075-T6 and 7178-T6 Aluminum Alloys," NASA TN D-7173, National Aeronautics and Space Administration, 1973.

DISCUSSION

C. E. Richards[1] *(written discussion)*—I would like to ask where the compliance measurements were taken and what differences, if any, may have been encountered if compliance measurements are taken from different faces or regions of test pieces.

In our experience,[2] we would expect, for example, compliance measurements obtained from the sides of single edge notched specimens (that is, the two

[1] Materials Division, Central Electricity Research Labs., Leatherhead, Surrey, England.

[2] Lindley, T. C. and Richards, C. E., 3rd International Conference on Fracture, Munich, 1973.

parallel surfaces intersecting the fatigue crack and perpendicular to the crack front) to be different from those obtained from, say, the front face (that is, the surface from which the starter notches are machined). I would appreciate any information you have on this.

Wolf Elber (author's closure)—In our tests on center-cracked thin sheet specimens, the compliance measurements are taken on the surface just ahead of the crack tip. The nonlinearity of the compliance curve is, indeed, a function of gage location. Our gage location maximizes the curvature just as the crack becomes fully open.

J. Schijve[3] *(written discussion)*—The original papers of Dr. Elber should be considered as a mile-stone in the development of the theory of fatigue crack propagation. His crack-closure model has significantly contributed to the understanding of variable-amplitude loading. The present paper is also promising for predicting crack growth under spectrum loading. The measurements of the crack opening stress during spectrum tests are of great interest. During the meeting he indicated that spectra should be classified into either "short" spectra or "long" spectra. It would be helpful if the meaning of these concepts could be defined in some more detail. In this respect it would also be appreciated if the number of cycles of the two spectra adopted in his tests could be indicated (that is, the recurrence period). Were both spectra symmetric with respect to positive and negative stress ranges?

The equivalent N approach apparently avoids a cycle-by-cycle calculation. However, a prediction on the same basic assumptions on crack closure could also be made by employing

$$\Sigma(\delta_a)_i = A\ \Sigma(\Delta K_{\text{eff}})_i^n$$

Would the result have been essentially the same?

Wolf Elber (author's closure)—The terms "short" spectra and "long" spectra can only be given relative and approximate definitions. I consider a spectrum "short," if the crack growth during one repeat interval is less than the plastic zone size created by the highest load in the spectrum. In this case, the fluctuations in crack-opening load are usually very small and the spectrum shows very little sequence effect. By corollary, a "long" spectrum is associated with crack growth larger than the maximum plastic zone size and can show significant sequence effects.

The spectra in my tests contained about 5000 cycles. They were assymetrical. The precise form can be derived from the tables of load maxima and associated load ranges.

Your summation equation indeed is the prime condition for my derivation, so the result would be identical.

R. I. Stephens[4] *(written discussion)*—The previous paper by Barsom and your

[3] Department of Aeronautical Engineering, Delft University of Technology, Delft, Netherlands.

[4] Materials Engineering Div., The University of Iowa, Iowa City, Iowa 52242.

own paper indicated that constant-amplitude fatigue crack growth behavior can predict crack growth rules and life in some complex loading histories. This implies sequence effects are not of primary concern in these spectra. Would the author include his presented explanation of this situation in the discussion?

Wolf Elber (author's closure)—There may indeed be a large group of spectra that encompass the majority of industrial applications, which could be considered "short" spectra. Sequence effects for those spectra would then be at worst secondary effects.

T. R. Brussat[5] *(written discussion)*—Progress in understanding and predicting crack growth under spectrum loading has been impeded by a general hesitation to identify and separate the important and less important features of a loading history and to appropriately simplify the history to a manageable form. This paper has succeeded in demonstrating how three primary features of a random spectrum loading history can be preserved in the equivalent constant-amplitude loading history.

The author correctly limits his approach to "short" spectrum loading histories, wherein the crack growth between any two consecutive repetitions of the maximum spectrum load is a very small fraction of the overload-effected zone, so that the opening stress, S_{op}, remains constant. It is well-known that service loading histories for aircraft structure often include very high tensile or compressive loads that occur only a few times during the crack growth life. The temporary changes in S_{op} caused by these overloads (and underloads) introduce major discontinuities in the slope of the crack length-time (a versus N) curve. This differs from the smooth a-N curve that is characteristic of constant-amplitude loading. Thus, it is clear that the author's approach does not apply to "long" spectrum loading histories.

The following is suggested to extend the equivalent constant-amplitude approach to long spectrum loading histories. A short spectrum loading history is created by removing all infrequent overloads (and underloads) from the long history. This short history is then replaced by the equivalent constant amplitude loading history using the author's approach. Finally, the infrequent overloads and underloads are reinserted into the loading sequence.

This simplified loading history is expected to display the correct failure mode and critical crack size. In addition, S_{op} will vary in the appropriate manner, and the a-N curve will have the appropriate shape. In general, the extent of retardation due to the infrequent overloads will be somewhat overestimated, but this source of error would be expected to be small for spectrum loading histories of practical interest.

Using this extension of the author's approach it would be possible to estimate fatigue crack growth for even the most complex "long" spectrum loading history using retardation modeling that has up to now been applicable only to simple sequences of constant-amplitude loading with intermittent overloads and underloads.

[5] Stress Department, Lockheed-California Company, Burbank, Calif. 91520.

For aircraft structure, variations in service usage lead to significant differences in the number of infrequent overloads that occur among various fleet members. This, in turn, may lead to large deviations from the crack growth obtained from one test or analysis conducted using a single arbitrarily selected overload sequence. Multiple spectrum testing to cover this source of variation would usually be unfeasible. It would now appear to be feasible, however, to conduct multiple analyses. These analyses would operate upon the equivalent constant-amplitude loading history with various numbers of overloads, inserted at various times, covering the range of possible service histories. These analyses, supplementary to a single spectrum test result, could form a basis for improved assessment of structural reliability.

Wolf Elber (author's closure)—I agree with Mr. Brussat that his proposed modifications would simplify his particular problems. It was Mr. Brussat's integrating calculation scheme which first stimulated my search for a simple calculation scheme. This chain may develop a few more links.

L. A. Imig[1]

Crack Growth in Ti-8Al-1Mo-1V with Real-Time and Accelerated Flight-by-Flight Loading

REFERENCE: Imig, L. A., "Crack Growth in Ti-8Al-1Mo-1V with Real-Time and Accelerated Flight-by-Flight Loading," *Fatigue Crack Growth Under Spectrum Loads, ASTM STP 595*, American Society for Testing and Materials, 1976, pp. 251–264.

ABSTRACT: Crack growth in Ti-8Al-1Mo-1V was measured and calculated for real-time and accelerated simulations of supersonic airplane loading and heating. Crack-growth rates calculated on the assumption that an entire flight could be represented by a single cycle predicted the experimental rates poorly. Calculated crack-growth rates were slower than the experimental rates for all tests with flight-by-flight loading. For room-temperature accelerated tests, the calculated rates agreed well with the experimental rates; but the calculations became progressively less accurate for progressively more complex test conditions (tests that included elevated temperature). Calculations of crack growth using the crack-closure concept can probably be improved through study of crack-opening stresses using finite-element models that account for variable-amplitude loading, residual stresses, and temperature effects. The calculations of crack growth could also be improved through detailed studies of material properties and interactions among stress, temperature, and time as appropriate for the real-time operating conditions of a supersonic transport airplane.

KEY WORDS: fatigue (materials), stress cycle, high temperature tests, supersonic transports, titanium alloys, flight simulation, axial stress, accelerated tests, crack initiation, crack propagation

Practical aspects of fatigue-crack growth are a concern shared by both researchers and designers. Evidences of that concern are the many conferences held by the American Society for Testing and Materials (ASTM) to discuss and interchange ideas about crack growth. Crack growth related to airplane materials and structures has been studied predominantly for subsonic airplane flight conditions [*1,2*][2] for recent examples; but crack growth for materials and conditions representing supersonic flight also requires study to stay abreast of advancing flight capabilities. (Such advancement has led to the Anglo-French Concorde and the Russian Tu-144 supersonic airplanes.) The objectives of the present paper were to determine the effects on crack growth of the real-time and temperature environment of simulated Mach 3 flight, and to assess the

[1] Research engineer, NASA Langley Research Center, Hampton, Va. 23665.

[2] The italic numbers in brackets refer to the list of references appended to this paper.

applicability of the crack-closure and linear summation methods to crack-growth calculations for these flight-simulation tests.

Experimental Considerations

Materials and Specimens

The crack-growth tests for this investigation were conducted on duplex-annealed Ti-8Al-1Mo-1V, titanium alloy sheet which was 1.27-mm thick. The tensile properties of the sheet agreed closely with those from Ref *3* for this alloy.

The fatigue specimens made from the sheet titanium alloy are shown in Fig. 1. The central notch produced a stress-concentration factor of 4.1. Parallel

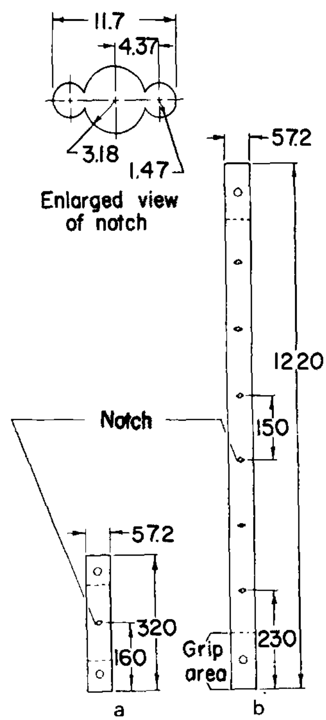

FIG. 1—*Configurations of fatigue specimens. Dimensions are in millimeters. Sheet thickness is 1.27 mm: (a) accelerated tests and (b) real-time tests.*

reference lines spaced at 1.27 mm were photographically placed on accelerated test specimens for use in recording crack lengths.

Stress Sequences

The present fatigue tests used programed variable-amplitude stress sequences (flights) representing the stresses expected in the lower wing skin of a commerical supersonic transport during its operation. The flights were derived [*4*] considering atmospheric turbulence, flight maneuvers, and landing as sources of wing load. Reference *4* describes the formulation of variable-amplitude flights whose largest amplitude was calculated to occur, on the average, once per flight, once in five flights, once in a hundred flights, and so forth. The stresses within the flights were determined separately for the climb, cruise, and descent segments of flight as shown in Fig. 2 for the flight whose largest amplitude occurred once per flight. The design mean stress referred to in Fig. 2 represents the stress in a lower wing skin during level unaccelerated flight at maximum airplane mass.

The flights developed in Ref *4* are called Type A flights. They were simplified to produce an additional sequence of variable-amplitude flights called Type G flights, see Fig. 2*b*. Type G flights produced variable-amplitude tests. The flights consisted of a single cycle having the same maximum and minimum stresses as each of the flights from which they were taken.

Fatigue Tests

Two kinds of fatigue tests, called "real-time" and "accelerated," were conducted to compare crack growth for the realistic time and temperature environment of a supersonic airplane relative to the crack growth from fatigue tests which neglect time and temperature effects. Both the real-time and accelerated tests employed identical sequences of stress amplitudes within the flights. In accelerated Type A tests, both the stress sequence within each flight and the order in which the flights were applied were scheduled automatically by a computer; the flights of Fig. 2*a* were applied at a rate of about 2 s each, and the test was conducted either at room temperature or constant elevated temperature. In real-time tests, the flights were inscribed on charts for a chart-following device; each flight, Fig. 2*c*, lasted about 96 min and included a 90-min-long elevated temperature cycle.

All fatigue tests employed hydraulically-actuated, closed-loop, servocontrolled fatigue testing machines [*5*] which operated 24 h a day. The specimens were loaded axially. Stresses for accelerated tests were based on the initial net area at the test section of each single notch specimen; for real-time tests, stresses were based on the average net area of each six-notch specimen. In a given six-notch specimen, the individual net areas of the notches were within 1 percent of the average area.

Crack-Growth Recording—Specimens for real-time tests were visually inspected approximately monthly for crack initiation. After cracks were discovered, their growth was logged weekly by an optical inspection with a 10-power microscope. In accelerated tests, crack growth was recorded by a 70-mm camera which simultaneously photographed the specimen and a flight counter. A special command included in the sequence of flight loads activated the camera and advanced the film by one frame. The image on the film was approximately full size and crack lengths were determined from the spacing of the reference lines on the specimen.

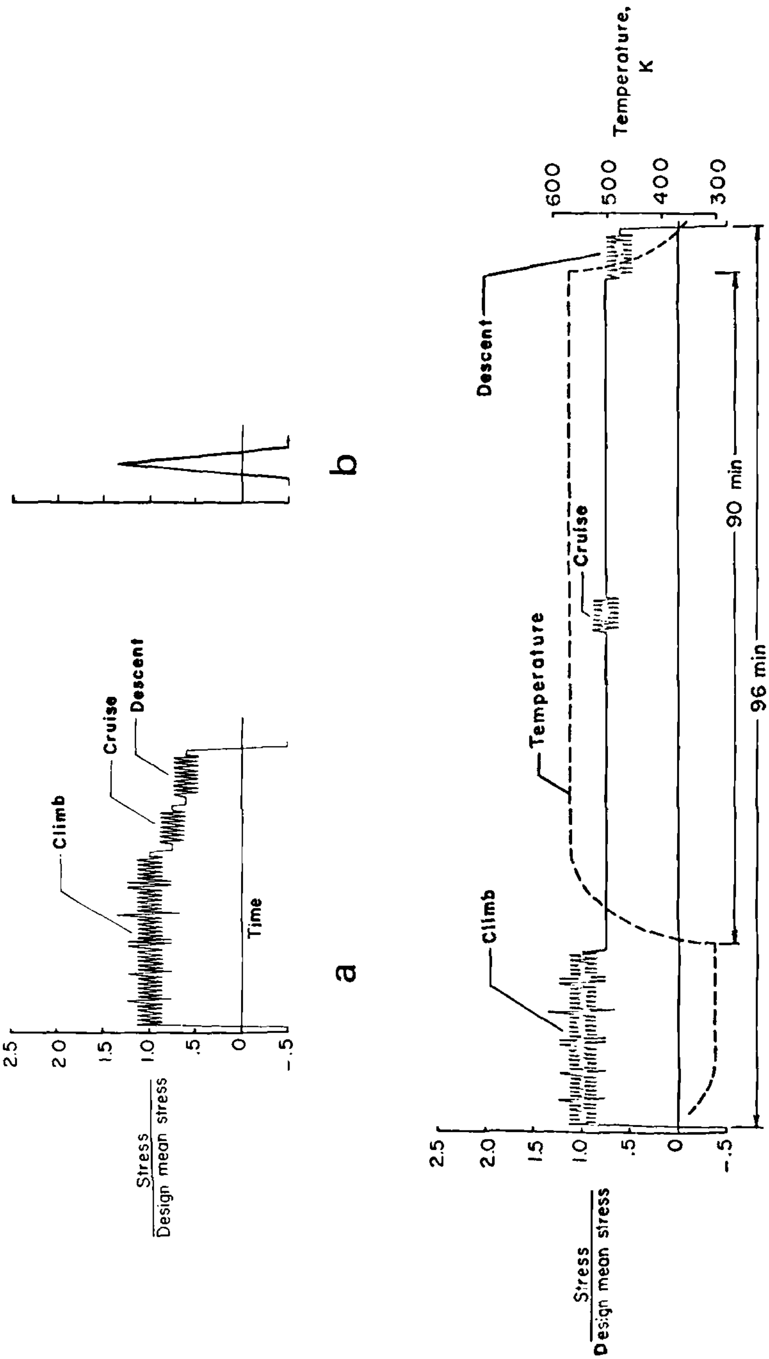

FIG. 2—*Flights for accelerated and real-time tests: (a) a Type A flight for accelerated tests, (b) a Type G flight for accelerated tests, and (c) a Type A flight with cyclic temperature for real-time tests.*

Test Conditions—The Type A flights were used in tests with design mean stresses of 172, 207, and 241 MPa, as shown in Table 1. One accelerated test was

TABLE 1 – *Test program and results. Duplex-annealed Ti-8Al-1Mo-1 V, 1.27 mm thick.*

			Crack Initiation[a]		Crack Growth[b]	
Stress Sequence	Design Mean Stress, MPa	Fatigue Life, flights	Period, flights	Percentage of Total Life, flights	Period, flights	Percentage of Total Life, flights
			Accelerated Tests at Room Temperature[c]			
	172	137 158	127 000	93	10 160	7
A	207	18 540	13 300	72	5 240	28
	241	7 472	5 300	71	2 170	29
	172	105 988	78 000	74	27 990	26
G	207	57 290	40 300	70	16 990	30
	241	22 290	12 000	54	10 290	46
			Accelerated Tests at 560 K[c]			
	172	36 243	25 500	70	10 740	30
A	207	12 498				
	241	4 580	2 850	62	1 730	38
			Real-Time Tests[d]			
	172	19 014	12 000	63	7 010	37
A	207	10 420	8 100	78	2 320	22
	241	5 093				

[a] For cracks extending 1 mm from the notch.

[b] For cracks from 1 mm long until failure.

[c] One test at each design stress.

[d] Median value from test.

conducted at room temperature (300 K) and one at 560 K for each design stress. In real-time tests, the temperature was cycled from 300 to 560 K in each flight (see Fig. 2*c*).

Type G flights were used on one set of room-temperature accelerated tests (see Table 1). Tests with Type G stress sequences were conducted as a potential aid in analyzing the crack growth in tests with Type A stress sequences.

Crack-Growth Analysis

Crack growth from both constant-amplitude tests [*6*] and the present variable-amplitude tests was analyzed in terms of growth rate and stress intensity. The analyses are discussed in the two following sections.

Constant-Amplitude Tests

The crack-growth data for constant-amplitude tests of Ti-8Al-1Mo-1V [*6*] were analyzed using the crack-closure concept of Ref *7* to define an effective stress-intensity factor. According to that concept, the crack is closed during part of each load cycle and therefore cannot grow during that time; thus, the applied stress range ΔS is reduced to an effective stress range of $U\Delta S$. The factor U was determined [*7*] for crack growth at positive R values in an aluminum alloy. For expediency, the same factor U was used in this paper to analyze the constant-amplitude data from Ref *6*. Effective ranges of stress intensity were calculated from $\Delta K_{eff} = U\Delta S\sqrt{\pi a}$, where the values of a are average crack lengths for the increments of crack growth [*6*], and $U = 0.5 + 0.4R$ $(R \geq 0)$ [*7*]. A least-squares technique using the relation $\Delta a/\Delta N = A\,[\Delta K_{eff}]^n$ produced a good correlation between crack-growth rate and ΔK_{eff} as shown in Fig. 3 for tests at room temperature and 560 K, respectively. The best-fit constants determined for the two test temperatures are given in the following tabulation.

Test Temperature	A	n
Room Temperature	5.5×10^{-8}	3.15
560 K	1.1×10^{-7}	2.72

These values were used to make the following calculations of crack growth for the present variable-amplitude tests.

Variable-Amplitude Tests

Crack-growth rates for the present variable-amplitude tests were calculated in three ways:

1. by assuming one cycle per flight, and using effective stress intensity,
2. by considering only the stresses exceeding the crack-opening level and using effective stress intensity (the "crack-closure method"), and
3. by considering all stresses in the flight, and using the conventional stress intensity, ΔK (the "linear-summation method").

Factors to account for the narrow specimen width and the eccentricity of the individual cracks at the two ends of the notch (see Fig. 4) were used to calculate the stress intensities. The width of the specimen was accounted for by the factor $\sqrt{\sec\,(\pi a/W)}$ [*8*], and eccentricity was accounted for by factors L interpolated from the tabular values in Ref *9*. Thus, the expression for stress intensity was $U\Delta SL\sqrt{\pi a \sec\,(\pi a/W)}$, where a is the average crack length for the current growth increment, L is the factor for either the long or the short crack, as appropriate, and $U = 1$ to calculate conventional stress intensity. The stress concentration due to the notch in the specimen was neglected because it influenced the stress intensity by less than about 3 percent for the present calculations [*10*].

For all three methods of calculating crack growth, the stresses selected were from flights of the severity shown in Fig. 2, because they represented about 80

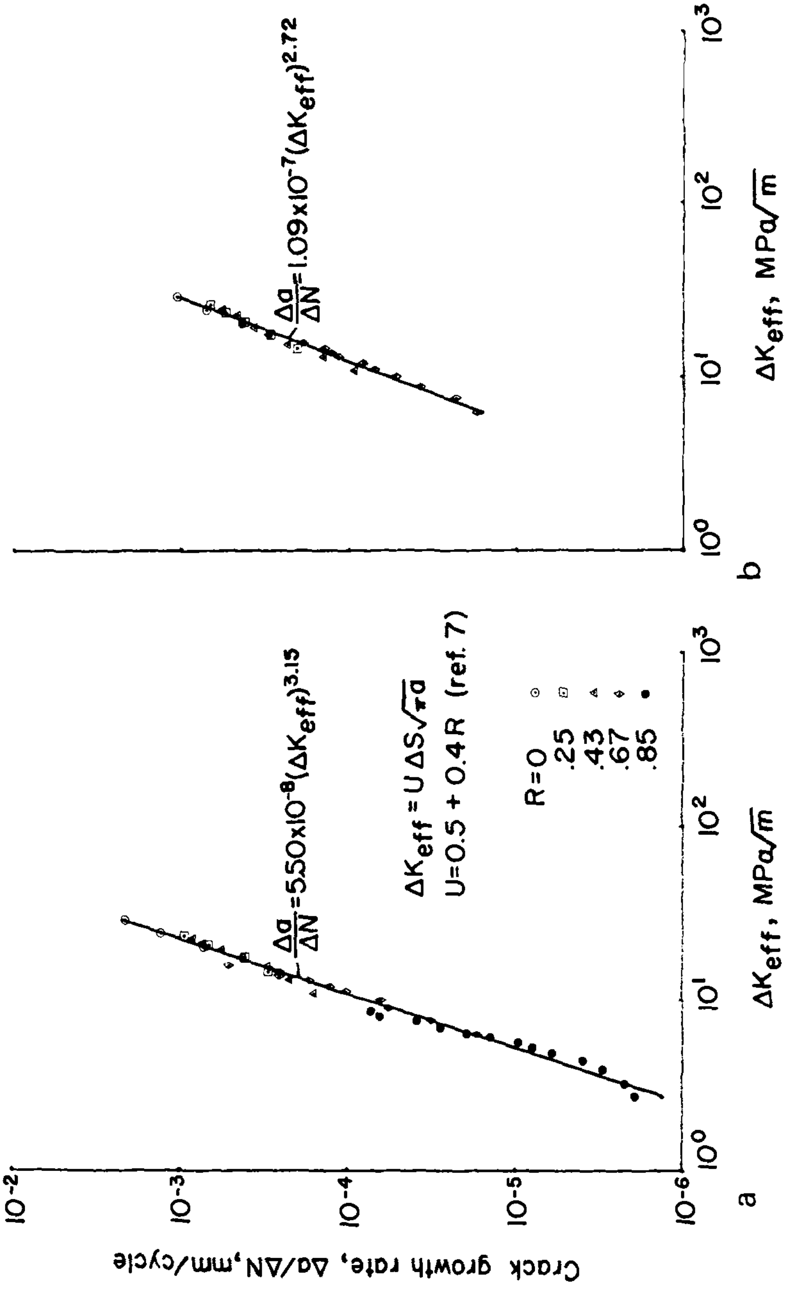

FIG. 3—*Correlation between crack-growth rate and ΔK_{eff} for constant-amplitude fatigue tests of duplex-annealed Ti-8Al-1Mo-1V, 1.27 mm thick. Data from Ref 6: (a) tests at room temperature and (b) tests at 560 K.*

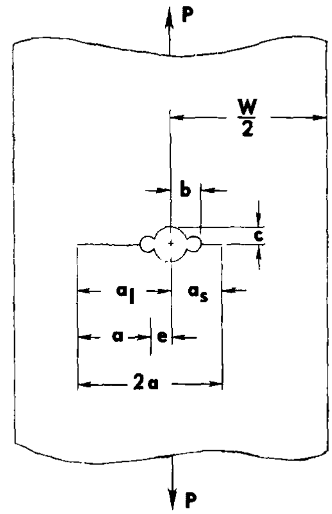

FIG. 4—*Crack and geometric nomenclatures for calculating crack eccentricities.*

percent of the flights applied. All three calculations also assumed that cracks would grow at the rates determined in constant-amplitude tests for the same values of stress intensity.

One Cycle per Flight—This calculation assumed that a single cycle between the minimum and maximum stresses in the flight (the ground-air-ground cycle) produced all the crack growth. Both Type A and Type G tests were analyzed in this way using effective stress intensity. The R value for the ground-air-ground cycle is −0.37. The effective stress range for constant-amplitude tests, with negative R values, was determined by elastoplastic, finite-element analysis of a cracked sheet in Ref *11*. Those calculations produce $U = 0.54$ for the present tests ($R = -0.37$). For this first method, crack-growth rates (growth increments per flight) were calculated from $\Delta a = A\ (\Delta K_{\text{eff}})^n$ using A and n from the previous section, and using the average crack length from each increment of the experimental crack growth, in ΔK_{eff}. Experimental rates were assumed to be constant during each increment of crack growth.

Crack Closure—For this method, effective stress intensities were calculated for all stress cycles fully exceeding the crack-opening stress. Only the stress cycles in climb fully exceed the crack-opening stress when $U = 0.54$. The cycles in cruise are only partially above (and were neglected), and the cycles for descent are below the crack-opening stress. Therefore, the effective stress range selected was from the maximum stress of each cycle to, arbitrarily, the minimum stress for the smallest amplitude of the climb segment. As Fig. 2*a* shows, the climb segment of Type A flights had 30 cycles of small amplitude, 6 cycles of an intermediate amplitude, and 1 cycle of large amplitude. Thus, for this method, crack growth per flight was calculated from

$$\Delta a = A\ [30(\Delta K_{\text{eff}})_1{}^n + 6(\Delta K_{\text{eff}})_2{}^n + (\Delta K_{\text{eff}})_3{}^n]$$

where the subscripts correspond to the three ranges of the effective stress, and the other nomenclature is the same as previously described.

The values of A and n used in the calculations depended on the kind of test. For accelerated tests, the calculations used the values of A and n corresponding to the constant test temperature. For real-time tests, each flight included a temperature cycle, but the temperature for the climb segment of each flight was near room temperature; therefore, values of A and n for room temperature were used.

Linear Summation—This calculation summed the crack growth for the complete range of each cycle in the flight, including the ground-air-ground cycle. Crack growth was calculated using ΔK. To calculate crack growth using ΔK, a different value of $\bar{A}$ was required for each stress range in the flight. The $\bar{A}$'s were obtained by factoring the term U from the expression for ΔK_{eff}, and combining U with the value of A determined earlier in this paper for constant-amplitude data. Thus, $\Delta a/\Delta N = AU^n\ (\Delta K)^n = \bar{A}(\Delta K)^n$. The values of $\bar{A}$ obtained using $U = 0.5 + 0.4R$ [7] and the constant-amplitude data from Ref 6 are shown in Fig. 5. A value of $\bar{A}$ was determined for each stress range in the flight. The previously

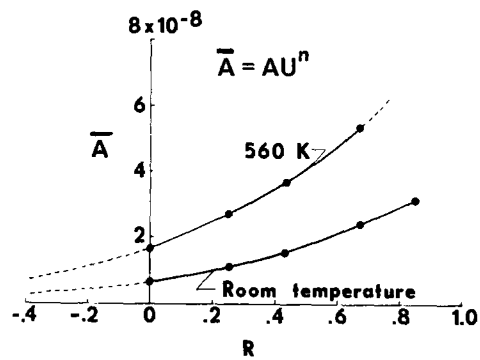

FIG. 5—*Relations between* $\bar{A}$ *and* R *for constant-amplitude fatigue tests of duplex-annealed Ti-8Al-1Mo-1V, 1.27 mm thick. Data from Ref 6.*

determined values of the exponent n were retained. The crack-growth rates per flight were calculated from

$$\Delta a = 30\bar{A}_1\ (\Delta K_1)^n + 6\bar{A}_2\ (\Delta K_2)^n + \dots$$

where the subscripts on $\bar{A}$ and ΔK correspond to the various stress amplitudes, the number of terms in the equation corresponds to the number of different amplitudes, and the coefficient of each term is the number of cycles for each amplitude.

Results and Discussion

The test results, presented in Table 1, are discussed in terms of both crack initiation and crack growth.

Crack-Initiation Periods

The smallest cracks detectable from the film records of room-temperature accelerated tests, or from observations of the real-time tests, were usually less than 1 mm long; but the cracks were about 2 mm long before becoming detectable on film records of accelerated tests at 560 K.

In most tests, cracks at the two ends of the notch initiated at different times. Therefore, in general, an eccentricity factor was required to calculate stress intensity for these cracks, as described earlier. The values given in Table 1 for accelerated tests are for the first crack to initiate. For real-time tests, the values are for the first crack at the notch having the median life.

To establish a consistent base of comparison, the number of flights to produce a crack 1 mm long (see Table 1) was determined from plotted curves of crack length versus number of flights for each test. For hot accelerated tests, the curves were extrapolated. Table 1 indicates that most of the cracks reached a length of 1 mm (initiated) at between 60 and 80 percent of the total life. In all of the accelerated tests, the crack initiation periods were consistently larger fractions of total lives for lower design mean stresses. The data for real-time tests show the opposite trend, but its significance cannot be adequately determined because data are available for only two real-time tests.

Crack-Growth Periods

The periods of crack growth in Table 1 are differences between the fatigue lives and the initiation periods. The crack-growth periods for Type A accelerated tests at the two temperatures were about the same, consistent with the crack-growth periods for constant-amplitude tests of this alloy [*6*] for the same temperatures. For a given design stress, the growth periods for real-time tests were somewhat shorter than for the accelerated tests.

The growth periods for Type A tests were much shorter (growth rates were faster) than for Type G tests. The faster rates for Type A tests indicate that the small stress cycles contributed significantly to the crack growth.

Crack-Growth Rates

The calculated crack-growth rates are plotted against the experimental rates from the persent tests in Figs. 6 and 7. The points in each figure represent the rates for both the long and short cracks and for all design stresses. The solid line in each figure is a least-squares linear fit of all the points. The dashed lines indicate where the points would lie if the calculated rates equaled the experimental rates.

Type G Tests—Figure 6 shows the crack-growth rates for Type G tests where both the tests and calculations simulated the flights by a single cycle. As shown by the slope of the solid line, the calculated rates were faster than the experimental rates by an average of about 70 percent. That result should be expected qualitatively, because the higher stresses in fifth flights, 100th flights,

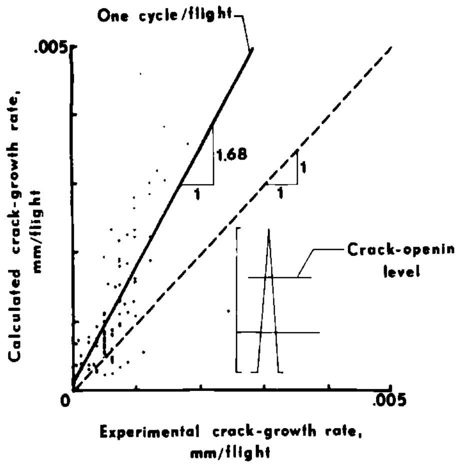

FIG. 6—*Experimental and calculated crack-growth rates for Type G fatigue tests of duplex-annealed Ti-8Al-1Mo-1V, 1.27 mm thick.*

and so forth, probably retarded the crack growth, and these higher stresses were not accounted for in the calculations.

Type A Tests—The experimental crack-growth rates for Type A tests and the rates calculated in the three ways discussed earlier are shown in Fig. 7. Parts *a*, *b*, and *c* of Fig. 7 contain the rates for accelerated tests at room temperature, accelerated tests at 560 K, and real-time tests, respectively. The top parts of Figs. 7*a*, 7*b*, and 7*c* compare the experimental rates to those calculated, assuming the flight could be represented analytically as a single cycle; the center parts compare the experimental rates to those calculated, accounting for only the cycles exceeding the assumed crack-opening level (all the cycles in the climb segment of each flight); the bottom parts compare the experimental rates to those calculated, using linear summation of the crack-growth contributions of all cycles in the flight.

Figure 7 shows better agreement between calculated and experimental rates for room-temperature accelerated tests (Fig. 7*a*) than for elevated temperature or real-time tests (Figs. 7*b* and *c*). It shows that the flights were poorly represented in the calculations by a single cycle (top row of figures). It shows that the rates calculated by the crack-closure and the linear summation methods were about equal for each test condition (center and bottom figures).

The present calculations using linear summation and other calculations of linear fatigue damage both predicted longer fatigue lives (slower damage accumulation) than the experiments produced [*5*]. In contrast, Refs *1* and *2* reported that linear summation calculations for crack growth indicate higher crack-growth rates than their experiments on 2024-T3 and 7075-T6 aluminum alloys. These different observations probably result from the interaction effects of the spectrums on the materials, the relative severities of the spectrums, or the combined effects. As shown in Fig. 8, the spectrum from Ref *1* contains

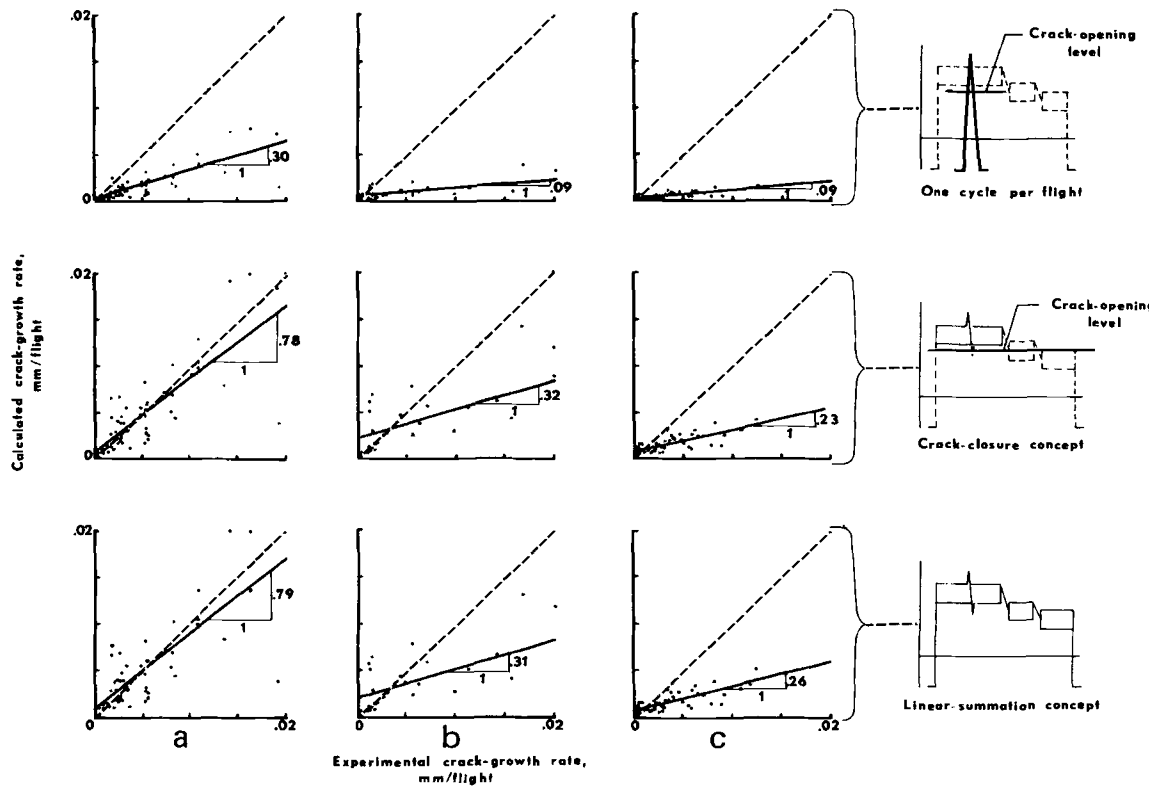

FIG. 7—*Experimental and calculated crack-growth rates for Type A fatigue tests of duplex-annealed Ti-8Al-1Mo-1V, 1.27 mm thick: (a) accelerated tests at room temperature, (b) accelerated tests at 560 K, and (c) real-time tests.*

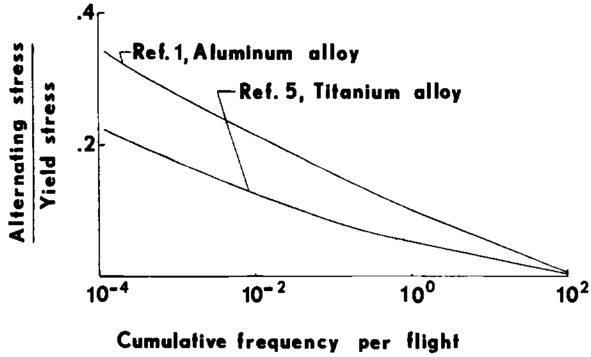

FIG. 8–*Gust spectrums.*

significantly higher stresses than the present spectrum, relative to the yield strengths of the two materials. Conceivably, the higher relative stresses in the infrequent flights of Ref *1* produced larger delays in crack growth than in the present tests.

In contrast to the good agreement between calculated and experimental rates for the room-temperature tests, the calculated crack-growth rates for accelerated tests at 560 K and for real-time tests were much slower than the experimental rates. This discrepancy is difficult to explain for the hot accelerated tests because the calculation method was identical to that for room-temperature tests, and the supporting constant-amplitude data for both temperatures seemed equally well correlated. Possibly, the high loads in the infrequent flights produced less retardation at 560 K than at room temperature. For the real-time tests, Fig. 7*c*, insufficient information is available about local high-stress creep, stress-strain relations, crack-opening stresses, and their interactions during cycles of temperature, to properly predict crack growth. A first attempt to calculate local stresses at the notch for real-time flights [*12*] indicated only slight differences between the stresses for real-time flights and those for room-temperature flights. Thus, much basic study will probably be required before crack growth can be calculated accurately for this type of loading.

Overall, the present calculations indicate that the linear summation and crack-closure concepts produced the best calculations of crack growth. The calculations by both methods could probably be improved by considering a crack-growth relation which allows the rate to accelerate at high values of stress intensity [*13*], and by considering the plasticity and stress distribution effects induced by the notch [*14*]. In addition, calculations with the crack-closure concept could probably be improved through further study of the crack-opening stress levels for variable temperature and loading.

Concluding Remarks

Crack growth in Ti-8Al-1Mo-1V was measured and calculated for real-time and accelerated simulations of supersonic airplane loading and heating. Crack-growth rates, calculated on the assumption that an entire flight could be represented by a single cycle, predicted the experimental rates poorly. Calculated crack-growth rates were slower than the experimental rates for all tests with flight-by-flight loading. For room-temperature accelerated tests, the calculated rates agreed well with the experimental rates; but the calculations became progressively less accurate for progressively more complex test conditions (test that included elevated temperature). Calculations of crack growth using the crack-closure concept can probably be improved through study of crack-opening stresses using finite-element models that account for variable-amplitude loading, residual stresses, and temperature effects. The calculations of crack growth could also be improved through detailed studies of material properties and interactions among stress, temperature, and time as appropriate for the real-time operating conditions of a supersonic transport airplane.

References

[*1*] Schijve, J., Jacobs, F. A., and Tromp, P. J., "Fatigue Crack Growth in Aluminum Alloy Sheet Material Under Flight Simulation Loading. Effects of Design Stress Level and Loading Frequency," NLR-TR-72018U, National Aerospace Laboratory, Amsterdam, Feb. 1972.

[*2*] Brussat, T. R. in *Damage Tolerance in Aircraft Structures, ASTM STP 486*, American Society for Testing and Materials, 1971, pp. 122–143.

[*3*] "Metallic Materials and Elements for Aerospace Vehicle Structures," Department of Defense, MIL-HDBK-5A, 1966.

[*4*] Imig, L. A. and Illg, Walter, "Fatigue of Notched Ti-8Al-1Mo-1V Titanium Alloy at Room Temperature and 550 F (560 K) With Flight-by-Flight Loading Representative of a Supersonic Transport," NASA TN D-5294, National Aeronautics and Space Administration, 1969.

[*5*] Imig, L. A. and Garrett, L. E., "Fatigue-Test Acceleration With Flight-by-Flight Loading and Heating to Simulate Supersonic-Transport Operation," NASA TN D-7380, National Aeronautics and Space Administration, 1973.

[*6*] Hudson, C. M., "Studies of Fatigue Crack Growth in Alloys Suitable for Elevated Temperature Applications," NASA TN D-2743, National Aeronautics and Space Administration, 1965.

[*7*] Elber, Wolf in *Damage Tolerance in Aircraft Structures, ASTM STP 486*, American Society for Testing and Materials, 1971, pp. 230–242.

[*8*] Brown, W. F. and Srawley, J. E., *Plane Strain Crack Toughness Testing of High Strength Metallic Materials, ASTM STP 410*, American Society for Testing and Materials, 1966, p. 78.

[*9*] Isida, M., "Crack Tip Stress Intensity Factors for the Tension of an Eccentrically Cracked Strip," Dept. of Mechanics, Lehigh University, Bethlehem, Pa., 1965.

[*10*] Newman, J. C., Jr., "An Improved Method of Collocation for the Stress Analysis of Cracked Plates With Various Shaped Boundaries," NASA TN D-6376, National Aeronautics and Space Administration, 1971.

[*11*] Newman, J. C., Jr., "A Finite-Element Analysis of Fatigue Crack Closure," presented at the Eighth ASTM National Symposium on Fracture Mechanics, Providence, R. I., Aug. 1974.

[*12*] "Cyclic-Stress Analysis of Notches for Supersonic Transport Conditions," Boeing Aerospace Co., NASA CR-132387, National Aeronautics and Space Administration, 1974.

[*13*] Forman, R. G., Kearney, V. E., and Engle, R. M. in *Transactions*, American Society of Mechanical Engineers, Series D, *Journal of Basic Engineering*, Vol. 89, No. 3, Sept. 1967, pp. 459–464.

[*14*] Crews, J. H., Jr., and White, N. H., "Fatigue Crack Growth From a Circular Hole With and Without High Prior Loading," NASA TN D-6899, National Aeronautics and Space Administration, 1972.

Life Prediction and Applications

D. V. Nelson[1] *and H. O. Fuchs*[2]

Prediction of Fatigue Crack Growth Under Irregular Loading

REFERENCE: Nelson, D. V. and Fuchs, H. O., "Prediction of Fatigue Crack Growth Under Irregular Loading," *Fatigue Crack Growth Under Spectrum Loads, ASTM STP 595*, American Society for Testing and Materials, 1976, pp. 267–291.

ABSTRACT: Fatigue crack growth under irregular loading is calculated from constant-amplitude test data. The results of such calculations are compared with measurements of crack growth in modified compact tension specimens made of two commonly used structural steels and subjected to three different irregular load histories, each applied at several load levels.

Two crack growth rate relations are utilized: I, the Forman relation, and II, a relation based on an effective stress intensity range concept. The Forman relation is used with two different methods of "counting" load ranges, that is, crack growth is calculated: (*a*) for all rising tensile load ranges as they occur in the load history and (*b*) for the load history condensed by a method which forms *overall* ranges and includes only the top decile of all rising tensile ranges. Crack growth rate Relation II is used only with counting Method *a*. The three resulting prediction methods are designated I*a*, I*b*, and II. Methods I*a* and I*b* disregard sequence effects, while Method II includes them.

Predictions of crack growth using Methods I*a* and I*b* agree with average test lives to within a factor of two in nearly all cases, with the exception of those instances where large compressive loads cause gross yielding and accelerated growth. Predictions based on Method II are superior to those for I*a* and I*b* when such gross yielding occurs and are comparably good for the other cases investigated here.

KEY WORDS: crack propagation, predictions, loads (forces), stresses, crack initiation, stress ratio, retarding, residual stress, fatigue (materials), fracture properties, crack closure, compression

Data obtained from constant-amplitude tests permit the calculation of crack growth under irregular loading. Virtually all predictions of fatigue crack propagation to date have been concerned with load histories which can be characterized by cycles. For simulated aircraft loadings, crack growth has been calculated for varying layers of cycles, with attempts to account for crack growth retardation due to periodic tensile overloads [*1–4*].[3] For random loadings, particularly those with load spectra describable by the Rayleigh distribution function, crack growth has been characterized in terms of equivalent

[1] Research assistant, Mechanical Engineering Dept., Stanford University, Stanford, Calif. 94305; now with General Electric Co., Sunnyvale, Calif. 94086.

[2] Professor, Mechanical Engineering Dept., Stanford University, Stanford, Calif. 94305.

[3] The italic numbers in brackets refer to the list of references appended to this paper.

root-mean-square cycles [*5–7*]. However, little consideration has previously been given to crack propagation for those irregular loadings where the definition of a cycle is not straightforward. A similar problem exists in the prediction of crack initiation, where various "cycle counting" methods [*8–12*] have been developed for selecting damaging "events" (for example, large overall ranges interrupted by smaller ranges) in irregular load histories. Constant-amplitude fatigue data are then used to predict the crack initiation damage of such events. A similar type of approach will be applied here to the prediction of crack propagation for the same histories for which initiation was calculated in Ref *12*.

Previous crack growth predictions have also neglected the possible effects of compressive loadings. A number of experimental investigations [*13–15*] have shown that compressive overloads can increase crack growth rate, while other studies [*14–17*] have found that if a tensile overload is followed immediately by a compressive overload, the effects of crack growth retardation are greatly diminished. Furthermore, Stephens [*15*] has recently found that retardation can be reduced by application of cycles with compressive loading following single tensile overloads. A new prediction method with the ability to account for important load sequence effects due to both tensile and compressive overloads will be presented. The effect of compressive loadings which cause gross yielding will be given special consideration.

All predictions are made using a linear elastic fracture mechanics approach. The following items are needed for this purpose: (*a*) a forecast of loading, including not only the magnitude but sequence of loads as well; (*b*) a relation between stress intensity, K, and loading for a given component geometry and anticipated type and size of crack, which will be referred to as a "K-calibration" for the sake of brevity; (*c*) constant-amplitude crack growth rate data ($\Delta a/\Delta N$ versus ΔK) for a given metal, including knowledge of fracture toughness, K_c, threshold stress intensity, ΔK_{th}, and stress ratio, R, effects on growth; and (*d*) a way of using these items. Item *d* is the main concern of this paper.

Input Data for Predictions

Load Histories

Three distinctly different irregular load histories were used in this study and are depicted in Fig. 1. These histories have recently been used in an extensive crack initiation and propagation test program of the SAE Fatigue Design and Evaluation Committee [*18*]. Each history was applied repeatedly in testing, so that test data were reported in terms of blocks (that is, repetitions of the history). Due to their contrasting nature, these load blocks are especially useful for evaluation of prediction methods. The suspension history, with 2506 reversals, has a strong compressive bias. The transmission (or axle) history, with 1710 reversals, has a tensile bias with frequent reversals into compression. The bracket history, with 5936 reversals, is a narrow-band, random loading with little or no mean bias.

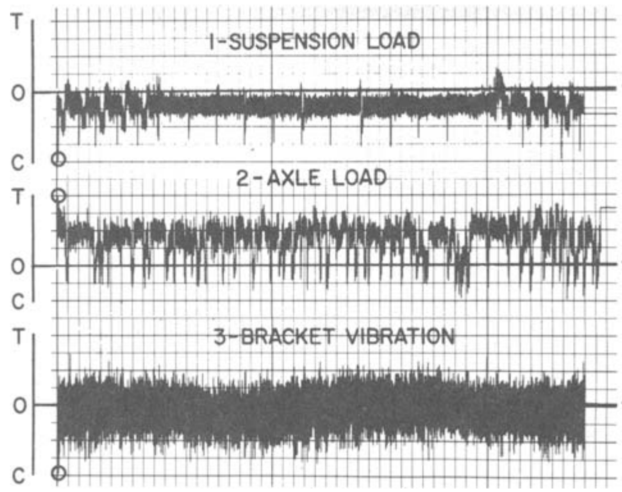

FIG. 1–*Three irregular load blocks representative of ground vehicle service (courtesy of the Cumulative Damage Division of the SAE Fatigue Design and Evaluation Committee).*

Specimen and Materials

The specimen used in the SAE test program was a modified compact tension type with a large keyhole notch [*18*]. Two commonly used structural steels, U. S. Steel Man-Ten and Bethlehem RQC-100, were tested. Mechanical properties and estimated fracture toughness values for these steels are given in Table 1.

TABLE 1 – *Mechanical properties and fracture toughness of U.S. Steel Man-Ten and Bethlehem RQC-100.*

	Man-Ten	RQC-100
Monotonic yield strength (0.2%), MPa (ksi)	324 (47)	815 (118)
Cyclic yield strength (0.2%), σ'_{ys}, MPa (ksi)	324 (47)	620 (90)
Ultimate tensile strength, MPa (ksi)	565 (82)	863 (125)
Reduction in area, %	67	44
Fracture toughness,[a] MPa $\sqrt{m}$ (ksi $\sqrt{in.}$)	121 (110)	154 (140)

[a] Estimated from knowledge of critical crack lengths and corresponding maximum tensile loads for tests reported in Ref *18*.

K-*Calibration*

The K-calibration was derived from experimental measurements [*19*] of specimen compliance (C) at various normalized crack lengths (a/W) ranging from 0.35 to 0.72. First, these data were divided into two intervals: (a/W) from 0.35 to 0.53 and from 0.53 to 0.72. Data in each interval were fitted by a cubic function in a least-squares sense and subject to the constraints that at (a/W) = 0.53, the two adjoining functions have equal values, slopes, and curvatures. This produced a single continuous curve (with continuous first and second derivatives) which represented the overall trend of the scattered data without introducing inflections in the fitted curve. A K-calibration in the form (K/P) = $f(a/W)$ was then derived using Eqs 1 and 2.

$$G = \frac{P^2}{2B}\left(\frac{\partial C}{\partial a}\right) \tag{1}$$

$$K = \sqrt{G\,E} \text{ (plane stress)} \tag{2}$$

where

G = elastic strain energy release rate,
E = modulus of elasticity,
B = specimen thickness, and
P = applied loading.

The experimentally derived K-calibration compares favorably with an analytical (boundray collocation) calibration [*20*] for a compact tension specimen of similar geometry. In particular, the experimental calibration is 5 percent lower than the analytical calibration at (a/W) = 0.35. The difference between the two K-calibrations diminishes as (a/W) increases, and they converge at (a/W) $\approx$ 0.6. For (a/W) greater than 0.72, the analytical K-calibration was used for predictions since no experimental data were available for larger (a/W) values.

Constant-Amplitude $\Delta a/\Delta N$ *versus* ΔK *Data*

Measurements of crack length versus cycles [*21*] under constant amplitude, R = 0, loading for both Man-Ten and RQC-100 were made using compact tension specimens (ASTM Standard Method of Test for Plane-Strain Fracture Toughness of Metallic Materials (E 399-72)) machined from the same heats of steel as the modified compact tension specimen. The "raw" crack growth data were converted to $\Delta a/\Delta N$ versus ΔK form using an incremental-polynomial data-fitting technique [*22*].

Crack growth rate data were available only in the range of $\Delta a/\Delta N$ from about 5×10^{-7} to 3×10^{-5} cm/cycle for both metals. The threshold stress intensity and fracture toughness values and possible stress ratio effects were not determined.[4] This lack of data might be a serious hindrance to predicting crack

[4] Further tests are planned by the Fracture Mechanics Division of the SAE Fatigue Design and Evaluation Committee to determine these data.

growth. Yet, it provided an opportunity to examine the capability of the prediction methods to perform with limited input data, a situation typical of engineering practice.

For both Man-Ten and RQC-100, $\Delta a/\Delta N$ at $\Delta K = 10$ MPa$\sqrt{m}$ is roughly 10^{-7} cm/cycle. In addition, threshold stress intensities for a number of other steels fall in the range of 5 to 15 MPa$\sqrt{m}$ [*23*]. Thus, two values of ΔK_{th}, 5.5 and 11.0 MPa$\sqrt{m}$, were used in this work to examine the effect of ΔK_{th} on predictions.

Crack Growth Rate Relations

An important consideration in any crack growth prediction is the selection of a growth rate relation. For irregular loadings, the ability of such relations to account for stress ratio effects on crack growth rate is of particular concern. Two relations were used here.

The Forman relation [*24*], that is,

$$\Delta a/\Delta N = \frac{A(\Delta K)^n}{(1-R)K_c - \Delta K} \tag{3}$$

where $R = K_{min}/K_{max}$, was selected because of its ability to predict possible stress ratio effects using only $R = 0$ data, all that was available for Man-Ten and RQC-100. Whether it adequately predicts such effects for these metals remains to be investigated experimentally. Constants A and n in Eq 3 were determined by a linear least-squares fit of log $[(\Delta a/\Delta N)(K_c - \Delta K)]$ versus log (ΔK) using $R = 0$ data for Man-Ten and RQC-100.

A crack growth rate relation based on an effective stress intensity range concept was also used, that is,

$$\Delta a/\Delta N = \frac{A(\Delta K_{eff})^n}{K_c - K_{max}} \tag{4}$$

where ΔK_{eff} is an effective stress intensity range equal to $(K_{max} - K_{res})$ or $(K_{max} - K_{min})$ if K_{min} is larger than K_{res}. The K_{res} term is a "residual stress intensity" which corresponds at least conceptually to the crack opening stress described by Elber [*25*]. In this work, K_{res} was taken as $q(K_{max} - \Delta K_{th})$, where q is a fraction. Threshold stress intensity range was included in the $(K_{max} - \Delta K_{th})$ term to make K_{res} vanish as K_{max} approaches ΔK_{th}; however, this condition is not an essential element of the growth rate relation and, with hindsight, could probably be discarded.

In general, the q value is likely to vary from metal-to-metal, for different specimen geometries and thicknesses, and will even increase with increasing K_{max}, as suggested by the studies of Newman [*26*] and Schijve [*27*]. As a first approximation, q was considered a constant.

The ΔK_{eff} term in Eq 4 will be used to account for both stress ratio effects and load sequence effects such as crack retardation. Keeping this in mind, values of q suitable for exploratory purposes were estimated as follows. The application of a single tensile overload of sufficient magnitude, K_{ol}, in constant-amplitude ($R = 0$) loading, K_{ca}, will usually cause crack arrest. The ratio (K_{ol}/K_{ca}) varies between two and three for a number of metals [*13,17, 28–33*]. If ΔK_{eff} is to account for crack arrest or retardation, then q should be taken as the reciprocal of (K_{ol}/K_{ca}), thus varying between 0.35 and 0.50. Constants A and n in Eq 4 were fitted for both "extreme" values of q by the same procedure used to calibrate Eq 3.

The use of Eq 4 to account for load sequence effects will be described in detail later. First, its ability to predict stress ratio effects on crack growth will be considered.

Equation 4 was calibrated with $R = 0$ growth rate data, K_c and ΔK_{th} values for aluminum alloys 2024-T3 and 7075-T6 [*34*] and titanium alloy Ti-6Al-4V [*35*]. In all cases, a value of $q = 0.35$ was used for exploratory purposes. Stress ratio effects were then predicted and compared with test data. Figure 2 shows such a comparison for 2024-T3 and is typical of the agreement between predictions and test results for all three metals. Unfortunately, no comparable stress ratio data exist for Man-Ten or RQC-100 to allow Eq 4 to be checked for these metals.

Crack Growth Predictions for Constant-Amplitude Loading

Before considering the prediction of crack growth for the three irregular loadings, predictions based on Eqs 3 and 4 for constant-amplitude loading

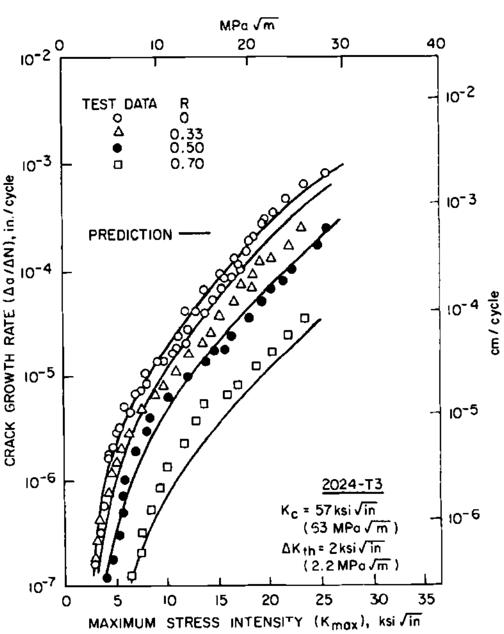

FIG. 2—*Comparison of predictions with test data for stress ratio effects on fatigue crack growth rate in 2024-T3 [34].*

applied to the modified compact tension specimen will be compared with available test data [18]. All predictions were based on growth from an initial crack length of 33 mm, as measured from the specimen load line (or 2.5 mm from the specimen notch tip).

Predictions were first made for fully-reversed loadings. Only the tensile half-cycle was considered in computing ΔK. For RQC-100, predictions were within experimental scatter for tests with a 17.8 kN load amplitude and within 20 percent of total crack propagation life for single tests at 13.4 and 15.6 kN load amplitudes. For these load amplitudes, predictions were the same for $\Delta K_{th} = 5.5$ and 11.0 $\text{MPa}\sqrt{\text{m}}$. For Man-Ten, predictions were within 10 percent of total life for a single test with 8.9 kN load amplitude and were again insensitive to ΔK_{th}.

Although only limited constant-amplitude test data were available for comparison, these predictions were reassuring. They suggested that the limited $\Delta a/\Delta N$ versus ΔK data generated for Man-Ten and RQC-100 and the experimentally derived specimen K-calibration were probably adequate for making reasonable predictions for the irregular loadings.

Predictions were also made for two single constant-amplitude tests conducted at stress ratios of $R = 0.17$ and 0.20 for Man-Ten, at maximum load levels of 26.7 and 22.3 kN, respectively. In both cases, predictions based on Eqs 3 and 4 were about a factor of 2.5 too conservative, indicating that perhaps stress ratio effects were being predicted which do not actually occur in Man-Ten. To gain some insight into this possibility, predictions were also made using the Paris relation, $\Delta a/\Delta N = A\ (\Delta K)^n$, which does not account for stress ratio effects. Predictions based on this relation agreed very closely with those based on Eqs 3 and 4 for the fully-reversed tests. As expected, however, the Paris relation predicted less growth for the two stress ratio tests with Man-Ten. Yet, it still predicted too much growth, by a factor of about 1.5. It is conceivable that the high tensile loadings in these two tests created compressive residual stresses in the vicinity of the specimen notch, the influence of which may have retarded initial crack growth beyond 33 mm. In any case, it is difficult to draw conclusions based on the results of only two tests.

Prediction of Crack Growth for Irregular Loadings

All prediction methods were based on the following two key assumptions: (a) that compressive loadings cause no growth and (b) that only rising tensile load ranges cause growth. The first assumption seems physically plausible, since under compressive loading, a crack tip should be shut and therefore unable to produce growth. The second assumption is supported by fractographic studies of McMillan and Pelloux [36], which showed that crack growth apparently occurs only during the rising portion of load cycles. Based on the first assumption, the three irregular load blocks described previously were converted to blocks containing only tensile loadings, as illustrated in Fig. 3.

Each prediction method also utilized the following procedure to compute and sum crack growth. First, an initial crack length, a_0, was selected. The first rising

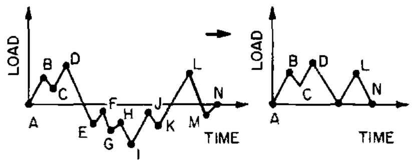

FIG. 3—*Conversion of an irregular load sequence to only its tensile loadings.*

load range in a given block was converted to a corresponding stress intensity range. Crack growth for the first range, $(\Delta a/\Delta N)_1$, was computed, giving a new crack length $a_1 = a_0 + (\Delta a/\Delta N)_1$. Next, the second rising load range was converted to a stress intensity range using a_1. Growth due to this range, $(\Delta a/\Delta N)_2$, was computed giving $a_2 = a_1 + (\Delta a/\Delta N)_2$. This process was continued throughout the entire load block. The sum of growth for a block gave a growth rate per block associated with the initial crack length, a_0, that is, $(\Delta a/\Delta\text{block})$ at a_0. This procedure was repeated for a number of selected crack lengths, a_i, which, in turn, allowed construction of a curve of crack length versus blocks by a simple numerical integration of

$$\text{blocks} = \int_{a_0}^{a_f} (\Delta a/\Delta\text{block})^{-1}\, \Delta a \tag{5}$$

*Prediction Method I*a

Equation 3 was used to calculate growth for each rising load range in a given block. No growth was calculated for ranges with ΔK less than ΔK_{th}. As mentioned before, two values of ΔK_{th} (5.5 and 11.0 MPa$\sqrt{\text{m}}$) were used, which provided information on the sensitivity of predictions to ΔK_{th} at various extreme load levels. This method, of course, neglects possible load sequence effects.

*Prediction Method I*b

This prediction method is the same as I*a* except that crack growth was calculated for load blocks which were first condensed to 10 percent of their original number of reversals by the Ordered Overall Range Method [*11,12*] before compressive loads were removed. This method of condensing irregular load blocks selects overall ranges and screens out smaller ranges which interrupt the overall ranges, as illustrated in Fig. 4. It is qualitatively similar to "rainflow" cycle counting [*8*], except that it condenses a loading while preserving its sequence. The size of ranges which are screened out is taken as a fraction of the largest overall range in a given load sequence. Fractions are selected depending on the extent to which one wishes to condense a sequence. The method was originally developed for use in making crack initiation predictions, where long-life damage, D, varies with stress range, ΔS, to a high power, for example,

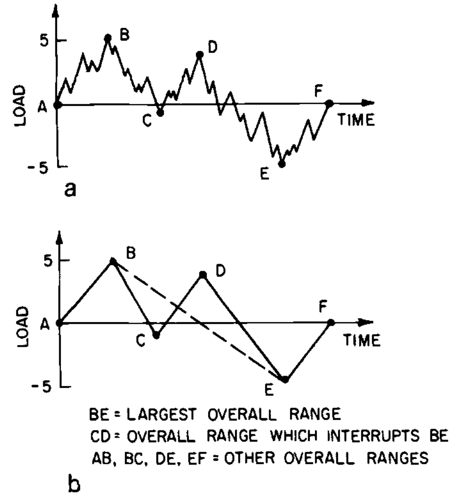

FIG. 4—*Selection of overall ranges in an irregular load sequence (*a*), screening out smaller interrupting ranges which are less than 40 percent of the largest overall range; (*b*) corresponding condensed sequence.*

$D \propto (\Delta S)^{10}$, and thus the damage of smaller ranges relative to larger overall ranges could be neglected in most cases without undue loss of accuracy. For crack propagation, damage usually varies with stress intensity range to a lower power, for example, $D \propto \Delta a/\Delta N \propto (\Delta K)^3$, and thus smaller ranges are relatively more damaging than their counterparts for long-life crack initiation. However, the use of condensed load blocks may still offer substantial savings of test and computing time for crack propagation studies without an unreasonable sacrifice of accuracy, especially in view of such uncertainties as scatter in experimental data, approximate knowledge of stress intensity factors for complex geometries and real flaws, etc.

A second purpose of using condensed load blocks was to investigate how crack growth, calculated on the basis of overall ranges, would compare to that calculated range-by-range (for every range), as done with Method I*a* (see Fig. 5).

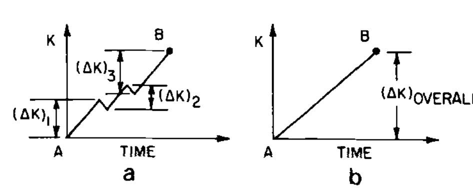

FIG. 5—*Range-by-range (*a*) and overall range (*b*) methods of calculating crack growth, which poses the question of how crack growth due to $(\Delta K)_1$, $(\Delta K)_2$, and $(\Delta K)_3$ compares to that for $(\Delta K)_{overall}$.*

Prediction Method II

This prediction method uses the ΔK_{eff} term in Eq 4 to account for the following possible load sequence effects: (*a*) crack retardation, (*b*) the decrease of retardation by sufficiently large compressive overloads, and (*c*) the acceleration of crack growth rate by gross yielding in compression (but not in tension).

The general philosophy of using ΔK_{eff} to account for such effects is illustrated in Fig. 6. The ΔK_{eff} for the cycles from Points A to B is that which

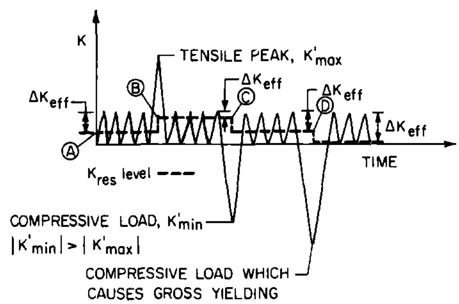

FIG. 6—*Illustration of the use of an effective stress intensity range concept to account for various sequence effects in a simple variable-amplitude loading.*

would normally be active in the absence of large tensile or compressive overloads. At Point B, a large tensile peak occurs, causing the K_{res} level to increase to $q(K'_{max} - \Delta K_{th})$. As a simplification, the effects of "delay and decay" of retardation [*13,28,29*] are not shown. The ΔK_{eff} for the cycles from Points B to C is reduced, producing retarded crack growth for these cycles.

At Point C, a large compressive load is applied. Based on test results [*14–17*] mentioned earlier which show that compressive overloads tend to eliminate crack retardation, the K_{res} level is returned to the normal level associated with the next loading, which in this case happens to be the same as that at Point A. Retarded crack growth ceases, and the growth rate is returned to normal values. In this work, any compressive load greater than or equal to a previous tensile overload was assumed to destroy the retarding effect of the tensile overload.

At Point D, a compressive overload large enough to cause gross yielding in compression occurs. To try to account for the increase in growth rate which is likely to result from such yielding, the K_{res} level is reduced to zero, increasing ΔK_{eff} (as long as a crack tip is within the compressively yielded zone). Recent X-ray diffraction measurements [*37*] have shown that the usual compressive residual stresses in front of a crack tip are eliminated in a specimen subjected to gross yielding in compression. Without such residual stresses to exert a clamping influence on a growing crack, growth rate should be accelerated in accordance with crack closure concepts. Note that throughout all of this, the assumption that compressive loadings do not cause growth directly is maintained. It is proposed, however, that large compressive loadings may greatly influence the ability of tensile loadings to cause growth through the mechanism of residual stresses.

The ΔK_{eff} term could also be used to try to account for the acceleration of crack growth due solely to the application of compressive overloads even in the absence of gross yielding. However, this was not done here because other effects seemed to be much stronger in the given load histories.

Since tensile peaks are so closely spaced in the load blocks considered here and since the blocks are applied repeatedly in testing, it was assumed, as a further simplification, that the highest tensile peak in each block would establish a $K'_{res} = q(K'_{max} - \Delta K_{th})$, where K'_{max} and K'_{res} are the applied and "residual" stress intensities associated with the highest peak. As noted previously, two values of q, 0.35 and 0.50, were used to see the effect on predictions. As another simplification, since large compressive loads occur frequently in the load blocks, it was assumed that K'_{res} due to the highest tensile peak would be eliminated if $|K'_{min}|$ was greater than $|K'_{max}|$, where K'_{min} is a "stress intensity" associated with the largest compressive load in a block.

The effect of gross yielding in compression was taken into account as follows. The elastic compressive stress distribution in the modified compact tension specimen, based on simple beam theory and as determined by finite elements, is shown in Fig. 7 for the case of −40.0 kN loading with Man-Ten. Under

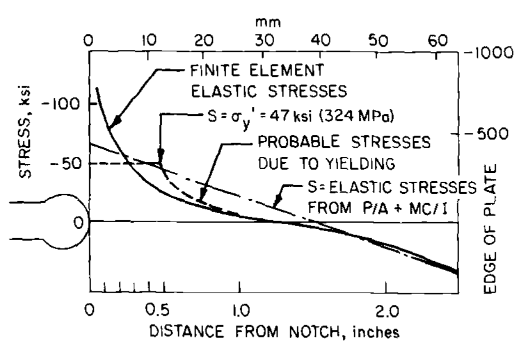

FIG. 7—*Finite element and simple beam theory estimates of elastic stresses in the modified compact tension specimen plus an estimate of the yield zone size in compression for Man-Ten at −9.0 kips (−40.0 kN) load level.*

compression, it was assumed that a crack closes completely and that the specimen behaves as if no crack were present. It was further assumed that if for any crack length, the nominal, elastic compressive stress at the crack tip, S (based on simple beam theory), exceeded the cyclic yield strength, then K_{res} would drop to zero, producing accelerated growth. This assumption gives only a rough approximation to the size of the zone of gross yielding in compression for this specimen, but it is suitable for exploratory purposes. When the crack tip grows out of the influence of this zone, K_{res} is returned to the normal level associated with the next loading.

No crack growth was calculated, of course, for load ranges with ΔK_{eff} less than ΔK_{th}. Predictions were made only for full load blocks, as with Method I*a*.

Comparison of Predictions with Test Results for Irregular Loadings

Predictions were made only for those tests in which gross yielding in tension did not occur so as not to violate the usual limits of applicability of linear elastic fracture mechanics upon which the prediction methods are based. All predictions were based on growth from an initial crack length of 33 mm.

Predictions at various extreme load levels are compared with average test life to fracture in Table 2. To save space, only plots of crack growth versus blocks for selected cases are shown in Figs. 8 through 12.

Transmission (Axle) Load History

Predictions were made at extreme load levels of +15.6 and +35.6 kN for Man-Ten and at +35.6 kN for RQC-100.

Method I*a* predictions are overly conservative for the Man-Ten tests for both ΔK_{th} values but are well within a factor of two of average test life. Figure 8 illustrates this for the +15.6 kN extreme load level. On the other hand, Method I*a* predictions are exceptionally good for the RQC-100 test.

Method I*b* predictions are in excellent agreement with test data for the Man-Ten tests. As shown in Fig. 8, predictions are within experimental scatter and are also relatively insensitive to ΔK_{th} at the +15.6 kN extreme load level (which is not the case for Method I*a*). For RQC-100, Method I*b* predictions fail to account for enough growth yet are still within a factor of two of average test life.

Method II predictions with $q = 0.35$ "bracket" experimental scatter for the two ΔK_{th} values, as shown in Fig. 9 for Man-Ten at +15.6 kN extreme load level. The prediction with $q = 0.50$ and $\Delta K_{th} = 5.5$ MPa$\sqrt{m}$ is within experimental scatter while that with $\Delta K_{th} = 11.0$ MPa$\sqrt{m}$ is nonconservative by about a factor of two. For Man-Ten with +35.6 kN extreme load level, Method II predictions with $q = 0.35$ are overly conservative for both ΔK_{th} values, but are still within a factor of two of average test life. Predictions with $q = 0.50$ are within experimental scatter for both ΔK_{th} values. For RQC-100, Method II predictions with $q = 0.35$ are exceptionally good, while with $q = 0.50$, they fail to account for enough growth but are still within a factor of 1.4 of average test life.

Bracket Load History

Predictions were made for Man-Ten at extreme load levels of −13.4 and −15.6 kN, and for RQC-100 at −15.6 and −35.6 kN.

Method I*a* predictions are overly conservative for the Man-Ten tests for both ΔK_{th} values but are within a factor of two of average test life. Predictions based on this method are quite good for RQC-100 at −35.6 kN extreme load level, as

TABLE 2 – *Ratio of predicted to average test life.*

Load History		Transmission								Bracket								Suspension							
Prediction Method		Ia		Ib		II $q = 0.35$		II $q = 0.50$		Ia		Ib		II $q = 0.35$		II $q = 0.50$		Ia		Ib		II $q = 0.35$		II $q = 0.50$	
ΔK_{th}, ksi$\sqrt{in.}$ (MPa$\sqrt{m}$) / Extreme Load, kips (kN)		5 (5.5)	10 (11)	5 (5.5)	10 (11)	5 (5.5)	10 (11)	5 (5.5)	10 (11)	5 (5.5)	10 (11)	5 (5.5)	10 (11)	5 (5.5)	10 (11)	5 (5.5)	10 (11)	5 (5.5)	10 (11)	5 (5.5)	10 (11)	5 (5.5)	10 (11)	5 (5.5)	10 (11)
Man-Ten	3.0(13.4)	No Tests								0.45	0.80	0.90	1.10	0.40	0.90	0.40	0.90	No Crack Initiation							
	3.5(15.6)	0.65	0.90	1.05	1.05	0.80	1.40	1.20	2.10	0.50	0.70	0.95	1.05	0.45	0.65	0.45	0.65	No Tests							
	6.0(26.7)	No Tests								No Tests								1.55	2.00	2.35	3.00	1.40	2.00	1.40	2.00
	8.0(35.6)	0.60	0.60	0.90	0.90	0.60	0.60	0.85	0.85	No Predictions								No Tests							
	9.0(40.0)	No Tests								No Tests								8.5	9.4	13.2	14.6	4.6	5.7	3.4	4.2
RQC - 100	3.5(15.6)	No Crack Initiation								0.15	0.20	0.25	0.30	0.15	0.20	0.15	0.20	No Tests							
	6.0(26.7)	No Tests								No Tests								0.45	0.60	0.65	0.90	0.40	0.60	0.40	0.60
	7.0(31.2)	No Tests								No Tests								0.60	0.70	0.90	1.05	0.60	0.65	0.60	0.65
	8.0(35.6)	0.95	0.95	1.55	1.55	1.00	1.00	1.40	1.40	0.90	0.90	1.70	1.70	0.85	0.85	0.85	0.85	No Tests							
	9.0(40.0)	No Tests								No Tests								0.60	0.70	0.90	1.05	0.55	0.65	0.55	0.65
	16.0(71.2)	No Predictions								No Predictions								12.4	12.5	19.1	19.3	5.8	5.8	3.9	3.9

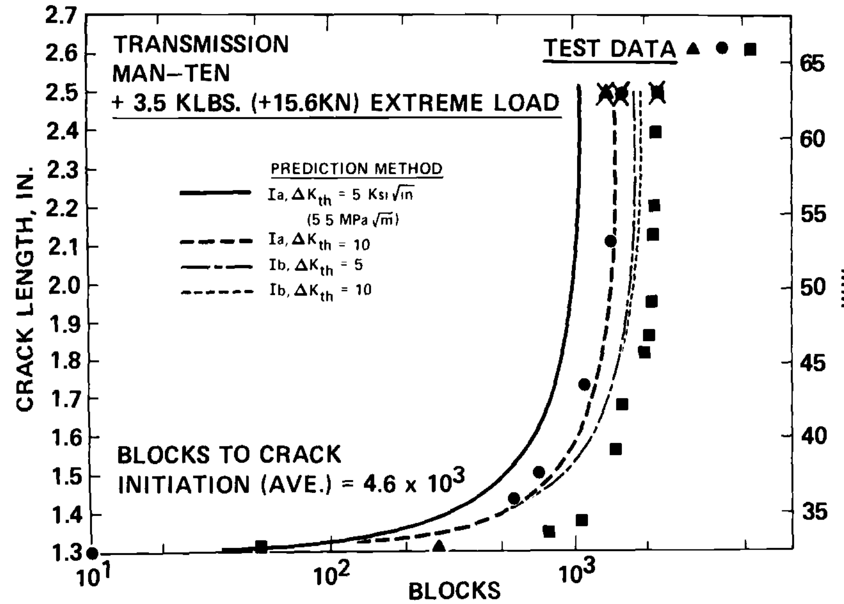

FIG. 8—*Comparison of Methods Ia and Ib predictions with test data for the transmission history with Man-Ten at +3.5 kips (+15.6 kN) extreme load level.*

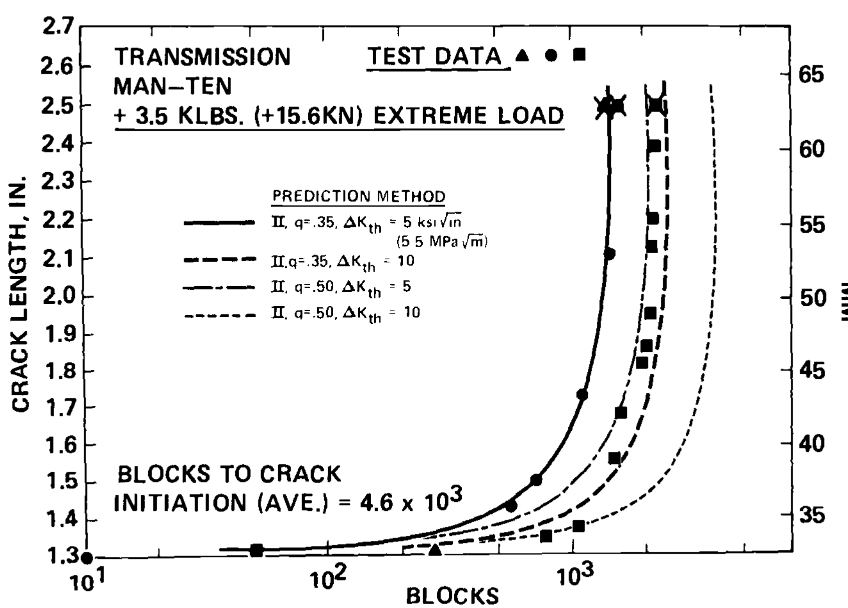

FIG. 9—*Comparison of Method II predictions with test data for the transmission history at +3.5 kips (+15.6 kN) extreme load level.*

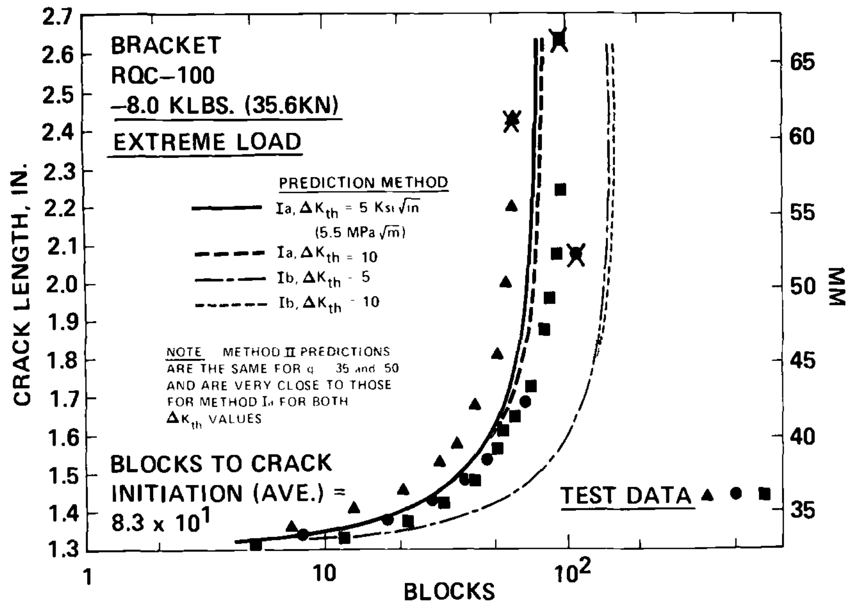

FIG. 10—*Comparison of Method Ia and Ib predictions with test data for the bracket history with RQC-100 at −8.0 kips (−35.6 kN) extreme load level.*

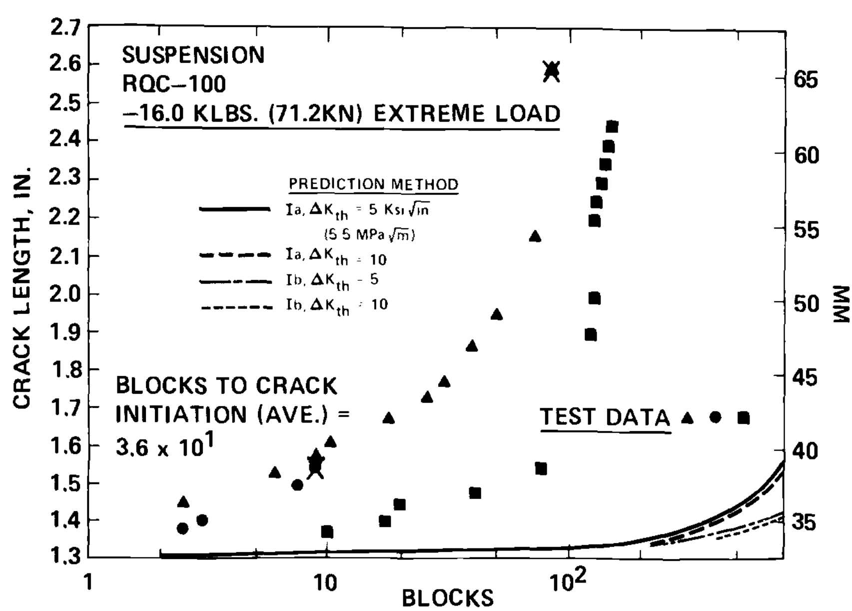

FIG. 11—*Comparison of Method Ia and Ib predictions with test data for the suspension history with RQC-100 at −16.0 kips (−71.2 kN) extreme load level.*

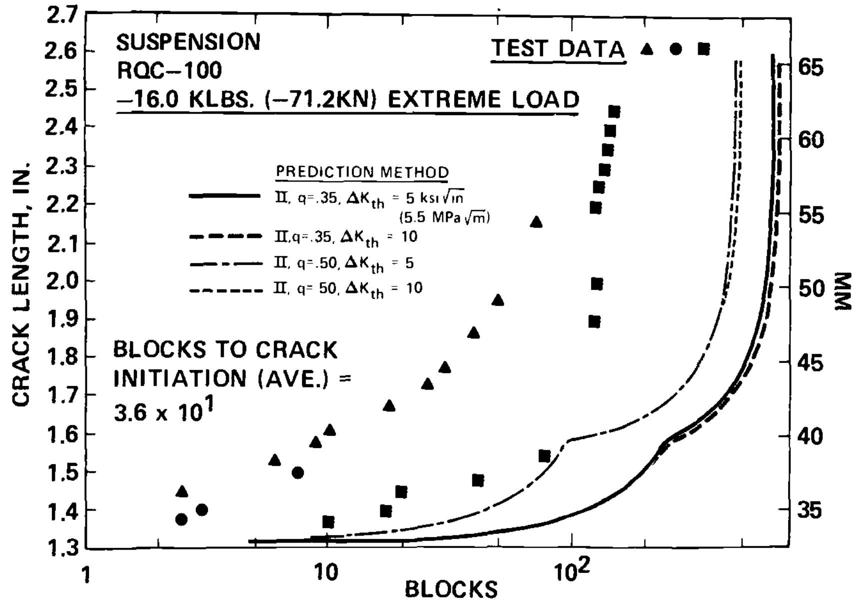

FIG. 12—*Comparison of Method II predictions with test data for the suspension history with RQC-100 at −16.0 kips (−71.2 kN) extreme load level.*

shown in Fig. 10; however, five to six times too much growth is calculated at the −15.6 kN extreme load level, depending on the ΔK_{th} value used.

Method I*b* predictions are in excellent agreement with the Man-Ten test results; however, for RQC-100 at the −35.6 kN extreme load level, they fail to account for enough growth, as shown in Fig. 10, but are still within a factor of two of average test life. Method I*b* predictions are somewhat better than those for I*a* at the −15.6 kN extreme load level with RQC-100 but are still three to four times too conservative.

Method II predictions are the same for $q = 0.35$ and 0.50 in all cases and are very close to those for Method I*a* for both ΔK_{th} values.

Suspension Load History

Predictions were made for Man-Ten at extreme load levels of −26.7 and −40.0 kN, and for RQC-100 at extreme load levels of −26.7, −31.2, −40.0, and −71.2 kN.

Method I*a* predictions fail to account for enough growth for the Man-Ten tests. For the −26.7 kN extreme load level, predictions are nonconservative by about a factor of two (in terms of total life). At the −40.0 kN extreme load level, predictions are nearly an order of magnitude nonconservative. In both cases, initial crack growth was more rapid than later growth. For the −26.7 kN extreme load level, growth from 33 to 36 mm took only about 400 blocks while that from 38 to 41 mm took about 3000 blocks. For the −40.0 kN extreme load level, growth from 33 to 38 mm took about 25 blocks, while that from 41 to 46 mm took about 200 blocks. The influence of compressive yielding at the notch may well be causing this initial accelerated growth. In contrast to the results for Man-Ten, Method I*a* predictions for RQC-100 tend to be overly conservative but are generally within a factor of two of average test life for the −26.7, −31.2, and −40.0 kN extreme load level tests. At −71.2 kN extreme load level, predictions fail to account for enough growth by over an order of magnitude, as shown in Fig. 11. In this case, as with the −40.0 kN test for Man-Ten, gross yielding in compression but not in tension occurred. Again, initial crack growth was accelerated.

Method I*b* predictions are even more nonconservative than those for Method I*a* for the Man-Ten tests and for the −71.2 extreme load level tests with RQC-100, as shown in Fig. 11. On the other hand, Method I*b* predictions agree better with test results for RQC-100 at −26.7, −31.2, and −40.0 kN extreme load levels.

Method II predictions are the same for $q = 0.35$ and 0.50 and agree very closely with Method I*a* predictions for all tests except those at extreme load levels of −40.0 kN for Man-Ten and −71.2 kN for RQC-100. In both cases, predictions based on this method try to account for the acceleration of crack growth due to gross yielding in compression. Method II predictions are clearly better than those for Method I, as shown in Fig. 12. However, they still fail to account for enough growth. The discontinuity in the crack growth prediction curves indicates the point where the effects of compressive yielding are predicted to cease. Note that if these effects were allowed to continue for another 3 mm or so beyond this point, which they actually may, then the predictions would agree quite well with total crack propagation life. However, they would still fail to account for enough of the initial accelerated growth.

Discussion

Predictions based on Methods I*a* or I*b* were almost always within a factor of two of average test life with the exceptions of the suspension load history when gross yielding in compression occured and the bracket history with RQC-100 at −15.6 kN extreme load level. Method I*b* predictions always accounted for less growth than those based on Method I*a*, but never by more than a factor of two. It is interesting to note that in many cases, predictions based on Method I*b* were in better agreement with test data than those based on Method I*a*, particularly for the transmission and bracket load histories with Man-Ten.

In general, reasonably good predictions could be obtained from a limited amount of $R = 0$, constant-amplitude $\Delta a/\Delta N$ versus ΔK data, and by estimating stress ratio effects and using assumed values of ΔK_{th}. This is significant for a realistic design situation where the use of incomplete data is often necessary.

Use of condensed histories offers several advantages: (*a*) substantial savings of test and computing time (in this case, a factor of ten reduction) may be achieved without undue loss of accuracy in view of experimental scatter, and (*b*) the effect of ΔK_{th} on predictions is minimized. Furthermore, condensed load blocks (by neglecting smaller load variations) are composed of overall ranges virtually all of which have $R \approx 0$. Thus, stress ratio data need not be known precisely to predict growth using condensed blocks. This point and Item *b* are significant because to determine ΔK_{th} and stress ratio effects for a particular metal involves considerable testing and expense.

The fact that Methods I*a* or I*b* produced fair predictions although they neglect load sequence effects suggests, of course, that the load histories considered here do not produce significant sequence effects. In addition, the assumption that only tensile loadings cause growth appears reasonable in all cases studied here with the notable exception of the suspension history tests when gross yielding in compression occurred.

The success of Methods I*a* and I*b*, which neglect the effects of load sequence, should be viewed with some caution. For load histories with occasional large overloads, tensile or compressive, they may produce overly conservative or dangerously nonconservative predictions.

Method II predictions are comparable to those for Method I for the transmission and bracket histories and are clearly superior for the suspension history when gross yielding in compression occurs.

The use of an effective stress intensity range concept to account for the acceleration of crack growth by sufficiently large compressive loading, especially that which causes gross yielding, has a worthwhile potential. It is consistent with crack closure concepts and experimental measurements of the destruction of compressive residual stresses at a crack tip by high compressive loadings, especially in lower yield strength metals.

Finally, the calculation of crack growth range-by-range compared to using overall ranges warrants further investigation. For example, tests should be conducted to see how crack growth for a load sequence such as that shown in Fig. 13*a* compares to that shown in Fig. 13*b*. Such test results would provide a good check on the suitability of crack propagation prediction methods for irregular loadings.

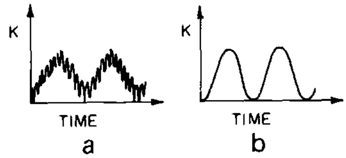

FIG. 13—*Two load sequences for which comparative crack growth tests should be conducted.*

Conclusions

1. For the load histories studied here, predictions based on Method I*a* (calculating growth range-by-range with full histories and using the Forman

relation) were within a factor of two of average crack propagation test life in nearly all cases and were always on the conservative side, with the notable exception of the suspension load history when gross yielding in compression occurred.

2. The use of condensed load histories with Method I*b* (calculating growth with overall ranges and neglecting smaller load variations) also produced comparably good predictions.

3. Predictions based on Method II, which tries to account for possible load sequence and stress ratio effects, were essentially the same as those for Method I*a* for the bracket and transmission histories but were considerably better for the suspension history when gross yielding in compression occurred.

Acknowledgments

Financial support from the Association of American Railroads, Deere & Company, and the National Science Foundation through the Stanford Center for Materials Research and the cooperation, encouragement, and advice of the members of the Fracture Mechanics Division of the SAE Fatigue Design and Evaluation Committee and of the reviewers of this paper are gratefully acknowledged.

References

[1] Katcher, M., *Engineering Fracture Mechanics*, Vol. 5, 1973, p. 793.

[2] Wheeler, O. E., *Journal of Basic Engineering, Transactions*, ASME, Vol. 94, Series D, No. 1, March 1972, p. 181.

[3] Willenborg, J., Engle, R. M., and Wood, H. A., "A Crack Growth Model Using an Effective Stress Intensity Concept," Technical Memorandum AFFDL-TM-73-137-FBR, Air Force Flight Dynamics Lab, Dayton, Ohio, 1971.

[4] Gallagher, J. P. and Stalnaker, H. D., "Methods for Analyzing Fatigue Crack Growth Rate Behavior Associated with Flight-by-Flight Loading," paper presented at the AIAA/ASME/SAE 15th Structures, Structural Dynamics and Materials Conference, Las Vegas, Nev., April 1974.

[5] Barsom, J. M. in *Progress in Flaw Growth and Fracture Toughness Testing, ASTM STP 536*, American Society for Testing and Materials, 1973, p. 147.

[6] Smith, S. H. in *Structural Fatigue in Aircraft, ASTM STP 404*, American Society for Testing and Materials, 1966, p. 74.

[7] Swanson, S. R., Cicci, F., and Hoppe, W. in *Fatigue Crack Propagation, ASTM STP 415*, American Society for Testing and Materials, 1967, p. 312.

[8] Endo, T., Mitsunaga, K., Takahashi, K., Kobayashi, K., and Matsuishi, M., "Damage Evaluation of Metals for Random or Varying Load," paper presented at the 1974 Symposium on Mechanical Behavior, Kyoto, Japan.

[9] Dowling, N. E., "Fatigue Failure Predictions for Complicated Stress-Strain Histories," Report No. 337, Department of Theoretical and Applied Mechanics, University of Illinois, Urbana, Ill., Jan. 1971.

[10] Schijve, J., "The Analysis of Random Load-Time Histories with Relation to Fatigue Tests and Life Calculations," *Fatigue of Aircraft Structures*, MacMillan Co., New York, 1963.

[11] Fuchs, H. O., Nelson, D. V., Burke, M. A., and Toomay, T. L., "Shortcuts in Cumulative Damage Analysis," Paper No. 730565, presented at the SAE Automobile Engineering Meeting, Detroit, Mich., May 1973.

[12] Nelson, D. V. and Fuchs, H. O., "Predictions of Cumulative Damage Using Condensed Load Histories," Paper No. 750045, presented at the SAE Automotive Engineering Congress and Exposition, Feb. 1975.

[13] Rice, R. C. and Stephens, R. I. in *Progress in Flaw Growth and Fracture Toughness Testing, ASTM STP 536*, American Society for Testing and Materials, 1973, p. 95.
[14] Hsu, T. M. and Lassiter, L. W. "Effects of Compressive Overloads on Fatigue Crack Growth," paper presented at the AIAA/ASME/SAE 15th Structures, Structural Dynamics and Materials Conference, Las Vegas, Nev., April 1974.
[15] Private communication, R. I. Stephens, Materials Engineering Division, University of Iowa, Iowa City, Iowa.
[16] Schijve, J., "Fatigue Crack Propagation in Light Alloy Sheet Material and Structures," Technical Report No. MP-195, National Aerospace Laboratory, The Netherlands, Aug. 1960.
[17] Wei, R. P., Shih, T. T., and Fitzgerald, J. H., "Load Interaction Effects on Fatigue Crack Growth in Ti-6Al-4V Alloy," NASA CR-2239, National Aeronautics and Space Administration, April 1973.
[18] Bussa, S. L. and Tucker, L. E., "The SAE Cumulative Fatigue Damage Test Program," Paper No. 750038, presented at the SAE Automotive Engineering Congress and Exposition, Detroit, Mich., Feb. 1975.
[19] Private communication, R. C. Rice, Battelle Memorial Institute, Columbus, Ohio.
[20] Srawley, J. E. and Gross, B., *Engineering Fracture Mechanics*, Vol. 4, 1972, p. 587.
[21] Private communication, D. R. Galliart, Materials Research, Deere & Company, Moline, Ill.
[22] Private communication, N. E. Dowling, Westinghouse Research Labs, Pittsburgh, Pa.
[23] Donahue, J., Clark, H. McI., Atanmo, P., Kumble, R., and McEvily, A., *International Journal of Fracture Mechanics*, Vol. 8, No. 2, June 1972, p. 209.
[24] Forman, R. G., Kearney, V. E., and Engle, R. M., *Journal of Basic Engineering, Transactions*, ASME, Vol. 89, Series D, No. 3, 1967, p. 459.
[25] Elber, W. in *Damage Tolerance in Aircraft Structures, ASTM STP 486*, American Society for Testing and Materials, 1971, p. 230.
[26] Newman, J. C., Jr., and Armen, H., Jr., "Elastic-Plastic Analysis of a Propagating Crack under Cyclic Loading," AIAA Paper No. 74-366, presented at the AIAA/ASME/SAE 15th Structures, Structural Dynamics and Materials Conference, Las Vegas, Nev., April 1974.
[27] Schijve, J., *The Accumulation of Fatigue Damage in Aircraft Materials and Structures*, AGARD-AG-157, NATO Advisory Group for Aerospace Research and Development, 1972, p. 75.
[28] Von Euw, E. F. J., Hertzberg, R. W., and Roberts, R. in *Stress Analysis and Growth of Cracks, ASTM STP 513*, American Society for Testing and Materials, 1973, p. 113.
[29] Gallagher, J. P. and Hughes, T. F., "Influence of Yield Strength on Overload Affected Fatigue Crack Growth Behavior in 4340 Steel," Technical Report AFFDL-TR-74-27, Air Force Flight Dynamics Lab, Dayton, Ohio, 1974.
[30] Corbly, D. M. and Packman, P. F., *Engineering Fracture Mechanics*, Vol. 5, 1973, p. 479.
[31] Trebules, V. W., Jr., Roberts, R., and Hertzberg, R. W. in *Progress in Flaw Growth and Fracture Toughness Testing, ASTM STP 536*, American Society for Testing and Materials, 1973, p. 113.
[32] Hudson, C. M. and Raju, K. N., "Investigation of Fatigue Crack Growth under Simple Variable Amplitude Loading," NASA TN D-5702, National Aeronautics and Space Administration, 1970.
[33] Jones, R. E., *Engineering Fracture Mechanics*, Vol. 5, 1973, p. 585.
[34] Hudson, C. M., "Effect of Stress Ratio on Fatigue Crack Growth in 7075-T6 and 2024-T3 Aluminum Alloy Specimens," NASA TN D-5390, National Aeronautics and Space Administration, 1969.
[35] Fitzgerald, J. H. and Wei, R. P., *Journal of Testing and Evaluation*, Vol. 2, No. 2, March 1974, p. 67.
[36] McMillan, J. C. and Pelloux, R. M. N. in *Fatigue Crack Propagation, ASTM STP 415*, American Society for Testing and Materials, 1967, p. 505.
[37] X-Ray Diffraction Division, SAE Fatigue Design and Evaluation Committee, unpublished test results, April 1974.

DISCUSSION

C. E. Richards[1] *(written discussion)*–I have three questions or discussion points concerning this paper.

1. Following our work which is presented in this symposium (P. J. Bernard, T. C. Lindley, and C. E. Richards), I would suggest that we would require at least two empirical laws for irregular loading–one for plane stress and one for plane strain conditions. Conditions between these extremes would require even more complex combinations of these expressions.

2. Concerning the assumption in Nelson and Fuchs' analysis that only the rising load is the only important part of the fatigue cycle, Laird has presented a model where both the rising and falling parts of the fatigue cycle are important to fatigue crack growth.

3. I do not see how one can argue that crack closure can completely explain the large effect of R ratio ($\sigma_{min}/\sigma_{max}$) on threshold values of ΔK for fatigue crack growth, ΔK_0, when it has been shown that environment can have such a large influence on ΔK_0. For instance, by testing in vacuo, it has been shown that under these circumstances R ratio has little or no effect on ΔK_0 (C. J. Beeves et al at Birmingham University, Dept. of Physical Metallurgy and Science of Materials, England).

D. V. Nelson and H. O. Fuchs (authors' closure)–In this paper, we have presented several methods of crack growth prediction for review and improvement by others. We appreciate the comments of the discussers. We are aiming at a method which can be used in design and which must therefore neglect some effects in order to remain reasonably simple.

Regarding Dr. Richards' first point of discussion, we agree that crack growth and load sequence effects such as retardation will vary under different types of multi-axial stress or strain. Plane stress and plane strain are, or course, merely special cases of multi-axial stress or strain which happen to be more convenient for analysis. In our paper we avoided much of this problem by making predictions based on constant-amplitude test data from specimens with the same degree and pattern of multi-axiality. The prediction of crack growth for specimens of varying thickness or subject to more general multi-axial loading conditions is a topic for future studies.

Regarding the second point of discussion, we note that in Laird's model,[2] both the rising and falling parts of a cycle are important, but in very different ways. New crack surfaces are created during the rising part; crack tip

[1] Central Electricity Research Laboratories, Leatherhead, Surrey, England.

[2] Laird, C. in *Fatigue Crack Propagation, ASTM STP 415*, American Society for Testing and Materials, 1967, p. 131.

re-sharpening occurs during the falling part. We believe that increments of crack extension are best related to the ΔK values associated with rising load ranges. Re-sharpening may well influence subsequent growth; the effect of the falling range is implied in the use of ΔK instead of K_{max}.

In response to the third point, we note that the crack closure concept has been used previously as a possible explanation for the effect of R-ratio on threshold stress intensity range for tests conducted in air.[3] We appreciate Dr. Richards' reminder that environment often has an important effect on crack growth behavior. We believe that crack closure is a very useful concept but do not want to imply that it can explain all effects observed under different environmental conditions.

C. C. Osgood[4] *(written discussion)*—These methods appear to predict life with reasonable conservatism for the cases considered, but with one notable exception: that wherein the mean stress was at a significant level in compression. This condition, together with the lack of recognition of compressive applied stress by the methods would seemingly lead to over-prediction, the severity of which may be related to the ratio of the total compression to the residual compression left after the previous tension.

The difference in responses of Man-Ten and of RQC-100 may be partially explained by Figs. 14 and 15 which show the difference in initiation time (or blocks) for the two steels. The rather high ordinate location of most of the

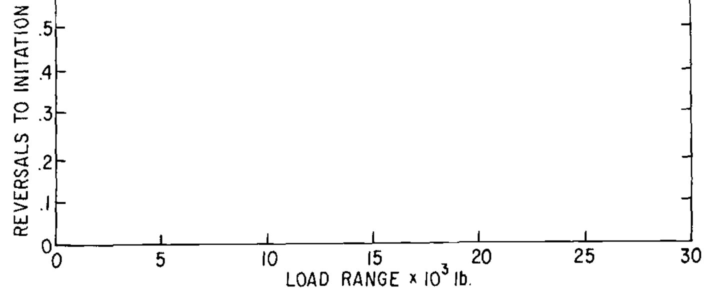

FIG. 14—*Ratio of initiation to total reversals versus load range at constant amplitude.*

[3] Schmidt, R. A. and Paris, P. C. in *Progress in Flaw Growth and Fracture Toughness Testing, ASTM STP 536*, American Society for Testing and Materials, 1973, p. 79.

[4] Forrestal Labs, Princeton University, Princeton, N. J. 08540.

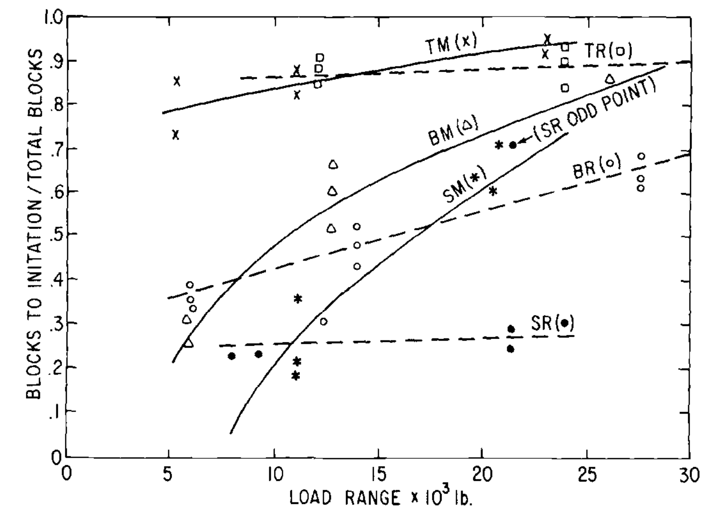

FIG. 15–*Ratio of initiation to total blocks versus load range at variable amplitude.*

curves indicates that the crack length of 0.1 in. (originally defined as "initiation") is itself too long with respect to the crack length at failure.

D. V. Nelson and H. O. Fuchs (authors' closure)–Dr. Osgood's plots of crack initiation blocks divided by total blocks to fracture shown in Figs. 14 and 15 are most interesting. They put into perspective the relative amount of life spent in crack propagation versus initiation (for a "transition" crack length of 0.25 mm (0.1 in.)), which is significant for design purposes.

The question: "When has a crack been initiated and starts to propagate?" has often been asked but has not been discussed in the literature. We propose the following operational definition: "A crack has completed its initiation and begun its propagation when the damage per cycle or per block calculated from the local shear stress ranges at a notch (based on the stress distribution in the uncracked part) becomes less than the damage calculated from stress intensity ranges (based on crack length and nominal stresses)." The influence of residual stresses must be included in both sets of computations.

Figures 16 and 17 illustrate this definition and show that the "transition" crack length will depend on load level, stress ratio, notch stress gradient, material, and size of the part. In these figures, damage per cycle or block is taken as $(1/N_f)$ for the crack initiation (I) curves, and as $(\Delta a/W\ \Delta N)$ for the propagation (P) curves, where N_f is the life to failure at the calculated local stress range, a is crack length, W is the width of the part, and N is the number of cycles. In Fig. 16, the indices 1, 2, and 3 indicate three levels of loading, with 1 being the lowest and 3 the highest. For crack propagation, damage increases with load and crack length; for initiation, damage is proportional to another power of load (a higher power at long life, a lower power at short life) and usually decreases with crack length because of the notch stress gradient. For the curves assumed in Fig. 16, the "transition" crack length is greater for higher loads.

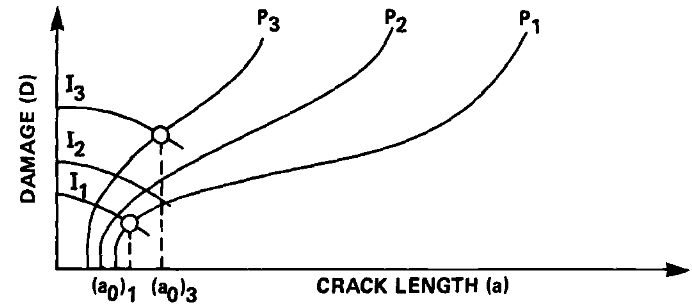

FIG. 16—*Schematic of the variation of crack initiation (I) damage and propagation (P) damage with crack length and load level for a notched part.*

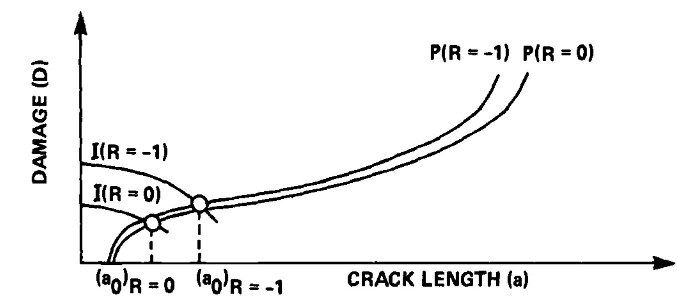

FIG. 17—*Schematic of the variation of crack initiation (I) damage and propagation (P) damage with crack length and stress ratio at a given maximum load level for a notched part.*

Figure 17 shows how the "transition" length would vary for a given maximum load at stress ratios of $R = -1$ (fully-reversed loading) and $R = 0$ (fluctuating tension). The propagation damage is only slightly larger at $R = -1$ than at $R = 0$. In this case, the "transition" length would be larger for $R = -1$ than $R = 0$ loading.

If a complete, correct theory of fatigue were available, we would not be concerned with a "transition" from crack initiation to propagation. Infinitesimal cracks on smooth parts and the local progress of fatigue damage at the tip of larger cracks would be considered in one complete formulation. Due to our current ignorance and because of greater convenience, we use two distinct theories. In the early stages of fatigue, we consider primarily the effect of local shear stresses at a notch root and compute damage from smooth specimen test data. In the later stages, we consider mainly the tensile stress field in the vicinity of a crack tip and compute damage from crack growth rate test data. This approach has worked quite well here for the bracket and transmission load histories, using a somewhat arbitrary "transition" crack length of 2.5 mm (0.1 in.). We doubt that calculations with another "transition" length would improve the results noticeably.

For the suspension history, we agree that improvements in our prediction methods are desirable. We did recognize the effect of gross yielding in compression in Method II and thus arrived at better predictions, but additional work is needed to achieve more reliable predictions when the influence of compressive loading is significant.

S. R. Varanasi[1] *and I. C. Whittaker*[1]

Structural Reliability Prediction Method Considering Crack Growth and Residual Strength

REFERENCE: Varanasi, S. R. and Whittaker, I. C., "**Structural Reliability Prediction Method Considering Crack Growth and Residual Strength,**" *Fatigue Crack Growth Under Spectrum Loads, ASTM STP 595*, American Society for Testing and Materials, 1976, pp. 292–305.

ABSTRACT: An analysis method to estimate structural reliability based on crack growth and residual strength of aircraft structures is presented. The method is based on linear elastic fracture mechanics theory and allows for the variability of crack initiation and growth found in the experimental data of various metals. At a reference stress intensity factor, the central tendency and the variance values of material crack-growth parameters are determined. Combinations of these parameters are selected by Monte Carlo simulation techniques, and are used to describe the characteristically stochastic behavior of crack growth in a material. This description of material crack-growth behavior is then applied to the typical case of the built-up skin-stringer configuration of fail-safe type airplane structures to predict the number and size of cracks in a fleet at any time during its life. Thus, inspection routines may be established based on realistic fleet performance, to provide suitable levels of structural reliability for a fleet of airplanes during its operational lifetime.

KEY WORDS: crack propagation, fatigue (materials), predictions, analyzing, residual stress, aircraft, structural analysis, fleet reliability

The integrity of aircraft structures had been considered, originally, to be a function only of the demonstrated static strength. Recently, the emphasis has changed to include fatigue evaluation techniques and damage tolerance methods as part of the structural integrity task.

Application of these differing technologies often results in inconsistent requirements which are resolved by arbitrary procedures. To rationalize the influence of these requirements on design, a study [*1,2*] [2] was accomplished on the interaction of static strength, fatigue damage initiation and crack growth, residual strength, and the environmental load exposure. This paper extends the analysis model [*1,2*] by utilizing a realistic airplane structural configuration for crack growth and residual strength calculations. The resultant analysis scheme provides a methodology to evaluate or weigh the design and operational

[1] Specialist engineers, Stress and Fatigue Research Group, Boeing Commercial Airplane Company, Seattle, Wash. 98124.

[2] The italic numbers in brackets refer to the list of references appended to this paper.

parameters of a modern aircraft structure. This analysis involves the modeling of the material and structural characteristics in the presence of a fatigue crack, and the modeling of procedures for inspecting the structure for possible damage. Thus, this modeling of the complex interaction of material characteristics, structural design configuration, operational load exposure, and operational inspection provides a measure of the reliability of a structure at any time.

The results of some exploratory parametric studies using this reliability analysis system are presented to illustrate some of these interactions.

Analytical Development

This analysis model presumes that a fatigue crack will initiate in some critical piece of structure due to a spectrum of loads through service usage. The crack will propagate at a rate dependent on the material, structural geometry, and applied loads, until it is either detected during an inspection, or is arrested by some design feature, or the structure fails.

Thus, the essential elements of a structural reliability analysis system are:

1. A crack initiation and growth model to calculate the time to crack initiation and subsequent growth to a critical size for a realistic structural configuration.
2. A residual strength model to calculate the strength of the structure in the presence of a crack of a given length.
3. A structural inspection and crack detection model which calculates the probability of detecting a crack and repairing it during a scheduled inspection.
4. A loading model which calculates the probability of a load, which is greater than or equal to the strength of the structure, occurring within some particular time.

The residual strength of structure diminishes as the crack grows, but the chance of detection improves with increase in crack size. This dependency of residual strength and inspection functions on crack size places considerable emphasis on the utilization of a crack-growth model in the reliability analysis.

Crack Growth Model

A model of crack development must consider crack initiation and growth to critical size. The time to initiation will be different for each structure, even though nominally identical structures of the same material are subjected to the same applied loads. Despite the use of very sensitive detection methods, the fatigue crack is known to have proceeded through an incubation phase and a physically ascertainable growth even before it reaches detectable size. Thus, a practical assumption of initial crack size includes the incubation and stress intensity threshold crack-growth phases. In this paper a crack is said to be initiated whenever it reaches a size which can be detected.

Following the lead of Refs *3* and *4*, it is assumed the crack initiation life to detectable size is a random variable N_0 with an extreme value distribution, namely, a two-parameter Weibull distribution with given characteristic life β and shape parameter α

$$N_0 \sim \mathrm{W}(\alpha,\beta)$$

Linear fracture mechanics theory is applied in the crack-growth phase following initiation. For the sake of simplicity, a constant-amplitude crack-growth model relating the crack-growth rate, $\Delta a/\Delta N$, to the stress intensity factor, K, by a power law is assumed

$$\Delta a/\Delta N = A\,K^n \tag{1}$$

In Eq 1, the proportionality constant, A, and the exponent, n, are determined from crack-growth tests of simple specimens of a material. Test data indicates that the values of A and n exhibit variability between identical specimens of the same material. For convenience, the crack-growth Eq 1 is expressed as

$$\log \Delta a/\Delta N = \log A + n \log K \tag{2}$$

Literature [5,6] provides information on typical observed values for the material constants in Eq 2. Figure 1 illustrates the variability of observed values

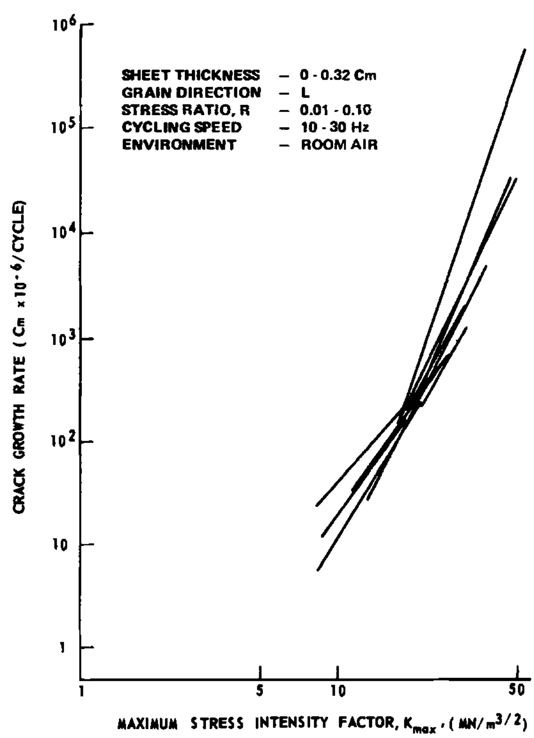

FIG. 1—*Fatigue crack growth behavior of 2024-T3 bare aluminum alloy sheet.*

in similar specimens for the two parameters–the slope, n, and the intercept, log A. In order to determine empirically the stochastic relationship between these two parameters, it may be observed that Fig. 1 shows the representative data in the form

$$y = d + nx \tag{3}$$

where

$$y = \log \Delta a/\Delta N, x = \log K, \text{ and } d = \log A$$

If K_R denotes a material reference stress intensity factor, and $\kappa = \log K_R$, it may be seen from Fig. 1 that, about this reference value, there is a variation in the slope, that is, the exponent, n, and a small varaiation in the growth rate. This is illustrated schematically in Fig. 2. This variation in slope and growth rate may

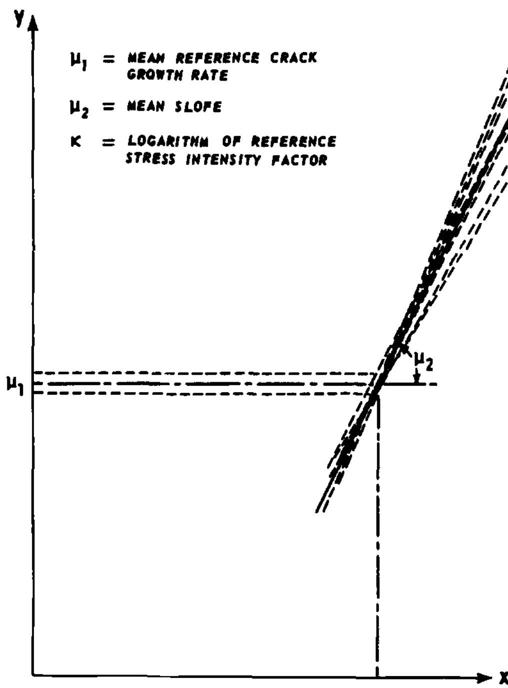

FIG. 2–*Schematic of crack-growth simulation.*

be expressed, using capital letters to denote random variables, as

$$y = D + \Lambda(x - \kappa) \tag{4}$$

where D and Λ are jointly determined once measurements are made on a test specimen. Over the population of such specimens, these values would have a distribution which is presently unknown. Presuming this stochastic variability to be the result of multitudinal influences makes the assumption of normal distribution plausible. These are specified as

$$D \sim N(\mu_1, \sigma_1{}^2)$$

$$\Lambda \sim N(\mu_2, \sigma_2{}^2)$$

Here the parameters governing the distributions of D and Λ, namely the mean, μ, and the variance, σ^2, are chosen to simulate the crack-growth behavior observed experimentally. Use of Eqs 1 and 4 results in

$$A = \frac{10^D}{K_R{}^\Lambda} \tag{5}$$

$$n = \Lambda$$

which define the material crack-growth behavior completely.

This description of material crack-growth behavior is then applied to the typical case of the built-up skin stringer configuration of a fail-safe type airplane structure. This is done by considering a stiffened sheet with riveted and uniformly-spaced stringers, containing a symmetrical crack centered at a stringer. The stiffened sheet is subjected to a remote applied stress, S, normal to the length of the crack (Fig. 3). The stress factor for the stiffened sheet is

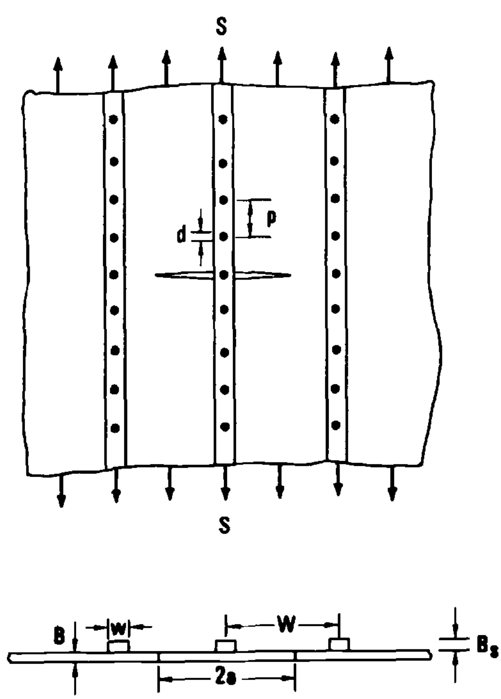

FIG. 3—*Stiffened sheet with uniformly-spaced stringers and a stringer-centered crack.*

calculated by superimposing stress intensity factors for the fastener forces and the remotely applied stress [7,8]. The effects of parameters such as stiffener spacing and stiffening amount, fastener spacing, size and flexibility, and crack length on the stress intensity factor of a stiffened sheet is given conveniently by a stress intensity correction factor γ. This factor is defined to be the ratio of stress intensity factors of the cracked sheet with and without the stringers.

Thus, with the generation of three random variables N_0, D, and Λ from their respective distributions and the calculation of the structural stress intensity factor, it is possible to compute the crack growth simulating one structure's life.

Residual Strength Model

It is presumed that the strength of a structure remains constant until the initiation of a fatigue crack. As the crack propagates, the residual strength of the cracked component diminishes until the structure fails under the applied load. Current structural design philosophy emphasizes the fail-safe approach, where materials with slow crack-growth rates and good fracture properties are often used in conjunction with positive crack stoppers. Crack stoppers provide a means of arresting the crack at some predetermined fail-safe length, say a_1. Thus, the fail-safe length defines the lower limit of the residual strength (fail-safe residual strength). This fail-safe residual strength is a design constraint; it is usually substantiated by test or analysis or both; and it is available, therefore, as an input parameter for this analysis procedure.

There is a critical value of the stress intensity factor, usually labeled K_c for plane stress conditions, which defines the critical crack length, a_c, for a specified loading condition. This length is essentially a material parameter and for a single-element, monolithic type structure, it defines the fail-safe length. In the case of built-up, skin-stiffener type airplane structure, the critical crack length is generally considered to be only a function of the skin material and load. However, the fail-safe length is also a function of the structural geometry, the location of tear-straps, or other similar crack stopping devices. Using considerations such as these, the following residual strength model is proposed.

Let $L(a)$ be the residual strength of some structure containing a fatigue crack of length a. The original strength of the structure is assumed to remain constant until the initiation of a crack of length a_0.

Therefore let

$$L(a) = \delta_u \text{ for } a \leq a_0 \tag{6}$$

$$L(a) = \delta \text{ for } a = \min(a_c, a_l)$$

where δ_u is the ultimate strength parameter, δ is the fail-safe residual strength parameter, a_c is material critical crack length, and a_l is fail-safe length. These strength design parameters are usually related to the design limit strength of the structure, δ_ℓ, as follows

$$0 < \delta < \delta_\ell < \delta_u$$

Furthermore, on current fail-safe airplane structures, typically: $\delta_u = 1.5\ \delta_\ell$. Taking into account the foregoing definitions, the residual strength of a structure containing a fatigue crack of length a, is given by

$$L(a) = \delta_u - \left\{K(a)/K_c\right\} \left\{\delta_u - \delta\right\} \quad \text{for } a > a_0 \tag{7}$$

Structural Reliability Model

Typical airplane operational procedures require the periodic examination of the structure as part of its structural integrity program. In the event that any damage is detected, the structure is repaired. Thus, the reliability of an airplane fleet, as a function of time, can be maintained at a high level. These operational variables of structural inspection and damage detection are considered, together with the structural performance variables of life to damage initiation, crack-growth, and corresponding residual strength degradation, in a developed reliability analysis system [*1,2*]. For the sake of conciseness, in this paper only the essential elements of this reliability analysis system are outlined as follows.

Reliability of a structure is defined to be one minus the probability of failure of a structure subjected to the imposed conditions of fatigue crack initiation and growth to critical size under a cumulative loading environment, periodic inspections, and repairs. Fleet reliability is defined to be the reliability of the weakest structure in the fleet and is given by the product of the individual reliabilities of structures in the fleet.

The probability of failure of a structure can be simply described as follows:

$$\left\{\begin{array}{l}\text{Probability of}\\ \text{failure of a}\\ \text{structure}\end{array}\right\} = 1 - \left\{\begin{array}{l}\text{Probability of}\\ \text{survival of a}\\ \text{structure when}\\ \text{a crack is}\\ \text{undetected}\end{array}\right\} - \left\{\begin{array}{l}\text{Probability of}\\ \text{detection and repair}\\ \text{of a structure before}\\ \text{failure}\end{array}\right\}$$

In other words, at anytime during a service interval between inspection periods, a structure has either failed or survived. Structural survival is due to one or the other of the following separate situations.

1. The structure survives because the strength of the structure in the presence of an undetected crack exceeds the imposed loads. The probability of structural survival in this situation is determined from load occurrence probability and residual strength of a structure.
2. The structure survives because the crack is detected and repaired before failure. The probability of structural survival in this situation is determined from a crack detection model which takes into account the variables such as crack length and quality of inspection.

Results

The results of some exploratory applications of the reliability analysis system are discussed in this section. Constant-amplitude, crack-growth test data are obtained for 2024-T3 bare aluminum alloy sheet specimens. For each specimen, a least square fit of a straight line relationship in log-log scale between the stress intensity factor and the crack-growth rate is obtained from the experimental crack size versus cyclic life data (Fig. 1). These fitted data are used to calculate the central tendency and variance values for the slope and intercept parameters of the crack-growth model described earlier. Monte Carlo simulation techniques have been utilized to select random combinations of these two parameters. Each combination of the parameters defines a simulated crack-growth relation for the material. Figure 4 shows a single set of simulated data and the bounds from

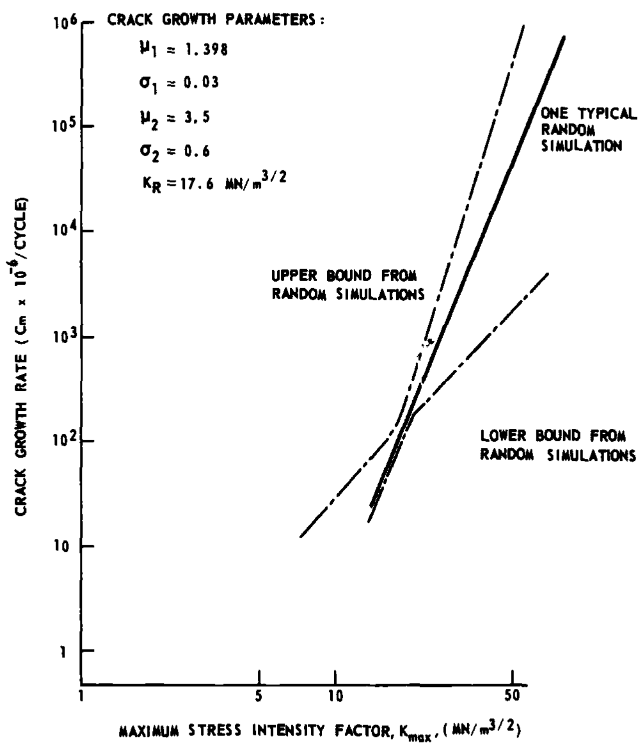

FIG. 4—*Simulation of 2024-T3 bare sheet crack-growth rate behavior.*

2000 such simulations, along with the central tendency and variance values for the two crack-growth parameters used in this simulation. A comparison of the results of Fig. 4 with those of Fig. 1 demonstrates quite clearly the realism of the crack-growth model.

The structural representation used in this analysis for a typical case of the built-up skin-stringer configuration of a fail-safe type airplane is that of a stiffened sheet with uniformly-spaced stringers, containing a crack centered at a stringer (Fig. 3). Typical values of the structural parameters such as stiffener size, spacing and stiffening amount, fastener spacing, and size are used in this example to calculate the stress intensity factor of this stiffened sheet. The fasteners attaching stringers to the sheet are assumed to be rigid for this analysis. However, provision is made in the analysis to include the effect of fastener flexibility on the stress intensity factor of a stiffened sheet. The results are shown in Fig. 5 where the stress intensity correction factor, γ, is plotted against

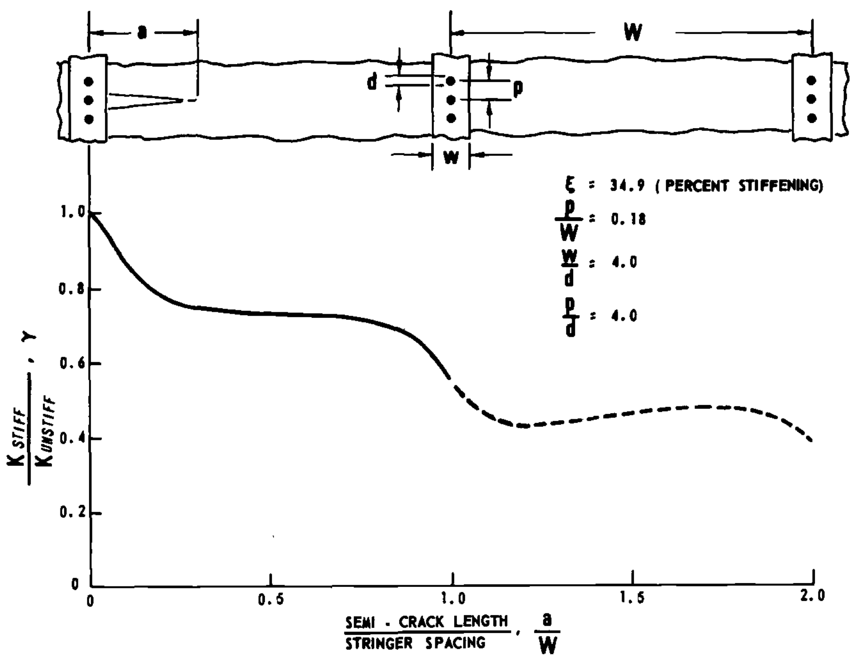

FIG. 5—*Stress intensity correction factor for a stiffened sheet.*

nondimensionalized crack length, for a symmetrical crack centered at a stringer. It can be seen from this figure that the effect of stringers is to lower the stress intensity factor for a stiffened sheet compared to an unstiffened sheet. The fail-safe crack length assumed here is 35.5 cm (a crack length spanning two-bays).

The interaction between the time to initiation of a detectable crack, the crack-growth, and residual strength models is illustrated in Fig. 6. The results shown here have been based on the assumptions that the characteristic life to a fatigue crack (0.25 cm in length) in a critical detail in the structure is 60 000 ground-air-ground cycles; the threshold size for crack detection is 0.08 cm; the maximum distance between positive crack stoppers is 35.5 cm; and the fail-safe residual strength of the structure containing a crack of this magnitude is 80 percent of the limit strength. It is further presumed that the structural material is 2024-T3 bare aluminum alloy with crack-growth parameters from Fig. 4 and a critical stress intensity factor, K_c, of 77 $MN/m^{3/2}$. Finally, the applied loads data are based on recorded velocity-acceleration-altitude (VGH) data from large

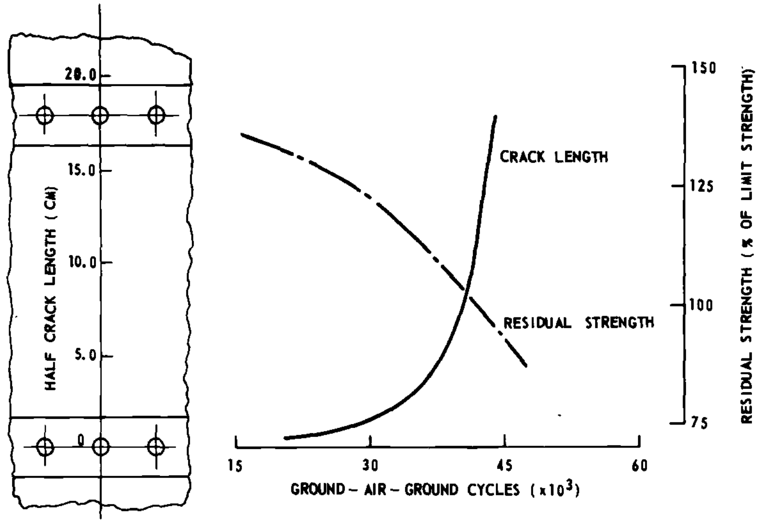

FIG. 6—*A simulation of structural crack growth and residual strength.*

jet transport airplanes [*2*]. Power spectral density techniques are used with these data to develop structural loading histories, both operational and extreme. The operational loads are used in the determination of the characteristic life to initiation, β, as well as the stress intensity factor for crack-growth. For the examples presented, the operational stress variation of 0–137.9 MN/m^2 is used. The extreme loads are used to determine the probability of an overload occurrence in the calculation of the probability of structural survival. Figure 6 shows an example of the crack propagation and residual strength values given by a single random simulation based on the hypothetical parameters just defined. This particular example was one of the more extreme cases, that is, early crack initiation life, selected from the very many simulations performed at each computation. It demonstrates how the life to detectable crack can be low despite the initial assumption of the 60 000 cycles characteristic life. This figure also helps to illustrate the cycle-dependent nature of both crack length and residual strength, with the former an increasing function and the latter a decreasing one.

Several parametric studies based on the previously discussed models in conjunction with the reliability analysis system [*1,2*] have been conducted, and some of the results are now presented to illustrate the scope of application. The baseline example case assumes a fleet of 300 structures of which one-quarter, namely, 75 structures, are examined at each of the inspection periods, which are scheduled at 7500 ground-air-ground cycle intervals, and repaired when found to be cracked.

The impact of characteristic initiation life on fleet reliability is shown in Fig. 7 where fleet reliability is plotted as a function of ground-air-ground cycles for three assumed characteristic initiation lives (β = 60 000, 30 000, and 1000) for a fail-safe type aircraft with a fail-safe residual strength equal to 80 percent of the limit strength. As would be expected, Fig. 7 shows that the fleet reliability decreases as the characteristic initiation life decreases. It may also be noted that

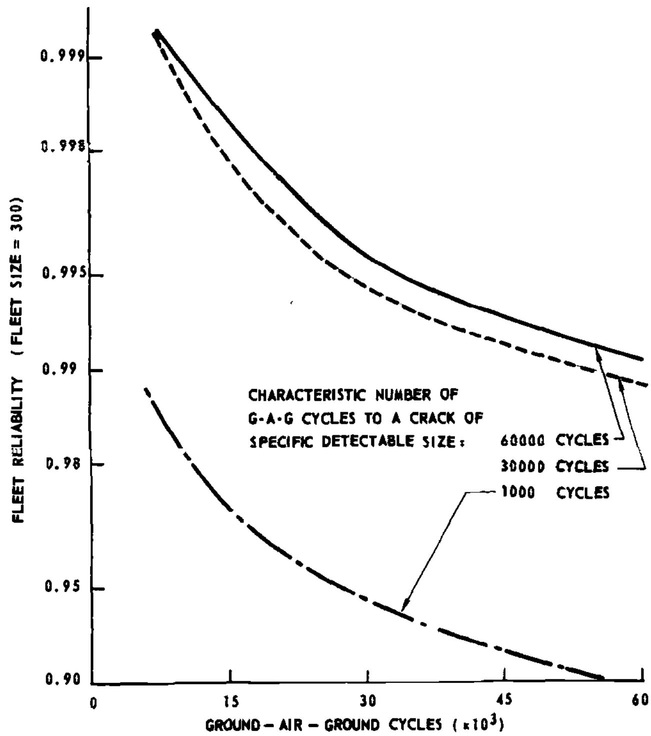

FIG. 7–*Effect of initiation life on fleet reliability.*

the fleet reliability does not drop to zero even with a low characteristic initiation life of 1000 cycles. This is due to the fact that although a majority of the airplanes in the fleet now develop cracks, the probability of detection and strength renewal at scheduled inspections is also higher. Furthermore, the residual strength of the cracked structure remains high due to fail-safe design.

The effect of fail-safe residual strength constraint on fleet reliability is shown in Figs. 8 and 9. Fail-safe residual strength is the strength of the structure when it contains a crack of fail-safe size (see prior discussion). Single load path, monolithic structures, without a similar provision for arresting a growing crack, are termed safe-life structures. These safe-life structures are not considered to possess any significant residual strength when fatigue crack reaches critical proportions. In this analysis, fail-safe type structures possess residual strength which is 80 percent of its limit strength. This represents a residual strength level which is common in current fail-safe airplane structural design. In contrast, the safe-life structure has been assumed to possess a residual strength which is 10 percent of its limit strength. The reliability of a safe-life structure designed to

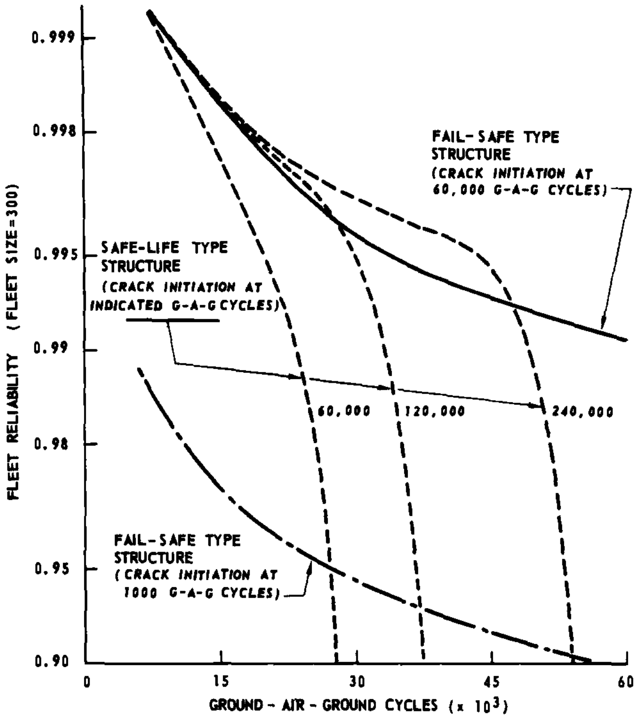

FIG. 8—*Effect of residual strength on fleet reliability.*

the same characteristic life to initiation as the fail-safe structure (60 000 ground-air-ground cycles) is presented in Fig. 8. To facilitate the comparison, some of the results for the fail-safe structure shown in Fig. 7 are repeated. It is clear from Fig. 8 that the reliability of the safe-life structure is much less than the equivalent fail-safe structure. However, safe-life reliability can be improved by increasing the characteristic life to initiation as illustrated.

The importance of the crack detection and residual strength parameters is clearly illustrated in Fig. 9. Here, all the cases illustrated are identical except for the particular variable noted against each case. A comparison has also been made between assumption of a stochastic behavior for crack-growth and the application of a discrete (average) crack-growth rate. It can be seen that in this example the fleet reliability based on the deterministic crack-growth behavior is optimistic. However, it is also clear that for the particular set of parameters assumed for these examples, the difference between the results of stochastic and discrete crack-growth rate assumptions is not large. It must be realized that as the input parameters vary, the influence of the stochastic crack-growth behavior on structural reliability can increase or diminish. For example, an assumed large value of characteristic life to initiation tends to reduce the importance of the crack-growth phase. As a result, the effect of crack-growth variability on structural reliability will be minimal.

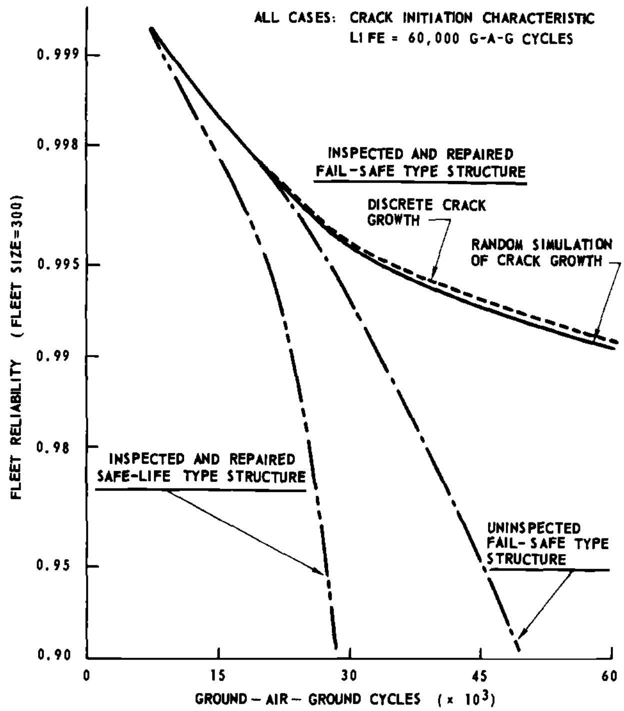

FIG. 9—*Effect of major parameters on fleet reliability.*

These few examples have been presented to illustrate how the crack initiation, growth, detection, and residual strength models, discussed earlier, can be applied in an analysis to determine the structural reliability of a fleet of airplanes. Although these examples have been presented against a quantitative background for clarity, their main intent is to demonstrate qualitatively the impact and interaction of the various elements on structural reliability.

Conclusions

The development of an interdisciplinary analysis system for calculating the structural reliability of a fleet of airplanes during its operational life has been discussed. This system has been applied to hypothetical, but plausible, examples to illustrate the impact of a few of the major elements on structural reliability. With the assumption of a reliability criterion, this system will allow an optimum selection of parameters which define structural material and configuration, crack initiation, crack-growth, and inspection frequency. Although the initial application of this system has been to airplane structures, it is anticipated that it can be extended with minor modifications to other structures which have similar design and operational characteristics.

References

[1] Whittaker, I. C. and Saunders, S. C., "Application of Reliability Analysis to Aircraft Structures Subject to Fatigue Crack Growth and Periodic Structural Inspection," AFML-TR-73-92, Air Force Materials Laboratory, Wright-Patterson AFB, Dayton, Ohio, 1973.

[2] Whittaker, I. C., and Saunders, S. C., "Exploratory Development on Application of Reliability Analysis to Aircraft Structures Considering Interaction of Cumulative Fatigue Damage and Ultimate Strength," AFML-TR-72-283, Air Force Materials Laboratory, Wright-Patterson AFB, Dayton, Ohio, 1973.

[3] Freudenthal, A. M., "Reliability Analysis Based on Time to the First Failure," 5th ICAF Symposium, Aircraft Fatigue Design and Operational Aspects, Melbourne, Australia, May 1967.

[4] Whittaker, I. C. and Besuner, P. M., "A Reliability Analysis Approach to Fatigue Life Variability of Aircraft Structures," AFML-TR-69-65, Air Force Materials Laboratory, Wright-Patterson AFB, Dayton, Ohio, 1969.

[5] Donaldson, D. R. and Anderson, W. E., "Crack Propagation Behavior of Some Airframe Materials," *Proceedings*, Crack Propagation Symposium, Cranfield, England, Sept. 1961.

[6] McEvily, A. J., Jr., and Illg, W., "The Rate of Crack Propagation in Two Aluminum Alloys," NACA Technical Note 4394, Sept. 1958.

[7] Poe, C. C., Jr., "Stress Intensity Factor for a Cracked Sheet with Riveted and Uniformly Spaced Stringers," NASA TR R-358, National Aeronautics and Space Administration, Washington, D. C., 1971.

[8] Varanasi, S. R. and Carlson, C. M., "CRISP–A Computer Program for the Analysis of Cracks in Stiffened Panels," The Boeing Commercial Airplane Company Document D6-41314, Feb. 1974.

H. D. Dill[1] *and C. R. Saff*[1]

Spectrum Crack Growth Prediction Method Based on Crack Surface Displacement and Contact Analyses

REFERENCE: Dill, H. D. and Saff, C. R., "Spectrum Crack Growth Prediction Method Based on Crack Surface Displacement and Contact Analyses," *Fatigue Crack Growth Under Spectrum Loads, ASTM STP 595*, American Society for Testing and Materials, 1976, pp. 306–319.

ABSTRACT: A method for prediction of crack growth behavior has been developed, based on evaluations of stress intensity caused by crack surface contact. The potential interference of the crack surfaces is determined from analyses of elastic displacements during loading and unloading and of the permanent deformation left in the wake of a growing crack. The potential interference is treated as a wedge acting behind the crack tip and the contact stresses created by this wedge are computed through an elastic-plastic analysis. The effective stress intensity range used for crack growth prediction is found by subtracting the stress intensity caused by these contact stresses from the applied stress intensity range. Comparisons of crack growth behavior predicted by this method and that measured in constant amplitude tests, with and without high loads, and in block spectrum tests have shown that the method accounts for load interaction effects in these cases. These effects include delayed retardation following high loads, crack growth acceleration during high loads, and dependence of growth rates on number of high loads.

KEY WORDS: crack propagation, fatigue (materials), stress analysis, predictions, loads (forces)

A method for prediction of crack growth behavior has been developed, based on analysis of crack surface contact stresses. Several experimental investigations [*1–8*][2] have indicated the existence of crack surface contact prior to complete unloading of the cracked material. Crack surface contact increases the minimum stress intensity range effective for propagating the crack. The concept of an effective stress intensity range influenced by crack surface contact is attractive as a basis for spectrum crack growth prediction since it qualitatively explains many observed load interaction effects. These effects include delayed retardation following high loads, crack growth acceleration during high loads, and dependence of growth rates on number of high loads.

This method of crack growth analysis is based on evaluations of stress intensity caused by crack surface contact. An analysis of crack surface

[1] Project strength engineer and strength engineer, respectively, McDonnell Aircraft Company, St. Louis, Mo. 63166.

[2] The italic numbers in brackets refer to the list of references appended to this paper.

displacements during loading and unloading is used to determine the permanent plastic deformation left in the wake of the growing crack. The potential interference of the crack surfaces is determined from an analysis of the interference free displacement remaining at minimum load, in conjunction with the analysis of the permanent deformations. The contact stresses behind the crack tip are found by treating the potential interference as a wedge between the surfaces and performing an elastic-plastic analysis of the stresses caused by this wedge. The effective stress intensity range used for crack growth prediction is found by subtracting the stress intensity caused by these contact stresses from the applied stress intensity range. Comparisons of crack growth behavior predicted by this method and that measured in constant amplitude tests, with and without high loads, and in block spectrum tests have shown that the method accounts for load interaction effects in these cases.

Crack Surface Displacement Analyses

An analysis method has been developed to determine displacements along the crack surfaces caused by loading and unloading during a single load cycle. The displacement analysis is based upon the Dugdale model [9] of the plastic zone, treating the plastic zone as an extension of the elastic crack surface over which a constant yield stress acts. The plastic zone size is determined to be that length of constant yield stress such that the stress intensity caused by the yield stress equals the applied stress intensity; hence there is no singularity at the extended tip. The crack surface displacement at K_{max} is found from the superposition of the Westergaard solution [10] for elastic displacement near the crack tip and the displacement due to the constant yield stress of the plastic zone [11,12]. The Westergaard solution for displacements under remote loading is shown in the upper portion of Fig. 1. The constant yield stress of the plastic zone tends to reduce the Westergaard displacement by the amount shown in the middle portion of Fig. 1. The resultant displacement is shown in the lower portion.

The displacements during unloading are similarly shown in Fig. 2. During unloading, the reversed plastic zone stress is increased to twice the yield stress used during loading, accounting for an elastic stress range equal to the difference of tensile and compressive yield stresses.

The crack surface displacements at the minimum applied load, shown in Fig. 3, are found by subtracting the displacements occurring during unloading from those at maximum load. Even when the minimum load is zero, the crack surface remains wedged open by the stress distributions within the plastic zone, when permanent plastic deformations caused by prior crack growth are not considered.

To qualitatively understand the residual plastic deformation left in the wake of a growing crack, consider a ligament of material ahead of the crack tip being traversed by a crack as in Fig. 4. The ligament accrues plastic deformation as it is encompassed by the plastic zone of the crack. As the crack tip passes through the ligament, the plastic deformation remains as a displacement of the crack

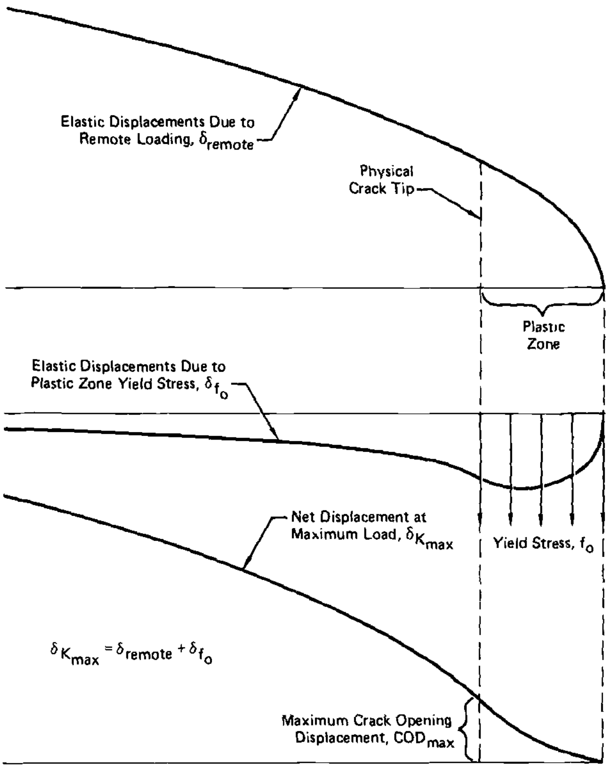

FIG. 1—*Elastic crack surface displacements at maximum load.*

surface due to permanent extension of the ligament. This is referred to as the plastic crack surface in Fig. 4.

The bottom portion of Fig. 4 shows that the elastic surface is propped apart by the plastic deformation ahead of the crack tip. However, the extended plastic crack surfaces will interfere upon unloading. The interference is visualized as though the surfaces were allowed to pass through each other. The potential interference of either surface is the displacement of that surface past the centerline of the crack.

In modeling the residual deformation and surface interference, the plastic deformation at the crack tip at minimum load is considered to be equal to the crack opening displacement (COD) at that load [*11,13*]. This crack opening displacement, as obtained from Rice [*11*], is approximated as

$$COD_{K_{min}} = \alpha\,(K_{max}^2 - \frac{1}{2}\Delta K^2)/2Ef_0 \qquad (1)$$

where $\alpha = 1$ for plane stress, $\alpha = (1 - \nu^2)/2$ for plane strain, and $f_0 = \sigma_{ys}$ = yield stress.

This deformation exists just behind the crack tip as well since material

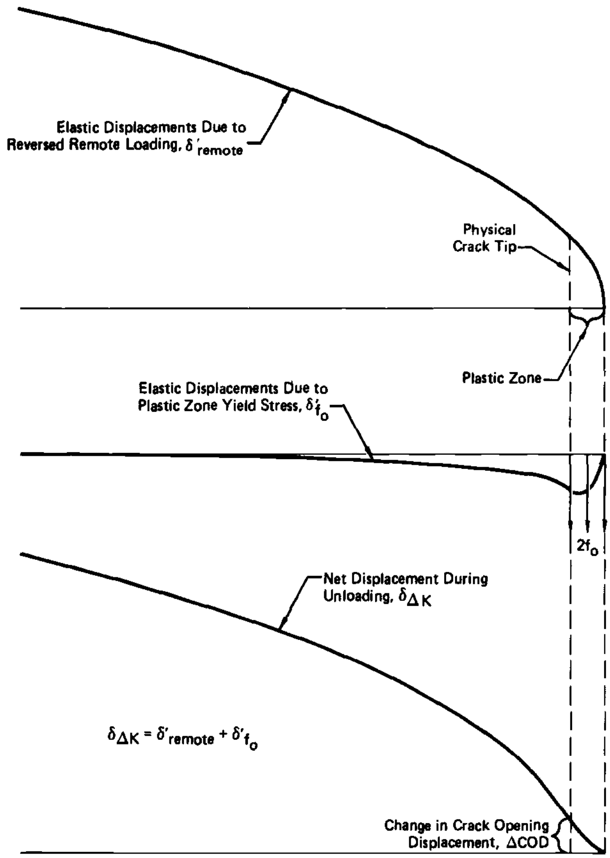

FIG. 2–*Elastic crack surface displacements during unloading.*

adjacent to the crack tip, both ahead and behind, is compressed to this value on unloading. Correlation with constant-amplitude closure stress intensity data from Elber [*1*] shows that a closer approximation to the permanent plastic deformation is

$$\delta_{residual} = \alpha\,(K^2_{max} - 0.4\,\Delta K^2)/2Ef_0 \tag{2}$$

The potential interference is the difference between the permanent plastic deformation and the minimum displacement of the elastic surface as shown in Fig. 5.

Contact Stress Analyses

The potential interference acts as a wedge behind the crack tip, creating a stress intensity at the crack tip. To determine the stresses behind the tip caused by this wedge, a simple contact stress model of closure was developed. This

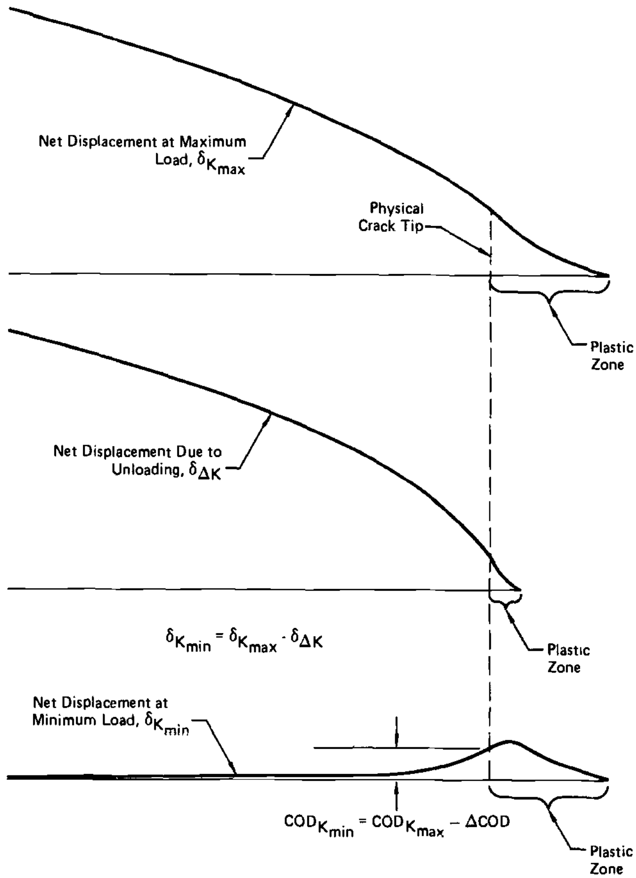

FIG. 3—*Elastic crack surface displacements at minimum load.*

model, symbolized in Fig. 6, uses 25 constant stress elements to idealize the wedge. Bueckner's weight function approach [*14*] was used to develop an influence coefficient matrix for the displacement-stress relationship between elements. The analysis is iterative so that a solution is determined wherein the maximum contact stress is limited to the yield stress and there is no tensile contact stress. A typical example of this analysis is summarized on Fig. 7 showing crack surface displacements and stresses following 0.635 mm of growth after a single overload. This plot shows the analytical displacements at K_{max} and K_{min}, permanent plastic deformation, potential interference, and contact stresses behind the crack tip.

The stresses determined from interference are used to compute the contact stress intensity occurring at the minimum load, the effective minimum stress intensity, and the effective stress intensity range.

Figure 8 shows a comparison of the results obtained using this model and Elber's test data [*1*].

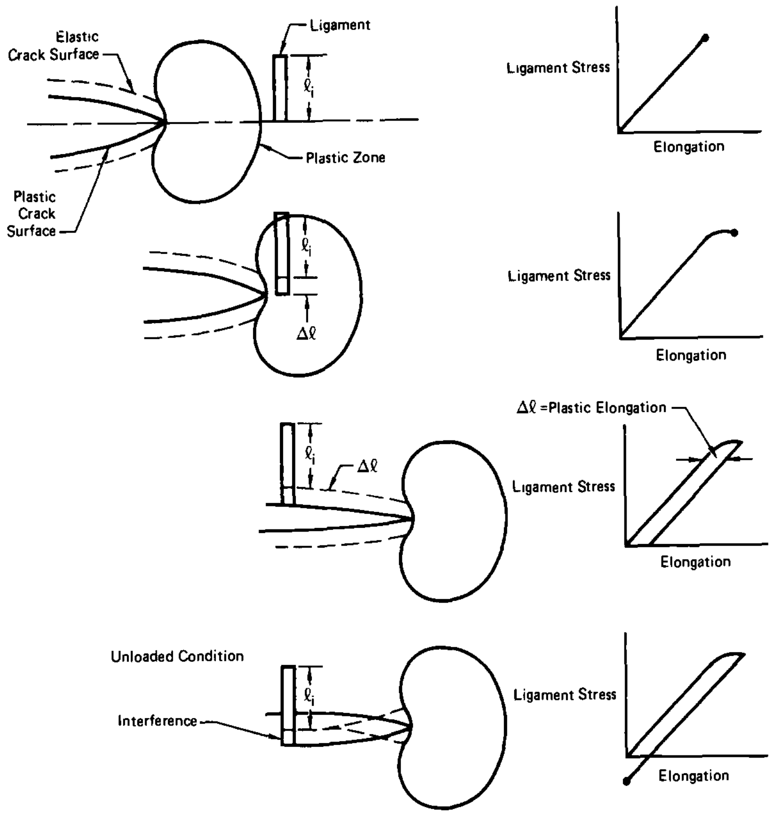

FIG. 4—*Crack closure phenomenon caused by interference of crack surfaces.*

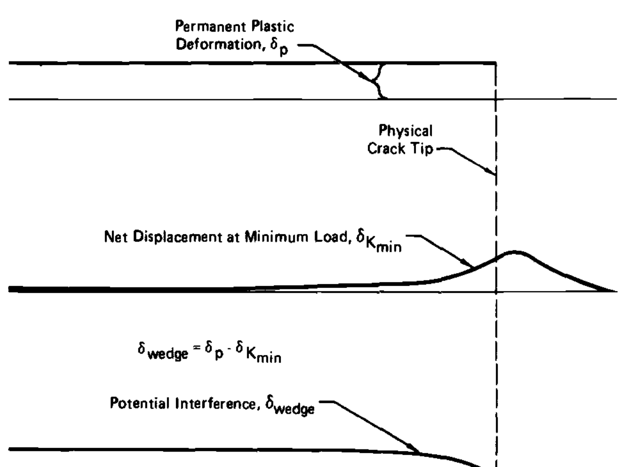

FIG. 5—*Potential interference at minimum load under constant-amplitude cycling.*

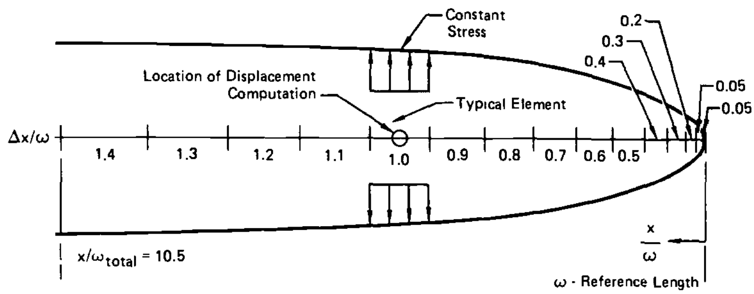

- 25 x 25 Influence Coefficient Matrix Derived Through Bueckner's Weight Function Approach
- Maximum Stress Limited to Yield
- No Tensile Stresses
- Displacements and Stress Intensity Computed for Input Values of K_{max}, K_{app}, E, and f.

FIG. 6—*Contact stress model of closure.*

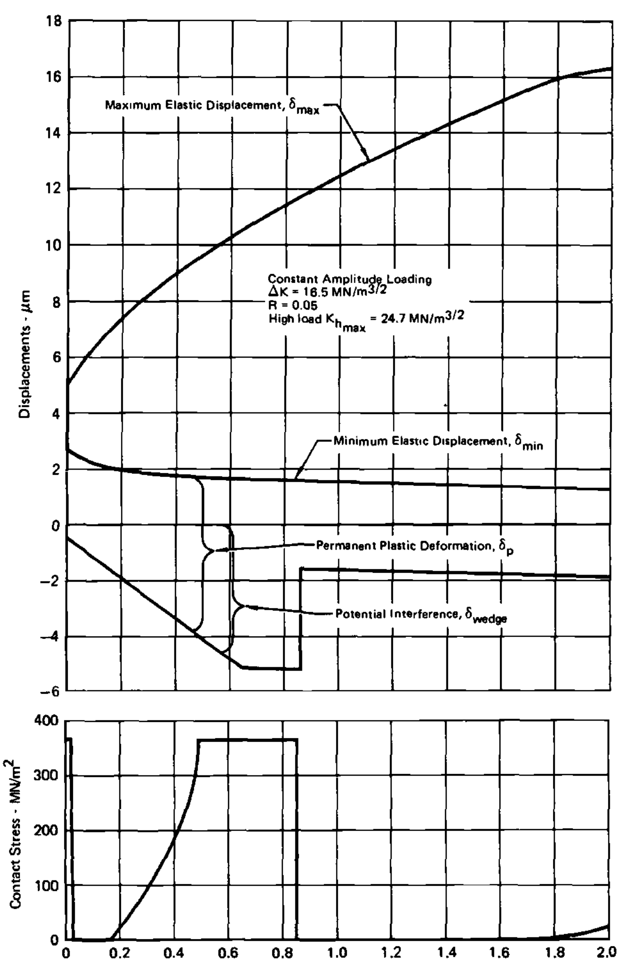

FIG. 7—*Crack surface displacements and stresses 0.635 mm after a single high load.*

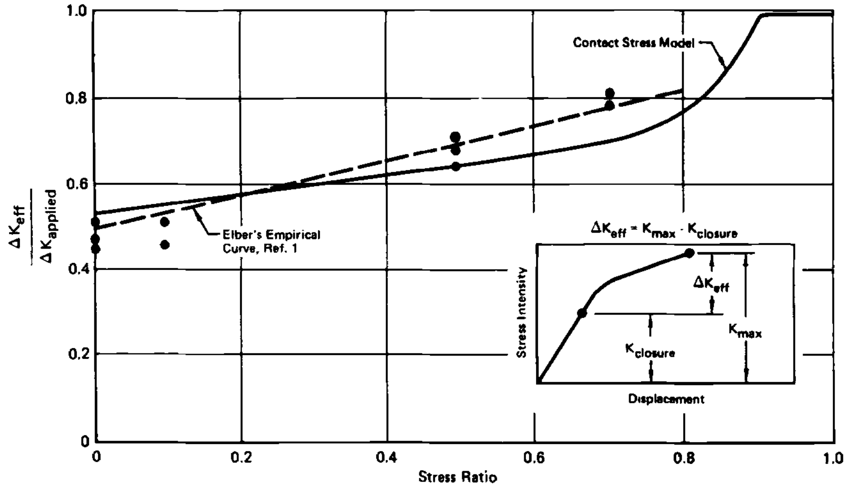

FIG. 8—*Comparison of crack growth models in constant-amplitude loading.*

Constant-Amplitude Crack Growth

Input to the growth analyses includes the sigmoidal da/dN–ΔK curve for a stress ratio, R, of zero. This curve is subsequently modified to be a da/dN–ΔK_{eff} curve, through results of analyses of closure as typified by Fig. 8. Crack growth for R ratios other than zero are determined using the ΔK_{eff} appropriate for that R ratio. To estimate the crack growth rate increase which occurs when K_{max} approaches K_c, a factor magnifying the crack growth rate is used

$$\frac{da}{dN} = \frac{da}{dN}\bigg|_{\Delta K_{eff}} \left\{\frac{K_c}{K_c - K_{max}}\right\} \tag{3}$$

This magnification is similar to the modification made by Forman [*15*].

The usefulness of the contact stress model of crack closure to explain the effects of stress ratio is indicated in Fig. 9. This figure shows the correlation of analytical constant-amplitude crack growth and test results reported by Schijve, Broek, and de Rijk [*16*]. The crack growth curves shown are for stress ratios of 0.202, 0.428, and 0.546, Curves 1, 2, and 3, respectively. The large differences in constant-amplitude growth rates shown in Fig. 9 are due to testing at different stress ranges, with mean stress held constant and stress amplitude varied between tests, rather than solely due to stress ratio effects. Currently, the model treats negative stress ratios as $R = 0$ with $\Delta K = K_{max}$.

Crack Growth Following High Loads

Figure 10 shows comparisons of predicted crack growth rates using the contact stress model and test results for constant-amplitude cycling with multiple high loads. The data of Trebules, Roberts, and Hertzberg [*3*] were generated from thin compact tension specimens of 2024-T3 aluminum. These

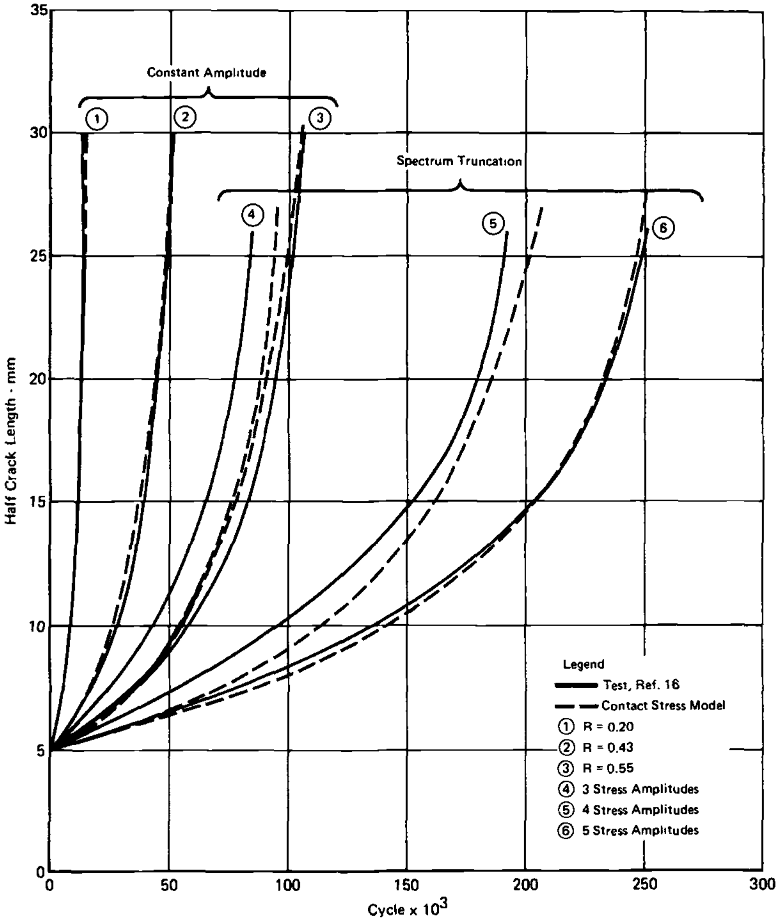

FIG. 9—*Comparison of analysis with constant-amplitude and spectrum truncation tests.*

comparisons show good correlation with the delay recorded in test. The analysis predicts a longer delay in retardation following a single high load than that recorded in test. The minimum growth rate predicted agrees well with the empirical curves. For multiple high loads the agreement between analysis and theory is very good for both delay and minimum growth rate.

As indicated in Fig. 10, current crack propagation models do not explain these phenomena very well. Wheeler's model [*17*] is based on plastic zone size interaction and can be "tuned," through a retardation exponent, to match results for a particular spectrum and specimen geometry. However, the model can not vary retardation with the number of high load cycles and does not predict delayed retardation.

T. R. Porter [*18*] has reported test results for eight variations in the number of high loads repeatedly applied during constant-amplitude testing. These tests

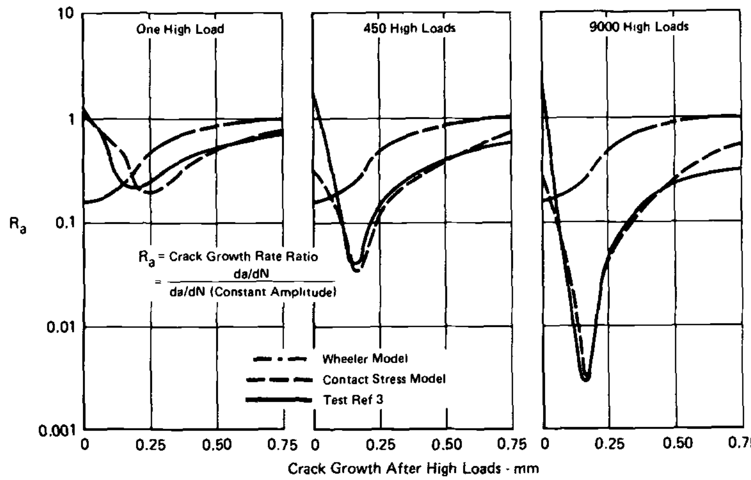

FIG. 10—*Comparison of measured and predicted crack growth following high loads.*

were performed on center cracked panels of 7075-T6 aluminum. Crack growth analyses using the contact stress model are shown with the test data in Fig. 11. Correlation of analysis and test results is consistently good, indicating the ability of the model to account for the effects of high loads on constant-amplitude crack growth.

Blocked Spectrum Crack Growth

To determine the ability of the analysis technique to account for the effects of variations in blocked spectra on crack growth, the test results reported by Schijve, Broek, and de Rijk [*16*] were selected. Three test series were performed using a base spectrum block having three stress amplitudes applied with a constant mean stress, Curve 4, Fig. 9. The two additional spectra were generated by adding first a lower stress amplitude, Curve 5, and then a higher stress amplitude, Curve 6. The test specimens consisted of center cracked panels of 2024-T3 clad aluminum with a 4-mm diameter hole and 1-mm notches used as a crack starter.

Correlation of the contact stress model analysis with test results is presented in Fig. 9. Also shown is correlation of the analysis with constant-amplitude results. Note that the analytical curves for both constant amplitude and spectrum crack growth were generated using the contact stress model and the same *da/dN* curve. The correlation shown in Fig. 9 indicates the usefulness of this analysis technique for prediction of spectrum crack growth.

Conclusions

A method for prediction of spectrum crack growth behavior has been developed based on analysis of crack surface contact stresses. Based on the

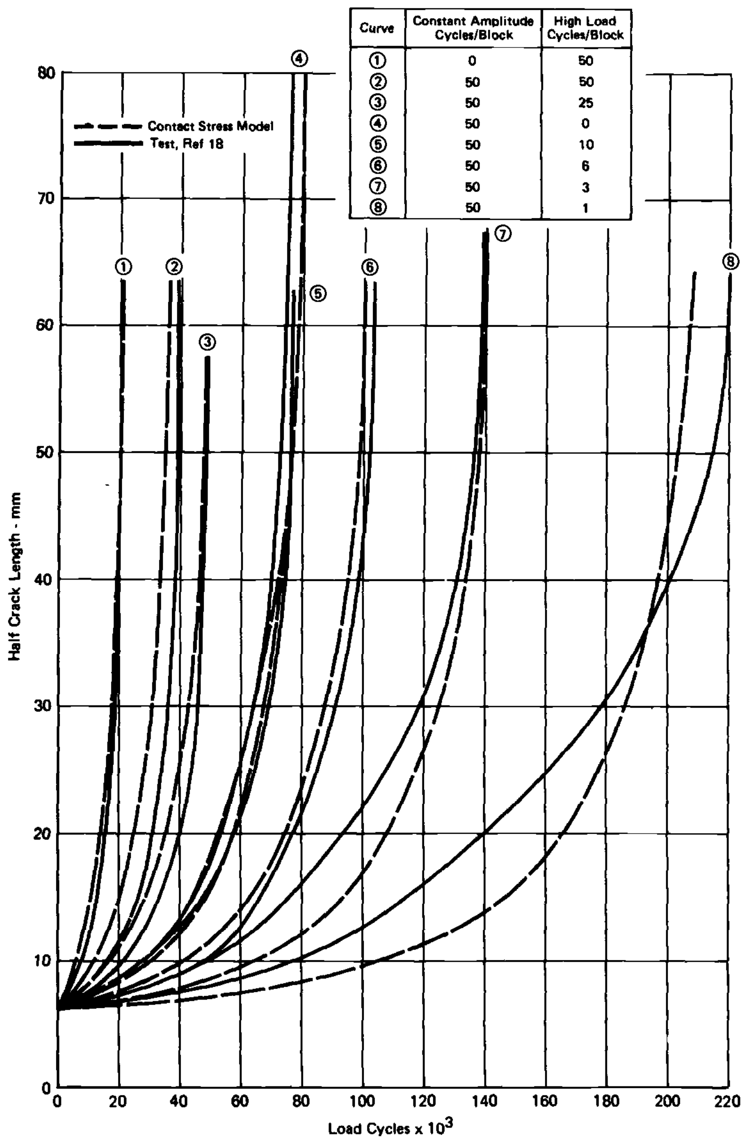

FIG. 11—*Comparison of analysis and constant-amplitude tests with multiple high loads repeatedly applied.*

correlation between test and analysis presented herein, the method appears to be capable of explaining:

1. stress ratio effects on constant-amplitude crack growth,
2. effects of single and multiple high loads on constant-amplitude crack growth, and
3. effects of truncation and other variations of blocked spectra on fatigue crack growth.

References

[1] Elber, W. in *Damage Tolerance in Aircraft Structures, ASTM STP 486*, American Society for Testing and Materials, 1971, pp. 230–242.

[2] von Euw, E. F. J., "Effect of Overload Cycle(s) on Subsequent Fatigue Crack Propagation in 2024-T3 Aluminum Alloy," Ph.D. thesis, Lehigh University, Bethlehem, Pa., 1971.

[3] Trebules, V. W., Roberts, R., and Hertzberg, R. W. in *Progress in Flaw Growth and Fracture Toughness Testing, ASTM STP 536*, American Society for Testing and Materials, 1973, pp. 115–146.

[4] McMillan, J. C. and Pelloux, R. M. N. in *Fatigue Crack Propagation, ASTM STP 415*, American Society for Testing and Materials, 1967, pp. 505–535.

[5] Probst, E. P. and Hillberry, B. M., "Fatigue Crack Delay and Arrest Due to Single Peak Tensile Overloads," AIAA Paper No. 73-325, AIAA Dynamics Specialists Conference, Williamsburg, Va., 19-20 March 1973.

[6] Corbly, D. M. and Packman, P. F., *Engineering Fracture Mechanics*, Vol. 5, 1973, pp. 479–497.

[7] Ho, C. L., Buck, O., and Marcus, H. L. in *Progress in Flaw Growth and Fracture Toughness Testing, ASTM STP 536*, American Society for Testing and Materials, 1973, pp. 5–21.

[8] Jones, R. E., *Engineering Fracture Mechanics*, Vol. 5, 1973, pp. 585–604.

[9] Dugdale, D. S., *Journal of Mechanics and Physics of Solids*, Vol. 8, 1960, pp. 100–104.

[10] Westergaard, H. M., *Journal of Applied Mechanics*, Vol. 6, 1939, pp. A-49–A-53.

[11] Rice, J. R. in *Fatigue Crack Propagation, ASTM STP 415*, American Society for Testing and Materials, 1967, pp. 247–309.

[12] Rice, J. R., *International Journal of Solids and Structures*, Vol. 8, 1972, pp. 751–758.

[13] Adams, N. J. I., *Engineering Fracture Mechanics*, Vol. 4, 1972, pp. 543–554.

[14] Bueckner, H. F., *Zeitschrift fuer Angewandte Mathematik und Mechanik*, Vol. 50, 1970, pp. 529–546.

[15] Forman, R. C., Kearney, V. E., and Engle, R. M., *Journal of Basic Engineering, Trans. ASME*, Series D, Vol. 89, No. 3, 1967, pp. 459–464.

[16] Schijve, J., Broek, D., and de Rijk, P., "Fatigue Crack Propagation Under Variable Amplitude Loading," National Aerospace Laboratory, NLR T. N. M. 2094, Dec. 1961.

[17] Wheeler, O. E., "Spectrum Loading and Crack Growth," ASME Paper No. 71 – Met-X, 1971.

[18] Porter, T. R., "Method of Analysis and Prediction of Variable Amplitude Fatigue Crack Growth," *Engineering Fracture Mechanics*, Vol. 4, 1972.

DISCUSSION

Otto Buck[1] *(written discussion)*—We used the Dugdale model too, some time ago.[2] It uses an infinitely thin strip of material only. That means it does not describe the real situation at all. So, I wonder why the results you obtained look so good? Could you comment on that?

H. D. Dill and C. R. Saff (authors' closure)—We use the Dugdale model to define plane stress plastic zone size and crack opening displacement because it incorporates the material properties thought to be important in governing plastic

[1] Science Center, Rockwell International, Thousand Oaks, Calif. 91360.

[2] Ho, C. L., Buck, O., and Marcus, H. L. in *Progress in Flaw Growth and Fracture Toughness Testing, ASTM STP 536*, American Society for Testing and Materials, 1973, p. 5.

zone size, and it exhibits the expected load-displacement characteristics. In plane strain conditions, characteristic of thick materials, we use plastic zone sizes and crack opening displacements shown by Rice[3] to be roughly one half of those predicted by the Dugdale model. Using these assumptions, the contact stress model predicts a lower closure stress intensity, less retardation, and less delay in minimum retardation under plane strain conditions than under plane stress. By selecting an appropriate assumption of plane stress or plane strain we have been able to correlate with data from several materials.

C. E. Richards[3] *(written discussion)*–In the plane stress model you employed, it is relatively easy to visualize the "sucking in" of material from the free surfaces to create net tensile strain in regions where the crack has passed which in turn leads to compressive stresses in tensile cyclic loading. However, in plane strain conditions I find it less easy to visualize what happens metallurgically that creates net tensile strains. Do you have any suggestions?

A member of the audience suggested that the net tensile strains required to give compressive closure in zero-tension or tension-tension loading may arise from one or both of the following effects. The net tensile strain may be caused by nonlinear elasticity in the atom core regions of heavily worked material. This may result in up to 2 percent strain. The second possibility is that the two fatigue surfaces behind the crack tip may not "fit" exactly. For example, in striation fatigue growth there may be "hill-hill" interference rather than "hill-valley" matching. Nevertheless, there would be differences metallurgically between net strains produced under plane stress and plane strain conditions.

Another member from the audience confirmed this and described evidence that closure stresses in plane stress were about 50 percent of K_{max} whereas in plane strain the value was lower at about 30 percent of K_{max}.

H. D. Dill and C. R. Saff (authors' closure)–J. R. Rice[4] has documented an approach toward understanding the differences in plastic zone plane stress and plane strain conditions in terms of slip or tensile yielding on discrete surfaces emanating from the crack tip. He refers to the discussion of Hahn and Rosenfield[5] in which plane stress plastic flow ahead of flat through-the-thickness cracks in thin sheets tends to consist of two intersecting 45 deg shear bands. The plasticity is then localized to a narrow region of height roughly equal to sheet thickness. Rice models plane strain plastic flow as in-plane sliding on two discrete surfaces inclined at angles $\pm\theta$ with the crack line. Perhaps his discussion will give some insight into the mechanisms of plane stress and plane strain plastic zone formation.

In the same reference Rice shows that the plastic zone size and crack opening displacement are roughly half as large for plane strain conditions as compared to plane stress conditions. We have incorporated this relationship into our model

[3] Central Electricity Research Laboratories, Leatherhead, Surrey, England.

[4] Rice, J. R. in *Fatigue Crack Propagation, ASTM STP 415*, American Society for Testing and Materials, 1967, pp. 247–309.

[5] Hahn, G. T. and Rosenfield, A. R., *Acta Metallurgica*, Vol. 13, No. 3, 1965.

and results indicate that, under constant-amplitude loading conditions with zero minimum stress, closure will occur at 46.7 percent of K_{max} in plane stress and 33.1 percent in plane strain. This seems to agree with the trends noted.

L. F. Impellizzeri[1] *and D. L. Rich*[1]

Spectrum Fatigue Crack Growth in Lugs

REFERENCE: Impellizzeri, L. F. and Rich, D. L., "Spectrum Fatigue Crack Growth in Lugs," *Fatigue Crack Growth Under Spectrum Loads, ASTM STP 595*, American Society for Testing and Materials, 1976, pp. 320–336.

ABSTRACT: Analytical and experimental investigations were conducted to determine the crack growth behavior in lug joints subjected to a randomized flight-by-flight spectrum. Specific objectives were to evaluate capabilities for analyzing spectrum crack growth in lugs and to assess the effects on crack growth of K_{Ic} and cold working the material surrounding the lug holes. Stress intensity solutions were developed for cracks radiating from lug holes using Bueckner's weight function approach for various stress distributions surrounding the lug hole. The stress distributions were determined using an elastic/plastic finite element analysis. Included in these analyses were residual stress distributions following either large lug loads or mandrel hole enlargement. Spectrum crack growth calculations were made using the resulting stress intensity values and the Wheeler retardation crack growth model.

Lug specimens were fabricated from two heats of 6Al-4V mill annealed titanium representative of material having low and high fracture toughness levels. Basic mechanical properties including ultimate and yield strength, percent elongation, and reduction in area and fracture characteristics, including K_{Ic} and constant-amplitude crack growth rates, were determined for each heat of material. EDM cuts in the lug specimens were used as points of stress concentration where precracks were developed by low-level constant-amplitude fatigue loading. The lug holes of selected specimens were cold worked to determine the effect of compressive residual stresses on the crack growth rate. Plots of crack growth versus spectrum hours were obtained for each specimen by post-failure examination of the fracture surfaces using the scanning electron microscope.

KEY WORDS: crack propagation, fatigue (materials), cyclic loads, aircraft, tensile properties, mathematical prediction, strain energy methods, stress analysis, residual stress, plastic deformation, inspection, titanium alloys

Structural fatigue very often initiates in areas of high load transfer due to the superimposed stress concentration caused by the fastener bearing load. In many structural joints, the magnitude of this fastener bearing load can be minimized by transferring the load through a row of fasteners and tapering the mating parts to soften the "hot spot" at the end fastener. This reduces the percentage of total load transferred by each individual fastener and thereby reduces the ratio of bearing stress to tension stress. In some structural joints, however, the geometry

[1] Section chief–Strength and lead engineer–Strength, respectively, McDonnell Aircraft Company, McDonnell Douglas Corporation, St. Louis, Mo. 63166.

of the design dictates that 100 percent of the load be transferred through a single fastener or pin. This type of structural joint is, of course, called a lug.

The elastic gross section stress concentration factor for a typical lug is about five compared to about three for a fastener hole with zero bearing load. The degradation in crack initiation life due to this high stress concentration factor is significant. The degradation in crack growth life is even more serious because of the large diameter of the lug hole. This is explained by the nature of a lug, transferring 100 percent of the load through a single fastener or pin, which requires the pin and therefore the lug hole to be large in diameter. Typical fastener holes in aircraft structure are on the order of 6 mm in diameter, but lug holes in aircraft structure are very often on the order of 50 mm in diameter. The stress gradient for the larger diameter lug hole is much more shallow, that is, the stress remains relatively high for larger distances from the edge of the hole simply because of the larger diameter. While a 2-mm crack emanating from a 50-mm lug hole would still be in the highly stressed region and therefore significantly affected by the lug hole, a 2-mm crack emanating from a 6-mm fastener hole would be much less affected by the presence of the fastener hole.

The purpose of this paper is to present empirical crack growth characteristics for a 6Al-4V annealed titanium lug subjected to a typical fighter aircraft flight-by-flight fatigue spectrum, and to compare these spectrum crack growth test results to analytical calculations.

Test Program

The objectives of the test program were to determine basic material properties, for example, yield strength, fracture toughness, and da/dN as well as flight-by-flight spectrum crack growth data for a lug. Test variables included two toughness levels of 6Al-4V mill annealed titanium, two crack types, and three mandrel interference levels for cold working to induce compressive residual stresses around the lug hole. Materials, specimens, fatigue spectrum, and test results are detailed in the following paragraphs.

Basic Material Properties

Two heats of 6Al-4V mill annealed titanium forgings were obtained to evaluate the effect of fracture toughness on crack growth characteristics. Heat 1 consisted of three pieces of a 67 by 360 by 1220-mm forging which was forged from a billet having an oxygen content of 0.175 percent and was representative of low to medium toughness material. Heat 2, representative of high toughness material, was forged as a single piece 150 by 230 by 910-mm forging from a billet having an oxygen content of 0.152 percent.

Standard tensile and fracture toughness tests were conducted on specimens taken from each heat of material. Fracture toughness was determined using compact tension specimens, 31.75 mm thick, with all testing in conformance with ASTM Test for Plane Strain Fracture Toughness of Metallic Materials (E

399-72). All test values were valid with the two heats showing a distinct difference in toughness levels, 66 and 88 MN/m$^{3/2}$. Constant-amplitude crack growth data were obtained by testing two wedge opening loaded specimens from each heat. The specimens had a thickness of 31.75 mm and a width of 125 mm. The constant-amplitude crack growth rates were very similar for the two heats of material, the only difference being for high ΔK.

Lug Specimen

Figure 1 shows the detailed geometry of the lug specimens. They were fabricated from the mill annealed 6Al-4V titanium described previously and are

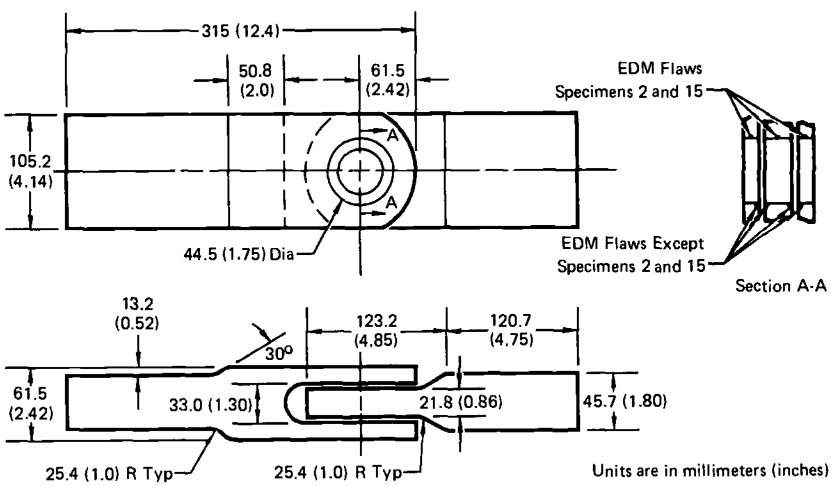

FIG. 1–*Lug specimen.*

representative of typical wing spar-to-fuselage bulkhead attachments in fighter aircraft structure. Twelve lug specimens, including both the male and female parts, were machined from Heat 1 and three from Heat 2. As indicated in Fig. 1, the mouth of the female lug is 33.0 mm, while the male lug is 21.8 mm thick, producing a total 11.2-mm gap. The purpose of the gap is to allow for ease of wing-to-fuselage assembly in a three-spar, three-bulkhead combination where manufacturing tolerances can build up. Seven of the twelve Heat 1 specimens were assembled unsymmetrically with the 11.2-mm gap all on one side. The remaining five Heat 1 specimens and three Heat 2 specimens were assembled symmetrically with 5.6-mm gap on each side. The assembly of all 15 specimens included a 3.2-mm-thick beryllium copper bushing installed in both the male and female lug. The bushings were installed with a very mild 0.10-mm diametral interference which, coupled with its relative thinness and low stiffness, produced no appreciable residual stress. The steel pins were installed with a very slight clearance providing a "neat fit."

Electrical discharge machined (EDM) flaws were used as points of stress concentration for precrack development. The EDM flaws, as indicated in Fig. 1, were located at the hole wall midway between the lug surfaces for one specimen from each heat, and at the corner of the hole wall and lug surfaces for the other 13 specimens. The corner flaws in the female lugs were located on the inside surface which is the higher stressed surface because of secondary bending. The corner flaws in the male lugs were located on both surfaces. The EDM flaws were approximately 0.50-mm radius quarter-circle and 0.50-mm radius semi-circle for the corner flaw and midway flaw, respectively. All specimens were precracked by constant-amplitude cycling at 55 percent design limit load; the precrack size for each specimen was about 3-mm radius.

Four of the Heat 1 specimens were cold worked after precracking. A split sleeve process was utilized wherein a steel mandrel is pulled through a 0.46-mm-thick stainless steel sleeve installed in the lug hole. The split in the sleeve is located at the back side of the lug. The lug hole is reamed to the final 44.45-mm-diameter size after cold working. The amount of material removed by the reaming operation is nominally 0.60 mm on the diameter. The diametral interference of the mandrel for cold working was 0.91 mm for two of the specimens, 0.69 mm for the third specimen, and 0.46 mm for the fourth. The extent of residual compressive stress introduced by the cold working is given in the section on analytical techniques.

Flight-by-Flight Spectrum Definition

All of the lug specimens were tested to a fighter aircraft flight-by-flight spectrum. The positive and negative cumulative peak exceedances per 1000 h are given in Fig. 2 in terms of percent design limit load. Design limit load (DLL) for

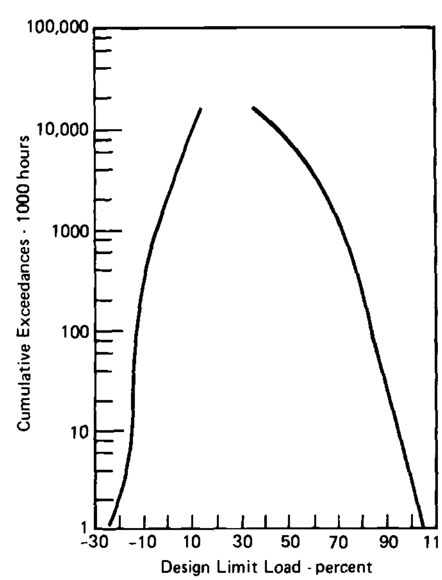

FIG. 2—*Fatigue spectrum positive and negative cumulative peak exceedances.*

the lug specimens was 509 330 N which corresponds to a gross section stress of 223 MN/m^2 in the male lug. The flight-by-flight spectrum includes 365 fighter missions and 355 attack missions in 1000 h. A ground load is applied between each flight to simulate take-off and landing loads. The higher positive and negative cycles are randomly selected for inclusion in a particular mission. The highest positive cycle applied once per 1000 h is 105 percent DLL; it is applied approximately one tenth of the way through a 1000 h sequence. The spectrum includes higher load levels applied less frequently. A 115 percent DLL cycle is applied after 2000 h and every 4000 h thereafter. A 125 percent DLL cycle is applied after 8000 h and every 16 000 h thereafter.

Spectrum Test Results

In addition to the 15 lug specimens that are the subject of this paper, lug specimens of the same geometry were also tested in an earlier program but without flaws or precracks. Those specimens were cycled without failure for 64 000 h to the spectrum defined in the preceding paragraph, and then statically failed at approximately 240 percent DLL.

The detailed test results for the 15 precracked lugs are presented in Table 1. The precrack sizes shown represent post-test measurements made by viewing the fracture surfaces; it is a measurement giving crack depth perpendicular to the lug hole surface. As indicated earlier, there was more than one precrack introduced into each lug specimen. The EDM flaws were located in both the male and female parts. The precrack size given in Table 1 is for the failure origin, so it is either in the male or female lug depending on which failed. As shown in Table 1, the failures were equally divided between the male and female lug suggesting a rather well balanced design. The gross section design limit tension stress in the male lug is 223 MN/m^2, while the comparative tension stress in each ear of the female lug is 184 MN/m^2. However, the male lug is in double shear, whereas each ear of the female lug is in single shear which subjects it to bending stresses. Strain gage measurements on the female lug indicate the combination of tension plus bending gives 239 MN/m^2 on the critical inside surface.

The data in Table 1 show that, with an 0.51-mm EDM flaw, the lug specimen sustained 50 000 h without failure. This specimen was tested without a visible precrack to determine the effect of the EDM flaw. The largest precrack introduced into a non-cold-worked lug specimen was 4.57 mm; that specimen failed after 4542 h. Table 1 indicates a potent beneficial effect resulting from the cold-working operation. Three of the four cold-worked specimens were cycled for 50 000 h without failure and one of them had a 6.35-mm precrack. The one cold-worked specimen that did fail had a relatively low mandrel interference. It is shown in the section on analytical techniques that the 0.46-mm interference level produces a rather ineffective level of compressive residual stress. All of the cold-worked specimens were tested in the unsymmetrical configuration with 11.2-mm gap on one side. The effect of the unsymmetric

TABLE 1 – *Spectrum test results.*

Specimen Number	Mandrel Interference, mm (in.)	Precrack Size, mm (in.)	Crack Growth, Life-Hours[c]
1	...	0.51 (0.02)	50 000 NF
2[a]	...	2.03 (0.08)	12 133 M
3	...	2.54 (0.10)	7 745 F
4	...	2.79 (0.11)	7 023 F
5	...	4.57 (0.18)	4 542 F
6[b]	...	2.29 (0.09)	5 139 F
7[b]	...	2.79 (0.11)	5 740 M
8[b]	...	4.06 (0.16)	7 228 M
9[b]	0.46 (0.018)	1.52 (0.06)	8 000 F
10[b]	0.69 (0.027)	3.05 (0.12)	50 000 NF
11[b]	0.91 (0.036)	2.79 (0.11)	50 000 NF
12[b]	0.91 (0.036)	6.35 (0.25)	50 000 NF
13	...	1.78 (0.07)	10 931 M
14	...	2.79 (0.11)	6 000 M
15[a]	...	3.05 (0.12)	6 000 M

[a] These specimens had midway crack; all others had corner crack.

[b] These specimens tested with 11.1 mm (0.44 in.) gap on one side; all others tested symmetrically with 5.6 mm (0.22 in.) gap on each side.

[c] NF indicates no failure. M indicates failure in male lug. F indicates failure in female lug.

loading is minimal on the male lug and only slightly more significant on the higher loaded ear of the female lug. The crack growth life of the female lugs tested unsymmetrically was somewhat less than the female lugs tested symmetrically. For example, Specimen 3 tested symmetrically and with a 2.54-mm precrack sustained 7745 h, while Specimen 6 tested unsymmetrically and with a 2.29-mm precrack sustained 5139 h.

Specimens 1 through 12 in Table 1 are from Heat 1 and Specimens 13 through 15 are from Heat 2. As indicated previously, the material K_{Ic} for Heat 1 is 66 $MN/m^{3/2}$ while the material K_{Ic} for Heat 2 is 88 $MN/m^{3/2}$. The higher fracture toughness for Heat 2 did not provide slower constant-amplitude crack growth except for high ΔK. The same trend of no appreciable difference between Heat 1 and Heat 2 is demonstrated in Table 1 for spectrum crack growth. For example, Specimen 7 from Heat 1 with a 2.79-mm precrack sustained 5740 h. This compares to Specimen 14 from Heat 2, also with a 2.79-mm precrack, which sustained 6000 h.

Analytical Techniques

The objective of the analysis presented in this paper was to determine the adequacy of developed techniques in terms of correlation with spectrum crack growth data for lugs. The analysis techniques included a combination of Bueckner's weight function for an edge crack, a geometry correction factor, and finite element solutions giving lug stress distributions. These were utilized to obtain the stress intensities for the loads applied in the flight-by-flight fatigue spectrum and for those resulting from mandrel hole enlargement. The Wheeler plastic zone model was used for determining crack growth retardation.

Approximate Weight Function for a Hole

Bueckner's weight function [*1*][2] is given by the following relation

$$m(x,a) = \frac{H}{2K}\frac{\partial u(x,a)}{\partial a}$$

where H equals E for plane stress and $E/1 - \nu^2$ for plane strain, K is the stress intensity, and $u(x,a)$ is the crack opening displacement at x for a crack of length a. The weight function was shown to be unique by Bueckner [*1*] and by Rice [*2*] for a given structural geometry and crack size regardless of the stresses acting on the structure, that is, it is independent of the loading condition. The integral of the product of this function and the stress distribution along the crack boundary gives the stress intensity, or in equation form

$$K = \int_a p(x)\, m(x,a)\, dx$$

where $p(x)$ is the stress distribution that would exist along the crack boundary if the crack were not there. Since the weight function is independent of the loading condition, it can be determined for one condition and then utilized to obtain the stress intensity for another.

The present development of the weight function for a hole utilizes the exact weight function derived by Bueckner [*3*] for an edge crack in a semi-infinite plate. This function is modified by a geometry correction factor to obtain the desired result. The final equation for the approximate weight function for a hole is

$$m(x,a) = m_{ec}\,\Phi_1\,\Phi_2\,\Phi_3$$

where

$$m_{ec} = (a-x)^{-1/2}\ \left[1 + 0.6147\left(1 - \frac{x}{a}\right) + 0.2502\left(1 - \frac{x}{a}\right)^2\right]\ [\sqrt{2/\pi}]$$

$$\Phi_1 = 1 - 0.6449\left(\frac{a}{R}\right) + 0.8964\left(\frac{a}{R}\right)^2 - 0.7327\left(\frac{a}{R}\right)^3$$

$$+ 0.3335\left(\frac{a}{R}\right)^4 - 0.0781\left(\frac{a}{R}\right)^5 + 0.0073\left(\frac{a}{R}\right)^6$$

Φ_2 and Φ_3 are given in the Appendix.

[2] The italic numbers in brackets refer to the list of references appended to this paper.

The term m_{ec} is Bueckner's weight function for an edge crack in a semi-infinite plate, and x is measured from the edge of the plate toward the crack tip. The term Φ_1 is the geometry correction factor, and R is the hole radius. The geometry correction factor was obtained as the ratio of the stress intensity for a crack emanating from one side of a hole in an infinite plate to the stress intensity for an edge crack in a semi-infinite plate. The stress intensities for both of these configurations were of course determined for the same loading, uniform pressure on the crack faces. The stress intensity determined for the crack emanating from the hole was obtained numerically [4]. The preceding equation for Φ_1 was obtained by point to point matching of the two stress intensity solutions in the range $a\mathrm{R} \leq 3$; therefore, the weight function can only be considered accurate for $a/\mathrm{R} \leq 3$.

It should be recognized that since the geometry correction factor Φ_1 was determined as the ratio of stress intensities for a particular loading condition, uniform pressure on the crack faces, that the resulting weight function is not necessarily accurate for other loading conditions. To evaluate its accuracy, the weight function $m_{ec}\ \Phi_1$ was utilized to compute the stress intensity for a crack emanating from one side of a hole in an infinite plate subjected to uniform tension applied at a large distance from the hole. This is a significantly different loading condition than uniform pressure on the crack faces. The resulting curve of stress intensity versus crack length is compared to Bowie's [5] accepted standard solution and Grandt's [6] approximate solution in Fig. 3. Both curves are within 7 percent of the Bowie prediction. Another approximate solution was developed by Hall et al [7] using superposition principles. It is within 2 percent of the Bowie curve for one crack and 7 percent for two cracks for $a/\mathrm{R} \geq 0.05$.

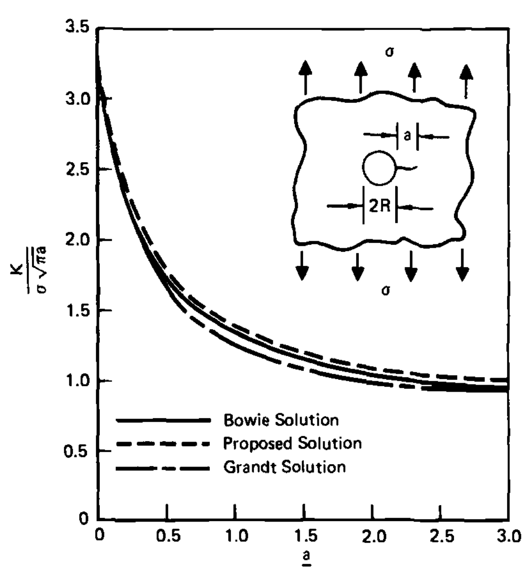

FIG. 3—*Correlation with Bowie stress intensity solution.*

The present solution is slightly on the conservative side, that is, for the same crack length it predicts a somewhat higher stress intensity than Bowie. The fact that the stress intensity calculated herein compares favorably with the accepted standard for a loading distribution significantly different from the one for which it was developed suggests that reasonable accuracy could be expected for other loading distributions.

The quantity m_{ec} Φ_1 represents the weight function for a crack emanating from one side of a hole in an infinite plate. The term Φ_2 provides the necessary adjustment factor to account for the case of cracks emanating from both sides of a hole in an infinite plate. The term Φ_3 gives the correction factor for finite width effects. The accuracy of the product of these factors was determined by comparison to Newman's [8] solution for cracks emanating from both sides of a hole in finite width plates with width/diameter = 2 and 4. The present solutions were within 4 percent of both of Newman's solutions.

Calculations of Lug Stress Intensity

The analytical technique described in the previous section provides a method of computing the stress intensity for cracks in holes for any loading condition. The additional information required for this analysis is the lug stress distribution that would exist along the crack boundary if the crack were not there. Figure 4

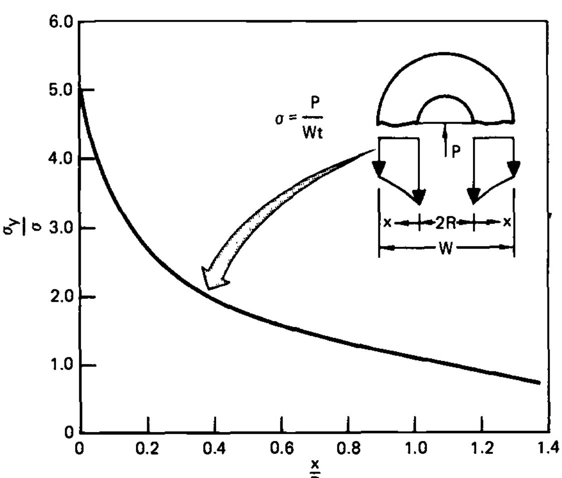

FIG. 4—*Elastic stress distribution in loaded lug.*

gives that distribution based on a two-dimensional finite element solution for a pin loaded lug with the geometry of the titanium specimens discussed in the first part of this paper. The through-the-thickness variation in stress is considered to be small due to the relatively large diameter of the lug hole compared to its thickness. The steel "neat fit" pin was also modeled for the finite element analysis to produce the correct pin bearing pressure on the inside surface of the lug hole. The resulting stress intensity versus crack length is given in Fig. 5. It should be noted that the stress intensity given in Fig. 5 includes a 1.13 front face correction factor which corresponds to Bueckner's [*3*] derivation for an edge crack.

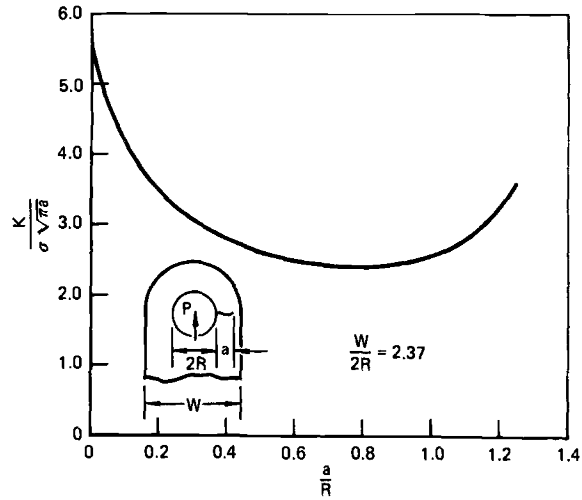

FIG. 5—*Stress intensity solution for a through crack in a lug.*

Four of the lug specimens were cold worked prior to testing with a split sleeve technique as mentioned earlier. The resulting compressive residual stresses produced by the three different levels of mandrel interference are given in Fig. 6. These stress distributions were obtained by elastic/plastic analysis [*9*] assuming

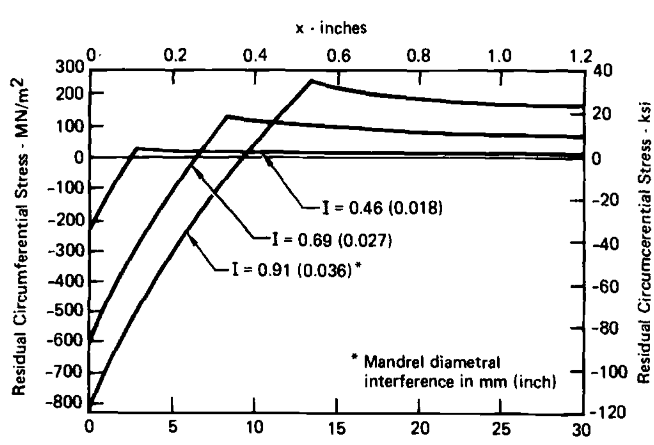

FIG. 6—*Residual stresses after cold-work expansion of holes.*

a "donut shaped" configuration with the outside diameter equal to the width of the lug. An elastic/plastic finite element solution using the actual lug geometry was also obtained for the 0.91-mm mandrel interference which verified the validity of the donut-shape assumption. The residual stress intensities versus crack length for the three different mandrel interference levels are given in Fig. 7. It is of interest to note that the residual stress intensity remains negative

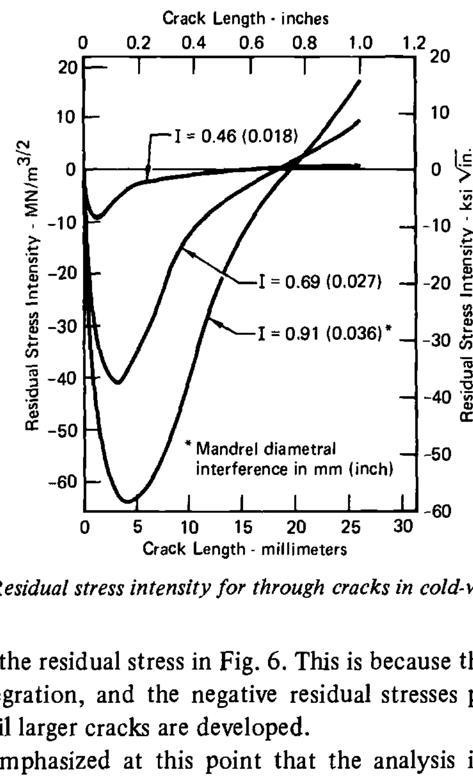

FIG. 7—*Residual stress intensity for through cracks in cold-worked lugs.*

farther out than the residual stress in Fig. 6. This is because the stress intensity is obtained by integration, and the negative residual stresses predominate in this computation until larger cracks are developed.

It should be emphasized at this point that the analysis in this paper is not extended beyond linear elastic fracture mechanics. Although an elastic/plastic analysis technique was utilized to obtain the residual stress distributions in Fig. 6, the residual stresses themselves are elastic and were simply used as the distribution $p(x)$ required for Bueckner's elastic weight function approach to compute stress intensities. The basic idea for the cold-worked specimens is that K_{max} and K_{min} for each cycle in the flight-by-flight spectrum are determined by adding the stress intensity from Fig. 7 to the stress intensities from Fig. 5 for each cycle's maximum and minimum stress. This is simply a superposition technique valid for elastic systems. As long as the sum of the residual stresses and the stresses produced by the externally applied loads do not cause yielding, the solution should be reasonably accurate. In the absence of any compressive residual stresses, the highest loads in the flight-by-flight spectrum produce stresses only slightly greater than tension yield at the edge of the lug hole. Therefore, when this tension stress field is added to the large compressive residuals produced by the mandrel operation, the sum is below the elastic limit.

The stress intensities versus crack length given in Figs. 5 and 7 are for through-the-thickness cracks as indicated on the graphs. Throughout most of the spectrum crack growth life of the subject lug specimens, the crack was not through the thickness but rather a quarter circle or semi-circle corresponding to the shape of the corner flaw or midway flaw, respectively, introduced by electrical discharge machining (EDM). The flaw shape parameter, Q, [*10*] was utilized to account for this difference. It was assumed that the stress intensity was equal to the quantity $1/\sqrt{Q}$ multiplied times the through-the-thickness stress intensities given in Figs. 5 and 7; a value of $Q = 2.47$ was used. Although this assumption is only accurate for short crack lengths, it provides a conservative, that is, greater than actual, estimate of the stress intensity. Comparison with a solution by Kobayashi [*11*] for an open hole with $a/R = 0.2$, and using this assumption resulted in about 4 percent disagreement. The slight variations in Q due to σ/σ_{ys} variations were included in the spectrum crack growth analysis.

Spectrum Crack Growth Analysis

The ΔK value for each cycle in the flight-by-flight spectrum was determined using the stress intensity computation procedures detailed in the previous section. These were then used to enter a curve of da/dN versus ΔK to obtain the crack extension for each cycle. The crack growth was thereby linearly summed on a cycle-by-cycle basis.

Stress ratio adjustments were made using Forman's equation [*12*]. There are many cycles in the spectrum where the valley is compression, but the stress ratio was assumed to be zero in these instances rather than negative. This is because the critical area in a lug is not put into compression during reversed loading, but simply put into a nearly zero stress condition. The stress ratio for all cycles in the spectrum is therefore either zero or a positive value. This is the case except for the cold-worked specimens. The stress ratio for many of the cycles is negative for these specimens because of the large residual stress intensity, as shown in the preceding section, especially for the 0.91-mm mandrel interference.

Crack growth retardation, due to periodically applied higher load levels, was taken into account using the Wheeler [*13*] plastic zone model. The size of the plastic zone in front of the crack tip was recomputed on every cycle. The magnitude of the Wheeler retardation parameter m used in the spectrum crack growth analysis was 2.98 based on the best fit of crack growth data from mill annealed 6Al-4V titanium unloaded hole specimens subjected to the same flight-by-flight fighter aircraft spectrum as the lug specimens.

Correlation with Fracture Surface Crack Growth Measurements

The fracture surfaces of the lug specimens were viewed with the scanning electron microscope to match individual striation spacings with particular load levels in the spectrum. This was done by knowing the sequence of load level magnitudes in the spectrum and relating that to the observed sequence of striation spacing widths. The resulting spectrum crack growth data for the male lugs are presented in Fig. 8 and for the female lugs in Fig. 9. The crack growth

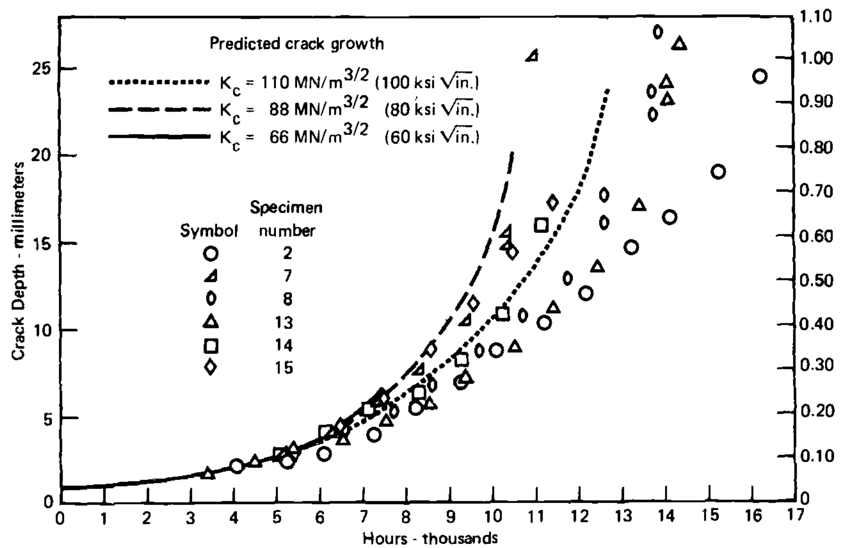

FIG. 8—*Crack growth in male lugs.*

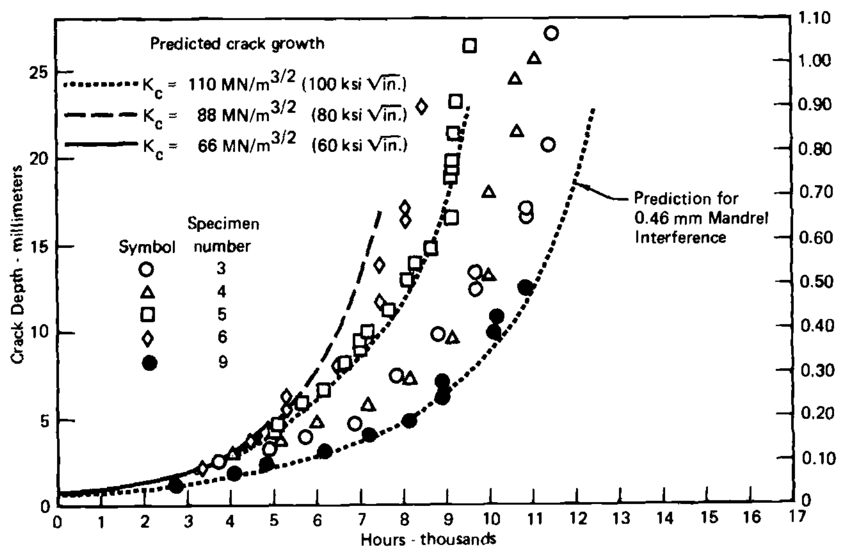

FIG. 9—*Crack growth in female lugs.*

data for each specimen are plotted starting with its precrack depth entered on the predicted curve. The variation in crack depth at failure indicated in both Figs. 8 and 9 is primarily due to the variation in the failing load resulting from the different load levels in the fatigue spectrum.

The three crack growth prediction curves in the two graphs of spectrum crack growth show the significant effect of the K_c assumption, at least in the later stages of growth. The question of what K_c value to assume is always a difficult one. It should be emphasized that this question does not relate primarily to what is the K_{Ic} value, but rather what is the extent of plane stress in the failure mode resulting in a K_c level significantly higher than the material plane strain fracture toughness. The K_c computed for the failing load of the male lugs for Heat 1 averaged 90.7 $MN/m^{3/2}$ and for Heat 2 averaged 97.1 $MN/m^{3/2}$. The K_c computed for the failing load of the female lugs for Heat 1 averaged 103.2 $MN/m^{3/2}$. None of the Heat 2 specimens failed in the female lug. This is simply because the EDM flaws and precracks were, by chance, larger in the male lugs. The K_c computed for the female lugs was, as expected, greater than that computed for the male lugs because they are thinner and plane stress conditions would be more operable. Although plane stress conditions were more predominant in the female lugs, plane stress was also active on the top and bottom edges of the male lug causing tunneling of the crack through the midplane of the male lug. This factor probably contributed to the average K_c value being greater than K_{Ic}.

The one cold-worked specimen that failed had a rather low 0.46-mm mandrel interference; the residual stress intensity for that specimen is shown in Fig. 7. Its spectrum crack growth data are represented by the solid circular symbols in Fig. 9. Using the superposition approach mentioned in the preceding section, that is, adding the residual stress intensity to the stress intensities due to the applied loading, gives the crack growth prediction curve shown in Fig. 9. Curves of precrack size versus predicted crack growth life for different mandrel interference levels are presented in Fig. 10. The dramatic benefit provided by the cold

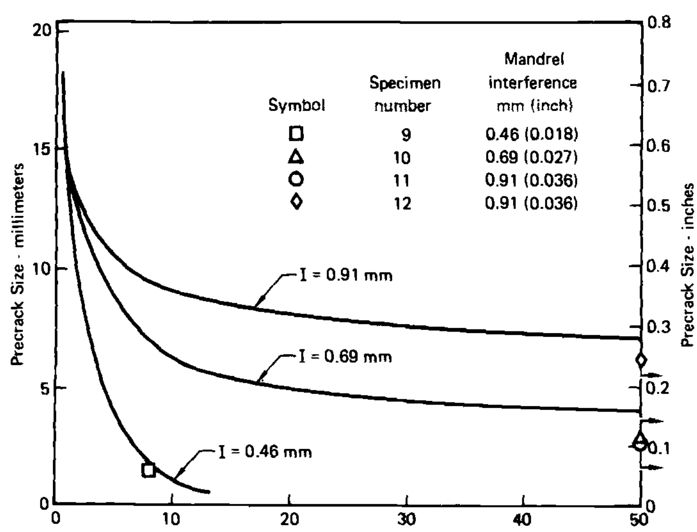

FIG. 10—*Precrack size versus crack growth life for cold-worked specimens.*

working, especially at the 0.91-mm mandrel interference level, is demonstrated in this graph and the test data correlate favorably with the curve.

Summary

Precracked lug specimens fabricated from mill annealed 6Al-4V titanium were tested to a flight-by-flight fighter aircraft fatigue spectrum. A number of the specimens were cold worked by mandrel hole enlargement to produce compressive residual stresses around the lug hole to retard crack growth. Comparisons of the crack growth life for the lug specimens indicated a potent beneficial effect due to cold working. For example, a non-cold-worked specimen with a 2.54-mm precrack failed after 7745 spectrum hours compared to a cold-worked specimen with a 6.35-mm precrack tested for 50 000 spectrum hours without failure.

An approximate weight function for a hole was developed to compute stress intensities for different stress distributions surrounding the lug hole. These stress intensity solutions were utilized to enter da/dN versus ΔK curves for annealed 6Al-4V to obtain data for spectrum crack growth analysis. The Wheeler plastic zone model was used for determining crack growth retardation due to periodically applied higher load levels. The magnitude of the retardation parameter m used in the analysis was 2.98 based on the best fit of crack growth data from unloaded hole specimens subjected to the same spectrum as the lugs. The resulting crack growth predictions correlated reasonably well with the spectrum test data obtained by scanning electron microscope examinations of the lug fracture surfaces.

Acknowledgment

The authors wish to extend special thanks to a colleague at McDonnell Aircraft Company, W. T. Fujimoto, who developed the approximate weight function for a hole utilized in this paper.

Appendix

The terms Φ_2 and Φ_3 are used to adjust the weight function for double cracks and to account for finite width effects, respectively. They are given by the following equations:

$$\Phi_2 = 1 \qquad \text{(single crack)}$$

$$\Phi_2 = \left\{ \frac{\sqrt{R+a}\left\{1 - \frac{2}{\pi}\tan^{-1}\left[\frac{R}{\sqrt{(R+a)^2 - R^2}}\right]\right\}}{\left\{\frac{1}{2}\sqrt{R+\frac{a}{2}}\left\{1 - \frac{2}{\pi}\tan^{-1}\left[\frac{2R-a}{\sqrt{2R+2)^2 - (2R-a)^2}}\right] + \frac{2}{\pi}\sqrt{1 - \frac{2R-a}{2R+a}^2}\right\}\right.} \right\} \qquad \text{(double crack)}$$

$$\Phi_3 = \sqrt{\frac{\sec\left\{\left(\frac{2R + a}{W - a}\right)\left(\frac{\pi}{2}\right)\right\}\sin\left\{\left(\frac{2R + a}{W - a}\right)\left(\frac{2a}{W}\right)\right\}}{\sec\left\{\left(\frac{2R}{W}\right)\left(\frac{\pi}{2}\right)\right\}\left\{\left(\frac{2R + a}{W - a}\right)\left(\frac{2a}{W}\right)\right\}}} \quad \text{(single crack)}$$

$$\Phi_3 = \sqrt{\frac{\sec\left\{\left(\frac{2R + 2a}{W}\right)\left(\frac{\pi}{2}\right)\right\}}{\sec\left\{\left(\frac{2R}{W}\right)\left(\frac{\pi}{2}\right)\right\}}} \quad \text{(double crack)}$$

The term Φ_2 was derived using an assumption that the crack or cracks and hole can be represented by a single effective through-the-thickness crack equal in length to the diameter of the hole plus the length of the crack or cracks. Stress intensities were then determined using this assumption with a uniform pressure applied over the original crack area [*14*]. The term Φ_2 then is simply a ratio of the solution for a crack emanating from two sides of the hole and the solution for a crack emanating from one side of the hole.

The term Φ_3 was determined using Isida's [*15*] finite width correction factors and the effective through-the-thickness crack length as just defined. Since the expression $m_{ec}\Phi_1$ gives the appropriate stress intensity for short cracks, the term Φ_3 is normalized by dividing the stress intensity for crack lengths of 2R+a and 2R+2a, by the stress intensity for a crack of length 2R. An important factor inherent in term Φ_3 is the correction which allows compilation of finite width effects for the crack emanating from only one side of the hole.

References

[*1*] Bueckner, H. F., "A Novel Principle for the Computation of Stress Intensity Factors," *Zeitschrift fur Angewandte Mathematik und Mechanik*, Vol. 50, No. 9, 1970, pp. 529–546.

[*2*] Rice, J. R., *International Journal of Solids and Structures*, Vol. 8, 1972, pp. 751–758.

[*3*] Bueckner, H. F., "Weight Functions for the Notched Bar," *Zeitschrift fur Angewandte Mathematik und Mechanik*, Vol. 51, 1971, pp. 97–109.

[*4*] Bueckner, H. F. and Giaever, I., "The Stress Concentration of a Notched Rotor Subjected to Centrifugal Forces," *Zeitschrift fur Angewandte Mathematik und Mechanik*, Vol. 46, 1966, pp. 265–273.

[*5*] Bowie, O. L., *Journal of Mathematics and Physics*, Vol. 35, 1956, pp. 60–71.

[*6*] Grandt, A. F., "Stress Intensity Factors for Some Thru-Cracked Fastener Holes," AFML-TR-74-71, July 1974.

[*7*] Hall, L. R., Shah, R. C., and Engstrom, W. L., "Fracture and Fatigue Crack Growth Behavior of Surface Flaws and Flaws Originating at Fastener Holes," AFFDL-TR-74-47, Vol. I, May 1974.

[*8*] Newman, J. C., Jr., "An Improved Method of Collocation for the Stress Analysis of Cracked Plates with Various Shaped Boundaries," NASA TN D-6376, Aug. 1971.

[*9*] Hoffman, O., *Introduction to the Theory of Plasticity for Engineers*, McGraw-Hill, New York, 1953, pp. 80–94.

[*10*] Brown, W. F., Jr., and Srawley, John E., *Plane Strain Crack Toughness Testing of High Strength Metallic Materials, ASTM STP 410*, American Society for Testing and Materials, Dec. 1967, p. 102.

[11] Kobayashi, A. S., "A Simple Procedure for Estimating Stress Intensity Factor in Region of High Stress Gradient," AD767404, Sept. 1973.

[12] Forman, R. G., Kearney, V. E., and Engle, R. M. "Numerical Analysis of Crack Propagation in Cycle-Loaded Structures," American Society of Mechanical Engineers, Paper No. 66-WA-MWT-4, 1966.

[13] Wheeler, O. E., "Spectrum Loading and Crack Growth," American Society of Mechanical Engineers, Paper No. 71-Met-X, 1971.

[14] Tada, H., Paris, P., and Irwin, G., *The Stress Analysis of Cracks Handbook*, Del Research Corporation, Hellertown, Pa., 1973, p. 5.11.

[15] Isida, M., *Transactions*, American Society of Mechanical Engineers, Series E, *Journal of Applied Mechanics*, Vol. 33, 1965, pp. 674.

Glossary

A Constant
a Crack length (half crack length in center-cracked specimens, or crack depth for surface flaws)
a_0 Initial crack length
a_f Final crack length
Δa^* Overload affected crack length increment
$\Delta a/\Delta N$ or da/dN Rate of fatigue crack growth
B Specimen thickness
B_N Net thickness in face-grooved specimen
C Compliance
c Half crack length at the specimen surface of surface-flawed specimens
E Young's modulus
f Frequency
G Strain energy release rate
K Stress intensity factor
K_I K for the opening mode (Mode I)
K_c Critical stress intensity for failure or fracture toughness
K_{Ic} Plane-strain fracture toughness
K_{Iscc} Apparent threshold K for stress corrosion cracking
K_{max} Maximum stress intensity factor in a loading cycle
K_{mean} Mean value of stress intensity factor in a loading cycle
K_{min} Minimum stress intensity factor in a loading cycle
K_{ol} Overload K
K_{op} Crack opening K
K_{rms} Root mean square stress intensity factor for a distribution
K_{ul} Underload K
ΔK Range of stress intensity factor in a loading cycle; $\Delta K = K_{max} - K_{min}$
ΔK_{eff} Effective range of stress intensity factor in a loading cycle
ΔK_{th} Threshold ΔK for fatigue crack growth
ΔK_{th}^* Overload affected ΔK_{th}
N Number of cycles
n Exponent in crack growth rate expression
N_D Number of cycles of delay
P Applied load
P_{max} Maximum applied load in a loading cycle
P_{min} Minimum applied load in a loading cycle
P_{op} Applied load above which the crack is fully open; crack opening load

P_r or ΔP Range of applied load in a loading cycle; $P_r = \Delta P = P_{max} - P_{min}$
P_{rd} Distribution of P_r
P_{rm} Modal value of P_r
Q Shape factor for surface flaws
R Stress ratio; $R = S_{min}/S_{max} = K_{min}/K_{max}$
r_y Plastic zone correction factor; $r_y = \frac{1}{2\pi}(K/\sigma_{ys})^2$
S Applied (gross-section) stress; $S = P/BW$
S_c Closure stress
S_{max} Maximum applied stress in a loading cycle
S_{mean} Mean value of applied stress in a loading cycle
S_{min} Minimum applied stress in a loading cycle
S_{op} Crack opening stress above which the crack tip is fully open
S_{rd} Distribution of S_r
S_{rm} Modal value of stress range S_r
ΔS or S_r Range of applied stress in a loading cycle; $S_r = \Delta S = S_{max} - S_{min}$
ΔS_{eff} Effective stress range
t Time or hold time (time at load)
T Temperature
U Effective stress or stress intensity range ratio; $U = \dfrac{\Delta S_{eff}}{\Delta S} = \dfrac{\Delta K_{eff}}{\Delta K}$
W Specimen width
ϵ Strain
ν Poisson's ratio
σ Stress
σ_u Ultimate strength
σ_{ys} Yield strength
τ Shear stress

Subscripts

Elemental Load Spectra

h High-load excursions (K_{hmax}, K_{hmin}, ΔK_h, N_h, t_h, t_h', f_h, R_h)
ℓ Low-load ($K_{\ell max}$, $K_{\ell min}$, ΔK_ℓ, N_ℓ, f_ℓ, R_ℓ)

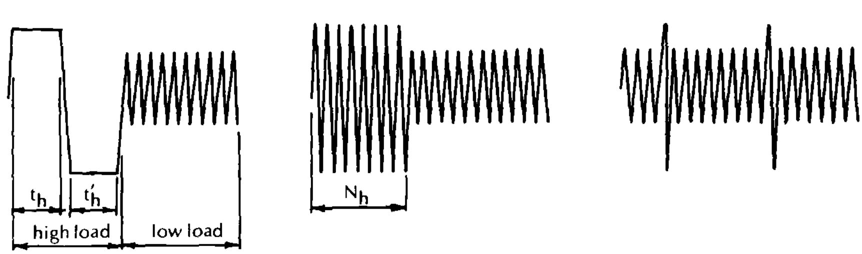

SINGLE HIGH-LOAD EXCURSION

MULTIPLE HIGH-LOAD EXCURSIONS

PERIODIC HIGH-LOAD EXCURSIONS

Block Programmed Loads

m block number
n load level within a given block

Typical Usage

$\Delta K_{m,n}$ stress intensity range for the n^{th} load level in the m^{th} load block